Developing New Hydrogen Bonded Alkaline Earth Metal-Organic Complexes

Hamdy, Louise

Award date:
2015

Awarding institution:
University of Bath

Developing New Hydrogen Bonded Alkaline Earth Metal-Organic Complexes

Louise Blythe Hamdy

A thesis submitted for the degree of Doctor of Philosophy

University of Bath

Department of Chemistry

April 2015

Table of Contents

List of Figures

List of Tables

Acknowledgements

I haven't said so in person, but I am truly grateful to my supervisor Chick Wilson for giving me the opportunity to move to Bath and join his research group, at a time when I really needed to shake up my life. I thank Chick for his guidance, enthusiasm and encouragement throughout my project, and for fooling me into believing that the research was entirely my own fantastic idea. I also thank Chick for his patience (read: tolerance) during my write-up, and for all his career advice.

Next I would like to thank the Wilson group alumni: András Kállay, Andrew Jones, Craig Wales and Alan Martin for my initiation into postgraduate research, for always being willing to share their knowledge, and for sheer entertainment value.

A huge thank you goes to all of the super-postdocs I have been fortunate to work with: Stephen Mansell and Will Gee for their assistance with practical work and Karen Robertson for her no-nonsense inorganic chemistry expertise. Special thanks go to Dyanne Cruickshank who helped me immensely with my crystallography and was extremely generous with her time, and likewise for Carlos Pinheiro. Thanks also to Lynne Thomas, especially for support during the early years. I would also like to acknowledge Paul Raithby, Andrew Burrows and their respective research groups for their assistance and for the use of their labs and equipment.

Next I would like to thank Alan Carver, Russel Barlow, Ed Aldred, Robert Stevens and Anneke Lubben for their technical and specialist support, Stephen Boyer for elemental analysis, Ann Hunter and staff at the NMSF for MS data, and Matt Dennis for answering all of my computing needs. I extend my thanks to all of the chemistry technical support staff.

Of course a massive thank you to all of the Wilson group ladies: Kate Wittering, Charlotte Jones, Lucy Saunders, Anneke Klapwijk and Lauren Agnew for creating such a supportive culture within the group and for all the good times. We often had far too much fun on school days, but frankly I think Alan's 'phi, chi, omega' dance has real educational value. Thanks also to all of our project students (including Alex Cousen, now PhD student) for always asking 'why?', for keeping us on our toes, and keeping us learning.

Finally, I thank my beloved family and friends, especially Hector, my parents, and the expats in Inverurie, for providing me with constant material and immaterial support, with minimal reciprocation of late.

I acknowledge the EPSRC and the University of Bath for funding, and I dedicate this work to Miss Laneres.

Abstract

This investigation addresses the understudied area of the research and development of hydrogen bonded metal-organic complexes featuring the alkaline earth metals magnesium and calcium. This work presents the crystal structures and thermal behaviour of a series of metal-organic and organic crystalline complexes synthesised from metal salts and pyridine carboxylic, dicarboxylic acid and chloranilic acid ligands, characterised primarily by X-ray diffraction.

Chapter 1 introduces crystal engineering, intermolecular interactions, and functional crystalline materials, followed by a literature review addressing metal-organic frameworks (MOFs), hydrogen bonded metal-organic complexes, magnesium MOFs and alkaline earth metal complexes synthesised from pyridine carboxylic, dicarboxylic and tricarboxylic acid and chloranilic acid.

Chapter 2 outlines the theory of the techniques used to analyse the synthesised materials, focusing on single crystal X-ray diffraction, followed by Chapter 3 which documents the sample preparation and the experimental details.

Chapter 4 describes the crystal structures of fourteen coordination complexes synthesised from magnesium and calcium salts and the three isomers of pyridine carboxylic acid. This work was carried out in order to identify structural trends such as the most common coordination geometries of the metal centres, the ways in which the ligands coordinate and any recurring hydrogen bonding motifs.

Chapter 5 discusses attempts to synthesise an alkaline earth metal analogue of a metal-containing 'metalloligand' of the formula $M(C_7H_4NO_4)_2(H_2O)_2$, in which the metal (M) is N,O-chelated by pyridine-2-carboxylate-4-carboxylic acid, and the subsequent combination of these materials with the diamines *o*-tolidine and *m*-xylylenediamine. This chapter also reports the structure of a magnesium coordination complex resulting from a hydrothermal reaction, and the subsequent transformation of this complex to a new crystal structure which contains the doubly deprotonated magnesium analogue of the originally targeted 'metalloligand'.

Chapter 6 describes the crystal structures of three complexes synthesised from pyridine carboxylic acids and chloranilic acid, and the complex resulting from the combination of one of these organic 'supramolecular ligands' with a copper salt. Finally, two new calcium-chloranilate coordination polymers are reported, one of which has an interesting anionic 3D structure.

Publication and Presentations

Publication:

'Self-assembly synthesis of precursors to potential open framework alkaline earth metal–organic complexes' L. B. Hamdy, P. R. Raithby, L. H. Thomas, C. C. Wilson., *New J. Chem.,* **2014**, 38, 2135-2143

Presentations:

1. April 2014, British Crystallographic Association (BCA) Spring Meeting, Loughborough, UK, **poster presentation**, 'Developing Magnesium and Calcium Metal-Organic Complexes and Hydrogen Bonded Networks'
2. August 2013, 28th European Crystallography Meeting (ECM28), Warwick, UK, **poster presentation**, 'Engineering Hydrogen Bonded Architectures of Magnesium-Organic Complexes'
3. July 2013, Advanced Complex Inorganic Nanomaterials (ACIN), Namur, Belgium, **oral presentation**, 'Engineering Extended Architectures using Metal Coordination in the Presence of Hydrogen Bonding'
4. June 2013, Afternoon of Science Research, University of Bath, **poster presentation**, 'Engineering Extended Architectures using Metal Coordination in the Presence of Hydrogen Bonding'
5. June 2013, Meeting of Minds, University of Bath, **oral presentation**, 'X-Ray Diffraction: Revealing the World on the Atomic Scale'
6. May 2013, Postgraduate Symposium, University of Bath, **oral presentation**, 'Engineering Extended Architectures using Metal Coordination in the Presence of Hydrogen Bonding'
7. March 2013, Third International Conference on Multifunctional, Hybrid and Nanomaterials (HYMA), Sorrento, Italy, **poster presentation**, 'Engineering Extended Architectures using Metal Coordination in the Presence of Hydrogen Bonding'
8. June 2012, Meeting of Minds, University of Bath, **oral presentation**, 'Engineering Extended Architectures using Metal Coordination in the Presence of Hydrogen Bonding'
9. June 2012, Afternoon of Science Research, University of Bath, **poster presentation**, 'Engineering Extended Architectures using Metal Coordination in the Presence of Hydrogen Bonding'

10. April 2012, British Crystallographic Association (BCA) Spring Meeting, Warwick, UK, **poster presentation**, ‘Engineering Extended Architectures Using Metal Coordination in the Presence of Hydrogen Bonding’

Chapter 1. Introduction

1.1. Objective

Single-crystal materials feature prominently in the development of modern technologies and therefore are of much interest to a wide spectrum of the scientific community.[1, 2] Inorganic-organic hybrid materials are attracting particular interest not only due to their fascinating molecular architectures, but also due to the fact that by applying the principles of crystal engineering, these structures are highly tuneable and can adopt a variety of functionalities.[3, 4] The objective of the work reported herein is to combine the structural flexibility afforded by a hydrogen bonded network,[5] with the benefits of a lightweight metal centre,[6] to develop new hydrogen bonded alkaline earth metal-organic complexes.

1.2. Crystal Engineering

Crystal engineering was first specifically spoken of by Schmidt.[7] In his 1971 paper on solid-state photochemistry, Schmidt regards the 'phase of crystal engineering' as the evolution of rules based on the theory of molecular packing to allow the rational development of solid state chemistry.[8] Desiraju echoes Schmidt's thoughts in his comprehensive definition of crystal engineering as 'the understanding of intermolecular interactions in the context of crystal packing and in the utilisation of such understanding in the design of new solids of desired physical and chemical properties.'[9] Crystal engineering is an interdisciplinary synthesis methodology applicable to the research and development of pharmaceuticals,[10] the study of biological molecules,[11] and it is fundamental to the design of functional crystalline materials with potential industrial applications.[12]

Crystal engineering is an extremely rapidly growing area of research which straddles various subjects including solid state chemistry and materials science.[2] Supramolecular chemistry encompasses aspects of crystal engineering since the crystal can be viewed as a supermolecule; Dunitz has described the crystal as the supermolecule 'par excellence'.[13] The category of supermolecules includes biological macromolecules which owe their three-dimensional structures to non-covalent interactions. Similarly, the structure of a molecular crystal is determined by the combined effects of intra- and intermolecular interactions[14] including ion-ion, ion-dipole, dipole-dipole, dispersion (London) forces and hydrogen (H-) bonding.[13] The concept of the 'supramolecular synthon' was introduced by Desiraju in 1995 to describe the spatial arrangement of intermolecular interactions to form structural motifs within the supermolecule.[15] These motifs, some examples of which are shown in Figure 1.1,

can be assembled with some degree of predictability through synthetic operations using intermolecular interactions by selective placement of functional groups, in a supramolecular equivalent of covalent synthesis.[15] Fyfe and Stoddart described a combination of these syntheses as 'supramolecular assistance to molecular synthesis' whereby discrete molecular entities comprised of covalent bonds are supported in the complex by non-covalent intermolecular interactions.[16]

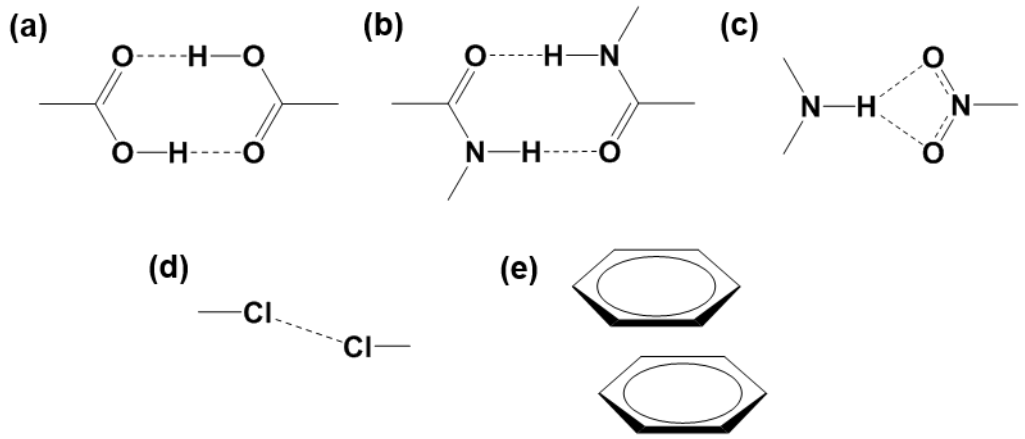

Figure 1.1. Supramolecular synthons: (a) Carboxyl dimer (b) Amide dimer (c) Bifurcated D-H···A/A H-bond whereby a hydrogen atom is attracted to both oxygen atoms of a nitro group. (d) Halogen bond between chlorine atoms. (d) π-π stacking interaction between two aromatic rings.

Desiraju highlights that the crucial difference between covalent and supramolecular synthesis is that the former is concerned with the connectivity of covalent bonds, whereas the latter is defined by geometrical and topological interaction connectivity resulting in patterns such as ribbons and sheets or features such as channels and pores.[15] Whitesides *et al*. describe the difference between the two syntheses in terms of the bonds involved: in covalent synthesis, enthalpy is the dominant factor and the bonds in the final products are kinetically stable, whereas in non-covalent synthesis the products are equilibrating structures, indicating a balance between enthalpy and entropy.[17]

Crystallisation is fundamentally a process of static, as opposed to dynamic, self-assembly, whereby the components do not dissipate energy and the system is at equilibrium.[18] The process can be viewed in terms of two distinct models of crystal packing which Desiraju describes as the geometric and chemical models.[2] The geometric model, first defined by Kitaigorodskii, assumes that crystal structures are primarily directed by optimal space filling close packing and directional intermolecular interactions are not weighted heavily in importance. This approach was supported in later work by Dunitz and Gavezzotti, in which

the analysis of six polymorphs of an organic crystal suggested that dispersion forces between molecules contributed more significantly toward the cohesive energy of the crystal than did intermolecular atom-atom contacts.[19] A highlight article by Dunitz and Schweizer on the crystal structure of alloxan stressed that there are infinite numbers of low energy crystal structures a given molecule may adopt, and it is inappropriate to attempt to predict or explain these in terms of interactions between non-bonded atoms.[20] Desiraju describes this as the 'thermodynamic crystal' since during the self-assembly process, the components of the system can orientate and re-orientate until an energy minimum is reached.[2]

The chemical model, in contrast, proposes that the crystal structure may be considered on the basis of directional intermolecular interactions.[2] This notion was originally put forward by Etter, with particular reference to H-bonds.[21] Etter proposed three general rules for H-bonding in organic crystals: (i) all good proton donors and acceptors are used in H-bonding; (ii) six-membered-ring intramolecular H-bonds form in preference to intermolecular H-bonds; (iii) the best proton donors and acceptors remaining after intramolecular H-bond formation form intermolecular H-bonds to one another. Further rules accounting for specific classes of functional groups were also presented, based on findings that certain functional groups showed a preference to particular H-bonding patterns. Desiraju calls the chemical model the 'kinetic crystal' since, theoretically, the strongest H-bond will form between the most acidic hydrogen and the most electronegative atom, followed by the inevitable formation of the second strongest interaction and so on during crystallisation.

Desiraju notes that neither the geometric nor the chemical model is applicable to every crystal structure, with contradictions to the theories and rules frequently arising. Therefore, the actual governing factors of crystallisation are likely to be a combination of both models and they need not necessarily be mutually exclusive. Desiraju claims that the supramolecular synthon concept represents a compromise between the geometric and chemical models since the supramolecular synthon embodies aspects of both geometrical and chemical recognition.[2] Studies on the crystal structures of substituted calixarenes by Bombicz and co-workers have shown that the supramolecular synthon can be engineered; the term 'synthon engineering' was proposed for the control of molecular packing *via* tuning of the synthons.[22] Furthermore, Desiraju suggests that the supramolecular synthon model may be the most practical as it is based on probabilities of particular synthons occurring, as opposed to quantitative energy measurements.[2]

1.2.1. Intermolecular Interactions

The very existence of solids and liquids is attributed to the effects of intermolecular interactions – forces that are fundamental to the crystallisation and dissolution of molecular crystals.[9] A crystal possesses a network of intermolecular interactions between the constituent molecules or ions that simultaneously attract and repel one another. In an energetically stable aggregate, the sum of the intermolecular interaction energies is attractive and the optimum geometry of the structure is a compromise between these interactions.[23] The non-covalent intramolecular interactions which occur in a molecular crystal affect the shape and conformation of the molecule, and in turn, influence the crystal packing.[14]

Electrostatic interactions, also called Coulombic or ionic interactions, arise from the permanent charge distribution in molecules. These constitute an important class of long-range intermolecular interactions in crystals,[9, 23] being the dominant forces in simple ionic crystals such as sodium chloride.[14] Van der Waals forces, including both dipole-dipole and dispersion (London) forces, are the most significant long-range interactions in crystals composed of non-polar molecules. Dispersion forces are present between all molecules including those with electrical multipole moments equal to zero since the electrons can effect an instantaneous polarity. This can induce temporary polarity in an adjacent molecule resulting in an attractive force. Dispersion forces are additive – their strengths are relative to the size and dependent on the shape of the molecule. They can especially influence the structure of molecular crystals if a highly polarisable function is present such as an aromatic ring or heteroatom.[9]

Hydrogen Bonds

Hydrogen bonds (herein usually abbreviated to H-bonds) are ubiquitous in nature, being responsible for the structure and properties of materials such as ice and water, and are widely present in biological systems, stabilising structures such as proteins and DNA. After van der Waals forces, H-bonds are the most frequently observed intermolecular interactions in molecular crystals and are very relevant to crystal engineering.

The concept of the H-bond has been touched upon by a number of scientists since the early 20th century with reference to the study of various materials, however it was Pauling who, in 1939, most formally introduced it in his book ‘The Nature of the Chemical Bond’: ‘Under certain conditions an atom of hydrogen is attracted by rather strong forces to two atoms instead of only one, so that it may be considered to be acting as a bond between them. This is called a hydrogen bond.’[24] The 2011 IUPAC definition of the hydrogen bond is ‘an

attractive interaction between a hydrogen atom from a molecule or a molecular fragment X–H in which X is more electronegative than H, and an atom or a group of atoms in the same or a different molecule, in which there is evidence of bond formation.'[25] In this work, an H-bond is written schematically as 'D-H···A' whereby 'D' represents the donor atom and 'A' the acceptor.

The H-bond is an electrostatic attraction which originates from the fact that the hydrogen atom possesses only one electron, and so it follows that H-bonding is unique to hydrogen.[26] This single electron engages in a covalent bond with the donor atom, and so greater relative electronegativity of the donor atom causes a local dipole in this bond which causes deshielding of the hydrogen atom bringing about an electrostatic attraction to any concentration of electron density of the acceptor.[27]

The nature of H-bonds varies considerably in strength, from weaker interactions comparable to van der Waals forces to those approaching the strengths of covalent bonds. Their energies cover a continuous scale from about 0.5 to 40 kcal mol^{-1} (approx. 2 – 167 kJ mol^{-1}) – one criterion by which H-bonds can be subdivided is according to their relative strengths (Table 1.1).[27] H-bonds can also be subdivided according to geometrical, thermodynamic and chemical properties, considering the nature of the donor and acceptor groups (however the resulting classifications are not necessarily consistent and often subjective).[26]

Neutral-neutral H-bonds, where neither the donor nor acceptor has a formal charge, can be weak to moderate in strength. Weak H-bonds arise from dipole-dipole electrostatic interactions where the hydrogen atom is covalently bonded to a relatively electroneutral atom such as carbon, e.g. C-H···O, or where the acceptor group is in the form of polarisable π-electrons, e.g. O-H···π. In moderate (or medium strength) H-bonds, the donor atom may be more electronegative relative to the hydrogen atom and the acceptor may have lone-pair electrons, e.g. N-H···O=C. The strongest H-bonds occur where there is an electron deficiency on the donor atom or excess in the acceptor such that they have a formal charge (charge-assisted H-bonds) e.g. H_3N^+-H···COO^-. Strong H-bonds are directional and often have a D-H-A angle close to 180°.[27]

Table 1.1. Properties of strong, moderate and weak hydrogen bonds.[27]

Property	Strong	Moderate	Weak
Bond energy (kJ mol^{-1})	63 – 167	17 – 63	< 17
D-H···A interaction	Mostly covalent	Mostly electrostatic	Electrostatic
Bond lengths	D-H ≈ H···A	D-H < H···A	D-H << H···A
H···A (Å)	~1.2 – 1.5	~1.2 – 2.2	2.2 – 2.3
D···A (Å)	2.2 – 2.5	2.5 – 3.2	3.2 – 4.0
Bond angles (°)	175 – 180	130 – 180	90 – 150

In this work, the maximum distance reported for an H-bond is taken to be the sum of the van der Waals radii of the donor and acceptor atoms, as published by Bondi,[28] plus a tolerance of 0.5 Å. The van der Waals radii and maximum H-bond distances of commonly encountered atoms and H-bonds are listed in Table 1.2. This quantitative system allows differentiation between interactions that could reasonably be assigned as weak H-bonds, and those which are more likely to be van der Waals in nature. On occasion in this work, an H-bond is reported which exceeds the maximum distance defined here, but where such an interaction has a very large angle (closer to 180°) indicating some degree of directionality, it is included in the structural analysis as a possible H-bond interaction.

Table 1.2. Atomic van der Waals radii of C, N, O and Cl, and maximum H-bond distances for common H-bonds reported in this work.

Atom	van der Waals radii	H-bond	Max. D···A distance
C	1.70 Å	O-H···O	3.54 Å
N	1.55 Å	N-H···O	3.57 Å
O	1.52 Å	C-H···O	3.72 Å
Cl	1.75 Å	C-H···Cl	3.95 Å

In crystalline structures, moderately strong H-bonds occasionally involve two acceptor atoms for one hydrogen atom so that the H-bond is bonded to three different atoms in the form D-H···AA (Figure 1.1(c)). If the three angles, D-H-A, A-H-A, A-H-D, sum to approx.

360° and the hydrogen atom lies within ~0.2 Å of the mean plane of the donor and acceptor atoms, such an arrangement is called a three-centred or bifurcated H-bond.[27] H-bonds of this configuration are encountered frequently in this work.

Halogen Bonds

The halogen bond is regularly observed in molecular crystals and can potentially be used to direct molecular recognition in crystal engineering. The definition of the halogen bond is the attractive interaction between an electrophilic halogen atom and a nucleophile, a general formula of which is 'D···X-Y' whereby 'D' is the electron donor (Lewis base, halogen bond acceptor), 'X' is the electron accepting halogen atom (Lewis acid, halogen bond donor) and 'Y' is the atom to which the halogen is covalently bonded, (C, N or another halogen atom).[29, 30] In the halogen bonds observed in this work, both 'X' and 'D' represent chlorine atoms covalently bonded to carbon atoms forming homogeneous halogen bonds in the form of Cl···Cl interactions (Figure 1.1(d)). It is also possible for 'D' to represent a metal-coordinated halide ligand which donates electrons to the empty σ* orbital of C-X,[4] forming halogen bonds of the form C-X···X'-M, the strengths of which can be tuned by changing the organic (-bonded) and inorganic halogen atoms.[31]

Halogen bonds arise due to the anisotropic distribution of electron density around an organic halogen atom which produces a region of positive electrostatic potential that increases with the polarizability of the atom.[29, 32] The attractive forces forming a halogen bond result in a D···X distance less than the sum of the van der Waals radii of the two atoms, with stronger interactions being shorter and more directional. The strength of the halogen bond donor and its tendency to form strong interactions increases with decreasing electronegativity, in the order F < Cl < Br < I.[29] Halogen bonds have energies ranging from 5 to 200 kJ mol^{-1} with Cl···Cl and $I^-\cdots I_2$ contacts being among the weakest and strongest halogen bonds, respectively.[30] Halogen bonds can be divided into two groups based on their geometrical characteristics (Figure 1.2): type-I and type-II halogen bonds.

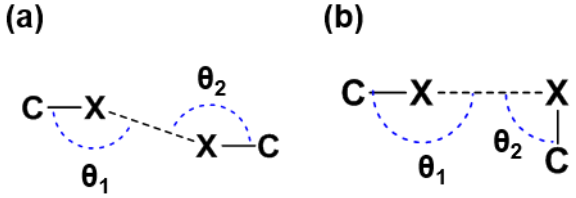

Figure 1.2. Halogen bonds. (a) Type-I halogen bond ($\theta_1 \approx \theta_2$). (b) Type-II halogen bond ($\theta_1 \approx 180°$, $\theta_2 \approx 90°$).[32]

Due to their similar properties to H-bonds such as their potential strength, specificity and directionality, halogen bonds may be regarded as potential supramolecular synthons and applied as such in the design of supramolecular architectures.[15] Their occurrence in conjunction with H-bonding,[33] and along with H-bonding, coordination bonds and π-π interactions[34] has been studied, and is an important consideration in drug development.[35]

π Interactions

Intermolecular interactions involving π-electrons include H-bonds in which π-electrons are the acceptor group. In this work, however, the most commonly encountered intermolecular interactions involving π-electrons are π-π (stacking) interactions between aromatic substituents as illustrated in Figure 1.1(e). In 1990, Hunter and Sanders modelled these interactions in terms of the charge distribution and attributed the overall attractive π-π interaction as the attraction between the negatively charged π-electron cloud of one aromatic group and the positively charged σ-framework of another. They rationalised that the geometry of the interaction, whether the aromatic groups are stacked (face-to-face or offset) or edge-to-face, is influenced by the electron-withdrawing/donating effects of any substituents of the aromatic ring.[36] In 2001, a review by Hunter *et al*. emphasised that π-π interactions are rather more complicated in comparison to well-defined single point interactions such as H-bonds. This is due to their having multiple points of intermolecular contact and so a greater contact surface area, increasing their susceptibility to van der Waals interactions. They can also have very variable geometries and can be influenced by a huge range of possible functional groups.[37] Such is the complexity and ambiguity of π-π interactions, that in 2012, Martinez and Iverson proposed that the terms 'π-stacking' and 'π-π interaction' no longer be used and that the Hunter and Sanders model be refined to account for substituent interactions. They asserted that the terms are misleading since they imply that (i) the interaction is specifically between π-electron clouds to result in stacking of the rings, and (ii) that these interactions are unique to aromatic groups and significant when compared to, and distinct from, the van der Waals forces that act upon all molecules. They suggest that the term 'aromatic donor–acceptor interactions' is most appropriate to describe face-to-face π-π interactions that occur under specific circumstances where there is an interaction between electron-rich and electron-deficient aromatics.[38]

In this work, π-π interactions are not considered to contribute significantly to the crystal packing of the reported structures, however, where there is some degree of overlap of aromatic rings, or conjugated systems, and the centroid-centroid distance is approx. 4 Å or less, they are reported in the interests of comprehensive and consistent structural analyses.

1.2.2. Polymorphism

Due to the supersaturated conditions under which crystal growth generally occurs, crystallisation is a kinetic phenomenon and as such, different crystal structures of the same molecule(s) are a possibility.[2] This is the phenomenon of polymorphism, which can be regarded as supramolecular isomerism. It presents a major challenge to, and is of huge research interest within, the subject of crystal engineering.[39] Polymorphism is a notoriously difficult phenomenon to define due to the varying factors and criteria that have to be taken into consideration, however the definition that generally prevails is that of McCrone who described a polymorph as 'a solid crystalline phase of a given compound resulting from the possibility of at least two different arrangements of the molecules of that compound in the solid state.'[40] Due to the focus of inorganic chemists and geologists on the structure-property relationships of inorganic compounds and minerals, polymorphism is widely recognised in inorganic materials such as calcium carbonate and titanium dioxide. Until a recent major increase in effort on this area, there was considerably less knowledge on the polymorphism of molecular crystals, partly due to the relative infancy of organic solid state chemistry compared with other disciplines, but also due to the difficulty of polymorph determination and control in inherently more flexible molecular systems.[41]

Any particular compound may potentially have polymorphic forms, but the conditions under which these polymorphs are stable may not be readily, if ever, encountered. Polymorphism is frequently exhibited by industrially relevant solids such as foodstuffs, personal care products, pharmaceuticals, dyes and explosives, and issues with the control of polymorphism can be encountered when these are manufactured in a repetitive process for which the precise production conditions are subject to slight variation. The formation of one crystalline phase over another is presumed to be initiated by the formation of critical nuclei of the new phase that grow preferentially under specific external environmental factors such as temperature.[39] In 2012, a study on the polymorphism of isonicotinamide found that the polymorphic form obtained from cooling crystallisation was dependent on the hydrogen bonding capacity of the solvent, illustrating how solvent effects have a major influence on the crystal nucleation process.[42]

Desiraju has drawn attention to a very intriguing aspect of polymorphism, in that despite the differences in energy between polymorphs of a material often being quite small, many organic crystals have not been found to be polymorphic, and it seems from this that the molecule often crystallises in a very selective manner.[43]

The capacity of crystalline substances to interconvert into another with potentially significant differences in chemical and physical behaviours has serious implications with regard to the

safety, production, stability, effectiveness and intellectual property protection of commercial products. Polymorphism is therefore an important and appealing area of research in crystal engineering.[23]

1.2.3. Crystallisation Techniques

Crystallisation with the aim of growing crystals suitable for X-ray diffraction, as opposed to the recrystallisation of a synthesised product for the purposes of increasing the purity and/or yield, generally requires more specific conditions in order to optimise the crystals' size and quality.

Evaporative crystallisation is a solution based technique whereby crystallisation is encouraged by the gradual evaporation of the solvent in which the compound(s) to be crystallised are dissolved until saturation of the solution. The rate of evaporation can be controlled through the temperature of the solution and/or by varying the size of the orifice(s) of the container. Evaporative crystallisation is the most frequently used technique throughout this work partly due to it requiring the least apparatus and that it can be carried out in small vials using very small quantities of reactants lending itself well to maximising the number of experiments accessible for a given amount of available sample. Furthermore, experiments carried out in small vials can easily be accommodated in hot-plates with custom DrySyn® adaptors for temperature control. Alternatively, a sealed vial can be used and crystallisation promoted by slow cooling of the solution.

Vapour diffusion crystallisation involves dissolving the compound(s) in one vial, placing this vial into a larger vial containing an antisolvent, and sealing the larger vial to allow the solvents to equilibrate. This technique requires careful selection of solvents with respect to their boiling points and the extent to which they can dissolve the compounds in order to promote crystallisation. If the solvent in the inner vial is more volatile, it diffuses into the antisolvent, and the concentration of the solute increases, while if the reverse is true, the antisolvent diffuses into the solvent, decreasing the concentration and affecting the solubility of the solute.

Crystallisation by solvent layering is achieved by dissolving a compound in one solvent and slowly layering a less dense solvent, in which the compound is less soluble, on top such that as the top layer slowly diffuses into the bottom layer, the consequent reduced solubility of the solute may promote crystallisation at the interface.[44]

Crystallisation from gels can also be utilised with success and is similar in principle to the layering technique as it involves diffusion between two layers. One compound is dissolved

in a solution with sodium metasilicate, for example, to form a gel, and a solution in which another compound is dissolved is layered on top of the gel. Crystallisation occurs by diffusional matter transfer between the layers, and since gravitational convection is prevented, the nuclei are more likely to be well separated and the crystals grow from all directions,[1] i.e. they are not compressed against the side of a vial.

1.3. Functional Crystalline Materials

Crystal engineering is a route towards the design of functional crystalline materials. This encompasses a huge range of materials with different molecular components, structures and functionalities, giving rise to different properties which can be utilised in a wide range of applications. Examples include materials for biomedical applications; a framework composed of non-toxic iron and the therapeutically active linker ligand nicotinic acid has highlighted their potential as drug delivery systems.[45] Polar materials can be used for non-linear optical applications,[46] and those possessing magnetic and photoluminescence have potential as molecular sensors and in electronic applications such as data storage.[47]

Porosity is one feature of functional crystalline materials that is attracting particular interest.[48] Porous materials have a very wide range of applications in gas adsorption and separation,[49] gas storage,[50, 51] the selective removal of contaminants from fuels,[52] and toxic gases from air,[53] catalysis,[54, 55] the encapsulation of guest species,[56, 57] and as molecular flasks with selective microenvironments.[58]

Porosity can be exhibited by a broad range of crystalline compounds, including those that are purely organic. Covalent organic frameworks (COFs),[59, 60] are crystalline materials composed of B, C, N, O and H connected into a rigid porous architecture by strong covalent bonds. It has been suggested that stable porous organic molecules in the form of discrete 'cages' of prefabricated covalent voids may have advantages over extended porous frameworks such as COFs, since the three-dimensional connectivity between the windows of the cages can be controlled by varying the cage vertex functionality.[61] Porosity can also be attained by organic crystalline molecules 'extrinsically' whereby the discrete molecular components do not have voids, but pack inefficiently, connected by intermolecular interactions, creating a porous network.[62] In general, extended frameworks are more stable towards solvent guest removal than are porous organic molecules/cages,[63] however, an extrinsically porous organic solid composed of H-bonded units of triptycene trisbenzimidazolone has been reported by Mastalerz and Oppel, which features 1D channels with a very high surface area, SA_{BET} of 2796 m^2g^{-1}.[64]

Porosity is also a structural feature of inorganic crystalline materials such as zeolites,[65] and can be designed into the structure of hybrid organic-inorganic materials that feature organic ligands coordinated to metal centres; this group of compounds can be broadly defined as 'metal-organic complexes'. These materials can be categorised on a scale with reference to the extent of their connectivity *via* coordination bonds. At one end are 0D complexes which feature discrete units of metal centres coordinated by organic ligands connected into the three-dimensional structure by non-covalent interactions such as H-bonds, halogen bonds, π-π interactions and van der Waals forces. Cook *et al*. have described such systems as supramolecular coordination complexes (SCCs).[66] At the other end of this scale are metal-organic frameworks (MOFs),[67] often referred to as 'coordination polymers', which are infinite networks composed of metal centres connected by bridging organic ligands *via* coordination bonds.[66] MOFs are often connected into 3D arrays through metal-ligand coordination; these MOFs are more likely to display the much sought-after microporous framework often associated with these materials. Located in the middle of the scale are 1D and 2D 'MOFs', whose exact classifications as MOFs and correct terminology is debatable,[67] however these can be referred to as 1D and 2D coordination polymers. The three-dimensional extended structure of these coordination polymeric chains and sheets is propagated in two directions or one direction, respectively, *via* intermolecular interactions between the infinite coordination polymeric units.

1.3.1. Metal-Organic Frameworks

MOFs constitute a very diverse range of crystalline materials which have a well-defined geometric structure with the metal centres or inorganic clusters acting as joints in a scaffold connected by organic ligands acting as struts.[67] Due to the specific coordination geometries of the d-block cations, MOFs most commonly feature transition metals. Main group metals feature to a lesser extent, while lanthanide MOFs are receiving increasing attention due to their luminescent properties.[68] MOFs can feature a diverse range of organic linkers; typically they are inflexible, polytopic ligands, frequently featuring phenyl- or ethynyl-containing molecules,[66] coordinating to the metal centres *via* carboxylate, azolate, pyridyl, amine, sulfonate, or phosphate donor groups,[69] with chelating ligands offering greater stability to the framework.[4] Halides, cyanide and thiocyanate ions can also act as linkers between metal centres.[48]

The predictable and well-defined geometries often adopted by the inorganic cluster 'nodes' gives rise to the concept of the secondary building unit (SBU). This term has been used with regard to zeolite structure analysis to describe the topological building units consisting

of up to 16 ‘T’ atoms (where ‘T’ are Si, Al, P etc.), whereby the primary building units are the individual TO_4 tetrahedra,[70] but has since been applied by Yaghi and co-workers to aid the understanding and prediction of the structures of MOFs.[71] These well-established, rigid molecular building blocks representative of the metal clusters can be assembled in situ into a predetermined target framework by combination with the organic ligands *via* coordination-driven self-assembly under specific synthetic conditions.[66, 67] Inorganic clusters feature multiple metal centres which can be bridged by carboxylate donor groups of the ligands, thus locking the ions into rigid, directional units that can form highly stable frameworks,[48] the properties of which are maintained and expressed in the final MOF structure. Examples of common SBUs of metal-carboxylate MOFs are shown in Figure 1.3. The strategy of recognising the necessary SBU for the targeted framework, and its utilisation in its design, has been termed ‘reticular synthesis’ and can be considered as a subclass of crystal engineering.[72] Organic links capable of coordinating to two or more metal centres can also constitute preformed SBUs.[67]

The geometry of the SBUs determine the framework topology of the MOF which can be assigned a net type.[67, 73] A net is a collection of nodes with a clearly defined connectivity or topology,[74] and a net type is inherent to every network structure. Therefore a net can be regarded as the blueprint for a structure,[73] and construction of the net can be achieved by correct application of the appropriate SBUs in what is referred to as the net-based approach to the construction of coordination polymers.[74]

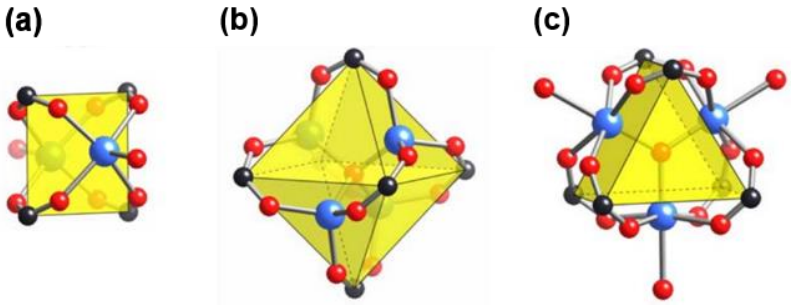

Figure 1.3. Common SBUs in metal carboxylate MOFs. (a) Square paddlewheel, (b) octahedral ‘basic zinc acetate’ cluster, (c) trigonal prismatic oxo-centred trimer. (Metal ions shown in blue, carbon atoms black, oxygen atoms red). Image obtained from Rowsell and Yaghi, 2004.[67]

MOFs are often synthesised using crystal growth techniques such as evaporative crystallisation, vapour diffusion and gel methods.[67] The coordination-driven self-assembly process by which MOFs form generally results in the thermodynamic product, therefore this process is aided by the kinetic reversibility of labile metal ions which will allow for reversible

metal-ligand bond formation.[66] For cases with low solubility of the precursors or use of a less labile metal ion, solvo/hydrothermal techniques may be employed, whereby the precursors are combined in solvents and placed inside a Teflon-lined stainless steel autoclave inside an oven. However, conditions such as temperature, concentration and solvent polarity have to be optimised to maintain the integrity of specific building blocks and promote the formation of target frameworks.[67]

The synthesis and study of MOFs is an attractive area of inorganic crystal engineering due to the potential to manipulate the properties of the materials, on a periodic scale, thus optimising their suitability for specific applications. One method of modification is through the simple substitution of the ligands in a reticular synthetic approach. This has been demonstrated by Eddaoudi *et al*. in their synthesis of an isoreticular series of sixteen materials, whereby use of a series of ditopic carboxylate linker ligands of different functionalities and dimensions connecting between inorganic octahedral $Zn_4O(CO_2)_6$ clusters resulted in the systematic variation of the pore size of the MOF, while maintaining the underlying topology of the original framework. One of the isoreticular series, IRMOF-6, proved to be an ideal material for CH_4 storage, with an uptake of 240 $cm^3\ g^{-1}$ at standard temperature and pressure.[75]

In situations where the bridging ligand has a reactive site, the MOF may be modified by a postsynthetic modification, such as (counter-) ion exchange,[76] or covalent transformations by organic synthesis.[66] Bloch *et al*. synthesised a MOF with open 2,2'-bipyridine coordination sites and demonstrated the material's ability to complex with Cu^{2+} which significantly enhanced the MOF's selectivity for the adsorption of CO_2 over that of N_2.[77]

Although they are probably the most versatile functional crystalline material of those described here, with wide-ranging applications from catalysis to drug delivery, gas adsorption is possibly the application most strongly associated with MOFs. Since gas adsorption requires materials of a high surface area to maximise uptake, much research carried out on MOFs aims to produce materials of high permanent microporosity, targeted to adsorb specific gases. To be deemed porous requires that the framework integrity is maintained on evacuation of guest solvent and that the framework withstands the reversible physisorption of guest molecules.[67]

High porosity can in principle be achieved using slim, expanded organic linker ligands,[78] however a porous MOF with a high surface area can lead to problems such as thermal and hydrothermal instability,[79] fragility of the structure and consequent framework collapse,[80] or the framework may be interpenetrated, whereby multiple identical frameworks intersect one another with maximum displacement, minimising pore space.[67] The problems of fragility

and interpenetration were overcome and the synthesis of MOFs possessing extremely high surface areas achieved by Furukawa *et al*.[78] Interpenetration of the networks was avoided by employing previous findings that interpenetration cannot occur if the network is not self-dual, in that the same net does not form if the linkers replace the nodes and vice versa, since this would involve linking sites of the same coordination that would not be viable.[81] Four MOF materials were synthesised and of these, MOF-210, composed of octahedral $Zn_4O(CO_2)_6$ units linked by 4,4′,4″-[benzene-1,3,5-triyl-tris-(ethyne-2,1-diyl)] tribenzoate and biphenyl-4,4′-dicarboxylate, showed an extremely high SA_{BET} of 6240 $m^2\ g^{-1}$. This is reportedly near the ultimate limit for a solid material as the volume-specific surface area is equal to that of cubic nanoparticles of edges 3 to 6 nm.[78]

Particular interest in designing MOFs to adsorb the potential vehicle fuel gases CH_4 and H_2, stems from these gases' suitability as clean fuels and the associated challenges of finding effective ways to separate, capture, and reversibly store them, while taking into account transportation requirements of safety and cost efficiency, which may be addressed by physisorption in a porous material.[82, 83] In light of the ever increasing global anthropogenic CO_2 emissions, environmental considerations are also behind the significant interest in MOFs designed to adsorb CO_2 gas produced by combustion of organic matter for the purposes of CO_2 capture, storage and utilisation,[84] by physisorption,[85] or by coordination to open metal sites.[86]

For all their potential in environmentally green chemistry, there has been a growing awareness that MOFs are often synthesised from petrochemical-derived feedstocks, expensive transition metals and harmful solvents. To break this trend, Smaldone *et al*. synthesised a MOF from renewable, and in some cases edible, natural products.[87] CD-MOF-1, $[(C_{48}H_{80}O_{40})(KOH)_2]_n$ was prepared by dissolving γ-cyclodextrin (γ-CD) with KOH in water and allowing vapour diffusion of methanol into the solution over the course of a week. The resulting MOF was constructed of unit cells of $(\gamma\text{-CD})_6$ cubes in which the secondary faces of the γ-CD units pointed outwards to make the six faces of the cube, inside of which there was a 1.7 nm sized pore. The cubes packed in a body-centred cubic arrangement. The eight-coordinate potassium ions assisted in the assembly of the structure through coordination by the primary faces of γ-CD tori *via* hydroxyl groups and glycosidic ring oxygen atoms, and the secondary faces *via* hydroxyl groups. CD-MOF-2 is an isostructural MOF, synthesised from rubidium hydroxide. The thermal stability of the guest-free MOFs as studied by thermogravimetric analysis (TGA) showed that CD-MOF-1 and CD-MOF-2 were stable up to 175 °C and 200 °C, respectively, indicating a thermally stable porous network. Their surface areas, SA_{BET} were 1220 $m^2\ g^{-1}$ and 1030 $m^2\ g^{-1}$, respectively.

CD-MOF-2 was later shown to display a high affinity for CO_2 which was attributed to chemisorption at the hydroxyl groups resulting in carbonic acid formation.[88]

The fixation of CO_2, along with the adsorption of H_2 and CH_4, by environmentally benign MOFs and other materials is an important area of research and a prime example of applied crystal engineering.

1.3.2. Hydrogen Bonded Metal-Organic Complexes

The work presented here focuses on metal-organic complexes of lower dimensional coordination connectivity (including 1D and 2D 'MOFs') that are connected primarily *via* H-bonds formed between the organic substituents. The 0D materials, consisting of discrete coordination units, are those that have been described as supramolecular coordination complexes (SCCs) by Cook *et al*.[66]

Combination of the coordination bond forming capabilities of a metal ion with the directional H-bonding abilities of the coordinated organic ligands possessing complementary H-bonding groups provides a 'bridge' between coordination polymers and supramolecular assemblies.[89] [90] Burrows *et al*. synthesised a range of transition metal complexes coordinated by ligands and connected intermolecularly by triple H-bonds formed between the H-bonding recognition sites of ligands in an analogous fashion to the H-bonding motif between cytosine-guanine nucleotide base pairs.[89] In a similar use of a predictable supramolecular synthon, Aakeröy *et al*. employed the dimeric oxime-oxime H-bonds between the oxime functionalities of pyridine-oxime ligands coordinated to Ag(I) to direct the formation of ordered H-bonded networks.[90] Both of these examples feature metal centres coordinated by ligands with peripheral functional groups with H-bonding functionalities. In the latter, the metal-ligand complexes are H-bonded directly, while in the former the complexes are connected *via* H-bonding to a linking ligand such as melamine with both H-bond donor and acceptor groups. The design of such metal-ligand motifs is fundamental to the development new H-bonded metal-organic complexes.

A versatile metal-ligand complex, or 'metalloligand,' has been synthesised by Kitagawa and co-workers that features a Cu centre, N,O-chelated by two pyridine-2-carboxylate-4-carboxylic acid ligands and axially coordinated by water molecules (Figure 1.4). The dianionic, singly hydrated form of this metalloligand was used as a building block in the assembly of 1D, 2D and 3D transition metal coordination polymers displaying various magnetic properties.[91]

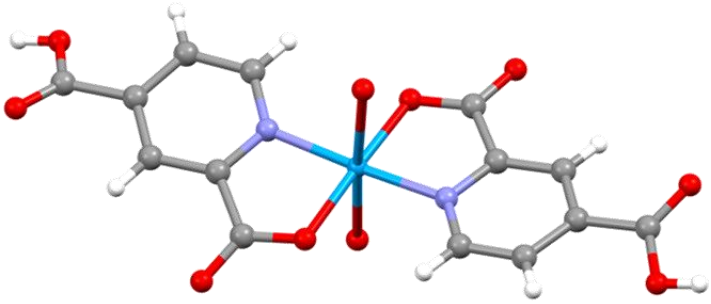

Figure 1.4. Formula unit of the Cu metalloligand (L^{Cu}) *bis-(pyridine-2-carboxylato-4-carboxyl)-diaqua-copper(II)* [**NELPEZ02**; CSD V5.35 October 2014] synthesised by Noro *et al*.[91] (hydrogen atom positions of axially coordinated water molecules not available).

The cobalt and nickel analogues of this complex have been synthesised by Beatty *et al*.[92] in order to be employed as metal-containing dicarboxylic acid reactants in a supramolecular assembly that imitates previously synthesised layered organic systems.[93] The ligand 2,4-pyridine dicarboxylic acid (2,4-pdca) was chosen as it is bidentate and able to chelate the metal centre, offering improved robustness and kinetic stability to the neutral metalloligand, and promoting reactivity at the peripheral carboxylic acid moieties.[92] The complexes $Co(C_7H_4O_4N)_2(H_2O)_2$, and $Ni(C_7H_4O_4N)_2(H_2O)_2$ were each combined with the primary amines benzylamine, 3,4-dimethylaniline, isopropylamine and 1-octylamine to result in precipitates which formed single crystals after recrystallisation from a warm methanol/water solution.

The syntheses resulted in architecturally consistent lamellar crystal structures with identical H-bonding patterns of ammonium-carboxylate charge-assisted H-bonds formed between the protonated amine groups and deprotonated carboxyl groups resulting in 2D H-bonded sheets lining the top and bottom of the layers in which the metal centres are centrally located. The N^+-H···O^- H-bonds to oxygen atoms of peripheral carboxylate groups range in D···A distance from approx. 2.65 Å to 2.79 Å, while the N^+-H···O^- H-bonds formed to the non metal-coordinating oxygen atom of the metal-coordinated carboxylate group are slightly longer with D···A distances from approx. 2.77 Å to 2.85 Å. H-bonds were also formed between the metal coordinated water ligands and both an oxygen atom of a peripheral carboxylate group and a non metal-coordinating oxygen atom of the metal-coordinated carboxylate group. Crucially, the distance between the planes on which the metal ions resided was dependent on the ammonium substituent, ranging from 9.92 Å to 13.24 Å, demonstrating that this feature could be controlled by the choice of cation.[92]

Research on lamellar H-bonded coordination networks was furthered by Chen and Beatty by the incorporation of guest molecules through increasing the flexibility of the aromatic ammonium component.[94] The Cu metalloligand, as synthesised previously by Noro *et al*.[91] (Figure 1.4), was crystallised with the aromatic primary amines 4-methylphenylethylamine, 4-chlorophenylethylamine, 4-bromophenylethylamine and DL-4-chlorophenylalaninol. As expected, proton transfer occurred from the peripheral carboxyl group to the amine group and charge-assisted H-bonds were formed, organising the structure into layers connected by 2D H-bonded sheets parallel to the *ab* plane, as observed previously.[92] The N^+-H···O^- H-bonds to oxygen atoms of peripheral carboxylate groups range in D···A distance from approx. 2.70 Å to 2.77 Å, while the N^+-H···O^- H-bonds formed to the non metal-coordinating oxygen atom of the metal-coordinated carboxylate group are slightly longer with D···A distances from approx. 2.86 Å to 2.93 Å. Unlike before however, acetone or water guest solvent molecules were included between layers, possibly permitted by the less efficient interlayer packing effected by the more flexible and bulky amines.

The material synthesised from DL-4-chlorophenylalaninol containing guest water molecules is shown in Figure 1.5. This material underwent a reversible structural transformation after cycles of dehydration/rehydration, removing and then replacing both its guest water molecules and water ligands, while the other three materials' structures were changed irreversibly. It was suspected that this was possible due to the hydroxyl group of the amine moving to interact with the metal centre and so stabilising an intermediate state during water loss. This observation supports the notion that such materials can be structurally dynamic solids and have potential applications as functional materials, e.g. as catalysts, for which intermediate states of the metal must be stabilised.[94]

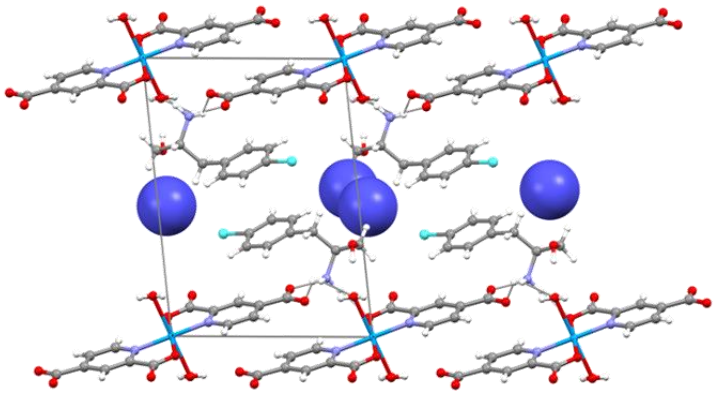

Figure 1.5. View down *a* axis showing packing of *[Cu($C_7H_3O_4N$)$_2$(H_2O)$_2$] [$C_9H_{13}ClNO$]$_2$.H_2O* [**DORCAP**; CSD V5.35 October 2014][94] (disordered guest water molecule shown in spacefill setting).

A later study was carried out by Beatty and co-workers in which the zinc analogue of the metalloligand was crystallised with the diamine 3,3'-dimethylbenzidine (*o*-tolidine). This resulted in a porous host-guest H-bonded network that was structurally stable to guest loss and re-uptake.[95] As predicted, proton transfer occurred from the peripheral carboxyl group to the amine group forming charge-assisted H-bonds organising the structure into alternate layers of the metalloligand 'pillared' by the diammonium dication, which were connected by 2D H-bonded sheets parallel to the *ab* plane in an identical fashion to those observed previously for the complexes featuring monoammonium counterions. During synthesis, 1 mL of a guest molecule was added to the reaction mixture and the structures were solved for complexes containing four different guests (*p*-xylene, nitrobenzene, hexanol and acetone) residing in the void spaces created between the 'pillars' formed by the diammonium substituents connecting between the dicarboxylate metalloligand layers. The complex accommodating an acetone solvent molecule disordered about a centre of inversion is shown in Figure 1.6. The host frameworks were practically identical regardless of which guest molecule had been added. The N^+-H···O^- H-bonds to oxygen atoms of peripheral carboxylate groups range in D···A distance from approx. 2.70 Å to 2.73 Å, and the N^+-H···O^- H-bonds formed to the non metal-coordinating oxygen atom of the metal-coordinated carboxylate group are slightly longer with D···A distances from approx. 2.75 Å to 2.77 Å. Due to the positioning of the diammonium substituents approximately on the {-121} plane, the void space is in the form of 1D channels parallel to the *a* direction, and do not extend along the *b* direction. The void space is approx. 8.27 Å – 8.51 Å along the *b* direction, as measured between neighbouring equivalent nitrogen atoms, infinite along the *a* direction, and approx. 10 Å along the *c* direction, although it can be inferred that this distance would be subject to the length of the diammonium substituent.

The complexes were subjected to heating under a vacuum to remove the guest molecules and sonicated in ethyl acetate to refill the channels, then treated to another cycle of heating under vacuum. At each stage the samples were analysed by PXRD. This showed that the framework was stable to guest removal and that the empty and filled frameworks were consistent. What small changes that were noted in the PXRD patterns were attributed to the flexibility of the H-bonded framework, but the samples remained crystalline even after repeated cycles of guest insertion and removal. The authors suggest that the flexibility and resilience of this framework is testament to the strength of the charge-assisted H-bonds, and that such materials have potential applications in guest exchange and separations.

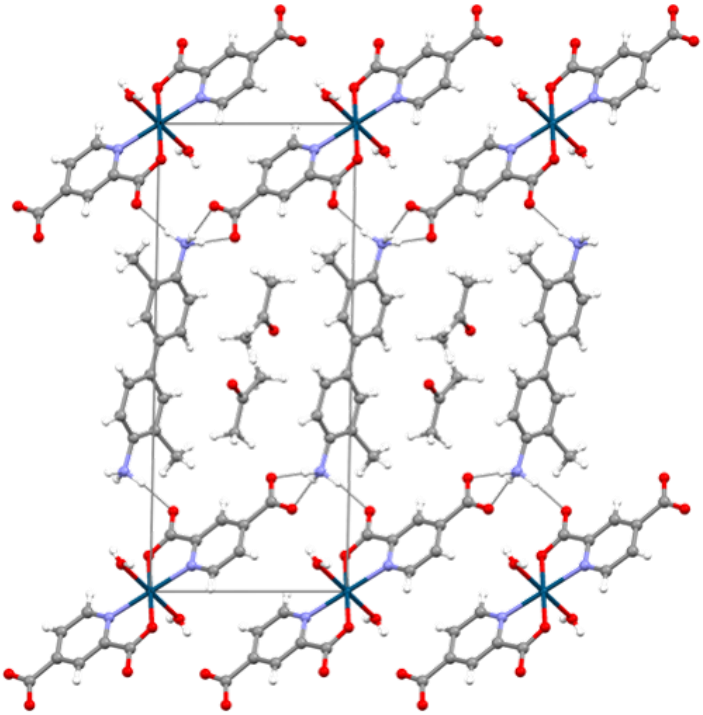

Figure 1.6. View down *a* axis showing packing of *[Zn($C_7H_3O_4N$)$_2$(H_2O)$_2$] [$C_{14}H_{18}N_2$].C_3H_6O* [**UZOYOY**; CSD V5.35 October 2014][95] (Acetone guest molecule is disordered about an inversion centre).

An interesting H-bonding system displaying 'guest' filled cavities was observed in the crystal structure of a 1D coordination polymer comprised of cadmium(II) thiocyanide units and 3-pyridine carboxylic acid (nicotinic acid), synthesised by Yang *et al*.[96] by the combination of aqueous solutions of $Cd(NO_3)_2.4H_2O$ and NH_4SCN added to a hot aqueous solution of nicotinic acid. The resulting complex, *catena-[bis-(trans-bis-(μ$_2$-thiocyanato)-bis-(nicotinic acid)-cadmium(II)) bis-(nicotinic acid) clathrate]* [**QIFLUM**; CSD V5.35 March 2015] features chains of $Cd_2(NCS^-)_2$ rings, with two nicotinic acid molecules coordinating to each metal centre. The chains are connected along the *c* direction by double H-bonds formed between the carboxyl groups of two inversely related nicotinic acid molecules coordinated to Cd(1), with D···A distances of 2.686(3) Å. The nicotinic acid molecule coordinated to Cd(2) formed a single H-bond of D···A distance 2.508(3) Å to the carbonyl oxygen atom of the carboxyl group of a guest nicotinic acid molecule, shown in red in Figure 1.7.

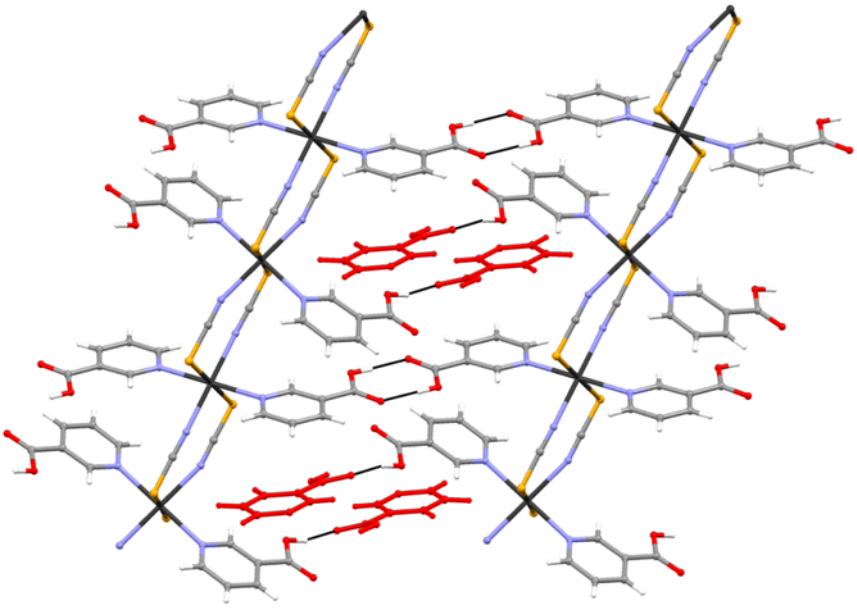

Figure 1.7. Crystal structure of **QIFLUM** showing two 1D polymeric chains connected by a double H-bond formed between carboxyl groups of coordinated nicotinic acid ligands, and guest nicotinic acid molecules (shown in red) H-bonded to coordinated nicotinic acid ligand.

1.4. Alkaline Earth Metal-Organic Complexes

The lighter group 2 elements, magnesium and calcium, are attractive choices of metals from which to synthesise new functional metal-organic complexes because they are abundant, inexpensive and non-toxic, unlike many of the transition and lanthanide metals that often feature in MOFs and related materials. Magnesium is especially interesting due to its additionally beneficial low formula weight giving it the potential to produce low density complexes, thus potentially improving the storage capacity per weight of adsorbent materials when compared to analogous materials featuring heavier metals. Furthermore, the Mg^{2+} ion shares some of the features of 3d transition metals which are typically used in MOFs. Its ionic radius is 72 pm, comparable to those of Zn^{2+} and Cu^{2+} at 74 pm and 73 pm, respectively,[97] and it tends to adopt an octahedral coordination,[98] which is useful for designing SBU's of predictable shape and directionality.

1.4.1. Magnesium MOFs

Although less explored than the transition metal MOFs, a number of magnesium MOFs have been reported,[99, 100] and due to the gravimetric advantage magnesium offers for gas storage materials, they have been especially studied with regard to gas adsorption.[101, 102,103]

Dincă and Long reported the synthesis and gas storage capacities of microporous $Mg_3(NDC)_3$ (NCD = 2,6-naphthalenedicarboxylate).[6] This MOF was stable to the removal of *N*,*N*-diethylformamide from its 1D channels. Although it showed a lower than expected storage capacity of H_2 at 2.3 mmol g^{-1} (1.7 mol/mol, 0.46 wt %) at 880 Torr and 77 K, it showed a very high isosteric heat of adsorption of 7.0 – 9.5 kJ mol^{-1}, attributed to the high van der Waals contact area associated with a very small pore size. The MOF was also found to act as an effective molecular sieve, selectively adsorbing H_2 or O_2 over N_2 or CO gas.

The magnesium analogue of a zinc MOF, *$[Zn_2(DHBDC)(DMF)_2].2H_2O$*, DHBDC = 2,5-dihydroxy-1,4-benzenedicarboxylate, known as MOF-74, (originally reported by Rosi *et al*. [**FIJDOS**; CSD V5.35 October 2014])[104] has been shown to be effective in the separation of CO_2 from CH_4.[86, 105] Zn-MOF-74, shown in Figure 1.8, has a honeycomb-like structure with 1D pores of diameter approx. 11 – 12 Å. Activation of Mg-MOF-74 by thermal removal of the solvent within the pores resulted in a high concentration of coordinatively unsaturated metal cations,[106] which are the primary sites of coordination of the guest molecules.[107] For the activated MOF, Dietzel *et al*. reported a surface area SA_{BET} of 1542 m^2 g^{-1} and a pore volume of 0.6 cm^3 g^{-1}. The CO_2 adsorption capacities of the nickel and magnesium analogues of MOF-74 were compared, and at 473 K they were found to be 26 wt% and 30 wt%, respectively. Since the actual amount of CO_2 adsorbed by each material was about equal, in this case, the higher wt/wt uptake for Mg-MOF-74 was attributed to the lighter weight of the metal.[105] In the same year, Britt *et al*. [86] also carried out gas adsorption studies on Mg-MOF-74. Separation experiments were carried out by introducing a flow of 20% CO_2 in CH_4 over the material and it was found that Mg-MOF-74 completely separated the CO_2 from the CH_4 stream, with no significant amounts of CH_4 adsorbed after saturation with CO_2. The authors reported an isosteric heat of adsorption of CO_2 of 39 kJ mol^{-1}, reflecting a strong physisorption interaction, but sufficiently low in energy for facile release. This was demonstrated by the full regeneration of Mg-MOF-74 under relatively mild conditions by purging with CH_4 at 80 °C. The authors cited the ease of regeneration of the activated MOF as advantageous for industrial CO_2 separation processes.[86]

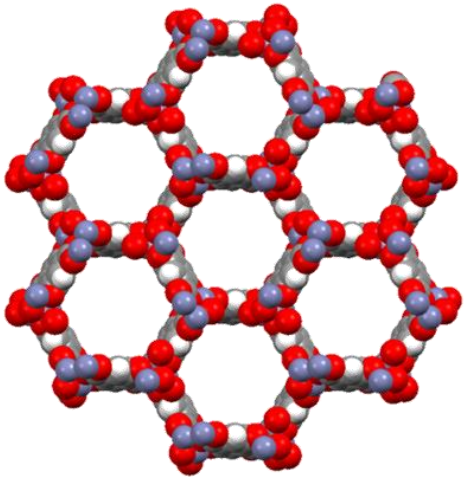

Figure 1.8. Zn-MOF-74 [**FIJDOS**][104] as viewed down the *c* axis, (protruding terminal DMF molecules and solvent water molecules in pores not shown).

1.4.2. Magnesium-Organic Complexes Featuring Pyridine Carboxylic Acid Ligands

Beatty and co-workers were successful in synthesising a range of interesting H-bonded structures with a high degree of control and predictability using 2,4-pyridine dicarboxylic acid. This finding forms the basis for the focus in the present work on synthesising alkaline earth metal-organic complexes using pyridine carboxylic acid ligands. These ligands are ideal for designing H-bonded coordination complexes owing to their H-bonding functionalities, multiple sites for metal-coordination, O,O'-chelation, and in the case of 2-pyridine carboxylic acid (picolinic acid) and 2,4-pyridine dicarboxylic acid, the potential to N,O-chelate to a metal centre, affording extra stability.

Complexes composed of magnesium and pyridine carboxylic acids have been reported. Picolinic acid has been used to synthesise the complex *bis-(pyridine-2-carboxylato)-diaqua-magnesium(II) 0.15-hydrate* [**UFAPEX**; CSD V5.35 March 2015] by Sharif *et al*.[108] The complex, illustrated in Figure 1.9(a), is a 0D metal-organic complex, and features a magnesium centre in a distorted octahedral environment, N,O-chelated by two picolinate ions and two water molecules. The supramolecular structure is extended by O-H···O and C-H···O hydrogen bonds, and π-π stacking between aromatic rings and C-H···π interactions. Picolinic acid also features in *bis-[(μ_2-pyridinium-2-carboxylato)-(pyridinium-2-caboxylato)-triaqua-magnesium(II)] tetrachloride dihydrate* [**NISJEE**; CSD V5.35 June 2014],[109] which is discussed in Chapter 4 as a comparison to one structure reported in this study.

Two 3D magnesium coordination polymers synthesised by solvothermal methods were reported by Liu *et al*. one of which featured nicotinic acid [**XEQLIQ**; CSD V5.35 March 2015]

and the other 4-pyridine carboxylic acid (isonicotinic acid) [**XEQLEM**; CSD V5.35 March 2015].[110] The complex featuring isonicotinic acid was also synthesised by He *et al*. along with an isomorphous structure featuring manganese in place of magnesium.[111] On soaking the complex in methanol for 12 hours, the authors noticed a transformation, reported as a single-crystal-to-single-crystal transformation, to a 0D complex *bis-(pyridine-4-carboxylato)-tetramethanol-magnesium(II)* [**HIVQIO**; CSD V5.35 March 2015]. The formula unit of this complex is shown in Figure 1.9(b). The packing is directed by both H-bonds and π-π stacking interactions of approx. 3.680 Å, as shown in Figure 1.9(c). The manganese complex did not undergo transformation under the same conditions, leading the authors to suggest that the binding energy of the Mn-O and Mn-N bonds are similar, while the binding energy of the Mg-O bond is greater than that of the Mg-N bond. The authors acknowledged that these observations were in agreement with Oliva and Cavallo's findings in their studies of the binding of Mg^{2+}, Mn^{2+}, and Co^{2+} on the nucleobase guanine.[112]

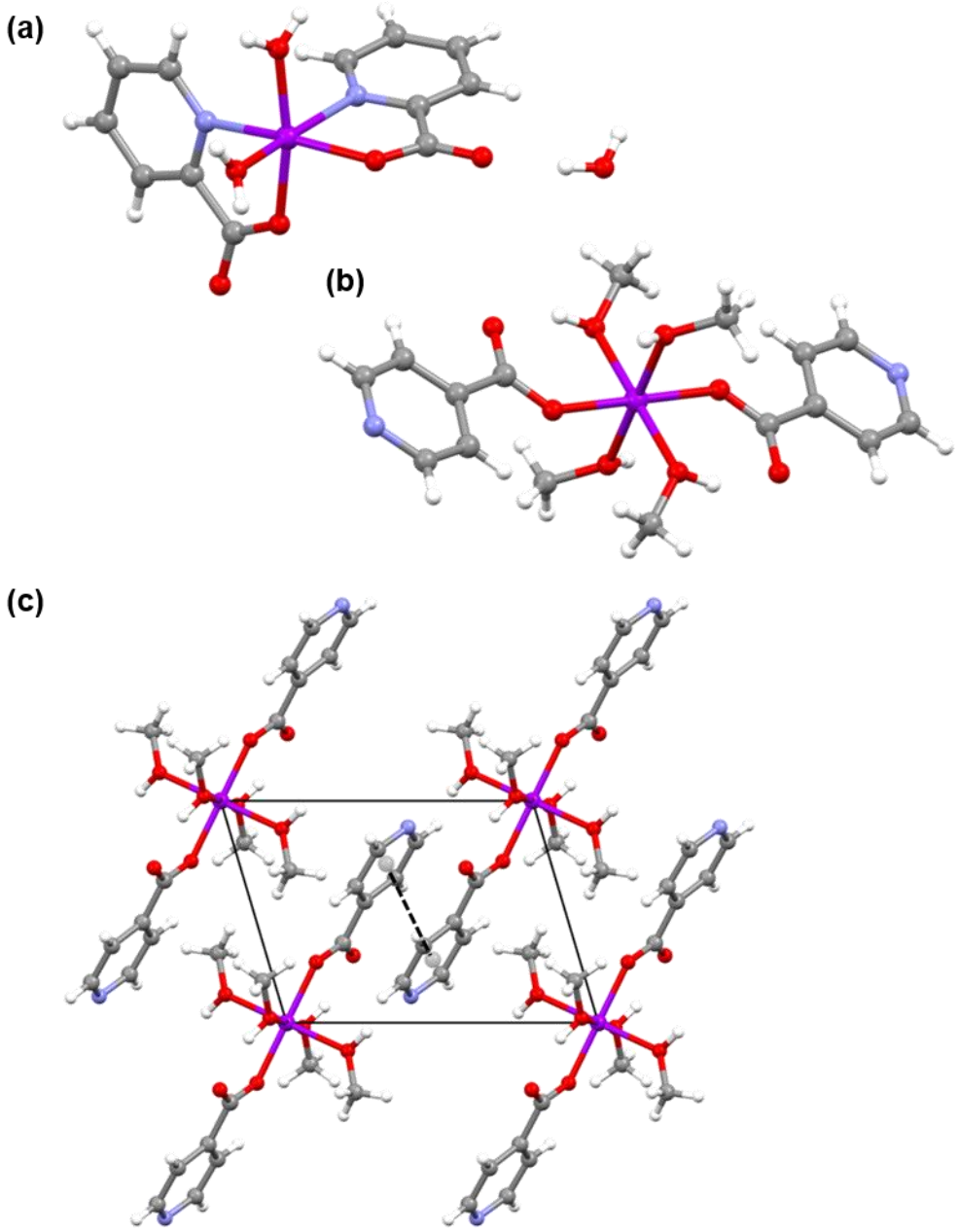

Figure 1.9. Mg complexes synthesised from pyridine carboxylic acids. (a) Formula unit of **UFAPEX**, (b) formula unit of **HIVQIO**, (c) View down the *b* axis showing π-π stacking interactions and packing of **HIVQIO**.

Chang *et al*. reported the structure of a complex synthesised from the hydrothermal reaction of 2,4-pyridine dicarboxylic acid and magnesium chloride hexahydrate dissolved in methanol with NaOH at 160 °C. The complex *bis-(pyridinium-2,4-dicarboxylato)-diaqua-magnesium(II)* [**ZIMJIQ**; CSD V5.35 March 2015] features a distorted octahedral

magnesium centre coordinated by a carboxylate oxygen atom of four pyridinium dicarboxylate ligands to form 2D coordination polymeric sheets.

The ligand 2,4-pyridine dicarboxylic acid has also been used to produce a 0D magnesium coordination complex. Mallick *et al*. synthesised *bis-[(μ$_2$-pyridine-2,4-dicarboxylato)-triaqua-magnesium(II)]* [**SUYLEE01**; CSD V5.35 October 2014] by the hydrothermal reaction of magnesium(II) acetate tetrahydrate and 2,4-pyridine dicarboxylic acid.[97] The formula unit, shown in Figure 1.10, features the doubly deprotonated organic ligand N,O-chelating the magnesium centre of octahedral geometry in a similar way to that observed in the Cu metalloligand reported by Noro *et al*.[91] and utilised extensively by Beatty and co-workers. The complex **SUYLEE01** differs from these metalloligands in that it contains two metal centres as opposed to one with the coordinating carboxylate oxygen atom bridging between the cations. In order to balance the charge, the organic ligands are therefore doubly deprotonated. This precludes the possibility of proton transfer from the metalloligand to another substituent, if this complex were to be used in a further crystallisation/synthesis experiment.

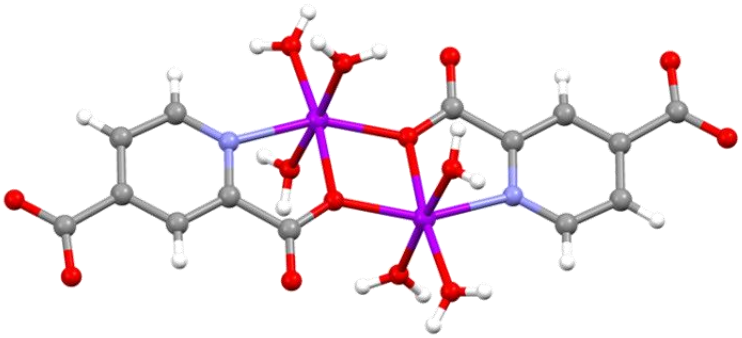

Figure 1.10. Formula unit of Mg metalloligand *bis-[(μ$_2$-pyridine-2,4-dicarboxylato)-triaqua-magnesium(II)]* (**SUYLEE01**) synthesised by Mallick *et al*.[97]

In the same paper as **SUYLEE01** was reported, the product of the solvothermal reaction between magnesium(II) acetate tetrahydrate and 3,5-pyridine dicarboxylic acid, an isomer of 2,4-pyridine dicarboxylic acid, was also presented. Mg-MOF-1, *catena-[(μ$_5$-pyridine-3,5-dicarboxylato)-aqua-magnesium(II)]* [**NABMUA**; CSD V5.35 March 2015] has a 3D chiral network of helical hexagonal channels along the *c* direction containing a network of Mg centres in an octahedral coordination environment, connected by the organic ligand and coordinated by guest water molecules facing towards the channels (Figure 1.11(a)). Taking into account the van der Waals radii of the atoms forming the 'walls' of the channels, the channels are 4 Å in diameter. Upon evacuation of the water molecules from the channels, the calculated void space increased from 11.9 % to 38.7 %, while the structure maintained

its thermal stability to temperatures in excess of 400 °C. This made available coordinatively unsaturated Mg sites which enabled the framework to adsorb H_2 and CO_2 reversibly and in preference to N_2. It was suggested that this was due to the kinetic diameter of N_2, at 3.64 Å being too large for the porous channels which were more accessible to the H_2 and CO_2 molecules with smaller kinetic diameters of 2.8 Å and 3.46 Å, respectively.[97]

This MOF and three other coordination networks of Mg and 3,5-pyridine dicarboxylate, synthesised by solvothermal methods, were reported by Banerjee *et al*.[113] Two of these complexes were 3D coordination polymers featuring 1D channels; one containing both coordinated and non-coordinated DMF molecules, and the other containing disordered, coordinated DMF molecules and non-coordinated water molecules. Synthesised by the hydrothermal reaction of magnesium(II) nitrate hexahydrate and 3,5-pyridine dicarboxylic acid dissolved in ethanol, the complex, *catena-[(μ_3-pyridine-3,5-dicarboxylato)-diaqua-magnesium(II)]* [**AVIPEB**; CSD V5.35 March 2015] differed from the other three reported in that, rather than being a 3D coordination polymer, it was composed of layers of 2D coordination polymeric sheets parallel to the *ab* plane: one such sheet is shown in Figure 1.11(b). The magnesium centre is in a pentagonal bipyramidal coordination geometry, coordinated by two water molecules and three organic ligands: two *via* both carboxyl oxygen atoms of one carboxyl group and the other *via* the pyridyl nitrogen atom. The 2D sheets are connected by H-bonds from the coordinated water molecules to coordinating carboxylate oxygen atoms. The authors attributed the different topologies of the complexes to the different coordination abilities of the solvents, noting that water had the highest affinity to coordinate, and thus coordinated preferentially compared to methanol and ethanol.

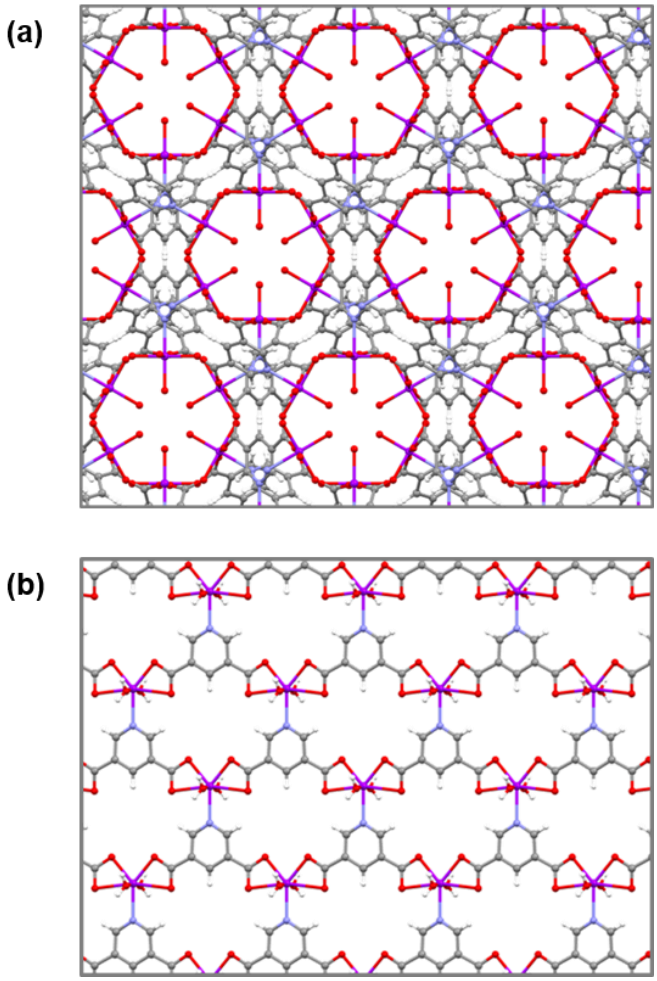

Figure 1.11. Packing of (a) **NABMUA** showing 1D channels parallel to the *c* axis and terminal water molecules protruding into the channels as viewed down the *c* axis. (b) One 2D polymeric sheet of **AVIPEB** as viewed down the *c* axis.

A range of alkaline earth metal coordination polymers were synthesised by Das *et al*. using the ligand 2,4,6-pyridine tricarboxylic acid.[114] 3D coordination polymers featuring Ca, Sr and Ba were synthesised by the reaction of the ligand and the according metal salt dissolved in water with a small amount of diethylamine, reacted in an autoclave at 180 °C. Two magnesium complexes of lower coordination dimensionality were also synthesised: one by the hydrothermal reaction of the ligand and a magnesium salt at 140 °C, *catena-[(μ_4-pyridine-2,4,6-tricarboxylato)-(μ_2-pyridine-2,4,6-tricarboxylato)-octaaqua-trimagnesium(II)]* [**YORYIO**; CSD V5.35 March 2015], with the other, *hexaaqua-magnesium(II) catena-[bis-(μ_2-pyridine-2,4,6-tricarboxylato)-tetraaqua-dimagnesium(II) dihydrate]* [**YORYOU**; CSD V5.35 March 2015] formed on further evaporation of the filtrate from the reaction with magnesium(II) nitrate hexahydrate.

YORYIO is composed of 1D coordination polymeric tapes, as illustrated in Figure 1.12(a). The organic ligands O,N,O'-chelate to the Mg centres of a distorted octahedral geometry, with one bridging between two metal centres, and one bridging between four. The chains are connected by H-bonds formed from the coordinated water ligands, and π-π stacking interactions between the aromatic rings. **YORYOU** is composed of 1D chains of the organic ligand, again O,N,O'-chelating and also O,O'-chelating, to bridge between two magnesium centres in a distorted pentagonal bipyramidal geometry as shown in Figure 1.12(b). These chains are connected by H-bonds from the coordinating water molecules, and also H-bonds *via* magnesium hexahydrate cations (not shown).

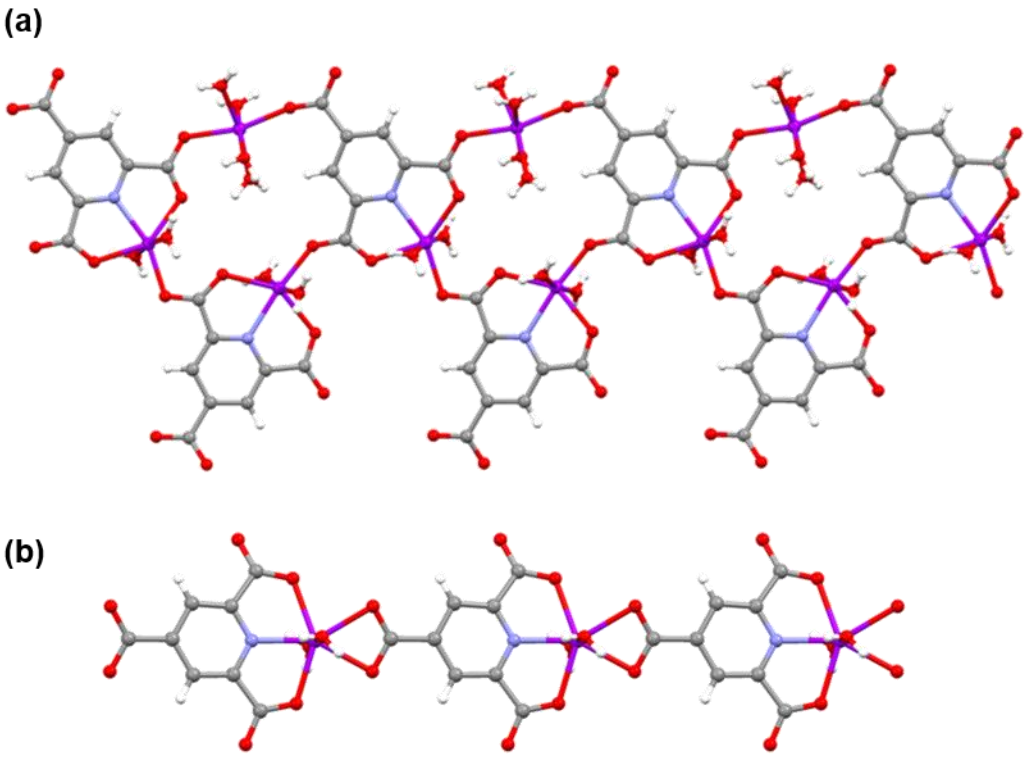

Figure 1.12. (a) 1D tape of **YORYIO**, as viewed down the *b* axis. (b) 1D chain of **YORYOU** parallel to the *b* axis as viewed down the *a* axis.

1.4.3. Calcium-Organic Complexes Featuring Pyridine Carboxylic Acid Ligands

Calcium complexes featuring pyridine carboxylic acid have also been reported. Gschwind *et al*.[115] utilised the multi-coordination abilities of nicotinic acid in the synthesis of a multitopic ligand designed to coordinate to two different metal centres. Reaction of nicotinic acid with tetraethylene glycol afforded a multitopic ligand, which when combined with calcium iodide and then copper iodide and allowed to crystallise, coordinated to the calcium centre through five oxygen atoms, and to the copper centre through the pyridyl nitrogen atoms of the two

nicotinic acid groups. This coordination behaviour is due to the tendency of hard bases to bind to hard acids in the form the oxygen donor atoms and the Ca^{2+} ion, and of soft bases to bind to soft acids in the form the nitrogen donor atoms and the Cu^{+} ion. The site specific coordination behaviour exhibited by the ligand was proposed as a possible route to forming stoichiometrically exact mixed metal oxides, as proven by thermal decomposition experiments.

A similar methodology to produce mixed metal oxides was proposed by Lazarescu *et al*. on preparing heterometallic coordination polymers synthesised from the combination of 2,3-pyridine dicarboxylic acid with calcium, barium and cobalt salts in aqueous solutions.[116] The heteronuclear cobalt complexes featuring calcium and barium were 1D and 3D coordination polymers, respectively. The homonuclear calcium complex, *catena-[(μ_3-pyridinium-2,3-dicarboxylato)-triaqua-(pyridine-2-carboxyl-3-carboxylato)-calcium(II)]* [**TUXLAA01**; CSD V5.35 March 2015] has previously been reported by both Barszcz *et al*.[117] and Starosta and Leciejewicz.[118] This complex is composed of 1D polymeric chains that run parallel to the *a* direction. It comprises eight coordinate calcium centres bridged along the *a* direction by coordination *via* two oxygen atoms of a carboxylate group, and connected along the *b* direction *via* coordination by one carboxylate oxygen atom of the other carboxylate group of 2,3-pyridinium dicarboxylate to form a 'ribbon'-like chain. The Ca centres are N,O-chelated by pyridine-2-carboxylic acid-3-carboxylate ligands (Figure 1.13).

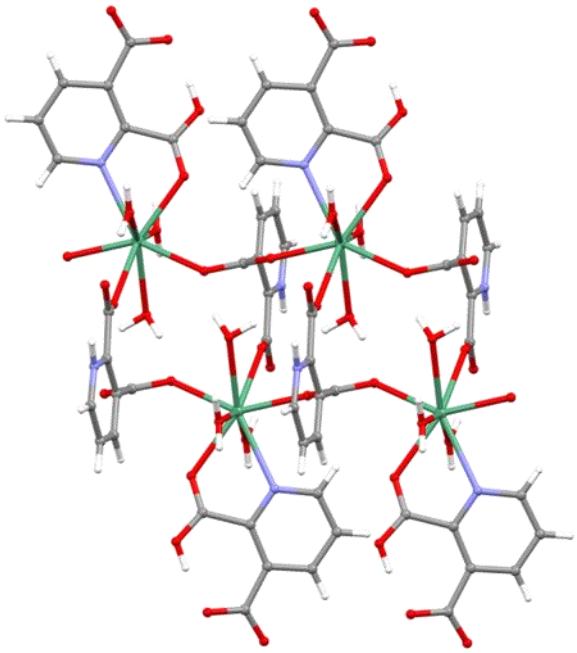

Figure 1.13. Crystal structure of **TUXLAA01** showing 1D chain parallel to the *a* axis.

Starosta and Leciejewicz also reported the structure of another 1D coordination polymeric chain composed of Ca centres bridged by 2,3-pyridine dicarboxylate ligands.[118] This structure, *catena-[bis-(μ$_2$-pyridine-2,3-dicarboxylato)-octaaqua-dicalcium(II)]* [**DOZDAY**; CSD V5.35 March 2015] features 1D coordination polymeric chains parallel to the *a* direction (Figure 1.14). The Ca centre is seven coordinate and is N,O-chelated by the ligand, which coordinates to the next ligand along the chain in the *a* direction *via* an oxygen atom of the second carboxylate group. It differs to **TUXLAA01** in that the metal ion and the ligand are present in a 1:1 ratio. Both complexes are extended into the 3D structure by extensive H-bonding interactions, primarily from the coordinated water molecules to the carboxylate oxygen atoms, and in the case of **TUXLAA0**, also from the pyridinium nitrogen atom to a water molecule.

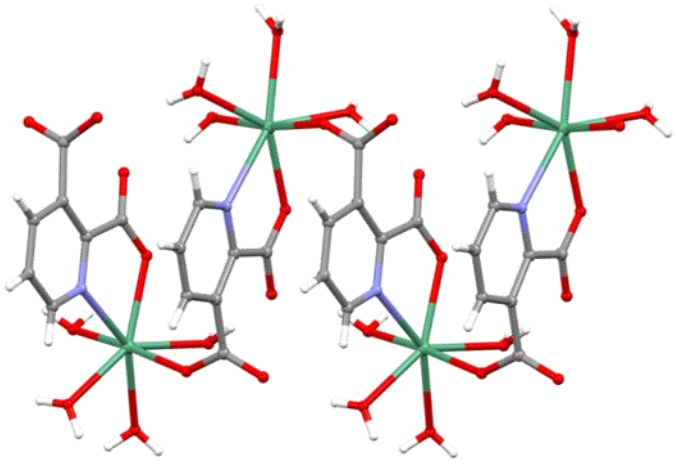

Figure 1.14. Crystal structure of **DOZDAY** showing 1D chain parallel to the *a* axis.

Starosta, Ptasiewicz-Bąk and Leciejewicz have reported the structures of two calcium complexes synthesised from the isomer of 2,3-pyridine dicarboxylic acid, 3,5-pyridine dicarboxylic acid. One structure, *(μ$_2$-pyridinium-3,5-dicarboxylato)-(pyridinium-3,5-dicarboxylato)-(pyridine-3-carboxyl-5-carboxylato)-nonaaqua-dicalcium(II) (pyridinium-3,5-dicarboxylate) hydrate* [**ALOXEE**; CSD V5.35 March 2015][119] (shown in Figure 1.15(a)) is a 0D coordination complex featuring one terminal seven-coordinate calcium centre, of 'nonspecific' geometry, coordinated by six water molecules and a carboxylate oxygen atom of one bridging 3,5-pyridinium dicarboxylate ligand. This ligand also coordinates, *via* an oxygen atom of its second carboxylate group, to a second seven-coordinate calcium centre of pentagonal bipyramidal geometry, which is coordinated by three water molecules, an oxygen atom of the carboxylate group of one 3,5-pyridinium dicarboxylate ligand and both carboxylate oxygen atoms of a pyridine-3-carboxylic acid-5-carboxylate ligand in a

bidentate fashion. The structure also features a non-coordinated 3,5-pyridinium dicarboxylate ion and a water molecule. The 3D structure is connected by H-bonds formed primarily from the coordinated water molecules to the carboxylate oxygen atoms and other water molecules, and from the pyridinium nitrogen atoms to carboxylate oxygen atoms. The second structure, *catena-[(μ$_2$-pyridine-3,5-dicarboxylato)-pentaaqua-calcium(II)]* [**ALOYEF**; CSD V5.35 March 2015][120] (shown in Figure 1.15(b)) is composed of 1D zigzag polymeric chains along the *c* direction of 3,5-pyridine dicarboxylate ligands bridging between seven coordinate calcium centres in a distorted pentagonal bipyramidal geometry, also coordinated by five water molecules. The chains are connected to adjacent chains by extensive H-bonding interactions from the coordinated water molecules to the carboxylate oxygen atoms.

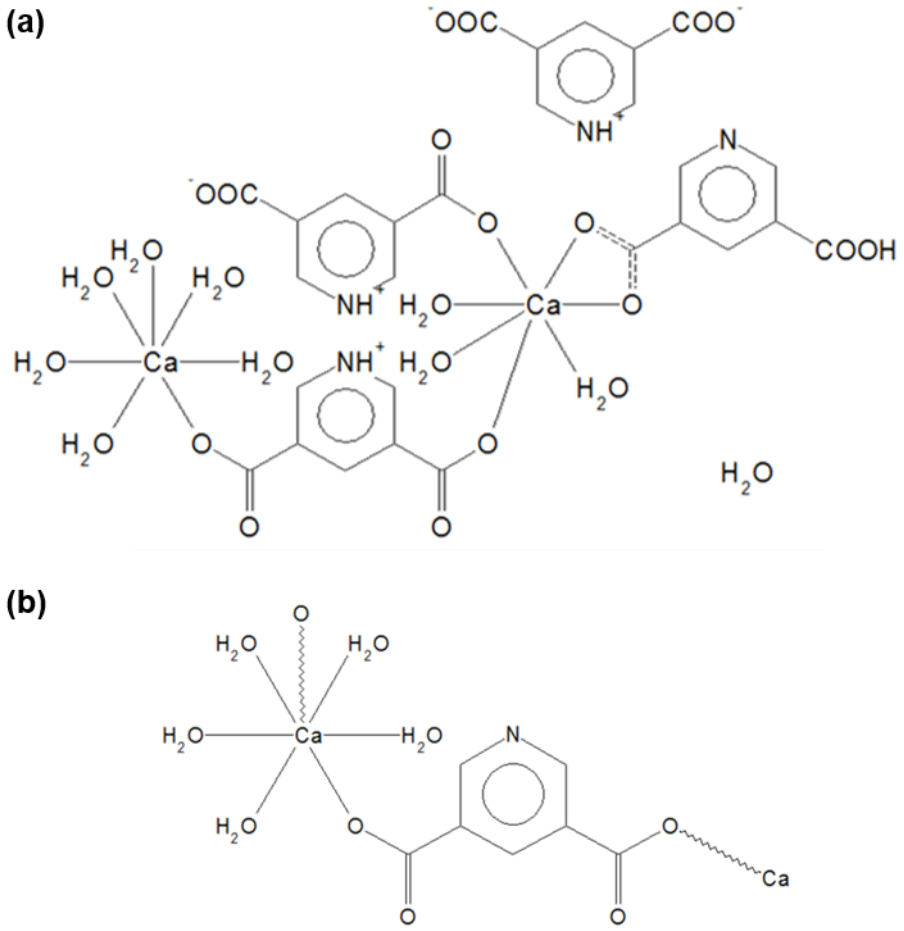

Figure 1.15. Crystal structures of (a) **ALOXEE** and (b) **ALOYEF**. (Coordinates for these structures are not available).

The crystal structure of a calcium complex synthesised from 2,6-pyridine dicarboxylic acid and its subsequent transformation into another structure has been reported by Kim *et al*.[121]

The initial complex, *catena-[bis-(μ$_3$-pyridine-2,6-dicarboxylato)-(μ$_2$-aqua)-diaqua-dicalcium(II)]* [**QQQAEA01**; CSD V5.35 March 2015], previously reported by Strahs and Dickerson in 1968,[122] was produced by the hydrothermal reaction of calcium(II) hydroxide, 2,6-pyridine dicarboxylic acid, DMF and nitric acid at 70 °C. **QQQAEA01** is composed of 1D helical polymeric chains parallel to the *c* direction chain with seven coordinate Ca centres in a pentagonal bipyramidal geometry (Figure 1.16(a)). The Ca centres are O,N,O'-chelated by one 2,6-pyridine dicarboxylate ligand, and coordinated by a carboxylate oxygen atom of two other organic ligands which O,N,O'-chelate to the next calcium centres along the chain, effectively bridging between the metal centres. The Ca centre is also coordinated by two water molecules: one terminal and one bridging to the next Ca centre along the chain. Heating of this complex to 310 °C under vacuum, followed by hydrothermal treatment at 70 °C yielded another 1D helical chain structure, *catena-[(μ$_2$-pyridine-2,6-dicarboxylato)-(μ$_2$-aqua)-diaqua-calcium(II)]* [**CAPICL**; CSD V5.35 March 2015], shown in Figure 1.16(b), with the chains running parallel to the *a* direction. **CAPICL** differs from **QQQAEA01** in that the Ca centres are eight coordinate, again O,N,O'-chelated by one 2,6-pyridine dicarboxylate ligand, but coordinated by a carboxylate oxygen atom of only one other organic ligand, bridging between the Ca centres. The metal centres are also coordinated by four water molecules as opposed to the two of **QQQAEA01**; two are terminal and two are bridging to the next Ca centre along the chain.

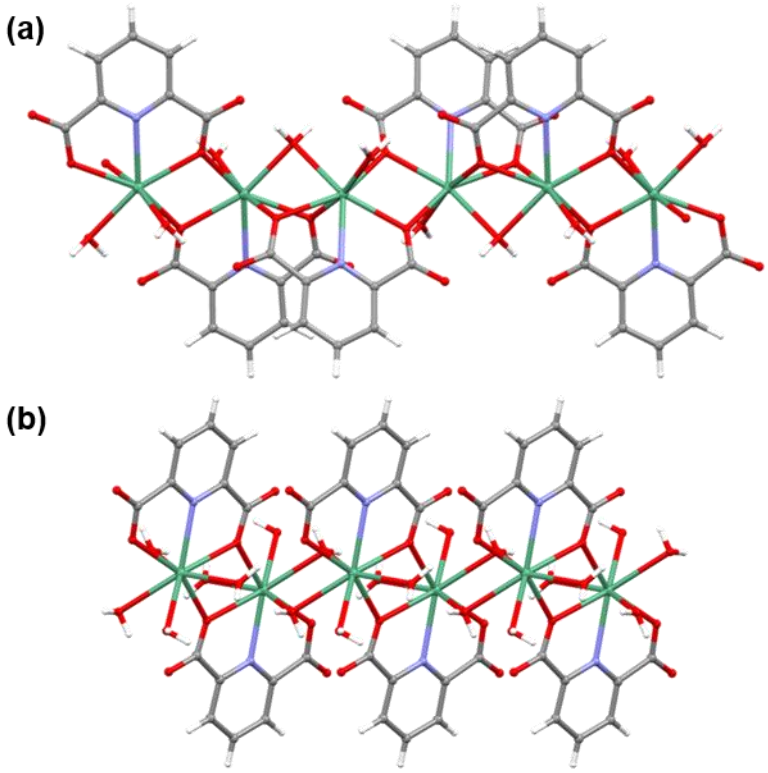

Figure 1.16. Crystal structures of (a) **QQQAEA01**, showing 1D chain, as viewed down the *a* axis and (b) **CAPICL**, showing 1D chain, as viewed down the *b* axis.

Starosta, Ptasiewicz-Bąk and Leciejewicz have reported other calcium complexes synthesised using 2,6-pyridine dicarboxylic acid. Two are composed of 1D polymeric chains, with one featuring an O,O'-chelating nitrate ion and exists in two polymorphic forms,[123] another featuring bridging water molecules,[124] and another reported complex is 0D.[125] Aghabozorg *et al*. also reported a calcium complex synthesised from 2,4,6-triamino-1,3,5-triazine and 2,6-pyridine dicarboxylic acid.[126] This complex is also 0D and the calcium centre is nine coordinate. In each of these complexes, as was observed in the complexes reported by Kim *et al*., the organic ligand O,N,O'-chelates the calcium centre.

1.5. Chloranilic Acid in Alkaline Earth Metal-Organic Complexes

Chloranilic acid, 2,5-dichloro-3,6-dihydroxy-1,4-benzoquinone is an interesting ligand for the synthesis of functional crystalline materials due to its versatility. Chloranilic acid can form a range of intermolecular interactions including H-bonds *via* the hydroxyl groups, halogen bonds *via* the chlorine atoms, and π-π stacking interactions *via* the conjugated system, and it can coordinate to, chelate and bridge between metal centres. Chloranilic acid

has been used in the synthesis of transition metal coordination complexes,[127, 128] and a number of alkali metal complexes have been reported by Molčanov and co-workers.[129-131]

For this work, it was decided to use chloranilic acid in the synthesis of new alkaline earth metal-organic complexes partly due to the fact that such structures barely feature in the Cambridge Structural Database (CSD),[132] as indicated in Table 1.3, and there have been no reported structures composed of magnesium and chloranilic acid/derivates.

Table 1.3. Metals which feature in inorganic complexes of chloranilic acid/derivatives. [CSD V5.35 March 2015].

Group	**Metals**
Group 1	Li (4), Na (6), K (1), Rb (1), Cs (1)
Group 2	**Be (1), Ba (1), Ca/Sn (4)**
Transition Metal	Sc (1), Cr(3), Mn (14), Fe (14), Co (15), Cu (34), Zn (2), Y (3), Zr (2), Mo (4), Ru (3), Rh (3), Pd (1), Ag (1), Cd (1), Lu (1) Re (1), Os (3)
Lanthanide	La (1), Ce (2), Pr (1), Nd (1), Eu (3), Gd (2), Tb (1), Yb (2)
Actinide	Th (1), U (2)
Group 13	Ga (1), In (1)
Group 14	Sn (3), (Ca/Sn (4)) Pb (1)

(Number in brackets indicates the number of complexes featuring that metal).

Beryllium coordinated by two chloranilate dianions has been reported by Burzlaff *et al*. in the crystal structure of *bis-(hexadecylpyridinium) bis-(chloranilato)-beryllate(II)* [**HIBMOU**; CSD V5.35 March 2015].[133] The beryllium centre is in a tetrahedral geometry, chelated by two oxygen atoms of two chloranilate dianions. The complex has a bilayer structure, with the pyridinium ring and the beryllium dichloranilate groups forming layers parallel to the *ab* plane, separated by the hexadecyl chains along the *c* direction.

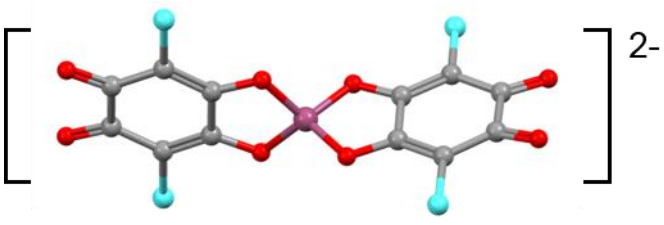

Figure 1.17. *Bis-(chloranilato)-beryllate(II)* anion of **HIBMOU**.

Abrahams *et al.* have reported a robust, porous coordination network formed from 2D polymeric sheets which was found to adsorb small guest molecules.[134] The complex *bis-(tetraethylammonium) catena-[tetrakis-(μ_2-chloranilato)-calcium(II)-tin(IV)]* [**BAKBAS**; CSD V5.35 March 2015] was synthesised from the reaction of $SnCl_4 \cdot 5H_2O$ and tetraethylammonium chloride dissolved in water added to chloranilic acid dissolved in methanol and left for two months in a soda-glass vial at room temperature. The calcium incorporated in the resulting crystals was believed to have leached from the reaction vials, however when the experiment was repeated using Ca salts and aqueous acetone, a better yield of the complex was obtained. **BAKBAS** features 2D anionic sheets with a square grid coordination network in which each metal centre is an eight coordinate 4-connecting node, chelated by the oxygen atoms of four chloranilate dianions. The sheets, one of which is shown in Figure 1.18, are parallel to the *ab* plane, and eclipse one another when viewed down the *c* direction so that the square windows form channels along the *c* direction.

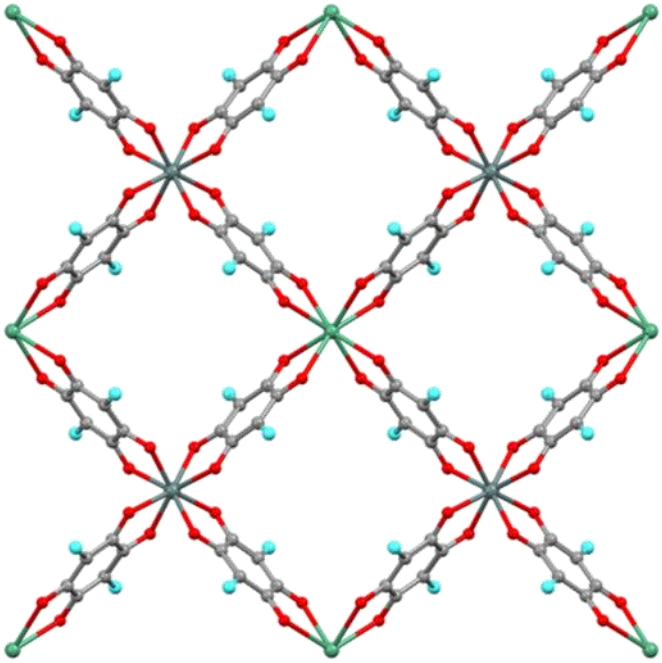

Figure 1.18. 2D polymeric sheet $[Sn(IV)Ca(II)(C_6O_4Cl_2)_4]$ of **BAKBAS**, as viewed down the *c* axis.

Between the sheets, balancing the charge, are disordered tetraethylammonium cations, and there are also guest acetone molecules. The structure was stable to the removal of the acetone guests and was found to then be able to take up either carbon disulfide or acetonitrile molecules, on immersion into the liquids. Adsorption experiments investigating the affinity of the desolvated structure for CO_2, N_2 CH_4 and H_2 were conducted, revealing that at 3000 kPa, each square cavity adsorbed approx. two CO_2 molecules at 273 K and at

2000 kPa each square cavity could adsorb approx. one molecule of N_2 at 195 K, approx. 2.4 molecules of H_2 at 77 K and approx. 1.0 molecule per cavity at 258 K.

A structure comprising barium and chloranilate dianions has been reported by Kashino *et al*.[135] Synthesis of *catena-[(μ₃-chloranilato)-(μ₂-aqua)-diaqua-barium(II)]* [**WOVMID**; CSD V5.35 March 2015] was carried out by combining chloranilic acid, sodium hydroxide, disodium metasilicate and acetic acid, and layering barium chloride dihydrate on top of the resulting gel. The crystal structure of **WOVMID** features an eight coordinate Ba centre coordinated by two bridging water molecules, two terminal water molecules and three chloranilate dianions; one by chelation *via* two oxygen atoms, and the other by coordination *via* one oxygen atom. This forms 2D zigzag polymeric sheets parallel to the *bc* plane (Figure 1.19(a) and (b)). The sheets are propagated along the *a* direction *via* H-bonds from the coordinated water molecules to the oxygen atom of the chloranilate dianion and by halogen bonds between Cl atoms of neighbouring 2D sheets.

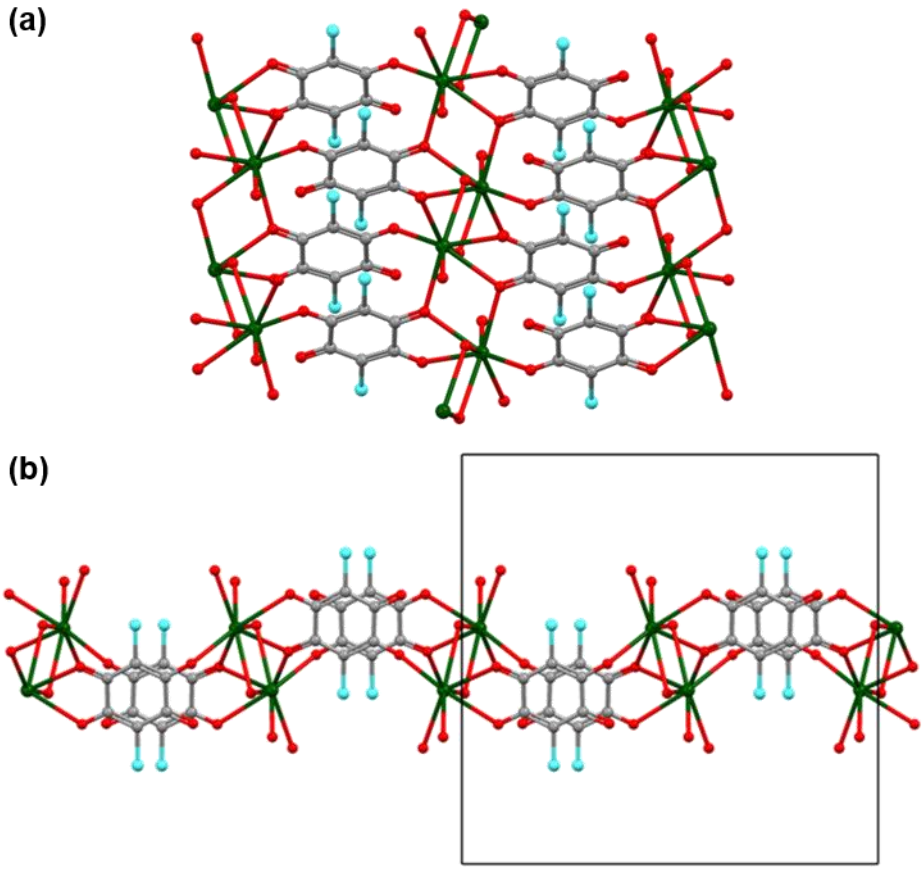

Figure 1.19. Crystal structure of **WOVMID**. (a) 2D polymeric sheet. (b) View down the *c* axis showing zigzag sheet.

1.6. Chloranilate and Hydrogen Chloranilate Supramolecular Ligands

Previous work carried out in the Wilson Group by Adam *et al*.[136] established a set of reliably reproducible bifurcated supramolecular motifs using the three methylpyridine isomers with chloranilic acid. This study formed the basis of an investigation in the present work to test the possibility of incorporating these motifs, synthesised with pyridine carboxylic acid isomers in place of methylpyridine isomers, into alkaline earth metal-organic complexes.

A range of salt and salt hydrate complexes were reported featuring methylpyridinium isomers and chloranilate dianions or hydrogen chloranilate ions, some of which are shown in Figure 1.20(a) – (e). In each case, the protonated pyridinium nitrogen atom forms a bifurcated H-bond to the oxygen atoms of the dianions or ions, forming a persistent supramolecular motif, with the distinct patterns dependent on the stoichiometry used in the crystallisation experiment.[136]

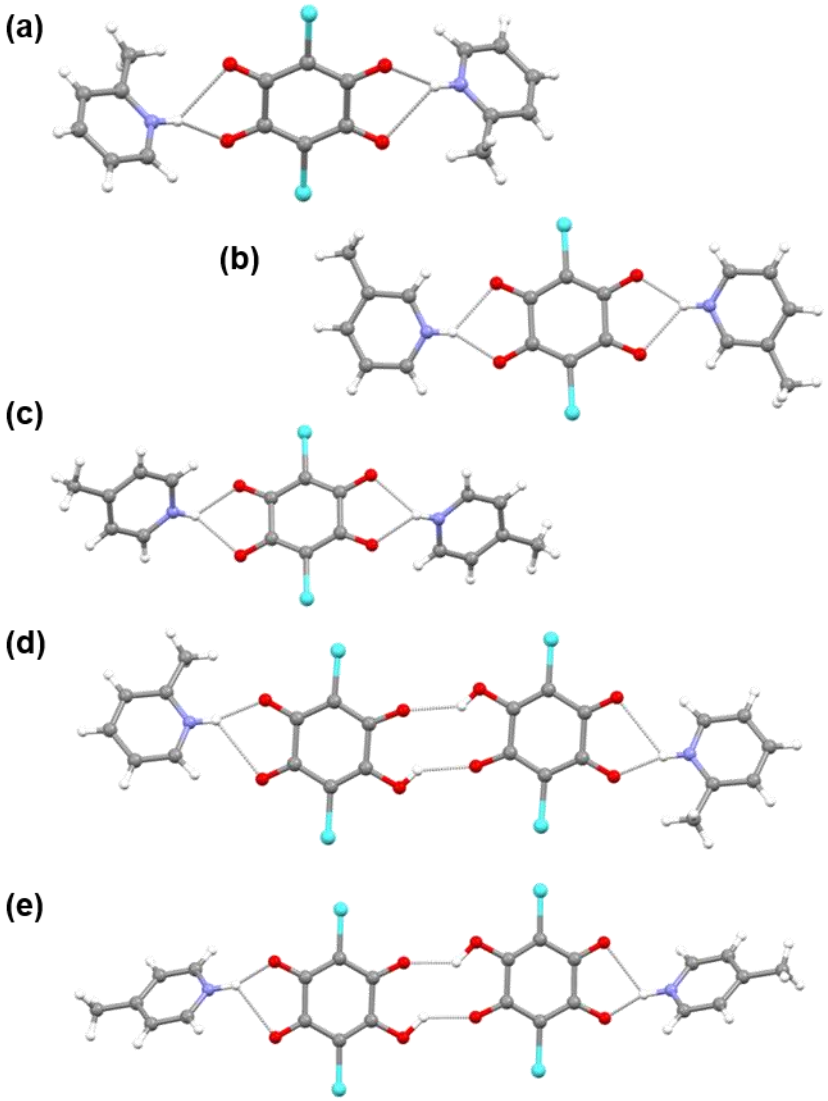

Figure 1.20. Complexes synthesised from methylpyridines and chloranilic acid. (a) **NUYBOZ01** $(C_6H_8N)_2(C_6Cl_2O_4)$, *bis-(2-methylpyridinium) chloranilate* (b) **VURWAH03** $(C_6H_8N)_2(C_6Cl_2O_4)$, *bis-(3-methylpyridinium) chloranilate* (c) **VURSUX02** $(C_6H_8N)_2(C_6Cl_2O_4)$, *bis-(4-methylpyridinium) chloranilate* (d) **NUYCEQ02** $(C_6H_8N)(C_6HCl_2O_4)$, *2-methylpyridinum hydrogen chloranilate* (e) **VURSOR** $(C_6H_8N)(C_6HCl_2O_4)$, *4-methylpyridinum hydrogen chloranilate*.

1.7. Ligands of Interest in Pure Form

One aspect of the work reported herein was to investigate the extent to which the H-bonding motifs of the starting ligands in their pure form were retained once coordinated to a metal centre. Due to the gentle conditions under which the complexes were synthesised by self-assembly, it might be expected that the H-bonding motifs could potentially be retained and therefore utilised as supramolecular synthons in later syntheses.

1.7.1. Pyridine Carboxylic Acids

Picolinic Acid

The crystal structure of picolinic acid has been reported by Hamazaki *et al*.[137] The acidic hydrogen atom displays positional disorder between the carboxyl group and the pyridyl nitrogen atom, with the site occupancy factors taken to be 0.5, such that the molecule is 50:50 disordered between the neutral and zwitterionic forms. The crystal structure is composed of dimers connected by the O-H···O H-bond of D···A distance 2.531(1) Å formed between the carboxyl groups, related through a centre of inversion. These dimers are connected to neighbouring pairs along the *a* direction through the N-H···N H-bond of D···A distance 2.850(1) Å, centred on a crystallographic two-fold rotation axis, to form zigzag chains along the *c* direction (Figure 1.21(a)). These chains are both reinforced and connected along the *a* direction by weaker C-H···O interactions. The picolinic acid molecules connected by the N-H···N H-bond are arranged at an angle of approx. 47.5° with respect to each other (Figure 1.21(b)). The structure is connected along the *b* direction *via* π-π stacking interactions of about 3.837 Å between the pyridine/pyridinium rings (Figure 1.21(c)).

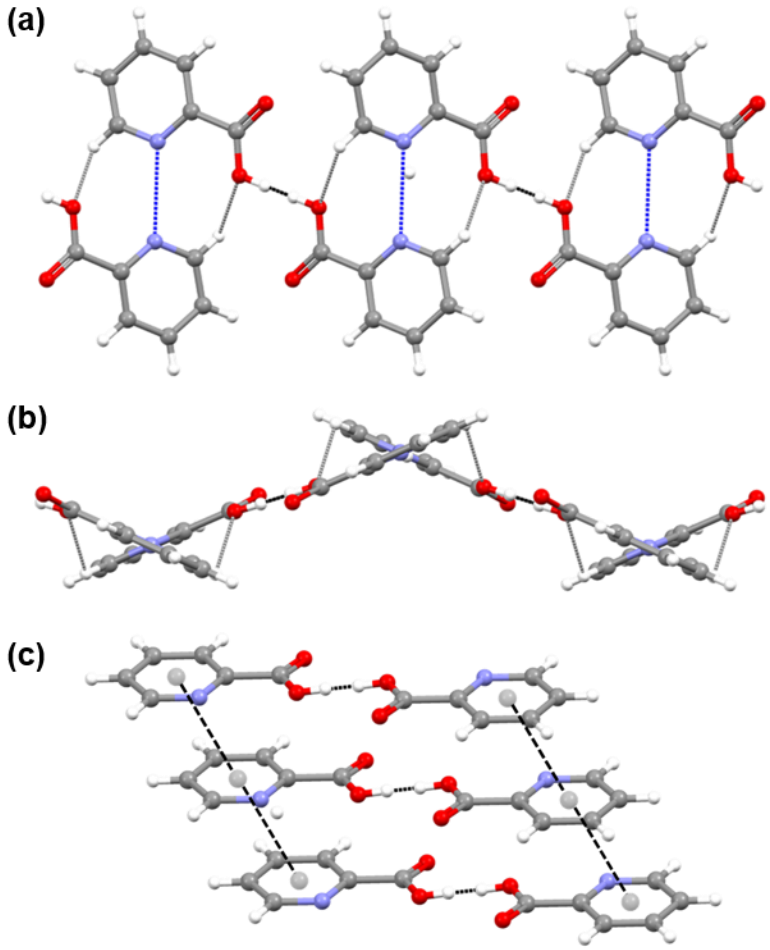

Figure 1.21. Crystal structure of pure picolinic acid [**PICOAC02**; CSD V5.35 June 2014]. (a) 1D H-bonded zigzag chain parallel to the *c* direction as viewed down the *b* axis, showing O-H···O (black), N-H···N (blue) and C-H···O (grey) H-bonds. (b) 1D H-bonded zigzag chain (as viewed down the reciprocal *a* axis). (c) π-π stacking interactions between neighbouring picolinic acid molecules along the *b* direction.

Nicotinic Acid

The crystal structure of nicotinic acid has been reported by Kutoglu and Scheringer.[138] The molecule is in its neutral form and connects along the *b* direction *via* an H-bond between the hydroxyl group of the carboxyl group to the pyridyl nitrogen atom, of D···A distance 2.602(1) Å, and a C-H···O H bond, to form 1D H-bonded chains (Figure 1.22(a)). These chains connect to others along the *a* direction *via* weak C-H···O interactions (Figure 1.22(a) and (b)), and along the *c* direction via π-π stacking interactions between the pyridyl rings of about 3.696 Å (Figure 1.22(c)).

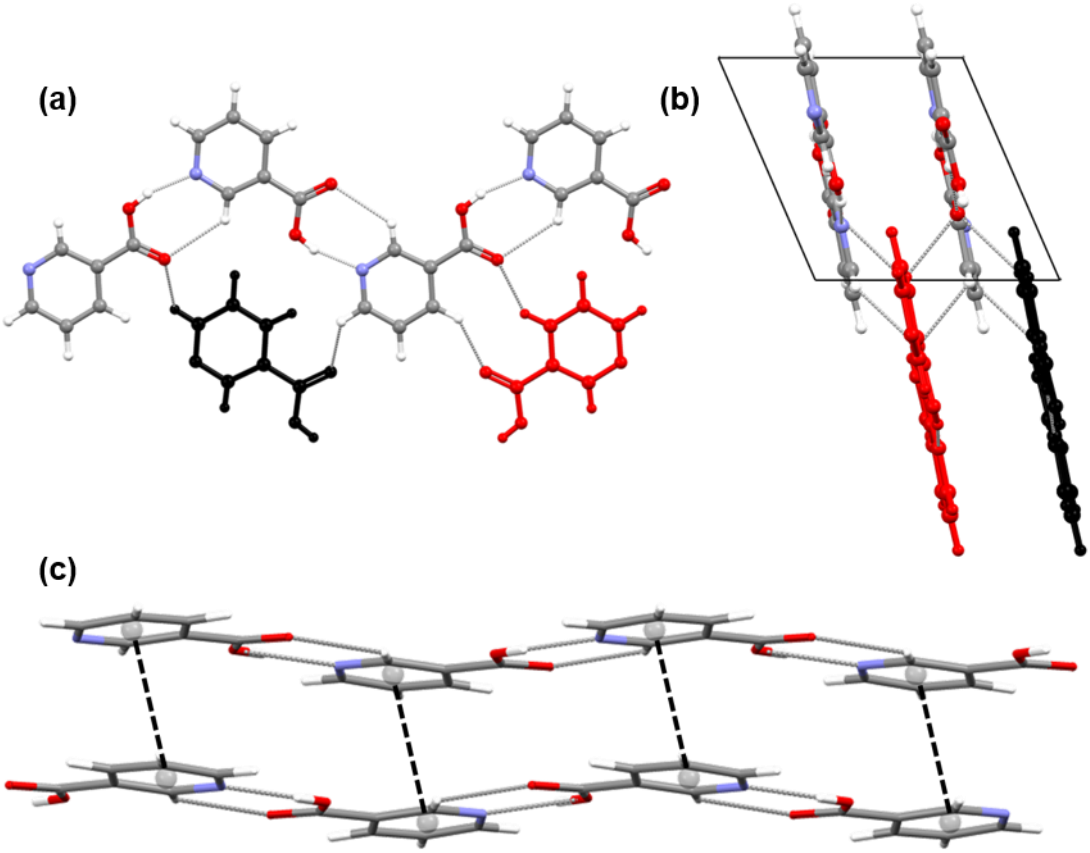

Figure 1.22. Crystal structure of pure nicotinic acid [**NICOAC02**; CSD V5.35 June 2014]. (a) 1D zigzag H-bonded chain parallel to the *b* direction (coloured by element), as viewed down the *c* axis, and H-bonds to molecules of neighbouring chains (coloured red and black) along the *a* direction. (b) View down the *b* axis showing four 1D chains and C-H···O H-bonds connecting between chains along the *a* direction. (c) π-π stacking interactions between the neighbouring chains coloured by element in (b), connecting chains along *c* direction, as viewed down the *a* axis.

Isonicotinic Acid

The crystal structure of isonicotinic acid has been reported by Takusagawa and Shimada.[139] Isonicotinic acid is has a very similar crystal structure to nicotinic acid in that the molecule is in its neutral form and makes 1D H-bonded chains that run parallel to the *b* direction through two H-bonds: one O-H···N H-bond from the hydroxyl group of the carboxyl group to the pyridyl nitrogen atom, of D···A distance 2.582(1) Å, and a weaker C-H···O H-bond (Figure 1.23(a)). Due to the carboxyl group being in the 4- position as opposed to the 3-position, the 1D chains are straight. The 1D H-bonded chains connect along the *c* direction *via* weak C-H···O interactions (Figure 1.23(b)), and along the *a* direction *via* π-π stacking interactions between the pyridyl rings of about 3.842 Å (Figure 1.23(c)).

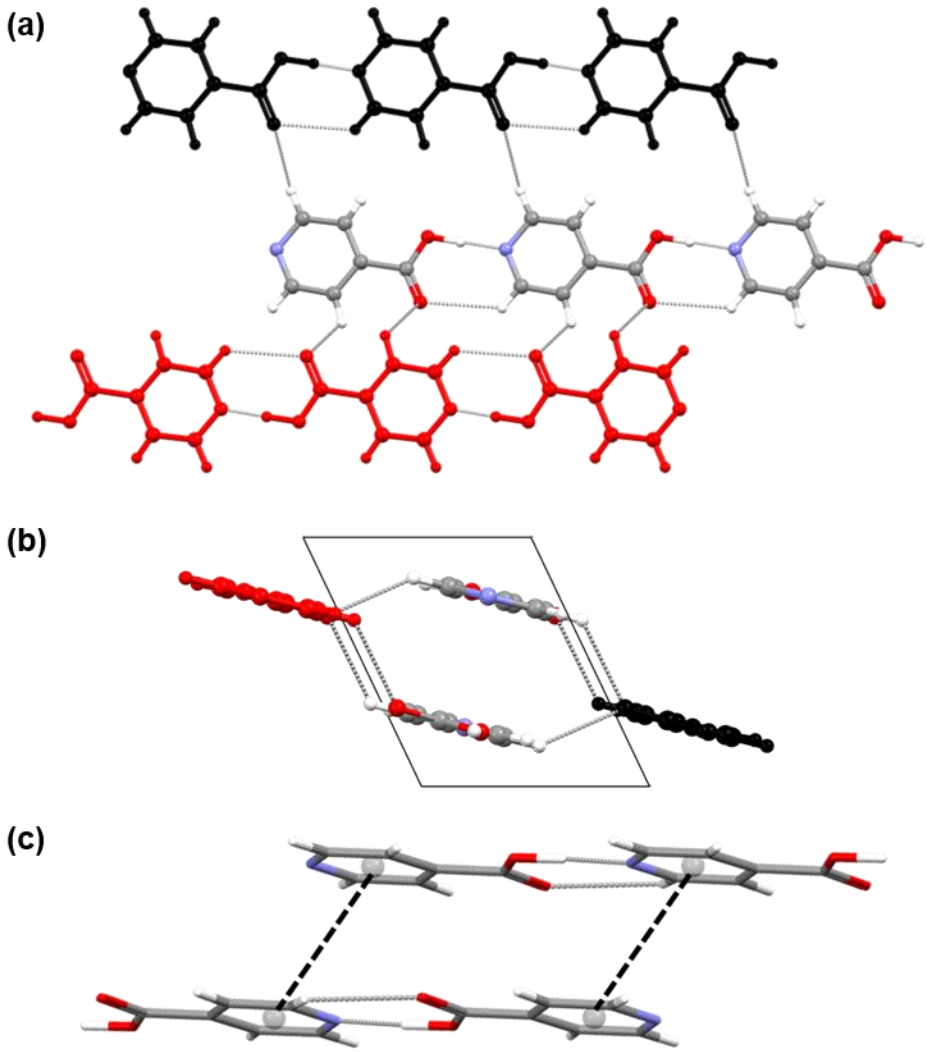

Figure 1.23. Crystal structure of pure isonicotinic acid [**ISNICA**; CSD V5.35 June 2014]. (a) Three 1D H-bonded chains connected by N-H···O and C-H···O bonds parallel to the *b* direction as viewed down the reciprocal *a* axis. (b) View down the *b* axis showing H-bonds connecting along the *c* direction. (c) π-π stacking interactions connecting molecules along the *a* direction.

2,4-Pyridine Dicarboxylic Acid

The crystal structure of 2,4-pyridine dicarboxylic acid has not been reported in its pure form (CSD V5.35, March 2015), however the structure of the hydrate has been reported by Sander *et al*.[140] In this structure, the organic molecule is in its zwitterionic form, while the crystal structure of the hydrate in which 2,4-pyridine dicarboxylic acid is in its neutral form is determined during this work and is reported in full in Appendix D.

1.7.2. Chloranilic Acid

Originally determined by in 1976 by Anderson,[141] the crystal structure of pure chloranilic acid was more recently re-determined at 100 K by Dutkiewicz *et al*.[142] The molecule is located on a centre of inversion and H-bonds are formed from each hydroxyl group to a carbonyl oxygen atom of a neighbouring molecule, O-H···O of D···A distance 2.752(2) Å, and angle 152(2)°. This forms a 2D H-bonded layer network (Figure 1.24(a)), which is parallel to the {202} plane (Figure 1.24 (b)), and connected to neighbouring layers *via* type-I Cl···Cl halogen bonds of distance 3.2838(8) Å, and angles C-Cl···Cl, of 152.96(6)°.

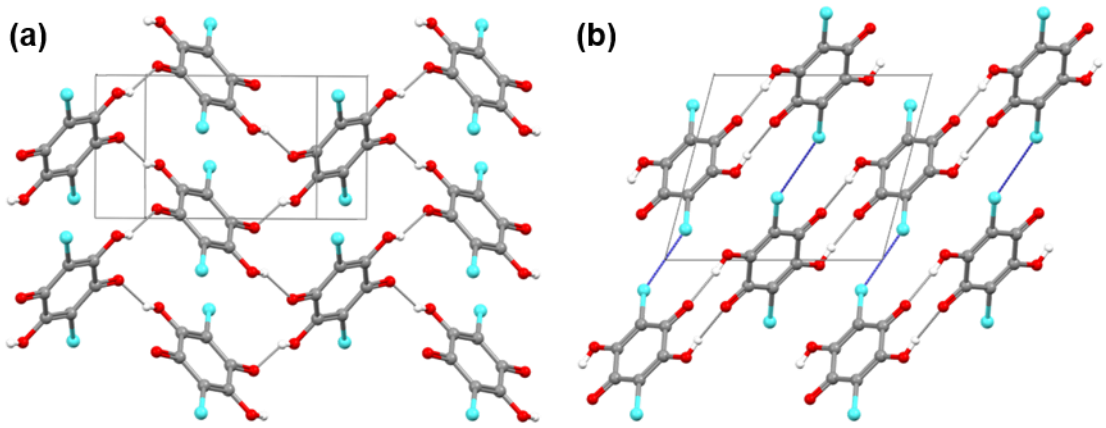

Figure 1.24. Crystal structure of pure chloranilic acid [**CLANAC11**; CSD V5.35 June 2014]. (a) View down the reciprocal *a** axis showing 2D H-bonded network. (b) View down the *b* axis showing 2D H-bonded motifs along the {202} plane, connected by Cl···Cl halogen bonds (blue).

1.8. Project Aims

The aim of this investigation is to synthesise and characterise a set of new supramolecular materials based on H-bonded group 2 metal-organic complexes, and to build an understanding of the factors that govern their formation and that lead to particular features in their motifs and networks. This thesis challenges the general reluctance to use alkaline earth metals in place of transition metals in the development of novel metal-organic complexes. That such materials featuring group 2 metals are less commonly reported is likely due to their unpredictable coordination geometries owing to their lack of d electrons rendering them unattractive candidates for use in the synthesis of MOFs and related inorganic-organic hybrid materials. However, research on magnesium and calcium metal-organic complexes in particular is worthwhile not only due to the metals' economic and environmental attributes, but also the benefit they offer in terms of developing lightweight materials. In view of the controlled 'development' of crystalline complexes, H-bonds are a

possible handle in directing their formation, and H-bonded networks have been proven to impart considerable stability, as well as flexibility, on metal-organic complexes, suggesting potential industrial applications for such materials.

This work documents a crystal engineering approach to developing new metal-organic complexes, by combining the advantages of a group 2 metal with the degree of control and resilience afforded by H-bonding. The organic ligands identified for use in this investigation were selected primarily for their H-bonding potential and their coordination capabilities, including N,O- and O,O'-chelation. The use of pyridine carboxylic and dicarboxylic acids allows a comparison between coordination from the oxygen and nitrogen donor atoms to the group 2 metal ions. The synthesised complexes can be analysed against related transition metal-organic complexes to study the effect of using the relatively hard acids, Mg^{2+} and Ca^{2+} metal ions, in place of transition metal ions with their different ionic structure.

Chapter 2. Theory and Methodology

2.1. Crystallography

Crystallography is a method used to determine the structure, or structural features, of crystalline materials by exposure to a beam of electromagnetic radiation such as X-rays or particles such as electrons or neutrons. It is based on the phenomenon of diffraction and the fact that the diffraction pattern of a crystal can be measured due to the constructive interference of diffracted waves by the regular repeating array of atoms. Crystalline materials and the theory of X-ray crystallography have been widely studied and discussed, notably by Stout and Jenson,[143] Massa,[144] Clegg *et al*.,[145, 146] Sherwood and Cooper,[147] and Dunitz.[148]

2.1.1. Crystalline Materials

A crystal is a highly ordered, three-dimensional pattern of atoms, molecules or ions arranged such that it can be described by a regular repeating structural motif which is in an identical environment throughout the crystal. The structural motif can be arbitrarily represented by a single point in space to produce a lattice point. These lattice points are arranged in a regular infinite array and together make up the crystal lattice of pure translation symmetry. The crystal lattice can be split into identical unit cells. The smallest translationally-repeating volume of the lattice, the primitive unit cell, is the volume associated with a single lattice point. The unit cell is a parallelopiped defined by the three lattice vectors, a, b, c, and three angles α, β, γ, between these vectors. The unit cell can be reproduced in three-dimensions to form the whole crystal.

The internal symmetry elements of a crystalline material are fundamental to the relationships between the unit cell parameters, i.e. the unit cell angles and axial lengths, and therefore, to which of seven crystal systems a material belongs. These crystal systems are: triclinic, monoclinic, orthorhombic, tetragonal, trigonal (rhombohedral or hexagonal), hexagonal and cubic, as listed in Table 2.1. The unit cell that best describes the crystal structure is that which shows the highest possible symmetry. Sometimes the smallest volume representative of the whole crystal, the primitive unit cell (P), is an oblique shape and it is more convenient and conventional to describe the crystal using a larger unit cell which corresponds to a higher symmetry crystal system, thereby simplifying its geometry by allowing it to contain more than one lattice point. This gives rise to the base centred (C, A or B, depending on which faces are centred), body-centred (I), face-centred (F) and

rhombohedral (R) unit cells; applying these lattice types divides the seven crystal systems into fourteen distinct Bravais lattices, illustrated in Figure 2.1.

Table 2.1. The seven crystal systems indicating the unit cell restrictions and Bravais lattice types.

Crystal System	**Characteristic Symmetry**	**Parameters**	**Lattice types**
Triclinic	None	$a \neq b \neq c$ $\alpha \neq \beta \neq \gamma$	P
Monoclinic	One 2-fold axis	$a \neq b \neq c$ $\alpha = \gamma = 90°; \beta > 90°$	P, C
Orthorhombic	Three 2-fold axes	$a \neq b \neq c$ $\alpha = \beta = \gamma = 90°$	P, C, I, F
Tetragonal	One 4-fold or $\bar{4}$ axis	$a = b \neq c$ $\alpha = \beta = \gamma = 90°$	P, I
Trigonal (rhombohedral)	One 3-fold or $\bar{3}$ axis	$a = b = c$ $(\alpha = \beta = \gamma \neq 90°)$	R
Trigonal (hexagonal)	One 6-fold or $\bar{6}$ axis	$a = b \neq c$ $\alpha = \beta = 90°; \gamma = 120°$	P
Hexagonal	One 6-fold or $\bar{6}$ axis	$a = b \neq c$ $\alpha = \beta = 90°; \gamma = 120°$	P
Cubic	Four 3-fold or $\bar{3}$ axes	$a = b = c$ $\alpha = \beta = \gamma = 90°$	P, I, F

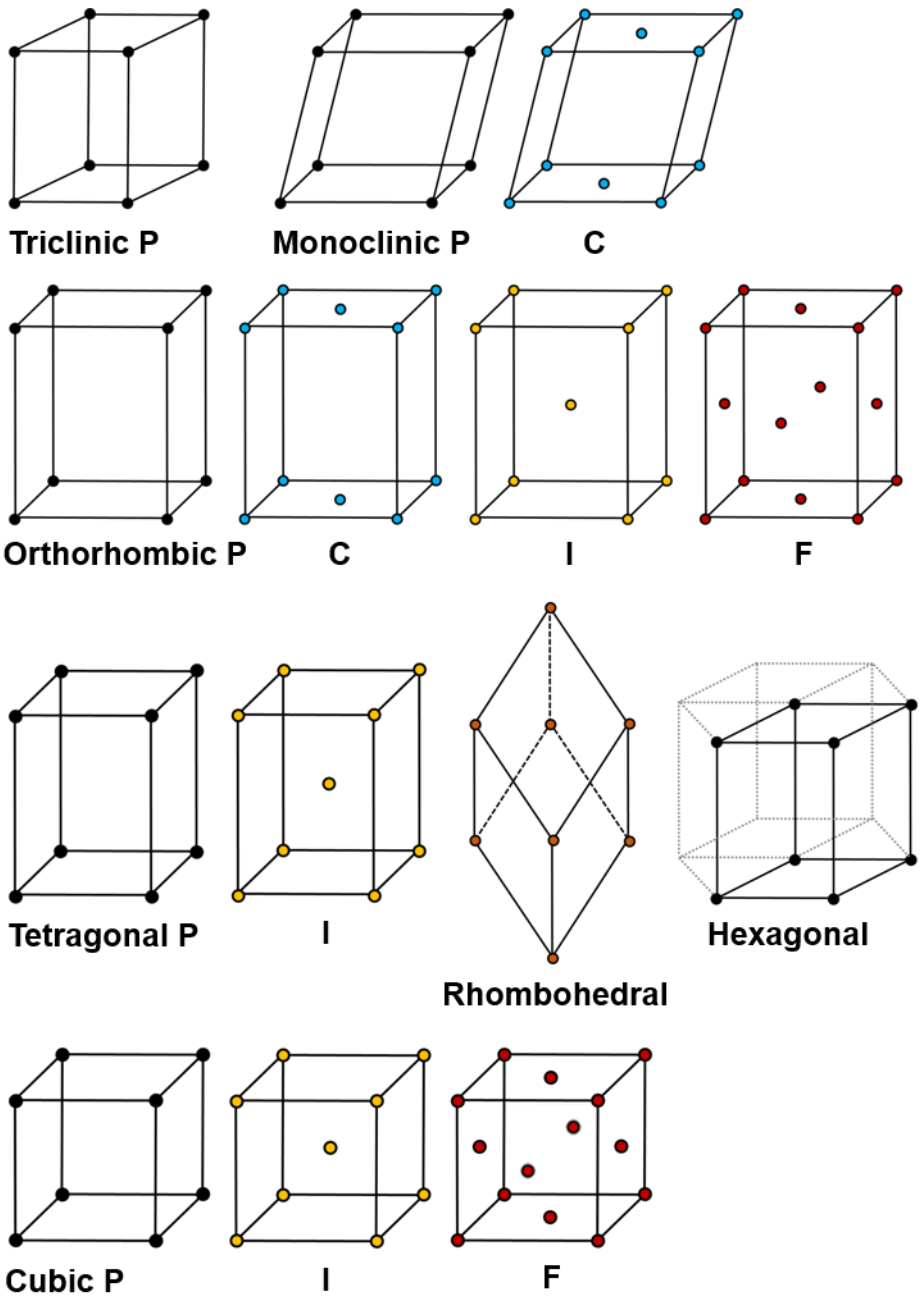

Figure 2.1. The 14 Bravais lattices.

The unit cell can also contain internal symmetry elements; the non-translational elements are: rotation, inversion, reflection and rotation-inversion, with rotational symmetry within the crystal lattice being restricted to one-, two-, three-, four-, and sixfold. These non-translational symmetry elements can be combined in 32 unique ways, resulting in the 32 crystallographic point groups, represented by the Hermann-Mauguin symbols. The unit cells of crystalline solids, in contrast to single molecules, also possess internal translational symmetry elements: the screw axis and glide plane. Incorporating these translational

symmetry elements with the 32 point groups repeated on a Bravais lattice gives a total number of exactly 230 different possible space groups describing the atomic structure of the crystal in terms of the asymmetric unit. The asymmetric unit, or basis, is a unique structural motif within the unit cell that can lead to the complete description of the crystal by the application of the internal unit cell symmetry and translation in the *a*, *b*, *c* lattice vectors. The space groups are well established and are recorded in the International Tables of Crystallography, Volume A.[149] Every possible crystal structure has a characteristic space group, however the space groups are not distributed equally: the majority of crystalline molecular materials have triclinic, monoclinic or orthorhombic space groups and about a third of all known crystal structures of molecular compounds have the monoclinic space group P $2_1/c$.[145]

Atomic positions within the unit cell can be given as fractional coordinates *x*, *y*, *z* of the *a*, *b*, *c* unit cell axes. Planes through the crystal can be described in terms of where they intercept the unit cell axes. The planes pass through points in the unit cell that are equivalent by translation in the crystal. Therefore there are sets of parallel lattice planes called *hkl* planes, whereby *hkl* are Miller indices. The intercepts of the plane on the *a*, *b*, *c* axes of the unit cell are 1/*h*, 1/*k* and 1/*l*. The reciprocals of these rational fractions give the *hkl* Miller indices. The planes parallel to the faces of the unit cell are the (100), (010) and (001) planes, since 0 indicates an intercept at infinity.

2.1.2. X-Ray Diffraction

The analytical technique of X-ray diffraction (XRD) evolved from the discovery of X-rays by Wilhelm Conrad Röntgen in 1895,[150] a breakthrough that earned him the first Nobel Prize in Physics in 1901. In 1912 Max von Laue ventured that X-rays, being waves of very short wavelength comparable to the interatomic distances of a crystal, as opposed to tiny particles, would interact with a crystal as a diffraction grating interacts with visible light.[151] Experiments carried out by two of his students, Walter Friedrich and Paul Knipping, proved his theory, and he was awarded the Nobel Prize in Physics in 1914 for his discovery. This development led to the first crystal structure determination by X-ray diffraction of rock salt, accomplished by father and son William Henry Bragg and William Lawrence Bragg in 1913.[152] Their research brought about the derivation of the Bragg Equation (Equation 2.1) a fundamental concept in the understanding of crystallography.[153, 154] In recognition of their ground-breaking achievement, the two Braggs were jointly awarded the Nobel Prize in Physics in 1915.

Single crystal XRD (scXRD) has become the most powerful method known today for obtaining structural information in the solid state. ScXRD allows the precise determination of the composition and structure of unknown compounds including conformation, connectivity and the finer details such as bond distances and angles along with intermolecular interactions and molecular packing in the crystal. It is used to study a wide range of crystalline materials including minerals, inorganic and organic molecules, and biological structures.

During an XRD experiment, X-rays, which have a wavelength of 50–300 pm, are directed onto and interact with a single crystal of the material under investigation. As the interatomic distances are in the same region as the wavelength of the X-rays at 100-300 pm (1-3 Å), the electrons within the atoms of the crystal scatter the X-rays in all directions; if this occurs without changing the wavelength, it is called elastic scattering or diffraction.

The scattered radiation can be detected by the use of an area detector such as a Charge Coupled Device (CCD) system or an image plate. It takes the form of a diffraction pattern of spots of different intensities. A diffraction spot is produced when waves scattered from successive *hkl* planes of a Miller index are in-phase and so cause constructive interference: hence the path difference between these scattered X-rays must be equal to an integral number of wavelengths. The scattering phenomenon can be regarded geometrically as reflection of the incident X-rays, where the angle of incidence equals the angle of reflection. Therefore, a diffraction spot arises for every Miller index at certain angles of incidence and reflection, θ, and these angles are determined by the wavelength of radiation, λ, and the inter-planar spacing, d_{hkl}. The Bragg Equation, shown in Equation 2.1, shows the relationship between these three variables and the derivation for this equation is shown in Figure 2.2. The four horizontal lines represent a set of *hkl* planes that are at distance, d_{hkl}, apart. The red arrows represent X-rays reflecting off these planes. Only angles of θ which result in the path difference between the two waves, n λ, shown in bold black lines, as an integral number of wavelengths, will result in constructive interference and therefore a diffraction spot.

$$n\lambda = 2d_{hkl}\sin\theta \qquad \textbf{Equation 2.1.}$$

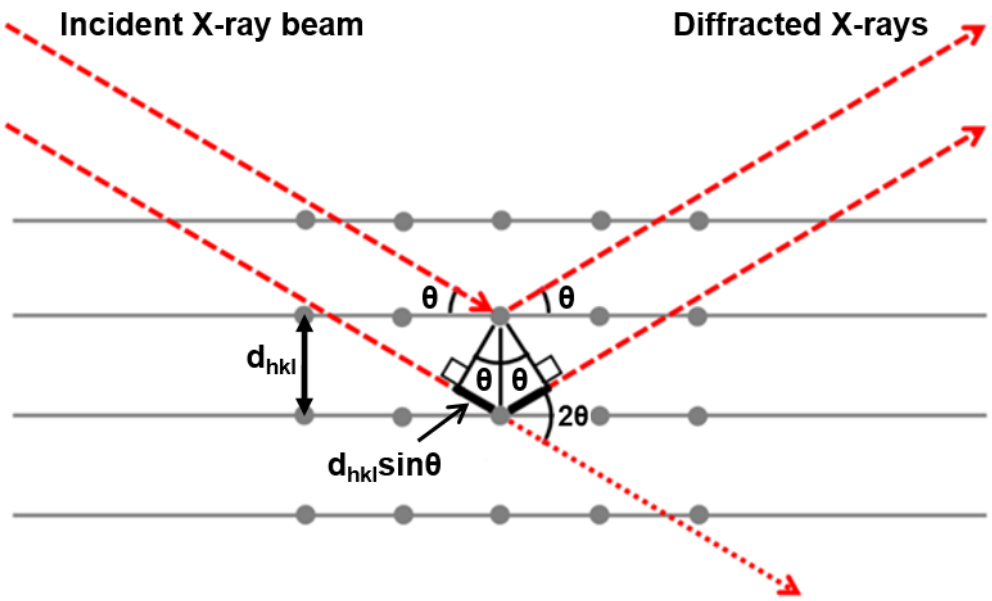

Figure 2.2. Derivation of the Bragg Equation.

2.1.3. Reciprocal Space

The Bragg Equation can be rewritten as sinθ = (nλ/2) (1/d). This shows that sinθ is inversely proportional to d, therefore crystal structures with large interplanar spacings will have a compressed diffraction pattern, and those with small interplanar spacings will have an expanded diffraction pattern. Since sinθ is directly proportional to 1/d, a lattice in reciprocal space can be constructed with an interplanar spacing of 1/d measured in units of $Å^{-1}$. The reciprocal lattice can be realised from the points with coordinates (*h*, *k*, *l*) located where the diffraction vectors normal to the corresponding *hkl* planes terminate at a distance of $1/d_{hkl}$, when taken to radiate from a single origin point.

The real-space and reciprocal lattices are related in terms of their vectors **a**/**a***, **b**/**b***, **c**/**c***, which correspond to the direction and magnitude of the unit cell axes. The definitions of the reciprocal axes are the vector products of the associated direct axes as shown in Equation 2.2.

$$\mathbf{a}^* = (\mathbf{b} \times \mathbf{c})/V \qquad \mathbf{b}^* = (\mathbf{a} \times \mathbf{c})/V \qquad \mathbf{c}^* = (\mathbf{a} \times \mathbf{b})/V \qquad \textbf{Equation 2.2.}$$

A geometrical interpretation of the Bragg Equation is the Ewald construction, or the sphere of reflection, which illustrates the conditions under which the Bragg Equation is fulfilled and reflection will occur for a given set of *hkl* planes. Figure 2.3(a) shows a 2D representation of the Ewald construction. A crystal, C, is oriented such that an angle θ is made between a set of *hkl* planes and the direction of the incident and diffracted X-ray beam. A sphere of radius 1/λ is positioned round the crystal, and the point where the transmitted X-rays pass

through this sphere is designated as the origin, O, of the reciprocal lattice. P is a point at which the diffracted X-ray beam exits the sphere and the reciprocal lattice vector OP is equivalent to the diffraction vector. The triangle QPO is right-angled and satisfies the Bragg Equation in that $\sin\theta = OP/OQ$, since $OP = 1/d$ and $OQ = 2/\lambda$. Therefore, where the reciprocal lattice point, P, or rather the endpoint of a reciprocal lattice vector, coincides with the surface of the sphere of reflection, a diffraction spot will occur, defined by the direction of the vector CP. Rotation of the reciprocal lattice about O will cause different reciprocal lattice points to come into contact with the sphere of reflection. This is put into effect by rotating the crystal about the point C during the diffraction experiment to measure diffraction spots corresponding to different sets of *hkl* planes.

Not all of the reciprocal lattice points are necessarily detectable by a given wavelength of X-ray radiation. A reciprocal lattice point further than a distance of $2/\lambda$ from O will not intersect the sphere of reflection at any orientation, limiting the number of diffraction peaks that can be observed. This forms the limiting sphere, as shown in Figure 2.3(b). The number of observable reflections can be adjusted by varying the wavelength: a shorter wavelength will increase the size of the spheres and so make it possible to detect a greater number of reflections, while a longer wavelength will reduce this number until no reflections are observable.

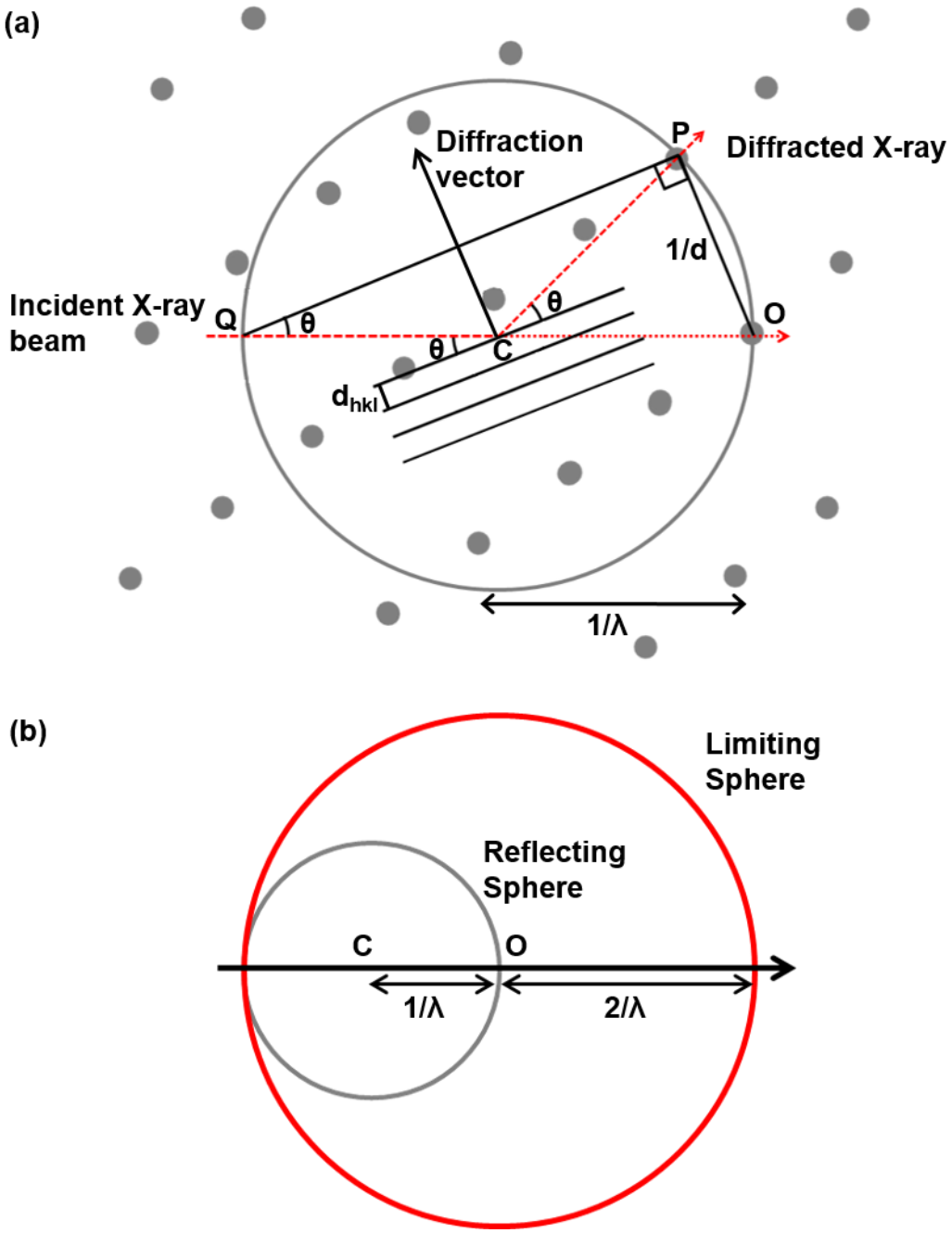

Figure 2.3. (a) The Ewald construction represented in 2D centred around a crystal, C, and superimposed by the reciprocal lattice with origin, O. (b) The Limiting Sphere with radius double that of the sphere of reflection.

2.1.4. Interpreting the Diffraction Pattern

Interpretation of the diffraction pattern ultimately produces a time-averaged electron density map indicating atomic positions, from which the crystal structure can be solved. The diffraction pattern is the result of scattering from the whole crystal under examination, and therefore represents the average unit cell. The diffraction pattern is a two-dimensional

projection of part of the three-dimensional reciprocal lattice and its appearance depends on the orientation of the crystal relative to the X-ray beam and the detector. The geometry of the diffraction pattern (the distances between spots and the angles between rows) relates to the crystal system while the symmetry of the diffraction pattern, evident in the positions and intensities of related diffraction spots, relates to the space group. The intensities of the diffraction spots provide information on the positions of atoms within the unit cell. Instances where *hkl* reflections have intensity, I_{hkl}, equal to 0, due to the destructive interference of scattered waves, are described as systematic absences as they arise from translational symmetry elements and allow the determination of the Bravais lattice type and space group of a crystal. There are specific conditions concerning the *hkl* indices under which these reflections will or will not be present.

Regardless of whether or not the crystal structure is centrosymmetric, a lattice (real or reciprocal) always features inversion symmetry, therefore, generally, the diffraction pattern also features inversion symmetry. Friedel's Law, as this trend is known, reduces the number of possible point groups representative of the symmetry of the diffraction pattern from 32, to the 11 which feature inversion symmetry; these are the 11 Laue classes. For the monoclinic crystal system, the point groups 2, *m* and 2/*m* will be indistinguishable from their diffraction patterns as they will all appear to relate to the point group 2/*m*.

2.1.5. Fourier Synthesis

X-rays are diffracted by individual electrons within the electron clouds of the atoms that form a crystal, with every constituent part of the crystal structure contributing to every diffraction spot in the resulting pattern. Atoms of the same element contribute similarly as defined by their atomic scattering factor, f_j. This is a measure of the amplitude of the scattered X-rays from an atom for a given reflection, and since it is dependent on electron density, it is unique to each element. Assuming the atom is spherical, f_j is a function of $\sin\theta/\lambda$. When $\sin\theta/\lambda = 0$, f_j is equal to the atomic number, but as $\sin\theta/\lambda$ increases, f_j diminishes. This is due to the greater phase shift of the scattered X-rays from discrete electrons resulting in destructive interference. This effect is more gradual for heavier elements relative to lighter elements since they contain more core electrons representing greater electron density. As the scattering is dependent on the number of electrons in an atom, heavy elements, when present in a crystal structure, dominate the calculated electron density map and lighter atoms such as hydrogen are less likely to be observed. The atomic scattering factors are also weakened by atomic vibrations, as defined by the atoms' anisotropic displacement parameters.

The structure factor, F_{hkl}, is a mathematical description of the resultant wave scattered from the atoms within the unit cell, according to their atomic scattering factors, corresponding to each *hkl* reflection in the diffraction pattern. The structure factor can be expressed in terms of N atoms in one unit cell, the atomic scattering factor and the fractional coordinates (x_j, y_j, z_j) of the j^{th} atom, according to Equation 2.3, which is termed the Fourier transform:

$$F_{hkl} = \sum_{j=1}^{N} f_j \exp[2\pi i(hx_j + ky_j + lz_j)] \qquad \textbf{Equation 2.3.}$$

The structure factor F_{000} corresponds to the in-phase scattering from all atoms in the direction of the transmitted X-ray beam where $\sin\theta/\lambda = 0$; therefore it has a phase of zero and since f_j is equal to the atomic number, the amplitude equals the number of electrons in the unit cell. This can be calculated using Equation 2.3 by substituting for the *hkl* indices (0 0 0).[145]

F_{hkl} is a complex number associated with an amplitude, $|F_{hkl}|$, and a phase, ϕ_{hkl}:

$$F_{hkl} = |F_{hkl}| \exp[i\phi\, hkl] \qquad \textbf{Equation 2.4.}$$

The intensities of the diffraction spots, I_{hkl}, are experimentally observable quantities, and therefore can be measured for each *hkl* reflection. Once corrected to account for factors including absorbance, extinction, crystal size and morphology, the amplitudes of the structure factors can be determined from the intensities of each *hkl* reflection, according to the relationship:

$$I_{hkl} \propto |F_{hkl}|^2 \qquad \textbf{Equation 2.5.}$$

The phases of the structure factors, however, are not obtained from the intensities of the *hkl* reflections, which brings about the 'phase problem'. The phases of the scattered waves depend on the relative positions of electron density within the unit cell, therefore, if the phases could be measured, the electron density could be calculated at given fractional coordinates, ρ_{xyz}, in units of e Å^{-3}. The electron density can be expressed in terms of the summation of the structure factors for the *hkl* reflections and the volume of the unit cell, according to Equation 2.6, which is termed the reverse Fourier transform:

$$\rho_{xyz} = \frac{\mathbf{1}}{\boldsymbol{V}} \sum_{h,k,l} F_{hkl} \exp[-2\pi i(hx + ky + lz)] \qquad \textbf{Equation 2.6.}$$

Equation 2.3 and 2.6 describe how the crystal structure represented by the diffraction pattern (from reciprocal space) and the electron density of the unit cell (in real space), are

related mathematically through Fourier transformation. Equation 2.6 is fundamental to the interpretation of crystallographic experiments. The process by which the electron density, ρ_{xyz}, is calculated for every point in the unit cell, (x, y, z), from the recombination of the structure factors is called Fourier synthesis.

2.1.6. Structure Solution

In order to carry out the Fourier synthesis of Equation 2.6, it is necessary to know, at least as approximate values, the phases, ϕ_{hkl}, corresponding to each structure factor amplitude, $|F_{hkl}|$. Structure solution, in effect, is the process of solving the phase problem and it can be achieved by several different methods using computer software programs.

Direct Methods

Direct methods are the most commonly used structure solution techniques and are generally employed for crystal structures composed of organic molecules or where there are no heavy atoms present. Direct methods utilise the relationships between structure factor amplitudes to directly determine phase information. These calculations are based on certain mathematical constraints regarding the electron density function which affect the structure factors associated with the unknown phases and the fact that the scattered waves must combine to represent these conditions.

The constraint stating that the electron density in real space is non-negative, $\rho_{xyz} \geq 0$, leads to inequality relationships. Harker-Kasper inequalities, dating from 1948, use the unitary structure factor, U_{hkl}, which is the observed structure factor normalised by the structure factor F_{000} to give a value from 0 to 1 indicating the fraction of electrons scattering in-phase for that reflection. Assuming the crystal is centrosymmetric, the inequality relationship between the *hkl* and the 2*h*2*k*2*l* reflections, Equation 2.7, allows the determination of the sign of the phase of U_{2h2k2l} where the intensities are sufficiently large.

$$U_{2h2k2l} \geq 2U^2_{hkl} - 1 \qquad \textbf{Equation 2.7.}$$

Unitary structure factor amplitudes greater than about 0.5 are generally sufficiently high to unambiguously assign U_{2h2k2l} as positive in order to satisfy the inequality relationship. However, the amplitudes are not always high enough, and U_{2h2k2l} cannot ever be unambiguously associated with a negative sign. These limitations of the application of inequality relationships necessitate other direct methods.

The fact that atoms must be in discrete positions brings about the constraint that electron density is located in concentrated regions of well-defined maxima. Regarding the atoms as points unaffected by thermal motion is achieved by calculation of E values, E_{hkl}, introduced by Karle and Hauptman, representing the ratio of the structure factor amplitudes, $|F_{hkl}|$, to the mean amplitude of all *hkl* reflections at the same resolution. Normalising the structure factors over the relevant θ range removes the fall-off in intensity due to the θ-dependence of the atomic scattering factor, and therefore the effect of atomic shape and vibration. For large values of E_{hkl}, Karle and Hauptman inequalities can restrict the values of phases. Furthermore, the distribution of the $|E_{hkl}|$ values indicate as to the presence or absence of a centre of symmetry in the space group.

In many crystal structures it is reasonable to regard the atoms as essentially equal, a constraint on which Sayre based the development of equality relationships between structure factors, applicable to centrosymmetric crystals. The Sayre Equation implies that the structure factor, F_{hkl}, can be determined as the product of all the pairs of structure factors whose indices sum to it – an infinite list – however, only some of these *hkl* reflections are measured. The strongest reflection pairs measured will contribute most significantly to the structure factor of the reflection being calculated, and if this reflection is also strong, it is very likely that the triplet relationship between the three reflections (Equation 2.8) will indicate the probable sign of the phase, in that if $F_{h'k'l'}$ and $F_{h-h',\ k-k',\ l-l'}$ have the same sign, F_{hkl} will be positive, and if they have different signs, F_{hkl} will be negative.

$$sF_{hkl} \approx sF_{h'k'l'} \cdot sF_{h-h',\ k-k',\ l-l'} \qquad \textbf{Equation 2.8.}$$

The probability of the correct phase being assigned decreases with increasing number of atoms in the structure due to the number of Fourier syntheses to be calculated, and so direct methods is most effective for crystals with less than 300 non-hydrogen atoms in the asymmetric unit.

In a similar way, but this time for non-centrosymmetric structures, rather than to calculate the sign of the phase, it is necessary to calculate the phase angle, ϕ_{hkl}. Triplet phase relationships are derived expressed as:

$$\phi_{hkl} \approx \phi_{h'k'l'} + \phi_{h-h'k-k'l-l'} \qquad \textbf{Equation 2.9.}$$

Large numbers of triplet relationships can be used to identify the phase of a reflection using the tangent formula, derived from the Sayre equation:

$$\tan(\phi(h)) \approx \frac{\sum_k |E(k)\, E(h\text{-}k)| \sin(\phi(k) + \phi(h\text{-}k))}{\sum_k |E(k)\, E(h\text{-}k)| \cos(\phi(k) + \phi(h\text{-}k))} \qquad \textbf{Equation 2.10.}$$

This summation is carried out over all available triplets and gives estimated phases for reflections. The automated phase determination process implemented in direct methods structural solution programs starts with a small set of known phases from the origin-fixing set, or assumed phases of strong reflections. The use of multi-solution methods is a strategy in which known phases are supplemented with various trial phases of other strong reflections. Repeated application of the tangent formula calculates and refines phases for the rest of the reflections in the dataset. Figures of merit are calculated for each set of phases obtained to indicate the likelihood of the solution being correct. Fourier synthesis based on the calculated phase values of the best figure of merit generates an electron density map which is examined for recognisable molecular features.

Patterson Synthesis

The Patterson function (Equation 2.11) is the Fourier synthesis of the relative intensities $|F_{hkl}|^2$. Replacing the structure factors with the products of each with their complex conjugate effectively sets the phases to zero.

$$P_{uvw} = \frac{1}{V} \sum_{h,k,l} |F_{hkl}|^2 \cos[2\pi(hu + kv + lw)] \qquad \textbf{Equation 2.11.}$$

The resulting Patterson map reveals relative interatomic separations by way of maxima representing interatomic vectors between every atom in the unit cell to every other atom. The self-vectors, from each atom to itself, have zero length and coincide on the unit cell origin, indicated by the strongest peak in the Patterson map. The interatomic vectors operate in both directions so for every pair of atoms there are two equal vectors related by inversion through the origin, therefore, the Patterson map is always centrosymmetric, regardless of the symmetry of the crystal structure. The intensity of a vector is proportional to the product of the atomic numbers of the two atoms involved, therefore the intensity of the origin peak is proportional to the sum of the squares of the atomic numbers of all the atoms in the unit cell. The next most prominent peaks will be those corresponding to interatomic vectors between any heavy atoms. Patterson synthesis is most effective when there are some heavier atoms within the structure, because, from their vectors, a set of self-consistent atomic positions can be deduced to build a model structure from which approximate phases can be calculated and Fourier synthesis carried out to generate an electron density map.

Symmetry elements are evident in the Patterson map in the form of local concentrations of maxima referred to as Harker lines or planes, providing the atoms are not actually located

on the symmetry element. Identification of vectors between heavy atoms related by symmetry often affords additional symmetry information on the structure.

Patterson synthesis can be applied in cases where the crystal contains molecules of known stereochemistry even if there are no heavy atoms present. A calculated Patterson map can be found for the known fragment and matched to the Patterson map for the whole structure. A rotation search is used to find the correct orientation of the fragment, and a translation search to find the correct position.

2.1.7. Structure Completion

Structure solution provides an initial model of the asymmetric unit based on the atomic positions of the non-hydrogen atoms, however, very often only some of these atoms have been located and the rest are absent. In order to locate these atoms to complete the phasing model, the reverse Fourier transform (Equation 2.6) is calculated using the observed structure factor amplitudes, $|F_o|$ and the calculated phases, ϕ_c, on which the initial model is based, as coefficients. This gives a new electron density map showing the positions of the atoms in the initial model, and new peaks which can be assigned atomic scattering factors to improve the model. This process of Fourier refinement is repeated until all of the non-hydrogen atoms are accounted for.

Difference Fourier maps can also be used to locate atoms and confirm atom assignments. These are generated by calculating the reverse Fourier transform using the calculated phases as before, but substituting the observed structure factor amplitudes by the differences between the observed and calculated structure amplitudes, $|F_o| - |F_c|$. In the difference Fourier map the positions of the atoms in the model are not shown, but missing atoms are represented as peaks. Difference Fourier maps are particularly useful for determining the positions of hydrogen atoms after refinement of the model containing the non-hydrogen atoms.

2.1.8. Structure Refinement

Structure refinement is the process by which the numerical parameters of the model structure are adjusted in order to optimise the agreement between the observed diffraction pattern and that which can be calculated from the Fourier transform (Equation 2.3) using the (x, y, z) atomic coordinates of the model structure. Hence, refinement optimises the agreement between the observed, F_o, and the calculated, F_c, structure factors, but since

the observed phases are not available, in practice, the amplitudes of the observed, $|F_o|$, and calculated structure factors, $|F_c|$, are compared.

Least-Squares Refinement

In a good single crystal XRD experiment, there are a considerably greater number of reflections than there are parameters to be defined, such that the parameters are said to be 'over-determined'. This allows for an error to be calculated for each parameter indicating the precision of the numerical value in the form of the estimated standard deviation (e.s.d.) or standard uncertainty (s.u.), with the variance being the square of the error. Refinement of the model structure is carried out using the least-squares method which solves for the parameters that minimise the sum of the squares (variance) of the (residual of the) differences between the two sets of structure factors, $|F_o|$ and $|F_c|$:

$$\text{min.} = \sum_{h,k,l} w(|F_o|^2 - |F_c|^2)^2 \qquad \textbf{Equation 2.12.}$$

Here, w, is the weight assigned to each reflection based on its relative reliability and is equal to the inverse of the variance of the calculated structure factor amplitude. ($|F_o| - |F_c|$) can be used instead of ($|F_o|^2 - |F_c|^2$), however the latter is more common as it allows the inclusion of very weak data for which the background may be stronger than the reflection. Least-squares refinement is an iterative process whereby incremental changes are made to the latest parameter values in each cycle until any changes are negligible relative to their standard deviations and the refinement has converged.

Refinable Parameters

The parameters that can be refined to improve the agreement between the calculated and observed structure factors include the overall scale factor, which places the calculated and observed data onto the same absolute scale, and the provisional parameters that define each atom in the model structure. These are the atomic coordinates (x, y, z) which locate the atom within the unit cell, the displacement parameters (U_{ij} values) which describe its vibrational thermal motion and a site occupancy factor which shows if the atom is on a symmetry element, and defines the extent to which it may be disordered.

To enhance the structural model's representation of the actual crystal structure, non-hydrogen atoms are refined anisotropically, with three displacement parameters and three parameters describing the directions of the axes of the resulting thermal ellipsoid. The

displacement parameters of atoms are influenced by the temperature at which the diffraction data was collected, and generally, thermal vibrations are reduced and therefore the model structure is more accurate, by carrying out the experiment under cryogenic conditions. If they can be located at all by X-ray diffraction, hydrogen atoms are only refined isotropically due to their having only one electron. This electron is naturally displaced towards the atom to which it is covalently bonded (the parent atom): this has the apparent effect of shortening the bond. In the case of H-bonds, in the model, the D-H and H···A bonds are usually effectively shorter and longer, respectively, than they are in reality. When measuring H-bonds the D···A distances are thus a more reliable geometric parameter. Often hydrogen atoms are not located or do not refine well but with knowledge of their expected environment, by adding a constraint, their positions can be calculated in relation to the parent atoms. Such hydrogen atoms are refined as riding atoms with isotropic displacement factors fixed to a factor of the value of that of the parent atoms'. Constraints can be used to refine any rigid group of known geometry and as they express a parameter in terms of its relationship with another, constraints reduce the number of freely refined parameters, increasing the data:parameter ratio.

Restraints, unlike constraints, are less absolute conditions imposed on molecular features of known geometry to promote the movement of atoms to more chemically reasonable positions. They increase the data:parameter ratio by providing additional data in the form of expected distances or angles whose differences from the observed measurements are included in the least squares sums along with appropriate weights for the geometric information.

Since the model structure is a time-averaged approximation of the unit cell, naturally occurring disorder is accounted for in the assignment of site occupancy factors. Where a site is, on average, occupied by different atoms, their site occupancies are constrained to sum to 1 and these parameters are refined with this constraint imposed.

Model Validation

The progress of least squares refinement, indicated by the extent to which the observed and calculated data are in agreement, is monitored by the calculation of the residual (R-) factor;

$$R = \frac{\Sigma \, | \, |F_o| - |F_c| \, |}{\Sigma \, |F_o|}$$ **Equation 2.13.**

and the weighted R-factor:

$$wR_2 = \sqrt{\frac{\Sigma\, w(F_o^2 - F_c^2)^2}{\Sigma\, w(F_o^2)^2}} \qquad \textbf{Equation 2.14.}$$

These values are multiplied by 100 to indicate the relative percentage deviation between the observed and calculated data. They decrease in magnitude as the structure is refined to convergence, by which point, the R-factor will typically have a value in the range of 0.02 – 0.07, and the weighted R-factor will be at least twice as large due to its sensitivity to small errors in the model. Another measure of the quality of the model is the 'goodness of fit,' S:

$$S = \sqrt{\frac{\Sigma\, w(F_o^2 - F_c^2)^2}{(n-p)}} \qquad \textbf{Equation 2.15.}$$

where n is the number of reflections, and p the number of parameters used in the refinement. A value of 1 indicates that the weighting scheme is appropriate and that the model is a good representation of the actual crystal structure, however it can be easily manipulated by adjusting the weighting scheme or the number of reflections used.

Crystal structure solution and refinement results in the identification of the crystal's Bravais lattice, space group, and a parameterised model of the asymmetric unit. From this model, bond distances and angles can be measured and the crystal packing can be visualised. The model is somewhat limited, however, in that since it represents electron density, it cannot specifically differentiate between atoms and lone pair or bonding electrons, therefore the model must be interpreted with reference to the relevant chemistry.

2.1.9. Powder X-Ray Diffraction (PXRD)

PXRD can be carried out on a polycrystalline powder of the material under investigation. The crystallites in the powder sample are generally randomly arranged in every orientation, however crystallites that have a pronounced platelet or needle morphology often show preferred orientation by which they tend to lie flat on a sample holder. This can be overcome by placing the sample in a glass capillary which is rotated during data collection. Each crystallite diffracts the incident X-ray beam as does a single crystal during a scXRD experiment such that many diffraction spots relating to the different crystallites are produced. Assuming the crystallites are randomly arranged, essentially all possible orientations of the crystal are represented by the powder sample, so every crystal plane is

simultaneously exposed to the X-ray beam in an orientation that satisfies the Bragg Equation (at the correct 2θ angle). The diffracted beams are in the direction of a number of cones centred around the incident and transmitted X-ray beam and so the spots form concentric circles of different 2θ values. A narrow cross section of these rings appears as a set of lines which is scanned by a detector and the data is presented as a graph of diffracted intensity against the angle 2θ. Thus, the diffraction pattern is a one-dimensional projection of part of the three-dimensional reciprocal lattice(s) of the crystallites, as illustrated in Figure 2.4. The shape of the peak relates to both experimental features and to sample features such as the crystallite size. The positions of the peaks are determined by the size, shape, and symmetry of the unit cell, and the peak intensities are determined by the atomic structure; this gives rise to a unique and characteristic pattern for every crystalline material and phase. Therefore, PXRD is extremely useful for the identification of phases in a sample. A crystalline sample can be ground into a powder and the resulting pattern can be compared to the patterns of the starting materials, datasets of known materials, or the simulated PXRD pattern of a single crystal from the sample under investigation for which the crystal structure has been solved. This comparison highlights whether the single crystal is representative of the bulk product or not, and what other materials may be present. In this work, PXRD is used solely to qualitatively asses the bulk sample composition, complementing the data obtained from scXRD.

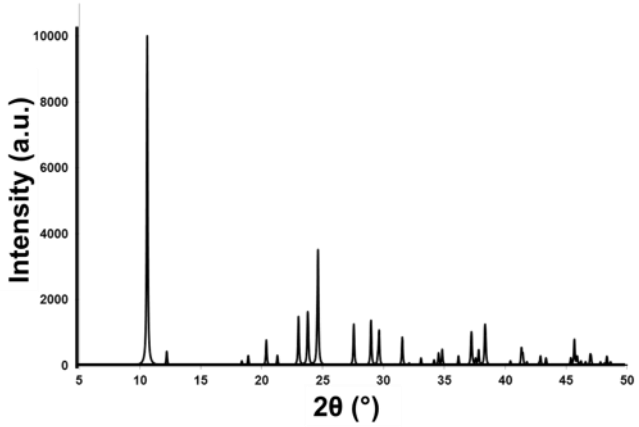

Figure 2.4. Example of a PXRD pattern showing peaks at specific values of 2θ.

PXRD is also a very useful technique to determine the degree of crystallinity of a sample or to study materials under non-ambient conditions (for example to look at a phase transformation as a function of temperature). For very high quality data collected under precisely controlled experimental conditions, quantitative information can be obtained regarding the sample composition and the crystallite size. When single crystals of the

material of interest cannot be grown in sufficient size and/or quality, but high quality PXRD data is available and an initial structural model can be deduced from other materials of known structure, PXRD offers a method by which to determine the crystal structure using Rietveld refinement.

2.2. Thermal Analysis

2.2.1. Differential Scanning Calorimetry (DSC)

DSC is a commonly applied thermoanalytical technique. The method is concerned with the measurement of energy changes upon heating or cooling the sample under investigation. In heat-flux DSC, the variant used in this work, the sample is placed in an aluminium pan, and an empty pan is used as the reference. The pans are inside a furnace, purged with an inert gas (Figure 2.5) and are connected by a very good heat flow path. The pans are subjected to a temperature ramp from the heat-flux plate below which adjusts the relative heat flows to keep the temperatures of the two pans as closely matched as possible throughout the experiment. Any difference in temperature between the sample and the reference, caused by enthalpy changes in the sample, is monitored. This temperature difference is proportional to the heat-flux difference between the pans.[155] The output of DSC analysis is represented as a DSC trace showing the energy difference, or heat flow, (expressed in mW) plotted against temperature (Figure 2.6). The DSC trace indicates the nature of the physical or chemical phenomena which may occur within the sample. Endothermic events such as a phase transition or melt, and exothermic events such as crystallisation, can be identified. DSC is frequently used in purity analysis, as separate components within a sample would be expected to have different melting points. The presence of different polymorphs can also be established (at least qualitatively) by identification of separate melting events. In this work, DSC is often used to record melting points of samples, and to give an indication as to their composition, as sometimes it is possible to identify excess starting materials by their melting points. DSC is used to explore the sample's thermal behaviour, and is often used in conjunction with hot stage microscopy (HSM).

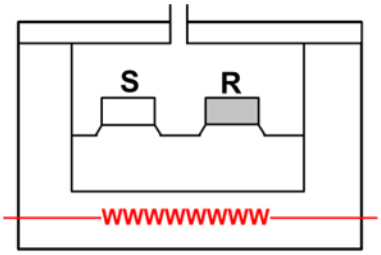

Figure 2.5. Schematic diagram of the heat-flux DSC apparatus, illustrating the sample (S) and the reference (R) materials.

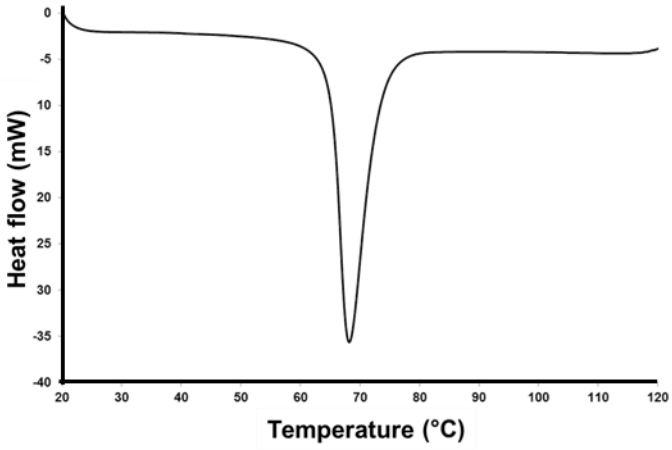

Figure 2.6. Example of a DSC trace showing an endothermic event (melt) at about 70 °C.

2.2.2. Hot Stage Microscopy (HSM)

HSM is a thermoanalytical technique combining microscopy with thermal analysis to visually record the behaviour of a material subjected to a controlled heating programme to allow the physical characterisation of a material as a function of temperature.[156] In this work, HSM is often used to determine the melting points, or at least melting ranges, of materials. Since the technique is generally applied to single crystals for which the crystal structure has been determined, it is helpful in unambiguously assigning the source of any melting events observed during DSC. However, the information obtained from HSM and DSC often do not correspond, indicating that the single crystal used for HSM is not representative of the bulk sample, in much the same way as the complementary information acquired from scXRD and PXRD can be used to qualitatively determine sample purity. HSM is also very useful to visualise and record events such as a colour change, phase transformation or recrystallisation from a melt and if the crystal is enclosed in inert oil, solvent evolution may be observed.

2.2.3. Thermogravimetric Analysis (TGA)

TGA is a common thermoanalytical technique in which a sample inside a sample holder pan is placed on a sensitive electromagnetic balance within a furnace, under an inert atmosphere. The sample is heated at a controlled rate and the loss in mass of the sample, relative to the initial mass, is recorded. The output of TGA analysis is represented as a thermogravimetric curve of sample mass, as a percentage of the initial mass, plotted against temperature. The trace features plateaus and steps indicating no change in weight, and mass loss, respectively. TGA is useful to determine at what temperature gaseous components may be lost from the sample, or to indicate the solvent content and the nature of that solvent since absorbed and constitutional solvent are likely to be lost at different temperatures.[155]

2.3. Elemental Analysis (CHN)

Elemental analysis is a technique used to determine the mass fractions of the elements carbon, hydrogen, nitrogen (hence 'CHN' analysis), and sometimes sulphur and halogens, to give information of the composition of a sample. The sample is placed inside a tin capsule and ignited inside a combustion reactor. The gaseous products are transported by a stream of carrier gas into a separation column and a thermal conductivity detector measures the concentrations of the elements.[157, 158]

2.4. Infrared (IR) Spectroscopy

IR spectroscopy can be used to obtain structural information about molecules contained within a sample by the identification of chemical bonds and functional groups. Chemical bond vibrations such as stretching and bending, which result in a change in the dipole moment, are excited by IR radiation. An IR spectrum of a sample is recorded by measuring the absorbance of the incident IR radiation, with a wavenumber range of about 400 – 4000 cm^{-1}. The absorbance value is calculated as a ratio of the measured intensity of the reference spectra such that the output spectrum of IR analysis is represented as % transmittance against the wavenumber of the radiation. The spectrum displays absorption bands at specific wavenumbers indicative of specific chemical bonds. For example, in this work, IR spectroscopy has been used to investigate the C=O stretching vibration of a carboxyl group, which is expected to appear as a strong absorption band between 1725 – 1665 cm^{-1}.[159]

Every molecule has many different ways in which to vibrate to absorb energy generating many absorption bands which gives rise to a fingerprint region at wavenumbers lower than about 1500 $cm^{-1.}$ The absorption bands in this region are unique to every polyatomic molecule since IR spectra are sensitive to the mass and structural differences between different molecules, and even different isomers, thus this region is very useful in positively identifying a compound when compared to spectra of known compounds stored on a database.[155]

2.5. Mass Spectrometry (MS)

MS is a sensitive technique for the analysis and identification of unknown compounds by determination of the structure, elemental composition, molecular mass, and formula. The instrument used to carry out MS is a mass spectrometer. Depending on the technique that is used, the sample is introduced as a solid or liquid first into a high vacuum region, or into an atmospheric ion source. Ionisation occurs by electron or chemical ionisation, and the ions are accelerated into the mass analyser, such as a quadrupole ion trap or time-of-flight mass analyser, within a high vacuum system. In quadrupole mass analysis the ions enter a quadrupole mass filter and oscillate in a plane perpendicular to oppositely charged rods. The ions are subsequently separated according to their *m/z*, in that ions of a particular *m/z* reach the detector at particular values of the DC and AC potentials. An electron multiplier detects the ions that pass through the mass analyser by measurement and amplification of the current induced by the collision of energetic particles with a dynode. The output of MS analysis is a mass spectrum showing the relative ion intensity (%) plotted against *m/z* and molecular fragments can be identified by matching the detected isotope pattern to the expected isotope pattern. In this work, MS is used to analyse the composition of a powder material, to determine if the target complex may have formed.[155]

Chapter 3. Experimental

3.1. Techniques and Instrumentation

3.1.1. Single Crystal X-Ray Diffraction (scXRD)

All of the structures presented in this work were determined from single crystal X-ray diffraction data using one of two laboratory diffractometers. Data were collected on a Rigaku R-axis/RAPID image plate diffractometer ("the Rigaku") at 100 K (unless otherwise stated) and the temperature was controlled using Oxford Cryosystems Cryostream low temperature device. Data were also collected on an Agilent Technologies Gemini A Ultra CCD diffractometer ("the Gemini") at 150 K, using an Oxford Diffraction Cryojet. Both diffractometers are equipped with graphite-monochromated MoK_α radiation (λ = 0.71073 Å) and operate at 50 kV and 40 mA.

Sample Selection

The content of the relevant sample vial was inspected under the microscope and crystals removed and placed in a small drop of inert oil (fomblin) on a glass slide. For diffraction, it was desirable to select good quality crystals with smooth faces and defined edges. The crystals were analysed under plane-polarised light to check for twinning. Single crystals displayed uniform optical extinction upon being rotated by 90°. The linear dimensions of the crystal should have been no longer than 0.5 mm as this is usually the maximum width of the uniform part of the X-ray beam. An ideal crystal had dimensions between 0.2 mm and 0.5 mm, but often platelet crystals with depths less than 0.1 mm were used if no more suitable crystals could be found. If necessary, crystals were cut to an appropriate size with a scalpel.

Unit Cell Determination

The crystal chosen for diffraction was either coated in fomblin or dabbed with a small amount of silicone grease and mounted on a glass fibre (if using the Rigaku) or a nylon loop (if using the Gemini), which was attached to the goniometer head. The position of the goniometer head was adjusted to ensure that the crystal remained centred in the X-ray beam at all orientations. A set of preliminary diffraction patterns were collected by exposure at different orientations to give a provisional unit cell and to check the quality of diffraction from the crystal. Four images were collected for this purpose when using the Rigaku,

whereas 15 images were collected on the Gemini on account of the smaller area of the CCD detector. The unit cell was determined by indexing either by the real-space method 'autoindexing' or by the reciprocal space method. During the indexing procedure, generally reflections resulting in spots with an I/σ(I) ≥ of 8 were used to calculate the scattering vectors. The shortest three non-coplanar vectors, assigned as **a***, **b*** and **c***, were selected to define the reciprocal unit cell, and therefore the provisional real-space unit cell. The orientation matrix, which relates the orientation of the reciprocal unit cell to the goniometer axes, was established from the coordinates of the vectors. The *hkl* indices of each vector could be determined to assess the accuracy of the proposed primitive unit cell. A full-matrix least-squares refinement incorporating various experimental corrections was carried out on the reflection list to determine the metric symmetry and the likely crystal system and provide estimated standard uncertainties of the reduced unit cell parameters. After refinement, the corresponding orientation matrix was used to predict the positions of reflections at particular angles. At this point, if the reduced cell parameters matched those of a starting material, a previously determined structure or a structure recorded in the CSD, no further data were collected from the crystal. Otherwise, a data collection strategy was calculated by the diffractometer software according to the symmetry of the proposed unit cell. If there was any doubt regarding the symmetry of the crystal during indexing, a data collection strategy based on the lower symmetry system was chosen; in this case if the crystal were of higher symmetry the equivalent reflections could be merged and there would be ample data for structure solution.

Data Collection

A typical data collection process would collect data up to a 2θ value of 55° to obtain a resolution of 0.77 Å. Often after data collection, reflections beyond a 2θ value of 52.75° were cut to give a data resolution of 0.8 Å and a completeness of close to 100 %. Ideally the data collection strategy would involve recording only the unique reflections therefore using the minimum amount of time, however in order to obtain more reliable data, symmetry-equivalents were often collected and the reflections averaged by merging the datasets. Collecting more data, and therefore increasing the redundancy of the symmetry-equivalent data available is beneficial for a good quality dataset and is useful when confirming the crystal symmetry and correcting data such as by applying absorption corrections. Typically, data collection took in the region of a few hours to about one day depending on the symmetry of the crystal, its diffracting quality, the intensity of the X-ray beam, and to some extent, the amount of time available on the diffractometer. The data were collected on the Rigaku using d*trek and processed using FSPROCESS, both within

the CrystalClear[160] software package. Data were collected and processed on the Gemini using CrysAlisPro.[161]

Data Reduction

After data collection, the raw frames were scanned by the computer software to calculate the intensities of each *hkl* reflection while accounting for background intensity. During the integration process, corrections such as the adsorption, Lorentz and extinction corrections were made. For data collected on the Rigaku, absorption corrections were applied using ABSCOR,[162] whereas for data collected on the Gemini, absorption corrections were applied using SADABS.[163] Finally, the structure factor amplitude was determined for each reflection and an *hkl* file containing all the *h*, *k*, *l* indices, $|F_o|^2$ and the standard uncertainty of each measured reflection intensity, $\sigma(F_o)^2$, was produced for use in structure solution.

Structure Solution and Refinement

(3), **(4)**, **(9)**, **(10)**, **(11)**, **(12)**, **(13)**, **(20)**, **(21)**, **(22)**: Data were collected on a Rigaku R-axis/RAPID image plate diffractometer at 100 K. Structure solution was carried out by direct methods using SHELXS-97[164] and followed by full-matrix least-squares refinement on F^2 using SHELXL-2013[164] within the WinGX software suite.[165] All non-hydrogen atoms were refined anisotropically. H atoms were located in difference Fourier density maps and refined isotropically, unless otherwise stated in the notes below outlining specific refinement details for some structures.

(9): The oxygen atom of the non-coordinated, disordered water molecule (site occupancy factor (s.o.f) = 0.5) was refined isotropically. The aromatic hydrogen atoms were fixed in idealised positions and refined with isotropic thermal parameters riding at 1.2 U_{iso} of the carbon or nitrogen atom to which it is covalently bonded. O-H distance restraints of 0.87 Å, and an H-H distance restraint of 1.39 Å were applied to the non-coordinated, disordered water molecule and the U_{iso} values of the hydrogen atoms were fixed to a value of 1.5 times those of the parent oxygen atoms.

(10): The aromatic hydrogen atoms covalently bonded to carbon atoms were fixed in idealised positions and refined with isotropic thermal parameters riding at 1.2 U_{iso} of the parent carbon. The U_{iso} values of the coordinated water molecules were fixed to a value of 1.5 times those of the parent oxygen atoms.

(12): The aromatic hydrogen atoms were fixed in idealised positions and refined with isotropic thermal parameters riding at 1.2 U_{iso} of the carbon atom to which they are

covalently bonded. The U_{iso} values of the coordinated water molecules were fixed to a value of 1.5 times those of the parent oxygen atoms.

(20): The water molecule displays positional disorder and the oxygen atom was taken to be distributed 50:50 between two possible sites (s.o.f = 0.5). The hydrogen atom H1 is disordered between two possible sites; as the hydroxyl group on the chloranilic acid, H1c, or as part of the water molecule, H1w, (s.o.f = 0.5). The U_{iso} values of the water hydrogen atoms H2 and H2W (s.o.f = 0.5), were fixed to a value of 1.5 times those of the parent oxygen atoms.

(1), **(5)**, **(6)**, **(7)**, **(8)**, **(17)**: Data were collected on a Rigaku R-axis/RAPID image plate diffractometer at 100 K, except **(5)** for which data were collected at 110 K. Structure solution was carried out by direct methods using SHELXS-2013[164] and followed by full-matrix least-squares refinement on F^2 using SHELXL-2013[164] within the WinGX software suite.[165] All non-hydrogen atoms were refined anisotropically unless otherwise stated. H atoms were located in difference Fourier density maps and refined isotropically.

(17): The oxygen atom of the disordered, non-coordinated water molecule (s.o.f = 0.5) was refined isotropically. O-H distance restraints of 0.87 Å were applied to all the water molecules, and the U_{iso} values of all the water hydrogen atoms were fixed to a value of 1.5 times those of the parent oxygen atoms.

(14), **(15)**: Data were collected on an Agilent Technologies Gemini A Ultra CCD diffractometer at 150 K. Structure solution was carried out by direct methods using SHELXS-97[164] and followed by full-matrix least-squares refinement on F^2 using SHELXL-2013[164] within the WinGX software suite.[165] All non-hydrogen atoms were refined anisotropically. H atoms were located in difference Fourier density maps and refined isotropically.

(2), **(16)**, **(18)**, **(19)**, **(23)**, **(24)**, **(25)**: Data were collected on an Agilent Technologies Gemini A Ultra CCD diffractometer at 150 K. Structure solution was carried out by direct methods using SHELXS-2013[164] and followed by full-matrix least-squares refinement on F^2 using SHELXL-2013[164] within the WinGX software suite.[165] All non-hydrogen atoms were refined anisotropically. H atoms were located in difference Fourier density maps and refined isotropically unless otherwise stated in the notes below outlining specific refinement details of some structures.

(2): The aromatic hydrogen atoms were fixed in idealised positions and refined with isotropic thermal parameters riding at 1.2 U_{iso} of the carbon or nitrogen atoms to which they are covalently bonded. O-H distance restraints of 0.87 Å were applied to the coordinated water molecules and the U_{iso} values of the coordinated water hydrogen atoms H8A, H8B, H9A and H9B were fixed to a value of 1.2 times those of the parent oxygen atoms.

(16): The aromatic hydrogen atoms were fixed in idealised positions and refined with isotropic thermal parameters riding at 1.2 U_{iso} of the carbon atoms to which they are covalently bonded. O-H distance restraints of 0.83 Å were applied to the coordinated water molecule. N-H distance restraints of 0.91 Å were applied to the ammonium groups. The U_{iso} values of all the water hydrogen atoms were fixed to a value of 1.5 times those of the parent oxygen atoms.

(19): The aromatic hydrogen atoms were fixed in idealised positions and refined with isotropic thermal parameters riding at 1.2 U_{iso} of the carbon atoms to which they are covalently bonded. O-H distance restraints of 0.85 Å were applied to the coordinated water molecules. O-H distance restraints of 0.86 Å were applied to the non-coordinated water molecules. H-H distance restraints of 1.37 Å were applied to all water molecules. The U_{iso} values of all the water hydrogen atoms were fixed to a value of 1.5 times those of the parent oxygen atoms.

(24): The methyl hydrogen atoms were fixed in idealised positions and refined with isotropic thermal parameters riding at 1.5 U_{iso} of the carbon atoms to which they are covalently bonded.

(25): The methyl hydrogen atoms were fixed in idealised positions and refined with isotropic thermal parameters riding at 1.5 U_{iso} of the carbon atoms to which they are covalently bonded.

PLATON[166] was used to verify assigned space groups and calculate geometrical parameters of the planes, H-bonds and π-π stacking interactions observed in the crystal structures. Refined structures were visualised using the crystal structure visualization program Mercury.[167] This was used to create the diagrams of the crystalline complexes presented in this work, for which thermal ellipsoids are set at the 50% probability level.

Table 3.1. Crystal data and structure refinement for **(1)** – **(5)**.

	(1)	**(2)**	**(3)**	**(4)**	**(5)**
Formula	$C_{12}H_{30}Cl_4Mg_2N_2O_{14}$	$C_{24}H_{52}Cl_8Mg_4N_4O_{24}$	$C_{12}H_{18}Ca_2N_6O_{20}$	$C_{12}H_{20}CaCl_2N_2O_9$	$C_{12}H_{18}MgN_4O_{14}$
M/g mol^{-1}	616.86	1161.64	646.26	447.28	466.61
Diffractometer	Rigaku	Gemini	Rigaku	Rigaku	Rigaku
T (K)	100	150	100	100	110
Space group	$P\bar{1}$	$P\bar{1}$	$P\bar{1}$	P $2_1/n$	$P\bar{1}$
a (Å)	8.5861(14)	8.4783(5)	7.1676(12)	14.9988(11)	6.1279(6)
b (Å)	8.6185(18)	9.1139(4)	7.6744(14)	7.5870(6)	8.1151(10)
c (Å)	9.857(2)	16.7213(9)	11.712(2)	16.6975(11)	9.4126(12)
α (°)	94.103(6)	79.473(4)	76.452(6)	90	89.443(5)
β (°)	101.236(5)	79.403(5)	88.434(6)	94.178(2)	86.609(4)
γ (°)	96.954(5)	81.140(4)	67.328(6)	90	88.628(4)
V (Å^3)	706.8(2)	1238.92(12)	576.51(18)	1895.1(2)	467.11(9)
Z	1	1	1	4	1
ρ_{calc} (g cm^{-3})	1.449	1.557	1.862	1.568	1.659
μ (mm^{-1})	0.522	0.585	0.607	0.66	0.181
θ Range (°)	3.04-27.48	2.78-26.23	3.07-27.48	3.01-27.48	3.30-27.48
Reflections collected	16374	10311	7557	23061	11191
Independent	3220	5000	2622	4332	2125
Observed > 2σ(I)	2941	3878	2299	3999	1808
R_{int}	0.0289	0.0329	0.027	0.0219	0.0278
Completeness (%)	99.6	99.9	99.6	99.9	99.9
Parameters	214	349	217	315	178
GooF	1.061	1.029	1.103	1.039	1.090
R_1 (observed)	0.0241	0.0363	0.0243	0.0215	0.0332
R_1 (all)	0.0275	0.0549	0.0303	0.0237	0.0401
wR_2 (all)	0.0598	0.0776	0.0645	0.0583	0.0888
$\rho_{max,min}$ (e Å^{-3})	0.346, -0.164	0.338, -0.325	0.388, -0.247	0.439, -0.191	0.412, -0.300

Table 3.2. Crystal data and structure refinement for **(6)** – **(10)**.

	(6)	**(7)**	**(8)**	**(9)**	**(10)**
Formula	$C_{12}H_{18}MgN_4O_{14}$	$C_{12}H_{18}MgN_4O_{14}$	$C_6H_{11}MgN_3O_{11}$	$C_6H_{15}CaCl_2NO_7$	$C_{12}H_{18}Ca_2N_6O_{20}$
M/g mol^{-1}	466.61	466.61	325.49	324.17	646.48
Diffractometer	Rigaku	Rigaku	Rigaku	Rigaku	Rigaku
T (K)	100	100	100	100	100
Space group	$P\bar{1}$	$P\bar{1}$	P $2_1/n$	C $2/c$	P $2_1/c$
a (Å)	6.9760(12)	4.7079(4)	9.9683(6)	11.484(2)	21.7842(13)
b (Å)	10.184(2)	7.0524(8)	6.8418(3)	16.858(4)	6.6762(4)
c (Å)	13.819(3)	14.1691(17)	18.8376(10)	6.8715(13)	18.7611(11)
α (°)	80.832(7)	94.124(4)	90	90	90
β (°)	83.325(6)	91.235(3)	103.938(2)	91.679(7)	114.523(4)
γ (°)	77.664(5)	102.963(3)	90	90	90
V (Å^3)	943.4(3)	456.92(9)	1246.92(11)	1329.7(5)	2482.4(3)
Z	2	1	4	4	4
ρ_{calc} (g cm^{-3})	1.643	1.696	1.734	1.619	1.73
μ (mm^{-1})	0.180	0.186	0.211	0.894	0.563
θ Range (°)	3.00–27.48	3.20-27.48	3.18-27.48	3.55-27.49	3.02-27.49
Reflections collected	22236	10795	15569	15122	29544
Independent	4289	2072	2829	1516	5570
Observed > 2σ(I)	3075	1805	2318	1349	4089
R_{int}	0.0463	0.021	0.0387	0.0323	0.058
Completeness (%)	99.8	99.8	99.4	99.8	98.8
Parameters	352	178	234	101	393
GooF	1.226	1.119	1.102	1.143	1.166
R_1 (observed)	0.0341	0.0277	0.0381	0.0262	0.0401
R_1 (all)	0.0583	0.0324	0.0471	0.0308	0.069
wR_2 (all)	0.0994	0.0751	0.0970	0.0573	0.1145
$\rho_{max,min}$ (e Å^{-3})	0.409, -0.343	0.306, -0.224	0.283, -0.301	0.679, -0.376	0.569, -0.626

Table 3.3. Crystal data and structure refinement for **(11)** – **(15)**.

	(11)	**(12)**	**(13)**	**(14)**	**(15)**
Formula	$C_{24}H_{36}Ca_3Cl_6N_4O_{16}$	$C_{12}H_{18}Ca_2Cl_2N_2O_9$	$C_{12}H_{10}CaCl_2N_2O_4$	$C_{12}H_8CaN_2O_4$	$C_{56}H_{62}N_8O_{10}$
M/g mol^{-1}	969.51	485.34	357.22	284.28	1007.13
Diffractometer	Rigaku	Rigaku	Rigaku	Gemini	Gemini
T (K)	100	100	100	150	150
Space group	$P\bar{1}$	I2	I 2/*a*	P $2_1/n$	C 2/*c*
a (Å)	8.2553(16)	6.1121(6)	8.5775(16)	9.0083(4)	21.1041(13)
b (Å)	8.7190(14)	7.1782(10)	9.6486(15)	16.8243(5)	7.1108(4)
c (Å)	14.734(3)	21.865(3)	17.671(4)	9.0574(5)	33.841(2)
α (°)	75.820(5)	90	90	90	90
β (°)	85.328(6)	93.652(8)	96.775(9)	119.649(7)	105.360(7)
γ (°)	84.474(5)	90	90	90	90
V (Å^3)	1021.6(3)	957.3(2)	1452.3(5)	1193.00(12)	4897.0(6)
Z	1	2	4	4	4
ρ_{calc} (g cm^{-3})	1.576	1.684	1.634	1.583	1.366
μ (mm^{-1})	0.865	0.923	0.815	0.537	0.095
θ Range (°)	3.09-27.48	3.41-27.48	3.19-27.49	2.87- 26.23	3.04-26.2
Reflections collected	25214	6187	9223	12585	15270
Independent	4676	2172	1667	2407	4925
Observed > 2σ(I)	4351	1807	1359	2049	3737
R_{int}	0.0327	0.034	0.0844	0.0392	0.0373
Completeness (%)	99.8	99.5	99.9	99.9	99.9
Parameters	313	139	117	204	458
GooF	1.05	1.128	1.124	1.042	1.021
R_1 (observed)	0.0212	0.0259	0.0536	0.0298	0.0425
R_1 (all)	0.0234	0.0432	0.0642	0.0396	0.0641
wR_2 (all)	0.0540	0.0658	0.1397	0.0688	0.0948
$\rho_{max,min}$ (e Å^{-3})	0.394, -0.195	0.474, -0.373	0.890, -0.549	0.300, -0.247	0.273, -0.215

Table 3.4. Crystal data and structure refinement for **(16)** – **(20)**.

	(16)	**(17)**	**(18)**	**(19)**	**(20)**
Formula	$C_{22}H_{24}CuN_4O_{10}$	$C_7H_{12}MgNO_{8.5}$	$C_7H_7MgNO_6$	$C_{14}H_{28}Mg_2N_2O_{19}$	$C_{18}H_{16}Cl_2N_2O_{10}$
M/g mol^{-1}	567.99	270.49	225.45	577.06	491.23
Diffractometer	Gemini	Rigaku	Gemini	Gemini	Rigaku
T (K)	150	100	150	150	100
Space group	$P\bar{1}$	P $2_1/c$	P $2_1/c$	$P\bar{1}$	P $2_1/c$
a (Å)	9.1890(6)	9.5610(8)	8.3533(4)	7.0638(6)	15.091(3)
b (Å)	9.6577(5)	8.3362(6)	10.1625(4)	8.9852(8)	3.6548(5)
c (Å)	13.4738(10)	13.9891(10)	10.1408(4)	9.6628(12)	17.587(3)
α (°)	83.393(5)	90	90	83.104(9)	90
β (°)	71.988(6)	102.135(7)	104.147(4)	75.593(9)	101.753(5)
γ (°)	77.606(5)	90	90	83.597(7)	90
V (Å^3)	1109.10(13)	1090.05(15)	834.75(6)	587.58(11)	949.6(3)
Z	2	4	4	1	2
ρ_{calc} (g cm^{-3})	1.701	1.648	1.794	1.631	1.718
μ (mm^{-1})	1.055	0.201	0.223	0.198	0.408
θ Range (°)	2.89-26.23	3.28–27.48	2.88-29.66	2.99-29.75	3.25-27.49
Reflections collected	8366	13467	4206	7669	9065
Independent	4460	2498	1991	7669	2176
Observed > 2σ(I)	3484	1414	1678	4917	1783
R_{int}	0.0370	0.0834	0.0326	0.0485	0.0556
Completeness (%)	99.8	99.9	99.9	99.9	99.4
Parameters	386	200	164	210	187
GooF	1.039	1.135	1.059	1.078	1.071
R_1 (observed)	0.0408	0.0787	0.0381	0.0627	0.0355
R_1 (all)	0.0603	0.1317	0.0485	0.1042	0.0458
wR_2 (all)	0.0873	0.2809	0.0893	0.1925	0.0883
$\rho_{max,min}$ (e Å^{-3})	0.410, -0.469	0.576, -0.851	0.487, -0.297	0.615, -0.856	0.597, -0.282

Table 3.5. Crystal data and structure refinement for **(21)** – **(25)**.

	(21)	**(22)**	**(23)**	**(24)**	**(25)**
Formula	$C_{18}H_{12}Cl_2N_2O_8$	$C_{18}H_{12}Cl_2N_2O_8$	$C_{18}H_{12}Cl_2Cu_2N_2O_{10}$	$C_{16}H_{16}CaCl_4N_2O_8$	$C_{30}H_{42}Ca_2Cl_4N_6O_{14}$
M/g mol^{-1}	455.20	455.20	614.28	546.19	932.65
Diffractometer	Rigaku	Rigaku	Gemini	Gemini	Gemini
T (K)	100	100	150	150	150
Space group	P $2_1/c$	P $2_1/n$	P$\bar{1}$	I $4_1/a$	P$\bar{1}$
a (Å)	13.934(2)	3.8675(2)	6.1624(4)	8.7092(3)	9.3514(10)
b (Å)	5.0186(6)	20.6622(8)	8.6804(6)	8.7092(3)	14.4656(14)
c (Å)	14.5084(15)	10.8360(8)	10.4701(9)	28.9919(11)	16.3045(18)
α (°)	90	90	99.311(6)	90	82.136(9)
β (°)	118.424(9)	92.608(7)	95.125(6)	90	73.721(10)
γ (°)	90	90	110.541(7)	90	80.081(9)
V (Å^3)	892.3(2)	865.02(8)	511.04(7)	2199.04(17)	2076.3(4)
Z	2	2	1	4	2
ρ_{calc} (g cm^{-3})	1.694	1.748	1.996	1.65	1.492
μ (mm^{-1})	0.419	0.432	2.406	0.818	0.601
θ Range (°)	3.19-27.48	3.51-27.48	2.90-26.23	2.81-27.09	2.86-29.38
Reflections collected	11238	10727	3779	3253	22293
Independent	2046	1958	3779	1203	9713
Observed > 2σ(I)	1845	1774	1686	995	5122
R_{int}	0.0564	0.0209	0.037	0.0445	0.0932
Completeness (%)	99.9	99.8	99.8	99.9	99.9
Parameters	160	160	178	75	541
GooF	1.069	1.118	1.069	1.312	1.073
R_1 (observed)	0.0415	0.0258	0.0448	0.1021	0.0812
R_1 (all)	0.0461	0.0285	0.0587	0.1175	0.1686
wR_2 (all)	0.1036	0.0698	0.0951	0.2449	0.1846
$\rho_{max,min}$ (e Å^{-3})	0.385, -0.438	0.376, -0.175	0.804, -0.479	0.843, -0.554	0.661, -0.519

3.1.2. Powder X-Ray Diffraction (PXRD)

The crystallisation preparations described above did not always result in a homogeneous product, and a single crystal for which the crystal structure was determined was not necessarily, and very often clearly not, representative of the bulk sample. For sample preparations in which the solvent was allowed to evaporate completely, single crystals of the product were commonly accompanied by powder, precipitate, oil or low quality crystals of potentially multiple crystalline forms. These unknown materials could be residual starting materials, hydrates, solvates or polymorphs of either or all starting materials or side products. In order to identify such materials, for the preparations resulting in a new crystalline complex as identified by single crystal XRD, the bulk sample was also analysed by PXRD where possible. This allowed qualitative assessment of the phase purity of the new complex by comparing its PXRD pattern calculated from the single crystal data, to the experimentally obtained PXRD pattern. The PXRD patterns of known starting materials or related complexes could also be compared against the experimental pattern to establish the composition of the bulk sample.

PXRD was carried out by removing as much of the sample as possible and grinding it into a homogeneous powder using a mortar and pestle. In some cases this did not yield a powder but rather a wet and sometimes sticky substance. If this occurred the mortar was placed in the drying oven at 50 °C to remove solvent from the sample. In a few cases this did not result in a dry powder and the sample could not be analysed by PXRD. In some cases where solvent was present in the vial containing the sample under investigation, either due to the vial being sealed or the solvent having not fully evaporated, the crystals were removed from the mother liquor and dried by either placing them in the mortar for a few minutes, placing them in the oven, or by squeezing dry in paper towel.

PXRD was carried out using a Bruker D8 Advance diffractometer equipped with graphite monochromated CuK_α radiation (λ = 1.5406 Å). Data were collected in the 2θ range 5–50°. Both transmission and reflection configurations were used. When using the transmission configuration, the sample was ground into a fine powder and inserted into a glass capillary tube which was mounted in the diffractometer and carefully centred. Data were collected with a scan rate of 2° min^{-1} and the capillary was rotated during the collection to minimise the effects of any preferred orientation. When using the reflection configuration, the finely powdered sample was placed on a small square cut from a glass slide and flattened with another glass slide or spatula, which was attached to the standard flat plate sample holder with a small piece of plasticine. Data were collected with a scan rate of 2.6° min^{-1} and the sample holder was rotated during the collection.

Capillary mode was used to obtain the PXRD pattern of the following starting materials and products:

Calcium(II) nitrate tetrahydrate, calcium(II) acetate hydrate, magnesium(II) nitrate hexahydrate, picolinic acid, isonicotinic acid, 2,4-pyridinedicarboxylic acid monohydrate, **(3)**, **(4)**, **(5)**, **(6)**, **(10)**, **(20)** (2:1), **(I4)**, **(9)**.

Flat-plate mode was used to obtain the PXRD pattern of all other starting materials and products.

3.1.3. Differential Scanning Calorimetry (DSC)

DSC was performed to analyse the thermal behaviour of the bulk sample. Heat flux DSC measurements were carried out using a TA Instruments Q20 DSC system. A 1–5 mg sample was weighted out from the sample vial from which single crystals were obtained. The sample was heated from ambient temperature at a rate of 10 °C min^{-1}, to 500 °C or until initial decomposition was observed. Melting points were derived from the onset point of endothermic events using the TA Universal Analysis software and are quoted to one decimal place.

3.1.4. Hot stage Microscopy (HSM)

Hot stage microscopy was used to determine the melting points of new materials and to qualitatively analyse thermal behaviour. HSM was performed using a Mettler Toledo FP82HT hot stage instrument. A single crystal for which the unit cell had been determined, or was identifiable by its characteristic appearance, was placed in a small drop of fomblin on a glass slide, covered with a thin glass slide cover, and fitted into the heating chamber. The sample was heated at a rate of 10 °C min^{-1}, (or occasionally 5 °C min^{-1}) to 350 °C or until the crystal melted.

3.1.5. Thermogravimetric Analysis (TGA)

TGA was performed on a Perkin Elmer precisely TGA 400 Thermogravimetric Analyser at the University of Bath. Samples were heated at 10 °C min^{-1} under a 20 mL min^{-1} flow of nitrogen gas.

3.1.6. Elemental Analysis (CHN)

Elemental analyses for carbon, nitrogen and hydrogen were performed by the Elemental Analysis service at London Metropolitan University using a Thermo Scientific (Carlo Erba) Flash 2000 Elemental Analyser, configured for % CHN.

3.1.7. Infrared spectroscopy (IR)

IR spectroscopy was carried out at the University of Bath. IR spectra were recorded for the neat sample using a Perkin Elmer precisely Spectrum 100 FT-IR Spectrometer fitted with a Universal ATR sampling accessory. Spectra were recorded at ambient temperature in the region 4000 – 650 cm^{-1}. The following abbreviations are used: w (weak), m (medium), s (strong) and b (broad).

3.1.8. Mass Spectrometry (MS)

MS was performed on samples dissolved in water or methanol on an Electrospray Quadrupole Time-of-Flight mass spectrometer (ESI-QTOF) in both positive and negative ion modes at the University of Bath. MS was also performed on a Thermofisher LTQ Orbitrap XL on solid samples by APCI (atmospheric pressure chemical ionisation) using ASAP (atmospheric solids analysis probe) and dissolved in methanol using negative nanospray, at the EPSRC National Mass Spectrometry Facility (NMSF) in Swansea, UK. Identification of ions was based on detected isotope patterns that mimicked the expected isotope pattern.

3.2. Sample preparation

All chemicals and solvents were purchased from Sigma-Aldrich, except from calcium(II) nitrate tetrahydrate, which was obtained from Alfa Aesar. All chemicals were used without further purification and all solvents were of reagent grade quality. The most commonly used method for crystal growth was the slow evaporation of solvent at set temperatures. Generally, the reagents/starting materials were weighed into 7 mL glass vials and dissolved in appropriate solvent(s) before combining, or dissolved together in the same vial. Generally, approx. 2 mL of solvent was initially added to the reagent(s) and the solvent was added dropwise thereafter until the reagent(s) dissolved in the minimum volume of solvent. Very often sonication with gentle heating was required to aid dissolution. The vial was covered with a hole-pierced lid and the contents allowed to evaporate and crystallise at a

set temperature. At 30 °C, 40 °C and 50 °C, the temperature was controlled using a hot-plate with custom DrySyn® adaptor, for experiments carried out at 4 °C the samples were placed in a fridge. For laboratory (room) temperature experiments, the samples were stored on an open shelf (termed the crystallisation shelf hereafter) and subject to small ambient temperature fluctuations, but were maintained at approximately 18 °C. Often the solvent evaporated completely but sometimes crystals were removed from the mother liquor for analysis once they were discovered to be present.

Frequently, different crystallisation experiments with the same reagent combination resulted in the same single crystal product, as confirmed by scXRD on samples from each vial.

3.2.1. Complexes in Chapter 4

Crystals of $[Mg(C_6H_5NO_2)(H_2O)_4]_2.4Cl.2H_2O$ **(1)** were prepared by adding an ethanol solution (approx. 2 mL) of picolinic acid (15 mg, 0.122 mmol, 123.11 g mol^{-1}) to a methanol solution (approx. 2 mL) of magnesium(II) chloride (12 mg, 0.126 mmol, 95.22 g mol^{-1}). The two solutions were combined by vortex mixing and solvent evaporation took place at lab temperature. After eight months the solvent had evaporated and clear, colourless, cuboidal crystals had formed.

(1) was also produced using the same reagent quantities as above by adding a dichloromethane (DCM) solution (approx. 2 mL) of picolinic acid to an aqueous solution (approx. 2 mL) of magnesium(II) chloride. The two solutions were combined by vortex mixing and solvent evaporation took place at lab temperature. Analysis found (calculated): C, 23.28 (23.36); H, 5.03 (4.91); N, 4.46 (4.54).

Crystals of $2[Mg(C_6H_5NO_2)(H_2O)_4]_2.8Cl$ **(2)** were prepared by adding an ethanol solution (approx. 2 mL) of nicotinic acid (15 mg, 0.122 mmol, 123.11 g mol^{-1}) to an ethanol solution (approx. 2 mL) of magnesium(II) chloride (12 mg, 0.126 mmol, 95.22 g mol^{-1}). The two solutions were combined by vortex mixing and solvent evaporation took place at lab temperature. After 26 months, the solvent had evaporated and shards of a clear, colourless crystalline material had formed.

(2) was also produced using the same reagent quantities as above by:

(i) Adding an isopropanol solution (approx. 2 mL) of nicotinic acid to an aqueous solution (approx. 2 mL) of magnesium(II) chloride. The two solutions were combined by vortex mixing and solvent evaporation took place at lab temperature.

(ii) Adding a tetrahydrofuran (THF) solution (approx. 2 mL) of nicotinic acid to an aqueous solution (approx. 2 mL) of magnesium(II) chloride. The two solutions were combined by vortex mixing and solvent evaporation took place at lab temperature.

(iii) Adding an ethyl acetate solution (approx. 2 mL) of nicotinic acid to an aqueous solution (approx. 2 mL) of magnesium(II) chloride. The two solutions were combined by vortex mixing and solvent evaporation took place at lab temperature.

(iv) Adding an isopropanol solution (approx. 2 mL) of nicotinic acid to an ethanol solution (approx. 2 mL) of magnesium(II) chloride. The two solutions were combined by vortex mixing and solvent evaporation took place at lab temperature.

Crystals of *$[Ca(C_6H_5NO_2)(H_2O)_2(NO_3)_2]_2$* **(3)** were prepared by adding an isopropanol solution (approx. 2 mL) of nicotinic acid (13 mg, 0.106 mmol, 123.11 g mol^{-1}) to an isopropanol solution (approx. 2 mL) of calcium(II) nitrate tetrahydrate (24 mg, 0.102 mmol, 236.15 g mol^{-1}). The two solutions were combined by vortex mixing and crystal growth took place at 4 °C. As in the solvent evaporation crystallisation experiments, the lid of the vial was pierced with holes. After five months, small, clear, colourless, very thin platelet crystals had formed in solution.

(3) was also formed using the same reagent quantities as above, and under the same conditions, except using acetone as the solvent in place of isopropanol.

Crystals of *$[Ca(C_6H_5NO_2)_2(H_2O)_5].2Cl$* **(4)** were prepared by adding an isopropanol solution (approx. 2 mL) of nicotinic acid (25 mg, 0.203 mmol, 123.11 g mol^{-1}) to an isopropanol solution (approx. 2 mL) of calcium(II) chloride (23 mg, 0.207 mmol, 110.99 g mol^{-1}). The two solutions were combined by vortex mixing and crystal growth took place at 4 °C. As in the solvent evaporation crystallisation experiments, the lid of the vial was pierced with holes. After four months a very large, clear, colourless, cuboidal crystal had formed in solution.

(4) was also formed by adding a THF solution (approx. 2 mL) of nicotinic acid (25 mg, 0.203 mmol, 123.11 g mol^{-1}) to an acetonitrile (ACN) solution (approx. 2 mL) of calcium(II) chloride (11 mg, 0.099 mmol, 110.99 g mol^{-1}). The two solutions were combined by vortex mixing and crystal growth took place at 4 °C. Again, the lid of the vial was pierced with holes.

Crystals of *$[Mg(C_6H_5NO_2)_2(H_2O)_4].2NO_3$* **(5)** were prepared by dissolving isonicotinic acid (15 mg, 0.122 mmol, 123.11 g mol^{-1}) and magnesium(II) nitrate hexahydrate (31 mg,

0.121 mmol, 256.41 g mol^{-1}) in approx. 5 mL isopropanol. The solution was mixed by vortex mixing and solvent evaporation took place at 50 °C. After two weeks the solvent had evaporated and a clear, colourless crystalline material had formed.

(5) was also produced using the same reagent quantities as above by adding an aqueous solution (approx. 2 mL) of isonicotinic acid to a methanol solution (approx. 2 mL) of magnesium(II) nitrate hexahydrate. The two solutions were combined by vortex mixing and solvent evaporation took place at lab temperature.

Crystals of $[Mg(C_6H_5NO_2)_2(H_2O)_4].2NO_3$ **(6)** were prepared by adding a DCM solution (approx. 2 mL) of picolinic acid (15 mg, 0.122 mmol, 123.11 g mol^{-1}) to an acetone solution (approx. 2 mL) of magnesium(II) nitrate hexahydrate (31 mg, 0.121 mmol, 256.41 g mol^{-1}). The two solutions were combined by vortex mixing, then the vial was uncapped and solvent evaporation took place in the fume hood at lab temperature. Small, clear, colourless crystals formed overnight.

(6) was also produced using the same reagent quantities as above by:

(i) Adding a DCM solution (approx. 2 mL) of picolinic acid to an acetone solution (approx. 2 mL) of magnesium(II) nitrate hexahydrate. The two solutions were combined by vortex mixing and solvent evaporation took place at lab temperature (using the usual hole-pierced lid on the vial).

(ii) Adding a DCM solution (approx. 2 mL) of picolinic acid to an acetone solution (approx. 2 mL) of magnesium(II) nitrate hexahydrate. The two solutions were dissolved by gentle shaking before combining and solvent evaporation took place at lab temperature (using the usual hole-pierced lid on the vial).

(iii) Adding a DCM solution (approx. 2 mL) of picolinic acid to an acetone solution (approx. 2 mL) of magnesium(II) nitrate hexahydrate. The two solutions were dissolved by sonication before combining and solvent evaporation took place at lab temperature (using the usual hole-pierced lid on the vial).

(6) was also produced by dissolving picolinic acid (32 mg, 0.260 mmol, 123.11 g mol^{-1}) and magnesium(II) nitrate hexahydrate (62 mg, 0.242 mmol, 256.41 g mol^{-1}) in a 25 mL beaker in approx. 10 mL DCM and approx. 10 mL acetone. The solution was mixed by sonication and solvent evaporation took place in the fume hood at lab temperature. The beaker was covered with hole-pierced parafilm.

Crystals of *[Mg($C_6H_5NO_2$)$_2$(H_2O)$_2$].2NO_3.2H_2O* **(7)** were prepared by adding a DCM solution (approx. 2 mL) of picolinic acid (15 mg, 0.122 mmol, 123.11 g mol^{-1}) to an acetone solution (approx. 2 mL) of magnesium(II) nitrate hexahydrate (31 mg, 0.121 mmol, 256.41 g mol^{-1}). The two solutions were combined by vortex mixing and solvent evaporation took place at lab temperature. After one month, the solvent had almost completely evaporated and small, clear, colourless, rounded cuboidal single crystals had formed. The crystals were aggregated around the side of the vial in varying sizes and uniformly distributed in the middle.

(7) was also produced using the same reagent quantities as above by:

(i) Dissolving picolinic acid and magnesium(II) nitrate hexahydrate in approx. 5 mL methanol. The solution was mixed by vortex mixing and solvent evaporation took place at 50 °C.

(ii) Adding an ethyl acetate solution (approx. 2 mL) of picolinic acid to a THF solution (approx. 2 mL) of magnesium(II) nitrate hexahydrate. The two solutions were combined by vortex mixing and solvent evaporation took place at lab temperature.

(iii) Adding an acetone solution (approx. 2 mL) of picolinic acid to an acetone solution (approx. 2 mL) of magnesium(II) nitrate hexahydrate. The two solutions were combined by vortex mixing and solvent evaporation took place at lab temperature.

(iv) Adding a DCM solution (approx. 2 mL) of picolinic acid to an acetone solution (approx. 2 mL) of magnesium(II) nitrate hexahydrate. The two solutions were combined by vortex mixing and crystal growth took place at 4 °C.

(v) Adding a DCM solution (approx. 2 mL) of picolinic acid to an acetone solution (approx. 2 mL) of magnesium(II) nitrate hexahydrate. The two solutions were combined by vortex mixing and solvent evaporation took place at lab temperature to yield **(8)**. Crystals of **(7)** formed following the addition of approx. 3 mL THF to **(8)** and complete evaporation of the solvent at lab temperature.

(7) was also produced by dissolving picolinic acid (30 mg, 0.244 mmol, 123.11 g mol^{-1}) and magnesium(II) nitrate hexahydrate (31 mg, 0.121 mmol, 256.41 g mol^{-1}) in approx. 6 mL methanol. The solution was mixed by vortex mixing and solvent evaporation took place at 50 °C.

(7) was also produced using the same reagent quantities as above by adding a DCM solution (approx. 4 mL) of picolinic acid to an acetone solution (approx. 2 mL) of

magnesium(II) nitrate hexahydrate. The two solutions were combined by vortex mixing and solvent evaporation took place at lab temperature.

(7) was also produced by adding a DCM solution (approx. 2 mL) of picolinic acid (15 mg, 0.122 mmol, 123.11 g mol^{-1}) to an acetone solution (approx. 4 mL) of magnesium(II) nitrate hexahydrate (62 mg, 0.242 mmol, 256.41 g mol^{-1}). The two solutions were combined by vortex mixing and solvent evaporation took place at lab temperature.

(7) was also produced by dissolving picolinic acid (25 mg, 0.203 mmol, 123.11 g mol^{-1}) and magnesium(II) nitrate hexahydrate (52 mg, 0.203 mmol, 256.41 g mol^{-1}) in approx. 7 mL of water. The solution was mixed by vortex mixing and solvent evaporation took place at 40 °C.

Crystals of $[Mg(C_6H_5NO_2)(NO_3)(H_2O)_3].NO_3$ **(8)** were prepared by dissolving picolinic acid (15 mg, 0.122 mmol, 123.11 g mol^{-1}) and magnesium(II) nitrate hexahydrate (62 mg, 0.242 mmol, 256.41 g mol^{-1}) in approx. 7 mL methanol. The solution was mixed by vortex mixing and solvent evaporation took place at 50 °C. After two weeks the solvent had evaporated and a clear, colourless crystalline material had formed around the edges of the vial.

(8) was also produced by adding a chloroform solution (approx. 2 mL) of picolinic acid (15 mg, 0.122 mmol, 123.11 g mol^{-1}) to an aqueous solution (approx. 2 mL) of magnesium(II) nitrate hexahydrate (31 mg, 0.121 mmol, 256.41 g mol^{-1}). The two solutions were combined by vortex mixing and solvent evaporation took place at lab temperature.

(8) was also produced using the same reagent quantities as above by adding a DCM solution (approx. 2 mL) of picolinic acid to an acetone solution (approx. 2 mL) of magnesium(II) nitrate hexahydrate. The two solutions were combined by vortex mixing and solvent evaporation took place at lab temperature.

Note: Solvent evaporation crystallisation experiments of picolinic acid/magnesium(II) nitrate hexahydrate in a 1:1 molar ratio in acetone and DCM were all found to produce **(6)**, **(7)** or **(8)** on different occasions. However, crystals of more than one of the different materials were never recorded to have been found in the same vial.

Crystals of $[Ca(C_6H_5NO_2)(H_2O)_4].2Cl.H_2O$ **(9)** were prepared by dissolving isonicotinic acid (15 mg, 0.122 mmol, 123.11 g mol^{-1}) and calcium(II) chloride (17 mg, 0.153 mmol,

110.99 g mol^{-1}) in approx. 7 mL isopropanol. The solution was mixed by sonication and a 2 mL aliquot was removed and placed in another glass vial. Crystal growth took place from this solution at 4 °C. After sixteen months, shards of a clear, pale yellow crystalline material had formed.

Crystals of *[Ca($C_6H_5NO_2$)(NO_3)$_2$(H_2O)$_2$]$_2$* **(10)** were prepared by adding an acetone solution (approx. 2 mL) of picolinic acid (13 mg, 0.106 mmol, 123.11 g mol^{-1}) to an acetone solution (approx. 2 mL) of calcium(II) nitrate tetrahydrate (24 mg, 0.102 mmol, 236.15 g mol^{-1}). The two solutions were combined by vortex mixing and solvent evaporation took place at lab temperature. After eleven days the solvent had evaporated and a thin, white, platelet featherlike crystalline material was found at the bottom of the vial with clear, slightly yellowish crystals of **(10)** around the side.

Crystals of *[(Ca($C_6H_5NO_2$)(H_2O)$_3$)$_2$Ca($C_6H_5NO_2$)(H_2O)$_2$$Cl_2$].4Cl* **(11)** were prepared by dissolving picolinic acid (15 mg, 0.122 mmol, 123.11 g mol^{-1}) and calcium(II) chloride (18 mg, 0.162 mmol, 110.99 g mol^{-1}) in approx. 5 mL isopropanol. The solution was mixed by sonication and solvent evaporation took place at 50 °C. After one week the solvent had evaporated leaving feathery, clear, colourless crystals on the bottom of the vial with some clear, colourless, chunky crystalline material from which the structure of **(11)** was found.

Crystals of *[Ca_2($C_6H_4NO_2$)$_2$(H_2O)$_5$].2Cl* **(12)** were prepared by adding a DCM solution (approx. 2 mL) of picolinic acid (13 mg, 0.106 mmol, 123.11 g mol^{-1}) to a methanol solution (approx. 2 mL) of calcium(II) chloride (12 mg, 0.108 mmol, 110.99 g mol^{-1}). The two solutions were mixed by sonication and solvent evaporation took place at lab temperature. After 15 months, small, clear, colourless cuboidal crystals were found in a clear, colourless oil.

Crystals of *[Ca($C_6H_5NO_2$)$_2$$Cl_2$]* **(13)** were prepared by adding an isopropanol solution (approx. 2 mL) of nicotinic acid (25 mg, 0.203 mmol, 123.11 g mol^{-1}) to an isopropanol solution (approx. 2 mL) of calcium(II) chloride (23 mg, 0.207 mmol, 110.99 g mol^{-1}). The two solutions were combined by vortex mixing and solvent evaporation took place at 30 °C. After three weeks the solvent had evaporated leaving a white powder precipitate and brittle, clear, colourless platelet crystals.

(13) was also produced using the same reagent quantities as above, and the same solvent, except solvent evaporation took place at lab temperature, 40 °C or 50 °C.

(13) was also formed using the same reagent quantities as before, by adding a DCM solution (approx. 2 mL) of nicotinic acid to an isopropanol solution (approx. 2 mL) of calcium(II) chloride. The two solutions were combined by vortex mixing and solvent evaporation took place at lab temperature.

Crystals of *[Ca($C_6H_4NO_2$)$_2$]* **(14)** were prepared by adding a methanol solution (approx. 2 mL) of nicotinic acid (15 mg, 0.122 mmol, 123.11 g mol^{-1}) to a DCM solution (approx. 2 mL) of calcium(II) acetate hydrate (10 mg, 0.063 mmol, 158.17 g mol^{-1}). The two solutions were combined by vortex mixing and solvent evaporation took place at lab temperature. After two weeks the solvent had evaporated and large, clear, colourless needle crystals had formed.

3.2.2. Complexes in Chapter 5

The 'intermediate' material (reaction of magnesium(II) acetate tetrahydrate and 2,4-pyridine dicarboxylic acid monohydrate) **(I1)**, was prepared by adding a methanol solution (30 mL) of 2,4-pyridine dicarboxylic acid monohydrate (300 mg, 1.795 mmol, 185.13 g mol^{-1}) to an aqueous solution (4 mL) of magnesium(II) acetate tetrahydrate (174 mg, 0.811 mmol, 214.45 g mol^{-1}). The clear solution was stirred at 50 °C and after 30 minutes a white precipitate had formed. The solution was stirred for a further two hours. The obtained white powder was filtered by vacuum filtration and dried in the oven at 100 °C for approximately one hour. Yield: 260 mg. (0.662 mmol, 392.59 g mol^{-1}, 82 %), calculated for $C_{14}H_{12}MgN_2O_{10}$. IR (neat, cm^{-1}): 3274 b, 2800 s, 2446 b, 1904 b, 1691 w, 1640 m, 1608 m, 1562 m, 1482 w, 1427 w, 1352 s, 1272 s, 1244 s, 1232 s, 1186 m, 1091 w, 1018 m, 897 w, 827 w, 766 m, 706 s, 671 s. Analysis found (calculated for $C_{14}H_{12}MgN_2O_{10}$): C, 42.20 (42.83); H, 3.21 (3.09); N, 6.41 (7.14). Mass spectrometry: measured *m/z* of $[M-H]^-$ = 333.0364, expected *m/z* of $C_7H_5NO_4.C_7H_4NO_4$ $[2M-H]^-$ = 333.0364. Measured *m/z* of $[M-H]^-$ = 355.0059, expected *m/z* of $C_{14}H_7MgN_2O_8$ $[M-2H_2O-H]^-$ = 355.0058.

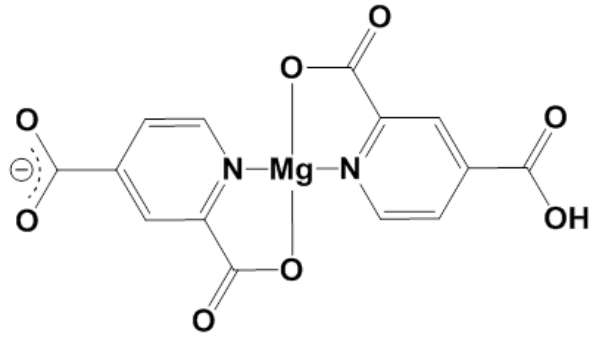

Figure 3.1. Ion identified by MS of **(I1)**: *Pyridine-2,4-dicarboxylate, pyridine-2-carboxylate-4-carboxylic acid-magnesium(II)*, *m/z* 355.0058.

The 'intermediate' material (reaction of magnesium(II) hydroxide and 2,4-pyridine dicarboxylic acid monohydrate) **(I2)**, was prepared by adding a methanol solution (30 mL) of 2,4-pyridine dicarboxylic acid monohydrate (150 mg, 0.810 mmol, 185.13 g mol^{-1}) to an aqueous solution of magnesium(II) hydroxide (47 mg, 0.806 mmol, 58.33 g mol^{-1}). The mixture of the two solutions was white and opaque. The mixture was stirred at 40 °C for about 20 minutes. The obtained flaky white powder was filtered by vacuum filtration, washed with methanol and water, and dried in the oven at 100 °C for one hour. Yield: 58 mg (0.148 mmol, 392.59 g mol^{-1}, 18 %), calculated for $C_{14}H_{12}MgN_2O_{10}$. Mass spectrometry: measured *m/z* of $[M+H]^+$ = 168.0291, expected *m/z* of $C_7H_6NO_4$ $[M+H]^+$ = 168.0238. Measured *m/z* of $[M-C_7H_4NO_4-H_2O+H]^+$ = 208.0032, expected *m/z* of $C_7H_6MgNO_5$ $[M-C_7H_4NO_4-H_2O+H]^+$ = 208.0091.

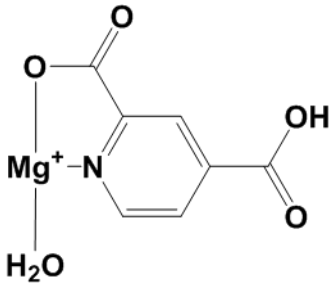

Figure 3.2. Ion identified by MS of **(I2)**: *Pyridine-2-carboxylate-4-carboxylic acid magnesium(II) hydrate*, *m/z* 208.0091.

The 'intermediate' material (reaction of copper(II) sulfate pentahydrate and 2,4-pyridine dicarboxylic acid monohydrate) **(I3)**, was prepared as described by Noro *et al.*,[168] for the synthesis of $C_{14}H_{12}CuN_2O_{10}$, but reduced to 10 % of the original quantities. A methanol solution (30 mL) of 2,4-pyridine dicarboxylic acid monohydrate (334 mg, 1.804 mmol,

185.13 g mol^{-1}) was added to an aqueous solution (5 mL) of copper(II) sulfate pentahydrate (250 mg, 1.001 mmol, 249.69 g mol^{-1}). Combining the two solutions resulted in a blue, opaque mixture. This was stirred at lab temperature for approximately 20 minutes. The obtained bright blue powder was filtered by vacuum filtration, washed with methanol and dried under dynamic vacuum. Yield: 317 mg (0.766 mmol, 413.81 g mol^{-1}, 75 %), calculated for $C_{14}H_{10}CuN_2O_9$. IR (neat, cm^{-1}): 3397 b, 3108 w, 3076 w, 2778 b, 2491 b, 1923 b, 1722 s,1632 s, 1607 s, 1561 m, 1476 w, 1433 w, 1281 s, 1257 s, 1181 s, 1118 w, 1094 m, 1035 m, 989 m, 978 m, 903 m, 874 m, 809 m, 763 s, 720 s, 683 s. Mass spectrometry: measured *m/z* of $[M\text{-}2H_2O\text{-}H]^-$ = 393.9496, expected *m/z* of $C_{14}H_7CuN_2O_8$ $[M\text{-}2H_2O\text{-}H]^-$ = 393.9504.

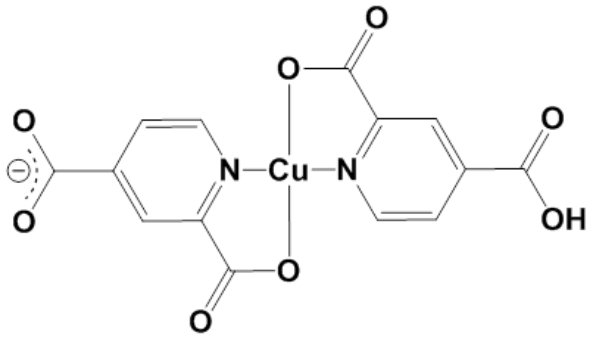

Figure 3.3. Ion identified by MS of **(I3)**: *(Pyridine-2,4-dicarboxylate, pyridine-2-carboxylate-4-carboxylic acid)-copper(II)*, *m/z* 393.9496.

Crystals of $(C_7H_3NO_2)_2(C_{14}H_{17}N_2)_2(C_{14}H_{18}N_2).2H_2O$ **(15)** were prepared by growth from a solution of **(I1)** (20 mg, 0.051 mmol, 392.59 g mol^{-1}) suspended in approx. 4 mL water, with 1 mL dimethylformamide (DMF), 1 mL toluene and a methanol solution of *o*-tolidine (2 mL, 0.0252 mol L^{-1}, 0.050 mmol, 212.29 g mol^{-1}) stirred and heated at 40 °C for about an hour. The vial was covered with hole-pierced parafilm and left in the fume hood. After three days clear, colourless platelet crystals were agglomerated and floating on the surface of the solution and resting at the bottom of the vial.

Crystals of $[Cu(C_7H_3NO_4)_2(H_2O)][C_8H_{14}N_2].H_2O$ **(16)** were prepared by growth from a solution of **(I3)** (22 mg, 0.051 mmol, 431.83 g mol^{-1}) suspended in 2 mL methanol, with 1 mL DMF, 1 mL water, 1 mL acetone and an aqueous solution of *m*-xylylenediamine (1.3 mL, 0.0379 mol L^{-1}, 0.049 mmol, 136.19 g mol^{-1}) stirred and heated at 40 °C for approximately one hour. The vial was sealed with a screw cap and placed in the fume hood. After nine days bright blue prismatic crystals had formed in the similarly blue solution. IR (neat, cm^{-1}): 3540 w, 3076 b, 2900 b, 2125 w, 1648 s, 1609 s, 1547 s, 1473 w, 1375 m, 1335 s, 1272 w,

1258 m, 1186 m, 1080 m, 1036 w, 881 w, 828 w, 807 w, 777 s, 730 s, 687 s. Analysis found (calculated): C, 46.43 (46.52); H, 4.36 (4.27); N, 9.76 (9.87).

The 'intermediate' material (reaction of magnesium(II) nitrate hexahydrate and 2,4-pyridine dicarboxylic acid monohydrate) **(I4)**, was prepared by dissolving 2,4-pyridine dicarboxylic acid monohydrate (15 mg, 0.081 mmol, 185.13 g mol^{-1}) and magnesium(II) nitrate hexahydrate (21 mg, 0.082 mmol, 256.41 g mol^{-1}) in approx. 5 mL methanol. The solution was mixed by vortex mixing and solvent evaporation took place at 30 °C. After six days the solvent had evaporated and a visually homogeneous product of clear, colourless, thin platelet crystals had formed. Single crystal XRD data could not be obtained due to the poor quality of the crystals. IR (neat, cm^{-1}): 2825 w, 2661 w, 2589 w, 2541 w, 1945 w, 1830 w, 1685 s, 1614 s, 1511 w, 1488 m, 1466 s, 1456 m, 1416 m, 1306 s, 1230 m, 1165 m, 1136 m, 1089 m, 918 m, 845 s, 750 s, 688 m.

Crystals of *$[Mg(C_7H_3NO_4)(H_2O)_4].0.5H_2O$* **(17)** were prepared in two steps. The first step involved the preparation of **(I4)**, as described above. The second step involved the addition of an aqueous solution of *m*-xylylenediamine (2.14 mL, 0.0379 mol L^{-1}, 0.081 mmol, 136.19 g mol^{-1}) to the entire product **(I4)** obtained from the first step, dissolved in approx. 4 mL methanol. The two solutions were combined by vortex mixing and solvent evaporation took place at 50 °C. After one week there were small, clear, colourless, rounded platelet crystals floating in solution and the vial was removed from heat and placed in the fume hood. IR (neat, cm^{-1}): 3696 m, 3152 b, 1626 m, 1597 s, 1547 m, 1476 m, 1433 m, 1383 s, 1362 s, 1351 s, 1241 m, 1196 w, 1094 w, 1022 w, 780m, 702 s. Analysis found (calculated): C, 31.19 (31.08); H, 4.48 (4.48); N, 5.34 (5.18).

(17) was also produced by:

(i) Growth from a turbid solution of **(I1)** (20 mg, 0.051 mmol, 392.59 g mol^{-1}) suspended in 4 mL ethanol, with 2 mL DMF, 4 mL water, 1 mL toluene and a methanol solution of *o*-tolidine (2 mL, 0.0252 mol L^{-1}, 0.050 mmol, 212.29 g mol^{-1}) stirred and heated at 40 °C for about an hour. The vial was covered with hole-pierced parafilm and left in the fume hood. After nine weeks small, clear colourless rounded platelet crystals of **(17)** had formed in solution.

(ii) Growth from a turbid solution of **(I1)** (20 mg, 0.051 mmol, 392.59 g mol^{-1}) suspended in 4 mL isopropanol, with 2 mL DMF, 2 mL water and a methanol solution of *o*-tolidine (2 mL, 0.0252 mol L^{-1}, 0.050 mmol, 212.29 g mol^{-1}) stirred and heated at 40 °C for about an hour. The vial was covered with hole-pierced

parafilm and left in the fume hood. After one month, agglomerates of long, clear, colourless, broad crystal shards of **(17)** had formed in solution.

(iii) Growth from a turbid solution of **(I1)** (20 mg, 0.051 mmol, 392.59 g mol^{-1}) suspended in 4 mL ACN, with 2 mL DMF, 2 mL water and a methanol solution of *o*-tolidine (2 mL, 0.0252 mol L^{-1}, 0.050 mmol, 212.29 g mol^{-1}) stirred and heated at 40 °C for about an hour. The vial was covered with hole-pierced parafilm and left in the fume hood. After one month small, clear, colourless needle crystals of **(17)** had formed on the bottom of the vial and also floating in solution.

(iv) Growth from a solution of **(I1)** (10 mg, 0.025 mmol, 392.59 g mol^{-1}) suspended in approx. 2 mL ACN, with 1 mL DMF, 1 mL water, 0.5 mL toluene and an aqueous solution of *m*-xylylenediamine (0.9 mL, 0.0379 mol L^{-1}, 0.034 mmol, 136.19 g mol^{-1}) stirred and heated at 50 °C for about two hours. The vial was sealed with a screw cap and left in the fume hood. After three weeks clear, colourless, flat, rounded crystals of **(17)** had formed in solution.

(v) Growth from a turbid solution of **(I2)** (10 mg) suspended in 1 mL ethanol, with 1 mL DMF, 1 mL water, and an aqueous solution of *m*-xylylenediamine (0.7 mL, 0.0379 mol L^{-1}, 0.027 mmol, 136.19 g mol^{-1}) stirred and heated at 50 °C for about two hours. The vial was sealed with a screw cap and left in the fume hood. After three months, small, rounded, clear, colourless crystals of **(17)** had formed in solution.

(vi) Growth from a turbid solution of **(I2)** (10 mg) suspended in 1 mL THF, with 1 mL DMF, 1 mL water, and an aqueous solution of *m*-xylylenediamine (0.7 mL, 0.0379 mol L^{-1}, 0.027 mmol, 136.19 g mol^{-1}) stirred and heated at 50 °C for about two hours. The vial was sealed with a screw cap and left in the fume hood. After three months, small, rounded, clear, colourless, platelet crystals of **(17)** had formed in solution.

(vii) Growth from a solution of **(I1)** (10 mg, 0.025 mmol, 392.59 g mol^{-1}) and 2,4-pyridine dicarboxylic acid monohydrate (5 mg, 0.027 mmol, 185.13 g mol^{-1}) suspended in approx. 2 mL ACN, with 1 mL DMF, 1 mL water and 0.5 mL toluene stirred at lab temperature for about one hour. The vial was sealed with a screw cap and left in the fume hood. After seven months, small rounded, clear, colourless, platelet crystals of **(17)** had formed in solution.

(viii) Growth from a solution of **(19)** (9 mg, 0.016 mmol, 577.06 g mol^{-1}) dissolved in approx. 2 mL ACN, 1 mL water, and 1 mL dilute acetic acid (1 mL, 0.0312 mol L^{-1}, 0.031 mmol) with a methanol solution of *m*-xylylenediamine (0.41 mL, 0.0379 mol L^{-1}, 0.016 mmol, 136.19 g mol^{-1}) stirred and heated at

50 °C for about two hours. The vial was covered with a two-hole pierced lid and left in the fume hood. After five months, small rounded, clear, colourless, platelet crystals of **(17)** had formed in solution.

(ix) Growth from a solution of **(19)** (10 mg, 0.017 mmol, 577.06 g mol^{-1}) dissolved in approx. 2 mL THF, with 1 mL DMF and 1 mL water with an aqueous solution of *m*-xylylenediamine acidified with acetic acid to about pH 4.11 (0.7 mL, 0.0253 mol L^{-1}, 0.018 mmol, 136.19 g mol^{-1}) stirred and heated at 50 °C for about one hour. The vial was sealed and left in the fume hood. After three weeks, small, clear, colourless crystals had formed in solution.

Crystals of *[Mg($C_7H_3NO_4$)(H_2O)$_2$]* **(18)** were prepared by the hydrothermal reaction, outlined by Mallick *et al.*,[97] of 2,4-pyridine dicarboxylic acid monohydrate (167 mg, 0.902 mmol, 185.13 g mol^{-1}) and magnesium(II) acetate tetrahydrate (214 mg, 0.998 mmol, 214.45 g mol^{-1}) dissolved, by sonication, in 5 mL water in an un-capped glass vial placed inside a Teflon-lined stainless steel autoclave. The mixture was heated in an oven from ambient temperature and maintained at 150 °C for 72 hours. The autoclave was allowed to cool back to room temperature slowly in the oven before being removed. The following day the autoclave was opened. The vial contained a clear, colourless solution, some white solid and large clear, colourless, prismatic crystals of **(18)**. IR (neat, cm^{-1}): 3231 b, 2162 w, 1980 w, 1868 w, 1693 w, 1627 s, 1600 s, 1560 s, 1481 m, 1441 m, 1397 s, 1362 s, 1247 m, 1087 m, 1020 m, 936 w, 915 w, 888 w, 848 w, 780 m, 697 s. Analysis found (calculated): C, 37.42 (37.30); H, 3.05 (3.14); N, 6.26 (6.21).

(18) was also produced by growth from a solution of **(19)** (10 mg, 0.017 mmol, 577.06 g mol^{-1}) dissolved in approx. 2 mL ethanol, with 1 mL DMF and 1 mL water with an aqueous solution of *m*-xylylenediamine acidified with acetic acid to pH 4.11 (0.7 mL, 0.0253 mol L^{-1}, 0.018 mmol, 136.19 g mol^{-1}) stirred and heated at 50 °C for about one hour. The vial was sealed and left in the fume hood. After three weeks, a large crop of clear colourless crystals of varying sizes had formed in solution.

(18) was also produced using the same reagent quantities as above, and under the same conditions, except using:

(i) Isopropanol in place of ethanol, and adding 1 mL toluene.
(ii) ACN in place of ethanol, and adding 1 mL toluene.
(iii) DMF in place of ethanol.

(18) was also produced by growth from a solution of **(19)** (10 mg, 0.017 mmol, 577.06 g mol^{-1}) dissolved in approx. 2 mL ethanol, with 1 mL DMF and 1 mL water with a

50:50 aqueous/methanol solution of *o*-tolidine acidified with acetic acid to pH 3.67 (2.8 mL, 0.0062 mol L^{-1}, 0.017 mmol, 212.29 g mol^{-1}) stirred and heated at 50 °C for about one hour. The vial was sealed and left in the fume hood. After three weeks, clear colourless crystals of varying sizes had formed in solution.

(18) was also produced using the same reagent quantities as above, and under the same conditions, except using:

(i) Isopropanol in place of ethanol.
(ii) DMF in place of ethanol, with no additional 1 mL DMF added.

Crystals of $[Mg(H_2O)_6][Mg(C_7H_4NO_4)_2(H_2O)_2].3H_2O$ **(19)** were prepared by an identical preparation to the first of those described for the preparation of **(18)**. On opening, the vial was found to contain a solid white mass of crystals of **(18)**. The vial was sealed with a cap and stored undisturbed at lab temperature. After 10 weeks there was a large, visually homogeneous mass of clear, colourless crystalline platelet shards of **(19)** in solution. IR (neat, cm^{-1}): 3325 b, 3201 b, 2321 b, 1948 w, 1668 w, 1638 m, 1598 s, 1545 m, 1478 w, 1433 w, 1379 s, 1343 s, 1232 m, 1192 m, 1092 m, 1020 m, 872 w, 824 w, 769 m, 725 m, 689 s. Analysis found (calculated): C, 29.16 (29.14); H, 4.51 (4.90); N, 4.91 (4.86).

(19) was also produced by growth from a solution after the hydrothermal reaction of 2,4-pyridine dicarboxylic acid monohydrate (259 mg, 1.399 mmol, 185.13 g mol^{-1}) and magnesium(II) acetate tetrahydrate (150 mg, 0.699 mmol, 214.45 g mol^{-1}) dissolved by sonication in 7 mL water in a glass vial placed inside a Teflon-lined stainless steel autoclave. The mixture was heated in an oven from 88 °C and maintained at 150 °C for 72 hours. The autoclave was allowed to cool back to room temperature in the oven before being removed. On opening, the vial was found to contain only a clear, colourless liquid. The vial was sealed with a cap and left on the crystallisation shelf at lab temperature. After one month the vial was found to contain two large clusters of clear, colourless, platelet shards of **(19)** in solution.

(19) was also produced by growth from a turbid solution of **(I1)** (20 mg, 0.051 mmol, 392.59 g mol^{-1}) suspended in 4 mL methanol, with 2 mL DMF, 4 mL water, 1 mL toluene and a methanol solution of *o*-tolidine (2 mL, 0.0252 mol L^{-1}, 0.050 mmol, 212.29 g mol^{-1}) stirred and heated to 40 °C for about an hour. The vial was covered with hole-pierced parafilm and left in the fume hood. After four months, tiny, clear, colourless platelet crystals of **(19)** had formed in solution.

(19) was also produced by growth from a solution of **(I1)** (10 mg, 0.025 mmol, 392.59 g mol^{-1}) suspended in about 2 mL ethanol, with 1 mL DMF, 1 mL water, 0.5 mL toluene and an aqueous solution of *m*-xylylenediamine (0.9 mL, 0.0379 mol L^{-1}, 0.034 mmol, 136.19 g mol^{-1}) stirred and heated at 50 °C for about two hours. The vial was sealed with a screw cap and left in the fume hood. After nine months, thin, flat, platelet crystals of **(19)** had formed in solution.

3.2.3. Complexes in Chapter 6

Crystals of $(C_6H_{5.5}NO_2)_2(C_6HCl_2O_4).2H_2O$ **(20)** were prepared by dissolving picolinic acid (5 mg, 0.041 mmol, 123.11 g mol^{-1}) and chloranilic acid (17 mg, 0.081 mmol, 208.98 g mol^{-1}) in approx. 5 mL acetone. The solution was mixed by vortex mixing and solvent evaporation took place at lab temperature. After two days the solvent had evaporated and a variety of crystalline materials had formed including clusters of thick, dark red needle crystals **(20)**. There were also large red crystals of chloranilic acid and orange/red platelet crystals of **(21)**.

(20) was also produced using the same reagent quantities as above, and under the same conditions, except using ethanol as the solvent in place of acetone. This also produced red crystals of chloranilic acid.

(20) was also produced by adding an aqueous solution (approx. 2 mL) of picolinic acid (10 mg, 0.081 mmol, 123.11 g mol^{-1}) to an ACN solution (approx. 2 mL) of chloranilic acid (8 mg, 0.038 mmol, 208.98 g mol^{-1}). The two solutions were combined by vortex mixing and solvent evaporation took place at 30 °C. This also produced a clear, colourless crystalline material round the sides of the vial. Analysis found (calculated): C, 45.57 (44.01); H, 3.27 (3.29); N, 6.43 (5.70).

(20) was also produced using the same reagent quantities as above and using ethanol as the only solvent. Solvent evaporation took place at lab temperature. This also produced a fine, white, feathery crystalline material.

(20) was also produced by adding an aqueous solution (approx. 2 mL) of picolinic acid (5 mg, 0.041 mmol, 123.11 g mol^{-1}) to an ACN solution (approx. 2 mL) of chloranilic acid (8 mg, 0.038 mmol, 208.98 g mol^{-1}). The two solutions were combined by vortex mixing and solvent evaporation took place at 30 °C.

Crystals of $(C_6H_5NO_2)_2(C_6H_2Cl_2O_4)$ **(21)** were prepared by dissolving picolinic acid (10 mg, 0.081 mmol, 123.11 g mol^{-1}) and chloranilic acid (8 mg, 0.038 mmol, 208.98 g mol^{-1}) in

approx. 5 mL acetone. The solution was mixed by vortex mixing and solvent evaporation took place at lab temperature. After two weeks the solvent had evaporated and clear orange/red crystals had formed. Analysis found (calculated): C, 45.26 (47.49); H, 2.71 (2.66); N, 5.82 (6.16).

(21) was also produced using the same reagent quantities as above, and under the same conditions, except using ethanol as the solvent in place of acetone.

Note: Picolinic acid/chloranilic acid crystallisation experiments in which either acetone or ethanol were used as solvents were often found to produce both crystals of **(20)** and **(21)**, as could be identified by visual inspection. Some repeat preparations of **(21)** resulted exclusively in **(21)** while others resulted in a visible mixture of both. Experiments using a water/ACN mixture as the solvent, and in which solvent evaporation took place at 30 °C, more reliably resulted in **(20)** and not **(21)**.

Crystals of **(20)** had variable physical appearances. Some crystals were in the form of large, dark, almost black, crystalline blocks. Other crystals were very dark red, flat needles, and formed clusters.

Crystals of $(C_6H_6NO_2)_2(C_6Cl_2O_4)$ **(22)** were prepared by adding an aqueous solution (approx. 2 mL) of nicotinic acid (10 mg, 0.081 mmol, 123.11 g mol^{-1}) to an ACN solution (approx. 2 mL) of chloranilic acid (8 mg, 0.038 mmol, 208.98 g mol^{-1}). The two solutions were combined by vortex mixing and solvent evaporation took place at 30 °C. After eight days the solvent had evaporated and a homogeneous product of long, thin, dark orange/red needle crystals had formed. Analysis found (calculated): C, 47.56 (47.49); H, 2.58 (2.66); N, 6.29 (6.16).

(22) was also produced by solvent evaporation in two steps. The first involved adding an aqueous solution (approx. 2 mL) of nicotinic acid (5 mg, 0.041 mmol, 123.11 g mol^{-1}) to an ACN solution (approx. 2 mL) of chloranilic acid (8 mg, 0.038 mmol, 208.98 g mol^{-1}). The two solutions were combined by vortex mixing and solvent evaporation took place at 40 °C to give the expected product $(C_6H_6NO_2)(C_6HCl_2O_4)$ [**PAZHOO**; CSD V5.35 May 2014].[169] The second step involved adding a methanol solution (approx. 2 mL) of **PAZHOO** (8 mg, 0.024 mmol, 332.10 g mol^{-1}) to a DMF solution (approx. 2 mL) of magnesium(II) chloride (2 mg, 0.021 mmol, 95.22 g mol^{-1}). The two solutions were combined by vortex mixing and solvent evaporation took place at lab temperature.

Crystals of *$[Cu_2(C_6H_4NO_2)_2(H_2O)_2(C_6Cl_2O_4)]$* **(23)** were prepared by solvent evaporation in two steps. The first step involved the preparation of **(20)**, as described previously, by adding an aqueous solution (approx. 2 mL) of picolinic acid (10 mg, 0.081 mmol, 123.11 g mol^{-1}) to an ACN solution (approx. 2 mL) of chloranilic acid (8 mg, 0.038 mmol, 208.98 g mol^{-1}). The two solutions were combined by vortex mixing and solvent evaporation took place at 30 °C. The second step involved the addition of an ACN solution (approx. 2 mL) of **(20)** (9.4 mg, 0.019 mmol, 490.22 g mol^{-1}) to an aqueous solution (approx. 2 mL) of copper(II) sulfate pentahydrate (5 mg, 0.020 mmol, 249.69 g mol^{-1}). The two solutions were combined by vortex mixing and solvent evaporation took place at 40 °C. After 19 days the solvent had evaporated and fine green needle crystals had formed. There were also a number of low-quality opaque orange crystals present in the vial.

(23) was also produced using the same experimental procedure as described above, except that the second solvent evaporation step took place at 30 °C or 50 °C.

Crystals of *$[Ca(C_6Cl_2O_4)_2].2C_2H_8N$* **(24)** were prepared by solvent evaporation in two steps. The first step involved adding an isopropanol solution (approx. 2 mL) of nicotinic acid (25 mg, 0.203 mmol, 123.11 g mol^{-1}) to an isopropanol solution (approx. 2 mL) of calcium(II) chloride (11 mg, 0.099 mmol, 110.99 g mol^{-1}). The two solutions were combined by vortex mixing and solvent evaporation took place at 30 °C to give the expected product *$[Ca(C_6H_5NO_2)_2Cl_2]$* **(13)**. The second step involved the addition of an isopropanol solution (approx. 3 mL) of **(13)** (15 mg, 0.042 mmol, 357.22 g mol^{-1}) to a DMF solution (approx. 3 mL) of chloranilic acid (9 mg, 0.043 mmol, 208.98 g mol^{-1}). The two solutions were combined by vortex mixing and sonication. The materials did not dissolve well and two layers formed: a yellow layer above a purple layer containing precipitate. Solvent evaporation took place at 40 °C. After six days, very dark red octahedral crystals of **(24)** had formed in a clear, slightly yellow solution and a clear colourless crystalline material was also present. The vial was sealed with a cap and removed from the hotplate.

Crystals of *$[Ca_2(C_6Cl_2O_4)_2(C_3H_7NO)_6]$* **(25)** were prepared by combination of the leftover solutions which were not used in a vapour diffusion crystallisation experiment during the preparation of **(A7)** (see Appendix D). These solutions were mixed by vortex mixing and sonication and solvent evaporation took place at 50 °C. This resulted in fine pink rectangular needle crystals of **(25)** as well as crystals of **(24)**.

(25) was also prepared by solvent evaporation using the initial quantities as for the preparation of **(A7)**, except without splitting the solutions in order to confirm the results

using known masses. This involved the addition of a DMF solution (approx. 3 mL) of **(13)** (10 mg, 0.028 mmol, 357.22 g mol^{-1}, prepared as outlined in the preparation of **(24)**) to a THF solution (approx. 3 mL) of chloranilic acid (6 mg, 0.029 mmol, 208.98 g mol^{-1}). The two solutions were combined by vortex mixing and sonication and solvent evaporation took place at 50 °C. After two weeks, the solution was bright yellow with pink needle crystals of varying sizes present in solution. After four weeks the solvent had evaporated and the vial contained pink needle crystals with a light brown precipitate.

Some preparations resulted in a mixture of both **(24)** and **(25)** as could be identified visually. These are:

(i) Nicotinic acid (5 mg, 0.041 mmol, 123.11 g mol^{-1}), calcium(II) chloride (2 mg, 0.018 mmol, 110.99 g mol^{-1}) and chloranilic acid (9 mg, 0.043 mmol, 208.98 g mol^{-1}) were each dissolved separately in approx. 2 mL of an equal isopropanol/DMF solvent mixture. The three solutions were combined by vortex mixing and sonication and solvent evaporation took place at 40 °C. After one month the solvent had evaporated and crystals of both complexes had formed.

(ii) Calcium(II) chloride (10 mg, 0.090 mmol, 110.99 g mol^{-1}) and chloranilic acid (38 mg, 0.182 mmol, 208.98 g mol^{-1}) were each dissolved separately in approx. 3 mL of an equal isopropanol/DMF solvent mixture. The two solutions were combined by vortex mixing and sonication and solvent evaporation took place at 40 °C. After one month the solvent had evaporated and dark red crystalline chunks, some clear colourless crystalline material, red crystals of (likely) chloranilic acid and pink needle crystals had formed.

(iii) Nicotinic acid (4 mg, 0.032 mmol, 123.11 g mol^{-1}), calcium(II) chloride (2 mg, 0.018 mmol, 110.99 g mol^{-1}) and chloranilic acid (6 mg, 0.029 mmol, 208.98 g mol^{-1}) were each dissolved separately in approx. 2 mL of an equal THF/DMF solvent mixture. The three solutions were combined by vortex mixing and sonication and solvent evaporation took place at 50 °C. After three weeks the solvent had evaporated and crystals of both complexes had formed.

(iv) Calcium(II) chloride (10 mg, 0.090 mmol, 110.99 g mol^{-1}) and chloranilic acid (19 mg, 0.091 mmol, 208.98 g mol^{-1}) were each dissolved separately in approx. 3 mL of an equal THF/DMF solvent mixture. The two solutions were combined by vortex mixing and sonication and solvent evaporation took place at 50 °C. After one week the solution contained many tiny pink needle crystals and dark red octahedrons. After three weeks the solvent had evaporated and clusters of dark red octahedral crystals had formed along with a green/brown substance.

(v) Nicotinic acid (22 mg, 0.179 mmol, 123.11 g mol^{-1}), calcium(II) chloride (10 mg, 0.090 mmol, 110.99 g mol^{-1}) and chloranilic acid (38 mg, 0.182 mmol, 208.98 g mol^{-1}) were each dissolved separately in approx. 6 mL of an equal THF/DMF solvent mixture. The three solutions were combined and distributed equally between two 17 mL vials. The resulting solutions were sonicated before being equally divided between two 7 mL vials. After two weeks crystals of both complexes had formed in solution. The vials were sealed with a cap and left undisturbed.

Chapter 4. Magnesium and Calcium Pyridine Carboxylic Acid Complexes

4.1. Introduction

This chapter describes the structure and thermal properties of new crystalline materials consisting of magnesium or calcium metal centres coordinated by picolinic acid, nicotinic acid or isonicotinic acid ligand derivatives. The majority of these complexes were synthesised during the earlier stages of this investigation to establish how the ligands and metals interact, and to analyse and compare their coordination and connectivity patterns. The extent to which the ligand-ligand interaction is influenced by metal coordination was also of interest.

The first six coordination complexes discussed here can be classified as 0D in that they are composed of discrete units of the coordination complex. The first three complexes feature a 1:1 ligand:metal ratio and are similar in their conformation in that they consist of molecular units of two metal centres bridged by the carboxylate groups of two pyridine carboxylic acid ligands resulting in an eight-membered ring. The ligands used are picolinic acid in **(1)**, and nicotinic acid in **(2)** and **(3)**. The next three complexes have a 2:1 ligand:metal ratio whereby the metal is coordinated by two pyridine carboxylic acid ligands *via* one carboxylate oxygen atom. **(4)** is a calcium and nicotinic acid complex, while **(5)** and **(6)** feature magnesium. These two complexes are constitutional isomers, accommodating different isomeric forms of the pyridine carboxylic acid ligand; isonicotinic acid in the case of **(5)** and picolinic acid in **(6)**. A complex featuring nicotinic acid and a magnesium centre which does not display organic ligand-metal coordination is discussed in Appendix D **(A1)**.

Structures **(7)** – **(12)** have a common 1D arrangement whereby the metal-organic ligand coordination *via* the carboxylate groups results in polymeric chains. In all cases these chains are connected to each other *via* H-bonding interactions either directly between coordinating ligands or *via* non-coordinated water molecules or nitrate counter ions. **(7)** is a 'molecular building block structural isomer'[170] of **(6)**, also featuring picolinic acid as the ligand, yet it displays very different connectivity. **(8)** differs from **(7)** in its ligand:metal ratio of 1:1. **(A2)** is an organic complex closely related to these four materials, discussed in Appendix D. The following four 1D complexes feature calcium metal centres. **(9)** involves isonicotinic acid bridging calcium centres and includes a water molecule disordered over two positions. **(11)**, **(10)** and **(12)** all have picolinic acid as the organic ligand, with the last of these differing in that picolinic acid displays N,O-chelation to the calcium centre.

The final two complexes reported in this chapter have higher dimensional connectivity and feature calcium and nicotinic acid. **(13)** is a 2D coordination polymer comprising layers of

calcium centres coordinated by four nicotinic acid ligands and two chloride ions. **(14)** displays 3D coordination connectivity and is comprised purely of nicotinic acid ligands bridging three calcium centres.

The carboxyl group of the pyridine carboxylic acid ligands was of particular interest as it was consistently involved in metal-coordination. The C-O distances and O-C-O angles of the carboxylate group were noted in each complex and compared to the C-O, C=O distances and O=C-O angles of the ligand in its pure form as shown in Figure 4.1. This allows the effect of deprotonation to the carboxylate group and its subsequent metal-coordination to be studied in the ligands of the new complexes.

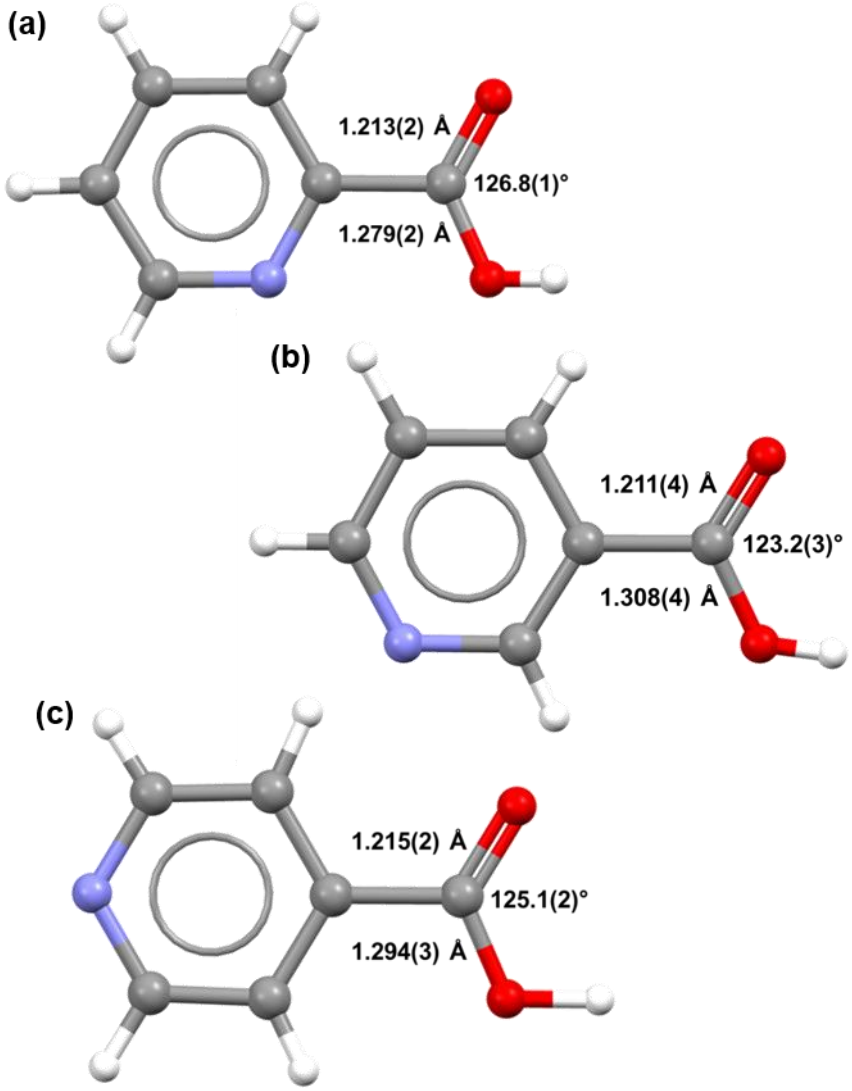

Figure 4.1. C=O and C-OH distances and O=C-O angles of the carboxyl group for the organic ligands in pure form, (a) picolinic acid, [**PICOLA02**; CSD V5.35 June 2014][137] (b) nicotinic acid [**NICOAC02**; CSD V5.35 June 2014][138] and (c) isonicotinic acid [**ISNICA**; CSD V5.35 June 2014].[139]

4.2. 0D Complexes

4.2.1. *Bis-[(μ_2-pyridinium-2-carboxylato)-tetraaqua-magnesium(II)] tetrachloride dihydrate* **(1)** *$[Mg(C_6H_5NO_2)(H_2O)_4]_2.4Cl.2H_2O$*

(1) was prepared by solvent evaporation of a 1:1 stoichiometric mixture of magnesium(II) chloride and picolinic acid dissolved in methanol and ethanol at lab temperature. The product was in the form of small, clear, colourless cuboidal crystals. Crystals of **(1)** were also produced by solvent evaporation of a 1:1 stoichiometric mixture of the starting materials dissolved in dichloromethane and water at lab temperature, the product of which was analysed by PXRD and compared to the calculated PXRD pattern from the scXRD determined structure and to those of the starting materials (Figure 4.2).[#]

As can be determined visually, there is some correlation between the experimentally obtained and calculated PXRD patterns, however the experimental PXRD pattern is not of high enough quality, possibly due to a very small sample quantity, to fully determine the composition of the bulk material of **(1)**.

[#] A general point to be made here is that when comparing experimentally obtained and calculated PXRD patterns it is common to observe a shift of the calculated pattern relative to the experimental pattern. This is due to the lower temperature at which the data are typically collected during scXRD (100-150 K for the structures reported here), compared to PXRD which is frequently carried out at lab temperature, (all PXRD patterns reported here are ambient temperature collections). The lower temperature of the scXRD experiment causes contraction of the lattice, hence of the d-spacing, shifting the pattern to higher 2θ values.

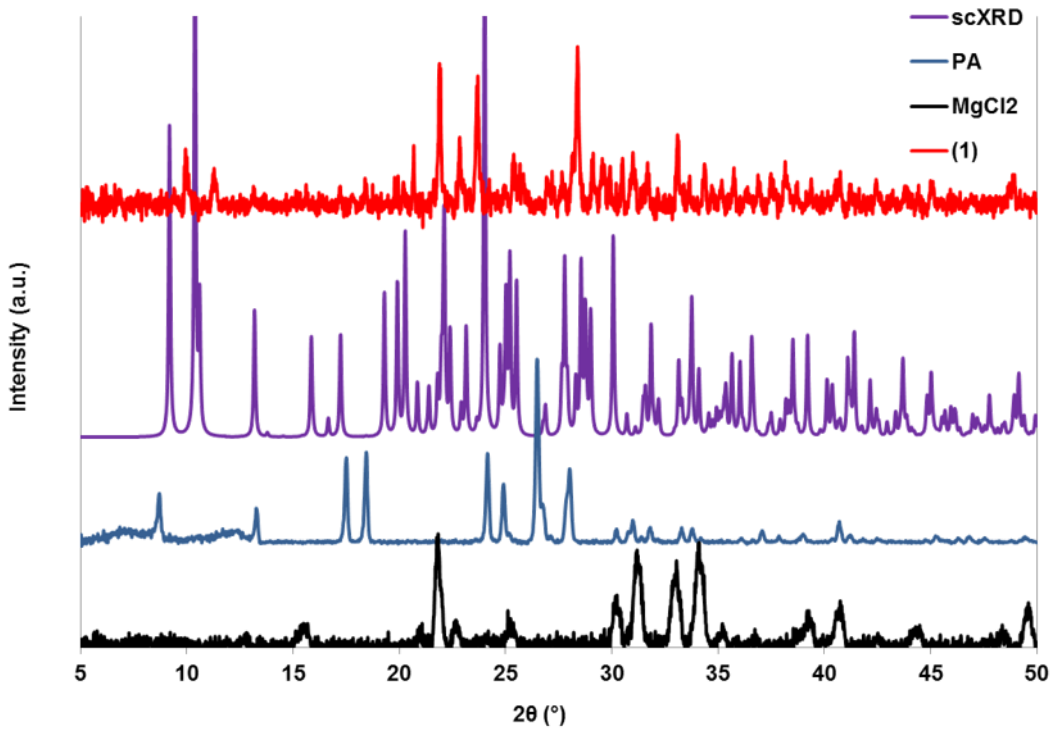

Figure 4.2. PXRD pattern of **(1)** compared to the calculated pattern (scXRD) and patterns of starting materials.

(1) comprises two zwitterionic picolinic acid ligands bridging two magnesium centres to form an eight-membered ring. The magnesium centres are coordinated to four water molecules and there are four non-coordinated chloride ions and two non-coordinated water molecules also within the formula unit (Figure 4.3(a)). A similar structure is reported by Karimov and Ismailova,[109] [**NISJEE**; CSD V5.35 June 2014]. These differ in that where **(1)** has a coordinated water molecule, **NISJEE** has a second picolinic acid ligand per metal centre, coordinated to magnesium *via* one carboxylate oxygen atom (Figure 4.3(b)).

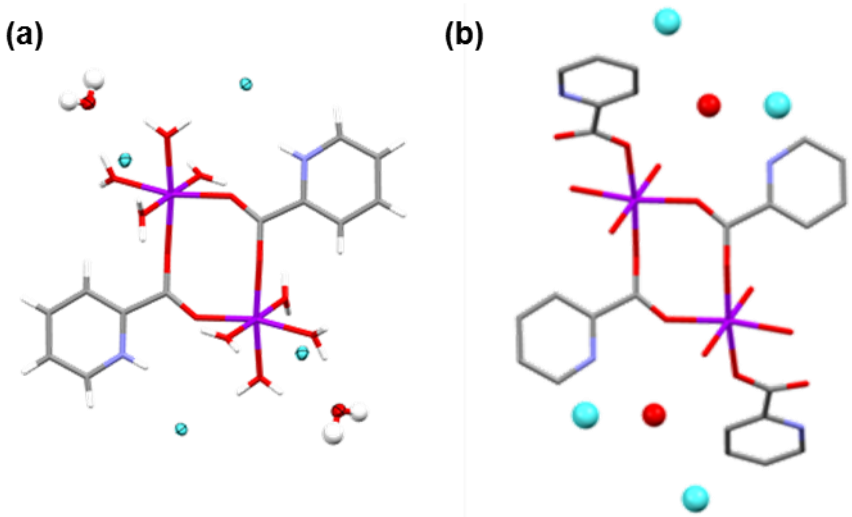

Figure 4.3. Formula unit of (a) **(1)** and (b) **NISJEE** (H atom positions not available).

Crystals with the unit cell parameters of **NISJEE** were found when checking the unit cell of crystals selected from the vial from which crystals of **(1)** were grown, several months after the structure of **(1)** had been determined. This suggests that either crystals of **NISJEE** were present at the time of the initial screening of crystals from the vial resulting in the discovery of **(1)**, or that the material converted to **NISJEE** over the following months. Similar evaporation crystallisation experiments using the solvent systems isopropanol and water, and THF and ethanol, both at lab temperature, resulted in crystals of **NISJEE**, however the duration of time between preparation and analysis was almost a year so it cannot be concluded with certainty whether **(1)** or **NISJEE** formed first. Figure 4.4 shows the PXRD pattern of **(1)** compared to the calculated patterns of both **(1)** and **NISJEE**. It is apparent that the experimental pattern of **(1)** has more common peaks with the calculated pattern of **NISJEE** than the calculated pattern of **(1)**, so it can be inferred that the product from these crystallisation experiments is a mix of closely related phases.

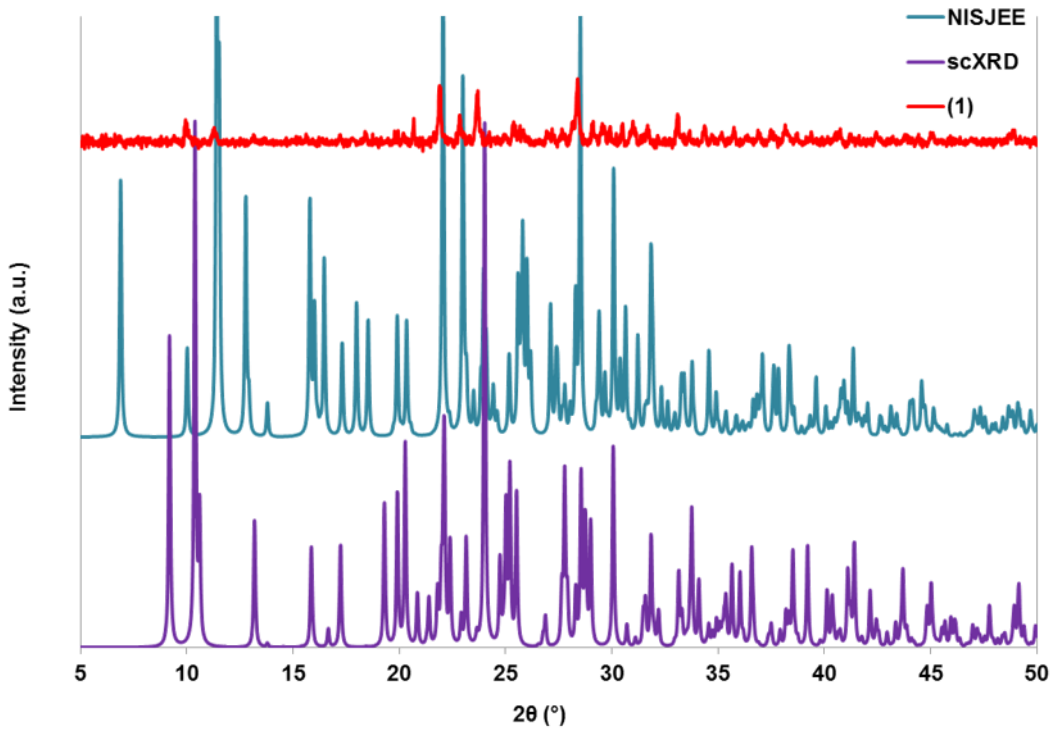

Figure 4.4. PXRD pattern of **(1)** compared to the calculated patterns of **(1)** (scXRD) and **NISJEE**.

The formula unit of **(1)** features two crystallographically equivalent magnesium centres related through an inversion centre. The magnesium centres are in a distorted octahedral geometry (Figure 4.5(a) and Table 4.1) with O-Mg-O angles ranging from 83.97(4)° for O3-Mg1-O2 to 98.93(4)° for O1-Mg1-O4$^{a\#}$, the latter being the angle formed between the metal and the two coordinating carboxylate oxygen atoms from two picolinic acid ligands.

Of the water ligands, the longest Mg-O distance is that of Mg1-O3 at 2.092(1) Å, while the shortest is that of Mg1-O5 of 2.045(1) Å, *trans* to the slightly longer Mg1-O6 of 2.056(1) Å. The Mg-O distances to the carboxylate oxygen atoms are quite different given the limited range of the Mg-O distances found in the complex. Mg1-O4^{a} is the shorter of the two at 2.015(1) Å compared to 2.067(1) Å for Mg1-O1.

Figure 4.5(b) shows the formula unit of **(1)** and its eight-membered ring conformation formed by the bridging picolinic acid ligands. The two magnesium centres and two carboxylate group atoms that make up the eight-membered ring are not coplanar and have a maximum deviation of ± 0.159(1) Å from their average plane.

[#] Superscript letters after atoms/centroids represent symmetry equivalent atoms/centroids; the symmetry operations corresponding to these are given under accompanying Figures or Tables close to their occurrence in the text.

The C-O distances of the carboxylate group are very similar at 1.242(1) Å and 1.246(1) Å for C1-O4 and C1-O1 respectively indicating that the negative charge of the carboxylate group is delocalised across the whole group. The angle of the carboxylate group of the bridging picolinic acid ligand in **(1)** (O1-C1-O4) is 129.0(1)°; the equivalent carboxylate group angle observed in **NISJEE** is 129.4(5)°. These angles are slightly wider than the O=C-O angle found in pure picolinic acid (126.8(1)°), likely as a result of distortion due to the metal coordination. In **(1)**, the carboxylate group and the pyridinium ring are twisted slightly from coplanarity with a O1-C1-C2-N1 torsion angle of 3.5(2)°.

Correlating the Mg-O coordination lengths to the Mg-O-C angles, it can be seen that the longer interaction Mg1-O1 is associated with the smaller angle of Mg1-O1-C1 at 138.59(8)°. Mg1^{a}-O4-C1 has an angle of 158.13(8)°, and features the shorter of the Mg-O coordination distances. The same situation is observed in **NISJEE**, with the longer Mg-O coordination of length 2.051(4) Å associated with the smaller Mg-O-C angle of 135.1(4)°, and the shorter Mg-O coordination of 2.037(4) Å associated with the larger Mg-O-C angle of 152.0(4)°. In **NISJEE** the C-O distances are more different to each other than in **(1)** with one being 1.218(7) Å and the other 1.242(6) Å.

(1) is composed of formula units connected through H-bonds. The formula units form distinct columns along the *a* and *c* directions, while when viewed down the *b* direction there is a slight overlap between the pyridinium rings of the formula units creating an H-bonded 2D motif parallel to the *ab* plane.

The chloride ions are non-coordinated to the metal centres and are fundamental to the connectivity of the crystal structure. Connecting formula units along the *a* direction, there are three H-bonds and for each one, Cl1 acts as the acceptor atom (Figure 4.5(c) and Table 4.2). The N-H group of the pyridinium ring forms the relatively weak H-bond N1-H1⋯Cl1^{a} with a D⋯A distance of 3.114(1) Å and an angle of 144(2)°. The H-bonds O2-H2B⋯Cl1^{a} and O3-H3B⋯Cl1^{b} have more linear angles of 177(2)° and 173(2)°, respectively, possibly due to H1 being covalently bonded to the larger and more rigid picolinic acid ligand as opposed to the coordinated water molecules featuring H2B and H3B, therefore their positions are likely to be more flexible. These H-bonds have equivalent D⋯A distances of 3.129(1) Å and 3.127(1) Å for O2-H2B⋯Cl1^{a} and O3-H3B⋯Cl1^{b}, respectively, which are indicative of moderate-weak strength H-bonds.

The columns of formula units are connected along the *c* direction through H-bonds from a coordinated water molecule and a C-H group of the picolinic acid ligand to the Cl1 ion, O5-H5A⋯Cl1^{g} and C6-H106⋯Cl1^{h}, and from two other coordinated water molecules to the oxygen atom of the non-coordinated water molecule, O2-H2A⋯O7^{f} and O3-H3A⋯O7^{f}

(Figure 4.5(d), Table 4.2). The latter two interactions are the stronger of these H-bonds with D···A distances of 2.808(2) Å and 2.752(2) Å and angles of 155(2)° and 164(2)° for O2-H2A···O7[f] and O3-H3A···O7[f], respectively. These angles are comparable to those of O5-H5A···Cl1[g] and C6-H106···Cl1[h], of 167(2)° and 157(1)°, respectively, however these H-bonds have longer D···A distances: O5-H5A···Cl1[g] is 3.161(1) Å and C6-H106···Cl1[h] is significantly longer at 3.675(2) Å; the latter is likely to be a very weak interaction.

The formula units are repeated in the *b* direction through H-bonds from two coordinated water molecules, the non-coordinated water molecule, and a C-H group to the Cl2 ion, and from the non-coordinated water molecule to the Cl1 ion (Figure 4.5(d) and Table 4.2). The H-bonds between coordinated water molecules and Cl2 are O5-H5B···Cl2, O6-H6A···Cl2[c] and O6-H6B···Cl2[a]. They have similarly medium-long D···A distances of 3.114(1) Å, 3.149(1) Å and 3.136(1) Å, respectively, and all have close to linear angles ranging from 173(2)° for O6-H6B···Cl2[a], to 178(2)° for O5-H5B···Cl2. In connecting the crystal structure along the *b* direction, the oxygen atom of the non-coordinated water molecule acts as a donor and makes two moderately weak H-bonds: O7-H7A···Cl1[d] with a D···A distance of 3.229(1) Å and an angle of 176(2)°, and O7-H7B···Cl2 of 3.143(1) Å and 163(2)°. C4-H104···Cl2[e] is a fairly weak H-bond from a C-H group to Cl2 and has a long D···A distance of 3.609(2) Å and an angle of 168(1)°. All of the metal coordinated water molecules in the crystal structure of **(1)** form two hydrogen bonds: the water molecule containing O5 and O6 forms two H-bonds to chloride ions and the water molecule containing O2 and O3 to one chloride ion and the non-coordinated water molecule. H-O-H angles of the water molecules range from 104(2)° for H3A-O3-H3B to 109(2)° for H5A-O5-H5B, which corresponds to the average H-O-H angle of 107.4° for magnesium coordinated water molecules, calculated from structures reported in the CSD from data collected at temperatures 100 and 173 K.

The linking of formula units along the *b* direction results in the slight overlap of pyridinium rings giving the impression of a 2D H-bonded motif parallel to the *ab* plane (Figure 4.5(e)). The centroid–centroid distance of (N1,C2,C3,C4,C5,C6) - (N1,C2,C3,C4,C5,C6)[i] is 4.282(1) Å and the centroid–centroid distance of (N1,C2,C3,C4,C5,C6) - (N1,C2,C3,C4,C5,C6)[e] is 5.226(1) Å (symmetry code: [i](2-x, -y,1- z)). The centroids of the pyridinium rings are offset at a centroid···centroid distance of 1.995 Å. Due to the long inter-centroid distance it is not likely that π-π interactions are major forces in governing the packing and rather it is extensive H-bonding interactions between water molecules and chloride ions which direct the crystal structure of **(1)**.

This would also appear to be true in the case of the crystal structure of **NISJEE**. The centroid – centroid distances of the parallel pyridinium groups are longer than those seen in **(1)**; therefore π-π interactions are unlikely to dominate the packing. H-bonds occur

between: the coordinated water molecules and the non-coordinated water molecule; the coordinated water molecules and both the chloride ions; the N-H group of the pyridinium ring and the non-coordinated water molecule; the non-coordinated water molecule and one of the chloride ions. In **(1)** the N-H group of the pyridinium ring H-bonds to a chloride ion, not the non-coordinated water molecule as in **NISJEE**. Also, in **(1)** the non-coordinated water molecule H-bonds to both of the chloride ions as opposed to just one, as seen in **NIJSEE**. Exclusive to **NISJEE** is an H-bond between a coordinated water molecule and the non-coordinated and deprotonated carboxylate oxygen atom of the coordinating picolinic acid ligand *cis* to the H-donating water molecule (Figure 4.6(a)). This H-bond occurs due to the presence of the second coordinated picolinic acid ligand and so cannot be present in **(1)**.

NISJEE has a similar structure to **(1)** in that the formula units form distinct columns that run along the *a* direction (Figure 4.6(b)), and columns along the *b* direction that show slight overlap of the carboxylate group of the additional (non metal-bridging) picolinic acid ligand (Figure 4.6(c)). In the *c* direction the formula units align in columns and show slight overlap of the pyridinium rings of the metal-bridging picolinic acid ligands (Figure 4.6(d)), similar to the situation in **(1)** when the structure is viewed down the *b* axis.

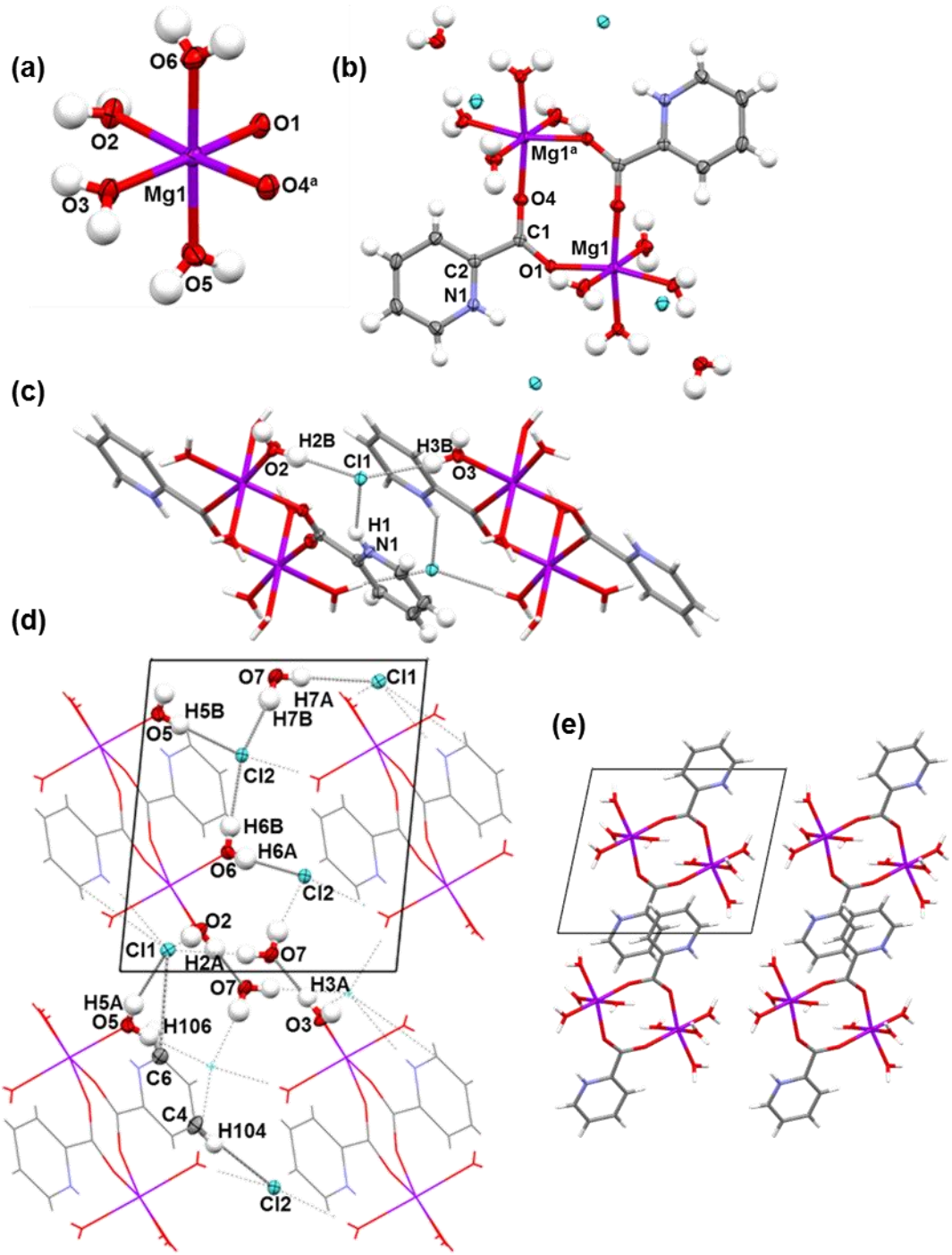

Figure 4.5. Crystal structure of **(1)**. (a) Octahedral Mg centre with four coordinating water molecules and two coordinating carboxylate oxygen atoms. (b) Formula unit showing bridging picolinic acid ligand and eight-membered ring conformation. (c) H-bonds between formula units connecting the structure along the *a* direction. (d) View down the *a* axis showing the H-bonds between formula units connecting the structure along the *b* and *c* directions. (e) View down the *b* axis showing two 2D H-bonded motifs parallel to *ab* plane with overlap between pyridinium rings. Symmetry codes: [a](1-x, -y,1- z)

Table 4.1. O-Mg-O angles and Mg-O distances in **(1)**.

Coordination	**O-Mg-O angle (°)**	**Interaction**	**Distance (Å)**
O6-Mg1-O1	95.50(4)	Mg1-O1	2.067(1)
O6-Mg1-O4[a]	86.90(4)	Mg1-O2	2.053(1)
O6-Mg1-O3	91.38(4)	Mg1-O3	2.092(1)
O6-Mg1-O2	85.41(4)	Mg1-O4[a]	2.015(1)
O5-Mg1-O1	84.78(4)	Mg1-O5	2.045(1)
O5-Mg1-O4[a]	91.67(4)	Mg1-O6	2.056(1)
O5-Mg1-O3	88.62(5)		
O5-Mg1-O2	96.01(5)		
O1-Mg1-O4[a]	98.93(4)		
O4[a]-Mg1-O3	92.51(4)		
O3-Mg1-O2	83.97(4)		
O2-Mg1-O1	85.52(4)		

Symmetry codes: [a](1-x, -y,1-z)

Table 4.2. Geometries of H-bonds in **(1)**.

D-H···A Interaction	D-H (Å)	H···A (Å)	D···A (Å)	D-H···A (°)
(Figure 4.5(c)) H-bonds connecting formula units along a direction.				
N1-H1···Cl1[a]	0.82(2)	2.41(2)	3.114(1)	144(2)
O2-H2B···Cl1[a]	0.86(3)	2.27(3)	3.129(1)	177(2)
O3-H3B···Cl1[b]	0.84(2)	2.30(2)	3.127(1)	173(2)
(Figure 4.5(d)) H bonds connecting formula units along b direction				
O5-H5B···Cl2	0.81(2)	2.31(2)	3.114(1)	178(2)
O6-H6A···Cl2[c]	0.77(3)	2.38(3)	3.149(1)	176(2)
O6-H6B···Cl2[a]	0.81(2)	2.33(2)	3.136(1)	173(2)
O7-H7A···Cl1[d]	0.80(2)	2.43(2)	3.229(1)	176(2)
O7-H7B···Cl2	0.80(2)	2.37(2)	3.143(1)	163(2)
C4-H104···Cl2[e]	0.91(2)	2.71(2)	3.609(2)	168(1)
(Figure 4.5(d)) H-bonds connecting formula units along c direction				
O2-H2A···O7[f]	0.79(2)	2.07(2)	2.808(2)	155(2)
O3-H3A···O7[f]	0.82(2)	1.95(2)	2.752(2)	164(2)
O5-H5A···Cl1[g]	0.81(2)	2.37(2)	3.161(1)	167(2)
C6-H106···Cl1[h]	0.92(2)	2.81(2)	3.675(2)	157(1)

Symmetry codes: [a](1-x,-y,1-z) [b](-x,-y,1-z) [c](x,-1+y,z) [d](1-x,1-y,1-z) [e](2-x,1-y,1-z) [f](1-x,-y,-z) [g](x,y,-1+z) [h](1+x,y,-1+z)

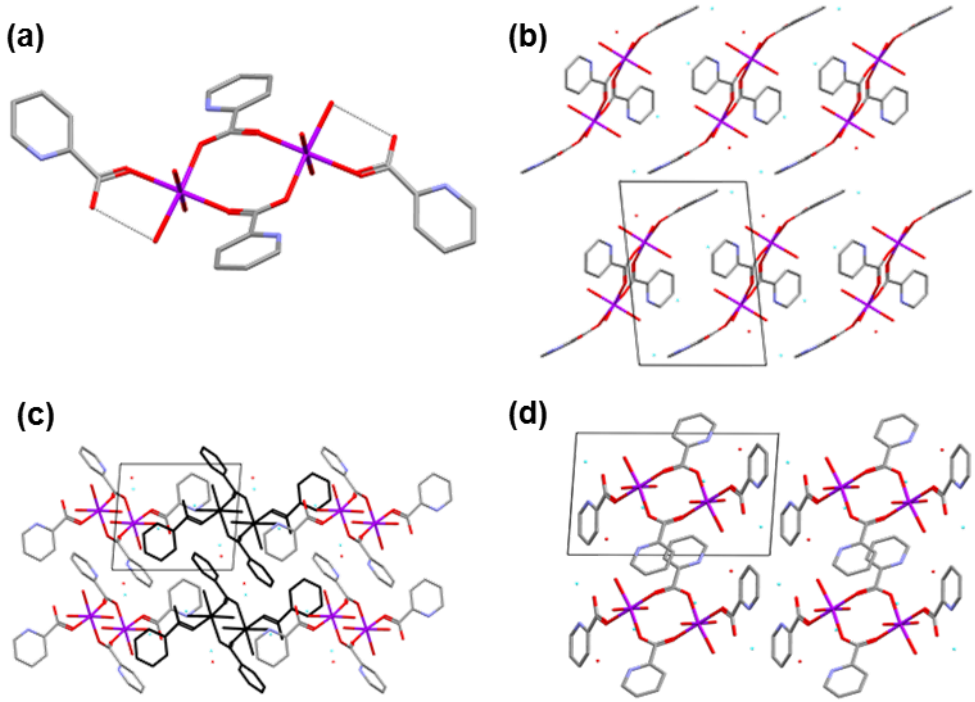

Figure 4.6. Crystal structure of **NISJEE** (hydrogen atom positions not available). (a) Formula unit showing intracomplex O-H···O bond, (non-coordinated water molecule and chloride ions removed). (b) View down the *a* axis showing formula units arranged into columns. (c) View down the *b* axis showing overlap between the non-bridging picolinic acid groups. (d) View down the *c* axis showing slight overlap between the pyridinium rings of bridging picolinic acid.

During HSM analysis, the melting point of **(1)** could not be determined but a considerable amount of bubbling from the sample crystals was evident, starting slowly at about 140 °C and vigorously from 170 °C. The sample was heated to 300 °C, but no melting was observed. DSC was carried out on the sample produced by solvent evaporation from dichloromethane and water at lab temperature (Figure 4.7). This showed an endothermic event from about 70 °C to 120 °C which could be attributed to the loss of water, followed by two melting peaks, one at 137.9 °C with a slight shoulder at about 141 °C; this can be attributed to the melting of (possibly excess) picolinic acid (m.p. 139 – 142 °C). Before decomposition of the sample, a second endothermic event occurs at 193.0 °C; this may be the melting point of **(1)**. Considering that **(1)** has a ligand:metal ratio of 1:1, it would not be expected that there would be considerable excess picolinic acid in the sample vial, which casts doubt upon the contents of the sample selected for DSC. Given that the PXRD pattern does not suggest that the single crystal is representative of the bulk sample, the melting transition observed at 193.0 °C in the DSC trace is not necessarily indicative of this material's melting point.

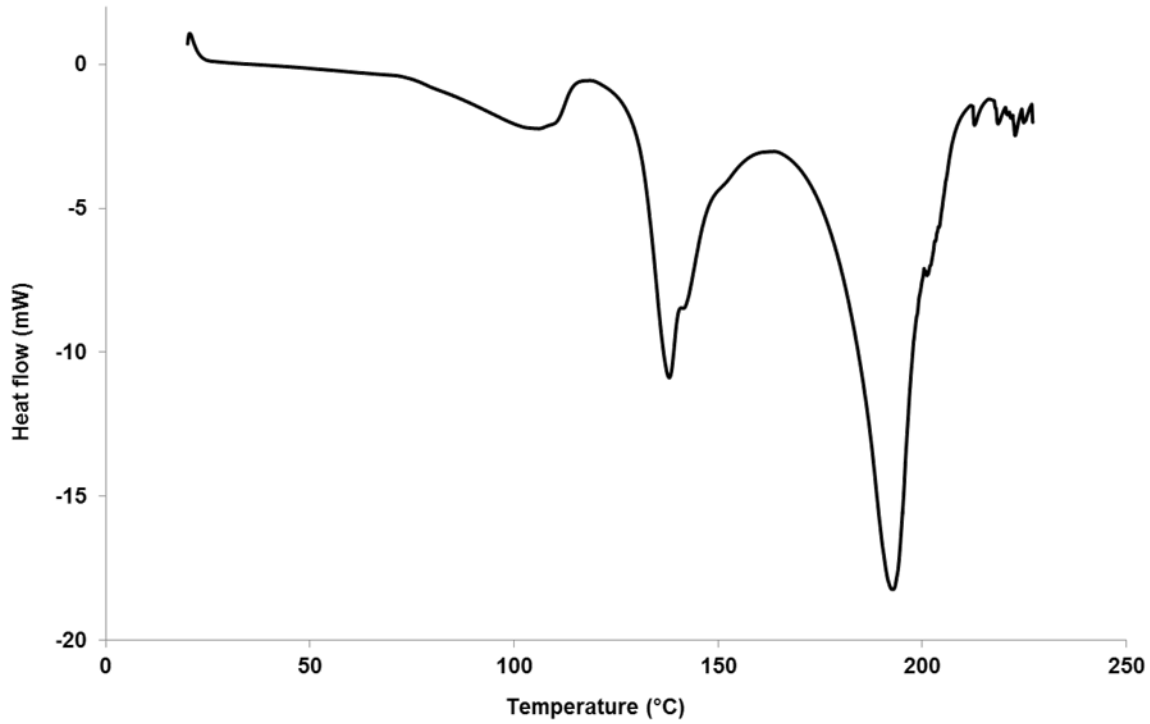

Figure 4.7. DSC trace of **(1)** on a 4.6 mg sample with a temperature ramp of 10 °C min^{-1}.

4.2.2. *Bis-[bis-((μ₂-pyridinium-3-carboxylato)-tetraaqua-magnesium(II))] octachloride* **(2)**
2[Mg($C_6H_5NO_2$)(H_2O)$_4$]$_2$.8Cl

(2) was prepared by solvent evaporation of a 1:1 stoichiometric mixture of nicotinic acid and magnesium(II) chloride dissolved in ethanol at lab temperature. The resulting product of large shards of a clear colourless crystalline material was not completely dry and a clear, colourless grease-like substance was also present. To obtain sufficient sample for PXRD analysis, the product of two of the other crystallisation experiments which resulted in crystals of **(2)** was also used (the conditions for which were solvent evaporation of a 1:1 stoichiometric mixture of the starting materials dissolved in isopropanol and water at lab temperature, and from isopropanol and ethanol at lab temperature). Although the resulting PXRD pattern is not informative (Appendix A, Figure A1), visually the crystalline material appeared homogeneous.

(2) is very closely related to **(1)**. The formula unit of **(2)**, (Figure 4.8(a)) features two residues of two octahedral magnesium centres related through an inversion centre and bridged by two crystallographically equivalent zwitterionic nicotinic acid ligands. To differentiate between them, the residues RMg1 and RMg2 are named after their corresponding metal centres. Each of the magnesium centres is also coordinated by four water molecules and there are eight non-coordinated chloride ions. In common with **(1)**, there are water

molecules in the crystal structure regardless of whether or not water was used in the evaporation crystallisation experiment; atmospheric water or that from wet solvent or reagents must have been incorporated during crystallisation. **(2)** differs from **(1)** in three main aspects: it contains two different metal-organic residues rather than one; the bridging ligand is nicotinic acid as opposed to picolinic acid; and it does not have a non-coordinated water molecule.

Similarly to **(1)**, the two magnesium centres in **(2)** have a distorted octahedral geometry with larger O-Mg-O angles formed between the two coordinating carboxylate oxygen atoms, and smaller angles formed between the water molecules *trans* to the carboxylate oxygen atoms (Figure 4.8(b) and (c), Table 4.3, Table 4.4). For Mg1, the largest angle is formed by the carboxylate oxygen atoms, $O11^{a}$-Mg1-O7 at 97.78(7)° and the smallest is formed by the water ligands *trans* to the carboxylate oxygen atoms, O8-Mg1-O10 at 82.00(7)°. In the case of Mg2 the largest angle is also formed by the carboxylate oxygen atoms, $O5^{b}$-Mg2-O1 at 99.92(6)°, but here the smallest angle is O1-Mg2-O2 at 80.82(7)°; this is the angle between one of the carboxylate oxygen atoms and the oxygen of the water ligand *trans* to the second carboxylate oxygen atom. The angle between the water ligands *trans* to the carboxylate oxygen atoms, O2-Mg2-O4, is 83.83(7)°. Mg1 has a less distorted octahedral geometry than Mg2 as the angles between the axial water ligands (if the carboxylate oxygen atoms are taken to be equatorial) and the equatorial oxygen atoms range between 85.86(7)° for O9-Mg1-O10 and 96.41(7)° for O12-Mg1-O7, *trans* to O9-Mg1-O10. In Mg2 there is a greater range in these angles with the smallest being 83.17(7)° for O3-Mg2-O4, and the largest being 98.57(6)° for O6-Mg2-O1: here again the largest angle is *trans* to the smallest. The two metal centres are similar with regards to the Mg-O bond distances in that the shortest of these is between the metal and the carboxylate oxygen atoms. This is different to **(1)** in which the two Mg-carboxylate oxygen atom distances have the shortest and second longest of the Mg-O coordination lengths. For Mg1 the Mg-carboxylate oxygen atom distances are 2.036(2) Å and 2.012(2) Å for Mg1-O7 and Mg1-$O11^{a}$, respectively. In Mg2 these distances are 2.033(2) Å and 2.019(2) Å for Mg2-O1 and Mg2-$O5^{b}$, respectively. The longest distance for each of the metal centres is to a water ligand *trans* to one of the carboxylate oxygen atoms, Mg1-O8 at 2.099(2) Å and Mg2-O4 at 2.101(2) Å.

The eight-membered ring conformations of each of the residues in the formula unit, RMg1 and RMg2, are shown in Figure 4.8(d) and (e). The atoms of the eight-membered rings made up by the two magnesium centres and two carboxylate groups do not lie on the same plane in either of the residues. In RMg1 the deviation from their average plane is ± 0.271(1) Å, while in RMg2 this deviation is greater at ± 0.386(1) Å. These deviations are greater than that observed for the eight-membered ring in **(1)** of ± 0.159(1) Å.

In RMg1 the O-C-O angle of the bridging nicotinic acid ligand, O7-C7-O11 is 127.2(2)° and the equivalent angle in RMg2, O1-C1-O5 is 126.8(2)°. In common with **(1)**, both of these angles are slightly wider in the complex than in the pure ligand (126.8(1)°). This widening can be attributed to the metal coordination distorting this group. The C-O distances in RMg1 are 1.245(3) Å and 1.253(3) Å for C7-O7 and C7-O11 respectively. In RMg2 the equivalent bond distances are 1.247(2) Å and 1.254(2) Å for C1-O1 and C1-O5 respectively; these distances are similar due to the delocalisation of the negative charge across the carboxylate group. The carboxylate group and the pyridinium rings of RMg1 and RMg2 are twisted slightly from coplanarity with a O7-C7-C8-C9 torsion angle of -3.7(3)° for RMg1, and a O1-C1-C2-C6 torsion angle of -2.0(3)° for RMg2.

In RMg1, the Mg1-O7 coordination distance of 2.036(2) Å is accompanied by the Mg1-O7-C7 angle of 137.6(2)°, and the Mg1-O11^{a} length of 2.012(2) Å by the Mg1^{a}-O11-C7 angle of 149.0(1)°. In RMg2, the Mg2-O1 distance of 2.033(2) Å is associated with the angle Mg2-O1-C1 of 141.0(1)° and the Mg2-O5^{b} distance of 2.019(2) Å with the Mg2^{b}-O5-C1 angle of 133.3(1)°. Thus, in RMg1, the bigger Mg-O-C angle is observed where the Mg-O distance is shorter, similar to the analogous situation in both **(1)** and **NISJEE**. In RMg2 however, the larger Mg-O-C angle is observed for the longer Mg-O coordination.

The two metal-organic residues of the formula unit, RMg1 and RMg2, are linked together along the {111} plane by H-bonds between the coordinated water molecules and the chloride ions (Figure 4.8(f)). However, in order to interpret the crystal structure of **(2)**, it is more practical to view the metal-organic residues separately rather than consider the formula unit as a whole.

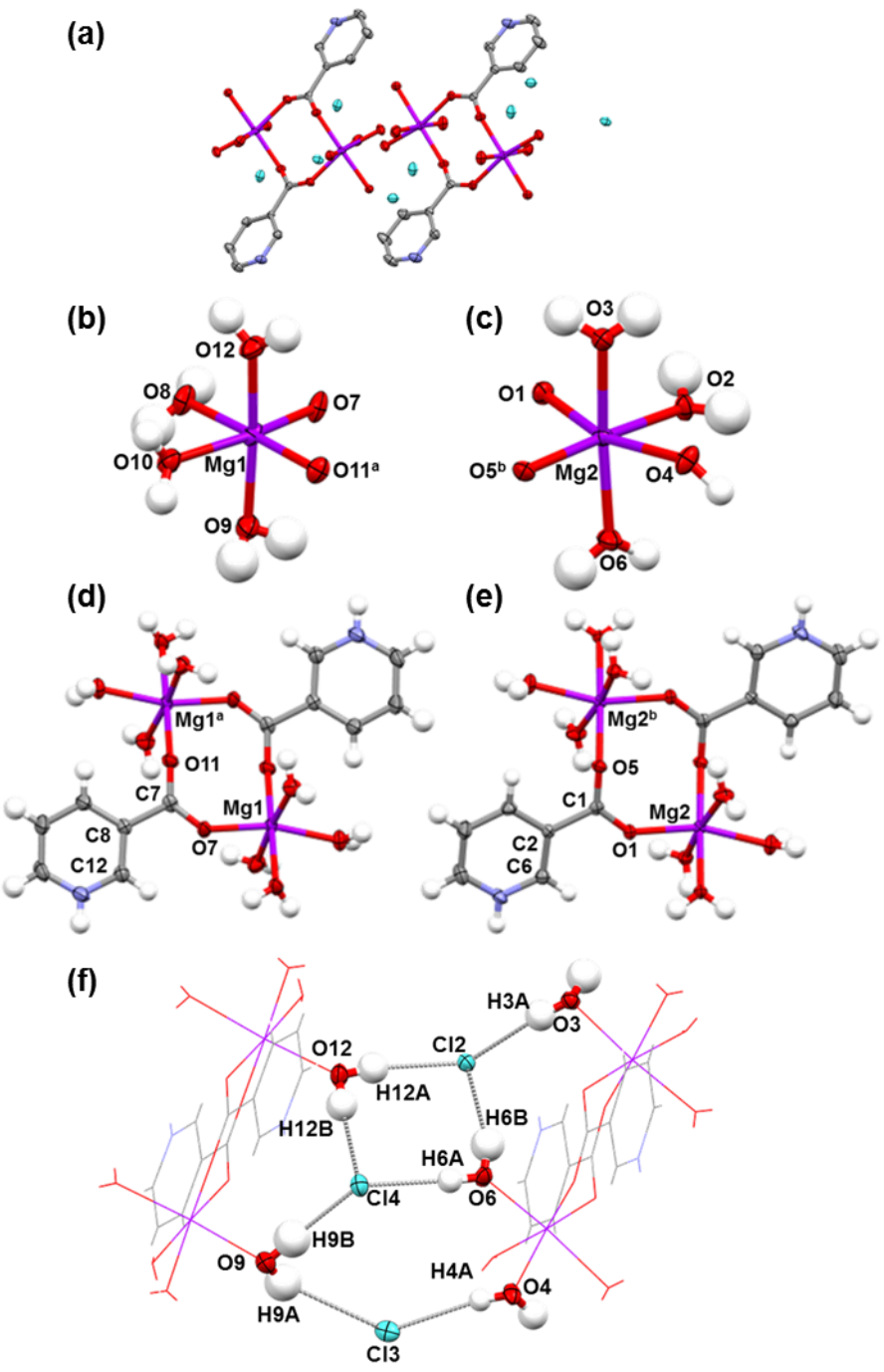

Figure 4.8. Crystal structure of **(2)**. (a) Formula unit of **(2)** (hydrogen atoms removed for clarity). (b) Octahedral Mg1 centre, and (c) Mg2 centre, each with two coordinating carboxylate oxygen atoms and four coordinating water molecules (H4B removed for clarity in (c)). (d) RMg1 residue showing bridging nicotinic acid ligand and eight-membered ring conformation. (e) RMg2 residue showing bridging nicotinic acid ligand and eight-membered ring conformation. (f) H-bonds within the formula unit. Symmetry codes: [a](1-x, 1-y, -z) [b](1-x, -y, 1-z).

Table 4.3. O-Mg-O angles and Mg-O distances involving Mg1 in **(2)**.

Coordination	**O-Mg-O angle (°)**	**Interaction**	**Distance (Å)**
O12-Mg1-O7	96.41(7)	Mg1-O7	2.036(2)
O12-Mg1-O8	91.68(7)	Mg1-O8	2.099(2)
O12-Mg1-O10	88.79(7)	Mg1-O9	2.095(2)
O12-Mg1-O11[a]	89.66(7)	Mg1-O10	2.084(2)
O9-Mg1-O7	89.25(7)	Mg1-O11[a]	2.012(2)
O9-Mg1-O8	89.49(7)	Mg1-O12	2.055(2)
O9-Mg1-O10	85.86(7)		
O9-Mg1-O11[a]	89.06(7)		
O7-Mg1-O8	83.19(7)		
O8-Mg1-O10	82.00(7)		
O10-Mg1- O11[a]	96.90(7)		
O11[a]-Mg1-O7	97.78(7)		

Symmetry codes: [a](1-x, 1-y, -z)

Table 4.4. O-Mg-O angles and Mg-O distances involving Mg2 in **(2)**.

Coordination	O-Mg-O angle (°)	Interaction	Distance (Å)
O3-Mg2-O1	89.70(6)	Mg2-O1	2.033(2)
O3-Mg2-O2	93.80(7)	Mg2-O2	2.074(2)
O3-Mg2-O4	83.17(7)	Mg2-O3	2.089(2)
O3-Mg2-O5[b]	89.19(7)	Mg2-O4	2.101(2)
O6-Mg2-O1	98.57(6)	Mg2-O5[b]	2.019(2)
O6-Mg2-O2	88.87(7)	Mg2-O6	2.064(2)
O6-Mg2-O4	89.23(7)		
O6-Mg2-O5[b]	88.08(7)		
O1-Mg2-O2	80.82(7)		
O2-Mg2-O4	83.83(7)		
O4-Mg2-O5[b]	95.84(7)		
O5[b]-Mg2-O1	99.92(6)		

Symmetry codes: [b](1-x, -y, 1-z)

The RMg1 and RMg2 residues align in distinct columns along the *b* direction (Figure 4.9(a)) and the *a* direction (Figure 4.10(a)). Along each of these directions, the residues are connected by H-bonding interactions to common chloride ions and the RMg1 and RMg2 residues are connected to each other by H-bonds, again *via* common chloride ions, save for one H-bond directly between the two units, to extend the structure along the *c* direction. Therefore it is apparent that the chloride counter ions in this structure are central to its connectivity. All of the chloride ions are involved in H-bonds which connect like residues along the *b* direction, and between RMg1 and RMg2 residues extending the structure along the *c* direction. Cl1 and Cl2 are the acceptor ions for H-bonds that connect RMg2 residues to each other along the *b* direction, but only Cl1 connects along the *a* direction. Similarly, Cl3 and Cl4 ions are involved in H-bonds linking RMg1 residues together along the *b* direction, and only Cl3 connects RMg1 residues along the *a* direction.

Linking RMg1 residues along the *a* direction, there are four H-bonds to Cl3 which also serve to connect the structure along the *b* and *c* directions (Figure 4.9(b), Table 4.5). Three of these interactions are between water ligands, O8-H8A···Cl3, O9-H9A···Cl3[d], and O10-

H10A···Cl3[e], and one is from the N-H group of nicotinic acid, N2-H102···Cl3[c]. O9-H9A···Cl3[d] is likely to be the weakest of these H-bonds due to its long D···A distance of 3.601(2) Å and angle of 150(3)°. N2-H102···Cl3[c] has the shortest of these H-bonds' D···A distances at 3.053(2) Å, and the second largest angle of 167°[#]. O8-H8A···Cl3 and O10-H10A···Cl3[e] are the most similar in length at 3.116(2) Å and 3.124(2) Å, respectively, however the latter has a more linear angle of 172(3)° compared to 164(2)° of O8-H8A···Cl3.

There are three H-bonds which associate RMg2 residues along the *a* direction for which Cl1 is the acceptor ion (Figure 4.9(c), Table 4.5), therefore these interactions also contribute to the extending of the structure along the *b* and *c* directions. O2-H2A···Cl1[f] and O4-H4B···Cl1[g] are formed between water ligands and Cl1, with D···A distances of 3.190(2) Å and 3.116(2) Å and angles of 165(3)° and 174(2)°, respectively, and are likely to be stronger interactions than C3-H103···Cl1[h] which is 3.649(2) Å in length and has an angle of 149°.

The structure is extended along the *b* direction *via* interactions involving all four chloride ions. RMg1 residues are connected through H-bonds to Cl3 that also connect along the *a* direction. Three H-bonds involving Cl4 also connect RMg1 residues along the *b* direction (Figure 4.10(b), Table 4.5). These bonds are all formed between water ligands and Cl4. O8-H8B···Cl4[i] is the weakest of these interactions with a D···A distance of 3.243(2) Å and an angle of 163(3)°, compared to the slightly shorter, and slightly more linear O9-H9B···Cl4[a] and O12-H12B···Cl4 with lengths of 3.054(2) Å and 3.154(2) Å and angles of 170(3)° and 173(3)°, respectively. It is interesting that the H9A-O9-H9B angle is the smallest involving the water ligands, at just 97(3)°; this angle may be compressed due to the positions of the Cl3 and Cl4 ions to which it forms O-H···Cl interactions.

RMg2 residues are linked along the *b* direction through interactions involving Cl1 and Cl2, (Figure 4.10(c), Table 4.5). Cl1 is also the acceptor in H-bonds connecting these residues along the *a* direction except in the case of the H-bond N1-H1···Cl1[j] which connects only along the *b* direction and contributes towards the connectivity along the *c* direction. This H-bond displays the shortest of these interactions with a D···A distance of 3.069(2) Å and an angle of 158°. Of the H-bonds to the Cl2 ion, the donor atom is always a water ligand oxygen atom and their lengths range from 3.156(2) Å for O6-H6B···Cl2[b] to 3.213(2) Å for O3-H3A···Cl2; O3-H3B···Cl2[f] has the most linear angle of 177(3)°.

The structure of **(2)** is propagated along the *c* direction by H-bonds involving all of the chloride ions and one H-bond between water ligands (Figure 4.11(a), Table 4.5). O2-H2B···O8[f] occurs directly between a donor water ligand of the RMg2 residue to a water

[#] In cases where an s.u. is not provided on H-bond distances or angles, the H atom involved has been fixed in a geometrically calculated position.

oxygen atom acceptor of RMg1. This is the shortest H-bond of all those observed in this structure at 2.821(2) Å, yet it has a relatively low angle of 151(3)°. The four H-bonds O4-H4A···Cl3^{f}, O6-H6A···Cl4^{b}, O10-H10B···Cl1 and O12-H12A···Cl2 are particularly involved in connecting between RMg1 and RMg2 residues. These interactions are all longer than 3 Å, in common with all the other H-bonds in this structure, and O6-H6A···Cl4^{b} has the largest angle of 177(3)°.

As for **(1)**, **(2)** is unlikely to display π-π stacking interactions. Figure 4.11(b) shows two of each of the RMg1 and RMg2 residues. The centroid – centroid distance between the parallel aromatic groups of the RMg1 residues is 4.631(1) Å, and between parallel aromatic groups of the RMg2 residues is 4.500(1) Å. The angle between the planes of the facing aromatic groups of the RMg1 and RMg2 residues is 5.9(1)° and the distance separating their centroids is 4.400(1) Å. These distances are too long to suggest that π-π stacking has any influence on the structure of **(2)**; it would appear that, in part due to the chloride ions present, H-bonds are the main driving force in its connectivity.

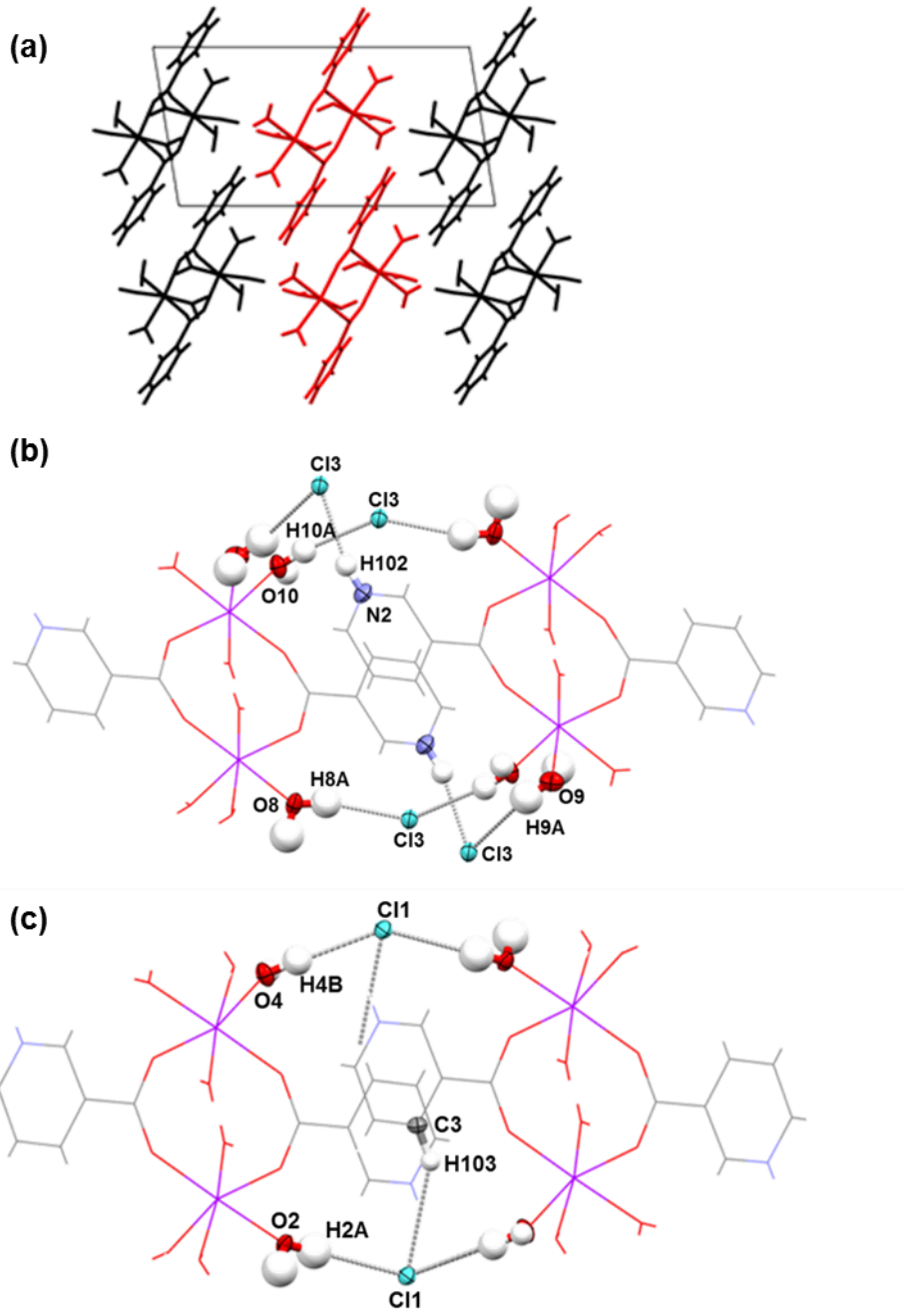

Figure 4.9. Crystal structure of **(2)**. (a) View down the *b* axis showing packing of RMg1 (black) and RMg2 (red) along the *a* and *c* directions. (b) H-bonds between RMg1 residues connecting the structure along the *a* direction. (c) H-bonds between RMg2 residues connecting the structure along the *a* direction.

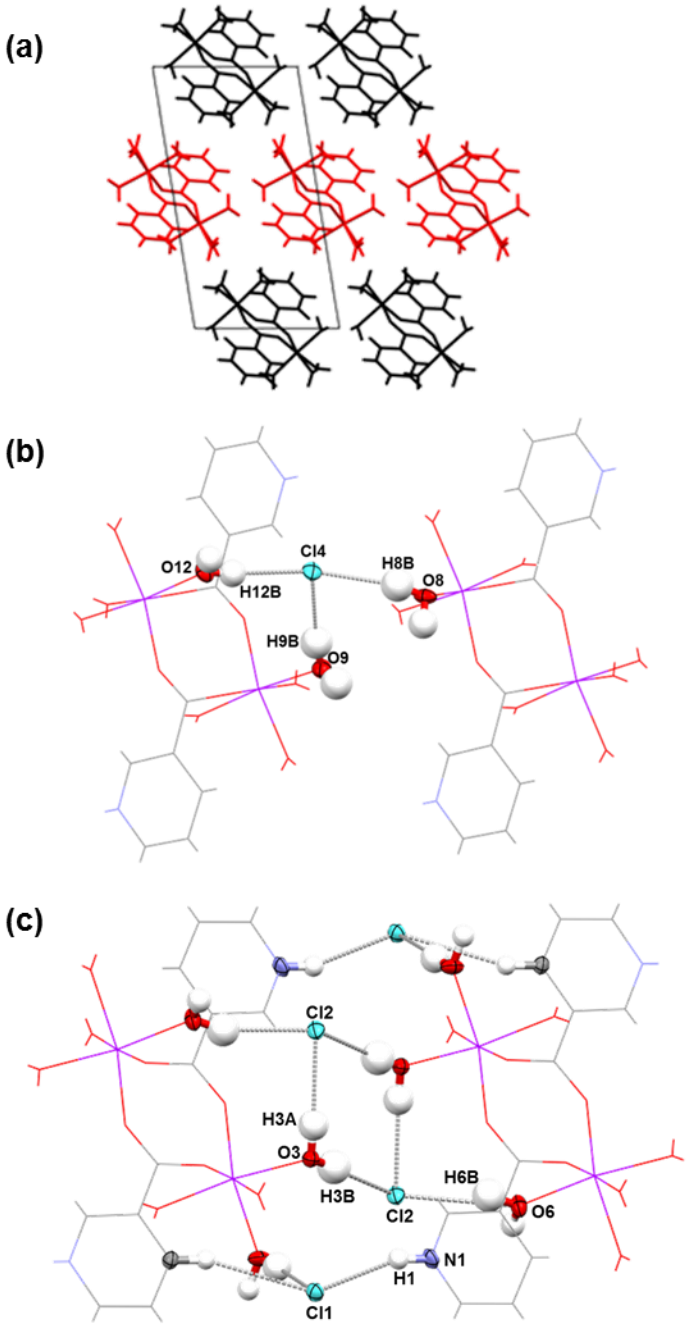

Figure 4.10. Crystal structure of **(2)**. (a) View down the *a* axis showing packing of RMg1 (black) and RMg2 (red) along the *b* and *c* directions. (b) H-bonds between RMg1 residues connecting the structure along the *b* direction, (omitting H-bonds to Cl3 that connect the structure along *a* direction). (c) H-bonds between RMg2 residues connecting the structure along the *b* direction (including unlabelled H-bonds that also connect the structure along the *a* direction).

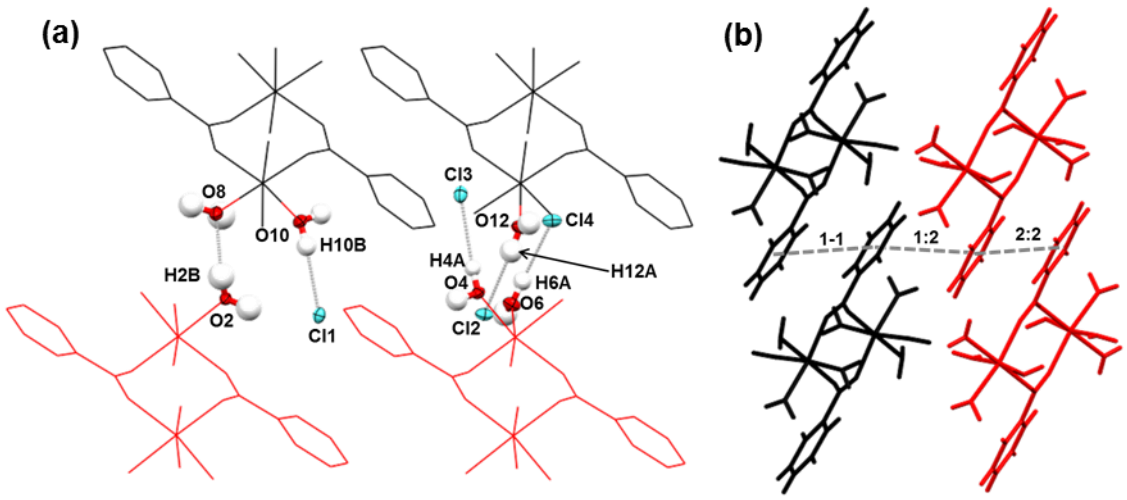

Figure 4.11. Crystal structure of **(2)**. (a) Selected H-bonds connecting RMg1 and RMg2 residues along the *c* direction. (b) View down the *b* axis showing aromatic group separations, RMg1 [1] (black) and RMg2 [2] (red).

Table 4.5. Geometries of H-bonds in **(2)**.

D-H···A Interaction	D-H (Å)	H···A (Å)	D···A (Å)	D-H···A (°)
(Figure 4.9(b)) H-bonds connecting RMg1 along a direction				
*N2-H102···Cl3[c]	0.86	2.21	3.053(2)	167
O8-H8A···Cl3	0.87(2)	2.27(2)	3.116(2)	164(2)
O9-H9A···Cl3[d]	0.81(3)	2.87(3)	3.601(2)	150(3)
O10-H10A···Cl3[e]	0.85(3)	2.28(3)	3.124(2)	172(3)
(Figure 4.9(c)) H-bonds connecting RMg2 along a direction				
O2-H2A···Cl1[f]	0.84(3)	2.37(3)	3.190(2)	165(3)
O4-H4B···Cl1[g]	0.88(3)	2.24(3)	3.116(2)	174(2)
*C3-H103···Cl1[h]	0.93	2.82	3.649(2)	149
(Figure 4.10(b)) H-bonds connecting RMg1 along b direction				
O8-H8B···Cl4[i]	0.84(2)	2.43(2)	3.243(2)	163(3)
O9-H9B···Cl4[a]	0.87(2)	2.20(2)	3.054(2)	170(3)
O12-H12B···Cl4	0.84(2)	2.32(2)	3.154(2)	173(3)
(Figure 4.10(c)) H-bonds connecting RMg2 along b direction				
*N1-H1···Cl1[j]	0.86	2.26	3.069(2)	158
O3-H3A···Cl2	0.85(2)	2.37(2)	3.213(2)	171(2)
O3-H3B···Cl2[f]	0.85(3)	2.36(3)	3.210(2)	177(3)
O6-H6B···Cl2[b]	0.85(2)	2.35(2)	3.156(2)	160(3)
(Figure 4.11(a)) H-bonds connecting RMg1 and RMg2 along c direction				
O2-H2B···O8[f]	0.83(2)	2.07(2)	2.821(2)	151(3)
O4-H4A···Cl3[f]	0.84(2)	2.44(2)	3.276(2)	171(2)
O6-H6A···Cl4[b]	0.84(3)	2.23(3)	3.066(2)	177(3)
O10-H10B···Cl1	0.87(2)	2.31(2)	3.166(2)	171(2)
O12-H12A···Cl2	0.84(2)	2.28(2)	3.111(2)	171(2)

Symmetry codes: [a](1-x,1-y,-z) [b](1-x,-y,1-z) [c](2-x,2-y,-z) [d](-1+x,1+y, z) [e](-1+x,y,z) [f](1-x,1-y,1-z) [g](-x,1-y,1-z) [h](1+x,-1+y,z) [i](x,1+y,z) [j](1+x,y,z) *H-bond features aromatic hydrogen atom fixed in idealised position.

A single crystal of **(2)** was analysed by HSM, indicating a melting range of 153 – 167 °C. This was not confirmed by DSC analysis which only showed decomposition starting at about 120 °C (Appendix A, Figure A2). However HSM did show the slow release of bubbles from about 66 °C and a large bubble released at approximately 130 °C. In the DSC trace there is a gradual decline from about 60 °C before decomposition.

4.2.3. *Bis-[(μ_2-pyridinium-3-carboxylato)-bis-(nitrato)-diaqua-calcium(II)]* **(3)**

$[Ca(C_6H_5NO_2)(H_2O)_2(NO_3)_2]_2$

(3) is a calcium containing complex, but in common with both **(1)** and **(2)** it is composed of discrete units which display an eight-membered ring structure in which two metal centres that are related through an inversion centre are bridged by two crystallographically equivalent carboxylate groups of the zwitterionic pyridyl carboxylic acid, which in this case is nicotinic acid, as in **(2)**. **(3)** differs from the previous two structures in that it features two coordinating water ligands, as opposed to four, and due to the different metal salt used as a starting material it does not have the chloride ions that were key to the H-bond networks in those complexes. Instead, the complex contains two chelating bidentate (κ^2) nitrate ions per metal centre. As in **(2)**, there are no non-coordinated water molecules in the structure.

(3) was prepared by growth from a solution of a 1:1 stoichiometric mixture of nicotinic acid and calcium(II) nitrate tetrahydrate dissolved in isopropanol at 4 °C in a vial with a hole-pierced lid. The resulting crystals were small, clear, colourless and very thin platelets. The crystals were stored in the fridge and after another seven months the solvent had evaporated and the dry material was analysed by PXRD. The single crystals in solution were clear and colourless, however the crystalline product, once dry, was a peachy-orange colour. The unit cell of a crystal from this dry material was determined, confirming that this orange material was still **(3)**. Figure 4.12 shows that the crystal selected for analysis by scXRD is quite representative of the bulk material, with good coincidence of the peaks of the experimental and calculated patterns. Some peaks may be due to the starting materials, but the strong peak at about 22° coincides especially well with an intense peak only of the calculated pattern, taking into account the expected shifting of this pattern to slightly higher 2θ values.

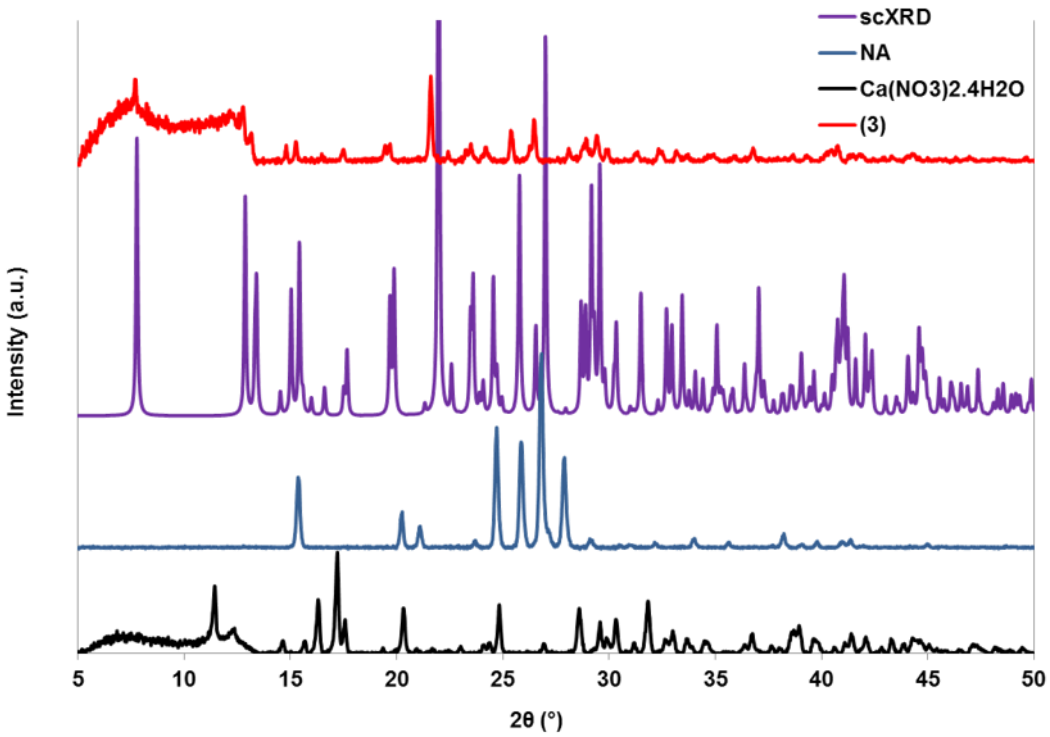

Figure 4.12. PXRD pattern of **(3)** compared to calculated pattern and patterns of starting materials.

The calcium centre in **(3)** is eight-coordinate (Figure 4.13(a), Table 4.6). The nitrate and water ligands are orientated similarly to their ligand pairs. The nitrate ions are bent slightly in towards each other about the coordinating oxygen atoms, and the angle between them as defined by the angles O8-Ca1-O5 and O9-Ca1-O6 are 74.57(4)° and 70.49(3)°, respectively. The angles formed between the coordinating oxygen atoms of the same nitrate ion and the calcium centre, O8-Ca1-O9 and O5-Ca1-O6, are 50.78(3)° and 49.66(3)°, respectively, as expected for this type of coordination. The distances between the nitrate oxygen atoms and the calcium centre are generally slightly longer, ranging from 2.480(1) Å for Ca1-O9 to 2.625(1) Å for Ca1-O6, compared to those between the calcium centre and the water molecules or carboxylate oxygen atoms. Of these coordination lengths, the water oxygen atom-calcium distances are longer at 2.431(1) Å and 2.387(1) Å for Ca1-O1 and Ca1-O2, respectively, while the calcium-carboxylate oxygen atom distances are the shortest at 2.390(1) Å for Ca1-O3 and 2.317(1) Å for Ca1-O4^{a}. This may contribute to the proximity of the water molecules to form the H-bond O2-H8···O1^{a} displayed within the formula unit (Figure 4.13(b), Table 4.7). O2-H8···O1^{a} is of medium length at 2.820(2) Å and the angle is 160(2)°. This is a moderately strong intramolecular

interaction, and it would seem that it constrains the metal-organic ligand coordination conformation.

The water ligands are not orientated perpendicular to the bridging nicotinic acid ligands. The angle between the water oxygen atoms, O1-Ca1-O2, is 143.35(4)° and is possibly contracted by the H-bond between the coordinated water ligands in the formula unit. The angles between each of the water oxygen atoms and each of the carboxylate oxygen atoms are less than 90°, possibly due to the distortion of the O1-Ca1-O2 angle affected by the intracomplex H-bond. O1-Ca1-O3 and O2-Ca1-O3 are 84.32(4)° and 84.01(4)°, respectively, while O1-Ca1-O4^{a} and O2-Ca1-O4^{a} are 79.88(4)° and 75.81(4)°, respectively.

The angle formed between the coordinating carboxylate oxygen atoms O3-Ca1-O4^{a} is 119.07(4)°, which may be optimal for the formation of the H-bond, and may also effectively compress the angle between the nitrate ions opposite the carboxylate oxygen atoms.

The formula unit of **(3)** is shown in (Figure 4.13(c)). The calcium centres and the two carboxylate group atoms that make up the eight-membered ring lie on a plane with a deviation of ± 0.055(1) Å. This is significantly less than the deviations from the average plane of the eight-membered rings in **(1)** (± 0.159(1) Å), and **(2)** (± 0.271(1) Å and ± 0.386(1) Å for RMg1 and RMg2, respectively). In **(3)** the atoms of the eight-membered ring are thus closer to coplanarity in comparison to the analogous rings in the previously discussed structures.

The carboxylate group angle (O3-C1-O4) is 124.2(1)°, which is closer to the O=C-O angle found in pure nicotinic acid (123.2(3)°) than the carboxylate group angles in both **(1)** and **(2)** are to the O=C-O angles of their respective ligands in pure form. The C-O distances are 1.241(2)° for C1-O4 and 1.260(2)° for C1-O3 which are comparable to the equivalent distances observed in the carboxylate groups in **(1)** and **(2)**.

The pyridinium ring and the carboxylate group are twisted from coplanarity with an O3-C1-C2-C4 torsion angle of −30.9(2)°. This twisting may be present to allow the two calcium centres and two carboxylate groups to be coplanar, and may result in the almost linear angle formed by Ca1^{a}-O4-C1 of 171.24(9)°. The other Ca-O-C angle, Ca1-O3-C1 is smaller at 109.81(1)°, which may be preferential to allow close interaction between the H-bonding water ligands. It is interesting to note that the greater distance of Ca1-O3 at 2.390(1) Å is associated with the smaller angle Ca1-O3-C1, and the shorter interaction Ca1-O4^{a} of 2.317(1) Å is associated with the significantly wider angle of Ca1^{a}-O4-C1. This pattern is observed in **NISJEE**, **(1)** and residue RMg1 of **(2)** but not in RMg2.

In the PXRD pattern of **(3)** (Figure 4.12), the most intense peak is the (1-10) at about 22°. The plane on which the eight-membered ring is located is close to this lattice plane (Figure 4.13(d)) being tilted to it by an angle of approx. 8.9°.

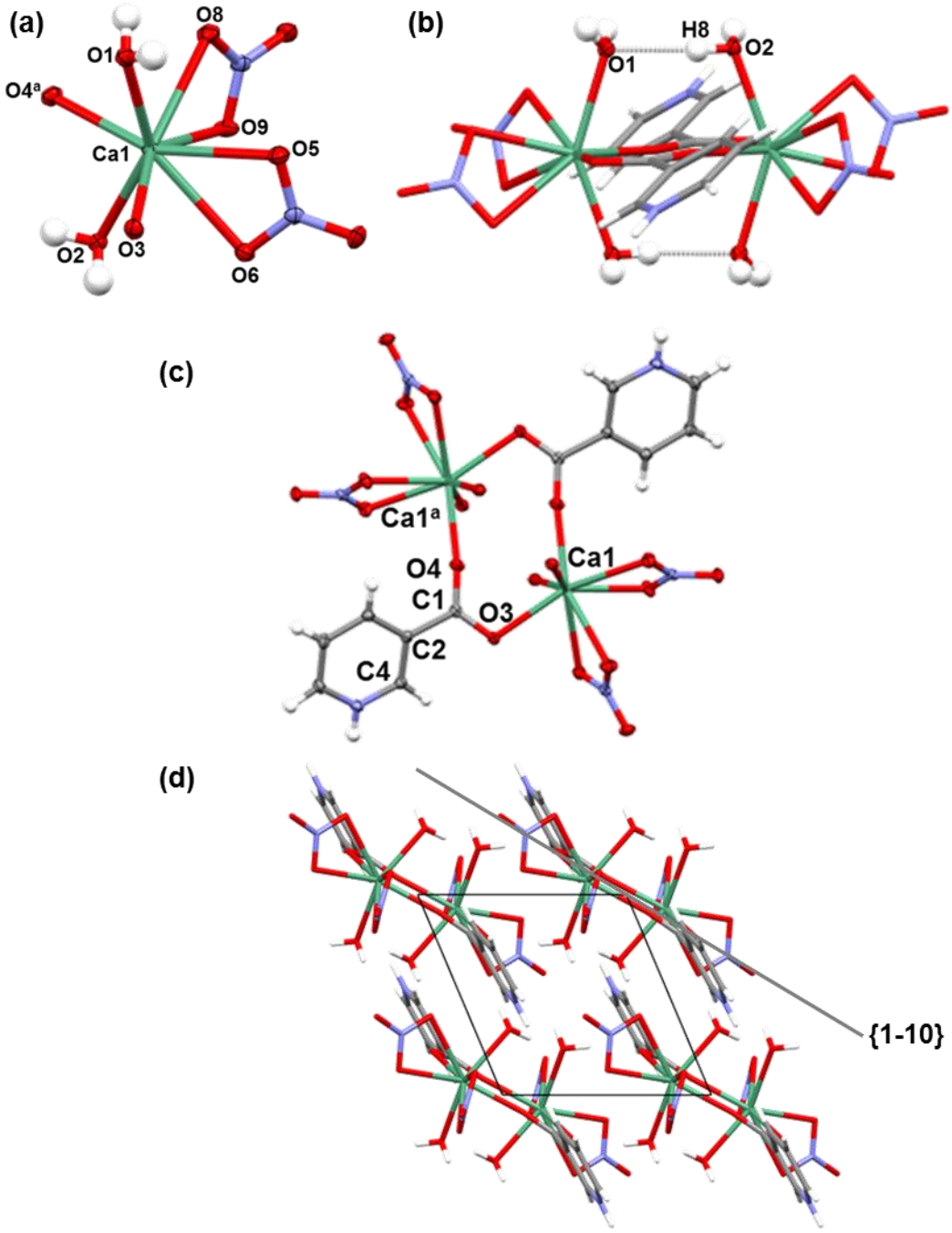

Figure 4.13. Crystal structure of **(3)**. (a) Eight-coordinate Ca centre with two coordinating nitrate ions, two coordinating carboxylate oxygen atoms and two coordinating water molecules. (b) Formula unit showing intracomplex H-bond O2-H8···O1[a]. (c) Formula unit showing bridging nicotinic acid ligand and eight-membered ring conformation (water hydrogen atoms removed for clarity). (d) View down the *c* axis showing crystal packing, and formula units aligned along {1-10} plane. Symmetry codes: [a](-x, -y, 1-z)

Table 4.6. O-Ca-O angles and Ca-O distances in **(3)**.

Coordination	O-Ca-O angle (°)	Interaction	Distance (Å)
O1-Ca1-O8	72.47(4)	Ca1-O1	2.431(1)
O1-Ca1-O9	123.15(3)	Ca1-O2	2.387(1)
O1-Ca1-O5	91.10(4)	Ca1-O3	2.390(1)
O1-Ca1-O6	135.49(4)	Ca1-O4[a]	2.317(1)
O1-Ca1-O3	84.32(4)	Ca1-O5	2.503(1)
O1-Ca1-O4[a]	79.88(4)	Ca1-O6	2.625(1)
O1-Ca1-O2	143.35(4)	Ca1-O8	2.553(1)
O2-Ca1-O3	84.01(4)	Ca1-O9	2.480(1)
O2-Ca1-O4[a]	75.81(4)		
O2-Ca1-O9	85.26(4)		
O2-Ca1-O8	128.60(4)		
O2-Ca1-O6	72.03(4)		
O2-Ca1-O5	121.52(4)		
O4[a]-Ca1-O8	80.59(4)		
O8-Ca1-O5	74.57(4)		
O5-Ca1-O3	82.57(4)		
O3-Ca1-O4[a]	119.07(4)		
O4[a]-Ca1-O9	92.63(4)		
O9-Ca1-O6	70.49(3)		
O6-Ca1-O3	72.05(3)		
O8-Ca1-O9	50.78(3)		
O5-Ca1-O6	49.66(3)		

Symmetry codes: [a](-x, -y, 1-z)

The packing of the crystal structure of **(3)** is directed by H-bond interactions between the water molecules and the N-H group and C-H groups of the pyridinium rings to the

carboxylate and nitrate oxygens. The formula units are arranged in layers parallel to the *bc* plane and are linked along the *a* direction by an H-bond between the water molecule of one formula unit and a carboxylate oxygen atom of the next, O1-H7···O3^{b} (Figure 4.14(a), Table 4.7). In this interaction, the oxygen atom O1 is the donor and O1 is also the acceptor in the H-bond within the formula unit (O2-H8···O1^{a}). O1-H7···O3^{b} is a moderately strong H-bond with a D···A distance of 2.684(2) Å and an angle of 168(2)°.

Extending the structure along the *b* direction, there are three H-bonds between formula units (Figure 4.14(b), Table 4.7). The coordinated nitrate ion of one formula unit accepts H-bonds from two water molecules coordinated to each of the Ca centres of the next formula unit along the *b* axis, O1-H6···O7^{c} and O2-H9···O6^{d}. The former H-bond is slightly longer with a D···A distance of 2.917(2) Å and an angle of 167(2)°. O2-H9···O6^{d} is the shorter interaction at 2.869(2) Å and has an angle of 162(2)°. The third H-bond is formed between the C-H group of a pyridinium ring to the oxygen atom of one of the H-bonding water molecules, C4-H5···O2^{d}. Although this H-bond has an angle of 171(1)°, it is slightly longer than the H-bonds involving the water molecules as donors at 3.280(2) Å, and since it features a carbon donor, it is likely to be a weaker interaction.

The formula units interact along the *c* direction through H-bonds between the pyridinium ring of one formula unit to the nitrate ion of the next one along the *c* direction (Figure 4.14(c), Table 4.7). H2 of C6 of the pyridinium ring, is attracted towards both O9 and O10 of the nitrate ion of the next formula unit, resulting in the H-bonds C6-H2···O9^{e} and C6-H2···O10^{e}. Neither of these are strong interactions, with the former having an angle of 147(2)° and D···A distance of 3.367(2) Å, while the latter has the shorter length of 3.056(2) Å and a very low angle of 122(1)°. H2 is located *ca*. 0.382 Å from the mean plane of C6, O9^{e} and O10^{e}, and the sum of the angles C6-H2-O10^{e}, O10^{e}-H2-O9^{e} and C6-H2-O9^{e} is approx. 320°. Therefore the H-bonds in which H2 participates do not definitively indicate a bifurcated H-bond. The H-bond C3-H1···O10^{e} is formed between another C-H group of the pyridinium ring to O10 of the nitrate ion. This is also a weak interaction with a small angle of 119(1)° and a D···A distance of 3.122(2) Å. The pyridinium ring also forms two H-bonds to the nitrate ion of the formula unit located along the *b* axis from the formula unit to which it H-bonds *via* C3 and C6, therefore connecting the structure along both the *b* and *c* directions (Figure 4.14(d), Table 4.7). Of these H-bonds, N3-H4···O10^{f} is the strongest with a D···A distance of 2.778(2) Å and an angle of 154(2)°. The second H-bond is from a C-H group and it is as expected a weaker interaction with a D···A distance of 3.205(2) Å and a slightly smaller angle of 148(1)°.

Thus it is evident that in an analogous manner to that in which the chloride counter ions were fundamental to the connectivity of the structures of **(1)** and **(2),** the coordinated nitrate

ions are central to the H-bonding interactions that influence the packing of **(3)**. Furthermore, the intracomplex H-bond O2-H8···O1[a] clearly exerts some influence over the shape of the formula unit, and therefore the entire crystal packing.

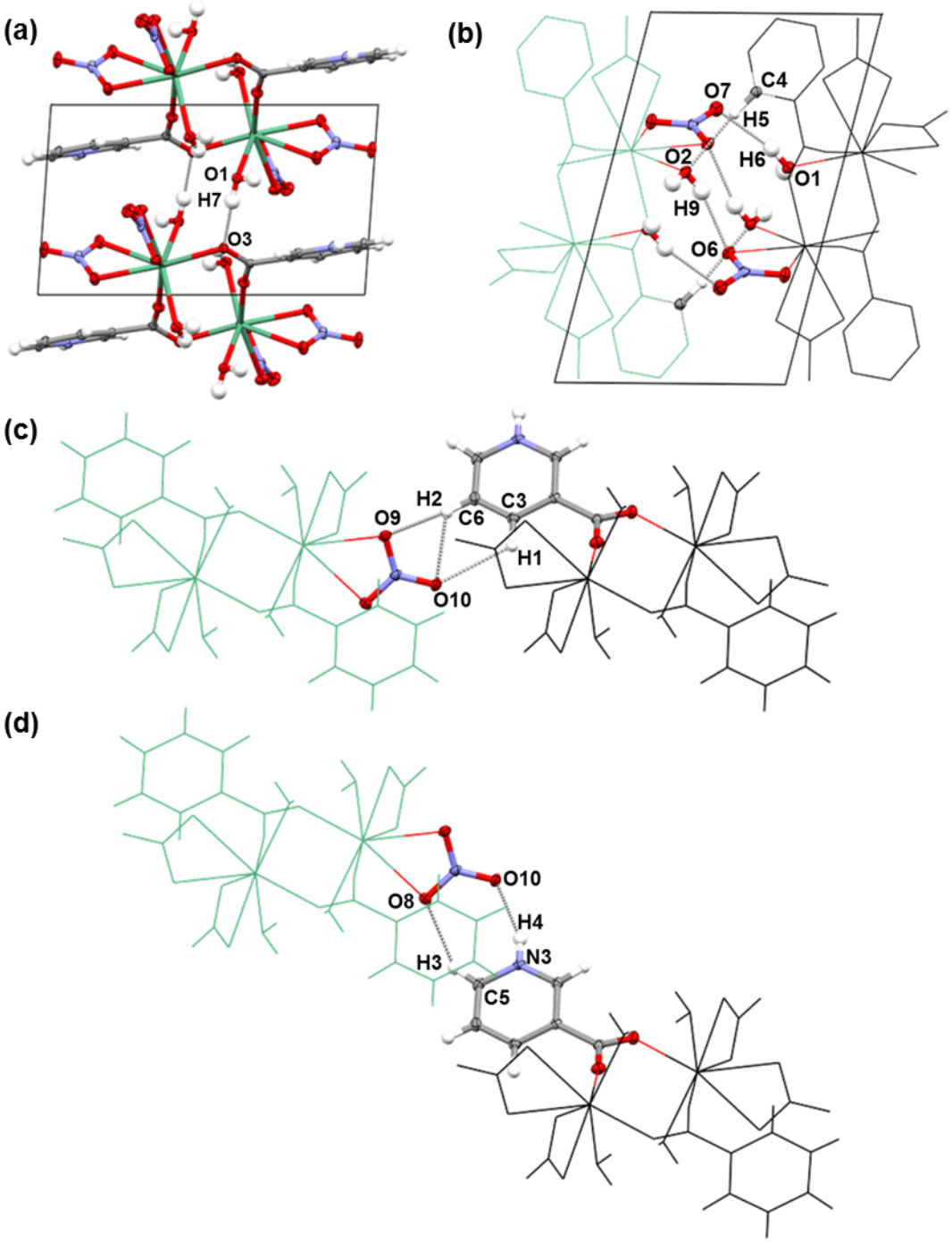

Figure 4.14. Crystal structure of **(3)**. (a) H-bond connecting formula units along the *a* direction. (b) H-bonds connecting formula units along the *b* direction. (c) H-bonds connecting formula units along the *c* direction. (d) H-bonds connecting formula units along the *b* and *c* directions.

Table 4.7. Geometries of H-bonds in **(3)**.

D-H···A Interaction	D-H (Å)	H···A (Å)	D···A (Å)	D-H···A (°)
(Figure 4.13(b)) Intracomplex H-bond within formula unit				
O2-H8···O1[a]	0.83(2)	2.02(2)	2.820(2)	160(2)
(Figure 4.14(a)) H-bond connecting formula units along a direction				
O1-H7···O3[b]	0.84(3)	1.85(3)	2.684(2)	168(2)
(Figure 4.14(b)) H-bonds connecting formula units along b direction				
O1-H6···O7[c]	0.81(2)	2.13(2)	2.917(2)	167(2)
O2-H9···O6[d]	0.80(2)	2.10(2)	2.869(2)	162(2)
C4-H5···O2[d]	0.95(2)	2.34(2)	3.280(2)	171(1)
(Figure 4.14(c)) H-bonds connecting formula units along c direction				
C3-H1···O10[e]	0.92(2)	2.57(2)	3.122(2)	119(1)
C6-H2···O9[e]	0.93(2)	2.55(2)	3.367(2)	147(2)
C6-H2···O10[e]	0.93(2)	2.46(2)	3.056(2)	122(1)
(Figure 4.14(d)) H-bonds connecting formula units along c and b directions				
N3-H4···O10[f]	0.86(2)	1.98(2)	2.778(2)	154(2)
C5-H3···O8[f]	0.94(2)	2.37(2)	3.205(2)	148(1)

Symmetry codes: [a](-x,-y,1-z) [b](1-x,-y,1-z) [c](x,-1+y,z) [d](-x,1-y,1-z) [e](x,y,-1+z) [f](x,1+y,-1+z)

HSM analysis of a single crystal of **(3)** gave a melting range of 109 – 116 °C. DSC analysis (Appendix A, Figure A3) also showed an endothermic event within this range, indicating a melting point of 111.1 °C. This is a lower melting range compared to that for **(2)** at 153 – 167 °C, and the possible melting point of **(1)** at 193.0 °C.

4.2.4. *Bis-(pyridinium-3-carboxylato)-pentaaqua-calcium(II) dichloride* **(4)**

$[Ca(C_6H_5NO_2)_2(H_2O)_5].2Cl$

(4) was first prepared by growth from a 1:1 stoichiometric mixture of nicotinic acid and calcium(II) chloride dissolved in isopropanol at 4 °C in a vial with a hole-pierced lid. When the experiment was repeated at lab temperature, 30 °C, 40 °C or 50 °C, another complex,

(13), was formed, which is discussed later. Figure 4.15(a) shows crystals produced from the experiment using isopropanol, still in solution. For this preparation, the crystals formed within four months, and after another six months the solvent had evaporated and the dry material was pale yellow in colour. The PXRD pattern obtained from this sample (Appendix A, Figure A4), is not the same as the calculated pattern, therefore the single crystal is not representative of the dry bulk material. The sample was prepared in a 1:1 molar ratio of calcium(II) chloride and nicotinic acid, yet **(4)** has a ligand:metal ratio of 2:1, therefore there may be excess $CaCl_2$ in the reaction vessel, but this is not apparent in the obtained PXRD pattern. The PXRD pattern of **(4)** shows a better match to the PXRD pattern of **(13)** (Appendix A, Figure A5), suggesting that once dry, the crystalline material converted to this complex. This would involve the loss of the coordinated water molecules and coordination to the chloride ions.

The calcium centre in **(4)** is seven-coordinate and has a distorted pentagonal bipyramidal structure (Figure 4.15(b), Table 4.8). It is coordinated to five oxygen atoms of water ligands and to two carboxylate oxygen atoms of two crystallographically different zwitterionic nicotinic acid ligands. The angles O5-Ca1-O3, O3-Ca1-O9, O9-Ca1-O8, O8-Ca1-O7 and O7-Ca1-O5 range from 67.76(3)° to 74.78(3)°, bracketing the expected value of 72° for the angle between equatorial ligands for complexes of this geometry. The angle formed between the axial substituents (O1 and O6) and the Ca centre is 169.40(3)°. The angles between O1, a carboxylate oxygen atom and the equatorial oxygen atoms are very close to 90°, with the biggest deviations exhibited by O1-Ca1-O8 with an angle of 84.13(3)°, and O1-Ca1-O7 of 101.54(3)°. The angles between O6, a water oxygen atom, and the equatorial ligands deviate slightly more from 90°, with O6-Ca1-O7 of 80.28(3)° and O6-Ca1-O5 of 103.23(3)°. The Ca-O distances for the carboxylate oxygen atoms constitute both the shortest and longest of the Ca-O distances; Ca1-O1 is 2.318(1) Å whereas Ca1-O3 has a distance of 2.438(1) Å. Ca1-O9 and Ca1-O8 have about equally long coordination distances of 2.439(1) Å and 2.436(1) Å, respectively.

The formula unit features two zwitterionic nicotinic acid ligands, each coordinating to the calcium centre *via* one carboxylate oxygen atom, while the other is non-coordinated, but still deprotonated - instead the nitrogen is protonated (Figure 4.15(c)). The C-O distances involving the metal-coordinated oxygen atoms are 1.240(1) Å for C7-O3 and 1.244(1) Å for C1-O1. The C-O distances involving the non metal-coordinated oxygen atoms are longer at 1.270(1) Å for C7-O4 and 1.259(1) Å for C1-O2. The O-C-O angles are 125.4(1)° and 125.3(1)° for O4-C7-O3 and O1-C1-O2, respectively. These are wider than the O=C-O angle in pure nicotinic acid (123.2(3)°) despite the carboxylate group not bridging metal centres. The carboxylate groups and the pyridinium rings are twisted quite significantly from

coplanarity with a O1-C1-C2-C3 torsion angle of -27.3 (2)°, and a O3-C7-C8-C9 torsion angle of 21.2(2)°.

The formula unit displays two intracomplex H-bonds (Figure 4.15(d), Table 4.9). These are formed between a C-H group of each nicotinic acid ligand and oxygen atoms of two water ligands, C3-H3···O7 and C9-H109···O6. These are weak interactions with long D···A distances of 3.508(2) Å and 3.298(2) Å, and relatively small angles of 130(1)° and 148(1)° for C3-H3···O7 and C9-H109···O6, respectively.

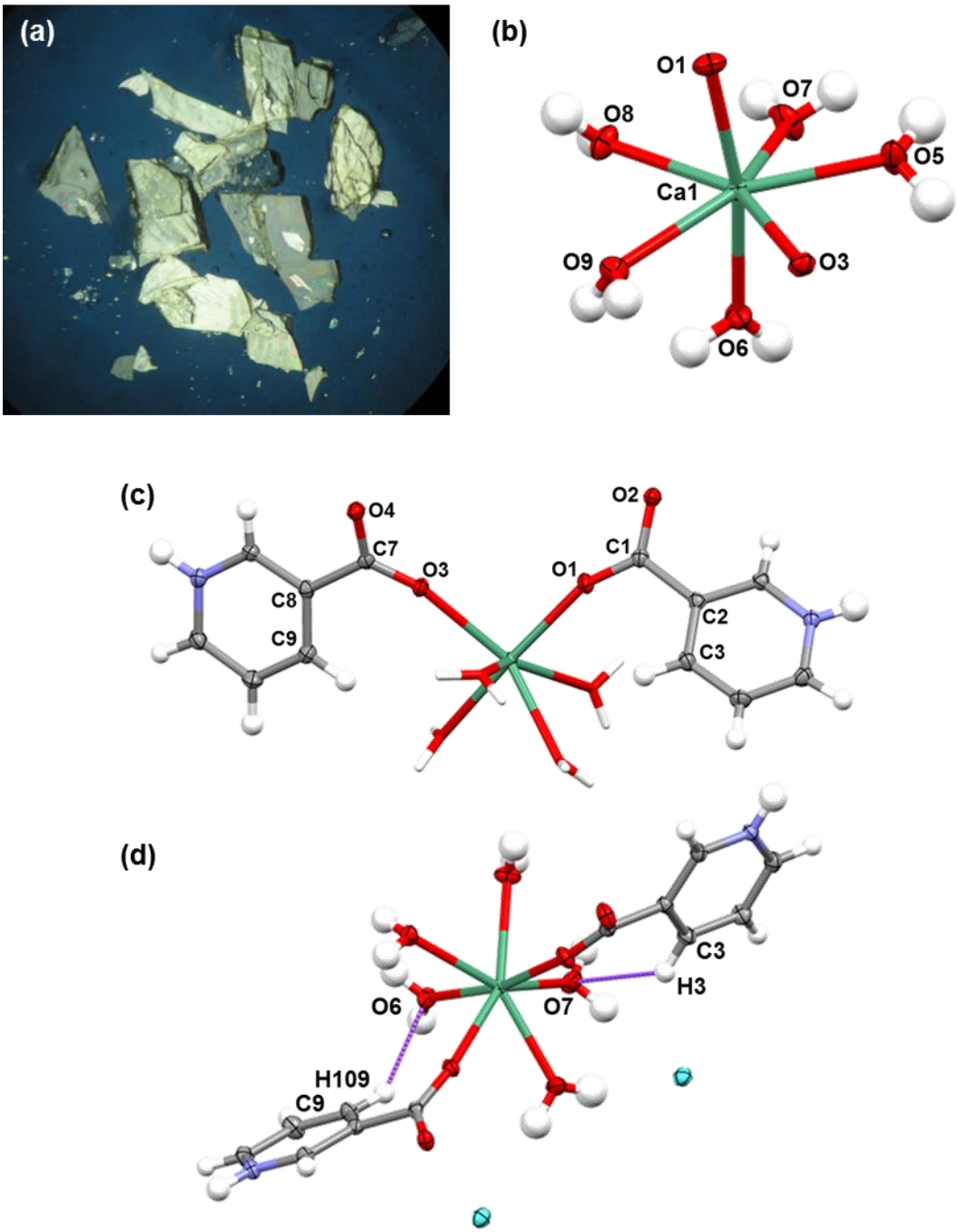

Figure 4.15. Crystal structure of **(4)**. (a) Crystals of **(4)** in solution. (b) Seven-coordinate Ca centre with five coordinating water molecules and two coordinating carboxylate oxygen atoms. (c) Formula unit showing carboxylate groups (chloride ions and one water ligand omitted for clarity). (d) Formula unit showing intracomplex H-bonds C3-H3···O7 and C9-H109···O6.

Table 4.8. O-Ca-O angles and Ca-O distances in **(4)**.

Coordination	O-Ca-O angle (°)	Interaction	Distance (Å)
O1-Ca1-O5	87.25(3)	Ca1-O1	2.318(1)
O1-Ca1-O3	89.67(3)	Ca1-O5	2.384(1)
O1-Ca1-O9	90.88(3)	Ca1-O3	2.438(1)
O1-Ca1-O8	84.13(3)	Ca1-O9	2.439(1)
O1-Ca1-O7	101.54(3)	Ca1-O8	2.436(1)
O6-Ca1-O5	103.23(3)	Ca1-O7	2.397(1)
O6-Ca1-O3	95.79(3)	Ca1-O6	2.350(1)
O6-Ca1-O9	81.95(3)		
O6-Ca1-O8	86.45(3)		
O6-Ca1-O7	80.28(3)		
O5-Ca1-O3	67.76(3)		
O3-Ca1-O9	73.97(3)		
O9-Ca1-O8	74.78(3)		
O8-Ca1-O7	73.14(3)		
O7-Ca1-O5	73.23(3)		
O1-Ca1-O6	169.40(3)		

The structure of **(4)** is composed of hydrogen bonded formula units. The metal-organic units are linked directly through H-bonds between: the N-H groups of the pyridinium rings and the non-coordinated carboxylate oxygen atoms; water ligands and non-coordinated carboxylate oxygen atoms; C-H groups of the pyridinium ring and a coordinated carboxylate oxygen atom, and to water ligands. However, the structure is primarily propagated *via* H-bonds to both of the non-coordinated chloride ions.

(4) is composed of H-bonded 2D motifs of metal-organic units along the {101} plane which are separated and linked by the chloride ions (Figure 4.17(a)). In order to interpret clearly the H-bonds that are formed within this structure however, it is more useful to look at how the H-bonds connect formula units in the *a*, *b* and *c* directions.

Figure 4.16(a) shows one formula unit (coloured by element) and the nearest neighbouring formula units along the *a* and *b* directions (coloured in black), as viewed down the *c* axis. The formula units align in a staggered manner and are linked through fifteen H-bonding interactions. These are listed in Table 4.9 and illustrated in Figure 4.16(b) which shows the same selection of formula units presented previously, except viewed down the *b* axis. Only the H-bonds in which the donor atoms originate from the central formula unit (coloured by element) are shown. These H-bonds connect the crystal structure along the *a* and *b* directions. There are two H-bonds in which a non-coordinated carboxylate oxygen atom is the acceptor: N1-H1···O4^{a} and O8-H8B···O2^{a}. The donor in the former is the protonated nitrogen atom of the pyridinium ring, and in the latter it is an oxygen atom of a water ligand. These are amongst the strongest of the H-bonds in this structure with H···A distances of 1.70(2) Å and 1.98(2) Å, D···A distances of 2.607(1) Å and 2.797(1) Å, and angles of 173(2)° and 165(2)° for N1-H1···O4^{a} and O8-H8B···O2^{a}, respectively. There is also an H-bond in which a coordinated carboxylate oxygen atom is the acceptor: C6-H106···O1^{a} is a far weaker interaction than those above as it has a carbon atom donor. Its relatively weak strength is apparent in its longer H···A distance of 2.93(2) Å, D···A distance of 3.505(1) Å and low angle of 121(1)°. There are six H-bonds formed between water ligands and chloride ions. These are all long and tending towards linear interactions with D···A distances ranging from 3.073(1) Å for O7-H7A···Cl1 to 3.188(1) Å for O9-H9B···Cl2^{b}. The latter displays the smallest angle of these bonds at 164(2)° and O5-H5A···Cl2 has the most linear angle at 178(2)°. There are seven H-bonds featuring a C-H group, five of which involve a chloride ion and two an oxygen atom as the acceptor. As well as forming an H-bond to O1^{a}, C6 also forms an H-bond to the oxygen atom of a water ligand, O5^{a}, from the same formula unit as O1^{a}, to form a bifurcated H-bond. C6-H106···O5^{a} has a comparable D···A distance to C6-H106···O1^{a} at 3.520(1) Å but a much wider angle of 165(1)°. There is another instance where a hydrogen atom of a C-H group is attracted to different acceptors but the H atom is not sufficiently coplanar as to be defined as bifurcated. C11-H11···Cl1^{d} and C11-H11···Cl1^{c} have fairly long D···A distances of 3.364(1) Å and 3.388(1) Å and low angles of 120(1)° and 138(1)°, respectively.

Weak interactions are formed between C-H groups of the pyridinium ring to the chloride ions. C3-H3···Cl1 and C10-H10···Cl2^{c} have long D···A distances of 3.633(1) Å and 3.888(1) Å and low angles of 140(1)° and 131(1)°, respectively.

The formula units are linked along the *c* direction through seven H-bonds, listed in Table 4.9 and shown in Figure 4.16(c), in which only the H-bonds originating from the formula units coloured by element are labelled. Four of these H-bonds are made directly between the metal-organic units and three are *via* the chloride ions. There are two H-bonds in which

the two non-coordinated carboxylate oxygen atoms of the same formula unit are the acceptors: N2-H2···O2^{e} and O9-H9A···O4^{e}. As would be expected, these are moderately strong interactions with D···A distances of 2.645(1) Å and 2.826(1) Å and wide angles of 179(2)° and 176(2)°, respectively. C12-H12···O1^{e} is a weaker H-bond formed between a C-H group of the pyridinium ring and the coordinated carboxylate oxygen atom paired with the non-coordinated oxygen atom acceptor of the H-bond N2-H2···O2^{e}. H12 is also attracted to an oxygen atom of a water ligand of the same formula unit as the acceptor O1^{e}, to form C12-H12···O9^{e}, indicating a bifurcated H-bond. Both of these are weak interactions with D···A distances of 3.404(1) Å and 3.445(1) Å and angles of 124(1)° and 159(1)° for C12-H12···O1^{e} and C12-H12···O9^{e}, respectively. The two H-bonds O7-H7B···Cl1^{f} and O8-H8A···Cl1^{b} are formed from water ligands to chloride ions. The former has the shorter D···A distance of 3.143(1) Å and larger angle of 168(2)°. The other chloride ion is also involved in the connectivity in the *c* direction through the H-bond C5-H105···Cl2^{g}. This is also a weaker interaction with a D···A distance of 3.533(1) Å and angle of 150(1)°.

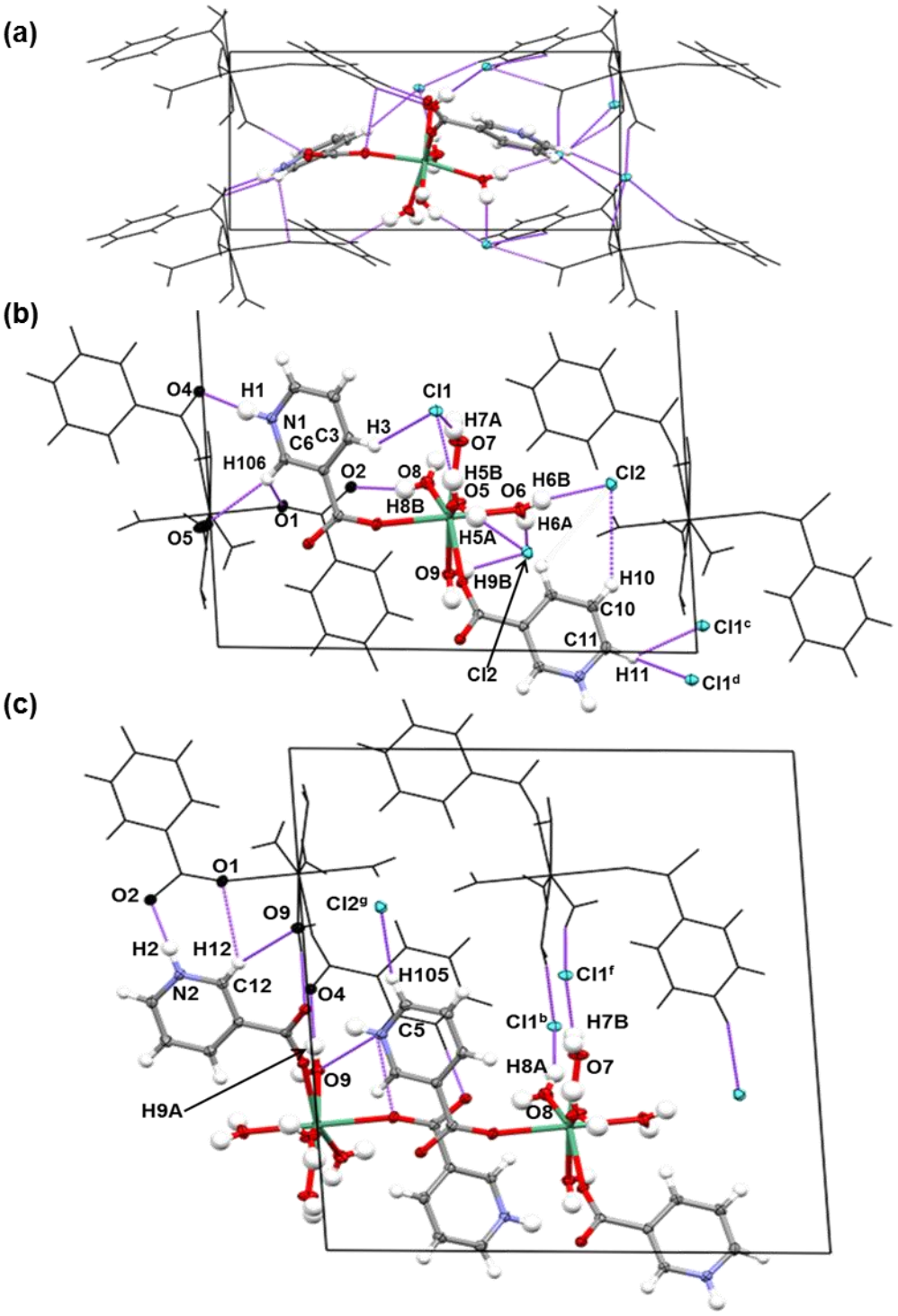

Figure 4.16. Crystal structure of **(4)**. (a) View down the *c* axis showing H-bonds connecting formula units along the *a* and *b* directions. (b) View down the *b* axis showing H-bonds connecting formula units along the *a* and *b* directions. (c) View down the *b* axis showing H-bonds connecting formula units along the *c* direction. Intracomplex H-bonds not included. Symmetry codes for selected Cl ions: [b](x, 1+y, z) [c](1½-x, ½+y, ½-z) [d](½+x, ½-y, -½+z) [f](1-x, 1-y, 1-z) [g](-½+x, ½-y, ½+z)

Table 4.9. Geometries of H-bonds in **(4)**.

D-H···A Interaction	D-H (Å)	H···A (Å)	D···A (Å)	D-H···A (°)
(Figure 4.15(d)) Intracomplex H-bonds within formula unit				
C3-H3···O7	0.94(2)	2.83(2)	3.508(2)	130(1)
C9-H109···O6	0.96(2)	2.45(1)	3.298(2)	148(1)
(Figure 4.16(b)) H-bonds connecting formula units along a and b directions				
N1-H1···O4[a]	0.92(2)	1.70(2)	2.607(1)	173(2)
O5-H5A···Cl2	0.89(2)	2.30(2)	3.183(1)	178(2)
O5-H5B···Cl1	0.85(2)	2.26(2)	3.090(1)	165(2)
O6-H6A···Cl2[b]	0.86(2)	2.23(2)	3.085(1)	170(2)
O6-H6B···Cl2[c]	0.78(2)	2.37(2)	3.140(1)	171(2)
O7-H7A···Cl1	0.87(2)	2.22(2)	3.073(1)	171(2)
O8-H8B···O2[a]	0.84(2)	1.98(2)	2.797(1)	165(2)
O9-H9B···Cl2[b]	0.82(2)	2.40(2)	3.188(1)	164(2)
C3-H3···Cl1	0.94(2)	2.86(1)	3.633(1)	140(1)
C6-H106···O1[a]	0.93(1)	2.93(2)	3.505(1)	121(1)
C6-H106···O5[a]	0.93(1)	2.61(1)	3.520(1)	165(1)
C10-H10···Cl2[c]	0.97(1)	3.18(2)	3.888(1)	131(1)
C11-H11···Cl1[d]	0.93(2)	2.80(2)	3.364(1)	120(1)
C11-H11···Cl1[c]	0.93(2)	2.64(2)	3.388(1)	138(1)
(Figure 4.16(c)) H-bonds connecting formula units along c direction				
N2-H2···O2[e]	0.93(2)	1.72(2)	2.645(1)	179(2)
O7-H7B···Cl1[f]	0.82(2)	2.34(2)	3.143(1)	168(2)
O8-H8A···Cl1[b]	0.81(2)	2.58(2)	3.299(1)	148(2)
O9-H9A···O4[e]	0.84(2)	1.98(2)	2.826(1)	176(2)
C5-H105···Cl2[g]	0.96(2)	2.66(2)	3.533(1)	150(1)
C12-H12···O1[e]	0.91(2)	2.82(2)	3.404(1)	124(1)
C12-H12···O9[e]	0.91(2)	2.58(2)	3.445(1)	159(1)

Symmetry codes: [a](½-x, ½+y, ½-z) [b](x, 1+y, z) [c](1½-x, ½+y, ½-z) [d](½+x, ½-y, -½+z) [e](1-x, 1-y, -z) [f](1-x, 1-y, 1-z) [g](-½+x, ½-y, ½+z)

The packing of **(4)** may also be influenced by π-π stacking interactions. Figure 4.17(a) shows the formula units arranged into H-bonded 2D motifs with slight overlap of the pyridinium rings. Figure 4.17(b) shows the π-π interactions between the aromatic groups. The centroid–centroid distance of (N2,C12,C8,C9,C10,C11) – (N1,C6,C2,C3,C4,C5,C6)^{d} is 4.605(1) Å, which is too long to constitute a π-π stacking interaction, however the centroid–centroid distance of (N2,C12,C8,C9,C10,C11) – (N1,C6,C2,C3,C4,C5,C6)^{h} is 3.895(1) Å, much closer to the separation expected for a significant π-π stacking interaction, although still longer than that observed in pure nicotinic acid.

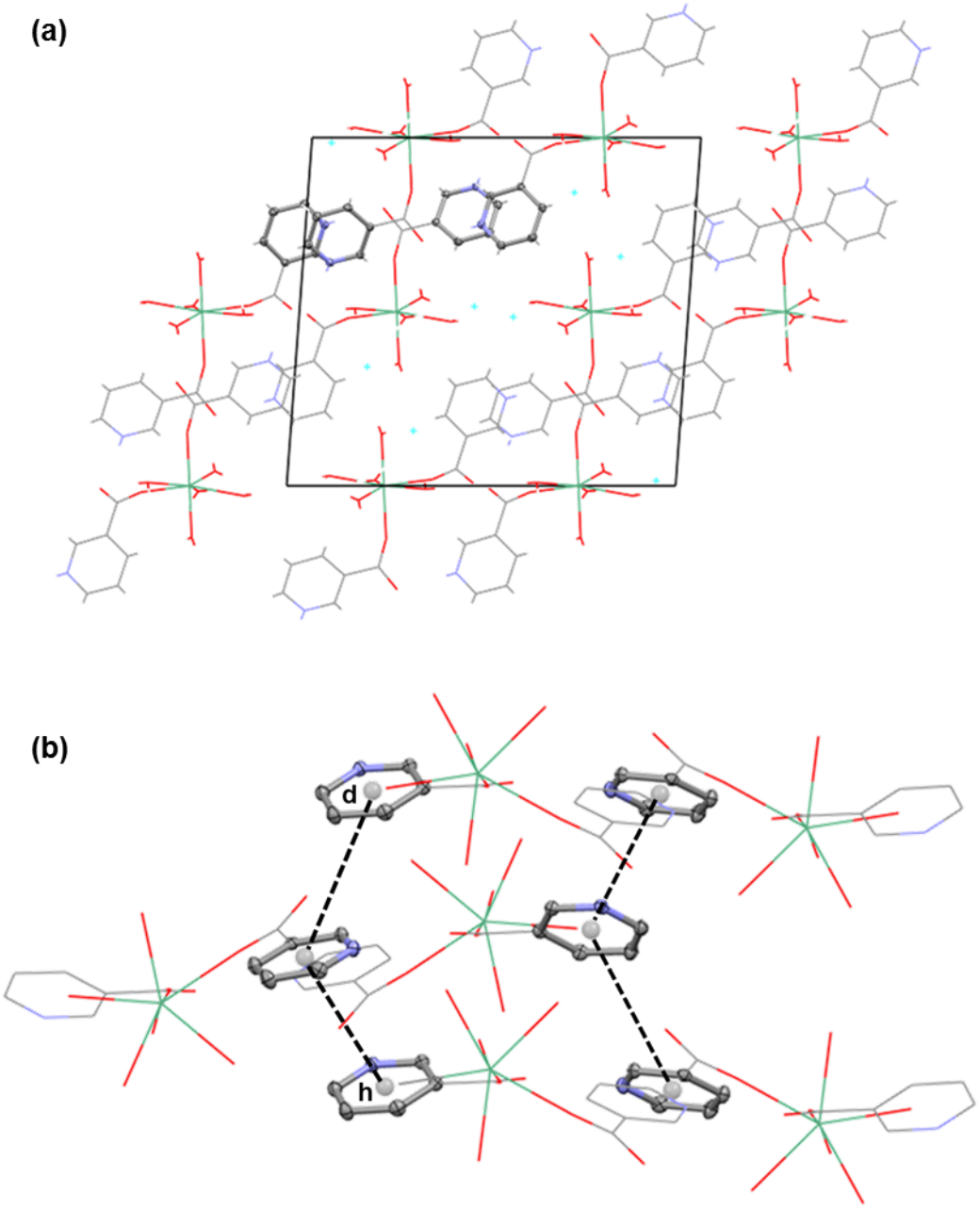

Figure 4.17. Crystal structure of **(4)**. (a) View down the *b* axis showing global packing and H-bonded 2D motifs of metal-organic units along the {101} plane with slight overlap of the pyridinium rings. (b) (View down the *a* axis) showing π-π stacking of pyridinium rings. Symmetry codes for centroid (N1,C6,C2,C3,C4,C5,C6): ^{d}(½+x, ½-y, -½+z) ^{h}(-½+x,1½ -y, ½-z)

HSM was carried out on a sample of **(4)**. At around 70 °C the clear and colourless crystal blackened and by *ca.* 150 °C the sample was bubbling vigorously. This continued and the sample reduced in size progressively until the temperature ramp was stopped at 375 °C. What remained of the sample was a cluster of tiny needles. DSC analysis gave a very

complicated trace of four separate endothermic events, which are difficult to interpret fully in terms of the isolated single crystal product (Appendix A, Figure A6).

4.2.5. *Bis-(pyridinium-4-carboxylato)-tetraaqua-magnesium(II) dinitrate* **(5)**

$[Mg(C_6H_5NO_2)_2(H_2O)_4].2NO_3$

(5) was prepared by solvent evaporation of a 1:1 stoichiometric mixture of isonicotinic acid and magnesium(II) nitrate hexahydrate dissolved in isopropanol at 50 °C. A clear, colourless crystalline material formed after two weeks from which a single crystal was cut for analysis by scXRD. The calculated PXRD pattern (Figure 4.18) indicates that the single crystal is not fully representative of the bulk material although several of the peaks do coincide with the experimentally obtained pattern. The ligand:metal ratio of the single crystal product is 2:1, therefore excess metal salt would be expected in the experimentally obtained PXRD pattern of the bulk product. Instead, there is more isonicotinic acid observed in this pattern with relevant peaks coinciding between the two patterns at about 16°, 26° and 28°.

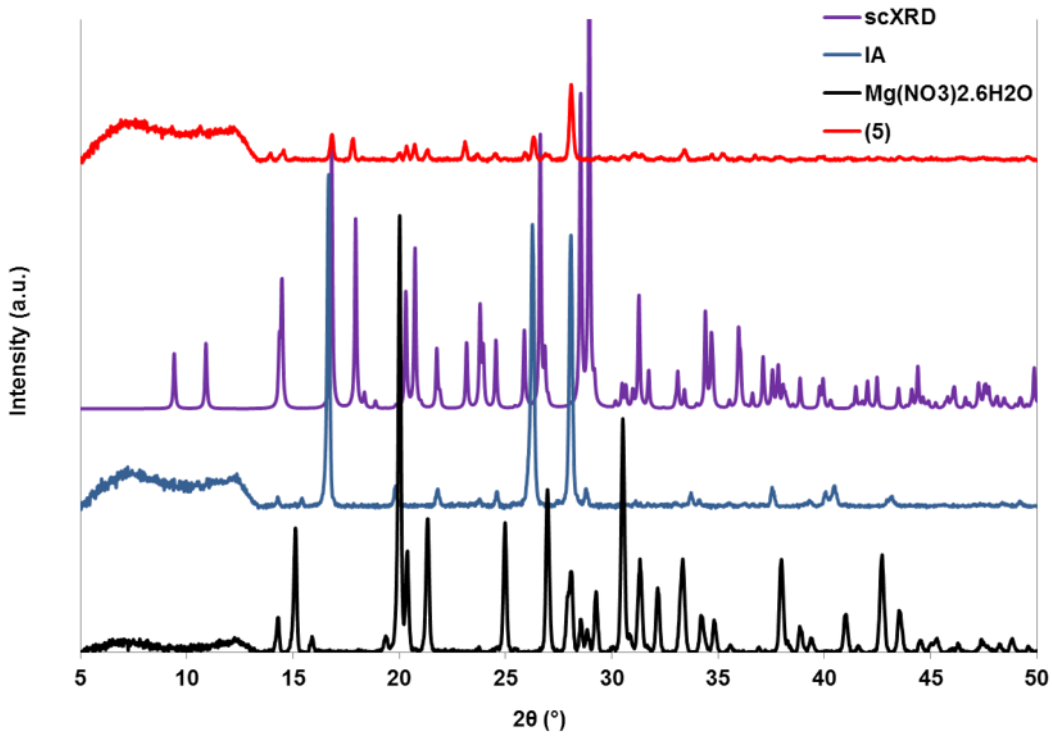

Figure 4.18. PXRD pattern of **(5)** compared to the calculated pattern and patterns of starting materials.

The formula unit of **(5)** consists of a magnesium centre coordinated by four water ligands and two zwitterionic isonicotinic acid ligands, each *via* one carboxylate oxygen atom, and

two non-coordinated nitrate ions. The magnesium centre is situated on an inversion centre and has a slightly distorted octahedral geometry (Figure 4.19(a) and Table 4.10). The O-Mg-O angles range from 85.26(4)° for O6/O6^{a}-Mg1-O7^{a}/O7 to 94.74(4)° for O6/O6^{a}-Mg1-O7/O7^{a}, and the Mg-O distances vary slightly from 2.040(1) Å, from the metal to the carboxylate oxygen atom, to 2.071(1) Å and 2.089(1) Å to the water ligands.

The metal-organic unit of **(5)** is strikingly similar to that of **HIVQIO** (Figure 1.9(b)) in which an octahedral magnesium centre is coordinated by two carboxylate oxygen atoms of two isonicotinate ions, and four methanol solvent molecules. Like in **(5)**, the Mg-O distances to the carboxylate oxygen atom are the shortest at approx. 2.014 Å, and those to the coordinated solvent are longer at approx. 2058 Å and 2.086 Å.

Due to deprotonation of isonicotinic acid in **(5)**, the C-O distances of the carboxylate group are more similar at 1.242(1) Å for C1-O4 and 1.252(2) Å for C1-O5, than for pure isonicotinic acid. However, the C-O distances in **(5)** show a different trend to those in **(4)** where the C-O distances involving the metal-coordinated oxygen atoms were shorter than those involving the non metal-coordinated oxygen atoms. In **(5)**, C1-O5 (the metal-coordinated oxygen atom) is longer than C1-O4 (non-coordinated), although there is a greater range in the C-O distances displayed by **(4)**. The angle O4-C1-O5 is 127.7(1)°, which is slightly wider than the O=C-O angle of the pure ligand (125.1(2)°), again, despite the carboxylate group not bridging between metal centres. The carboxylate groups and the pyridinium rings are twisted from coplanarity to a lesser extent than was observed in **(4)**, with a O5-C1-C2-C6 torsion angle of 16.6(2)°.

The formula unit contains two non-coordinated nitrate ions that are associated with the metal-organic unit through two H-bonds from two of the water ligands to two oxygen atoms of the nitrate ions (Figure 4.19(c) and Table 4.11). O6-H8⋯O2 and O7-H11⋯O1^{a} are moderately strong interactions with medium length D⋯A distances of 2.885(2) Å and 2.792(1) Å and very wide angles of 169(2)° and 175(2)°, respectively.

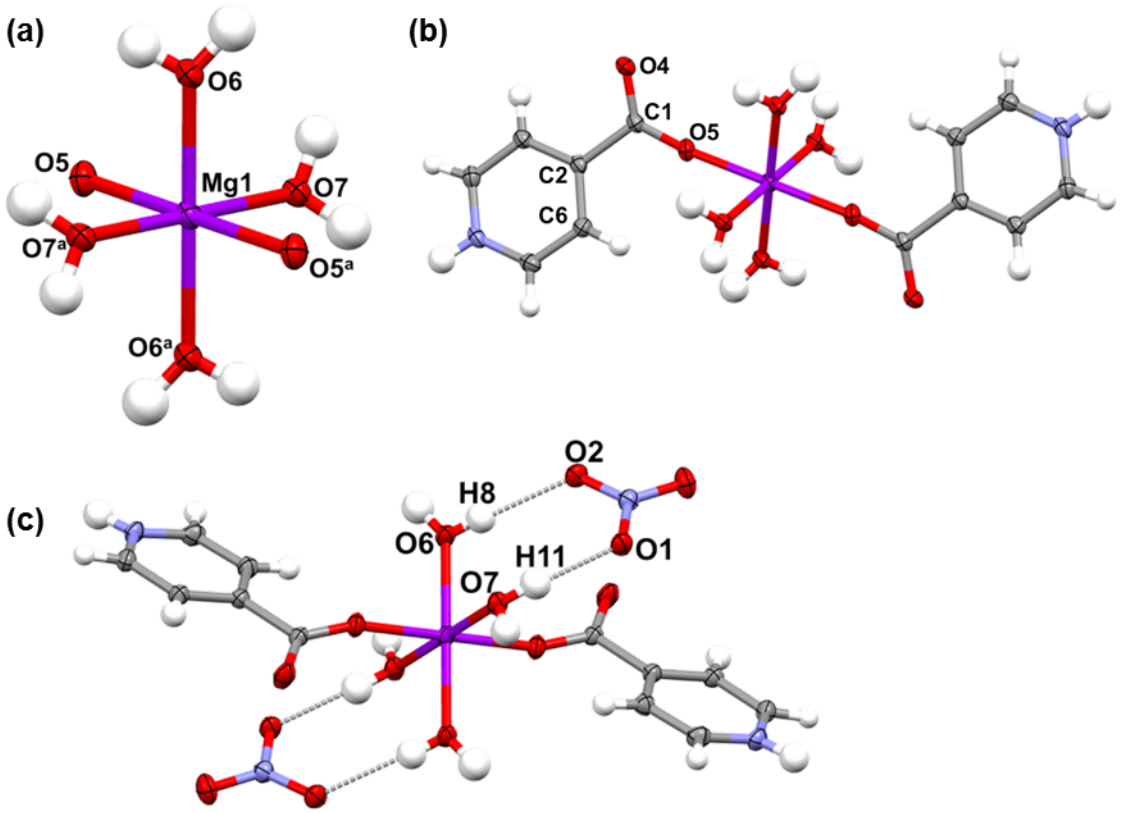

Figure 4.19. Crystal structure of **(5)**. (a) Octahedral Mg centre with two coordinating carboxylate oxygen atoms and four coordinating water molecules. (b) Formula unit (without nitrate ions) showing carboxylate coordination to Mg centre. (c) Formula unit showing H-bonds O6-H8···O2 and O7-H11···O1.

Table 4.10. O-Mg-O angles and Mg-O distances in **(5)**.

Coordination	O-Mg-O angle (°)	Interaction	Distance (Å)
O6/O6ª-Mg1-O5/O5ª	89.25(4)	Mg1-O5/O5ª	2.040(1)
O6/O6ª-Mg1-O7/O7ª	94.74(4)	Mg1-O6/O6ª	2.071(1)
O6/O6ª-Mg1-O5ª/O5	90.75(4)	Mg1-O7/O7ª	2.089(1)
O6/O6ª-Mg1-O7ª/O7	85.26(4)		
O5/O5ª-Mg1-O7/O7ª	91.46(4)		
O7/O7ª-Mg1-O5ª/O5	88.54(4)		

Symmetry codes: ª(-x,-y, -z)

The structure of **(5)** is directed by both H-bonding and π-π stacking interactions. The formula units are arranged into 2D H-bonded motifs parallel to the *bc* plane through H-bonding *via* the nitrate ion, supported by π-π stacking. These motifs are connected along the *a* direction by H-bonds directly between the metal-organic units and again *via* the nitrate ion.

There are seven H-bonds that arrange the formula units into the 2D H-bonded motif. Two of these are the H-bonds from the water ligands to the nitrate ion, mentioned previously. The oxygen atoms of the nitrate ion also accept H-bonds from the neighbouring formula units in both the *b* and *c* directions. This formula unit also forms H-bonds to the oxygen atoms of the water ligands of the next formula unit along the *c* direction (Figure 4.20(a)). The N-H group of the isonicotinic acid ligand forms a bifurcated H-bond to two of the oxygen atoms of the nitrate ion: N2-H7···O1^{b} and N2-H7···O3^{b}. The former is a moderately strong interaction as it has a D···A distance of 2.732(2) Å and an angle of 168(2)°. The latter is a longer and less linear interaction with a D···A distance of 3.329(2) Å and an angle of 133(2)°. O3^{b} also accepts an H-bond from the C-H group of the isonicotinic acid ligand, forming C5-H5···O3^{e} which is a very weak interaction of 3.275(2) Å and 119(1)°. Another C-H group of the same pyridinium ring forms the H-bonds C4-H4···O6^{c} and C4-H4···O7^{d} to the water ligands of the next formula unit along the *c* direction. These are also weak interactions with comparable D···A distances of 3.308(2) Å and 3.305(2) Å and angles of 124(1)° and 131(1)° for C4-H4···O6^{c} and C4-H4···O7^{d}, respectively.

The formula units are also linked by π-π stacking interactions between the pyridinium rings (Figure 4.20(b)). The centroid–centroid distance (N2,C2,C3,C4,C5,C6) - (N2,C2,C3,C4,C5,C6)^{b} is about 4.012 Å, and the centroid–centroid distance (N2,C2,C3,C4,C5,C6) - (N2,C2,C3,C4,C5,C6)^{d} is about 4.169 Å, in both cases longer than for the π-π stacking interactions observed in pure isonicotinic acid. The π-π stacking interactions exhibited by **HIVQIO** (Figure 1.9(c)) are likely a greater influence on the crystal packing than they are in **(5)**, since they are significantly shorter at approx. 3.680 Å.

The H-bonded 2D motifs are connected along the *a* direction through four H-bonds (Figure 4.20(c)). The non-coordinated carboxylate oxygen atom O4 is involved in three of these interactions where it accepts H-bonds from one C-H group of a pyridinium ring C6-H6···O4^{e}, and a water ligand O6-H9···O4^{f}, both originating from the next formula unit along the *a* direction, and from a C-H group of a pyridinium ring, C3-H3···O4^{g}, of one formula unit along both the *a* and *c* directions. The H-bonds from C-H groups are fairly weak interactions with D···A distances of 3.367(2) Å and 3.374(2) Å and angles of 150(1)° and 121(1)° for C3-H3···O4^{g} and C6-H6···O4^{e}, respectively. The H-bond from the water molecule, O6-H9···O4^{f}, is a shorter, linear and likely stronger interaction with a D···A distance of

2.684(1) Å and an angle of 175(2)°. The fourth H-bond connecting the 2D H-bonded motifs along the *a* direction is O7-H10···O2^{f}, which links from a water ligand of one formula unit, to the nitrate ion that is doubly H-bonded by the water ligands of the next formula unit along the *a* direction. Similarly to O6-H9···O4^{f}, this is a moderately strong interaction with a D···A distance of 2.745(1) Å and an angle of 168(2)°.

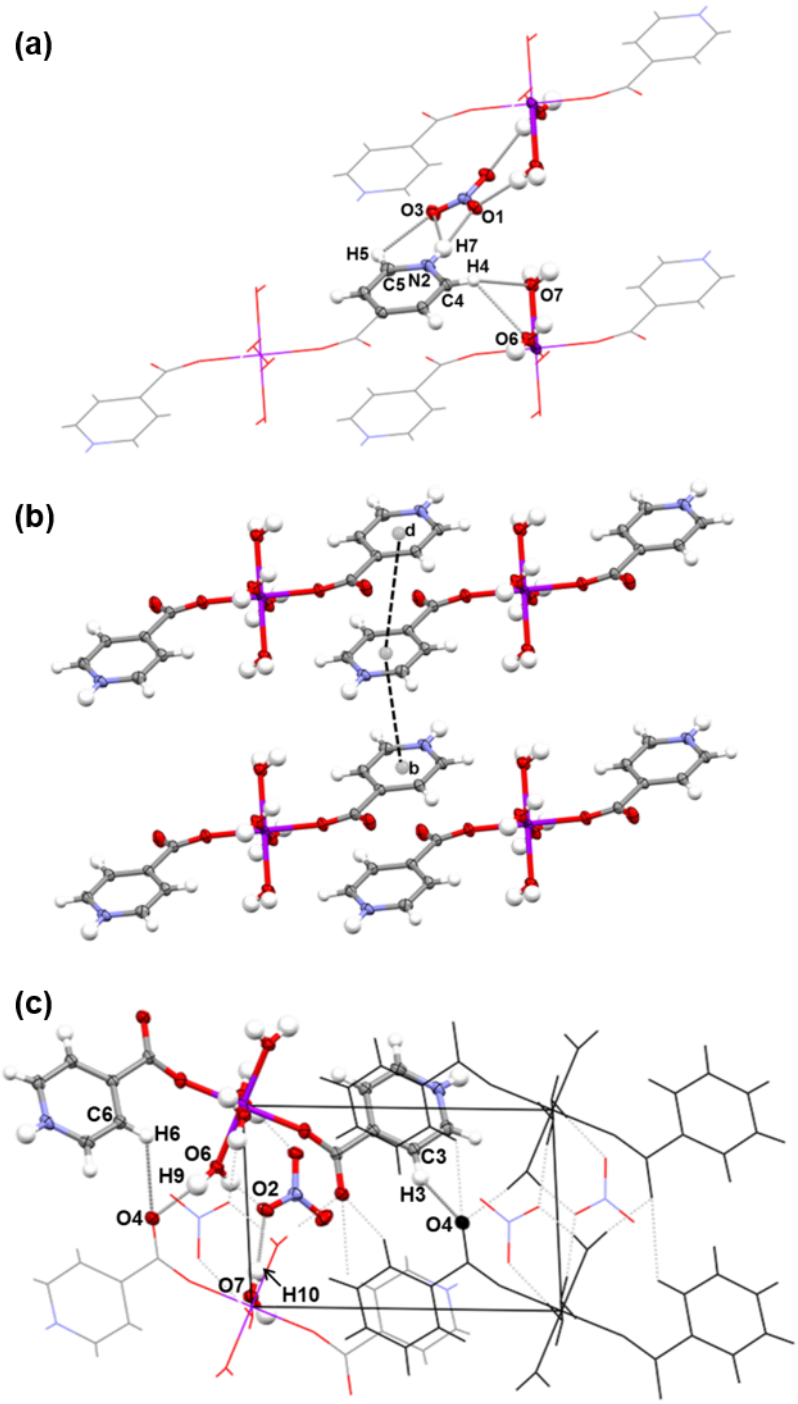

Figure 4.20. Crystal structure of **(5)**. (a) H-bonds and, (b) π-π stacking interactions connecting formula units along the *b* and *c* directions creating 2D motif parallel to the *bc* plane. (c) View down the *b* axis showing H-bonds connecting the 2D H-bonded motifs along the *a* direction. Symmetry codes for centroid (N2,C2,C3,C4,C5,C6): [b](-x, -1-y, 1-z) [d](-x, -y, 1-z)

Table 4.11. Geometries of H-bonds in **(5)**.

D-H···A Interaction	D-H (Å)	H···A (Å)	D···A (Å)	D-H···A (°)
(Figure 4.19(c)) H-bonds to nitrate ions in formula unit				
O6-H8···O2	0.78(2)	2.11(2)	2.885(2)	169(2)
O7-H11···O1[a]	0.86(2)	1.93(2)	2.792(1)	175(2)
(Figure 4.20(a)) H-bonds connecting π-π stacking formula units				
N2-H7···O1[b]	0.90(2)	1.85(2)	2.732(2)	168(2)
N2-H7···O3[b]	0.90(2)	2.65(2)	3.329(2)	133(2)
C4-H4···O6[c]	0.93(2)	2.70(2)	3.308(2)	124(1)
C4-H4···O7[d]	0.93(2)	2.62(2)	3.305(2)	131(1)
C5-H5···O3[e]	0.96(2)	2.70(2)	3.275(2)	119(1)
(Figure 4.20(c)) H-bonds connecting 2D tape motifs along a direction				
O6-H9···O4[f]	0.88(2)	1.81(2)	2.684(1)	175(2)
O7-H10···O2[f]	0.82(2)	1.94(2)	2.745(1)	168(2)
C3-H3···O4[g]	0.97(2)	2.49(2)	3.367(2)	150(1)
C6-H6···O4[e]	0.92(2)	2.80(2)	3.374(2)	121(1)

Symmetry codes: [a](-x,-y, -z) [b](-x, -1-y, 1-z) [c](x, y, 1+z) [d](-x, -y, 1-z) [e](-1+x, y, z)
[f](1-x, -y, -z) [g](1-x, -y, 1-z)

The thermal analysis of a single crystal of **(5)** by HSM revealed a melting range of 117 – 127 °C. DSC analysis (Figure 4.21) did show a broad endotherm from approx. 103 – 128 °C from which the melting point was determined to be 122.8 °C. There is another endothermic event apparent only in the DSC trace at 72.3 °C which cannot be assigned as the melting points of the starting materials (isonicotinic acid m.p > 300 °C; $Mg(NO_3)_2.6H_2O$ m.p 89 °C) but it is possible that it is associated with a phase transformation of a side product such as **(A5)** which is a simple isonicotinic acid nitrate salt discussed in Appendix D. The DSC trace of **(A5)** (Appendix D, Figure A56) shows an endothermic event at 67.1 °C, and in the HSM there is a clear smoothening of the crystal's edges between 68 °C and 75 °C. Due to the oily consistency of the bulk sample, a decent powder sample of **(A5)** could not be obtained in order to compare its PXRD pattern to that of **(5)**, but the calculated PXRD pattern can be

compared to both the calculated and experimentally obtained PXRD patterns of **(5)** (Appendix D, Figure A57). This shows some coincident peaks between **(A5)** (calculated) and **(5)** (experimentally obtained), specifically at about 23°, however there is better agreement between **(5)** (calculated) and **(5)** (experimentally obtained).

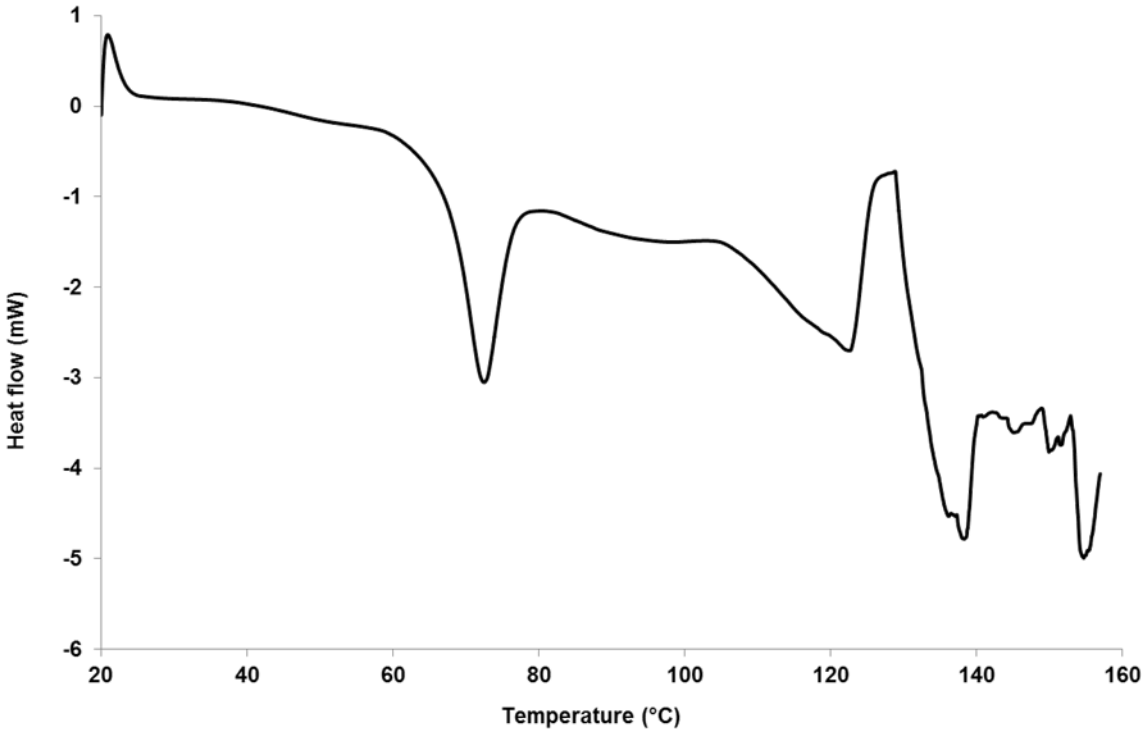

Figure 4.21. DSC trace of **(5)** on a 3.4 mg sample with a temperature ramp of 10 °C min^{-1}.

4.2.6. *Bis-(pyridinium-2-carboxylato)-tetraaqua-magnesium(II) dinitrate* **(6)**

$[Mg(C_6H_5NO_2)_2(H_2O)_4].2NO_3$

(6) was prepared by solvent evaporation of a 1:1 stoichiometric mixture of picolinic acid and magnesium(II) nitrate hexahydrate dissolved in DCM and acetone at lab temperature under slightly varying preparation permutations (see Experimental). Crystals of **(6)** formed within a few days and were colourless platelets. The experimentally obtained and calculated PXRD patterns of **(6)** do not match very well although there are coinciding peaks at about 20° and 26° (Figure 4.22). The strong peak at about 28° in the calculated pattern may be evident in the experimentally obtained pattern in the form of the relatively strong peak at approx. 27.5°, taking into account the expected shifting of the calculated pattern to slightly higher 2θ values. The ligand:metal ratio of the single crystal product is 2:1, therefore excess metal salt would be expected in the experimentally obtained PXRD pattern of the bulk sample, but there does not appear to be evidence of this.

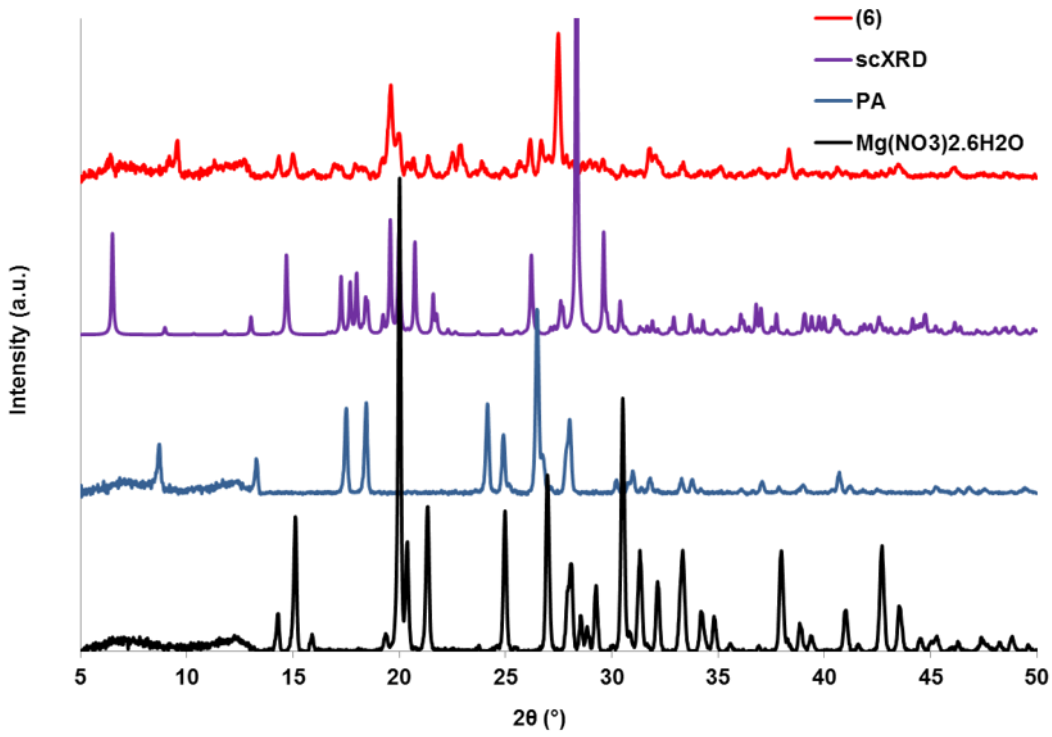

Figure 4.22. PXRD pattern of **(6)** compared to the calculated pattern and patterns of starting materials.

(6) is a constitutional isomer of **(5)**. The formula unit features a magnesium centre coordinated by four water ligands and two zwitterionic picolinic acid ligands, each *via* one carboxylate oxygen atom, and two non-coordinated nitrate ions. It differs from **(5)** only in that the nitrogen of the pyridine carboxylic acid is in the 2-position as opposed to the 4-position, however, the overall crystal structure is very different. H-bonds connect the formula units into 2D H-bonded motifs parallel to the *ab* plane which are connected along the *c* direction *via* the nitrate ions, but π-π stacking interactions do not occur in this structure as the distances between parallel aromatic groups are in excess of 6 Å.

The magnesium centre has a slightly distorted octahedral geometry (Figure 4.23(a) and Table 4.12). The O-Mg-O angles range between 85.92(6)° for O5-Mg1-O3 (between a water ligand and a carboxylate oxygen atom) to 96.60(6)° for O2-Mg1-O7 (between a carboxylate oxygen atom and a water ligand). The Mg-O distances to the carboxylate oxygen atoms are 2.053(1) Å and 2.073(1) Å for Mg1-O2 and Mg1-O3, respectively, which are on average slightly longer than the Mg-O distances to O6 and O7, water molecule oxygen atoms, at 2.046(1) Å and 2.069(1) Å, respectively. The remaining two Mg-O distances to water molecules are the longest of the coordination bonds at 2.106(1) Å for Mg1-O4 and 2.094(1) Å for Mg1-O5, these can therefore be referred to as the 'axial' ligands.

Figure 4.23(b) shows the formula unit of **(6)** omitting the two axial water ligands. The C-O distances and the O-C-O angles for each of the carboxylate groups are about equal. C20-O8 is 1.248(2) Å and C20-O2 is 1.251(2) Å and the angle O8-C20-O2 is 128.8(2)°. For the other ligand, C26-O3 is 1.253(2) Å, C26-O9 is 1.247(2) Å and the angle O3-C26-O9 is 128.6(2)°. As observed in both **(4)** and **(5)**, the O-C-O angle is slightly wider in the complex than it is in the pure organic ligand. The angle observed in **(6)** is closer to the O-C-O angle for the bridging picolinic acid ligand in **(1)**, although here one carboxylate oxygen atom is non-coordinated.

The picolinic acid ligands differ slightly in their O-C-C-N torsion angles between the carboxylate group and the pyridinium ring, in that one is twisted from coplanarity more than the other. O2-C20-C21-N17 has a torsion angle of −8.3(2)°, while O3-C27-C27-N16 is −4.7(2)°. The aromatic groups of the two picolinic acid ligands are not coplanar as their planes are related to one another by an angle of approx. 17°.

The formula unit features one intracomplex H-bond from a coordinated water molecule to a non-coordinated carboxylate oxygen atom, (Figure 4.23(b) and Table 4.13). O6-H6A···O9 has a medium-length D···A distance of 2.786(2) Å and a necessarily strained low angle of 148(2)° due to the restricted conformation. The H-O-H angle of the donating water molecule H6A-O6-H6B, is 114(2)°, which is wider than the average H-O-H angle of 107.4° for magnesium coordinated water molecules, due to the attractive force of the non-coordinated carboxylate oxygen atom, and the fact that the ligand also forms an H-bond *via* H6B to an oxygen atom of a nitrate ion.

The two non-coordinated nitrate ions in the formula unit are each H-bonded to the metal-organic unit through three H-bonds from both the N-H and a C-H group of the pyridinium ring and from a water ligand (Figure 4.23(b) and Table 4.13). Of these H-bonds O7-H7A···O10 is the strongest with a D···A distance of 2.667(2) Å and an angle of 172(2)°. O6-H6B···O13 and N16-H16···O10 are very similar in length and angle at 2.795(2) Å and 164(2)°, and 2.735(2) Å and 165(2)°, respectively, while as expected, the weaker interactions are from the C-H groups, C25-H25···O15 and C31-H31···O11, the latter of which has the shorter D···A distance of 3.200(2) Å and an angle of 146(2)°.

The formula units are arranged in a staggered manner into H-bonded motifs parallel to the *ab* plane (Figure 4.23(c)). The axial water ligands of the formula units H-bond to the non-coordinated carboxylate oxygen atom of the neighbouring formula units located along the *a* direction. These formula units form H-bonds back to the axial water ligands. The nitrate ions are also involved in connecting the formula units in the H-bonded motif by accepting H-bonds from the adjacent formula units. These ten interactions are illustrated in Figure

4.23(d) and listed in Table 4.13. The axial water ligand containing O4 is the donor in two H-bonds, O4-H4A···O9[a] and O4-H4B···O8[b], in both of which non-coordinated carboxylate oxygen atoms are the acceptors. These are moderately strong interactions with D···A distances of 2.709(2) Å and 2.696(2) Å, and angles of 174(2)° and 173(3)°, respectively. Similarly, the axial water molecule containing O5 is the donor in two H-bonds: one to a carboxylate oxygen atom, O5-H5A···O8[c], and one to an oxygen atom of a nitrate ion, O5-H5B···O14[d]. O5-H5A···O8[c] is the relatively stronger of the interactions with a shorter D···A distance of 2.763(2) Å and a wide angle of 176(2)°. O5-H5B···O14[d] is slightly longer at 2.906(2) Å and has an angle of 172(2)°. The two H-bonds from the equatorially coordinated water ligands to the neighbouring formula units' axial water ligands are O6-H6A···O5[d] and O7-H7B···O4[b]. Interestingly, although these H-bonds are formed between equivalent substituents, one is much stronger than the other. O7-H7B···O4[b] has a D···A distance of 2.872(2) Å and an angle of 175(2)°, comparable to the H-bonds from the water ligands to the non-coordinated carboxylate oxygen atoms. O6-H6A···O5[d] however, has a longer D···A distance of 3.049(2) Å and a significantly smaller angle of 114(2)°. This is most likely due to the conformation of the water ligand of the accepting oxygen atom, O5, influenced by the strong H-bonds that it makes, but it may also be affected by the strained intracomplex H-bond, O6-H6A···O9, which has a more strongly accepting atom, therefore asserting a greater attraction from the hydrogen atom.

The four other H-bonds linking the formula units into H-bonded motifs are from C-H groups of the pyridinium rings to the oxygen atoms of the nitrate ions. These nitrate ions are in turn, involved in H-bonds to the adjacent formula unit as discussed previously, considering the nitrate ions to be a part of this formula unit. These H-bonds are all weak interactions with D···A distances ranging from 3.094(2) Å for C29-H29···O12[f] to 3.350(2) Å for C28-H28···O12[f], and angles ranging from 114(1)° for C23-H23···O14[e], to 139(2)° for C29-H29···O12[f].

The H-bonded motifs are connected along the *c* direction by H-bonds involving the nitrate ions that are H-bonded as discussed previously to the metal-organic unit of the formula unit of which it can be considered a part (Figure 4.23(e) and Table 4.13). All of these H-bonds are formed between C-H groups of the pyridinium rings to an oxygen atom of the nitrate ions. There are bifurcated H-bonds formed by C24-H24, C25-H25 and C31-H31. C24-H24···O12[g] exhibits the longest D···A distance of 3.575(2) Å, and the largest angle of 173(2)°. C24-H24···O11[g] is shorter with a D···A distance of 3.132(2) Å but a smaller angle of 126(2)°. C25-H25 forms H-bonds to both of the nitrate ions through C25-H25···O11[g] and C25-H25···O15. The former is very slightly shorter with a D···A distance of 3.148(2) Å and has a much smaller angle at 114(1)°. C31-H31 also forms a bifurcated H-bond to the same

oxygen atoms of the nitrate ions as C25-H25. C31-H31···O15^{h} is the weaker of the interactions with a D···A distance of 3.237(2) Å and an angle of 120(1)°. O15^{h} also accepts the H-bond C30-H30···O15^{h} which has a similarly long D···A distance of 3.285(2) Å and angle of 125(2)° as the other carbon-donor H-bonds.

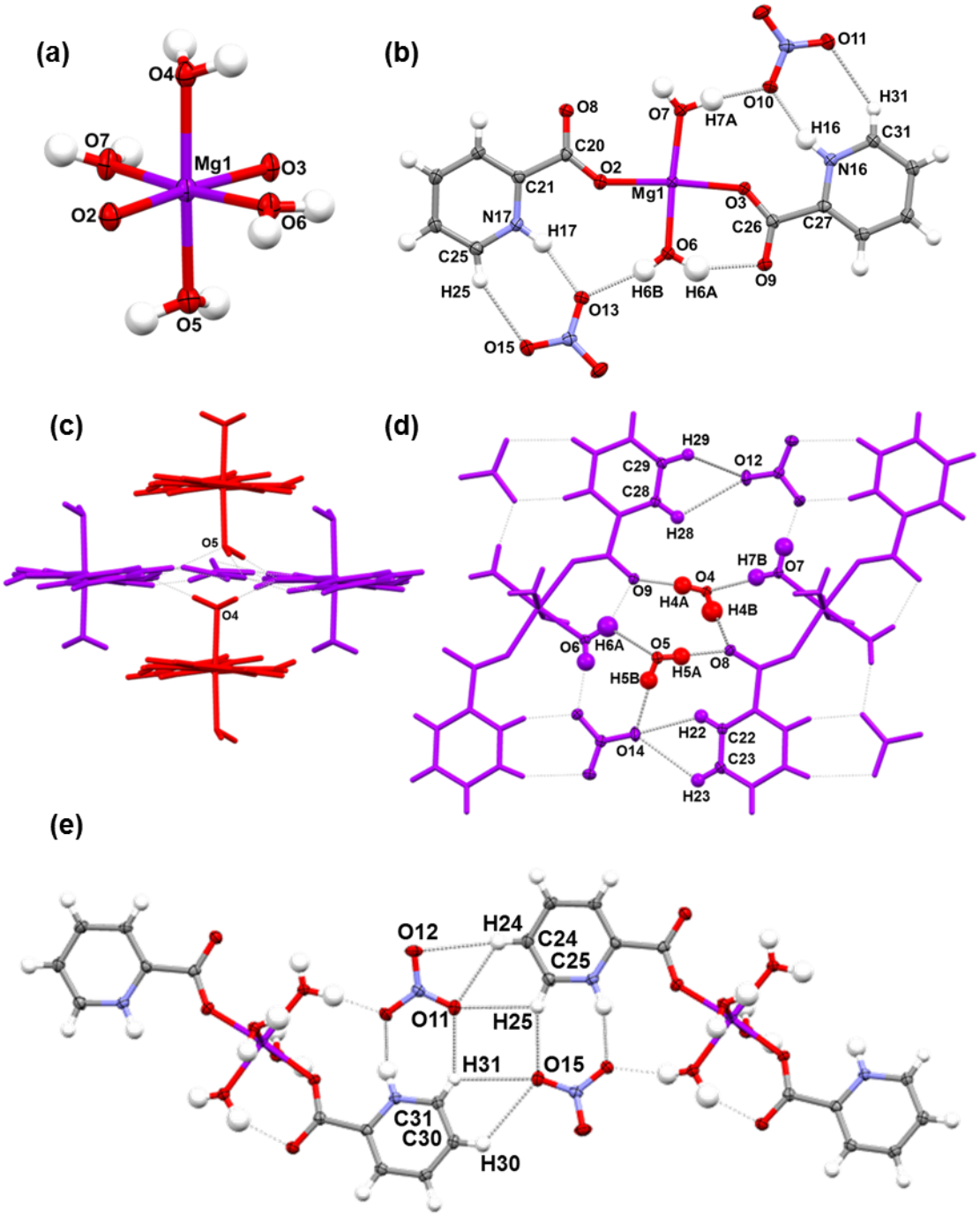

Figure 4.23. Crystal structure of **(6)**. (a) Octahedral Mg centre with two coordinating carboxylate oxygen atoms and four coordinating water molecules. (b) Formula unit showing coordinating carboxylate groups and H-bonds to non-coordinated nitrate ions, (axial water ligands removed for clarity). (c) Packing of formula units into the H-bonded motif parallel to the *ab* plane. (d) H-bonds connecting the formula units into the H-bonded motif parallel to the *ab* plane (nearest axially coordinated water molecule of red formula units located above and below purple formula units along the *a* axis shown only). (e) H-bonds connecting the H-bonded motifs along the *c* direction *via* the nitrate ions.

Table 4.12. O-Mg-O angles and Mg-O distances in **(6)**.

Coordination	O-Mg-O angle (°)	Interaction	Distance (Å)
O4-Mg1-O3	88.95(5)	Mg1-O2	2.053(1)
O4-Mg1-O6	88.86(6)	Mg1-O3	2.073(1)
O4-Mg1-O2	92.92(5)	Mg1-O4	2.106(1)
O4-Mg1-O7	87.89(6)	Mg1-O5	2.094(1)
O5-Mg1-O3	85.92(6)	Mg1-O6	2.046(1)
O5-Mg1-O6	94.57(5)	Mg1-O7	2.069(1)
O5-Mg1-O2	92.50(6)		
O5-Mg1-O7	88.36(6)		
O3-Mg1-O6	88.31(6)		
O6-Mg1-O2	87.00(6)		
O2-Mg1-O7	96.60(6)		
O7-Mg1-O3	88.19(6)		

Table 4.13. Geometries of H-bonds in **(6)**.

D-H···A Interaction	D-H (Å)	H···A (Å)	D···A (Å)	D-H···A (°)
(Figure 4.23(b)) H-bonds within formula unit				
O6-H6A···O9	0.93(3)	1.96(3)	2.786(2)	148(2)
O6-H6B···O13	0.87(2)	1.95(2)	2.795(2)	164(2)
O7-H7A···O10	0.94(2)	1.73(3)	2.667(2)	172(2)
N16-H16···O10	0.94(2)	1.82(2)	2.735(2)	165(2)
N17-H17···O13	0.92(2)	1.93(2)	2.810(2)	160(2)
C25-H25···O15	0.92(2)	2.39(2)	3.218(2)	149(2)
C31-H31···O11	0.92(2)	2.40(2)	3.200(2)	146(2)
(Figure 4.23(d)) H-bonds connecting formula units to create H-bonded motif				
O4-H4A···O9[a]	0.91(3)	1.80(3)	2.709(2)	174(2)
O4-H4B···O8[b]	0.87(3)	1.84(3)	2.696(2)	173(3)
O5-H5A···O8[c]	0.89(3)	1.87(3)	2.763(2)	176(2)
O5-H5B···O14[d]	0.87(2)	2.04(3)	2.906(2)	172(2)
O6-H6A···O5[d]	0.93(3)	2.55(2)	3.049(2)	114(2)
O7-H7B···O4[b]	0.85(2)	2.02(3)	2.872(2)	175(2)
C22-H22···O14[e]	0.93(2)	2.46(2)	3.104(2)	127(2)
C23-H23···O14[e]	0.94(2)	2.77(2)	3.269(3)	114(1)
C28-H28···O12[f]	0.96(2)	2.83(2)	3.350(2)	115(1)
C29-H29···O12[f]	0.99(2)	2.28(2)	3.094(2)	139(2)
(Figure 4.23(e)) H-bonds linking H-bonded motifs together				
C24-H24···O11[g]	0.94(2)	2.49(2)	3.132(2)	126(2)
C24-H24···O12[g]	0.94(2)	2.64(2)	3.575(2)	173(2)
C25-H25···O11[g]	0.92(2)	2.66(2)	3.148(2)	114(1)
C30-H30···O15[h]	0.91(2)	2.86(2)	3.285(2)	125(2)
C31-H31···O15[h]	0.92(2)	2.86(2)	3.237(2)	120(1)

Symmetry codes: [a](-x, 1-y, -z) [b](-x, 2-y, -z) [c](1-x, 2-y, -z) [d](1-x, 1-y, -z) [e](x, 1+y, z) [f](x, -1+y, z) [g](1+x, y, -1+z) [h](-1+x, y, 1+z)

A single crystal of **(6)** was analysed by HSM and the crystal melted in the range of 85 – 88 °C with no other events observed until the temperature ramp was stopped at 200 °C. DSC was carried out on the bulk sample (Appendix A, Figure A7). This showed a small endotherm at 84.9 °C, in agreement with the observations by HSM, but this is also close to the melting point of $Mg(NO_3)_2.6H_2O$ (m.p. 89 °C). A much stronger endotherm occurs at 130.9 °C, which is lower than the melting point of picolinic acid (m.p. 139 – 142 °C).

4.3. 1D Complexes

4.3.1. *Catena-[bis-(μ_2-pyridinium-2-carboxylato)-diaqua-magnesium(II)] dinitrate dihydrate* **(7)** *$[Mg(C_6H_5NO_2)_2(H_2O)_2].2NO_3.2H_2O$*

The complex **(7)** was obtained under a range of conditions. It was prepared by solvent evaporation of picolinic acid and magnesium(II) nitrate hexahydrate, in the various stoichiometric ratios 1:1, 1:2 or 2:1, dissolved in the solvent systems: DCM and acetone; methanol; acetone; water; THF and ethyl acetate, at various temperatures (see Experimental). Crystals of **(7)** also resulted from the addition of THF to crystals of **(8)**, and evaporation of the solvent over the course of three weeks. It was not established whether this was due to a process involving dissolution of **(8)** followed by the recrystallisation of **(7)**. The complex took various periods of time to form depending on the volatility of the solvent system used in the preparation. The product material was in the form of small, clear, colourless, smooth-sided and rounded cuboidal single crystals.

When the single crystals were initially harvested, the bulk material was frequently slightly wet with remaining saturated solvent and so obtaining a PXRD pattern was challenging. However from an experiment using a 1:1 molar ratio of picolinic acid and magnesium(II) nitrate hexahydrate dissolved in methanol and crystallised at 50 °C, a good PXRD pattern was obtained from the sample two and a half years after preparation. This indicates the apparent stability of the complex, since the experimentally obtained and calculated PXRD patterns (shown in Figure 4.24) match fairly well for this sample, with the intense peaks at about 13° and 19° coinciding. **(7)** has a ligand:metal ratio of 2:1, so it would be expected that excess magnesium(II) nitrate hexahydrate might be observed in the bulk sample PXRD pattern, as was expected in the cases of **(5)** and **(6)**. There are some coinciding peaks between the PXRD patterns of **(7)** and $Mg(NO_3)_2.6H_2O$ between 29° and 33°, but the more intense peaks at lower 2θ values do not match.

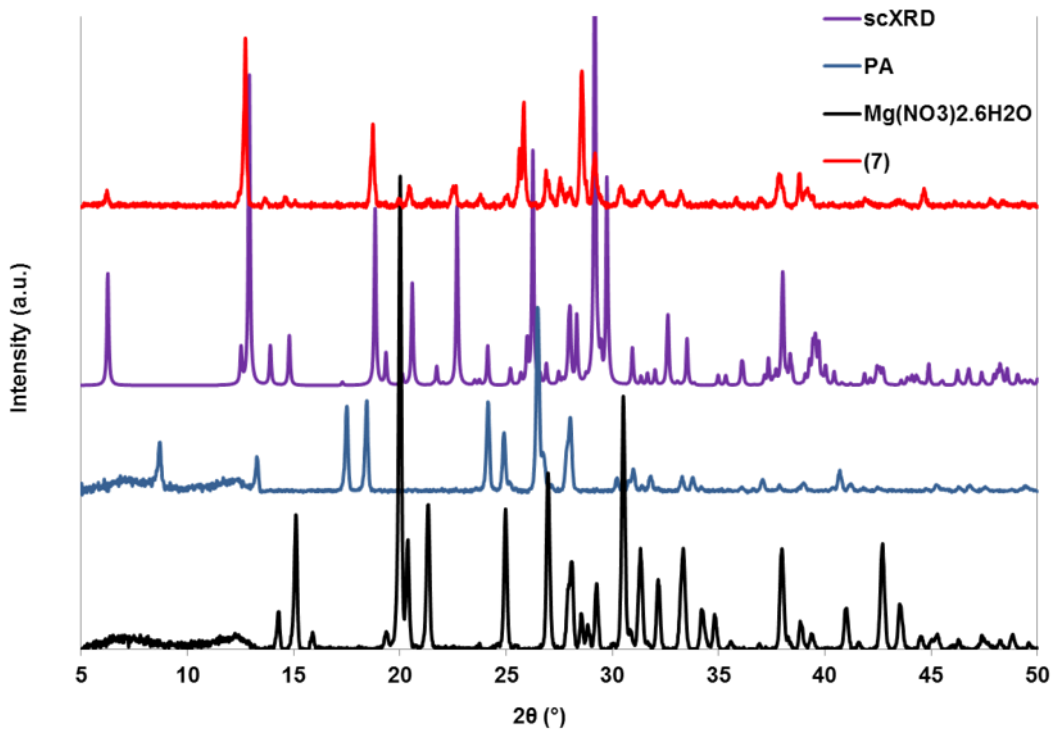

Figure 4.24. PXRD pattern of **(7)** compared to calculated pattern and patterns of starting materials.

The formula unit of **(7)** is composed of a magnesium centre, two zwitterionic picolinic acid ligands, two metal-coordinated water molecules, two non-coordinated nitrate ions and two non-coordinated water molecules. **(7)** has the same formula as both **(6)** and **(5)**. The structure of **(7)** differs from **(6)** in that it contains non-coordinated water molecules, but more significantly it is a coordination polymer as opposed to an H-bonded 0D metal-organic complex. The primary structure is a chain of magnesium centres, bridged to one another by two picolinic acid ligands through coordination by the carboxylate oxygen atoms so that each magnesium centre is coordinated to four picolinic acid ligands (Figure 4.25(a)). **(7)** and **(6)** may be described as molecular building block structural isomers,[170] while **(7)** and **(5)** are constitutional isomers.

Single crystals of **(7)** and **(6)** were never found in the same vial, although they could be prepared under identical experimental conditions. Their PXRD patterns are compared and discussed later in this chapter.

The magnesium centre has crystallographic inversion symmetry and has a slightly distorted octahedral geometry (Figure 4.25(b) and Table 4.14). The O-Mg-O angles range from 84.50(3)° for O5/O5^{b}-Mg1-O6^{a}/O6^{c} to 95.50(3)° for O5/O5^{b}-Mg1-O6^{c}/O6^{a}; these are the angles formed between the water ligands and the carboxylate oxygen atom, O6. The Mg-

O distances to the carboxylate oxygen atoms are essentially equivalent at 2.060(1) Å for Mg1-O1/O1^{b} and 2.063(1) Å for Mg1-O6^{a}/O6^{c}. The coordination distance of the oxygen atoms of the water ligands Mg1-O5/O5^{b}, is longer at 2.071(1) Å.

(7) features a similar eight-membered ring conformation as was observed in **(1)**, **(2)** and **(3)**, formed by the carboxylate group of picolinic acid bridging two magnesium centres (Figure 4.25(c)). The C-O distances of the carboxylate group are 1.242(1) Å for C6-O6 and 1.251(1) Å for C6-O1. The O1-C6-O6 angle is 129.3(1)° which is more comparable to the equivalent angle in **(1)** of 129.0(1)° than the O=C-O angle of pure picolinic acid (126.8(1)°). This can again be attributed to constraint imposed by metal-coordination, enabled by deprotonation. **(7)** differs slightly from **(1)** however, in that the Mg-carboxylate oxygen atom distances are more equal.

The carboxylate group and the pyridinium ring are twisted slightly from coplanarity with a O1-C6-C1-N1 torsion angle of -17.2(2)°, similar to the magnitude of that observed in **(5)**.

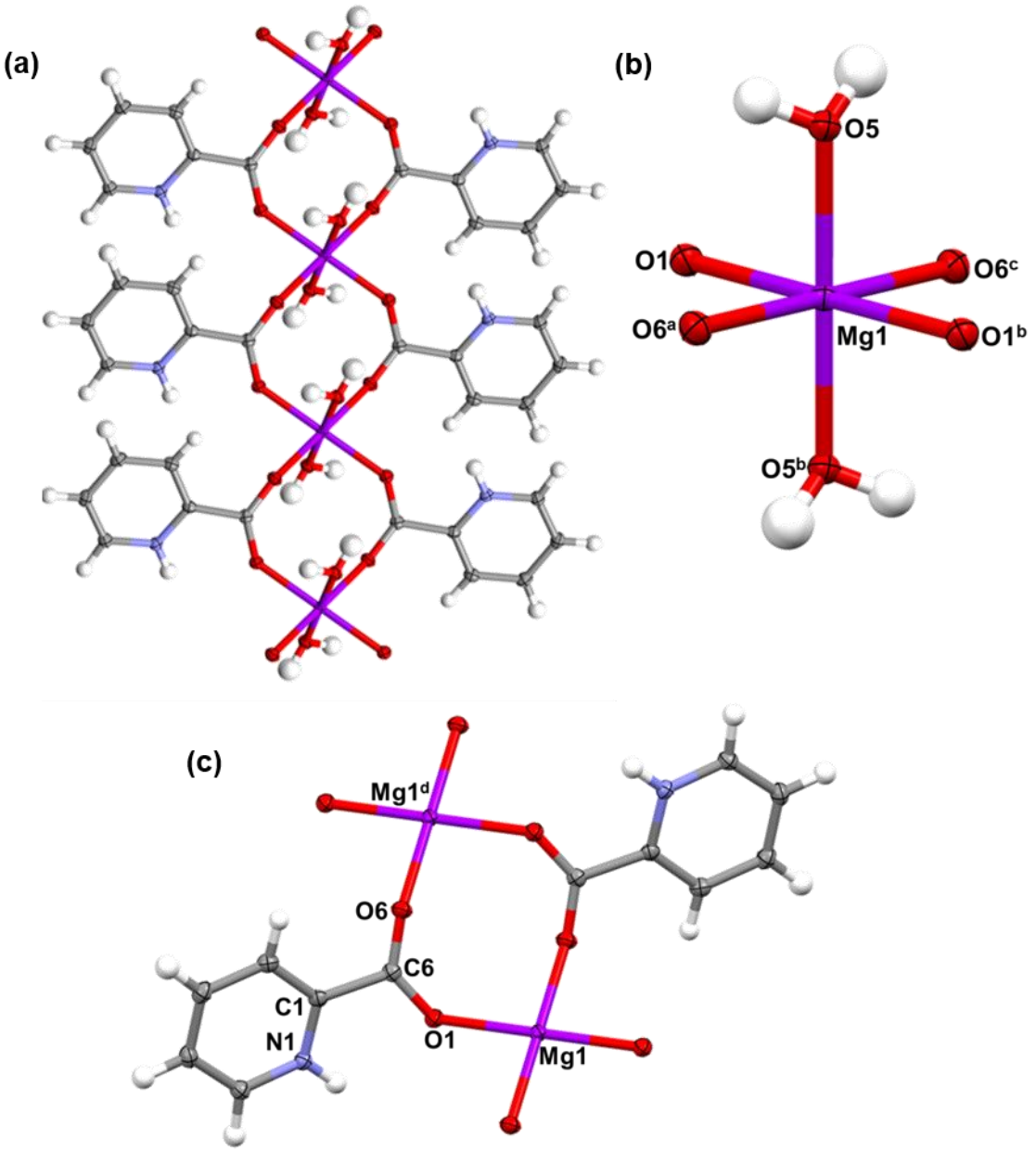

Figure 4.25. Crystal structure of **(7)**. (a) 1D chain of Mg centres bridged by two picolinic acid ligands (non-coordinated water molecules and nitrate ions excluded for clarity). (b) Octahedral Mg centre with four coordinating carboxylate oxygen atoms and two coordinating water molecules. (c) Section of the 1D chain showing the bridging picolinic acid ligand and eight-membered ring conformation (coordinated water molecules excluded for clarity). Symmetry codes: [a](1+x, y, z) [b](1-x, -y, -z) [c](-x, -y, -z) [d](-1+x, y, z)

Table 4.14. O-Mg-O angles and Mg-O distances in **(7)**.

Coordination	O-Mg-O angle (°)	Interaction	Distance (Å)
O5/O5^{b}-Mg1-O1/O1^{b}	92.28(3)	Mg1-O1/O1^{b}	2.060(1)
O5/O5^{b}-Mg1-O6^{a}/O6^{c}	84.50(3)	Mg1-O6^{a}/O6^{c}	2.063(1)
O5/O5^{b}-Mg1-O1^{b}/O1	87.72(3)	Mg1-O5/O5^{b}	2.071(1)
O5/O5^{b}-Mg1-O6^{c}/O6^{a}	95.50(3)		
O1/O1^{b}-Mg1-O6^{c}/O6^{a}	93.78(3)		
O6^{c}/O6^{a}-Mg1-O1^{b}/O1	86.22(3)		

Symmetry codes: ^{a}(1+x, y, z) ^{b}(1-x, -y, -z) ^{c}(-x, -y, -z)

The 1D chains that make up the structure of **(7)** run parallel to the *a* direction and are stacked along the *b* direction, connected through H-bonds *via* the nitrate ions and non-coordinated water molecules (Figure 4.26(a) and (b), and Table 4.15). The pyridinium ring forms H-bonds through the N-H and C-H groups to the nitrate ion and to the non-coordinated water molecule. N1-H1⋯O3 is one of the strongest interactions present in this structure with a D⋯A distance of 2.844(1) Å and an angle of 170(1)°. The bonds from the C-H groups of picolinic acid are weaker, and in the case of H5 and H2, the hydrogen atoms are directed towards two acceptors: H5 towards the nitrate ions along both the *b* and *c* directions, and H2 towards the nitrate ion and non-coordinated water molecule connecting between chains. Therefore these are longer and less direct interactions with D⋯A distances ranging from 3.184(2) Å for C5-H5⋯O2 to 3.611(1) Å for C2-H2⋯O7^{g}. The latter bond has a larger angle of 164(1)°, while C2-H2⋯O4^{f} has the lowest angle of 117(1)°. C3-H3⋯O4^{f} and C5-H5⋯O2 have angles of 132(1)° and 135(1)° respectively.

The non-coordinated water molecule is central to the linking of the 1D chains. It forms four H-bonds: one to the coordinated water molecule, O7-H7B⋯O5^{d}, one to a coordinating carboxylate oxygen atom, O7-H7B⋯O1^{c}, and two to two of the oxygen atoms of the nitrate ion, O7-H7A⋯O3^{b} and O7-H7A⋯O4^{b}; the latter two interactions constitute a bifurcated H-bond in which O7-H7A⋯O4^{b} is the stronger of the two interactions with a D⋯A distance of 2.829(1) Å and a very linear angle of 175(2)°.

The coordinated water molecule not only accepts an H-bond, but also acts as the donor in two interactions to the non-coordinated water molecule. O5-H5A⋯O7^{e} and O5-H5B⋯O7

are both moderately strong interactions with D···A distances of 2.787(1) Å and 2.776(1) Å and angles of 169(2)° and 171(2) °, respectively.

The 1D chains are connected along the *c* direction through H-bonds from the pyridinium ring to the nitrate ions (Figure 4.26(c) and (d), and Table 4.15). C4-H4 forms a bifurcated H-bond to the oxygen atoms of the nitrate ion. C4-H4···O2^{h} and C4-H4···O4^{h} are both weak interactions with D···A distances of 3.220(2) Å and 3.641(1) Å and angles of 114(1)° and 161(1)°, respectively. C5-H5 also participates in linking the structure along the *c* direction through C5-H5···O2^{h}, a weak interaction with a D···A distance of 3.104(1) Å and angle of 120(1)°, complementing C5-H5···O2 to form a bifurcated H-bond.

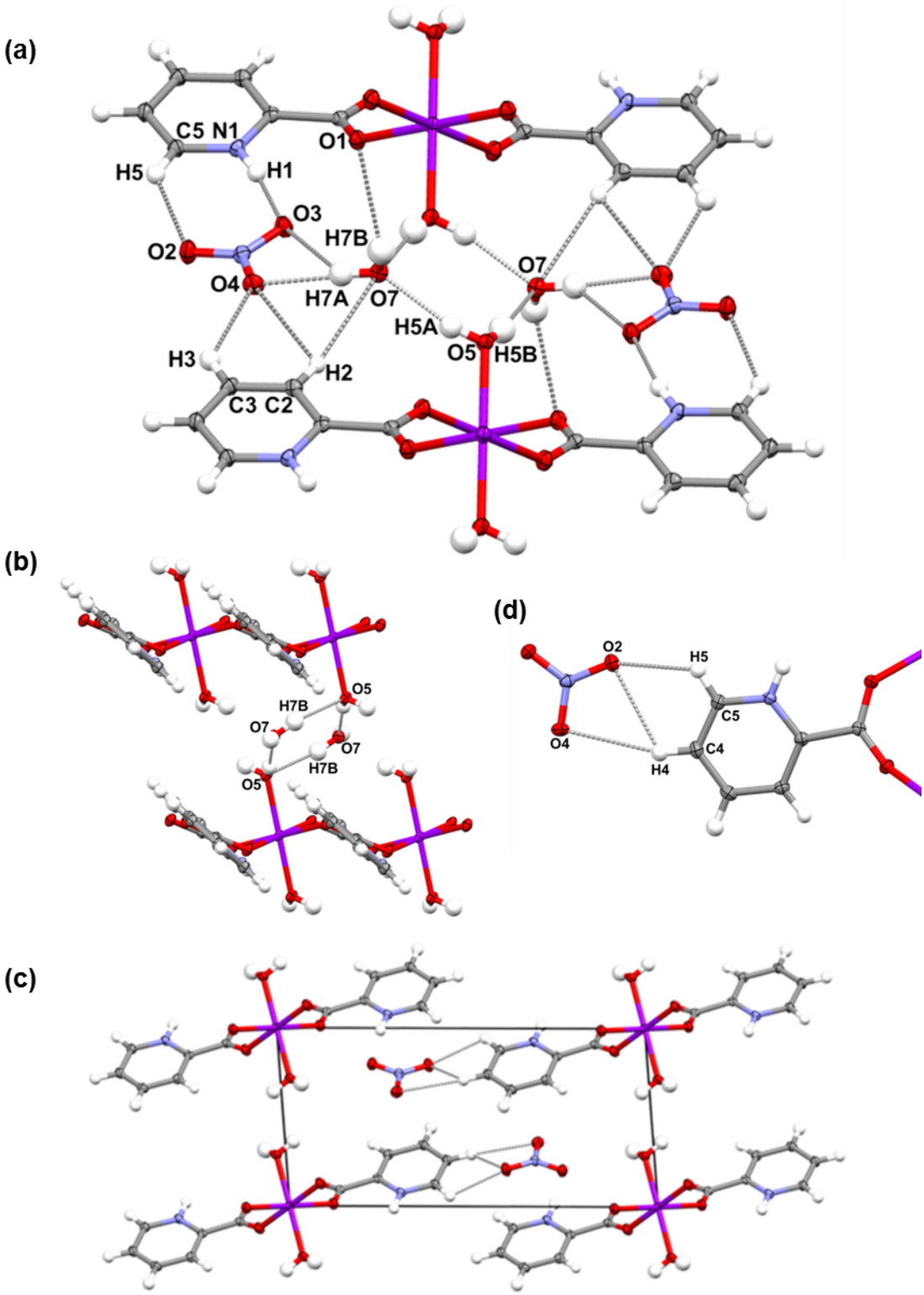

Figure 4.26. Crystal structure of **(7)**. (a) View down the *a* axis, straight down chain, and (b) showing H-bonds connecting 1D chains along the *b* direction. (c) View down the *a* axis showing H-bonds connecting 1D chains along the *c* direction, with (d) showing a zoomed view of (c), illustrating the H-bonds connecting the 1D chains.

Table 4.15. Geometries of H-bonds in **(7)**.

D-H···A Interaction	D-H (Å)	H···A (Å)	D···A (Å)	D-H···A (°)
(Figure 4.26(a) and (b)) H-bonds connecting 1D chains along a direction				
N1-H1···O3	0.90(2)	1.96(2)	2.844(1)	170(1)
O5-H5A···O7[e]	0.83(2)	1.97(2)	2.787(1)	169(2)
O5-H5B···O7	0.84(2)	1.94(2)	2.776(1)	171(2)
O7-H7A···O3[b]	0.85(2)	2.64(2)	3.231(1)	128(2)
O7-H7A···O4[b]	0.85(2)	1.98(2)	2.829(1)	175(2)
O7-H7B···O1[c]	0.84(2)	2.49(2)	3.059(1)	126(2)
O7-H7B···O5[d]	0.84(2)	2.21(2)	2.979(1)	152(2)
C2-H2···O4[f]	0.93(2)	2.88(1)	3.403(1)	117(1)
C2-H2···O7[g]	0.93(2)	2.71(1)	3.611(1)	164(1)
C3-H3···O4[f]	0.98(2)	2.55(1)	3.285(1)	132(1)
C5-H5···O2	0.99(2)	2.41(2)	3.184(2)	135(1)
(Figure 4.26(d)) H-bonds connecting 1D chains along c direction				
C4-H4···O2[h]	0.96(2)	2.70(1)	3.220(2)	114(1)
C4-H4···O4[h]	0.96(2)	2.72(2)	3.641(1)	161(1)
C5-H5···O2[h]	0.99(2)	2.49(2)	3.104(1)	120(1)

Symmetry codes: [b](1-x, -y, -z) [c](-x, -y, -z) [d](-1+x, y, z) [e](-x, -1-y, -z) [f](-2+x, -1+y, z) [g](-1-x, -1-y, -z) [h](1-x, -y, -1-z)

The melting point of **(7)** was found to be in the range of 80 – 91 °C by analysis of a single crystal by HSM. It is interesting that despite the chains of coordination polymer formed by this complex, which it would be thought could impart thermal stability, the melting point is in the same range as that of **(6)**, which is a complex of discrete units connected primarily by moderate strength H-bonds. This could be testament to the stabilisation afforded by the extensive H-bonding present in **(6)**, however further stabilisation still by the H-bonding present in **(7)** is not observed.

DSC was carried out on the bulk sample of a 1:1 ligand:metal preparation that was shown to result in **(7)** (Appendix A, Figure A8). This showed a broad endotherm at 78.9 °C, indicating a close agreement with the melting range observed by HSM. However this is a broad peak, and given that the melting point of $Mg(NO_3)_2.H_2O$ is 89 °C, if there was remaining starting material in the sample, as suggested by PXRD for a 1:1 sample preparation, it may not be possible to distinguish between its melting, and that of **(7)**.

4.3.2. *Catena-[(μ_2-pyridinium-2-carboxylato)-nitrato-triaqua-magnesium(II)] nitrate* **(8)**

$[Mg(C_6H_5NO_2)(NO_3)(H_2O)_3].NO_3$

(8) was prepared by solvent evaporation of a 1:2 stoichiometric mixture of picolinic acid and magnesium(II) nitrate hexahydrate dissolved in methanol at 50 °C. On two occasions this material was also formed during experiments in which the starting materials were used in equimolar ratios, including a preparation which on separate repeats produced either **(6)** or **(7)** (see Experimental). In common with **(6)** and **(7)**, **(8)** was a clear, colourless material, however rather than small discrete crystals, the product was in the form of large conglomerates of flat crystals. The PXRD pattern of **(8)** was taken from the preparation in which the ligand:metal ratio was 1:2. The single crystal product, however, unlike the previous two structures, has a 1:1 ligand:metal ratio. Therefore it could be expected that excess magnesium(II) nitrate hexahydrate may be detected in the PXRD pattern of this sample (Figure 4.27). There are coinciding peaks of the metal salt and **(8)** at about 15°, 20°, 25°, 27° and 31°, however **(8)** better matches the calculated PXRD pattern, albeit that there are certain peaks missing, in particular that at about 11°.

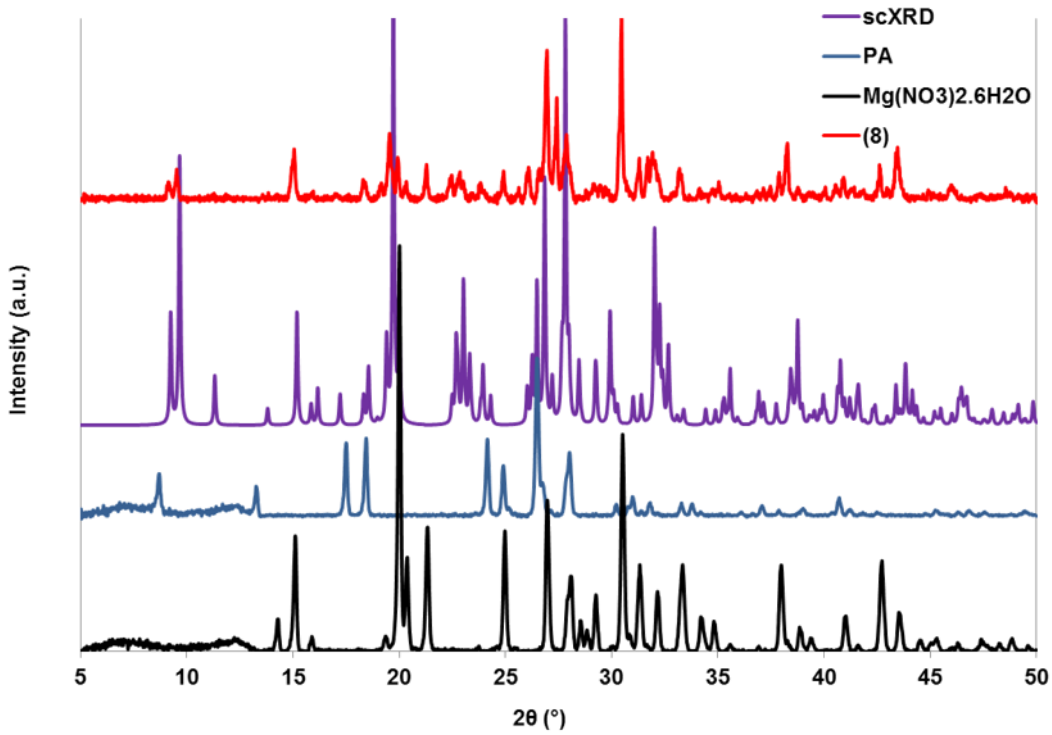

Figure 4.27. PXRD pattern of **(8)** compared to calculated pattern and patterns of starting materials.

There is a close relationship between the four coordination complexes **(6)**, **(7)**, **(8)** and **(A2)** (*pyridinium-2-carboxylate pyridinium-2-carboxylic acid nitrate*, Appendix D). All of these complexes could be produced using exactly the same quantities of the same starting materials, although single crystals of two or more different complexes were never found simultaneously in the same vial preparation. However, one experiment which yielded single crystals of **(8)**, once dry, was treated with a few mls of THF and subjected to another sequence of solvent evaporation and subsequently formed crystals of **(7)** (see Experimental). The experimentally obtained PXRD patterns of the bulk samples of each of the four complexes are shown together for comparison in Figure 4.28. It is clear that **(7)** and **(8)** have more mutually distinct patterns than that of **(A2)** which very closely resembles **(6)**, such that it can be said that the bulk materials are the same.

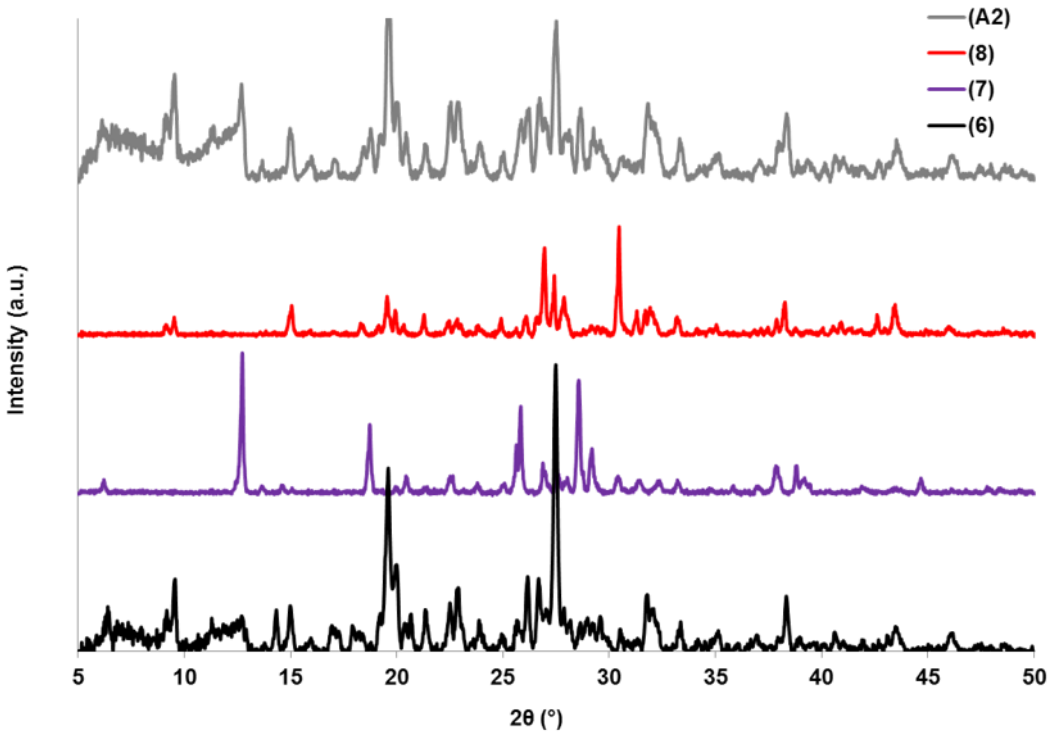

Figure 4.28. PXRD patterns of **(6)**, **(7)**, **(8)** and **(A2)**.

(8) is a coordination polymer composed of 1D chains, illustrated in Figure 4.29(a). Unlike **(7)**, however, the primary structure consists of magnesium centres bridged by only one picolinic acid ligand through the carboxylate oxygen atoms, hence the ligand:metal ratio of 1:1. The formula unit features a magnesium centre, a coordinating zwitterionic picolinic acid ligand, a coordinating nitrate group and three coordinating water molecules. In common with **(7)** there is a non-coordinated nitrate ion but in contrast there is one less water molecule in total and no non-coordinated water molecules.

The magnesium centre of **(8)** has a slightly distorted octahedral geometry (Figure 4.29(b) and Table 4.16), as is common for these magnesium-organic structures. The O-Mg-O angles range from 86.01(5)° for O2-Mg1-O7 to 94.14(5)° for O2-Mg1-O8, both angles between the carboxylate oxygen atom O2 and the oxygen atoms of two coordinating water molecules. The Mg-O distance to the coordinating oxygen atom of the nitrate ion, O3, is the longest at 2.133(1) Å, and those to the water ligands are 2.053(1) Å, 2.040(1) Å and 2.069(1) Å for Mg1-O7, Mg1-O8 and Mg1-O10, respectively. The Mg-carboxylate oxygen atom distances are the shortest and second longest of the Mg-O distances: Mg1-O2 is 2.076(1) Å while Mg1-O9, orthogonal to Mg1-O2, is 2.030(1) Å. This may be an effect of steric hindrance due to the fact that Mg1-O9 lies in the direction of the 1D chain. Mg1-O2

on the other hand is positioned perpendicular to the 1D chain, and therefore has less steric constraint.

The bridging picolinic acid ligand is shown in Figure 4.29(c). The C-O distances of the carboxylate group are 1.257(2) Å for C15-O2 and 1.241(2) Å for C15-O9. Once again, the shorter bonding distance is observed between the atoms lying in the direction of the 1D chain, and the shorter Mg-O distance is associated with the larger Mg-O-C angle; the angle Mg1^{a}-O9-C15 is 159.1(1)°. The angle Mg1-O2-C12 is 133.7(1)° due to the positioning of the next magnesium centre about the 2-fold screw axis.

The O-C-O angle O2-C15-O9 is 127.5(2)° . This is smaller than the bridging carboxylate angle of either **(7)** of 129.3(1)°, **(1)** of 129.0(1)° or **NISJEE** of 129.4(5)°, but it is slightly wider than the O=C-O angle of pure picolinic acid (126.8(1)°). This suggests that when the carboxylate group is bridging magnesium centres the O-C-O angle is widened, and this effect is greater when two carboxylate groups are bridging the metal centres. The carboxylate group and the pyridinium ring are twisted from coplanarity with a O2-C15-C16-N21 torsion angle of 26.5(2)°.

The 1D chains of **(8)** run in the *b* direction. Within the chains there are intracomplex H-bonds between the coordinating water ligands and an oxygen atom of the coordinated nitrate ion, O10-H1···O4, and to each of the carboxylate group oxygen atoms, O8-H6···O2^{b} and O8-H6···O9 (Figure 4.29(d) and Table 4.17). O10-H1···O4 and O8-H6···O2^{b} are moderately strong interactions with D···A distances of 2.723(2) Å and 2.867(2) Å and angles of 149(3)° and 154(3)°, respectively. O8-H6···O9 is a more constrained interaction and has a slightly longer D···A distance of 3.074(2) Å and a very low angle of 117(2)°.

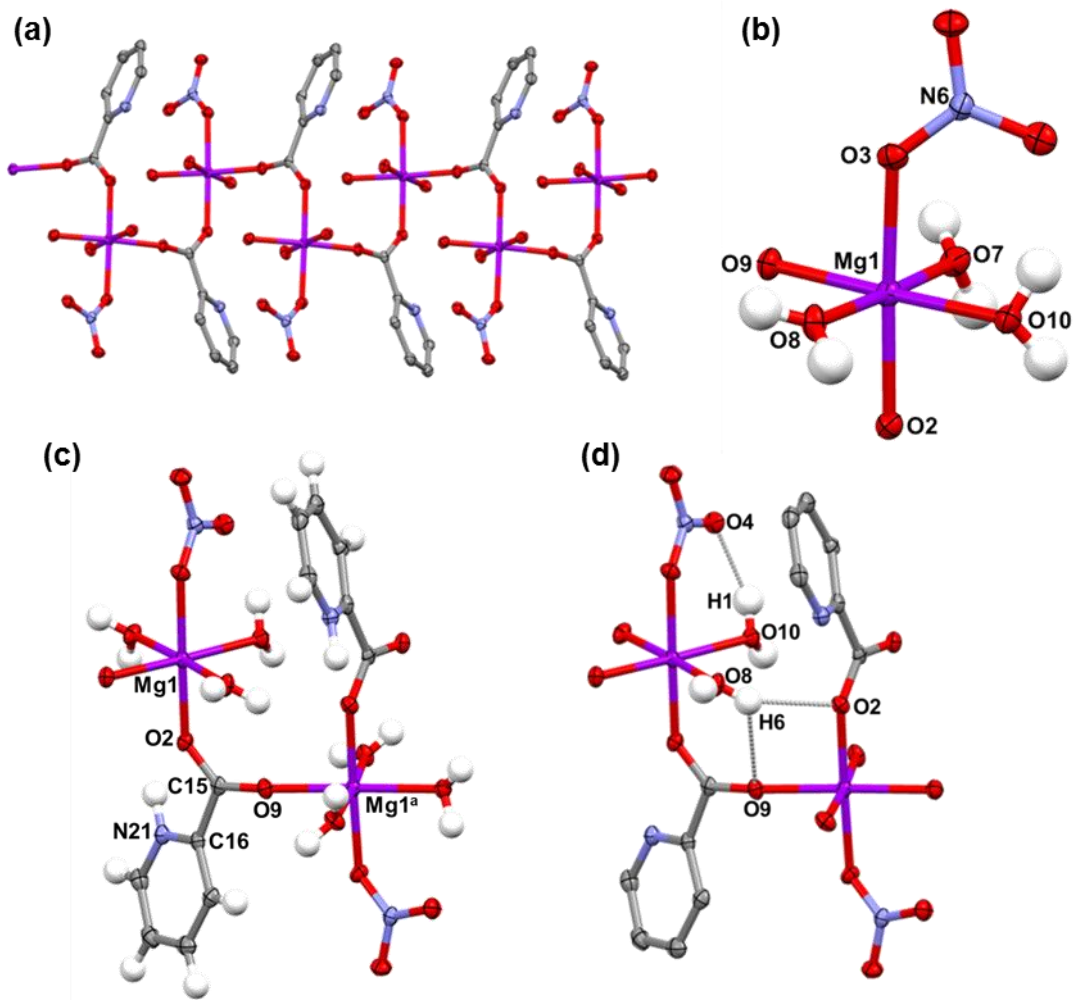

Figure 4.29. Crystal structure of **(8)**. (a) 1D chain of Mg centres bridged by one picolinic acid ligand (H atoms removed for clarity). (b) Octahedral Mg centre with two coordinating carboxylate oxygen atoms, one coordinating nitrate ion and three coordinating water molecules. (c) Section of 1D chain showing the bridging picolinic acid ligand. (d) Section of 1D chain showing intracomplex H-bonds (only H atoms of water ligands involved in H-bonds are shown). Symmetry codes: [a](½-x, ½-y, ½-z)

Table 4.16. O-Mg-O angles and Mg-O distances in **(8)**.

Coordination	O-Mg-O angle (°)	Interaction	Distance (Å)
O3-Mg1-O7	92.88(5)	Mg1-O2	2.076(1)
O3-Mg1-O10	89.48(5)	Mg1-O3	2.133(1)
O3-Mg1-O8	87.09(5)	Mg1-O7	2.053(1)
O3-Mg1-O9	88.64(5)	Mg1-O8	2.040(1)
O2-Mg1-O7	86.01(5)	Mg1-O9	2.030(1)
O2-Mg1-O10	88.82(5)	Mg1-O10	2.069(1)
O2-Mg1-O8	94.14(5)		
O2-Mg1-O9	93.09(5)		
O7-Mg1-O10	92.67(5)		
O10-Mg1-O8	91.16(6)		
O8-Mg1-O9	87.52(6)		
O9-Mg1-O7	88.64(5)		

The structure of **(8)** is composed of 1D chains parallel to the *b* direction, H-bonded to neighbouring chains along the *a* and *c* directions. Figure 4.30(a) shows H-bonds propagating the structure along the *a* direction (Table 4.17). These H-bonds are formed between the N-H and C-H groups of the pyridinium ring to the non-coordinated and coordinated nitrate ions and coordinated water ligands, and between the water ligands to the coordinated and non-coordinated nitrate ions.

N21-H12···O14^{c} is an H-bond from picolinic acid to an oxygen atom of the non-coordinated nitrate ion. It is among the strongest of the H-bonds in this structure with a D···A distance of 2.790(2) Å and an angle of 174(2)°. It is accompanied by the weaker H-bond C20-H11···O12^{c}, where the acceptor is another oxygen atom of the nitrate ion, which has a longer D···A distance of 3.359(2) Å and a smaller angle of 130(2)°. O14^{c} is also the acceptor in the H-bond O7-H5···O14^{c}, which is formed by a coordinated water molecule. This is a moderately strong interaction of 2.733(2) Å and 167(3)°. These H-bonds are also involved in connecting the structure along the *c* direction due to their interaction with the nitrate ion which is a central component to the extension along this direction. The third oxygen atom of the nitrate group, O13, is the acceptor of two H-bonds from the next picolinic acid ligand

along the *a* direction: C19-H10···O13[g] and C18-H9···O13[g]. These are equally weak H-bonds with D···A distances of 3.612(3) Å and 3.622(3) Å and angles of 121(2)° and 124(1)°. C18-H9 also interacts with O7, the oxygen atom of a water ligand. C18-H9···O7[f] is a slightly shorter and more linear H-bond than the previous two with a D···A distance of 3.452(2) Å and angle of 145(2)°. C17-H8···O4[f] is formed to the coordinated nitrate ion of the next 1D chain along the *a* direction. It has an angle of 163(2)° and a long D···A distance of 3.288(2) Å.

The water ligands containing O7 and O10 form H-bonds to oxygen atoms of coordinated nitrate ions. O7-H4 forms H-bonds to two oxygen atoms of the same nitrate ion, O7-H4···O4[d] and O7-H4···O5[d]. The former is the weaker of the two bonds with a D···A distance of 3.112(2) Å and an angle of 130(2)°, while O7-H4···O5[d] is a moderately strong interaction with a D···A distance of 2.854(2) Å and an angle of 170(2)°. Together these constitute a bifurcated H-bond. As well as the intracomplex H-bond, O10-H1 also forms an H-bond to O5 of the nitrate ion located along the *b* direction from the nitrate to which O7-H4 H-bonds. O10-H1···O5[e] is a weak interaction with a D···A distance of 3.168(2) Å and an angle of 128(2)°. O10-H1···O4 and O10-H1···O5[e] also make up a bifurcated H-bond.

The non-coordinated nitrate ion is important in the propagation of the structure along the *c* direction. It accepts H-bonds from the N-H and C-H groups of the pyridinium ring, N21-H12···O14[c] and C20-H11···O12[c], discussed previously, and also accepts H-bonds from water molecules, O8-H7···O12[h], O8-H7···O13[h], O10-H3···O12 and O7-H5···O14[c], the latter discussed previously. The H-bonds involved in connecting the structure along the *c* direction are listed in Table 4.17 and illustrated in Figure 4.30(b) and (c), where in (c) one of the two non-coordinated nitrate ions related through an inversion centre has been removed for clarity. O8-H7 forms a bifurcated H-bond to two oxygen atoms of the nitrate ion. O8-H7···O13[h] is the stronger component of the bifurcated H-bond with a D···A distance of 2.789(2) Å and an angle of 170(3)°. O10-H3···O12 is also a moderately strong interaction with a slightly longer D···A distance of 2.843(2) Å and a smaller angle of 164(3)°. The 1D chains are H-bonded directly by C20-H11 which forms an H-bond to an oxygen atom of the coordinated nitrate ion of the next 1D chain along the *c* direction, C20-H11···O5[i]. This is a moderately weak H-bond with a D···A distance of 3.156(2) Å and an angle of 152(2)°. As H11 is also involved in the interaction C20-H11···O12[c], this completes another bifurcated H-bond within this structure.

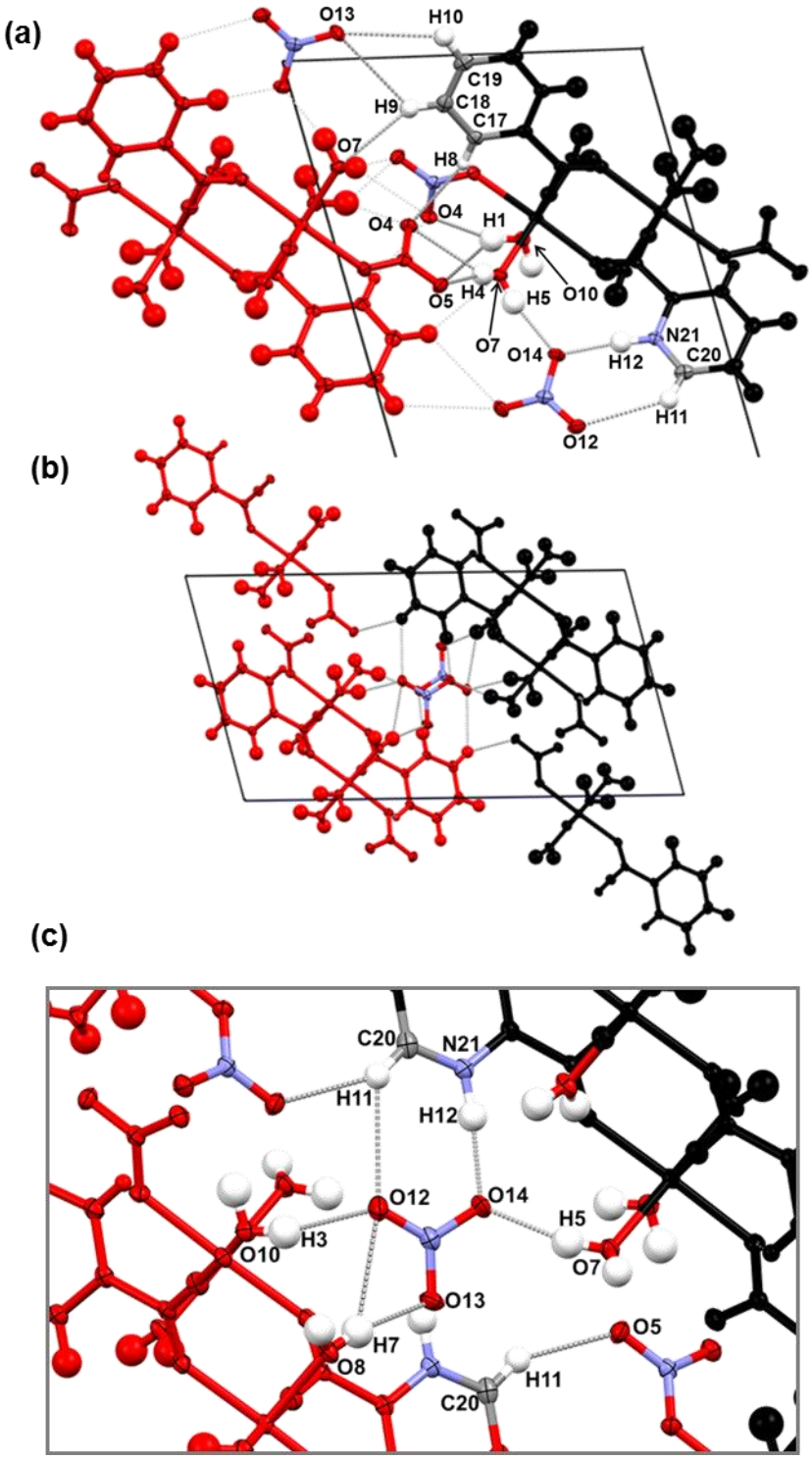

Figure 4.30. Crystal structure of **(8)**. (a) View down the *b* axis showing H-bonds connecting 1D chains along the *a* direction. (b) View down the *b* axis showing H-bonds connecting 1D chains along the *c* direction, with (c) showing a zoomed view of (b), illustrating the H-bonds connecting 1D chains (one non-coordinated nitrate ion omitted for clarity).

Table 4.17. Geometries of H-bonds in **(8)**.

D-H···A Interaction	D-H (Å)	H···A (Å)	D···A (Å)	D-H···A (°)
(Figure 4.29(d)) H-bonds within 1D chain				
O10-H1···O4	0.86(3)	1.95(3)	2.723(2)	149(3)
O8-H6···O2[b]	0.79(3)	2.14(3)	2.867(2)	154(3)
O8-H6···O9	0.79(3)	2.64(3)	3.074(2)	117(2)
(Figure 4.30(a)) H-bonds connecting 1D chains along a direction				
N21-H12···O14[c]	0.97(3)	1.82(3)	2.790(2)	174(2)
O7-H4···O4[d]	0.84(3)	2.51(3)	3.112(2)	130(2)
O7-H4···O5[d]	0.84(3)	2.02(3)	2.854(2)	170(2)
O7-H5···O14[c]	0.87(3)	1.88(3)	2.733(2)	167(3)
O10-H1···O5[e]	0.86(3)	2.57(3)	3.168(2)	128(2)
C17-H8···O4[f]	0.89(2)	2.42(2)	3.288(2)	163(2)
C18-H9···O7[f]	0.99(2)	2.60(2)	3.452(2)	145(2)
C18-H9···O13[g]	0.99(2)	2.98(2)	3.622(3)	124(1)
C19-H10···O13[g]	0.99(2)	2.99(2)	3.612(3)	121(2)
C20-H11···O12[c]	0.95(2)	2.66(2)	3.359(2)	130(2)
(Figure 4.30(c)) H-bonds connecting 1D chains along c direction				
O8-H7···O12[h]	0.84(3)	2.64(3)	3.285(2)	136(2)
O8-H7···O13[h]	0.84(3)	1.96(3)	2.789(2)	170(3)
O10-H3···O12	0.85(3)	2.02(3)	2.843(2)	164(3)
C20-H11···O5[i]	0.95(2)	2.29(2)	3.156(2)	152(2)

Symmetry codes: [b](½-x, ½+y, ½-z) [c](1-x, 1-y, 1-z) [d](1½-x, -½+y, ½-z) [e](1½-x, ½+y, ½-z) [f](-1+x, y, z) [g](-x, 1-y, 1-z) [h](½-x, -½+y, ½-z) [i](-½+x, ½-y, ½+z)

Analysis of a single crystal of **(8)** by HSM indicated a melting point in the range of 120 – 133 °C. The bulk sample of the preparation in which the ligand:metal ratio was 1:2 was analysed by DSC (Figure 4.31). Following a small endotherm at 76.3 °C, there is a larger

endotherm at 86.8 °C which likely indicates the melt of residual $Mg(NO_3)_2.6H_2O$ (m.p. 89 °C). A broad shallow endotherm at 121.4 °C is observed before decomposition. If this is taken to be the melting point of **(8)**, it is higher than that of **(6)** and, surprisingly, of **(7)**, despite the latter containing 1D doubly organic-ligand-bridged metal coordination polymeric chains. The melting point of **(8)** is more comparable to that of **(5)** at 122.8 °C. Although **(8)** has greater metal-coordination connectivity than **(5)**, the latter may be stabilised by, albeit fairly weak, π-π stacking interactions.

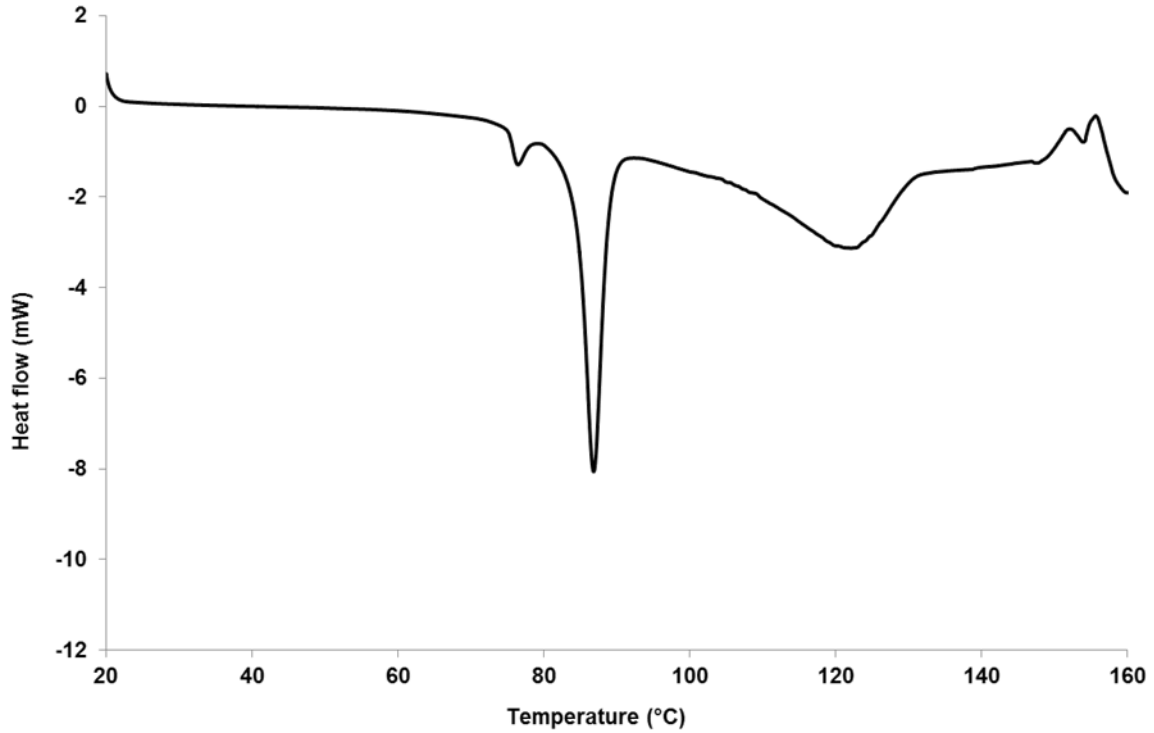

Figure 4.31. DSC trace of **(8)** on a 2.4 mg sample with a temperature ramp of 10 °C min^{-1}.

4.3.3. *Catena-[(μ_3-pyridinium-4-carboxylato)-tetraaqua-calcium(II)] dichloride hydrate* **(9)**
$[Ca(C_6H_5NO_2)(H_2O)_4].2Cl.H_2O$

(9), **(10)**, **(11)** and **(12)** are 1D coordination polymers, as were **(7)** and **(8)**. These structures however, feature calcium as opposed to magnesium centres again, bridged by pyridine carboxylic acid ligands.

(9) was prepared by growth from a solution of an approximately 4:5 stoichiometric ratio of isonicotinic acid and calcium(II) chloride dissolved in isopropanol at 4 °C in a vial with a hole pierced lid. The product was in the form of champagne-coloured, clear, crystalline shards. About five months after the crystals had been found and the structure determined, the unit cell of a crystal from the same sample was determined, confirming that the material was still **(9)**. The dry material was analysed by PXRD on the bulk sample one month later

(Appendix A, Figure A9). Although visually the crystalline material appeared homogeneous, the experimentally obtained PXRD pattern does not show much agreement with the calculated PXRD pattern from the single crystal structure. The complicated thermal behaviour of **(9)** recorded by DSC (Appendix A, Figure A10) and HSM (Appendix A) suggested that the material is not stable above 50 °C. The PXRD sample was prepared by oven drying at 50 °C, and the heating may have affected its composition and so it is not a fair representation of the as-prepared bulk sample.

The calcium centre in **(9)** is eight-coordinate (Figure 4.32(a), Table 4.18) and is situated on a 2-fold rotation axis. There are four coordinating water molecules and four coordinating carboxylate oxygen atoms of three different zwitterionic isonicotinic acid ligands, also on a 2-fold rotation axis. The ligand coordinates to three calcium centres *via* the carboxylate oxygen atoms. It coordinates to two Ca centres *via* one carboxylate oxygen atom to extend the 1D chain along the *c* direction, and to one Ca centre *via* both carboxylate oxygen atoms in the *b* direction, Figure 4.32(b).

The two Ca-O coordination interactions have different distances. The Ca-O distance concerning the coordination parallel to the *c* direction, Ca1-O1/O1^{a}, is 2.348(1) Å compared to the Ca-O coordination in which the oxygen atoms are of the same carboxylate group, Ca1-O1^{b}/O1^{c}, is 2.675(1) Å. The Ca-O distances to the water ligands are more equal than those to the carboxylate oxygen atoms, and lie between those distances: Ca1-O2/O2^{a} is 2.453(1) Å and Ca1-O3/O3^{a} is 2.423(1) Å.

The coordinating carboxylate and water oxygen atoms can be viewed as forming two semi-circles around the Ca centre aproximately perpendicular to one another: O3/O3^{a}-Ca1-O1/O1^{a} is 88.75(4)° and O3/O3^{a}-Ca1-O1^{a}/O1 is 92.52(4)° (Figure 4.32(a), Table 4.18). The water ligands are more spread out from each other than are the carboxylate oxygen atoms, evident in the wider angles O3/O3^{a}-Ca1-O2/O2^{a} of 69.40(4)° and O2-Ca1-O2^{a} of 73.71(6)°. The angle between the carboxylate oxygen atoms O1^{b}-Ca1-O1^{c} is necessarily small at 48.63(5)° due to the oxygen atoms being of the same carboxylate group of the zwitterionic isonicotinic acid ligand situated on the 2-fold rotation axis, while O1/O1^{a}-Ca1-O1^{c}/O1^{b} is wider at 68.50(4)°. The coordination along the *c* direction, O1-Ca1-O1^{a} is almost linear at 175.15(5)° whereas the water ligands that are directed perpendicular to the *c* direction are closer together, with O3-Ca1-O3^{a} displaying a lower angle of 149.84(6)°.

Since the isonicotinic acid ligand is on a 2-fold rotation axis, both the C-O distances are identical at 1.252(1) Å for C1-O1 and C1-O1^{d}, Figure 4.32(c). The angle O1-C1-O1^{d} is 123.2(2)°, smaller than the O=C-O angle in the pure ligand (125.1(2)°). This is likely due to the fact that both of the oxygen atoms of the carboxylate group chelate the metal centre,

narrowing this angle. The carboxylate group and the pyridinium ring are twisted from coplanarity with an O1-C1-C2-C3 torsion angle of 43.55(9)°. This may be due to steric effects in that there would be insufficient space for both a planar ligand and the water ligands of O2 and O2[a] to be situated alternately along the 1D chains. The twisting may also assist in the formation of the intracomplex H-bond C3-H3···O2, between a C-H group of the pyridinium ring and a coordinated water molecule, although this is a weak interaction with a D···A distance of 3.256(2) Å and an angle of 127° (Table 4.19).

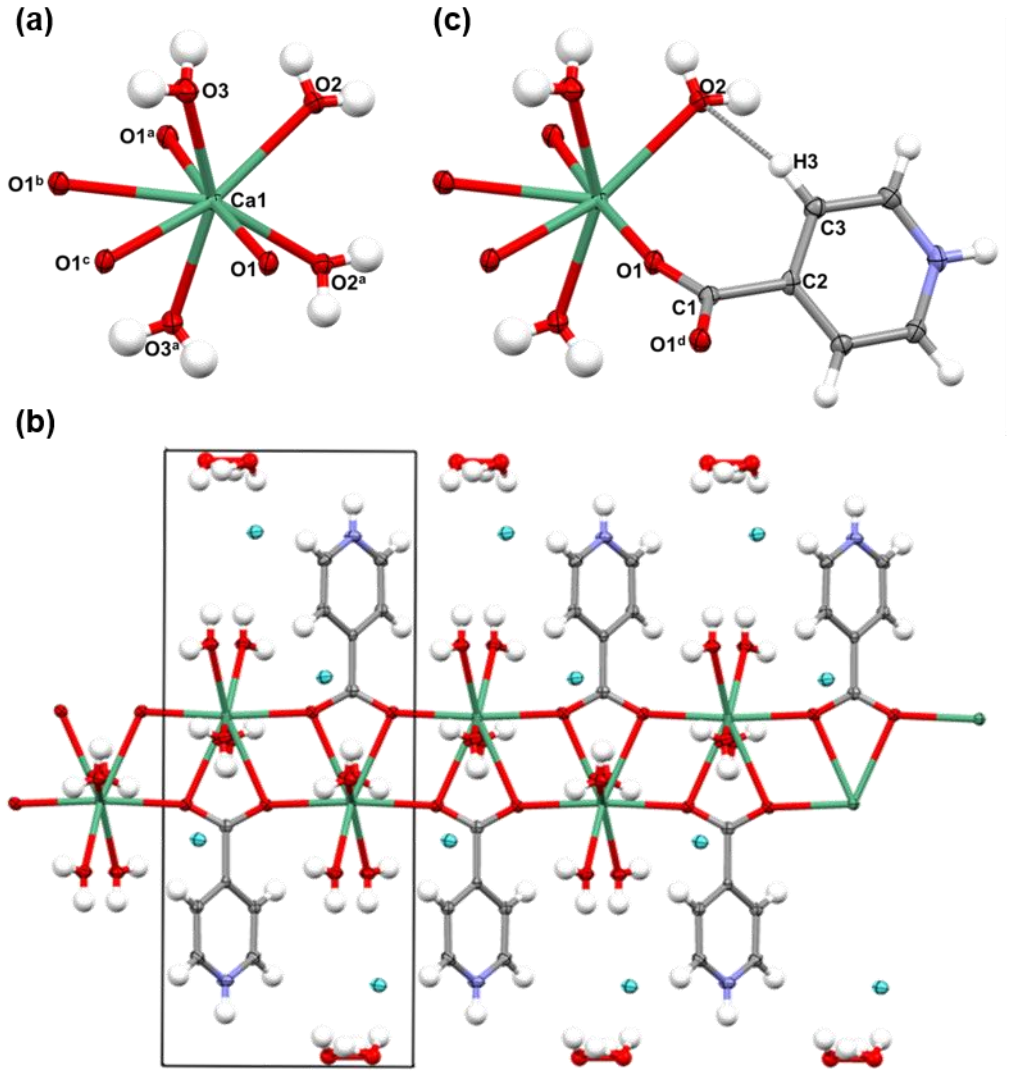

Figure 4.32. Crystal structure of **(9)**. (a) Eight-coordinate Ca centre with four coordinating carboxylate oxygen atoms and four coordinating water molecules. (b) View down *a* axis, showing the 1D chain parallel to *c* direction, with the isonicotinic acid ligand bridging three Ca centres, showing non-coordinated chloride ions and non-coordinated, disordered water molecules. (c) Ca centre and one coordinating isonicotinic acid ligand showing intracomplex H-bond C3-H3···O2, (one water ligand omitted for clarity). Symmetry codes: [a](1-x, y, ½-z) [b](x, -y, -½+z) [c](1-x, -y, 1-z) [d](1-x, y, 1½-z)

Table 4.18. O-Ca-O angles and Ca-O distances in **(9)**.

Coordination	O-Ca-O angle (°)	Interaction	Distance (Å)
O3/O3[a]-Ca1-O1/O1[a]	88.75(4)	Ca1-O1/O1[a]	2.348(1)
O3/O3[a]-Ca1-O1[a]/O1	92.52(4)	Ca1-O1[b]/O1[c]	2.675(1)
O3/O3[a]-Ca1-O1[b]/O1[c]	72.94(4)	Ca1-O2/O2[a]	2.453(1)
O3/O3[a]-Ca1-O1[c]/O1[b]	79.59(4)	Ca1-O3/O3[a]	2.423(1)
O3/O3[a]-Ca1-O2/O2[a]	69.40(4)		
O2-Ca1-O2[a]	73.71(6)		
O1/O1[a]-Ca1-O1[c]/O1[b]	68.50(4)		
O1[b]-Ca1-O1[c]	48.63(5)		
O1[a]/O1-Ca1-O2/O2[a]	80.40(4)		
O1[a]/O1-Ca1-O2[a]/O2	95.68(4)		
O1-Ca1-O1[a]	175.15(5)		
O3-Ca1-O3[a]	149.84(6)		
O3/O3[a]-Ca1-O2[a]/O2	140.19(4)		

Symmetry codes: [a](1-x, y, ½-z) [b](x, -y, -½+z) [c](1-x, -y, 1-z)

The packing of the 1D chains of **(9)** is illustrated in Figure 4.33(a). The chains are connected along the *a* and *b* directions by six H-bonds from the coordinated and non-coordinated water molecules to the chloride ions, as shown in Figure 4.33(b) and listed in Table 4.19. The non-coordinated water molecule lies on the 2-fold rotation axis and exhibits 50:50 disorder between two positions; it forms an H-bond to the chloride ion either through H5A or H5B. O4-H5A···Cl1[a] and O4-H5B···Cl1 are of equal length with D···A distances of 3.104(3) Å and 3.108(2) Å, respectively, but the latter has a more linear angle of 168(4)° compared to the angle of the former of 131(3)°. The H-bonds formed by the coordinated water molecules are generally slightly longer, with D···A distances ranging from 3.146(2) Å for O3-H3A···Cl1[h] to 3.256(2) Å for O3-H3B···Cl1[g], and large angles, from 153(2)° for O2-H2B···Cl1 to 172(2)° for O2-H2A···Cl1[g].

The formula units are also linked along the *b* direction *via* H-bonds from the N-H group of the pyridinium ring to the non-coordinated disordered water molecule situated on the 2-fold

rotation axis, N1-H1···O4^{e}/O4^{f}, (Figure 4.33(c) and Table 4.19). The water molecules are arranged alternately along the *c* direction on the same 2-fold rotation axis as is the isonicotinic acid ligand to which it is H-bonded. The D···A distance from N1 to either O4^{e} or O4^{f} is 2.687(3) Å, but when measured from N1 to the centroid of the two oxygen atoms the D···A distance is approx. 2.611 Å. The D-H···A angle to the oxygen atom in either position is approx. 160°. This is a moderately strong interaction which plays a central role in propagating the crystal structure in the *b* direction, and requires that both a non-coordinated water molecule is present, and that the N-H group is para to the carboxylate group, i.e, this connectivity could only be exhibited by isonicotinic acid, the same H-bonding could not be observed for either picolinic or nicotinic acid.

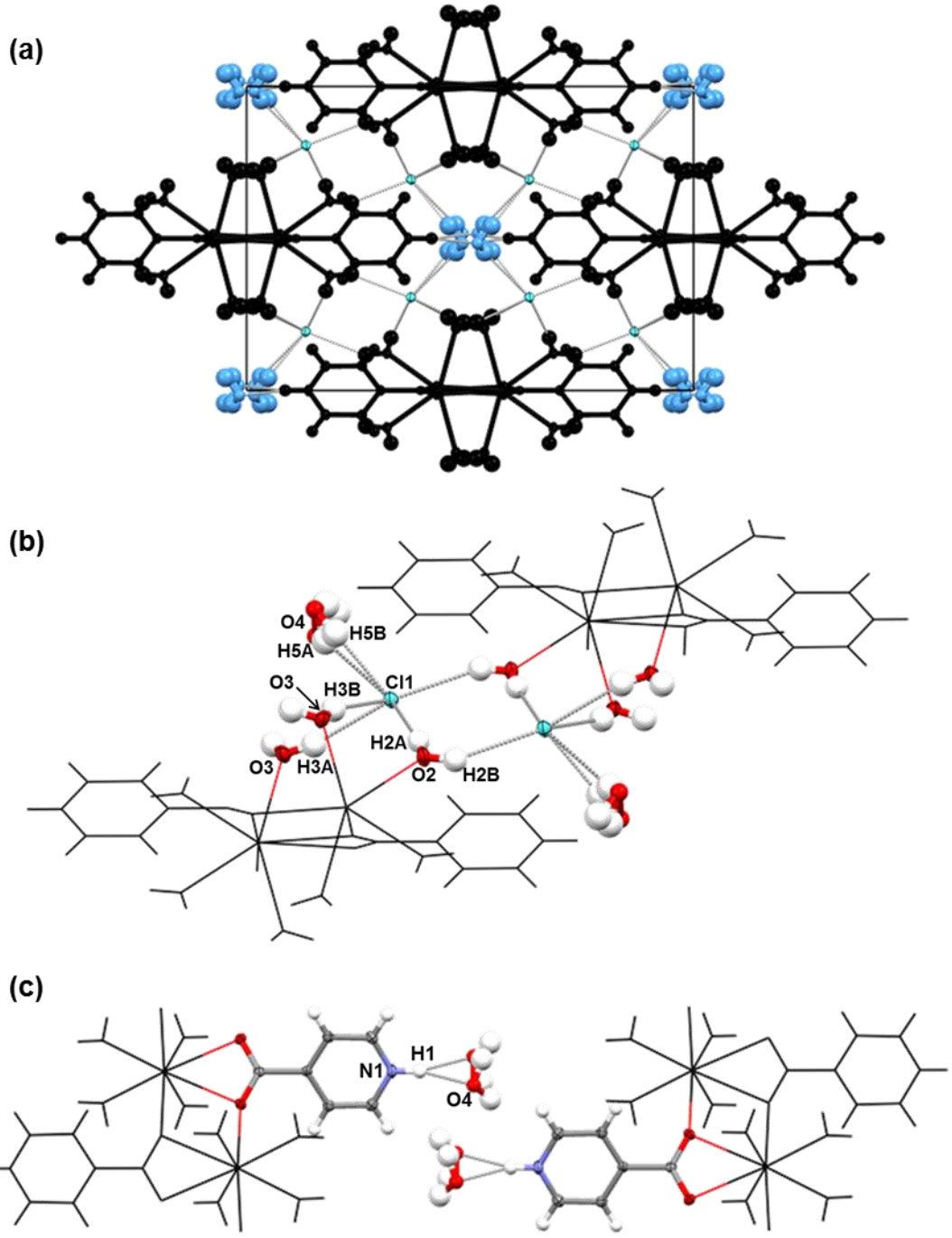

Figure 4.33. Crystal structure of **(9)**. (a) View down the *c* axis showing stacking of 1D chains along the *a* and *b* directions, connected by H-bonds *via* non-coordinated chloride ions and disordered water molecules (1D chains in black, water molecules in blue). (b) Detailing H-bonds connecting two 1D chains along the *a* direction *via* chloride ions. (c) Detailing H-bonds connecting 1D chains along the *b* direction *via* the H-bond N1-H1···O4^{e}/O4^{f}.

Table 4.19. Geometries of H-bonds in **(9)**.

D-H···A Interaction	D-H (Å)	H···A (Å)	D···A (Å)	D-H···A (°)
(Figure 4.32(b)) Intracomplex H-bond within 1D chain				
*C3-H3···O2	0.95	2.59	3.256(2)	127
(Figure 4.33(b) and (c)) H-bonds connecting 1D chains along both a and b directions				
*N1-H1···O4[e]/O4[f]	0.88	1.84	2.687(3)	160
O2-H2A···Cl1[g]	0.81(2)	2.35(2)	3.149(2)	172(2)
O2-H2B···Cl1	0.80(3)	2.45(2)	3.183(1)	153(2)
O3-H3A···Cl1[h]	0.82(3)	2.36(3)	3.146(2)	163(2)
O3-H3B···Cl1[g]	0.81(3)	2.48(3)	3.256(2)	162(2)
O4-H5A···Cl1[a]	0.87(3)	2.47(5)	3.104(3)	131(3)
O4-H5B···Cl1	0.87(4)	2.25(4)	3.108(2)	168(4)

Symmetry codes: [a](1-x, y, ½-z) [e](1-x, 1-y, 1-z) [f](x, 1-y, ½+z) [g](½-x, ½-y, -z) [h](½-x, -½+y, ½-z) *H-bond features aromatic hydrogen atom fixed in idealised position.

As was the case for **(1)**, **(2)** and **(4)**, the chloride ions are fundamental to the connectivity of the metal-organic units. In common with **(1)**, **(9)** does not display any H-bonds directly between metal-organic units (in this case the 1D chains), and so the counter ions act as common acceptors. The non-coordinated water molecules are also important in connecting the structure, acting as an acceptor for one metal-organic unit, and a donor in an H-bond to another.

4.3.4. *Catena-[bis-((μ$_2$-pyridinium-2-carboxylato)-bis-(nitrato)-diaqua-calcium(II))]* **(10)**

[Ca(C$_6$H$_5$NO$_2$)(NO$_3$)$_2$(H$_2$O)$_2$]$_2$

(10) is a constitutional isomer of **(3)**. The latter features two crystallographically equivalent calcium centres each coordinated by two water ligands and two bidentate nitrate ions. The metal centres are bridged by two crystallographically equivalent zwitterionic nicotinic acid ligands by coordination *via* the carboxylate oxygen atoms (Figure 4.13(c)). The crystalline structure of **(3)** is 0D in that it is composed of discrete units of the formula unit. **(10)**, in contrast, features two crystallographically inequivalent calcium centres each coordinated by two water ligands and chelated by two bidentate nitrate ions. Two crystallographically

inequivalent zwitterionic picolinic acid ligands alternately bridge between the calcium centres *via* the carboxylate groups to form a 1D coordination polymeric chain (Figure 4.35(a)). Both **(3)** and **(10)** were prepared from 1:1 stoichiometric mixtures of their respective pyridine carboxylic acid and calcium(II) nitrate tetrahydrate, and both have retained this ligand:metal ratio in the crystalline product. Crystals of **(10)** were grown in eleven days from an acetone solution at lab temperature. The PXRD pattern of the bulk product (Figure 4.34) shows some strong peaks that coincide with the calculated PXRD pattern at about 9°, 14°, 18°, 19°, and 27°, (taking into account the expected shifting of the calculated pattern to slightly higher 2θ values), suggesting that the single crystal is representative of the bulk product. However, much detail in the calculated pattern is absent in the experimentally obtained pattern, possibly due to poor sample quality or sample decomposition.

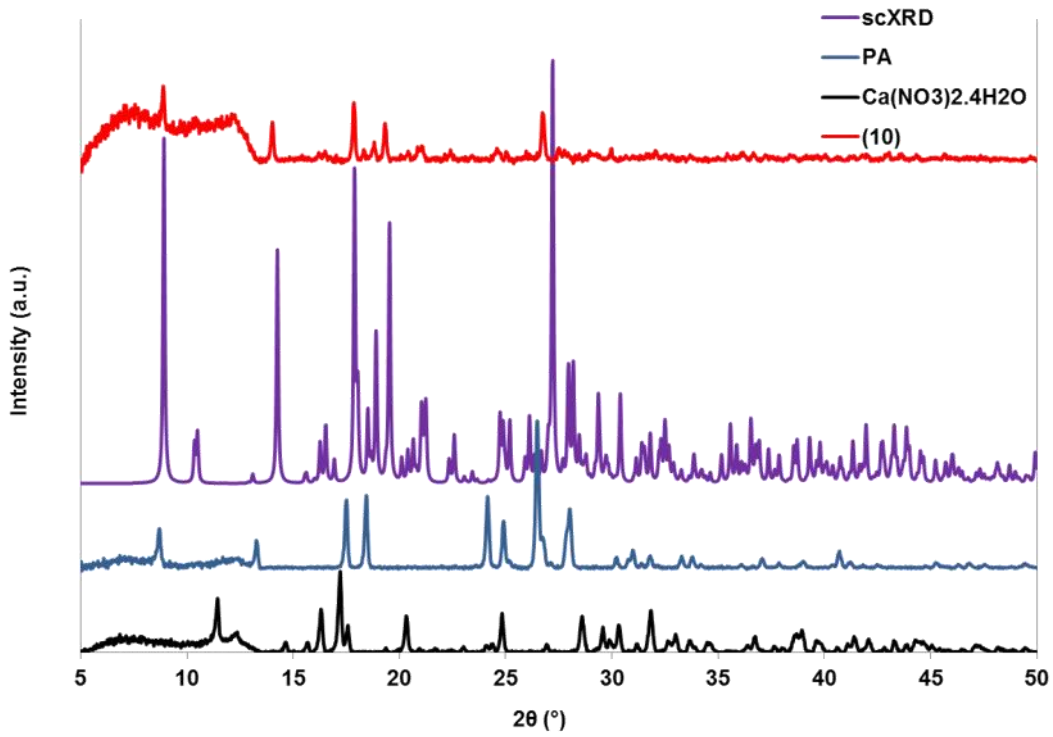

Figure 4.34. PXRD pattern of **(10)** compared to calculated pattern and patterns of starting materials.

Figure 4.35(b) and (c) show the two eight-coordinate calcium centres of **(10)**; their coordination geometries are listed in Table 4.20 and Table 4.21. The most striking difference between the two calcium centres in **(10)** and that of **(3)** is the orientation of the nitrate ions. While the nitrate ions of **(3)** were orientated similarly (see Figure 4.13(a)), the nitrate ions of **(10)** are more twisted relative to each other, in that the coordinating oxygen

atoms of one could be described as equatorial to the directions of the water ligands. This is evident in Ca1, in that the angles O17-Ca1-O13 and O17-Ca1-O14 are 86.91(8)° and 79.11(8)°, respectively, and the angles O16-Ca1-O13 and O16-Ca1-O14 are 91.42(9)° and 85.55(8)°, respectively. The differences between the angles formed between the same water ligands to each of the oxygen atoms of the other nitrate ion are much larger due to its orientation, which is similar to that of the nitrate ions in **(3)**: O16-Ca1-O10 is 70.60(8)°, O16-Ca1-O11 is 118.36(8)°, O17-Ca1-O10 is 126.09(8)° and O17-Ca1-O11 is 79.88(8)°. The same trend is observed for Ca2 in that O19-Ca2-O4 and O19-Ca2-O5 are 88.30(8)° and 93.82(8)°, respectively, and O18-Ca2-O4 and O18-Ca2-O5 are 76.56(8)° and 86.89(8)°, respectively, while O19-Ca2-O8 is 72.49(8)°, O19-Ca2-O7 is 118.95(8)°, O18-Ca2-O7 is 81.22(8)° and O18-Ca2-O8 is 126.13(8)°.

The angles between the coordinating carboxylate oxygen atoms, O20-Ca1-O1 and O3-Ca2-O2^{b} are 74.13(7)° and 73.65(7)°, respectively, significantly smaller than the equivalent angle observed in **(3)**, O3-Ca1-O4^{a}, of 119.07(4)°.

The angles formed between the calcium centre and the water ligands, O17-Ca1-O16 and O18-Ca2-O19, are 161.62(9)° and 159.82(9)°, respectively, which are slightly wider than the same angle in **(3)**, O1-Ca1-O2 at 143.35(4)°, however it is possible that this angle is influenced by the intracomplex H-bond within the formula unit (see Figure 4.13(b)).

The coordination distances from the calcium centres to the coordinating oxygen atoms of the nitrate ions vary between 2.507(2) Å for Ca1-O13 to 2.570(2) Å for Ca1-O10 in Ca1, and from 2.496(2) Å for Ca2-O7 to 2.623(2) Å for Ca2-O8 in Ca2. The coordination distances to the carboxylate oxygen atoms are similar at 2.388(2) Å for Ca1-O1, 2.409(2) Å for Ca1-O20, 2.393(2) Å for Ca2-O2^{b} and 2.400(2) Å for Ca2-O3. The Ca-O distances to the water ligands are similar for both Ca centres, but have the greatest range for Ca2: from 2.325(2) Å for Ca2-O18 to 2.361(2) Å for Ca2-O19.

Figure 4.35(d) shows the zwitterionic picolinic acid ligands bridging between the Ca centres. The carboxylate group angles O1-C1-O2 and O3-C7-O20 are both 127.2(3)°, which is slightly wider than the O=C-O angle of pure picolinic acid (126.8(1)°), possibly due to distortion by metal coordination. The C-O distances are different in each of the ligands: C1-O1 is 1.263(4) Å and C1-O2 is 1.241(3) Å; similarly, C7-O3 is 1.272(4) Å and C7-O20 is 1.238(4) Å. The ligands differ however, in their degree to which they exhibit coplanarity of the carboxylate group and the pyridinium ring. The torsion angle O2-C1-C2-N5 is 4.2(4)°, whereas the torsion angle O20-C7-C8-N6 is 23.9(4)°. The positioning of this pyridinium ring is favourable to the linearity of the intracomplex H-bond N6-H2⋯O1, a moderately strong

interaction with an angle of 177(4)° and a D···A distance of 2.712(4) Å, Figure 4.36(a). This H-bond is likely to be a significant influence on the adopted conformation.

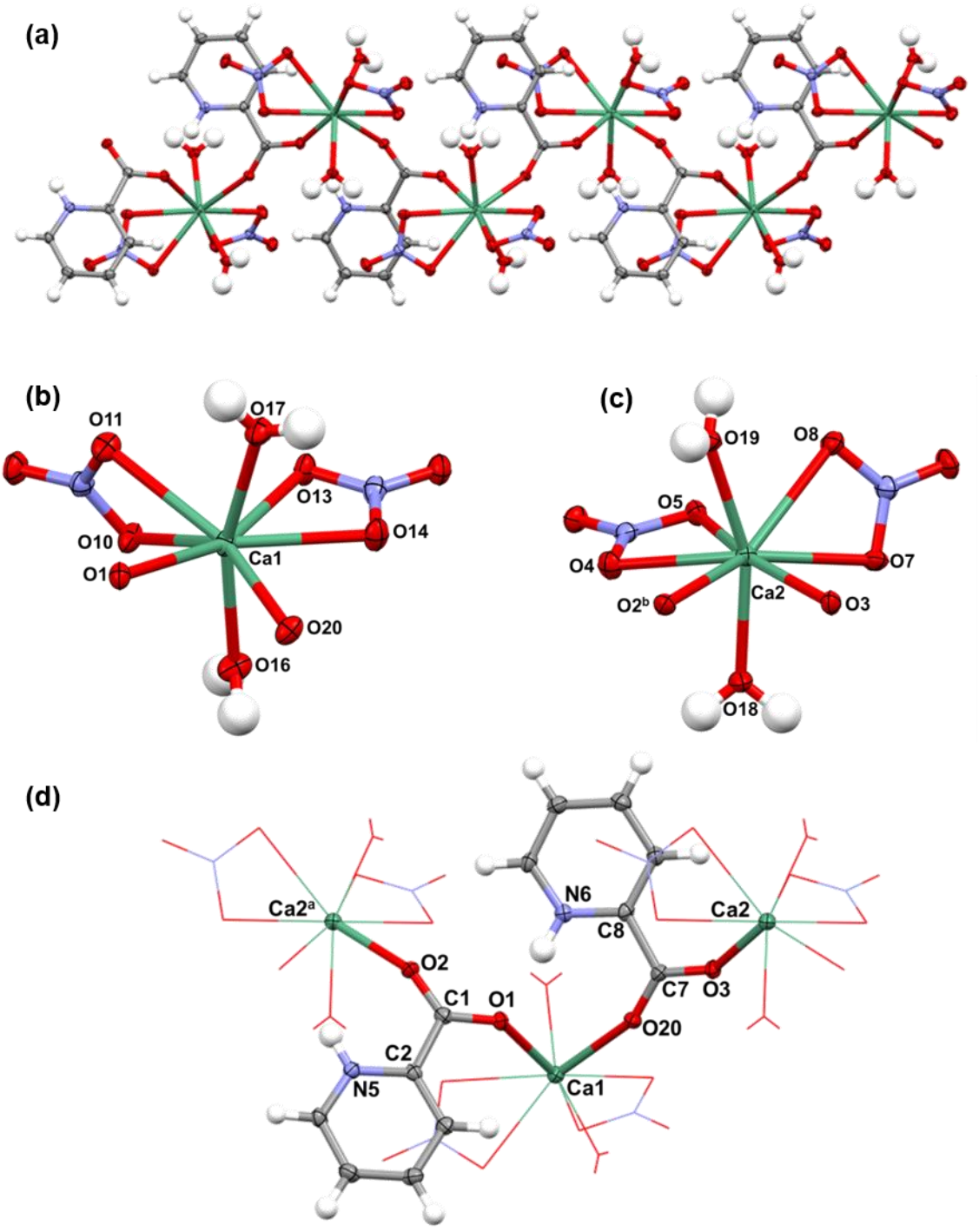

Figure 4.35. Crystal structure of **(10)**. (a) 1D chain parallel to the *c* direction. (b) Eight coordinate Ca1 centre, and (c) Ca2 centre, each with two coordinating carboxylate oxygen atoms, two coordinating nitrate ions and two coordinating water molecules. (d) Section of the 1D chain showing zwitterionic picolinic acid ligands bridging between metal centres. Symmetry codes: [a](x, ½-y, -½+z) [b](x, ½-y, ½+z)

Table 4.20. O-Ca-O angles and Ca-O distances concerning Ca1 in **(10)**.

Coordination	O-Ca-O angle (°)	Interaction	Distance (Å)
O17-Ca1-O1	86.96(8)	Ca1-O1	2.388(2)
O17-Ca1-O10	126.09(8)	Ca1-O10	2.570(2)
O17-Ca1-O11	79.88(8)	Ca1-O11	2.543(2)
O17-Ca1-O13	86.91(8)	Ca1-O13	2.507(2)
O17-Ca1-O14	79.11(8)	Ca1-O14	2.463(2)
O17-Ca1-O20	87.11(8)	Ca1-O16	2.337(2)
O16-Ca1-O1	99.95(9)	Ca1-O17	2.347(2)
O16-Ca1-O10	70.60(8)	Ca1-O20	2.409(2)
O16-Ca1-O11	118.36(8)		
O16-Ca1-O13	91.42(9)		
O16-Ca1-O14	85.55(8)		
O16-Ca1-O20	78.57(8)		
O11-Ca1-O13	87.51(7)		
O10-Ca1-O13	74.08(7)		
O13-Ca1-O14	51.42(7)		
O14-Ca1-O20	72.32(7)		
O20-Ca1-O1	74.13(7)		
O1-Ca1-O11	73.64(7)		
O1-Ca1-10	95.20(7)		
O10-Ca1-O11	50.02(7)		
O17-Ca1-O16	161.62(9)		

Table 4.21. O-Ca-O angles and Ca-O distances concerning Ca2 in **(10)**.

Coordination	O-Ca-O angle (°)	Interaction	Distance (Å)
O19-Ca2-O3	97.26(8)	Ca2-O2[b]	2.393(2)
O19-Ca2-O2[b]	78.34(8)	Ca2-O3	2.400(2)
O19-Ca2-O4	88.30(8)	Ca2-O4	2.541(2)
O19-Ca2-O5	93.82(8)	Ca2-O5	2.512(2)
O19-Ca2-O8	72.49(8)	Ca2-O7	2.496(2)
O19-Ca2-O7	118.95(8)	Ca2-O8	2.623(2)
O18-Ca2-O3	87.79(8)	Ca2-O18	2.325(2)
O18-Ca2-O2[b]	84.43(8)	Ca2-O19	2.361(2)
O18-Ca2-O4	76.56(8)		
O18-Ca2-O5	86.89(8)		
O18-Ca2-O7	81.22(8)		
O18-Ca2-O8	126.13(8)		
O7-Ca2-O3	76.55(8)		
O8-Ca2-O3	99.25(7)		
O3-Ca2-O2[b]	73.65(7)		
O2[b]-Ca2-O4	72.95(7)		
O4-Ca2-O5	50.65(7)		
O5-Ca2-O7	85.08(7)		
O5-Ca2-O8	70.01(7)		
O7-Ca2-O8	49.90(6)		
O18-Ca2-O19	159.82(9)		

Symmetry code: [b](x, ½-y, ½+z)

The 1D chains that form the structure of **(10)** run parallel to the *c* direction, and feature nine intracomplex H-bonds, illustrated in Figure 4.36(a) and listed in Table 4.22. The strongest interactions are N6-H2⋯O1 and N5-H1⋯O3[a], both formed between N-H groups of

pyridinium rings and coordinated carboxylate oxygen atoms. As N6-H2···O1 may influence the twisting of the picolinic acid ligand about the C7-C8 bond, N5-H1···O3[a] may also influence the conformation of the other picolinic acid, in that it too is very linear with an angle of 173(4)° and a moderate D···A distance of 2.744(3) Å. N6-H2 also forms the H-bond N6-H2···O2, making a bifurcated H-bond. This is a weaker interaction than that with O1 with a D···A distance of 3.544(4) Å and an angle of 128(3)°. The water molecules of O17 and O18 form H-bonds to coordinating oxygen atoms of the nitrate ions: O17-H17A···O4[a] and O18-H18A···O11[b]. These H-bonds have similar geometries, with D···A distances of 2.819(3) Å and 2.801(3) Å, and angles of 161(4)° and 166(5)°, for O17-H17A···O4[a] and O18-H18A···O11[b], respectively.

There are four intracomplex H-bonds within the 1D chain from C-H groups of the pyridinium ring. C12-H12 forms H-bonds to a coordinating carboxylate oxygen atom (O2) and to an oxygen atom of a water ligand (O19). Water oxygen atoms are the acceptors in the other C-H intracomplex H-bonds. C12-H12···O2 displays the smallest angle of 128° while the angles of other H-bonds range from 151° for C6-H6···O16[a] to 159° for C12-H12···O19[a]. The D···A distances of these bonds are long, from 3.434(4) Å for C12-H12···O19[a] to 3.554(5) Å for C9-H9···O19.

The 1D chains stack along the *b* direction and are connected through H-bonds *via* three nitrate ions, as shown in Figure 4.36(b) and (c), listed in Table 4.22. All of the coordinated water ligands partake in the connectivity of the chain in this direction, forming two H-bonds each, but only *via* one of the hydrogen atoms so that the water ligands form bifurcated H-bonds. Evidently, one interaction of the bifurcated H-bond is notably stronger than the other: O16-H16A···O15[c] has a D···A distance of 2.805(3) Å and an angle of 172(5)°, while O16-H16A···O13[c] has a D···A distance of 3.341(3) Å and an angle of 133(4)°. This trend is observed for each of the other water ligand H-bonds, with O17-H17B···O7[d], O18-H18B···O14[c], and O19-H19A···O6[d] having D···A distances of 2.848(3) Å, 2.749(4) Å and 2.854(3) Å, and angles of 170(5)°, 166(5)° and 166(4)°, respectively, while O17-H17B···O9[d], O18-H18B···O15[c], and O19-H19A···O5[d] have D···A distances of 3.346(4) Å, 3.536(4) Å and 3.355(4) Å, and angles of 136(4)°, 141(4)° and 132(4)°, respectively. The C-H···O H-bonds are equally weak interactions with D···A distances of 3.350(4) Å and 3.483(4) Å, and angles of 132° and 131°, for C3-H3···O13[c] and C9-H9···O5[d], respectively.

The structure of **(10)** is propagated along the *a* direction by H-bonding between parallel 1D chains, shown in Figure 4.37(a), with zoomed views of the H-bonds in (b) and (c), and the H-bonds listed in Table 4.22. The water molecules of O16 and O19 form bifurcated H-bonds to nitrate ions of the next chain along the *a* direction. O16-H16B···O10[e] and O19-H19B···O8[g] have D···A distances of 2.824(4) Å and 2.883(3) Å, and are very linear with

angles of 177(5)° and 176(4), respectively. The weaker components of each of the bifurcated H-bonds, O16-H16B···O12^{e} and O19-H19B···O9^{g}, have longer D···A distances of 3.344(3) Å and 3.414(4) Å, and smaller angles of 128(4)° and 113(4)°, respectively. The C-H groups C4-H4, C5-H5, C10-H10 and C11-H11 all form two H-bonds to nitrate ions: C5-H5 and C11-H11 to different ions, and C4-H4 and C10-H10 to oxygen atoms of the same nitrate ion. The C-H H-bonds to the nitrate oxygen atoms are generally weak with D···A distances ranging from 3.230(4) Å for C10-H10···O6^{g} to 3.502(5) Å for C5-H5···O12^{f}, and angles from 118° for C11-H11···O6^{g} to 159° for C4-H4···O13^{e}.

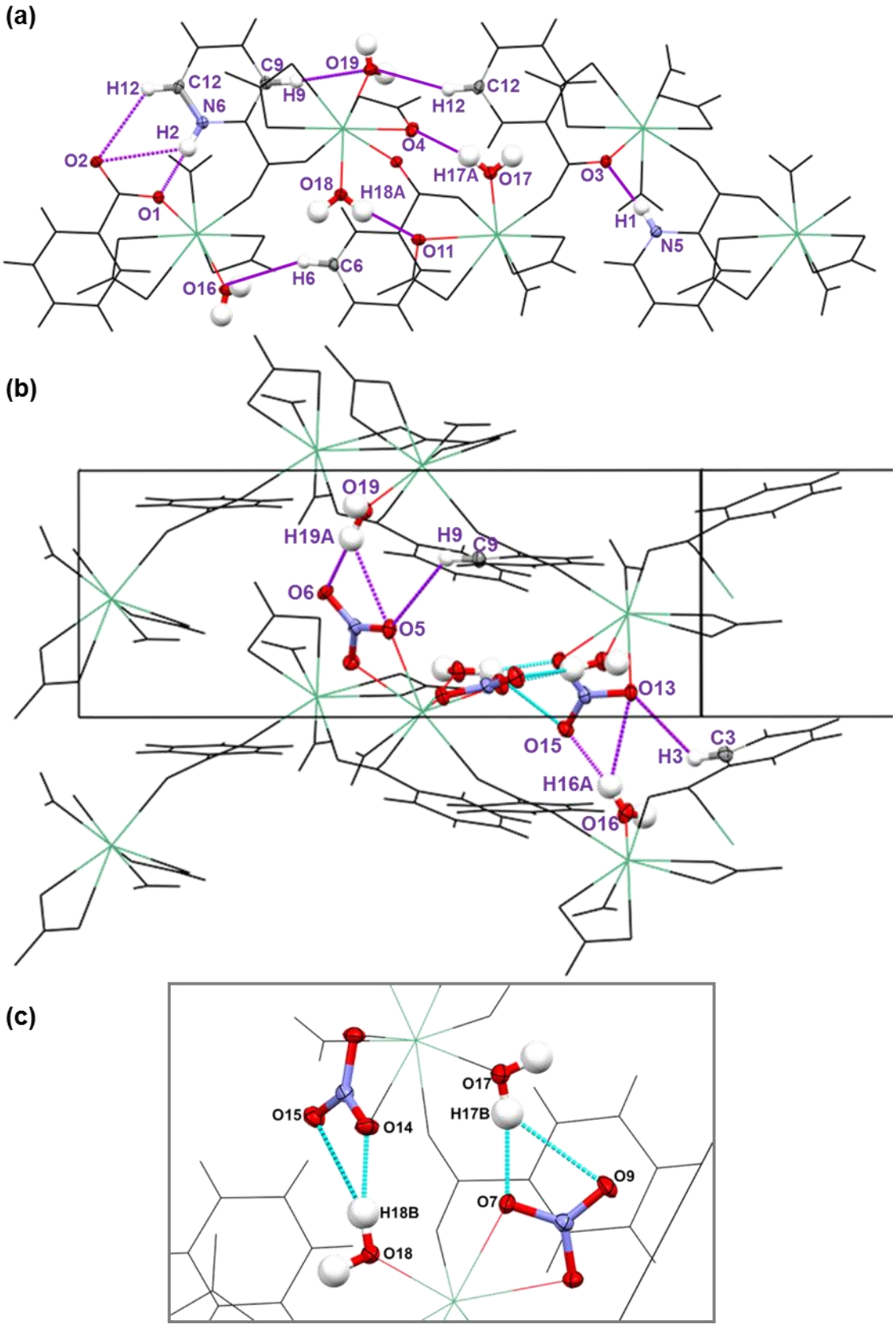

Figure 4.36. Crystal structure of **(10)**. (a) Intracomplex H-bonds within the 1D chain. (b) H-bonds connecting 1D chains along the *b* direction, with (c) showing a zoomed view of (b) viewed down the *b* axis, detailing the H-bonds illustrated in turquoise.

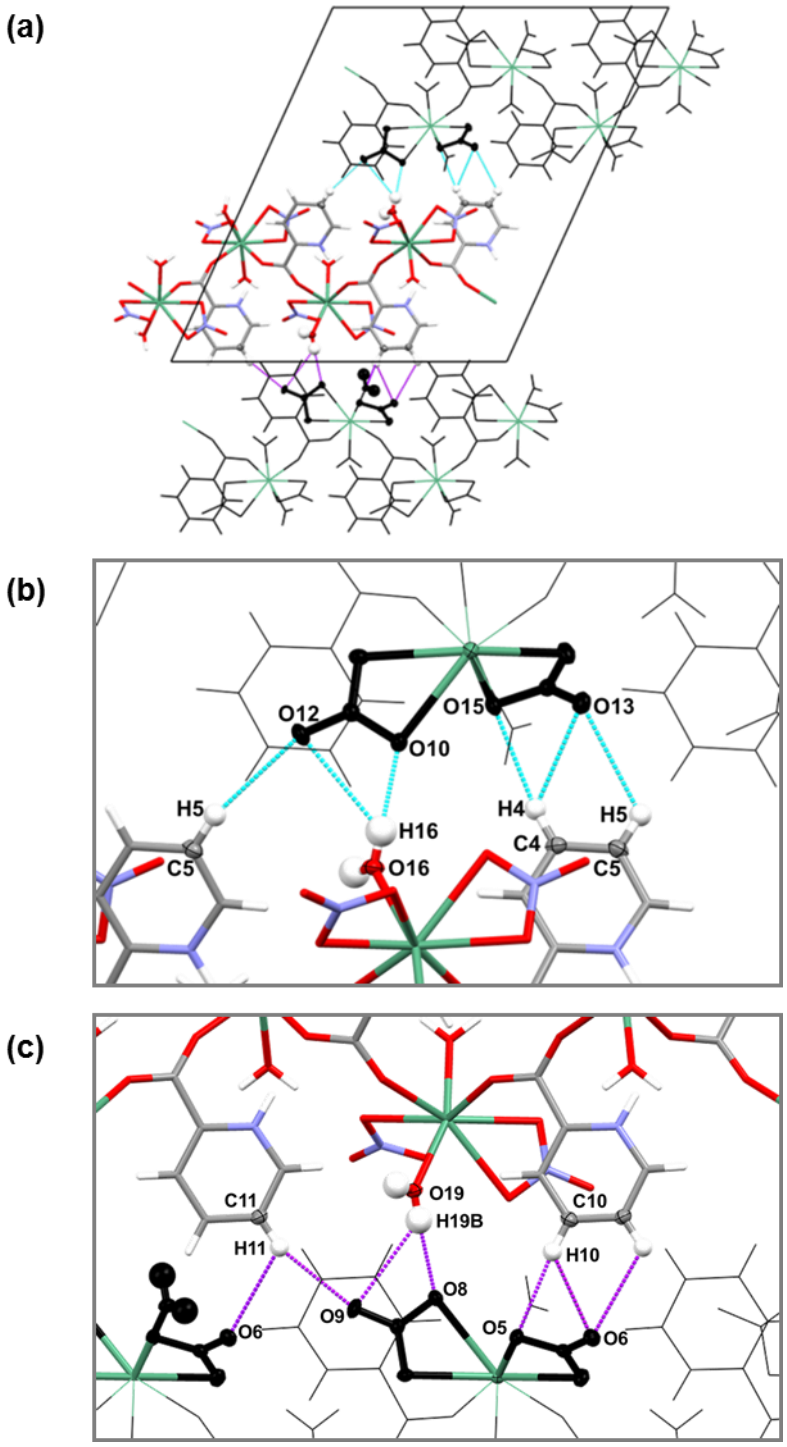

Figure 4.37. Crystal structure of **(10)**. (a) View down the *b* axis showing H-bonds connecting chains along the *a* direction, with (b) showing a zoomed view of (a) detailing the H-bonds illustrated in turquoise, and (c), showing a zoomed view of (a) detailing the H-bonds illustrated in purple (one water ligand of Ca2 has been omitted for clarity). Only H-bonds with donor atoms from the central chain (coloured by element) are shown, reciprocal H-bonds have been omitted for clarity.

Table 4.22. Geometries of H-bonds in **(10)**.

D-H···A Interaction	D-H (Å)	H···A (Å)	D···A (Å)	D-H···A (°)
(Figure 4.36(a)) Intracomplex H-bonds within 1D chain				
N5-H1···O3[a]	0.90(4)	1.85(4)	2.744(3)	173(4)
N6-H2···O1	0.92(5)	1.80(5)	2.712(4)	177(4)
N6-H2···O2	0.92(5)	2.90(4)	3.544(4)	128(3)
O17-H17A···O4[a]	0.85(5)	2.00(5)	2.819(3)	161(4)
O18-H18A···O11[b]	0.86(5)	1.96(5)	2.801(3)	166(5)
*C6-H6···O16[a]	0.95	2.58	3.439(4)	151
*C9-H9···O19	0.95	2.69	3.554(5)	152
*C12-H12···O2	0.95	2.82	3.492(5)	128
*C12-H12···O19[a]	0.95	2.53	3.434(4)	159
(Figure 4.36(b) and (c)) H-bonds connecting 1D chains along b direction				
O16-H16A···O13[c]	0.86(5)	2.70(5)	3.341(3)	133(4)
O16-H16A···O15[c]	0.86(5)	1.96(5)	2.805(3)	172(5)
O17-H17B···O7[d]	0.88(5)	1.98(5)	2.848(3)	170(5)
O17-H17B···O9[d]	0.88(5)	2.66(4)	3.346(4)	136(4)
O18-H18B···O14[c]	0.90(5)	1.87(5)	2.749(4)	166(5)
O18-H18B···O15[c]	0.90(5)	2.79(5)	3.536(4)	141(4)
O19-H19A···O5[d]	0.91(5)	2.67(5)	3.355(4)	132(4)
O19-H19A···O6[d]	0.91(5)	1.96(5)	2.854(3)	166(4)
*C3-H3···O13[c]	0.95	2.65	3.350(4)	132
*C9-H9···O5[d]	0.95	2.77	3.483(4)	131
(Figure 4.37(b)) H-bonds connecting 1D chains along a direction				
*C4-H4···O13[e]	0.95	2.50	3.404(4)	159
*C4-H4···O15[e]	0.95	2.65	3.325(4)	128
*C5-H5···O12[f]	0.95	2.69	3.502(5)	144
*C5-H5···O15[e]	0.95	2.83	3.407(3)	120
O16-H16B···O10[e]	0.82(5)	2.01(5)	2.824(4)	177(5)
O16-H16B···O12[e]	0.82(5)	2.78(4)	3.344(3)	128(4)
(Figure 4.37(c)) H-bonds connecting 1D chains along a direction				
*C10-H10···O5[g]	0.95	2.40	3.343(5)	170
*C10-H10···O6[g]	0.95	2.57	3.230(4)	127
*C11-H11···O6[g]	0.95	2.78	3.327(4)	118
*C11-H11···O9[h]	0.95	2.52	3.425(4)	158
O19-H19B···O8[g]	0.79(5)	2.09(5)	2.883(3)	176(4)
O19-H19B···O9[g]	0.79(5)	2.82(5)	3.414(4)	113(4)

Symmetry codes: [a](x, ½-y, -½+z) [b](x, ½-y, ½+z) [c](x, -1+y, z) [d](x, 1+y, z) [e](1-x, 1-y, 1-z) [f](1-x, ½+y, ½-z) [g](-x, -y, 1-z) [h](-x, ½+y, ½-z) *H-bond features aromatic hydrogen atom fixed in idealised position.

A single crystal of **(10)** was analysed by HSM and the melting range was found to be 106 – 120 °C. DSC analysis (Figure 4.38) showed an endothermic event indicating a melting point of 114.3 °C, and a second endothermic peak at 155.7 °C which does not relate to the melting point of either starting material (picolinic acid m.p. 139 – 142 °C; $Ca(NO_3)_2.4H_2O$ m.p. 44 °C), and could be decomposition of the melt. The melting point of **(10)** is comparable to that of **(3)** at 111.1 °C despite **(10)** having higher dimensional metal coordination in that it forms 1D chains as opposed to the discrete units of **(3)**. In **(3)**, however, the metal centres are doubly bridged by the zwitterionic nicotinic acid ligands, which possibly affords it relatively greater stability.

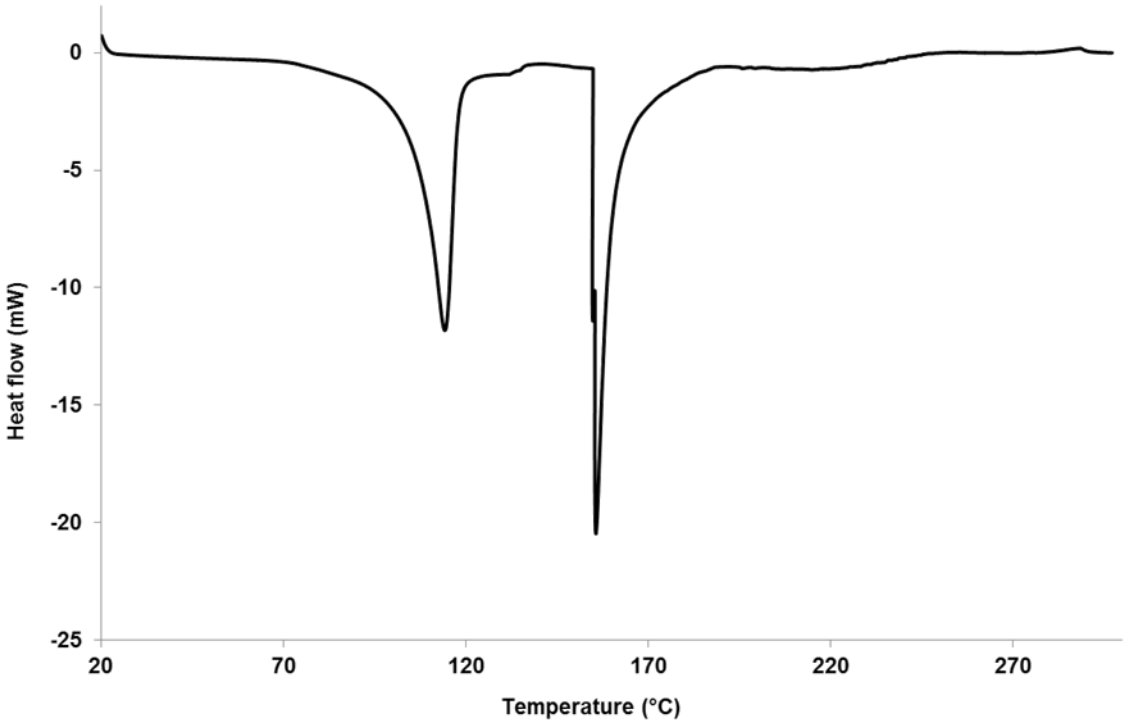

Figure 4.38. DSC trace of **(10)** on a 4.4 mg sample with a temperature ramp of 10 °C min^{-1}.

4.3.5. *Catena-[bis-((μ₂-pyridinium-2-carboxylato)-triaqua-calcium(II))-(μ₂-pyridinium-2-carboxylato)-dichloride-diaqua-calcium(II)] tetrachloride* **(11)**
$[(Ca(C_6H_5NO_2)(H_2O)_3)_2Ca(C_6H_5NO_2)(H_2O)_2Cl_2].4Cl$

(11) was prepared by solvent evaporation of a 3:4 stoichiometric mixture of picolinic acid and calcium(II) chloride dissolved in isopropanol at 50 °C. The chunky, clear colourless crystals formed within three days. The preparation was repeated using the different stoichiometric ratios 1:1, 2:1, 1:2, 3:1, 1:3, 3:2, 2:3 and 4:3, and although this was not an exhaustive investigation as the repeat experiments were carried out only once, it was only

the 3:4 preparation using 15 mg picolinic acid and 18 mg calcium(II) chloride which consistently produced good quality crystals of **(11)**. The PXRD pattern of the bulk product of a preparation resulting in **(11)**, shown in Figure 4.39, shows reasonable agreement between the experimentally obtained and calculated patterns, indicating a homogeneous yield of **(11)**.

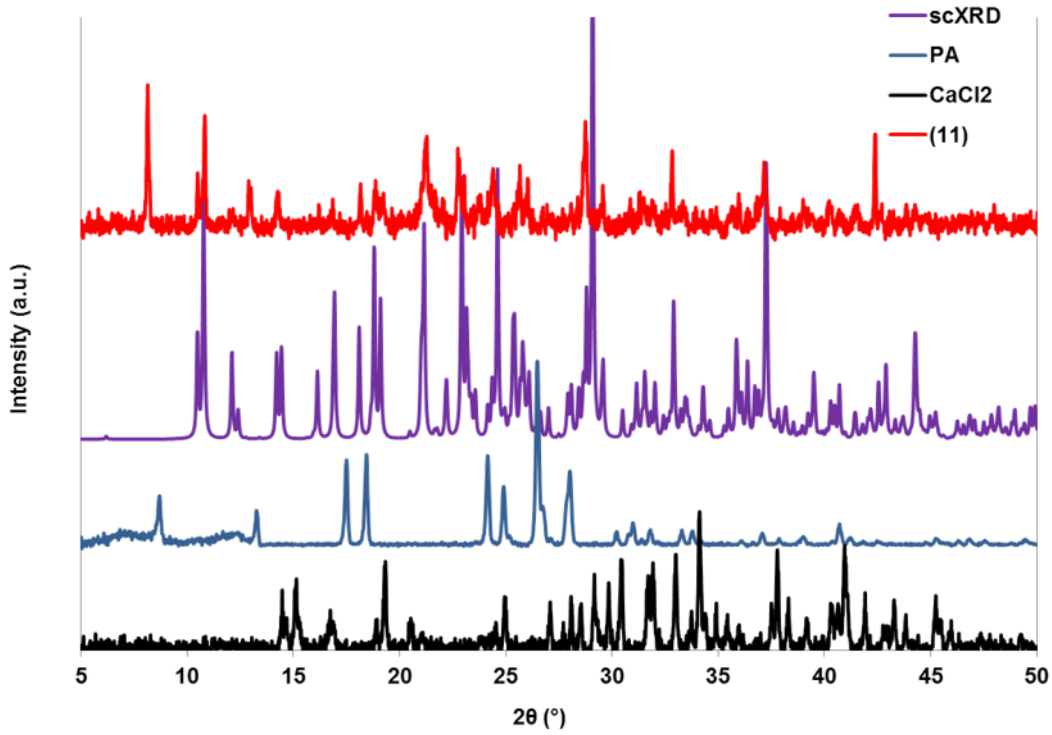

Figure 4.39. PXRD pattern of **(11)** compared to the calculated pattern and patterns of starting materials.

Interestingly, although prepared with a 3:4 ligand:metal ratio, the crystal structure of **(11)** features a ligand:metal ratio of 4:3. The formula unit of **(11)** features two crystallographically equivalent calcium centres, coordinated by three water molecules, and doubly bridged by two crystallographically equivalent zwitterionic picolinic acid ligands *via* the carboxylate oxygen atoms, in an arrangement akin to that observed in the formula units of **(1)**, **(2)** and **(3)**. Each of these calcium centres is singly bridged (*via* the carboxylate oxygen atoms) by a second zwiterionic picolinic acid ligand crystallographically inequivalent to the first, to another calcium centre, crystallographically inequivalent to the other two, which is also coordinated by two water molecules and two chloride ions. There are also two non-coordinated chloride ions present in the structure. The bridging of the calcium centres forms 1D coordination polymeric chains that run parallel to the *c* direction; the 1D chain is shown in Figure 4.40(a).

The calcium centres are shown in Figure 4.40(b) and (c) and their geometries are listed in Table 4.23 and Table 4.24. Both metal centres display a distorted octahedral geometry. Ca1 is located on an inversion centre and its ligand-Ca1-ligand angles have a lesser deviation from 90° than is seen for Ca2. The angles range from 85.97(3)° for Cl1/Cl1^{a}-Ca1-O8/O8^{a} to 94.03(3)° for Cl1/Cl1^{a}-Ca1-O8^{a}/O8. The coordinated chloride ion has a longer coordination distance than those for the carboxylate or water oxygen atoms, at 2.736(1) Å. The latter are more comparable, but the Ca-water oxygen atom distance is longer at 2.336(1) Å, while the Ca-carboxylate oxygen atom distance is 2.291(1) Å.

The octahedral geometry of Ca2 is more distorted than that of Ca1, with the O-Ca2-O angles ranging from 81.06(3)° for O2^{b}-Ca2-O5 to 100.85(4)° for O6-Ca2-O5. The Ca2-carboxylate oxygen atom distances are generally shorter than the Ca2-water oxygen atom distances, at 2.270(1) Å, 2.336(1) Å and the longer 2.364(1) Å, for Ca2-O1, Ca2-O2^{b} and Ca2-O3, respectively, while the distances to the water ligands are 2.325(1) Å, 2.405(1) Å and 2.362(1) Å for Ca2-O5, Ca2-O6 and Ca2-O7, respectively.

The zwitterionic picolinic acid ligands bridging between Ca centres are shown in Figure 4.40(d). The carboxylate group angles are different, with O3-C1-O4, bridging Ca1 and Ca2, having an angle of 127.0(1)°, and O1-C7-O2, bridging the doubly bridged Ca2 and Ca2^{b}, having an angle of 128.4(1)°. In both cases the O-C-O angle is greater than the O=C-O angle of pure picolinic acid (126.8(1)°). The C-O distances are more similar in the doubly bridging picolinic acid ligands with C7-O1 and C7-O2 having distances of 1.247(1) Å and 1.248(1) Å, respectively, while C1-O4 is 1.256(2) Å, and C1-O3 is 1.249(1) Å. The carboxylate groups and the pyridinium rings of the picolinic acid ligands are not coplanar. The torsion angle O2-C7-C8-N2 is 3.3(2)° and the torsion angle O4-C1-C2-N1 is 13.2(2)°. This is not as large as one of the equivalent torsion angles observed in **(10)**, O20-C7-C8-N6, of 23.9(4)°, but as was the case for **(10)**, the conformation of the pyridinium groups is likely to be affected by the intracomplex H-bonds, shown in Figure 4.41(a) and listed in Table 4.25. The torsion angle of O4-C1-C2-N1 may be influenced by the H-bonds N1-H1···Cl1 and C6-H6···Cl1, formed between the N-H and one of the C-H groups of the pyridinium ring to the coordinated chloride ion of Ca1. N1-H1···Cl1 has a D···A distance of 3.134(1) Å and an angle of 160(1)°, while C6-H6···Cl1 is a weaker interaction with a D···A distance of 3.674(1) Å and an angle of 106(1)°. The near coplanarity of O1-C7-O2 with its pyridinium ring may affect the H-bond C9-H9···O3; although this is a long interaction of 3.678(2) Å, the local geometry affords it a large angle of 172(1)°. Another intracomplex H-bond in **(11)**, O5-H5B···Cl1^{a}, is formed from a coordinated water ligand of Ca2 to the coordinated chloride ion of Ca1. This is a very linear interaction of 177(2)°, and again, a relatively long D···A distance of 3.127(1) Å.

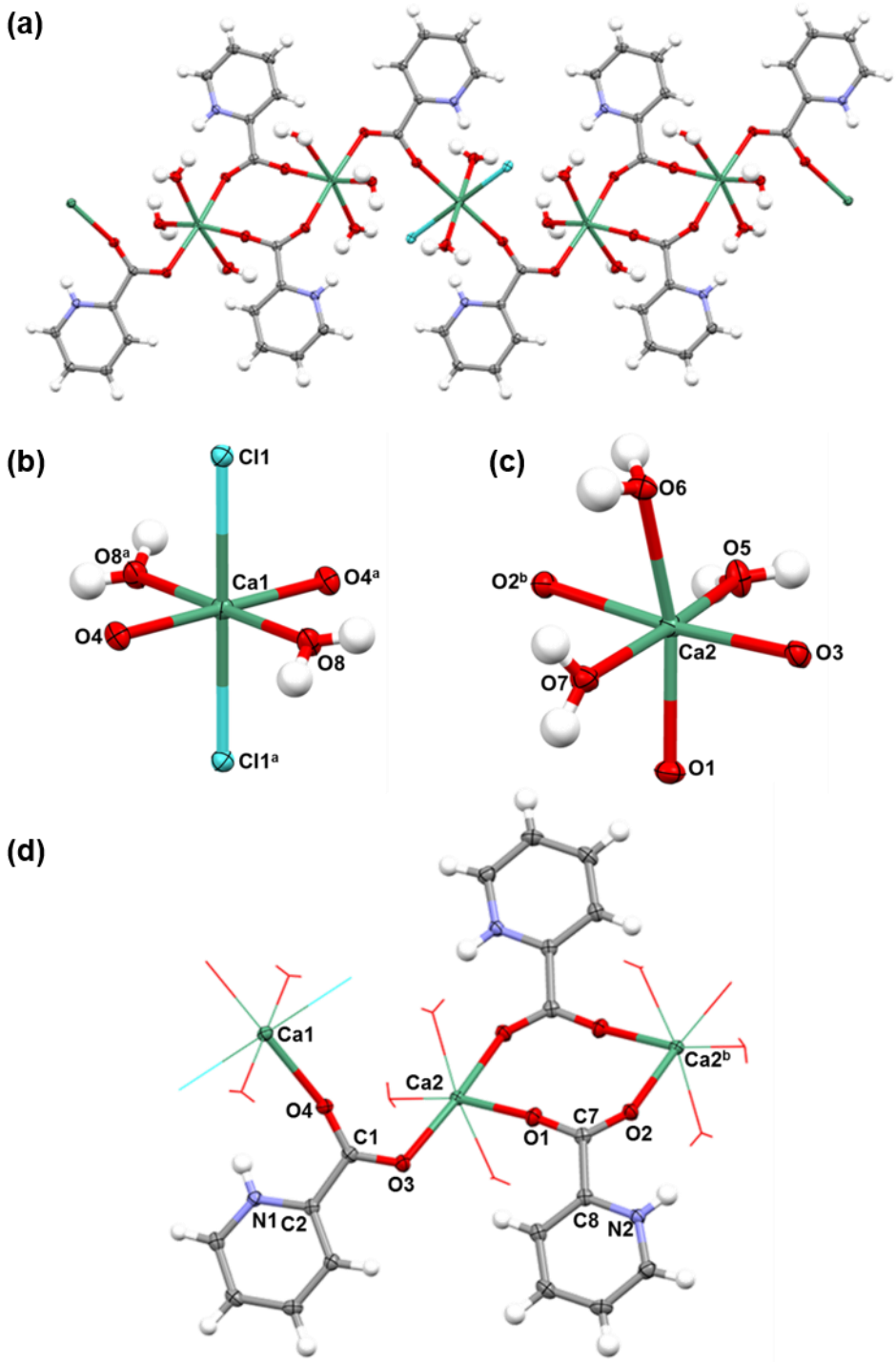

Figure 4.40. Crystal structure of **(11)**. (a) 1D chain parallel to the *c* direction. (b) Six coordinate Ca1 centre with two coordinating chloride ions, two carboxylate oxygen atoms and two water ligands. (c) Six coordinate Ca2 centre with three coordinating carboxylate oxygen atoms and three coordinating water ligands. (d) Section of the 1D chain showing zwitterionic picolinic acid ligands bridging between metal centres. Symmetry codes: [a](-x, 1-y, 1-z) [b](-x, 1-y, 2-z)

Table 4.23. O-Ca-O angles and Ca-O distances concerning Ca1 in **(11)**.

Coordination	O-Ca-O angle (°)	Interaction	Distance (Å)
Cl1/Cl1[a]-Ca1-O4/O4[a]	86.65(3)	Ca1-Cl1/Cl1[a]	2.736(1)
Cl1/Cl1[a]-Ca1-O4[a]/O4	93.35(3)	Ca1-O4/O4[a]	2.291(1)
Cl1/Cl1[a]-Ca1-O8/O8[a]	85.97(3)	Ca1-O8/O8[a]	2.336(1)
Cl1/Cl1[a]-Ca1-O8[a]/O8	94.03(3)		
O4[a]/O4-Ca1-O8/O8[a]	92.74(3)		
O4/O4[a]-Ca1-O8/O8[a]	87.26(3)		

Symmetry code: [a](-x, 1-y, 1-z)

Table 4.24. O-Ca-O angles and Ca-O distances concerning Ca2 in **(11)**.

Coordination	O-Ca-O angle (°)	Interaction	Distance (Å)
O6-Ca2-O2[b]	81.29(3)	Ca2-O1	2.270(1)
O6-Ca2-O5	100.85(4)	Ca2-O2[b]	2.336(1)
O6-Ca2-O3	92.88(3)	Ca2-O3	2.364(1)
O6-Ca2-O7	81.26(4)	Ca2-O5	2.325(1)
O1-Ca2-O2[b]	97.23(3)	Ca2-O6	2.405(1)
O1-Ca2-O5	95.14(4)	Ca2-O7	2.362(1)
O1-Ca2-O3	88.55(3)		
O1-Ca2-O7	82.33(4)		
O2[b]-Ca2-O5	81.06(3)		
O5-Ca2-O3	99.50(4)		
O3-Ca2-O7	88.14(3)		
O7-Ca2-O2[b]	91.61(3)		

Symmetry code: [b](-x, 1-y, 2-z)

The crystal structure of **(11)** is composed of 1D chains along the *c* direction, which stack along the *a* and *b* directions and H-bond to neighbouring 1D chains to form 2D H-bonded motifs parallel to the *ac* and *bc* planes. There are four H-bonds that are formed directly between acceptor and donor atoms of the 1D chains; otherwise the chains are linked by H-bonds *via* the non-coordinated chloride ions, in the same way as seen in the crystal structures of the 0D complexes **(1)** and **(2)**, synthesised from magnesium(II) chloride, and **(4)**, synthesised from calcium(II) chloride; these were also primarily connected by H-bonds *via* non-coordinated chloride ions.

Figure 4.41(b) shows the H-bonds formed between the 1D chains (listed in Table 4.25). C5-H5···O8^{c} and C6-H6···O6^{d} link the chains along the *a* direction. These are formed between C-H groups of the pyridinium ring of the picolinic acid ligand on one chain to two water molecules of the 1D chain along the *a* direction; one is coordinated to Ca1 and the other to Ca2. These are both weak H-bonds with D···A distances of 3.509(2) Å and 3.417(2) Å and angles of 112(1)° and 163(1)° for C5-H5···O8^{c} and C6-H6···O6^{d}, respectively. C6-H6 also forms an intracomplex H-bond to Cl1, and therefore H6 is part of a bifurcated H-bond. C11-H11···Cl1^{e} and C12-H12···Cl1^{e} are formed between the C-H groups of the pyridinium ring of the picolinic acid ligand of one chain, to the coordinated chloride ion of another chain located along the *b* direction. These interactions are weaker and longer than those linking chains along the *a* direction, with D···A distances of 3.897(2) Å and 3.537(2) Å and angles of 112(1)° and 140(1)°, for C11-H11···Cl1^{e} and C12-H12···Cl1^{e}, respectively.

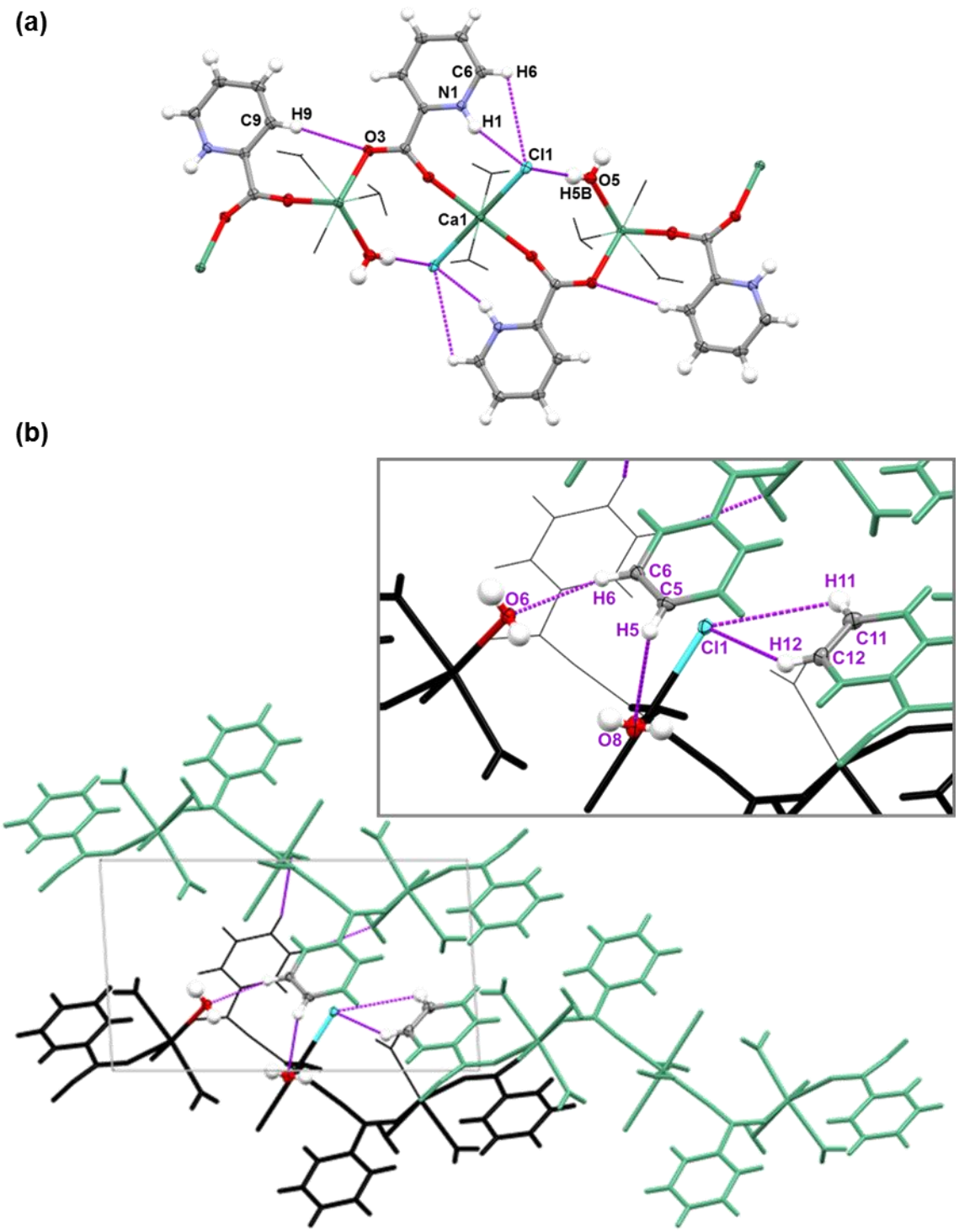

Figure 4.41. Crystal structure of **(11)**. (a) Intracomplex H-bonds within the 1D chain. (b) View down the *b* axis showing H-bonds formed directly between the 1D chains connecting the structure along both the *a* and *b* directions, (detailed in inset).

Each of the non-coordinated chloride ions are acceptors in multiple H-bonds, effectively connecting the 1D chains along the *a* and *b* directions. The H-bonds in which Cl2 is the acceptor linking neighbouring 1D chains along the *a* and *b* directions are illustrated in Figure

4.42(a) and (b), respectively, and listed in Table 4.25. These H-bonds are formed between the coordinated water molecules featuring O5, O6 and O7 and the C-H groups of the pyridinium ring of picolinic acid. Along the *a* direction, one 1D chain H-bonds to the Cl2 ion from two water molecules both coordinated to Ca2, O7-H7A···Cl2^{d}, and O6-H6B···Cl2^{d}, while the next chain along the *a* direction H-bonds to Cl2 from two water molecules coordinated to two different Ca2 centres, O7-H7B···Cl2^{f} and O5-H5A···Cl2^{a}. These four H-bonds have fairly long D···A distances, ranging from 3.127(1) Å for O7-H7A···Cl2^{d}, to 3.214(1) Å for O6-H6B···Cl2^{d}, and large angles, ranging from 167(2)° for O7-H7A···Cl2^{d}, to 175(2)° for O5-H5A···Cl2^{a}.

The 1D chain coloured in black in Figure 4.42(a) and (b), is connected to the next 1D chain along the *b* direction *via* Cl2, which accepts three H-bonds from C-H groups from the neighbouring 1D chain. C3-H3···Cl2^{g} and C4-H4···Cl2^{g} are weak interactions with D···A distances of 3.637(1) Å and 3.589(1) Å, and angles of 121(1)° and 127(1)°, respectively. C10-H10···Cl2^{g}, originating from the other picolinic acid ligand, is longer at 3.693(2) Å, yet significantly more linear with an angle of 176(1)°.

The H-bonds in which Cl3 is the acceptor link neighbouring 1D chains along the *a* and *b* directions, are illustrated in Figure 4.43(a) and (b), respectively, and listed in Table 4.25. The 1D chain illustrated in black H-bonds to Cl3 through four H-bonds: N2-H2···Cl3^{b} and C12-H12···Cl3^{b}, originating from the N-H and C-H groups of the pyridinium ring, and O6-H6A···Cl3 and O8-H8B···Cl3^{a}, originating from two water molecules coordinated to Ca2 and Ca1, respectively. C12-H12···Cl3^{b} is the weakest of these interactions with a D···A distance of 3.552(1) Å and angle of 110(1)°. This interaction completes the bifurcated H-bond in which C12-H12 participates while H12 is also involved in an interaction to Cl1 in C12-H12···Cl1^{e}, which connects 1D chains directly along the *b* direction. O6-H6A···Cl3 is relatively stronger, with a D···A distance of 3.121(1) Å and a large angle of 171(2)°. The next 1D chain along the *a* direction H-bonds to Cl3 through a C-H group of a pyridinium ring; C5-H5···Cl3^{d} is a weak interaction with a D···A distance of 3.692(1) Å and an angle of 151(1)°. Along the *b* direction, the next 1D chain H-bonds to Cl3 through a water molecule coordinated to Ca1; O8-H8A···Cl3^{h} is one of the strongest interactions relative to the others connecting the chains along the *a* and *b* directions via the chloride ions, with a D···A distance of 3.099(1) Å and an angle close to linear at 175(2)°.

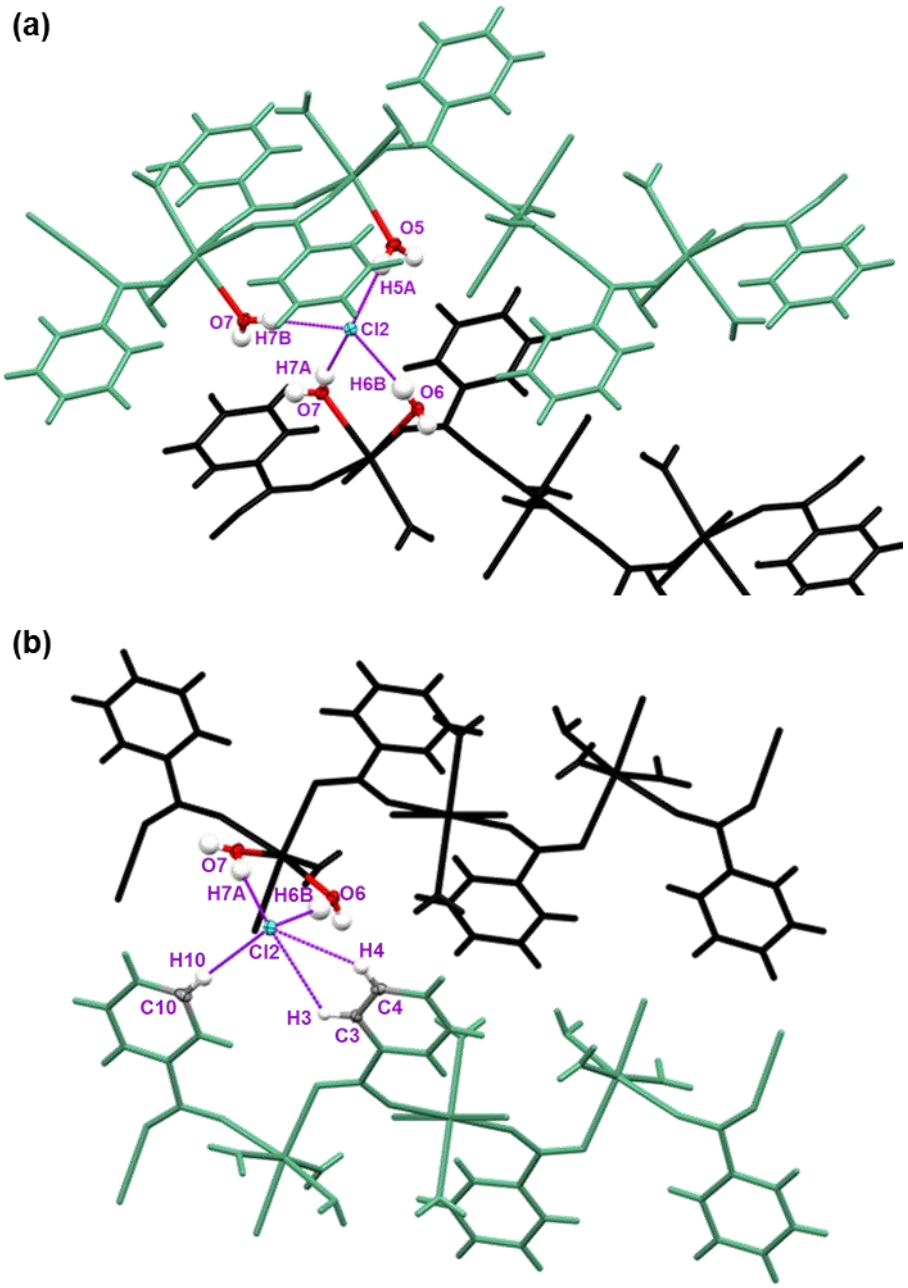

Figure 4.42. Crystal structure of **(11)**. (a) H-bonds to Cl2 connecting 1D chains along *a* direction. (b) H-bonds to Cl2 connecting 1D chains along *b* direction.

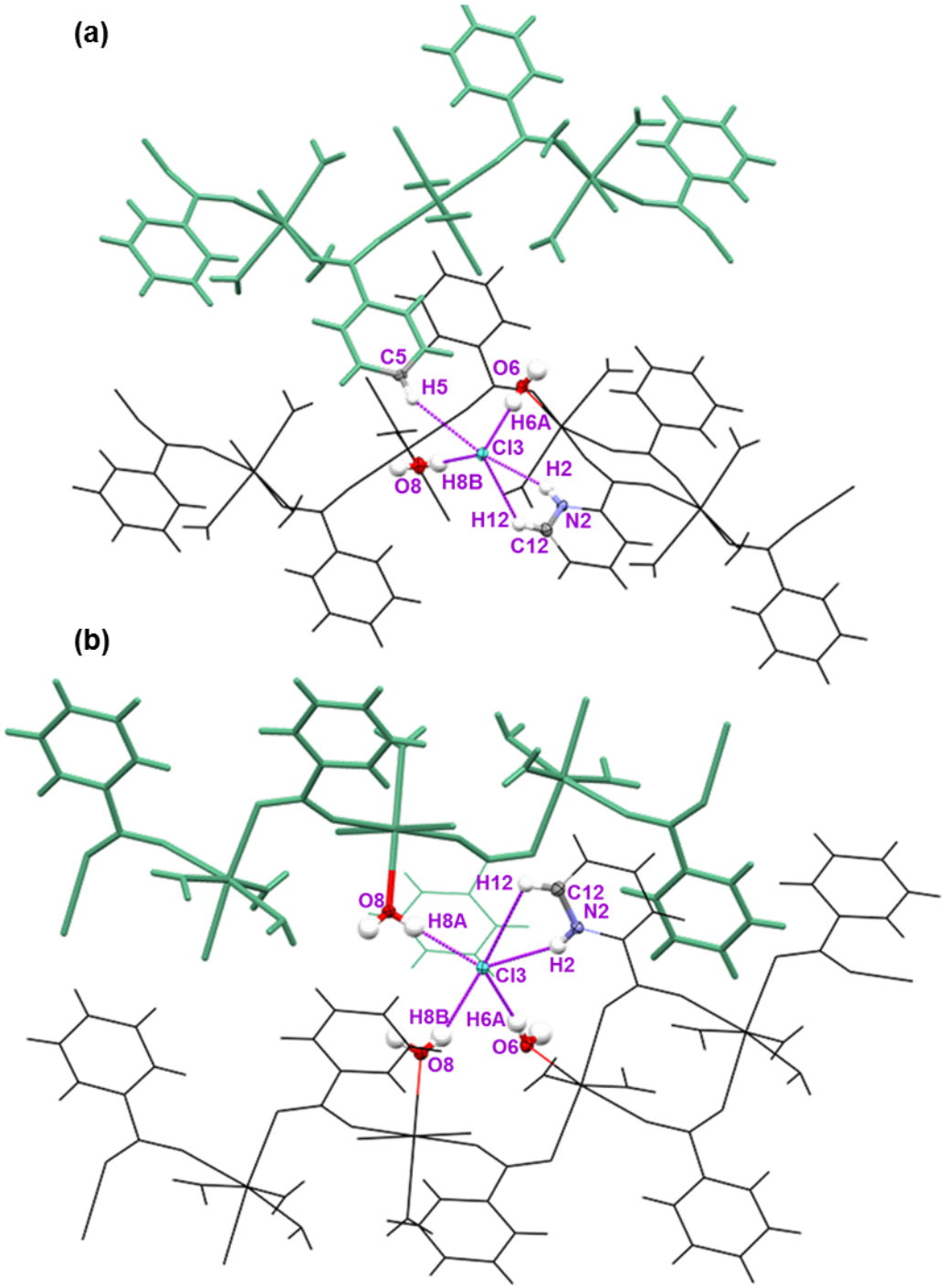

Figure 4.43. Crystal structure of **(11)**. (a) H-bonds to Cl3 connecting 1D chains along *a* direction. (b) H-bonds to Cl3 connecting 1D chains along *b* direction.

Table 4.25. Geometries of H-bonds in **(11)**.

D-H···A Interaction	D-H (Å)	H···A (Å)	D···A (Å)	D-H···A (°)
(Figure 4.41(a)) H-bonds within 1D chain				
N1-H1···Cl1	0.87(2)	2.30(2)	3.134(1)	160(1)
O5-H5B···Cl1[a]	0.83(2)	2.30(2)	3.127(1)	177(2)
C6-H6···Cl1	0.92(2)	3.32(1)	3.674(1)	106(1)
C9-H9···O3	0.92(2)	2.77(1)	3.678(2)	172(1)
(Figure 4.41(b)) H-bonds formed directly between 1D chains				
C5-H5···O8[c]	0.91(2)	3.07(1)	3.509(2)	112(1)
C6-H6···O6[d]	0.92(2)	2.53(2)	3.417(2)	163(1)
C11-H11···Cl1[e]	0.94(2)	3.44(2)	3.897(2)	112(1)
C12-H12···Cl1[e]	0.93(2)	2.77(2)	3.537(2)	140(1)
(Figure 4.42(a) and (b)) H-bonds formed to Cl2 connecting 1D chains along a and b directions				
O5-H5A···Cl2[a]	0.81(2)	2.33(2)	3.144(1)	175(2)
O6-H6B···Cl2[d]	0.81(2)	2.41(2)	3.214(1)	170(2)
O7-H7A···Cl2[d]	0.80(2)	2.35(2)	3.127(1)	167(2)
O7-H7B···Cl2[f]	0.82(2)	2.36(2)	3.181(1)	173(2)
C3-H3···Cl2[g]	0.93(2)	3.07(1)	3.637(1)	121(1)
C4-H4···Cl2[g]	0.97(2)	2.92(1)	3.589(1)	127(1)
C10-H10···Cl2[g]	0.94(2)	2.76(2)	3.693(2)	176(1)
(Figure 4.43(a) and (b)) H-bonds formed to Cl3 connecting 1D chains along a and b directions				
N2-H2···Cl3[b]	0.86(2)	2.33(2)	3.122(1)	152(2)
O6-H6A···Cl3	0.82(2)	2.31(2)	3.121(1)	171(2)
O8-H8A···Cl3[h]	0.83(2)	2.27(2)	3.099(1)	175(2)
O8-H8B···Cl3[a]	0.80(2)	2.42(2)	3.187(1)	162(2)
C5-H5···Cl3[d]	0.91(2)	2.87(1)	3.692(1)	151(1)
C12-H12···Cl3[b]	0.93(2)	3.12(2)	3.552(1)	110(1)

Symmetry codes: [a](-x, 1-y, 1-z) [b](-x, 1-y, 2-z) [c](1+x, y, z) [d](1-x, 1-y, 1-z) [e](x, -1+y, 1+z) [f](x, y, 1+z) [g](1-x, -y, 1-z) [h](x, -1+y, z)

HSM analysis of a single crystal of **(11)** gave a melting range of 128 – 138 °C. DSC analysis (Appendix A, Figure A11) shows two endothermic events: one small peak at 129.2 °C, within the melting range observed by HSM, and one larger peak at 148.1 °C. The melting point of picolinic acid (139 – 142 °C) lies between these temparatures and so it is not totally clear if either endothermic event can be attributed to its melt.

4.3.6. *Catena-[bis-(μ_3-pyridine-2-carboxylato)-tris-(μ_2-aqua)-diaqua-dicalcium(II)] dichloride* **(12)** *$[Ca_2(C_6H_4NO_2)_2(H_2O)_5].2Cl$*

Crystals of **(12)** were prepared by solvent evaporation of a 1:1 stoichiometric mixture of picolinic acid and calcium(II) chloride dissolved in DCM and methanol at lab temperature. The crystals were clear, colourless, brittle cuboids and formed in a clear, colourless viscous oil. For this reason a PXRD pattern was not obtained for the bulk sample as the necessary amount of a dry powder could not be acquired. Visually however, the crystalline material appeared homogeneous.

The structure of **(12)** features the same ligand:metal ratio as was used during preparation. The formula unit features two calcium centres, two picolinate ligands, five calcium-coordinated water molecules and two non-coordinated chloride ions. The structure of **(12)** is composed of 1D coordination polymeric chains that run parallel to the *a* direction, as shown in Figure 4.44(a) and (b). Unlike the pyridine carboxylic acid derived ligands observed in all of the structures **(1)** – **(11)**, the pyridine carboxylic acid is deprotonated to pyridine carboxylate; it is not zwitterionic. The picolinic acid ligand chelates the calcium centre *via* both the pyridyl nitrogen atom (N1) and one carboxylate oxygen atom (O2), (Figure 4.44(c), with the coordination geometries listed in Table 4.26). The coordination distance Ca1-N1 is 2.516(3) Å, while Ca1-O2 is shorter at 2.374(2) Å. O2 also coordinates to the next Ca centre along the *a* direction with a coordination distance of 2.400(2) Å, and the other carboxylate oxygen atom (O1) coordinates to the next Ca centre, again along the *a* direction, with a coordination distance of 2.368(2) Å. The angle formed by the bridging carboxylate oxygen atom O2, Ca1-O2-Ca1^a, is 99.93(8)°.

The picolinate ligand is a μ_3 bridging ligand. The carboxylate group angle O1-C1-O2 is 125.5(3)°, smaller than the O=C-O angle of pure picolinic acid (126.8(1)°). The C-O distances are not equal, possibly due to their different coordination behaviour: C1-O1 is 1.247(3) Å, and C1-O2, where O2 is the oxygen atom involved in chelation, is longer at 1.272(4) Å. The carboxylate group and the pyridyl ring are twisted from coplanarity with an O2-C1-C2-N1 torsion angle of 11.7(6)°.

Three of the water ligands also bridge between Ca centres as μ_2 bridging ligands, illustrated in Figure 4.44(d). These water ligands are all located on 2_1 screw axes. The Ca-O-Ca angles formed by these water ligands are all different: Ca1-O4-Ca1^c is 101.5(2)°, Ca1-O5-Ca1^c is 99.3(2)° and Ca1-O6-Ca1^a is 82.9(3)°.

The Ca centre is eight coordinate (Figure 4.44(e) and Table 4.26). It is coordinated by four oxygen atoms of water ligands, and by three different picolinate ligands; one of these coordinates by a nitrogen atom and a carboxylate oxygen atom (N,O-chelation), and the other two each *via* one crystallographically inequivalent carboxylate oxygen atom. Ca1-O6, where O6 is of a bridging water molecule, shows the longest coordination distance of 2.760(4) Å, followed by Ca1-N1 at 2.516(3) Å. Ca1-O5, and Ca1-O4, where O5 and O4 are also of bridging water molecules, are 2.480(3) Å and 2.441(3) Å, respectively. The coordination distance to the non-bridging water molecule, Ca1-O3, is identical to that of Ca1-O4. The angle formed by the two chelating atoms of picolinate, O2-Ca1-N1, is 66.61(8)°, and the angle formed between the two equivalent coordinating carboxylate oxygen atoms from two different picolinate atoms, O2^a-Ca1-O2, is 79.27(8)°.

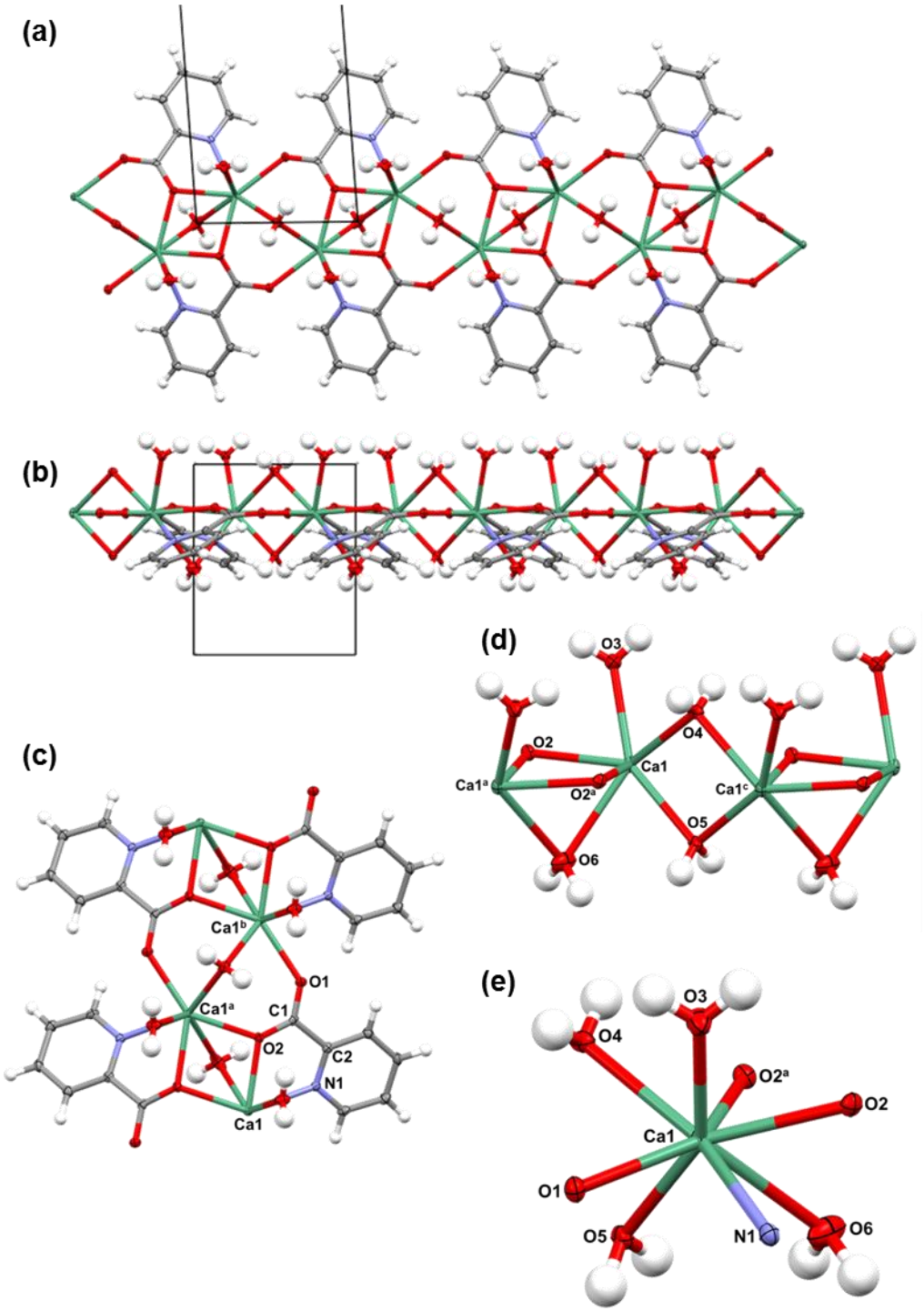

Figure 4.44. Crystal structure of **(12)**. (a) View down the *b* axis showing 1D chain parallel to the *a* direction. (b) View down the *c* axis showing the 1D chain. (c) Section of the 1D chain showing κ^2 N,O-chelating and μ_3 bridging picolinate ligand. (d) Section of the 1D chain showing coordinating water ligands and μ_2 bridging water ligands, and μ_2 bridging carboxylate oxygen atom (O2), (picolinate ligands omitted for clarity). (e) Eight coordinate Ca1 centre with one coordinating pyridyl nitrogen atom, three coordinating carboxylate oxygen atoms, and four coordinating water ligands. Symmetry codes: [a](1-x, y, 1-z) [b](-1+x, y, z) [c](2-x, y, 1-z)

Table 4.26. O-Ca-N/O and Ca-O-Ca angles, and Ca-N/O distances in **(12)**.

Coordination	O-Ca-N/O / Ca-O-Ca angle (°)	Interaction	Distance (Å)
O3-Ca1-N1	86.51(9)	Ca1-N1	2.516(3)
O3-Ca1-O1	83.19(9)	Ca1-O1	2.368(2)
O3-Ca1-O2	73.54(9)	Ca1-O2	2.374(2)
O3-Ca1-O2[a]	107.56(9)	Ca1-O2[a]	2.400(2)
O3-Ca1-O4	75.1(1)	Ca1-O3	2.441(3)
O5-Ca1-N1	108.5(1)	Ca1-O4	2.441(3)
O5-Ca1-O1	75.44(8)	Ca1-O5	2.480(3)
O5-Ca1-O2	135.7(1)	Ca1-O6	2.760(4)
O5-Ca1-O2[a]	78.85(7)		
O5-Ca1-O4	79.62(8)		
O5-Ca1-O6	72.07(8)		
O6-Ca1-N1	79.02(8)		
O6-Ca1-O1	131.2(1)		
O6-Ca1-O2	63.74(8)		
O6-Ca1-O2[a]	63.45(8)		
O6-Ca1-O4	130.87(6)		
N1-Ca1-O1	77.98(9)		
O1-Ca1-O4	75.51(8)		
O4-Ca1-O2[a]	72.35(6)		
O2[a]-Ca1-O2	79.27(8)		
O2-Ca1-N1	66.61(8)		
Ca1-O2-Ca1[a]	99.93(8)		
Ca1-O4-Ca1[c]	101.5(2)		
Ca1-O5-Ca1[c]	99.3(2)		
Ca1-O6-Ca1[a]	82.9(3)		

Symmetry codes: [a](1-x, y, 1-z) [c](2-x, y, 1-z)

The 1D coordination polymeric chains that make up **(12)** run parallel to the *a* direction. The chains are connected along the *b* direction *via* the non-coordinated chloride ion by the formation of five H-bonds from the coordinated water molecules of the chains, (Figure 4.45(a) and listed in Table 4.27). Each of the H atoms of each of the water molecules forms an H-bond to the chloride ion. These are all long, mostly close to linear interactions, the shortest of which is O5-H5···Cl1^{d} with a D···A distance of 3.091(3) Å, and which displays the most linear angle of 178(6)°, and the longest being O3-H3B···Cl1^{c} with a D···A distance of 3.453(3) Å and the smallest angle of 153(5)°.

Along the *c* direction, the chains are arranged in a staggered manner so that when viewed down the *c* axis, every chain will eclipse every second chain along this direction. As the bridging water ligands are located along the central spine of the 1D chain, it is the pyridyl groups that interact with the carboxylate oxygen atoms and non-bridging water ligand to connect the 1D chains along the *c* direction through H-bonds (Figure 4.45(b) and Table 4.27). The C-H group C4-H14 forms three H-bonds: one to the chloride ion, one to the water oxygen atom O3, and one to the carboxylate oxygen atom O1. The H-bonds C4-H14···Cl1^{e} and C4-H14···O1^{f} form a bifurcated H-bond. C4-H14···Cl1^{e} displays the slightly larger angle of 141° and the longer D···A distance of 3.707(4) Å, while C4-H14···O1^{f} has a shorter D···A distance of 3.515(5) Å and a smaller angle of 137°. The H-bond to O3 is a weaker interaction still: C4-H14···O3^{g} has a D···A distance of 3.546(4) Å and a very small angle of 114°. C5-H15 interacts weakly with O3; C5-H15···O3^{g} has a D···A distance of 3.455(5) Å and an angle of 120°.

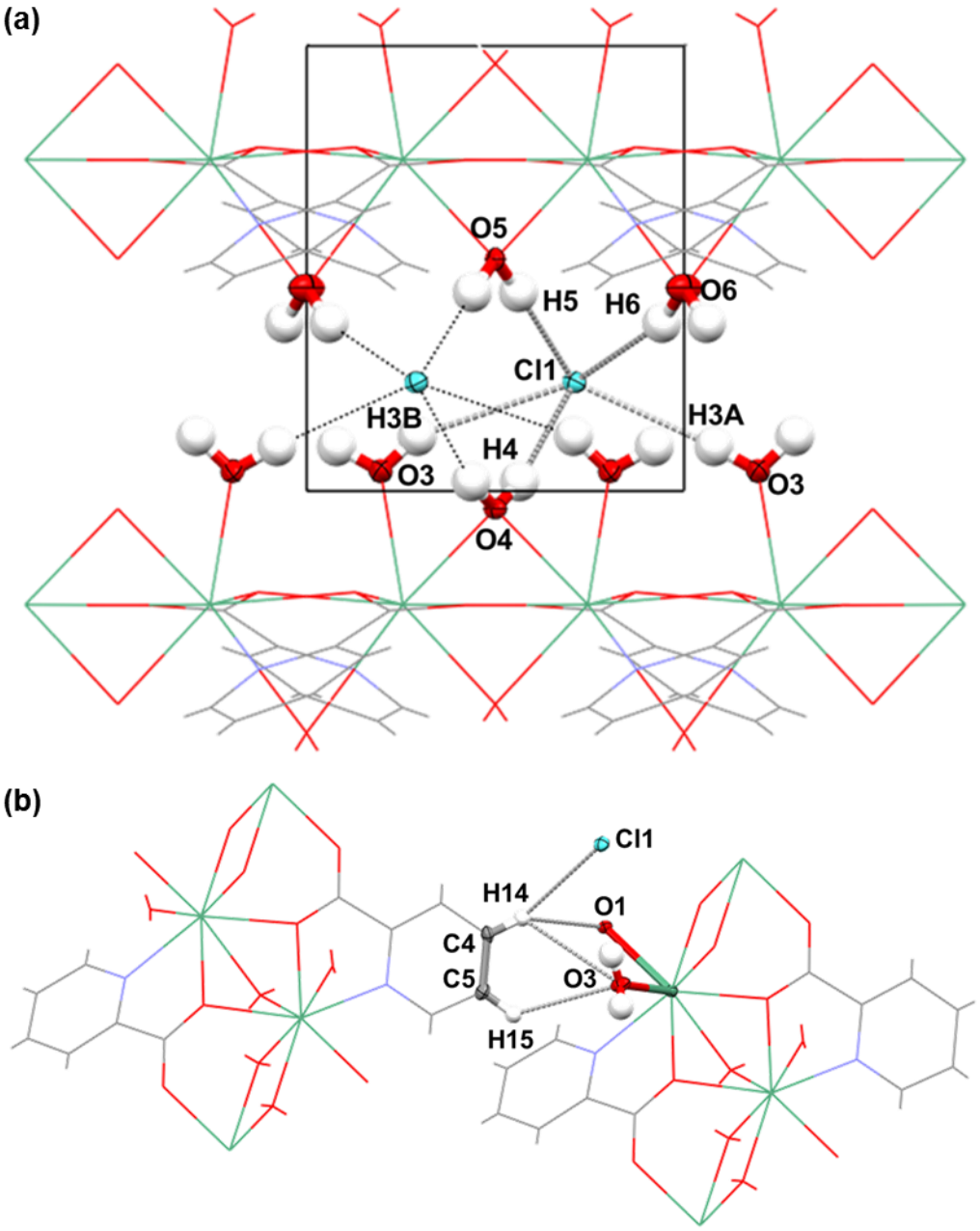

Figure 4.45. Crystal structure of **(12)**. (a) View down the *c* axis showing H-bonds connecting 1D chains along the *b* direction. (b) H-bonds connecting the 1D chains along the *c* direction.

Table 4.27. Geometries of H-bonds in **(12)**.

D-H···A Interaction	D-H (Å)	H···A (Å)	D···A (Å)	D-H···A (°)
(Figure 4.45(a)) H-bonds connecting 1D chains along b direction				
O3-H3A···Cl1[a]	0.82(5)	2.48(5)	3.297(3)	174(4)
O3-H3B···Cl1[c]	0.82(6)	2.70(6)	3.453(3)	153(5)
O4-H4···Cl1	0.81(6)	2.32(7)	3.125(3)	169(6)
O5-H5···Cl1[d]	0.87(7)	2.22(7)	3.091(3)	178(6)
O6-H6···Cl1[d]	0.97(5)	2.26(5)	3.202(3)	162(4)
(Figure 4.45(b)) H-bonds connecting 1D chains along c direction				
*C4-H14···Cl1[e]	0.95	2.92	3.707(4)	141
*C4-H14···O1[f]	0.95	2.76	3.515(5)	137
*C4-H14···O3[g]	0.95	3.05	3.546(4)	114
*C5-H15···O3[g]	0.95	2.88	3.455(5)	120

Symmetry codes: [a](1-x, y, 1-z) [c](2-x, y, 1-z) [d](x, 1+y, z) [e](-½+x, ½+y, ½+z) [f](½-x, ½+y, 1½-z) [g](1½-x, ½+y, 1½-z) *H-bond features aromatic hydrogen atom fixed in idealised position.

HSM of **(12)** using a ramp rate of 5 °C min^{-1} showed a smoothening of the crystal, possibly an initial melt, between about 80 – 96 °C before the crystal began to darken and fracture at roughly 120 °C. The DSC trace (Appendix A, Figure A12) shows a decomposition event at around 80 – 100 °C, and a second and more extreme decomposition event starting at about 135 °C.

4.4. Complexes with Higher Dimension Coordination Connectivity

4.4.1. *Catena-[bis-(μ_2-pyridinium-3-carboxylato)-dichloride-calcium(II)]* **(13)** *$[Ca(C_6H_5NO_2)_2Cl_2]$*

(13) was first prepared by solvent evaporation of a 1:1 stoichiometric mixture of nicotinic acid and calcium(II) chloride dissolved in isopropanol at 30 °C. Crystals of **(13)** were also formed when this evaporation crystallisation experiment was repeated at lab temperature using isopropanol, or an isopropanol and DCM mix, or in isopropanol at 40 °C or 50 °C.

When carried out in isopropanol at 4 °C, the crystallisation instead resulted in crystals of **(4)**. The resulting product was mostly a white precipitate containing a small amount of very small, clear, colourless, square-shaped platelet crystals that were brittle and crumbly that decomposed into tiny needle crystals within one week. **(13)** features a ligand:metal ratio of 2:1. In order to optimise its synthesis the experiment was repeated using a 2:1 stoichiometric ratio of nicotinic acid and calcium(II) chloride dissolved in a range of solvent systems and using a range of temperatures. The preparation using an ACN/THF mixture as the solvent, and crystallised at 4 °C, resulted in crystals of **(4)** rather than the targeted **(13)**. The only preparation using starting materials in a ligand:metal ratio of 2:1 that resulted in good quality crystals used the same conditions as the original preparation that produced **(13)**, namely crystallised at 30 °C from isopropanol solvent. This preparation resulted a fairly homogeneous sample of large, clear, colourless platelet crystals of **(13)** that were often hexagonal in shape, shown in Figure 4.47(a). The crystals from this sample decomposed into the familiar needles before a unit cell measurement could be obtained, however the PXRD pattern was obtained from the fresh sample. The pattern is shown in Figure 4.46 (in pink) and compared to the PXRD pattern of the original 1:1 sample (in red). The pattern of the 2:1 sample is different from, and of far better quality, to that of the 1:1 sample. It displays some common peaks with the calculated pattern of **(13)**, in particular the strong peak at about 10°. This strongly suggests that the 2:1 preparation resulted in crystals of **(13)**. The pattern does however exhibit some peaks that coincide with peaks relating to nicotinic acid starting material at about 25°, 26° and 27°.

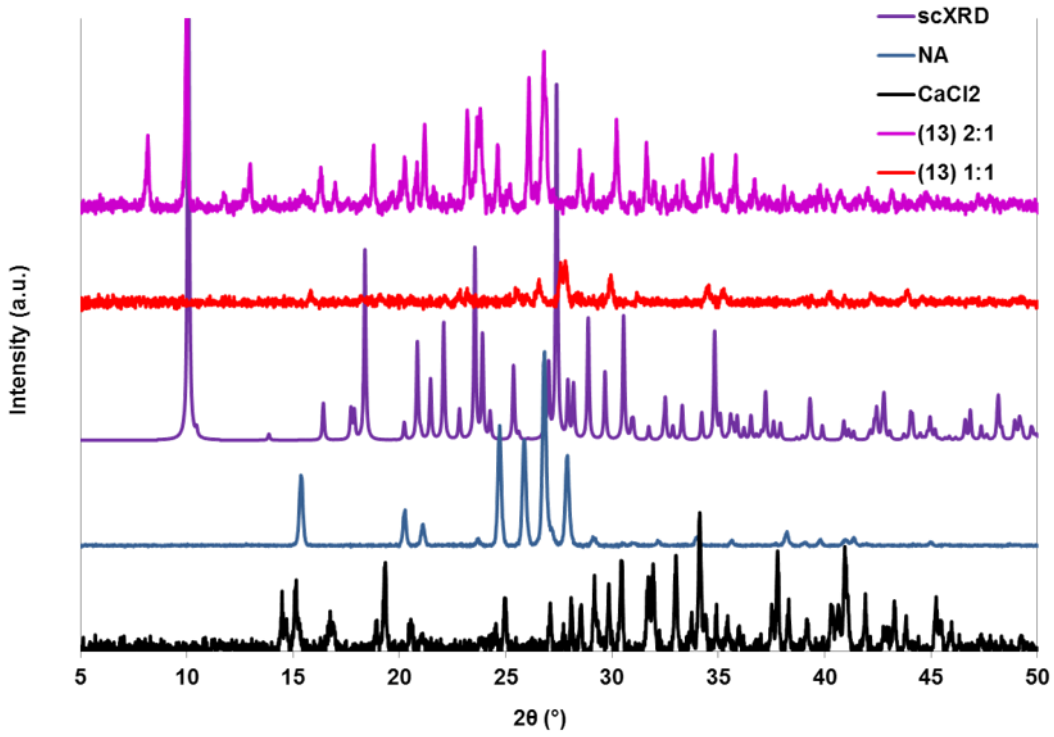

Figure 4.46. PXRD pattern of **(13)** compared to the calculated pattern and patterns of starting materials.

The crystal structure of **(13)** is composed of 2D coordination polymeric sheets, formed by the coordination of calcium centres by two chloride ions and four crystallographically equivalent zwitterionic nicotinic acid ligands *via* one carboxylate oxygen atom. The Ca centre is six coordinate, in an octahedral environment (Figure 4.47(b) and Table 4.28). The angles between the chloride ions and carboxylate oxygen atoms are all approx. 90°, ranging between 89.15(6)° for Cl1/Cl1^{a}-Ca1-O1^{a}/O1, to 90.85(6)° for Cl1/Cl1^{a}-Ca1-O1/O1^{a}. The coordination distances to the oxygen atoms are equal at 2.271(2) Å for both Ca1-O1/O1^{a} and Ca1-O2^{b}/O2^{c}. The coordination distance Ca1-Cl1/Cl1^{a} is longer at 2.745(1) Å.

The bridging nicotinic acid ligand is shown in Figure 4.47(c). The carboxylate group angle O1-C1-O2 is 125.6(3)°, wider than the O=C-O angle of pure nicotinic acid (123.2(3)°); this may be distorted due to the bridging between metal centres. The C-O distances of **(13)** are effectively equal at 1.246(3) Å and 1.247(4) Å for C1-O1 and C1-O2, respectively. The carboxylate group and the pyridinium ring are not coplanar, but slightly twisted with a O1-C1-C2-C3 torsion angle of 7.8(4)°.

The angles formed by the metal coordination, C1-O1-Ca1 and C1-O2-Ca1^{d}, are not equal with angles of 150.4(2)° and 159.8(2)°, respectively.

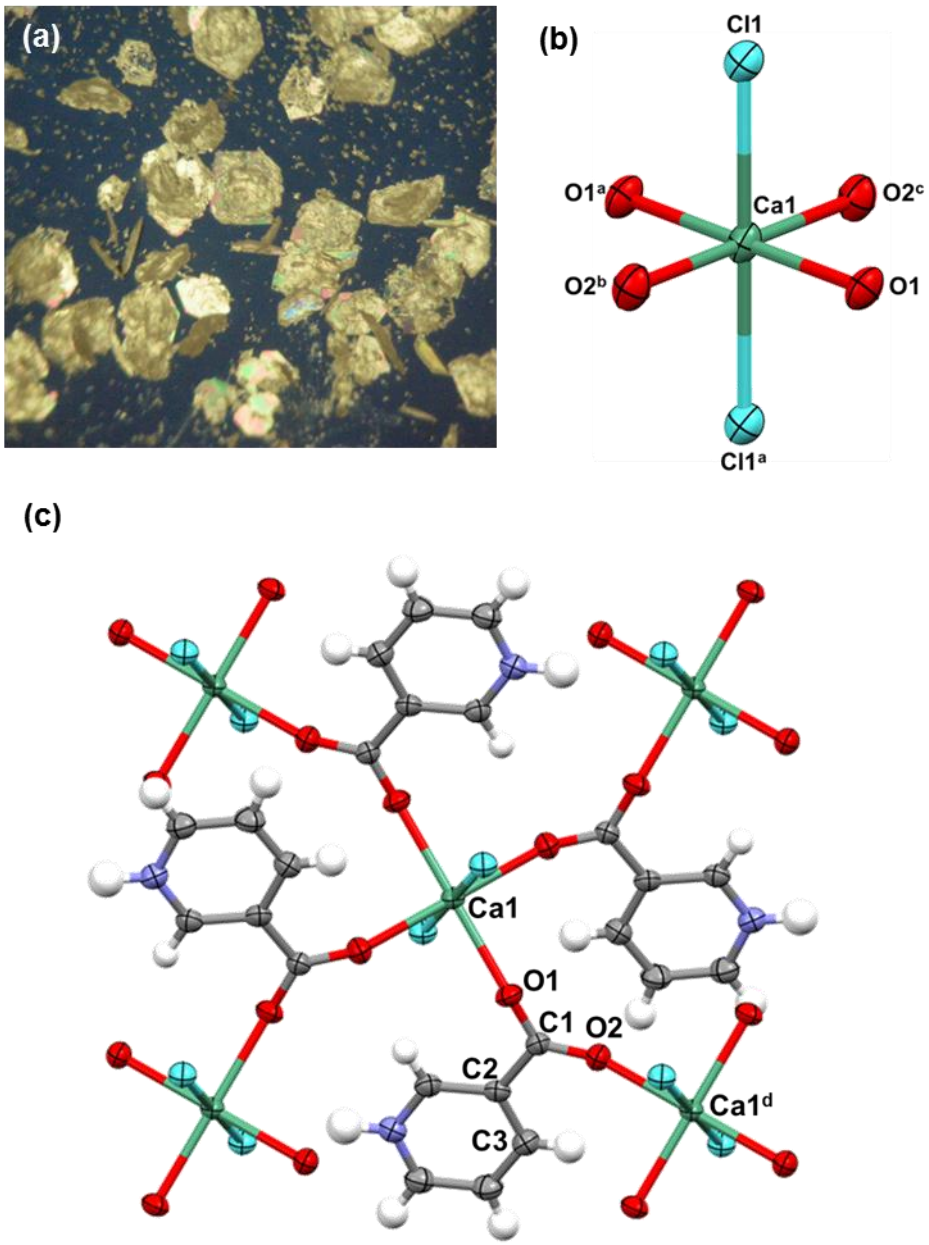

Figure 4.47. Crystal structure of **(13)**. (a) Crystals of **(13)** from the 2:1 ligand:metal preparation. (b) Octahedral Ca centre coordinated by two chloride ions and four carboxylate oxygen atoms. (c) Section of the 2D sheet, showing the Ca centre coordinated by four zwitterionic nicotinic acid ligands. Symmetry codes: [a](1½-x, ½-y, ½-z) [b](½+x, 1-y, z) [c](1-x, -½+y, ½-z) [d](1-x, ½+y, ½-z)

Table 4.28. Cl/O-Ca-O angles and Ca-Cl/O distances in **(13)**.

Coordination	Cl/O-Ca-O angle (°)	Interaction	Distance (Å)
Cl1/Cl1[a]-Ca1-O1/O1[a]	90.85(6)	Ca1-Cl1/Cl1[a]	2.745(1)
Cl1/Cl1[a]-Ca1-O1[a]/O1	89.15(6)	Ca1-O1/O1[a]	2.271(2)
Cl1/Cl1[a]-Ca1-O2[b]/O2[c]	89.16(6)	Ca1-O2[b]/O2[c]	2.271(2)
Cl1/Cl1[a]-Ca1-O2[c]/O2[b]	90.84(6)		
O1[a]/O1-Ca1-O2[c]/O2[b]	90.79(8)		
O2[c]/O2[b]-Ca1-O1/O1[a]	89.21(8)		

Symmetry codes: [a](1½-x, ½-y, ½-z) [b](½+x, 1-y, z) [c](1-x, -½+y, ½-z)

The 2D coordination polymeric sheets that make up the structure of **(13)** are parallel to the *ab* plane, on the {002} plane, thus producing the strong peak observed in the PXRD patterns at about 10°. The pyridinium ring forms seven moderately weak to weak H-bonds from each of the C-H groups and the N-H group, to chloride ions and carboxylate oxygen atoms belonging to the same sheet, as illustrated in Figure 4.48(a) and listed in Table 4.29. C3-H3 forms a bifurcated H-bond. C3-H3 H-bonds to Cl1 and O1, both coordinated to the same Ca centre to which the ligand is coordinated *via* O2. C3-H3···Cl1[d] is the longer interaction with a D···A distance of 3.942(4) Å, compared to C3-H3···O1[e] with a D···A distance of 3.614(4) Å, but has a much more linear angle of 171(3)°, as opposed to 118(3)° for C3-H3···O1[e]. C6-H6 forms two H-bonds: one to O2, a carboxylate oxygen atom of a neighbouring nicotinic acid ligand and one to Cl1, the chlorine atom coordinated to the same Ca centre to which the nicotinic acid ligand coordinates. These are long interactions with D···A distances of 3.565(3) Å and 3.422(3) Å angles of 171(3)° and 100(2)° for C6-H6···O2[c] and C6-H6···Cl1[a], respectively. C4-H4 and C5-H5 form H-bonds to the same chloride ion. These are very weak H-bonds with small angles of 105(3)° and 108(3)° and D···A distances of 3.752(4) Å and 3.629(4) Å for C4-H4···Cl1[f] and C5-H5···Cl1[f], respectively. The protonated nitrogen of the pyridinium ring forms the shortest H-bond within this structure, in which the acceptor is a chloride ion. N1-H1···Cl1[c] has a D···A distance of 3.042(3) Å and an angle of 165(4)°.

The 2D sheets are stacked along the *c* direction as shown in Figure 4.48(b); the sheets are connected by weak H-bonds formed between the C-H groups of the pyridinium ring to the chloride ion of the adjacent sheet (Figure 4.48(b) and (c) and Table 4.29). C4-H4···Cl1[g] and

C5-H5···Cl1^{g} are weak H-bonds with D···A distances of 3.609(4) Å and 3.464(4) Å and angles of 120(3)° and 129(3)°, respectively.

The pyridinium rings are positioned too far apart for π-π stacking interactions as the partially overlapping aromatic groups of the same 2D sheet have a centroid – centroid distance (C2,C3,C4,C5,N1,C6) – (C2,C3,C4,C5,N1,C6)^{f} of 4.824(2) Å and the overlapping aromatic groups of neighbouring 2D sheets have a centroid – centroid distance (C2,C3,C4,C5,N1,C6) – (C2,C3,C4,C5,N1,C6)^{h} of 4.277(2) Å. These centroid distances are significantly longer than the π-π stacking interactions observed in nicotinic acid in its pure form. The π-π separations are illustrated in Figure 4.48(d).

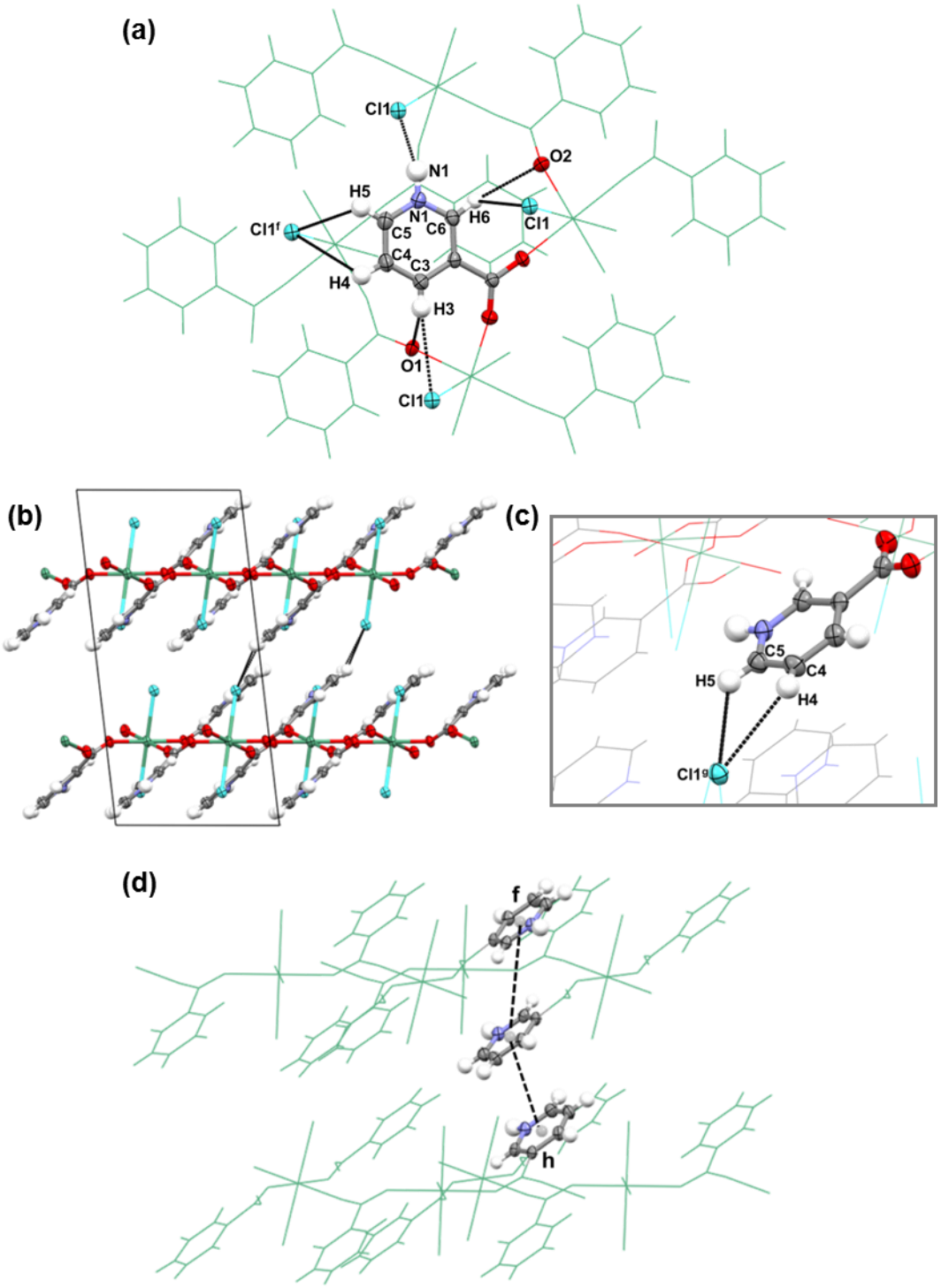

Figure 4.48. Crystal structure of **(13)**. (a) H-bonds within the 2D sheet. (b) View down the *b* axis showing 2D sheets parallel to the *ab* plane stacked along the *c* direction. (c) Detailing H-bonds connecting 2D sheets along the *c* direction. (d) π-π stacking separation between pyridinium rings of the same 2D sheet and between pyridinium rings of different 2D sheets. Symmetry codes for pyridinium groups and selected Cl ions: [f](½-x, ½-y, ½-z) [g](-1+x, ½-y, -½+z) [h](½-x, y, -z)

Table 4.29. Geometries of H-bonds in **(13)**.

D-H···A Interaction	D-H (Å)	H···A (Å)	D···A (Å)	D-H···A (°)
(Figure 4.48(a)) H-bonds within 2D sheet				
N1-H1···Cl1[c]	0.96(5)	2.11(5)	3.042(3)	165(4)
C3-H3···Cl1[d]	0.87(4)	3.08(4)	3.942(4)	171(3)
C3-H3···O1[e]	0.87(4)	3.12(4)	3.614(4)	118(3)
C4-H4···Cl1[f]	0.93(4)	3.40(4)	3.752(4)	105(3)
C5-H5···Cl1[f]	0.96(4)	3.22(4)	3.629(4)	108(3)
C6-H6···Cl1[a]	0.97(3)	3.11(4)	3.422(3)	100(2)
C6-H6···O2[c]	0.97(3)	2.60(3)	3.565(3)	171(3)
(Figure 4.48(c)) H-bonds connecting between 2D sheets				
C4-H4···Cl1[g]	0.93(4)	3.05(4)	3.609(4)	120(3)
C5-H5···Cl1[g]	0.96(4)	2.79(4)	3.464(4)	129(3)

Symmetry codes: [a](1½-x, ½-y, ½-z) [c](1-x, -½+y, ½-z) [d](1-x, ½+y, ½-z) [e](-½+x, 1-y, z) [f](½-x, ½-y, ½-z) [g](-1+x, ½-y, -½+z)

A single crystal of **(13)** did not appear to melt on heating to 375 °C when analysed by HSM, but the crystal visibly reduced in quality. The DSC trace for the bulk product of a sample obtained from a crystallisation preparation using starting materials in a ligand:metal ratio of 1:1 (Appendix A, Figure A13) shows a strong endothermic event with two minimas: one at 117.2 °C, and a slightly less intense and broader one at about 132 °C. These temperatures do not indicate melting points of either of the starting materials (nicotinic acid m.p. 236 – 239 °C; $CaCl_2$ m.p. 772 °C), and neither are they observed in the DSC trace of the closely related complex **(4)**.

4.4.2. *Catena-[bis-(μ_3-pyridine-3-carboxylato)-calcium(II)]* **(14)** *[$Ca(C_6H_4NO_2)_2$]*

(14) was prepared by solvent evaporation of a 2:1 stoichiometric mixture of nicotinic acid and calcium(II) acetate hydrate dissolved in methanol and DCM at lab temperature. Thick, clear, colourless needle crystals formed in two weeks. The PXRD pattern of the bulk sample (Figure 4.49) shows a good match to the calculated pattern, with coinciding peaks at about

12°, 15°, 19°, 22° and 25°, (taking into account the expected shifting of the calculated pattern to slightly higher 2θ values). The PXRD patterns indicates that the single crystal is fairly representative of the bulk sample, however some peaks may be due to residual nicotinic acid, in spite of the fact that the crystal structure features the ligands and metal in the same ratio in which the starting materials were used.

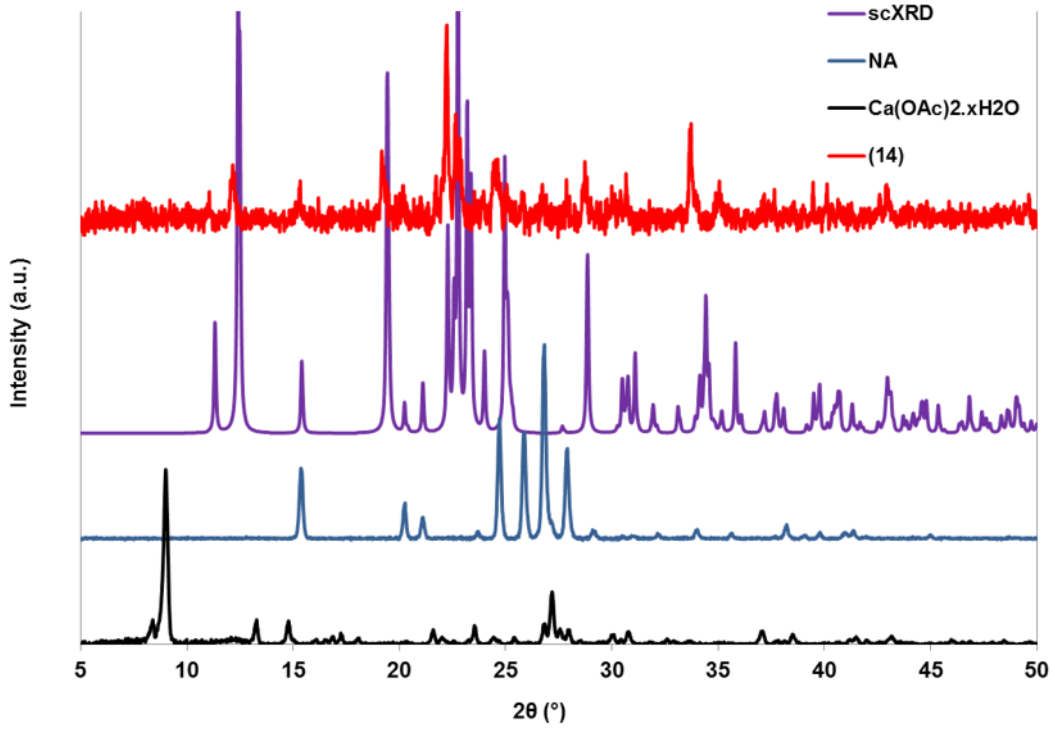

Figure 4.49. PXRD pattern of **(14)** compared to the calculated pattern and patterns of starting materials.

(14) has 3D coordination connectivity, but unlike the family of materials commonly termed traditional MOFs, it is not a porous framework. The formula unit features one calcium centre and two crystallographically inequivalent nicotinate ligands, which can be assigned as Nic1 and Nic2, according to their pyridyl nitrogen atoms, N1 and N2. The two μ_3 bridging nicotinate ligands form distinct 1D structural motifs that construct the three dimensional architecture of this complex through interconnection *via* coordination to the common calcium centre. The 1D structural motif featuring Nic1 is shown in Figure 4.50(a). Two alternating rings are formed by the coordination of Nic1 to the calcium centres: an eight-membered ring by coordination *via* both of the carboxylate oxygen atoms, O1 and O2, of two Nic1 ligands to two calcium centres, and a twelve-membered ring by coordination *via* one carboxylate oxygen atom, O2, and the pyridyl nitrogen atom, N1, of two Nic1 ligands to two calcium centres.

The 1D structural motif featuring Nic2 is shown in Figure 4.50(b). One ten-membered ring is formed by the coordination of both carboxylate oxygen atoms, O3 and O4, of one Nic2 ligand to two calcium centres, and by coordination *via* one carboxylate oxygen atom, O4, and the pyridyl nitrogen atom, N2, of another Nic2 ligand to the calcium centres.

The calcium centre of **(14)** is in a distorted octahedral environment, (Figure 4.50(c) and Table 4.30). The coordination distances between the calcium and the nitrogen atoms are the longest at 2.529(1) Å and 2.538(2) Å for Ca1-N1^{b} and Ca1-N2^{d}, respectively. Nic1 features the oxygen atoms which form the longest and shortest Ca-O coordination interactions, with Ca1-O1 having a distance of 2.266(1) Å, and Ca1-O2^{c} a distance of 2.325(1) Å. This may be due to the formation of the eight-membered ring that two Nic1 ligands form with two calcium centres. The Ca-O distances for the oxygen atoms of Nic2 are virtually equal at 2.289(1) Å for Ca1-O3 and 2.287(1) Å for Ca1-O4^{a}.

The angles between coordinating atoms vary between 82.00(5)° for O3-Ca1-N1^{b}, the angle formed between the coordinating pyridyl nitrogen atom of Nic1 and a carboxylate oxygen atom of Nic2, to 99.09(5)° for N1^{b}-Ca1-N2^{d}, the angle formed between the coordinating pyridyl nitrogen atoms of the two nicotinate ligands. The angle O2^{c}-Ca1-O1, within the eight-membered ring formed by Nic1, is 97.81(4)°. In the twelve-membered ring, the angle O2^{c}-Ca1-N1^{b} is significantly smaller at 84.47(4)°. The angles involving the coordination bonds in the ten-membered ring formed by Nic2, O4^{a}-Ca1-N2^{d} and O4^{a}-Ca1-O3, are 85.38(5)° and 96.71(4)°, respectively, again displaying a much smaller angle for those in which coordination by nitrogen is involved.

The nicotinate ligands are almost identical in their C-O distances but they differ slightly in their O-C-O angles, and quite significantly in the torsion angle formed between the carboxylate group and the pyridine ring. Nic1 has C-O distances of 1.255(2) Å and 1.252(2) Å for C1-O1 and C1-O2, respectively. Nic2 has C-O distances of 1.251(2) Å for C7-O3 and 1.255(2) Å for C7-O4. The O1-C1-O2 angle of Nic1 is 125.4(2)°, and the O3-C7-O4 angle of Nic2 is 124.8(2)°. In both cases the carboxylate group angle is wider than the O=C-O angle of pure nicotinic acid (123.2(3)°). The carboxylate group is twisted more from coplanarity for Nic1, with a O1-C1-C2-C3 torsion angle of -15.3(2)°, almost twice the O3-C7-C8-C9 torsion angle of Nic2, which is -7.2(2)°.

The eight-membered ring formed by Nic1 is comparable to those formed by two carboxylate groups and two metal centres in the discrete formula units of **(1)**, **(2)** and **(3)** and within the chain structures of **(7)** and **(11)**.

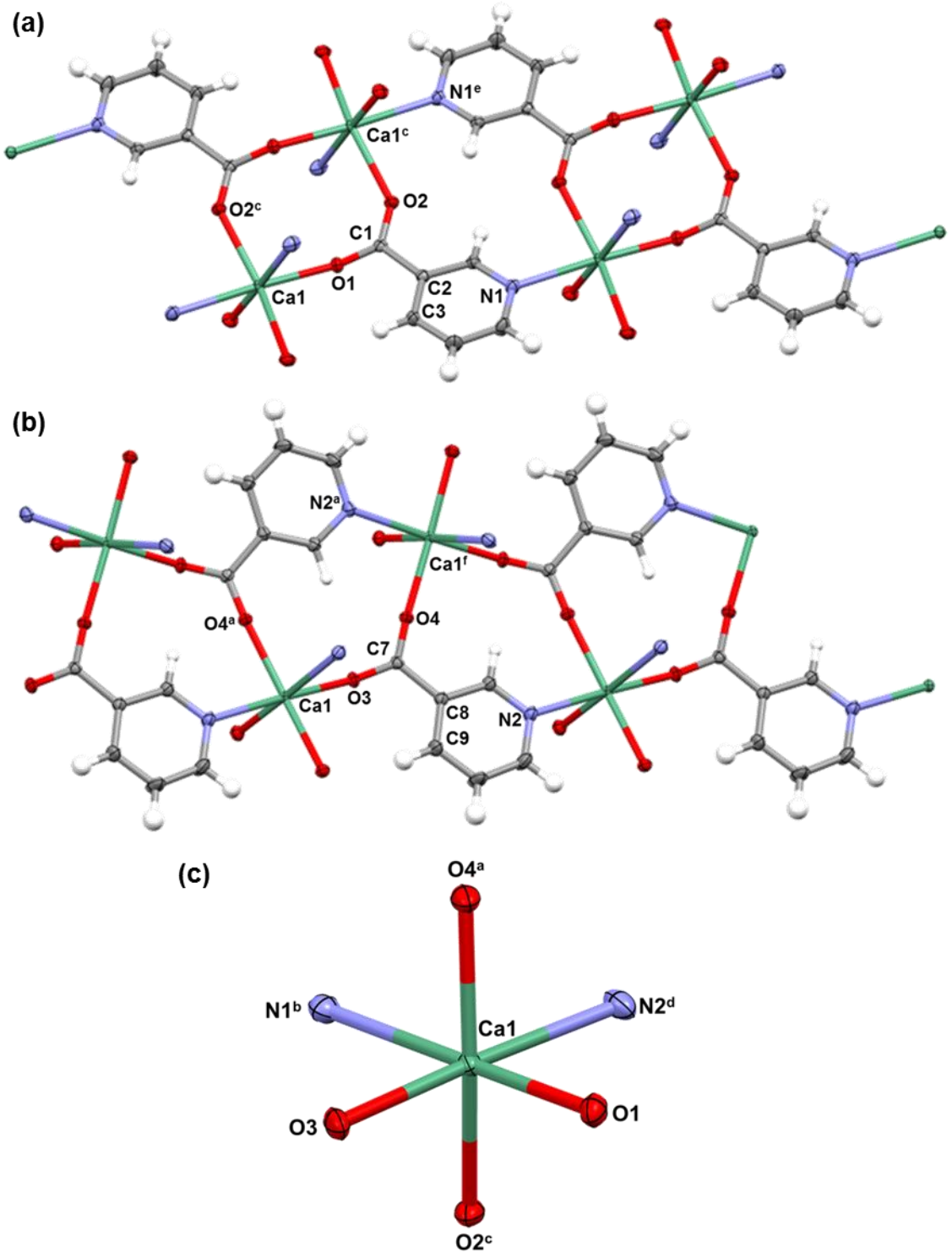

Figure 4.50. Crystal structure of **(14)**. (a) 1D structural motif featuring Nic1 ligands coordinated to Ca centres. (b) 1D structural motif featuring Nic2 ligands coordinated to Ca centres. (c) Octahedral Ca centre coordinated by two pyridyl nitrogen atoms and four carboxylate oxygen atoms. Symmetry codes: [a](½+x, 1½-y, ½+z) [b](-1+x, y, z) [c](2-x, 2-y, -z) [d](1+x, y, 1+z) [e](3-x, 2-y, -z) [f](-½+x, 1½-y, -½+z)

Table 4.30. N/N/O-Ca-N/O/O angles and Ca-N/O distances in **(14)**.

Coordination	N/N/O-Ca-N/O/O angle (°)	Interaction	Distance (Å)
O4[a]-Ca1-N1[b]	85.15(5)	Ca1-N1[b]	2.529(1)
O4[a]-Ca1-N2[d]	85.38(5)	Ca1-N2[d]	2.538(2)
O4[a]-Ca1-O1	93.03(4)	Ca1-O1	2.266(1)
O4[a]-Ca1-O3	96.71(4)	Ca1-O2[c]	2.325(1)
O2[c]-Ca1-N1[b]	84.47(4)	Ca1-O3	2.289(1)
O2[c]-Ca1-N2[d]	86.78(5)	Ca1-O4[a]	2.287(1)
O2[c]-Ca1-O1	97.81(4)		
O2[c]-Ca1-O3	91.35(4)		
N1[b]-Ca1-N2[d]	99.09(5)		
N2[d]-Ca1-O1	83.67(5)		
O1-Ca1-O3	95.33(5)		
O3-Ca1-N1[b]	82.00(5)		

Symmetry codes: [a](½+x, 1½-y, ½+z) [b](-1+x, y, z) [c](2-x, 2-y, -z) [d](1+x, y, 1+z)

The framework of **(14)** consists of 1D chains of alternating eight- and twelve-membered rings formed by Nic1 that form broken layers along the {002} plane, and 1D chains of ten-membered rings formed by Nic2 that form broken layers along the {20-2} plane. These chains are connected by the common octahedral calcium centres to which both Nic1 and 2 coordinate. Figure 4.51 illustrates this connectivity. The 1D chains cross each other at an angle of about 60°.

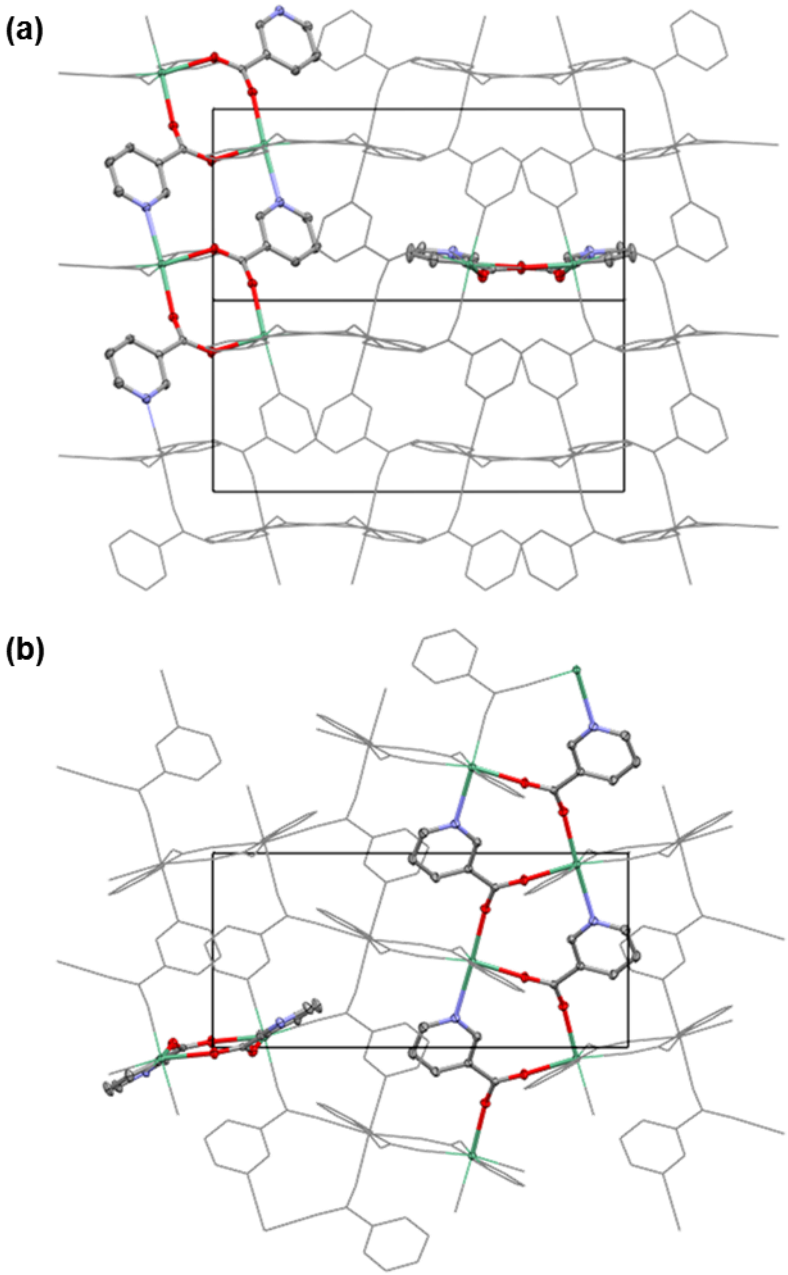

Figure 4.51. Crystal structure of **(14)**. (a) Global packing, showing 1D chains formed by Nic1 running in parallel to the *a* direction (left), and 1D chains formed by Nic2 aligned along the {20-2} plane, (right). (b) View down the *a* axis, showing different perspective to (a), more clearly showing the 1D chains formed by Nic2 (right).

Due to the three dimensional coordination connectivity of **(14)**, and the absence of any counter ions or water molecules, H-bonding is not a major contributor to the overall crystalline packing. There are H-bonds present however, all originating from the C-H groups of the pyridyl ring, and accepted by carboxylate oxygen atoms. These are illustrated in Figure 4.52(a) and (b), with respect to the 1D chain formed by Nic1 and 2, respectively, and in (c) with respect to the joining of the 1D chain motifs. All of the H-bonds are moderately

weak to weak interactions, with D···A distances ranging from 3.181(2) Å for C6-H6···O2^{e}, to 3.711(2) Å for C12-H12···O3^{f}, and angles from 117(2)° for C4-H4···O3^{a}, to 176(2)° for C3-H3···O4^{a}. C3-H3, C4-H4, C11-H11 and C12-H12 form H-bonds to two acceptors. C3-H3, C11-H11 and C12-H12 each H-bond to two carboxylate oxygen atoms of one nicotinate ligand, and C4-H4 H-bonds to two carboxylate oxygen atoms of two different nicotinate ligands. C3-H3, C4-H4 and C12-H12 are bifurcated H-bonds. C3-H3···O4^{a} is the shorter and more linear component of the interaction from C3-H3, with a D···A distance of 3.499(3) Å and the largest angle of 176(2)°. C3-H3···O3^{a} has a D···A distance of 3.525(2) Å and an angle of 135(2)°. H4 forms two interactions of very different angles. C4-H4···O1^{a} has an angle of 163(2)° and a D···A distance of 3.356(3) Å, while C4-H4···O3^{a} has an angle of 117(2)° and an D···A distance of 3.704(3) Å. The four H-bonds originating from C3 and C4 may be related to the greater twisting of the pyridyl ring of Nic1 from the plane of its carboxylate group. In the C12-H12 bifurcated H-bond, C12-H12···O3^{f} has a D···A distance of 3.711(2) Å and an angle of 170(2)°, and C12-H12···O4^{f} has a D···A distance of 3.218(2) Å and an angle of 131(1)°. C6-H6···O2^{e} is formed across the twelve-membered ring of the chain made up of Nic1 ligands. This H-bond has the shortest D···A distance, as noted above, and an angle of 131(2)°.

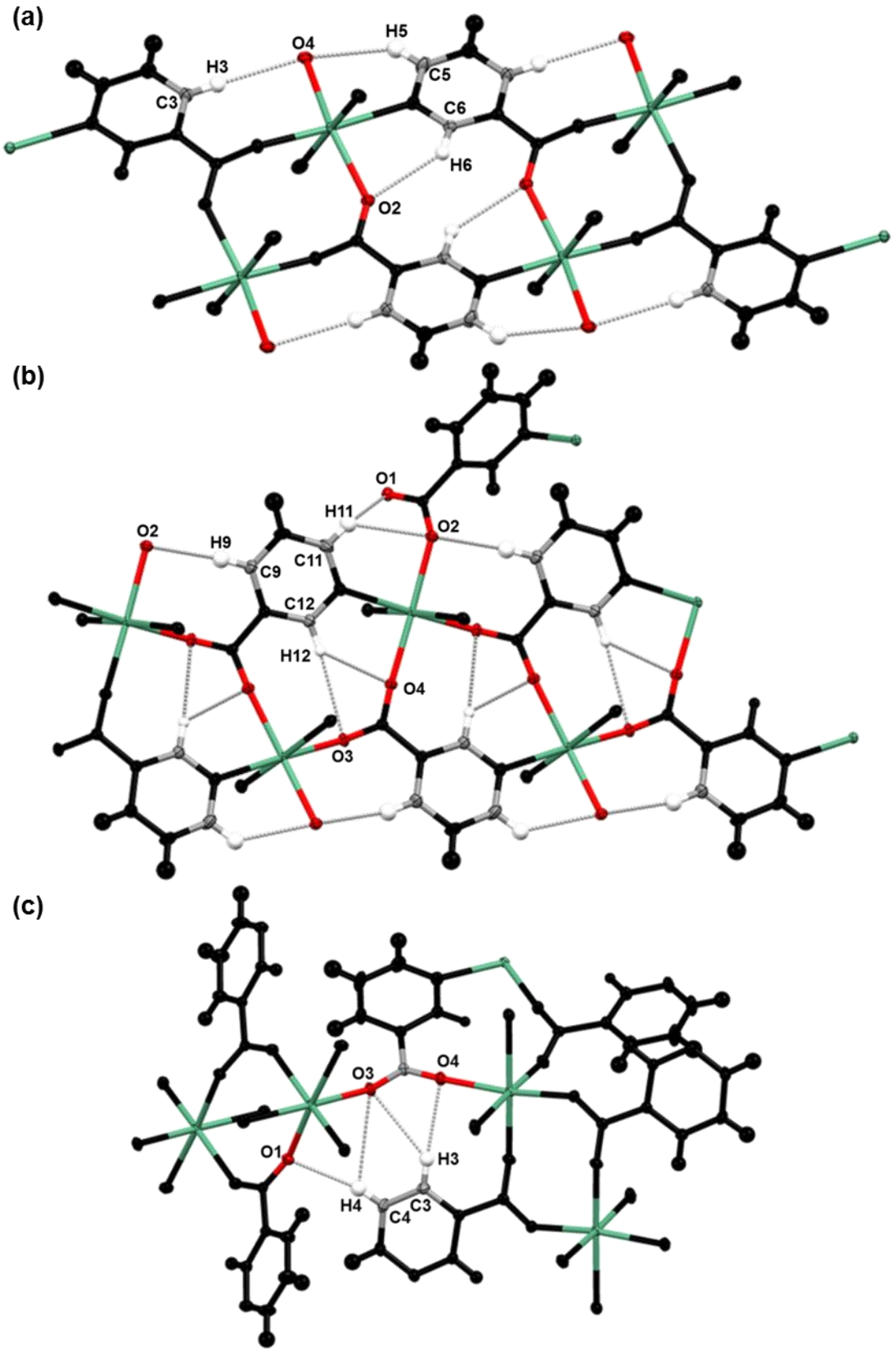

Figure 4.52. Crystal structure of **(14)**. (a) H-bonds with respect to the 1D chain formed by Nic1, and (b) Nic2. (c) H-bonds with respect to the joining of two 1D chain motifs.

Table 4.31. Geometries of H-bonds in **(14)**.

D-H···A Interaction	D-H (Å)	H···A (Å)	D···A (Å)	D-H···A (°)
C3-H3···O3[a]	0.93(2)	2.81(3)	3.525(2)	135(2)
C3-H3···O4[a]	0.93(2)	2.58(2)	3.499(3)	176(2)
C4-H4···O1[a]	0.95(2)	2.44(2)	3.356(3)	163(2)
C4-H4···O3[a]	0.95(2)	3.17(3)	3.704(3)	117(2)
C5-H5···O4[a]	0.97(2)	2.75(3)	3.368(3)	122(2)
C6-H6···O2[e]	0.95(2)	2.48(2)	3.181(2)	131(2)
C9-H9···O2[c]	0.94(2)	2.62(2)	3.512(2)	160(2)
C11-H11···O1[g]	0.96(2)	2.68(2)	3.442(3)	136(2)
C11-H11···O2[g]	0.96(2)	2.69(2)	3.368(2)	128(2)
C12-H12···O3[f]	0.95(2)	2.77(2)	3.711(2)	170(2)
C12-H12···O4[f]	0.95(2)	2.51(2)	3.218(2)	131(1)

Symmetry codes: [a](½+x, 1½-y, ½+z) [c](2-x, 2-y, -z) [e](3-x, 2-y, -z) [f](-½+x, 1½-y, -½+z) [g](1-x, 2-y, -1-z)

A single crystal of **(14)** was analysed by HSM and no melt was observed on heating to 375 °C. The DSC trace of the bulk sample (Appendix A, Figure A14) shows the strongest and most prominent endotherm at 218.7 °C. This is too low to indicate the melting of nicotinic acid (m.p. 236 – 239 °C). At about this temperature during HSM there was internal movement observed in the crystal, resembling bubbling.

4.5. Conclusions

Summary

The crystal structures of fourteen new metal-organic complexes have been presented: eight featuring magnesium and six featuring calcium metal centres. Of the magnesium complexes, four contain picolinic acid **(1)**, **(6)**, **(7)** and **(8)**, one nicotinic acid **(2)**, and one isonicotinic acid **(5)**: in each case the ligand is in its zwitterionic form. Of the three calcium complexes synthesised with picolinic acid, two feature the ligand in its zwitterionic form **(10)** and **(11)**, and in **(12)** the picolinate ion displays N,O-chelation to the metal centre. Four

calcium complexes were synthesised with nicotinic acid and in three of these the ligands are in their zwitterionic form **(3)**, **(4)** and **(13)**. The nicotinate ion of **(14)** coordinates to metal centres *via* the nitrogen atom of the pyridine ring in addition to the carboxylate oxygen atoms. There is one calcium complex featuring zwitterionic isonicotinic acid **(9)**.

Structural Trends

Six of the complexes exist as 0D molecular crystals composed of discrete units and six as 1D coordination polymers. The two structures of higher dimensional coordination connectivity are both synthesised from calcium salts and nicotinic acid. **(13)** is formed from 2D polymeric sheets and **(14)** has a 3D network.

Patterns have emerged as to the common coordination modes of these complexes. It was observed in **(1)**, **(2)** and **(3)** that two carboxylate groups bridge between two metal centres to form an eight-membered ring. This feature is also observed as part of the polymeric structure of **(7)**, **(11)**, **(12)** and **(14)**. **(11)** is interesting however, in that the two crystallographically equivalent calcium centres are bridged by two carboxylate groups of crystallographically equivalent ligands, while the crystallographically inequivalent calcium centres are singly bridged by a second ligand, in an alternate fashion. **(12)** is also slightly more complicated in that the two calcium centres are also doubly bridged by two coordinating water molecules. **(14)** has a higher coordination dimensionality and features the eight-membered ring as part of the 1D structural motif of the 3D structure.

It was noted that some complexes were related, either existing as constitutional isomers, as was the case for **(3)** and **(10)**, **(5)** and **(6)**, and **(5)** and **(7)**, or as 'molecular building block structural isomers', **(6)** and **(7)**. Transformation from **(8)** to **(7)** was observed, possibly *via* a dissolution/recrystallisation process. It is clear that there is a close relationship between **(6)**, **(7)**, **(8)** (and **(A2)**). These complexes could all potentially result from the same crystallisation experiment, however multiple crystalline forms in the same vial were not recorded simultaneously.

Metals

The magnesium centres are six coordinate and consistently have a distorted or slightly distorted octahedral geometry. The calcium centres vary from six coordinate with a near perfect octahedral geometry **(13)**, or distorted or slightly distorted octahedral geometry **(11)** and **(14)**, to seven coordinate **(4)**, and eight coordinate **(3)**, **(9)**, **(10)** and **(12)**. **(10)** and **(11)** feature two crystallographically inequivalent calcium centres, although the latter is

particularly interesting in that these metal centres have very different coordination environments.

Ligands

In all of these complexes, the carboxyl group of the pyridine carboxylic acid is deprotonated. Except for **(12)** and **(14)**, the pyridyl nitrogen atom is protonated to form the zwitterion. The organic ligands coordinate to the metal centres primarily *via* the carboxylate group due to the relatively hard base nature of the oxygen donor atoms and the hard acid character of the Mg^{2+} and Ca^{2+} ions. The carboxylate group bridges between two metal centres in all complexes except **(4)**, **(5)** and **(6)** in which only one carboxylate oxygen atom is metal-coordinating. The pyridyl ring is not protonated in either **(12)** or **(14)**, featuring picolinate and nicotinate, respectively, and both feature metal coordination from both the carboxylate group and the pyridyl nitrogen atom such that the ligands are μ_3 bridging. The isonicotinic acid ligand of **(9)** also bridges between three calcium centres except this is solely through the carboxylate group. The geometries of the organic ligands are listed in Appendix A, Table A1. In almost every instance, the O-C-O angle of the carboxylate group is wider than the O=C-O angle of the carboxyl group of the ligand in its pure form. In cases where the carboxylate group is bridging between metal centres this widening of the angle may be due to distortion from coordination in two directions. However, a widening is observed even in the complexes where no metal-bridging is displayed. The carboxylate group angle is smaller in **(9)** and **(12)** compared to the pure ligands. The former features coordination to three calcium centres, and the chelation of both oxygen atoms to the same central metal may act to compress the O-C-O angle. The latter may be influenced by the fact that one of the carboxylate oxygen atoms is partaking in N,O-chelation, and in effect is bridging two calcium centres.

The ligands in these metal-organic complexes do not retain the intramolecular interactions displayed by the materials in their pure forms. In the case of picolinic acid this is due to the fact that the ligand does not display disorder between the neutral and zwitterionic forms. Since the carboxyl group is always deprotonated to the carboxylate group the dimers observed in the pure form connected by O-H···O interactions are not formed, and since the pyridyl nitrogen atom is either protonated or involved in metal coordination, the N-H···N interactions are also not observed. The complexes featuring nicotinic and isonicotinic acid do not display intramolecular interactions characteristic of the pure ligands since they are all either zwitterionic or deprotonated, and the pure ligands are primarily connected by O-H···N H-bonds from the carboxyl group to form chains connected by π-π stacking

interactions. Metal coordination completely changes the way in which the ligands interact due to the carboxylate group wholly being given over to coordination and N-H and C-H groups more likely to form H-bonds to water molecules or counter ions than to other organic ligands. Where observed, π-π stacking interactions are longer in the metal-organic complexes than in the pure ligands.

H-Bonds

Every complex except for **(14)** features either chloride or nitrate counter ions, while every complex except from **(13)** and **(14)** feature coordinated water, with **(1)**, **(7)** and **(9)** additionally including non-coordinated water molecule(s). The counter ions and water molecules are central to the H-bonding interactions that connect these crystal structures. The counter ions, Cl^- and NO_3^-, act as H-bond acceptors while the water molecules act as both H-bond donors and acceptors. The pyridine carboxylic acid ligands form moderate to weak H-bonds from the N-H group, and weaker H-bonds from C-H groups of the pyridinium ring. The shortest H-bond reported here has a D⋯A distance of 2.607(1) Å and an angle of 173(2)°. It is an N-H⋯O H-bond between the pyridinium ring and a non-coordinating oxygen atom of a metal-coordinated carboxylate group of **(4)**.

Thermal Behaviour

There were difficulties in matching features in the DSC trace with occurences observed during HSM due to the inconsistencies in the thermal analysis results. This was attributed to sample impurity of the bulk samples used for DSC analysis, as the PXRD pattern often indicated that the single crystal from which structural data were obtained was not always representative of the bulk material. The structures with the highest dimensional coordination connectivity, **(13)** and **(14)**, were not found to melt during HSM up to 375 °C, which is likely due to their robust networks being connected in at least two directions by coordination bonds. By HSM, the 1D complexes were found to have variable approximate melting ranges from 80 – 91 °C for **(7)** to 128 – 138 °C for **(11)**. These melting ranges were not in excess of those of the 0D complexes: these ranged from 85 – 88 °C for **(6)** to 153 – 167 °C for **(2)**. Therefore, this study does not necessarily suggest there is greater thermal stability afforded by the higher dimensional metal-organic ligand coordination of the 1D complexes over the 0D complexes, possibly since the 0D complexes also display significant H-bonding interactions.

Chapter 5. Magnesium and Calcium Pyridine Dicarboxylic Acid Complexes and Addition of Diamines

5.1. Introduction

An obvious approach to impart further functionality into a group 2 metal-organic complex is to use more functionalised organic ligands. Chapter 4 confirmed that the pyridine carboxylic acid ligands preferentially coordinate to group 2 metal centres through the oxygen atoms of the deprotonated carboxyl group. In **(12)** it was observed that the picolinate ligand coordinated to the calcium centre by N,O-chelation *via* both a carboxylate oxygen atom and a pyridyl nitrogen atom. In **(14)**, the nicotinate ligand coordinated to three calcium centres, utilising the pyridyl nitrogen atom's coordination capability. Owing to their second carboxyl group functionality, pyridine dicarboxylic acids were selected for use in further experiments, specifically 2,4-pyridine dicarboxylic acid (2,4-pdca) in the form of 2,4-pyridine dicarboxylic acid monohydrate (2,4-pdcam). The multi coordination ability of this ligand has been utilised by Noro *et al.* in the synthesis of *bis-(pyridine-2-carboxylato-4-carboxyl)-diaqua-copper(II)* [**NELPEZ02**; CSD V5.35 October 2014] and its subsequent employment as a metalloligand.[91] This complex comprises a copper centre, N,O-chelated by two organic ligands with peripheral carboxyl functional groups, and coordinated by two water molecules (see Figure 1.4). The additional, non-coordinating carboxyl groups are capable of engaging in intermolecular interactions such as H-bonds. This complex, as well as its cobalt, nickel and zinc analogues, have been used by Beatty *et al.* in the development of 2D H-bonded coordination networks.[92, 94, 95]

Hence, the first step in developing new functional group 2 metal-organic complexes was to synthesise the target metalloligand (TM) – the group 2 metal analogue of $Cu(C_7H_4NO_4)_2(H_2O)_2$, illustrated in Figure 5.1. This would be a useful building block which could potentially be employed to introduce a group 2 metal into new metal-organic complexes. Once this complex could be established, the next step was to combine it with selected diamines to form a new crystalline complex in which charge-assisted H-bonds form between the peripheral carboxylate groups of the metalloligand and the ammonium groups of the protonated diamine in a similar fashion demonstrated by Beatty *et al*.[95]

Synthesis of the TM was first attempted by the preparation outlined by Noro *et al*., and also employed by Beatty *et al*. These preparations resulted in microcrystalline powders that were termed 'intermediates', **(I1)** – **(I3)**, (and **(I5)** – **(I7)** which were 'unsuccessful attempts' discussed in Appendix E). Single crystals were not obtained from these preparations. The ligand 3,5-pyridine dicarboxylic acid (3,5-pdca) was also used to produce intermediate

complexes – although N,O-chelation to a metal centre could not occur, it was used as a pyridine-based organic ligand of multi-coordination potential.

The next step was to combine the metalloligand with the diamine *o*-tolidine, as was used by Beatty *et al*.[95] or *m*-xylylenediamine. From these experiments three new crystal structures were obtained: **(15)** is an organic hydrate composed of 2,4-pyridine dicarboxylate ions and protonated *o*-tolidine ions; **(17)** is a hydrate in which a magnesium centre is N,O-chelated by one 2,4-pyridine dicarboxylate ion; and **(16)** is a copper-organic-organic hydrate in which the TM, minus one axial water molecule, forms an H-bonded network with *m*-xylylenediammonium.

Synthesis of the TM was also attempted by simple evaporative crystallisation techniques that had proven effective in producing new complexes on combining group 2 metal salts with pyridine carboxylic acids, reported in Chapter 4. Single crystals of the desired TM were not obtained, but crystals of pure 2,4-pyridine dicarboxylic acid monohydrate **(A3)** were formed and the structure (unreported in the literature) was solved (and discussed fully in Appendix D). Analysis of the bulk sample from another evaporative crystallisation experiment suggested that a new metal-organic complex had formed, establishing another 'intermediate'. **(I4)**, the reaction of magnesium(II) nitrate hexahydrate and 2,4-pyridine dicarboxylic acid monohydrate, was combined with *m*-xylylenediamine in an evaporative crystallisation experiment; this resulted in crystals of **(17)**.

Finally, two new magnesium-organic complexes prepared by reaction of magnesium aceatate tetrahydrate and 2,4-pdcam under hydrothermal conditions are reported. **(18)** is a 2D magnesium-organic complex and is the initial product of the reaction. Left in the mother liquor in a sealed vial at room temperature, this material undergoes transformation into **(19)** over several months. **(19)** is a 0D complex and contains the dianionic magnesium analogue of the TM.

This chapter describes the synthesis, structure and thermal properties of these new crystalline materials.

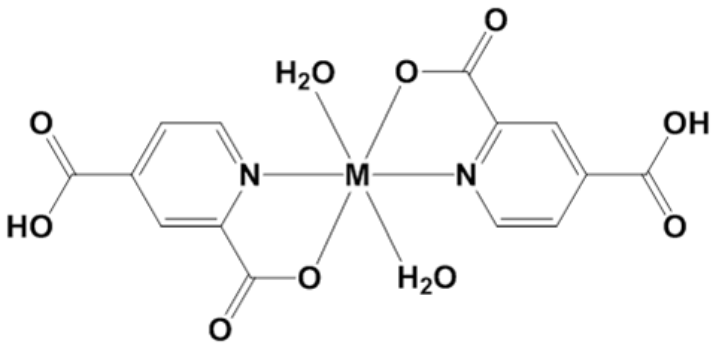

Figure 5.1. Target metalloligand (TM): *bis-(pyridine-2-carboxylate-4-carboxylic acid)-diaqua-M(II)*, where M = Mg or Ca.

5.2. Preparation of bis-(pyridine-2-carboxylato-4-carboxyl)-diaqua-Mg(II) and bis-(pyridine-2-carboxylato-4-caboxyl)-diaqua-Cu(II) 'Intermediate' Complexes

The preparations of **(I1)** – **(I3)** were based on that of $Cu(C_7H_4NO_4)_2(H_2O)_2$ outlined by Noro *et al*,[91] in which a 2:1 stoichiometric mixture of 2,4-pdcam and copper(II) sulfate pentahydrate was stirred in methanol and water to yield a blue powder.

5.2.1. *Reaction of magnesium(II) acetate tetrahydrate and 2,4-pyridine dicarboxylic acid monohydrate to give product* **(I1)**

(I1) was prepared by stirring a 2:1 stoichiometric mixture of 2,4-pdcam and magnesium(II) acetate hydrate in methanol and water at 50 °C. The PXRD pattern of the white powder product is shown in Figure 5.2. There are prominent peaks unique to **(I1)** at about 11°, 14°, 15° and 26°. The very prominent peak at about 24° coincides with a peak of the starting material 2,4-pdcam, however the larger peaks of this startng matrial are absent in the pattern of **(I1)**.

The PXRD pattern was also compared to those of the complexes **(17)**, **(18)** and **(19)** (Appendix B, Figure A15), and to the previously reported complexes *bis-[(μ_2-pyridine-2,4-dicarboxylato)-triaqua-magnesium(II)]* [**SUYLEE01**; CSD V5.35 October 2014][97] and *bis-(pyridinium-2,4-dicarboxylato)-diaqua-magnesium(II)* [**ZIMJIQ**; CSD V5.35 October 2014][171] (Appendix B, Figure A16) to check whether it was a previously prepared material or a known complex consisting of 2,4-pyridine dicarboxylate and magnesium. The PXRD pattern of **(I1)** shows some similarity with that of **(18)** with coinciding peaks at about 14°, 21° and 26°, but overall, the patterns do not match.

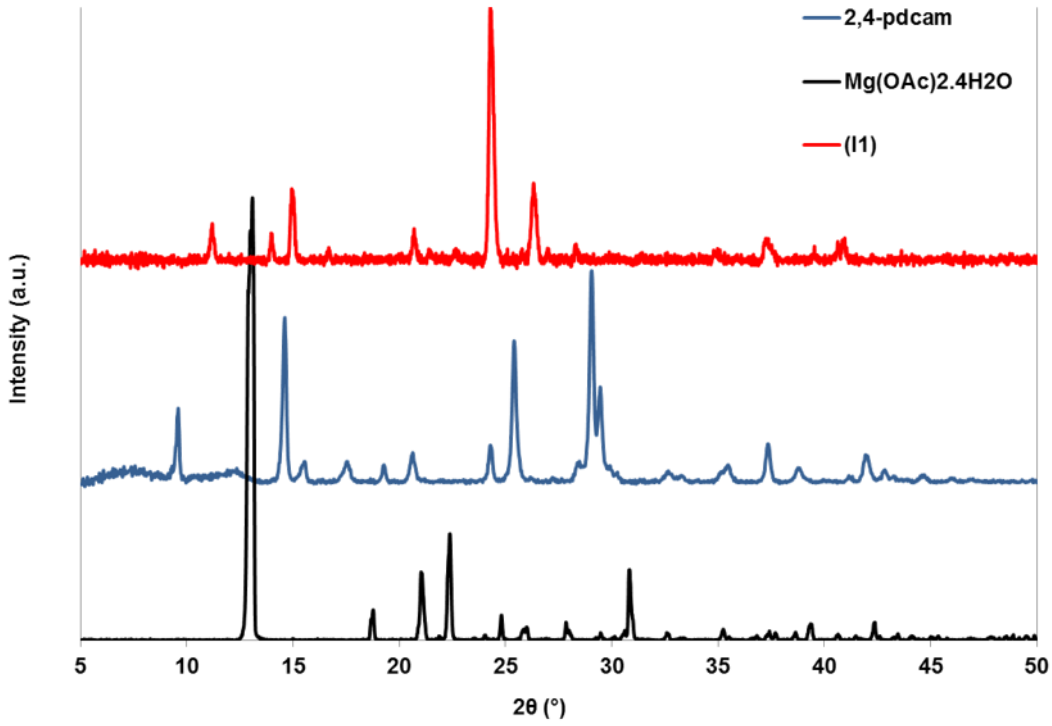

Figure 5.2. PXRD pattern of **(I1)** compared to the patterns of the starting materials.

The MS spectrum indicated an ion of *m/z* 355.0059 consistent with the presence of *pyridine-2,4-dicarboxylate, pyridine-2-carboxylate-4-carboxylic acid-magnesium(II)*, a fragment of the TM. Formaton of the complex was further supported by CHN analysis (see Experimental).

The thermal behaviour of **(I1)** was investigated by DSC (Appendix B, Figure A17). The trace shows a large endothermic event at 218.5 °C. The melting point of 2,4-pdcam is higher (m.p. 246 – 248 °C) and that of magnesium(II) acetate tetrahydrate lower (m.p. 72 – 75 °C), suggesting that this endothermic event, possibly a melt, is related to a new complex.

5.2.2. *Reaction of magnesium(II) hydroxide and 2,4-pyridine dicarboxylic acid monohydrate to give product* **(I2)**

(I2) was prepared by stirring a 1:1 stoichiometric mixture of 2,4-pdcam and magnesium(II) hydroxide in methanol and water at 40 °C. The PXRD pattern of the resulting white powder is shown in Figure 5.3. The peaks at about 19° and 38° match the peaks of magnesium(II) hydroxide, but the remaining peaks do not match those of 2,4-pdcam. When compared to the PXRD pattern of **(I1)** (Figure 5.4) it can be seen that there is a striking resemblance between the two patterns with matching peaks at about 11°, 14°, 15°, 21°, 24° and 26°

suggesting that the new complex formed in **(I1)** is also present in **(I2)** in a physical mixture also containing the magnesium(II) hydroxide starting material.

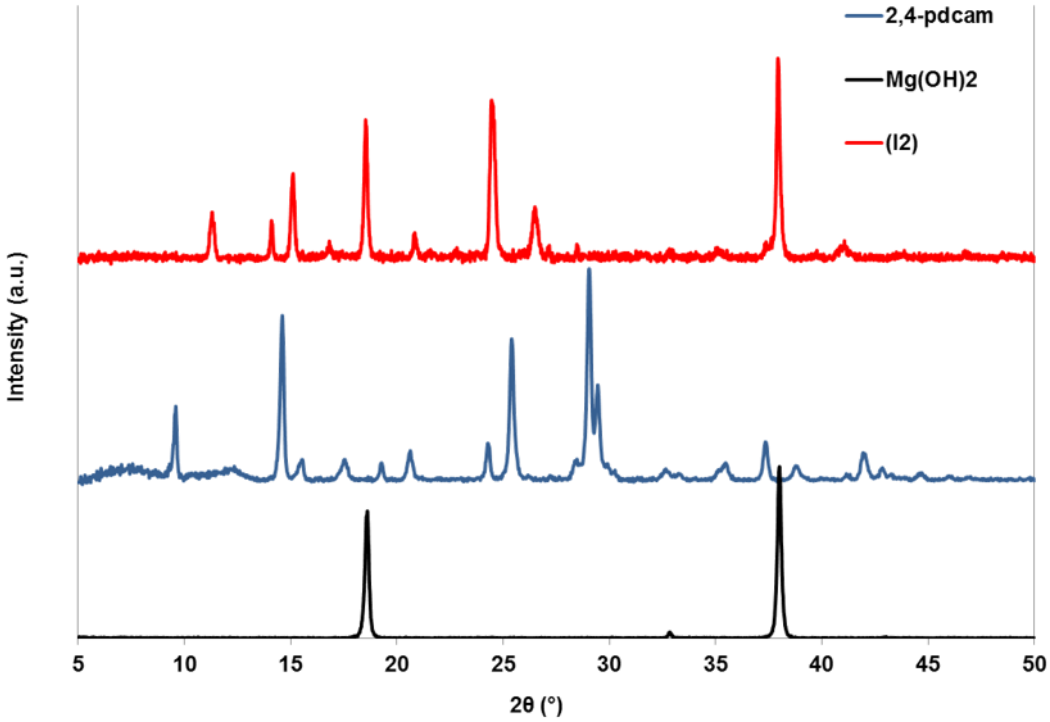

Figure 5.3. PXRD pattern of **(I2)** compared to the patterns of the starting materials.

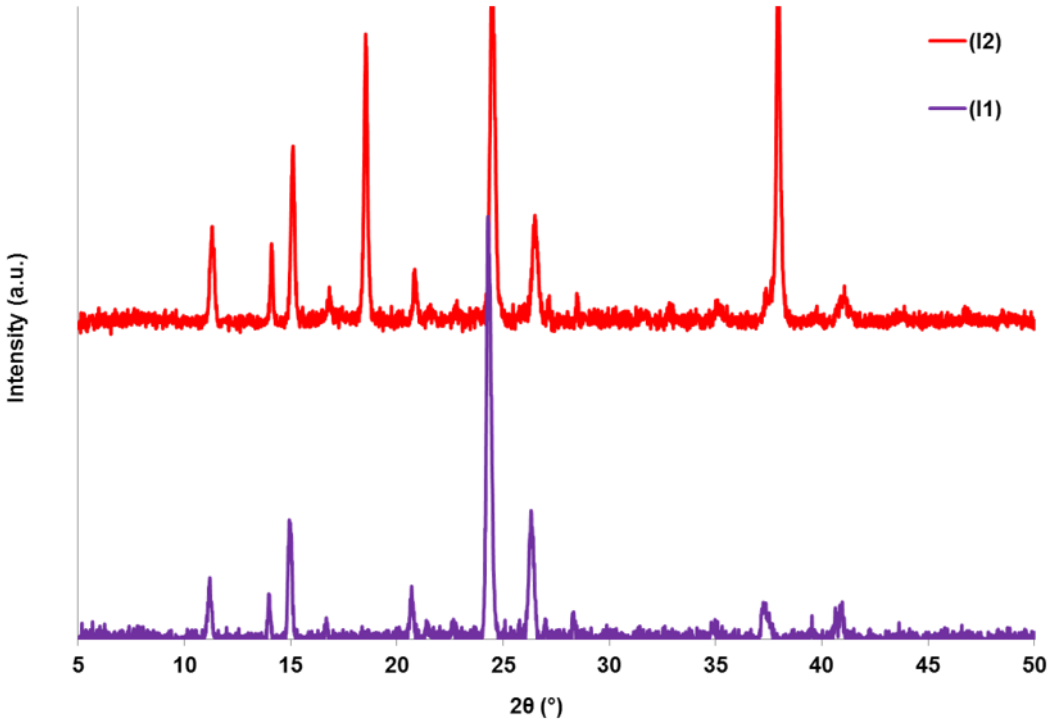

Figure 5.4. PXRD pattern of **(I2)** compared to that of **(I1)**.

Evidence that the TM was produced was obtained from the MS spectrum which indicated an ion of *m/z* 208.0032 suggesting the presence of *pyridine-2-carboxylate-4-carboxylic acid magnesium(II) hydrate*, a fragment of the TM, (see Experimental).

The DSC trace of **(I2)** (Appendix B, Figure A19) shows a large endothermic event at 218.0 °C, at the same temperature at which an endothermic event was observed in the DSC trace of **(I1)**. The melting point of $Mg(OH)_2$ is above 350 °C, eliminating its melt as the origin of this endotherm. Therefore, this provides further evidence that the complex formed in **(I1)** is also present in **(I2)**.

5.2.3. *Reaction of copper(II) sulfate pentahydrate and 2,4-pyridine dicarboxylic acid to give product* **(I3)**

(I3) was prepared as a control, to combine with the diamines in a similar fashion to the group 2 metal/pyridine dicarboxylic acid intermediates. A scaled-down version of the preparation outlined by Noro *et al*.[91] was carried out by stirring a 2:1 stoichiometric mixture of 2,4-pdcam and copper(II) sulfate pentahydrate in methanol and water at lab temperature. The PXRD pattern of the resulting blue powder product is shown in Figure 5.5. It corresponds to the calculated pattern of *bis-(pyridine-2-carboxylato-4-carboxyl)-diaqua-copper(II)* [**NELPEZ02**; CSD V5.35 October 2014].[91] This was further supported by MS, as the spectrum indicated an ion of *m/z* 393.9496 consistent with the presence of *pyridine-2,4-dicarboxylate, pyridine-2-carboxylate,4-carboxylic acid-copper(II)* (see Experimental).

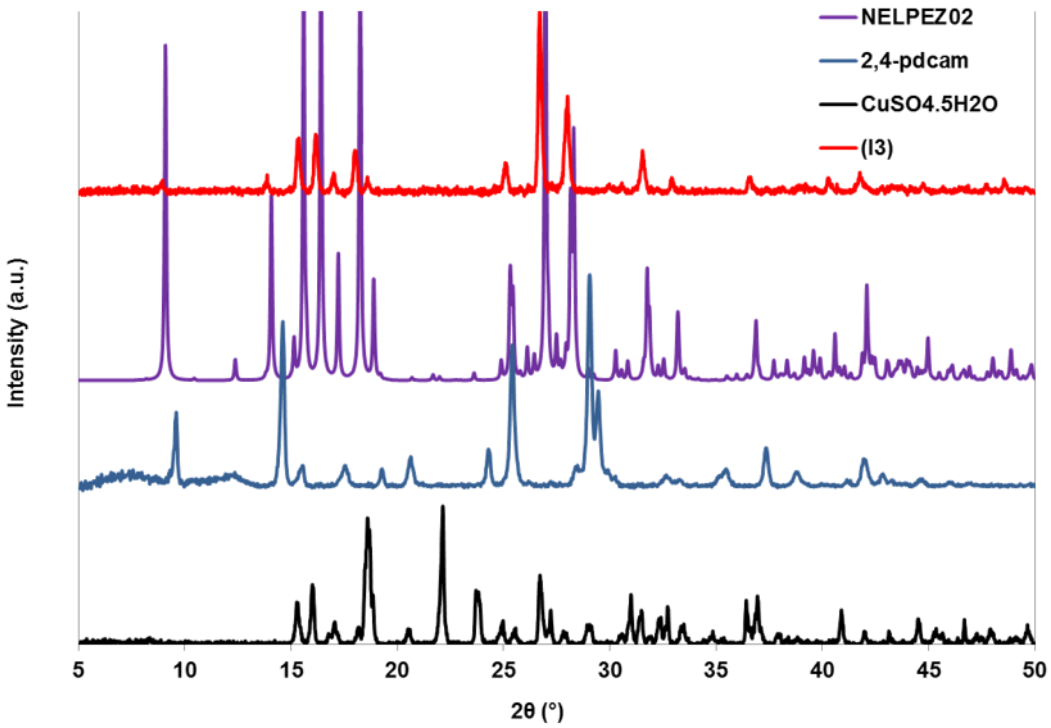

Figure 5.5. PXRD pattern of **(I3)** compared to the calculated pattern of **NELPEZ02** and patterns of the starting materials.

The thermal behaviour of **(I3)** was investigated by DSC (Figure 5.6). The trace shows a small broad endothermic event at 173.7 °C with a shoulder at about 182 °C, followed by a very strong endotherm at 317.1 °C. Neither of these events correspond to the thermal behaviours of the starting materials (2,4-pdcam m.p. 246 – 248 °C; $CuSO_4.5H_2O$ m.p. 110 °C, b.p. 150 °C).

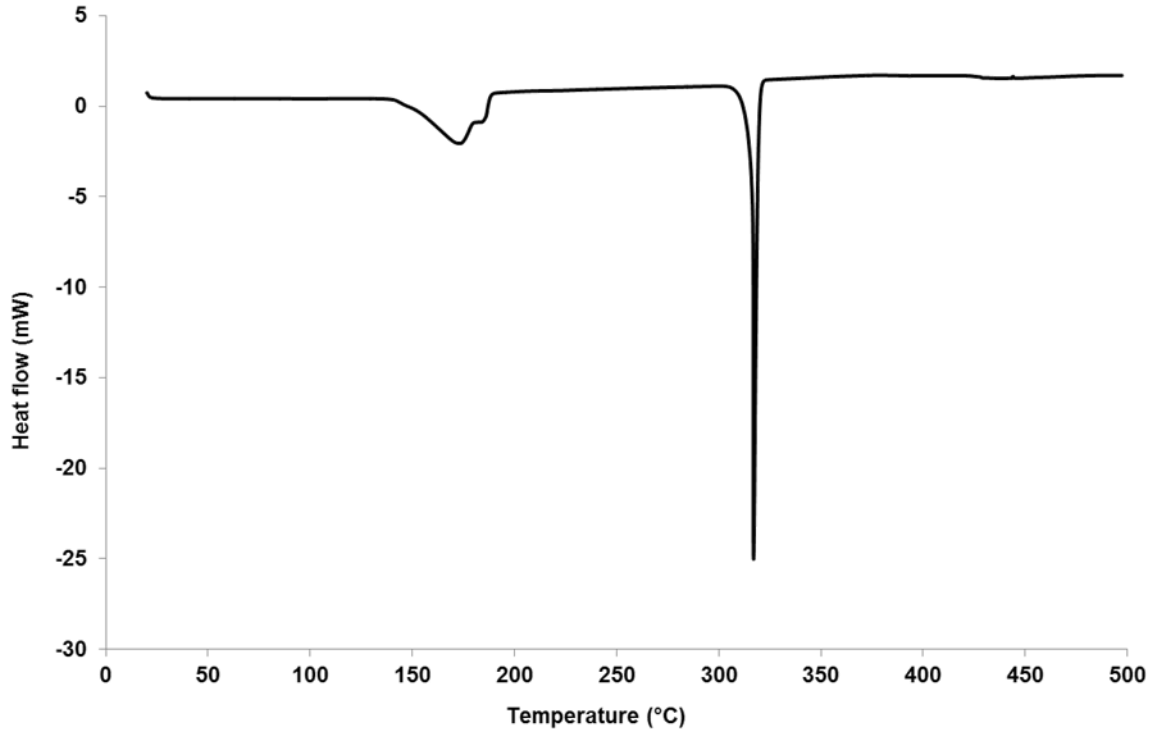

Figure 5.6. DSC trace of **(I3)** on a 1.5 mg sample with a temperature ramp of 10 °C min^{-1}.

5.3. Combination of Intermediates with Diamines

The complexes **(I1)** – **(I3)** (and **(I5)** – **(I7)**) were used in crystallisation experiments in which the intermediate was suspended in a solvent and a solution of a diamine was added. These experiments were carried out in glass vials, which were then either covered with hole-pierced parafilm, or sealed with caps, and then left in the fume hood to crystallise at lab temperature. Two new crystal structures were obtained from these experiments: the organic complex **(15)**, and the copper-organic complex **(16)**. Another crystal structure was obtained by growth from a 1:1 stoichiometric mixture of **(I1)** suspended in ACN and DMF, and an aqueous solution of *m*-xylylenediamine, dissolved with toluene and crystallised at lab temperature. The clear, colourless block crystals amongst a white glue-like substance were found to be an organic complex consisting of a 1:1 ratio of 2,4-pyridine dicarboxylic acid and *m*-xylylenediamine derivatives, however, the structure could not be fully solved in that the hydrogen atoms and an extensively disordered solvent molecule or counter ion could not be modelled. The data were collected again from another crystal but again, the structure could not be solved.

5.3.1. *Bis-(pyridine-2,4-dicarboxylate 3,3'-dimethylbiphenyl-4-amino-4'-ammonium) 3,3'-dimethylbiphenyl-4,4'-diammonium dihydrate* **(15)**

$(C_7H_3NO_2)_2(C_{14}H_{17}N_2)_2(C_{14}H_{18}N_2).2H_2O$

(15) was prepared by growth from a 1:1 stoichiometric mixture of **(I1)** suspended in water, and a methanol solution of *o*-tolidine, dissolved with DMF and toluene at 40 °C, then left at lab temperature. The clear, colourless platelet crystals that grew in solution were found to be purely organic: no magnesium originating from **(I1)** was incorporated into the crystals.

After four months, the solvent had evaporated and the PXRD pattern was obtained from the dry bulk sample (Figure 5.7). The pattern has some peaks consistent with the calculated PXRD pattern of the product **(15)**, at about 18°, 20°, 21°, 22°, 25° and 26°. The calculated pattern of the starting material *o*-tolidine was obtained from the single crystal data [**DADMBP**; CSD V5.35 October 2014].[172]

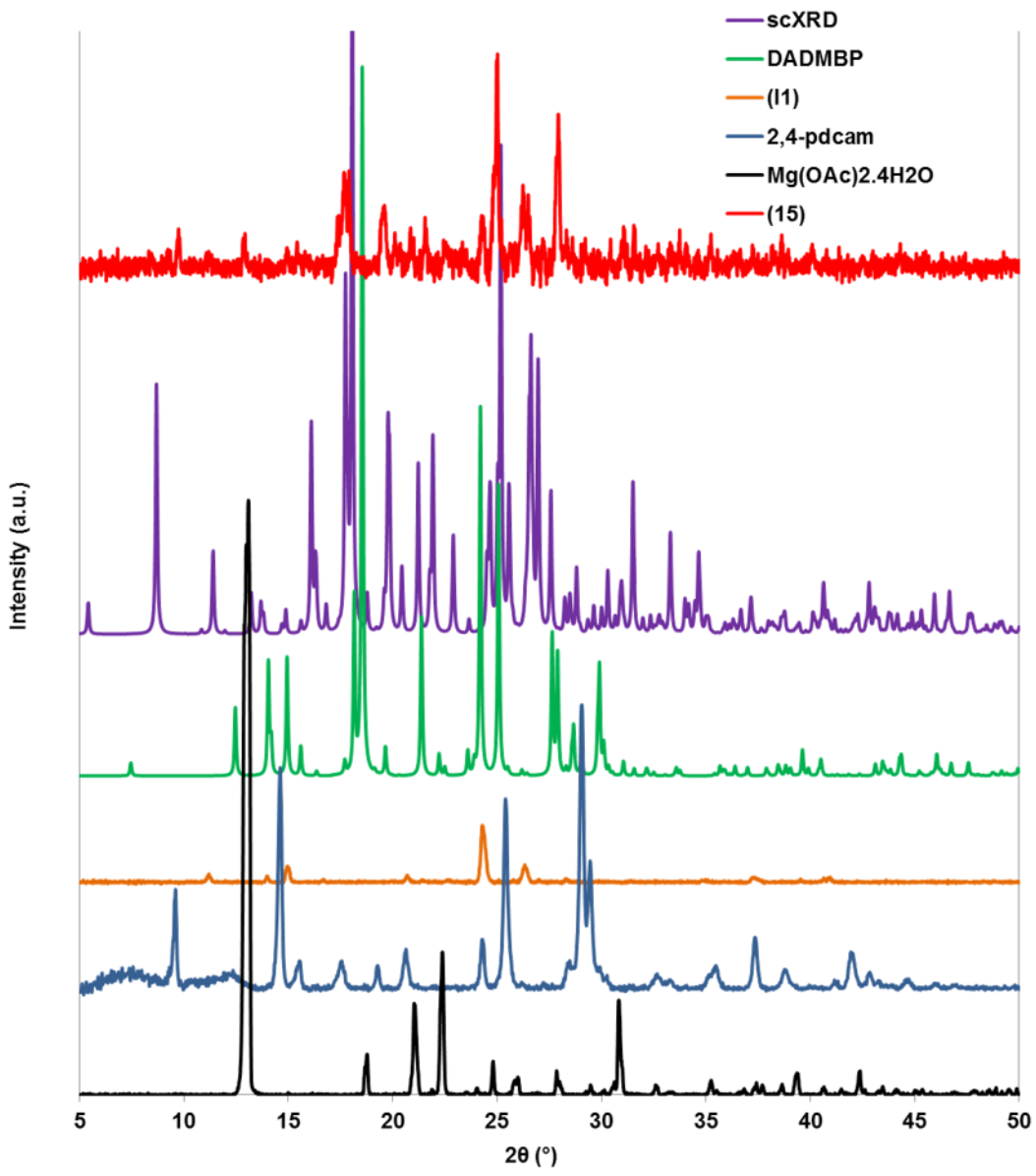

Figure 5.7. PXRD pattern of **(15)** compared to the calculated pattern and patterns of the starting materials.

The asymmetric unit of **(15)** features one 2,4-pyridine dicarboxylate ion, one 3,3'-dimethylbiphenyl-4-amino-4'-ammonium ion, half of one 3,3'-dimethylbiphenyl-4,4'-diammonium ion, and one water molecule. The 3,3'-dimethylbiphenyl-4-amino-4'-ammonium and 3,3'-dimethylbiphenyl-4,4'-diammonium ions are hereafter referred to as tol^{1+} and tol^{2+}, respectively.

The organic molecules of **(15)** are shown in Figure 5.8. One of the carboxylate groups of the 2,4-pyridine dicarboxylate ion has identical C-O distances of 1.256(2) Å for both C26-O3 and C26-O4 indicating the delocalisation of the negative charge. This carboxylate group

has an O-C-O angle of 126.7(2)°, larger than the O=C-O angles of 2,4-pdca in **(A3)** (2,4-pdcam, discussed in Appendix D) at 125.0(2)° and 125.4(2)°. The C-O distances of the other carboxylate group are different to one another at 1.247(2) Å and 1.269(2) Å for C22-O1 and C22-O2, respectively. This group has a smaller O-C-O angle of 124.7(2)°. The carboxylate groups are not coplanar with the pyridyl ring and differ in the degree to which they are twisted from coplanarity. The torsion angle O4-C26-C25-N1 is -9.6(2)°, while that of O2,C22-C23-C27 is much greater in magnitude at 40.4(2)°.

Tol^{1+} and tol^{2+} are oriented differently to each other. In each ion, the aromatic rings are not coplanar and in tol^{2+} they are twisted by -139.3(2)°, as measured by the torsion angle C20-C15-$C15^{a}$-$C20^{a}$. This is comparable to the equivalent torsion angle for *o*-tolidine in the pure form, **DADMBP**, which is about ±142°. In tol^{1+}, one aromatic group is twisted such that the torsion angle C14-C8-C4-C5 is -28.8(2)°, and the methyl substituents are on the same side of the ion.

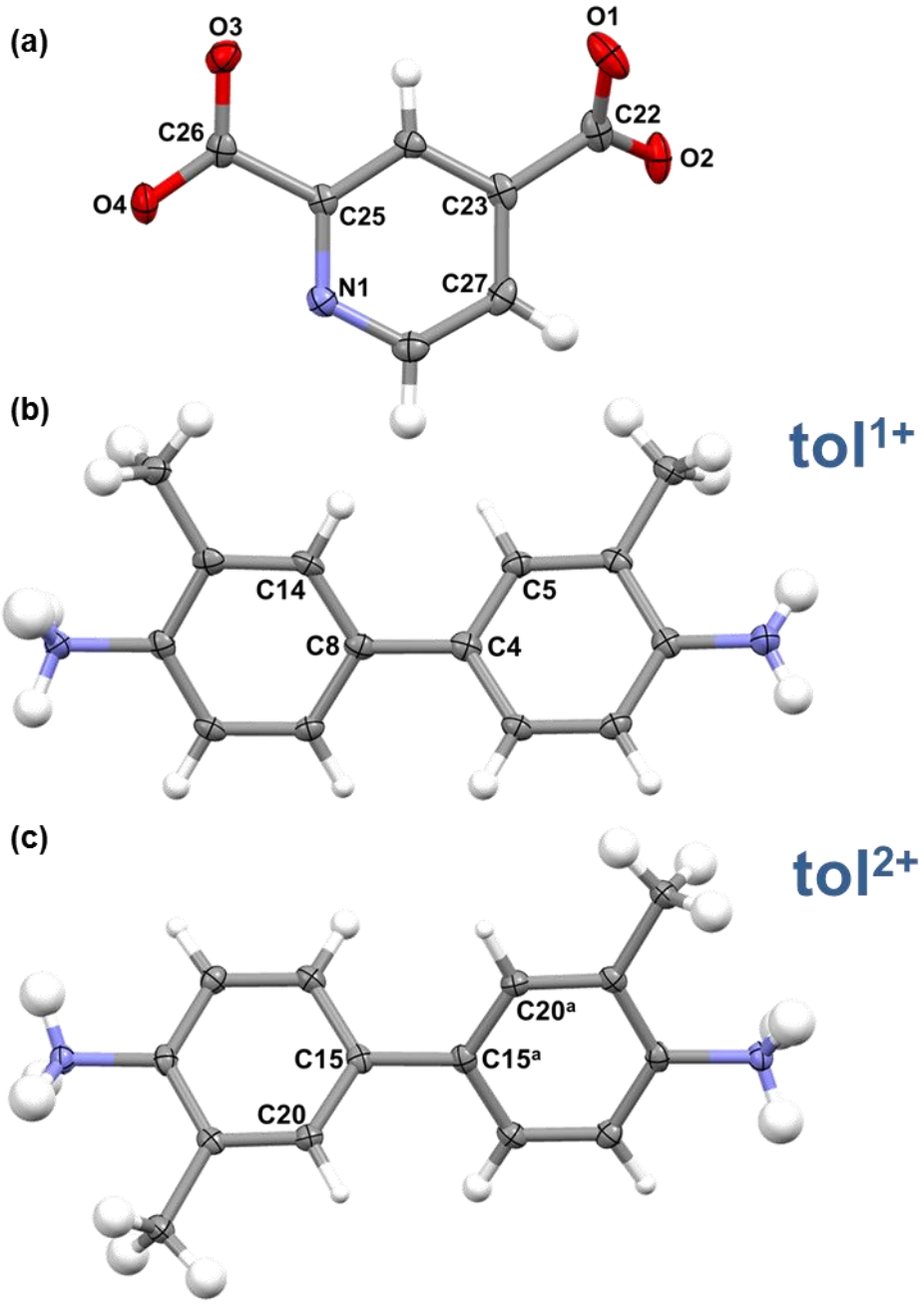

Figure 5.8. Crystal structure of **(15)**. (a) 2,4-pyridine dicarboxylate ion, (b) 3,3'-dimethylbiphenyl-4-amino-4'-ammonium ion, (c) 3,3'-dimethylbiphenyl-4,4'-diammonium ion. Symmetry code: [a](2-x, y, ½-z)

The structure of **(15)** is composed of 2D motifs of tol^{1+} and tol^{2+} ions parallel to the *ab* plane, separated along the *c* direction by 2D motifs of 2,4-pyridine dicarboxylate ions and water molecules, also parallel to the *ab* plane, as shown in Figure 5.9(a). The two motifs are connected by H-bonds from the *o*-tolidine ions to the 2,4-pyridine dicarboxylate ions and

water molecules, and from the water molecules to the 2,4-pyridine dicarboxylate ions (Figure 5.9(b)).

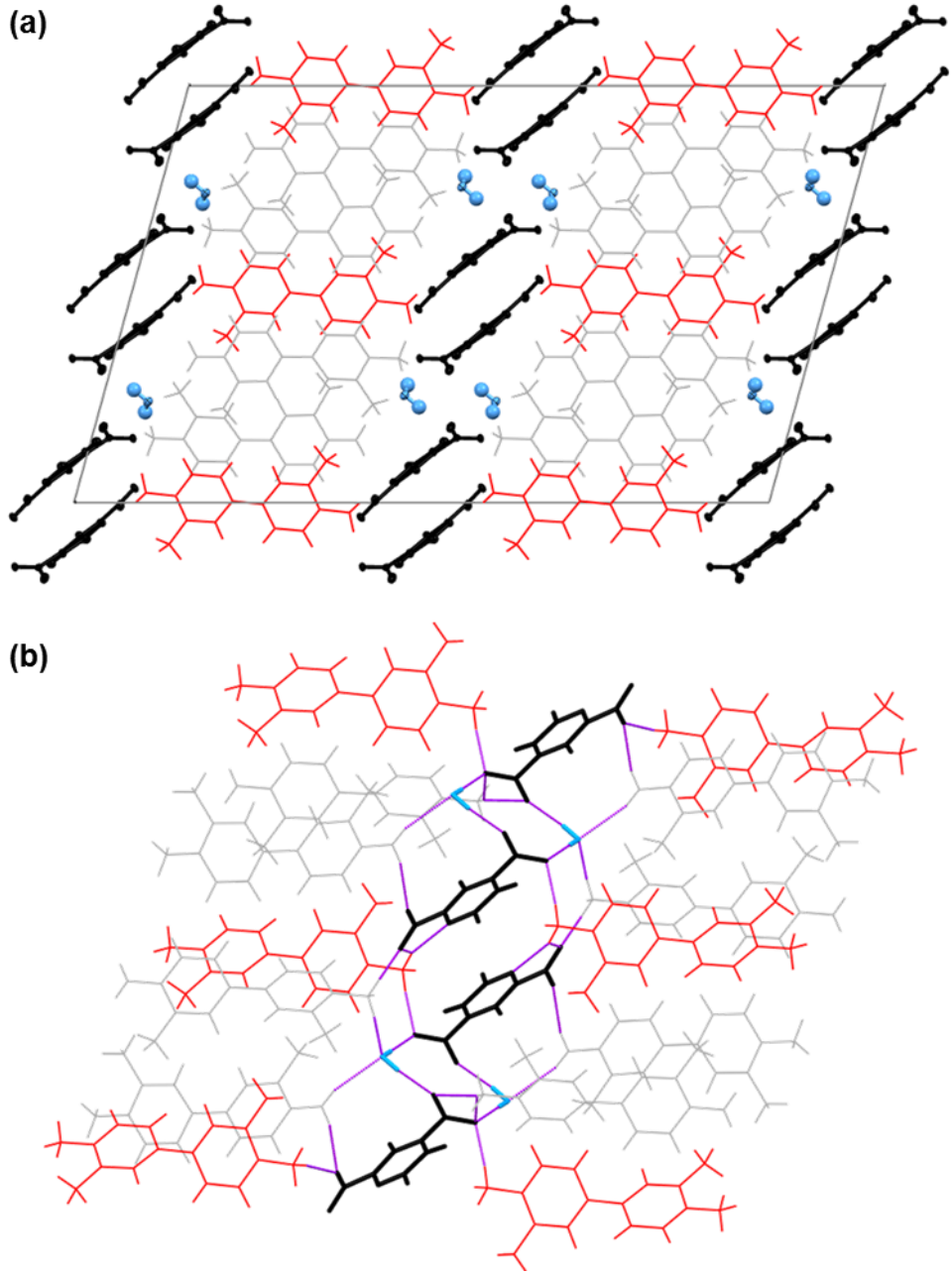

Figure 5.9. Crystal structure of **(15)**. (a) View down the *b* axis showing the global packing. (b) Selected H-bonds between substituents. Colours: 2,4-pyridine dicarboxylate ions (black), water molecules (blue), tol^{1+} (grey) and tol^{2+} (red).

Figure 5.10(a) shows the H-bonds formed from tol^{1+} to three adjacent 2,4-pyridine dicarboxylate ions, and two water molecules, connecting the structure along the *c* direction. The ammonium group forms four H-bonds: H2A is attracted to both carboxylate oxygen

atoms of one carboxylate group of one 2,4-pyridine dicarboxylate ion, and H2B forms an H-bond to one carboxylate oxygen atom of another ion, while H2C forms an H-bond in which the oxygen atom of the water molecule is the acceptor. N2-H2B···O4^{b} is the strongest of the interactions involving this group, with a D···A distance of 2.708(2) Å and a linear geometry with an angle of 179(2)°. The H-bond to water, N2-H2C···O5^{c}, is also a very linear interaction of medium length with a D···A distance of 2.799(2) Å and an angle of 174(2)°. N2-H2A···O1 and N2-H2A···O2 are slightly longer and less directional interactions of D···A distances of 2.871(2) Å and 3.148(2) Å and angles of 139(2)° and 151(2)°, respectively. O2 is also the acceptor to another, weaker H-bond from a methyl group of tol^{1+}. C13-H13B···O2 has a long D···A distance of 3.606(3) Å and an angle of 147(2)°. Similarly, the carboxylate oxygen atom, O4^{b}, is also the acceptor to an H-bond from a C-H group of the anilinium ring: C10-H110···O4^{b} has a shorter D···A distance of 3.411(2) Å but a smaller angle of 129(1)°.

The amine group forms two H-bonds: one in which the oxygen atom of a water molecule is the acceptor, N4-H4B···O5^{e}, and one in which a carboxylate oxygen atom of a 2,4-pyridine dicarboxylate ion is the acceptor, N4-H4A···O3^{d}. N4-H4B···O5^{e} has a longer D···A distance of 3.221(2) Å and a smaller angle of 157(2)° when compared to the H-bond involving the ammonium group and a water molecule, N2-H2C···O5^{c}. Similarly, when comparing N4-H4A···O3^{d} to the H-bond involving the ammonium group and just one carboxylate oxygen atom acceptor, N2-H2B···O4^{b}, N4-H4A···O3^{d} has a longer D···A distance of 3.054(2) Å and a smaller angle of 166(2)°. The apparently greater relative strength of the H-bonds involving the ammonium group when compared to those involving the amine group is likely due to charge-assistance in which both the donor and acceptor groups are charged.

O3^{d} also accepts an H-bond from a C-H group of the aniline ring, C2-H102···O3^{d}, which has comparable geometry to C10-H110···O4^{b}, with D···A distance 3.457(2) Å and angle 139(1)°.

The tol^{2+} ion forms H-bonds to six adjacent 2,4-pyridine dicarboxylate ions connecting the structure along the *c* direction, and to two tol^{1+} ions connecting the structure along the *b* direction. Figure 5.10(b) shows H-bonds to three 2,4-pyridine dicarboxylate ions and one tol^{1+} ion: H-bonds to the remaining ions are generated by 2-fold rotation symmetry. The ammonium group forms four H-bonds: two to carboxylate oxygen atoms of two 2,4-pyridine dicarboxylate ions and one bifurcated H-bond to a carboxylate oxygen atom and the pyridyl nitrogen atom of another ion. N3-H3B···O3^{b} and N3-H3C···O2 are similarly moderate-strong interactions with D···A distance of 2.755(2) Å and 2.793(2) Å and angles of 166(2)° and 163(2)°, respectively. The D···A distances of the bifurcated H-bond are slightly longer and the angles smaller: N3-H3A···O4^{f} has a D···A distance of 2.848(2) Å and an angle of 121(2)°, while N3-H3A···N1^{f} has a D···A distance of 2.961(2) Å and an angle of 155(2)°.

The methyl hydrogen atom, H21C, also interacts, albeit weakly, with $O4^{f}$ and $N1^{f}$. C21-H21C···$O4^{f}$ has a long D···A distance of 3.661(2) Å and a small angle of 137(2)°, while C21-H21C···$N1^{f}$ has a D···A distance of 3.443(2) Å and an angle of 128(2)°. A C-H group of the anilinium ring forms an H-bond to O2: C17-H17···O2 is a moderately weak interaction of D···A distance 3.401(2) Å and an angle of 138(1)°.

Connecting the structure in the *b* direction is the extremely weak H-bond C21-H21B···$N4^{b}$, formed between a methyl group of tol^{2+} to the nitrogen atom of the amine group of tol^{1+}. The length of this interaction is 3.738(3) Å, towards the maximum for a C-H···N H-bond, however the angle of 166(2)° indicates the directionality of this attractive interaction.

Figure 5.10(c) shows the H-bonds formed by the water molecule. The water molecule forms two H-bonds, each to one carboxylate oxygen atom of the same carboxylate group of two 2,4-pyridine dicarboxylate ions, connecting the structure along the *a* direction. O5-H5A···O2 and O5-H5B···$O1^{h}$ are similarly moderate-strong H-bonds with D···A distances of 2.784(2) Å and 2.758(2) Å and large angles of 170(3)° and 168(2)°, respectively.

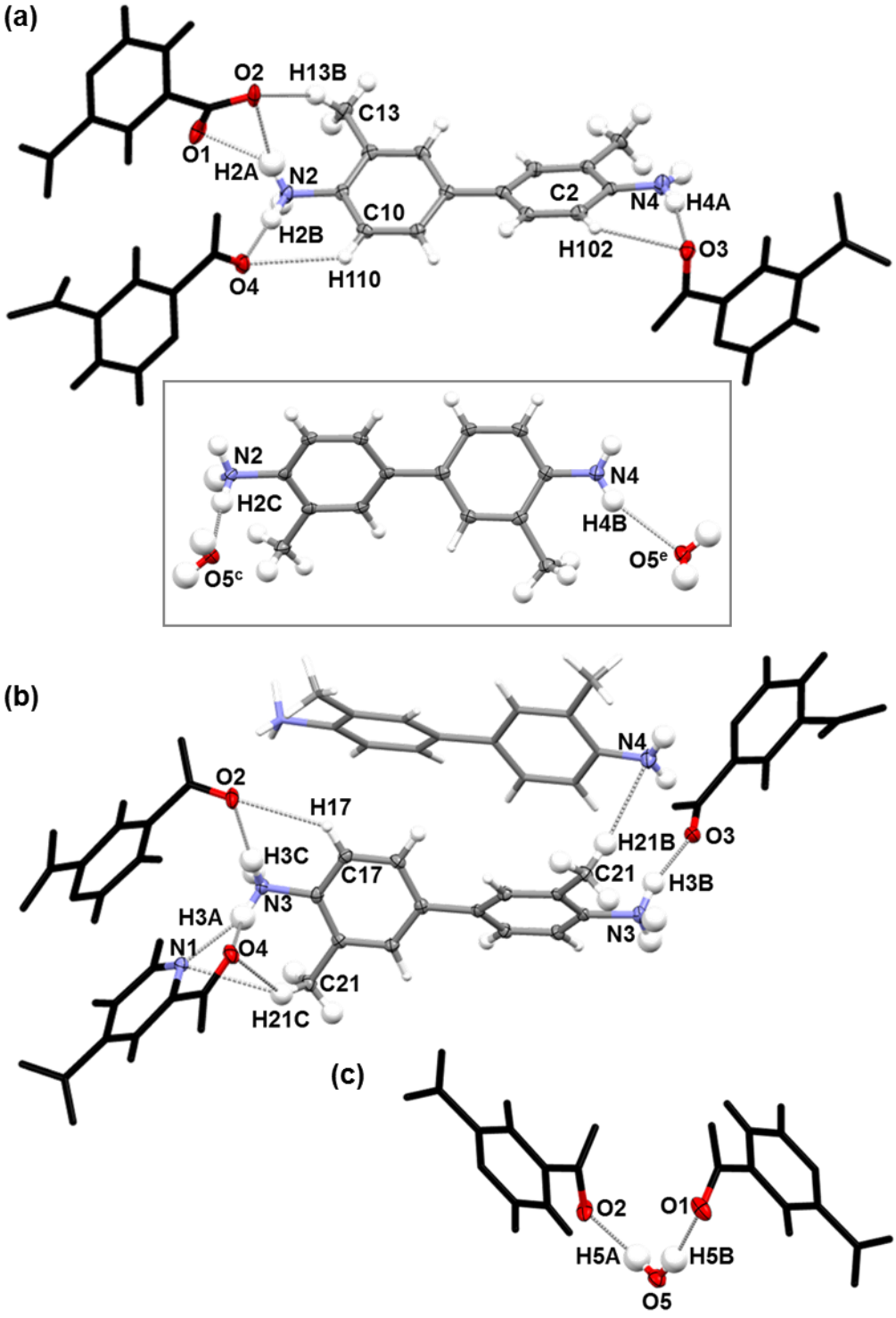

Figure 5.10. Crystal structure of **(15)**. (a) H-bonds from tol^{1+} to three 2,4-pyridine dicarboxylate ions, and two water molecules (inset). (b) H-bonds from tol^{2+} ion to six 2,4-pyridine dicarboxylate ions and two tol^{1+} ions, (only half of the H-bonded ions have been shown for clarity). (c) H-bonds between the water molecule and two 2,4-pyridine dicarboxylate ions. Symmetry codes for selected oxygen atoms: ^{c}(x, 1+y, z) ^{e}(1½-x, ½+y, ½-z)

Table 5.1. Geometries of H-bonds in **(15)**.

D-H···A Interaction	D-H (Å)	H···A (Å)	D···A (Å)	D-H···A (°)
(Figure 5.10(a)) H-bonds from tol^{1+}				
N2-H2A···O1	0.93(3)	2.11(2)	2.871(2)	139(2)
N2-H2A···O2	0.93(3)	2.30(3)	3.148(2)	151(2)
N2-H2B···O4^{b}	0.96(2)	1.75(2)	2.708(2)	179(2)
N2-H2C···O5^{c}	0.95(2)	1.85(2)	2.799(2)	174(2)
N4-H4A···O3^{d}	0.88(2)	2.19(2)	3.054(2)	166(2)
N4-H4B···O5^{e}	0.87(3)	2.40(2)	3.221(2)	157(2)
C2-H102···O3^{d}	0.97(2)	2.67(2)	3.457(2)	139(1)
C10-H110···O4^{b}	0.96(2)	2.72(2)	3.411(2)	129(1)
C13-H13B···O2	0.98(2)	2.74(2)	3.606(3)	147(2)
(Figure 5.10(b)) H-bonds from tol^{2+}				
N3-H3A···O4^{f}	0.96(2)	2.23(2)	2.848(2)	121(2)
N3-H3A···N1^{f}	0.96(2)	2.06(2)	2.961(2)	155(2)
N3-H3B···O3^{b}	0.97(2)	1.81(2)	2.755(2)	166(2)
N3-H3C···O2	0.97(2)	1.85(2)	2.793(2)	163(2)
C17-H17···O2	0.96(2)	2.62(2)	3.401(2)	138(1)
C21-H21B···N4^{b}	0.97(2)	2.79(2)	3.738(3)	166(2)
C21-H21C···O4^{f}	0.99(2)	2.88(2)	3.661(2)	137(2)
C21-H21C···N1^{f}	0.99(2)	2.75(2)	3.443(2)	128(2)
(Figure 5.10(c)) H-bonds from water molecule				
O5-H5A···O2	0.84(3)	1.95(3)	2.784(2)	170(3)
O5-H5B···O1^{h}	0.90(3)	1.87(3)	2.758(2)	168(2)

Symmetry codes: ^{b}(2-x, 1-y, -z) ^{c}(x, 1+y, z) ^{d}(x, 1-y, ½+z) ^{e}(1½-x, ½+y, ½-z) ^{f}(2-x, -y, -z) ^{g}(2-x, y, ½-z) ^{h}(1½-x, ½-y, -z)

Also connecting the structure along the *a* direction, are π-π stacking interactions of 3.936(1) Å between the pyridyl rings of the 2,4-pyridine dicarboxylate ions (Figure 5.11).

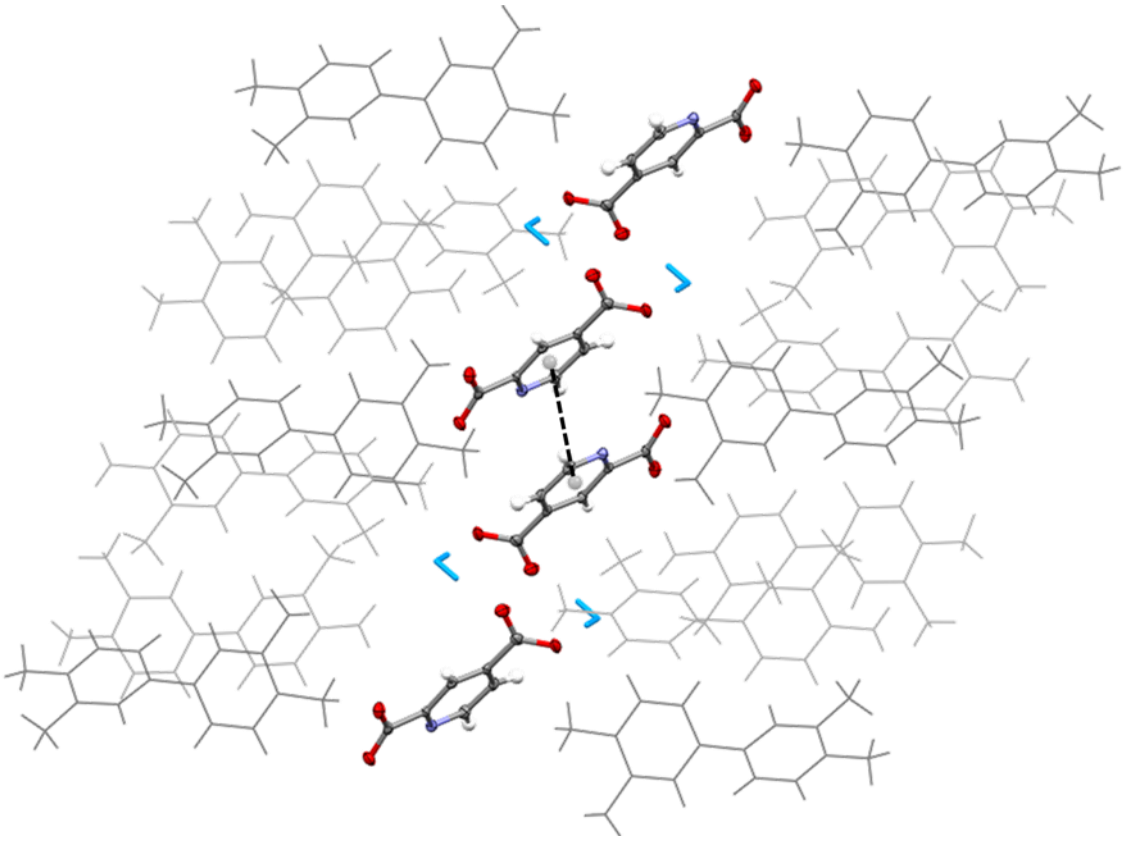

Figure 5.11. Crystal structure of **(15)**, showing π-π interactions between pyridyl rings of 2,4-pyridine dicarboxylate ions.

The thermal behaviour of **(15)** was investigated by HSM and DSC analysis. During HSM, the crystals underwent a phase transformation at about 138 °C during which the crystals smoothened at the corners and edges. This transformation immediately preceded a recrystallisation event between 140 – 148 °C, where small crystalline shards emerged from the original crystals, followed by a final melt at about 164 °C. The DSC trace (Figure 5.12) shows two endothermic events. The first, at 142.7 °C, has the broadest and most intense peak and coincides with the phase transition/recrystallisation event observed in HSM. The next peak, at 160.9 °C, is the melt of **(15)**.

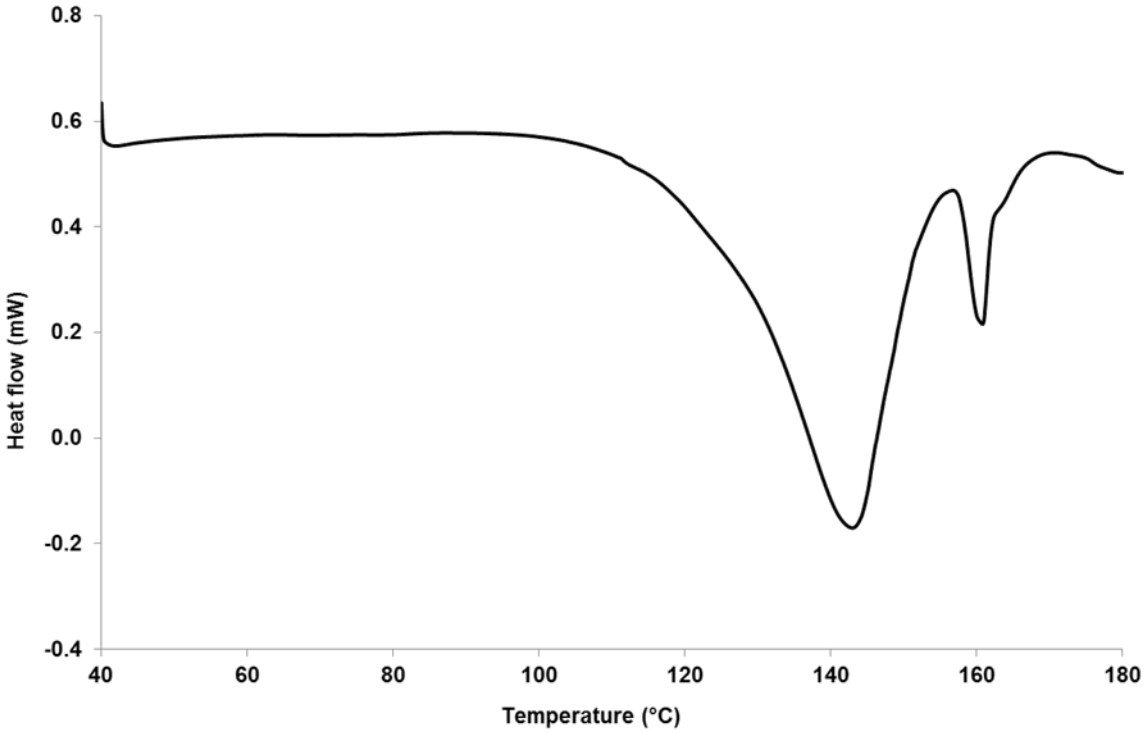

Figure 5.12. DSC trace of **(15)** on a 1.0 mg sample with a temperature ramp of 10 °C min^{-1}.

5.3.2. *1,3-xylylenediammonium bis-(pyridine-2,4-dicarboxylato)-aqua-copper(II) hydrate* **(16)** *$[Cu(C_7H_3NO_4)_2(H_2O)][C_8H_{14}N_2].H_2O$*

After many experiments in which a diamine added to a magnesium or calcium-containing intermediate complex was unsuccessful in producing a new group 2 metal-organic-organic complex, the copper-containing intermediate **(I3)** was combined with both *o*-tolidine and *m*-xylylenediamine in two crystallisation experiments.

(16) was prepared by growth from a 1:1 stoichiometric mixture of **(I3)** suspended in methanol, and an aqueous solution of *m*-xylylenediamine, dissolved with DMF and acetone at 40 °C, then left at lab temperature. Bright blue prismatic crystals formed in solution within nine days. When a methanol solution of *o*-tolidine was used in place of the aqueous solution of *m*-xylylenediamine, the reactants did not dissolve, and only a turbid greenish blue solution with a greyish blue precipitate resulted.

The PXRD pattern of the bulk sample obtained by vacuum filtration is shown in Figure 5.13. The experimentally obtained pattern does not match the calculated pattern.

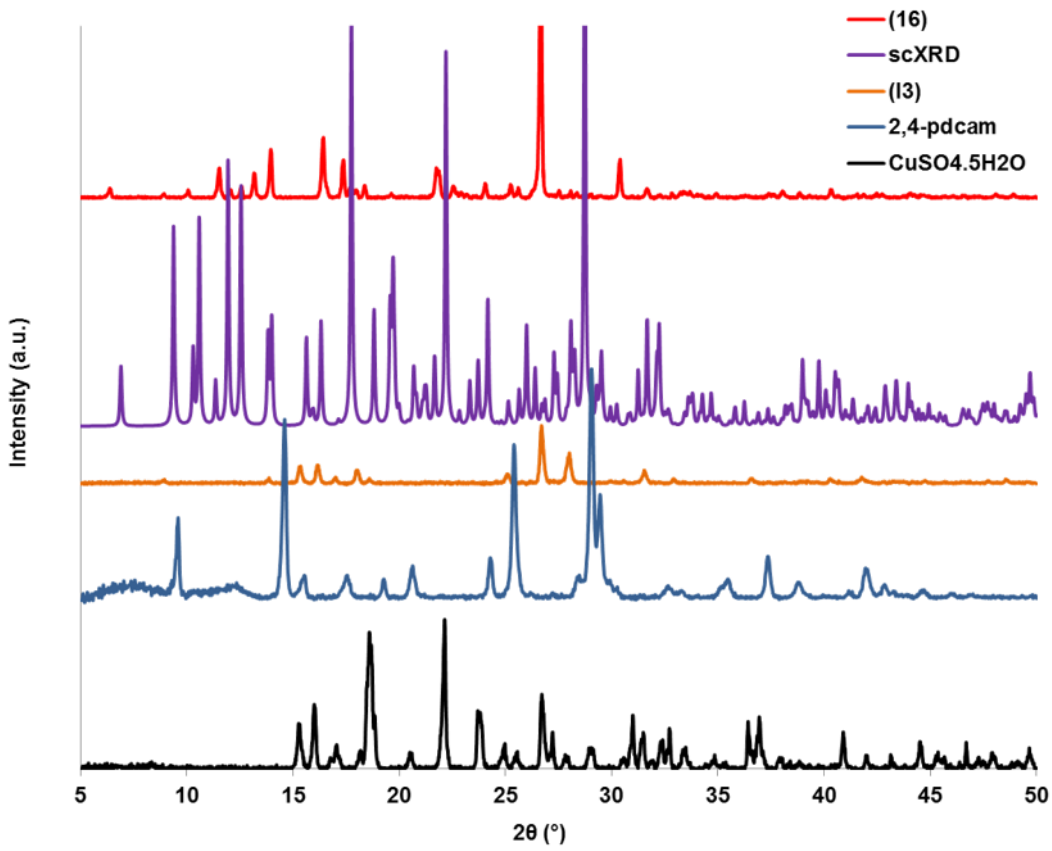

Figure 5.13. PXRD pattern of **(16)** compared to the calculated pattern and patterns of the starting materials.

The formula unit of **(16)** features three components, including one water molecule. The dication is *m*-xylylenediammonium, and the dianion consists of a copper centre N,O-chelated by two crystallographically inequivalent 2,4-pyridine dicarboxylate ligands by coordination *via* both the pyridyl nitrogen atom and one carboxylate oxygen atom. The $[Cu(C_7H_3NO_4)_2(H_2O)]^{2-}$ ion is illustrated in Figure 5.14(a) and its coordination distances and angles are listed in Table 5.2. The copper centre has a square pyramidal geometry. It is coordinated by the 2,4-pyridine dicarboxylate ligands at the equatorial positions and has one axially coordinated water molecule. The coordination distance to the water molecule is the longest at 2.250(2) Å, and those to the nitrogen atoms are the next longest at 1.995(2) Å and 1.992(2) Å for Cu1-N1 and Cu1-N2, respectively. The coordination distances to the carboxylate oxygen atoms are about 0.05 Å shorter than those to the nitrogen atoms, at 1.946(2) Å and 1.952(2) Å for Cu1-O4 and Cu1-O6, respectively. The angles between the water oxygen atom and the four other coordinating atoms show significant variation: O5-Cu1-N1 is 102.49(8)°, while O5-Cu1-O6 is 89.73(8)°. The angles formed between the coordinating nitrogen and oxygen atoms of the same ligand are very similar at 83.59(8)° for

O6-Cu1-N2 and 83.07(9)° for O4-Cu1-N1, while the angles formed between the nitrogen and oxygen atoms of different ligands have a greater difference: N1-Cu1-O6 is 97.84(9)° and N2-Cu1-O4 is 95.11(8)°. The base of the square pyramid is not flat: the angles N1-Cu1-N2 and O4-Cu1-O6 are 162.41(8)° and 178.32(7)°, respectively.

The carboxylate groups of the ligands have a very slightly different geometry depending on whether they are metal-coordinating or peripheral groups. The metal-coordinating groups have angles 125.3(3)° and 125.1(3)° for O6-C8-O7 and O4-C1-O3, respectively; more similar to the O=C-O angles of **(A3)**, (2,4-pdcam, discussed in Appendix D) at 125.0(2)° and 125.4(2)° than the angles of the peripheral groups which are slightly wider at 126.2(3)° for O8-C13-O9 and 126.3(3)° for O1-C6-O2. The metal-coordinating oxygen atoms have the longest C-O distances at 1.295(3) Å for C8-O6 and 1.285(3) Å for C1-O4. The C-O distances involving the non metal-coordinating oxygen atom of the metal-coordinating carboxylate group are shorter at 1.223(3) Å and 1.227(3) Å for C8-O7 and C1-O3, respectively. The C-O distances of the peripheral carboxylate groups show less variation: C6-O1 and C6-O2 are very similar at 1.250(3) Å and 1.257(3) Å, respectively, while the other carboxylate group has a greater difference between the C-O distances at 1.240(3) Å for C13-O8 and 1.276(4) Å for C13-O9, while still being less different than the C-O distances of the metal-coordinating carboxylate groups. The carboxylate groups are not coplanar with the pyridyl ring. The torsion angles for the peripheral carboxylate groups have the lowest and highest magnitudes at -2.5(4)° for O8-C13-C12-C14 and -6.7(4)° for O2-C6-C5-C7. The metal-coordinating carboxylate groups have smaller torsion angles at 4.9(3)° for C6-C8-C9-N2 and -3.1(3)° for O4-C1-C2-N1.

The structure of **(16)** is composed of layers of ions arranged into 2D H-bonded sheets on the {21-2} plane, producing the (21-2) peak in the calculated PXRD pattern at about 29°. The global packing of **(16)** is shown in Figure 5.14(b).

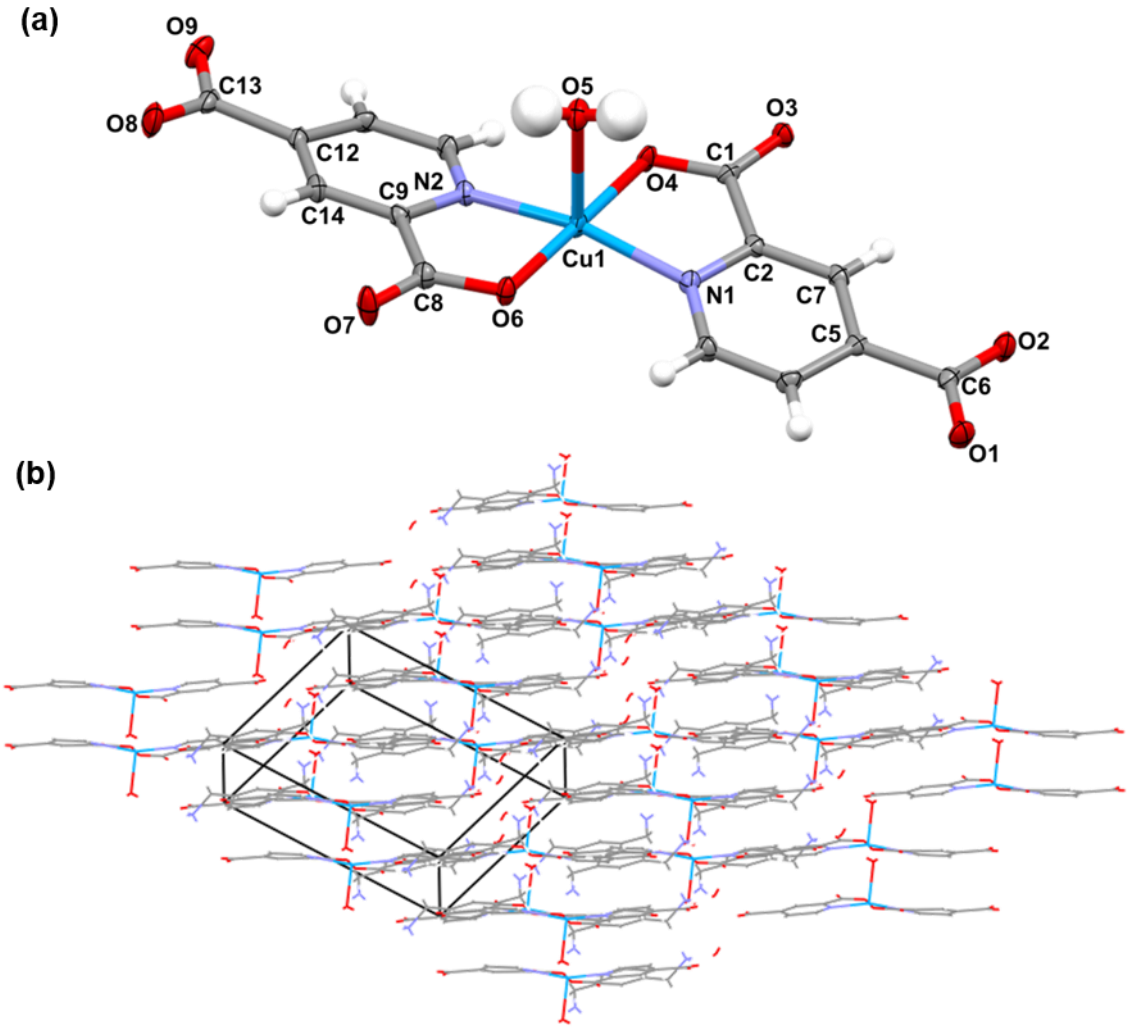

Figure 5.14. Crystal structure of **(16)**. (a) $[Cu(C_7H_3NO_4)_2(H_2O)]^{2-}$ ion showing the square-pyramidal Cu centre with two equatorial N,O-chelating 2,4-pyridine dicarboxylate ligands and one axial water ligand. (b) Global packing showing the layers of ions arranged into 2D H-bonded sheets on the {21-2} plane.

Table 5.2. N/N/O/O-Cu-N/O/N/O angles and Cu-N/O distances in **(16)**.

Coordination	N/N/O/O-Cu-N/O/N/O angle (°)	Interaction	Distance (Å)
O5-Cu1-N1	102.49(8)	Cu1-N1	1.995(2)
O5-Cu1-O6	89.73(8)	Cu1-N2	1.992(2)
O5-Cu1-N2	95.04(8)	Cu1-O4	1.946(2)
O5-Cu1-O4	91.44(8)	Cu1-O5	2.250(2)
N1-Cu1-O6	97.84(9)	Cu1-O6	1.952(2)
O6-Cu1-N2	83.59(8)		
N2-Cu1-O4	95.11(8)		
O4-Cu1-N1	83.07(9)		
N1-Cu1-N2	162.41(8)		
O4-Cu1-O6	178.32(7)		

The 2D H-bonded sheet is shown in Figure 5.15(a). The pattern features alternating chains of *m*-xylylenediammonium ions one ion across, and chains of $[Cu(C_7H_3NO_4)_2(H_2O)]^{2-}$ ions, two ions across, with non-coordinated water molecules situated between the chains. Figure 5.15(b) shows the H-bonding interactions responsible for connecting the ions within the 2D H-bonded sheet, (listed in Table 5.3). H-bonds are formed from the water molecule, and from the *m*-xylylenediammonium ion to the $[Cu(C_7H_3NO_4)_2(H_2O)]^{2-}$ ion, from the *m*-xylylenediammonium ion to the water molecule, and between neighbouring $[Cu(C_7H_3NO_4)_2(H_2O)]^{2-}$ ions. The oxygen atom of the water molecule accepts two H-bonds from crystallographically equivalent ammonium groups from two *m*-xylylenediammonium ions. These are moderately strong H-bonds with D···A distances of 2.924(3) Å and 2.795(4) Å and angles of 145(2)° and 167(3)° for N4-H4B···O10^{c} and N4-H4C···O10^{d}, respectively. The water molecule forms an H-bond to a peripheral carboxylate oxygen atom of a $[Cu(C_7H_3NO_4)_2(H_2O)]^{2-}$ ion. O10-H1B···O1^{a} is a moderately strong H-bond with a D···A distance of 2.782(3) Å and a close-to linear angle of 175(5)°. The *m*-xylylenediammonium ion forms H-bonds directly to the $[Cu(C_7H_3NO_4)_2(H_2O)]^{2-}$ ion *via* one ammonium group, one CH_2 group, and one C-H group of the benzyl ring. N3-H3A···O6^{b} is formed between the ammonium group and the metal-coordinating oxygen atom of the coordinating carboxylate group. It has a D···A distance of 2.897(3) Å and an angle of 153(2)°. C21-H21B···O7^{b} is

formed between a hydrogen of the CH_2 group next to the ammonium group, to the non metal-coordinating oxygen atom of the coordinating carboxylate group. This H-bond has a D···A distance of 3.066(3) Å and a low angle of 131(3)°. This accepting oxygen atom is also featured in the H-bond C19-H19···O7 from a C-H group of the benzyl ring, which has a D···A distance of 3.198(4) Å and an angle of 159°.

The $[Cu(C_7H_3NO_4)_2(H_2O)]^{2-}$ ions are connected along the 2D H-bonded sheet through very weak C-H···O interactions originating from the C-H group of the pyridyl ring to a peripheral carboxylate oxygen atom of a neighbouring $[Cu(C_7H_3NO_4)_2(H_2O)]^{2-}$ ion, related through a centre of inversion. C10-H10···O9^{e} is a very long interaction at 3.771(4) Å, but has a fairly large angle of 161° suggesting that it may be significant.

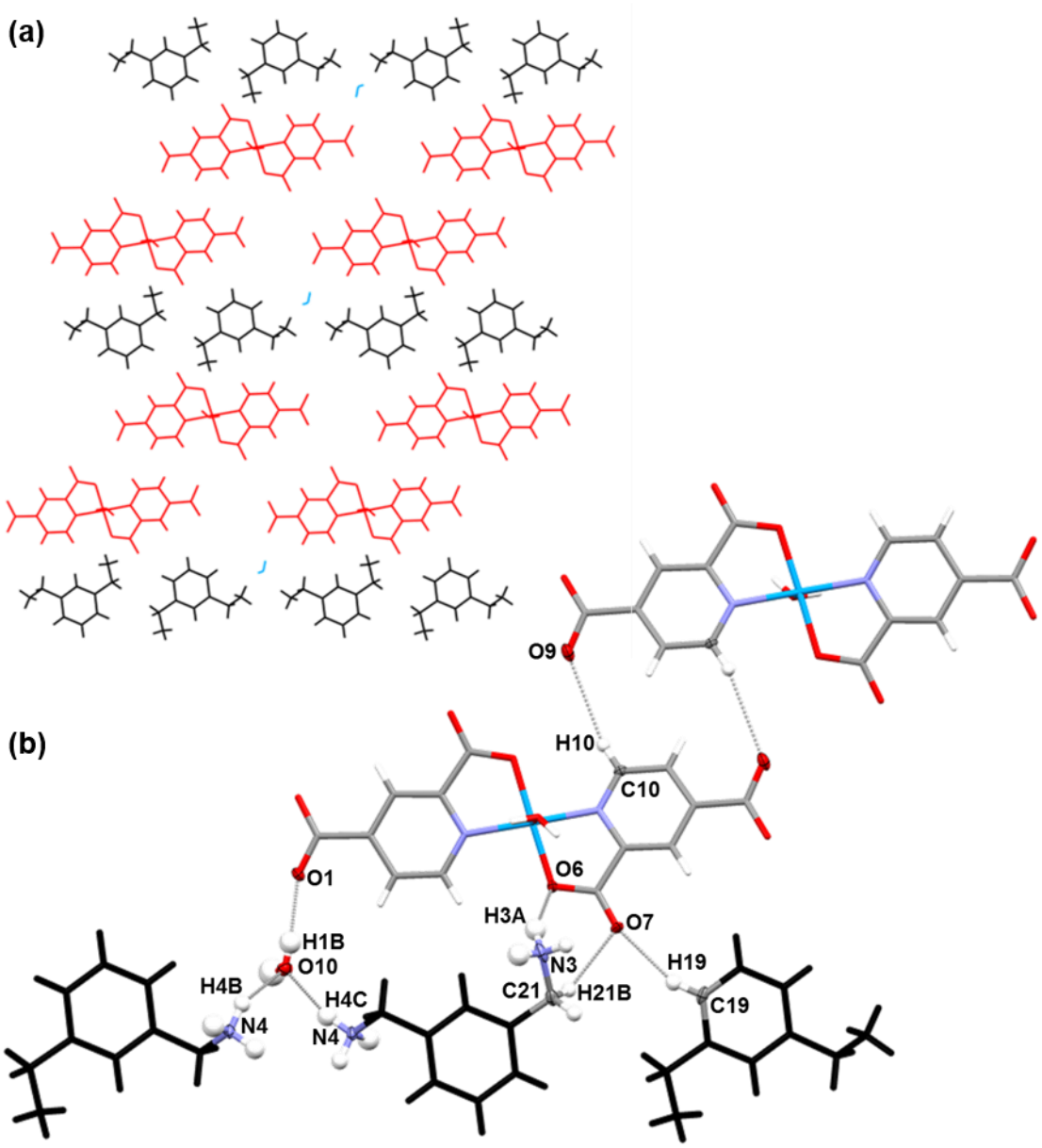

Figure 5.15. Crystal structure of **(16)**. (a) 2D H-bonded sheet. Colours: $[Cu(C_7H_3NO_4)_2(H_2O)]^{2-}$ ions (red), *m*-xylylenediammonium ions (black), water molecules (blue). (b) H-bonds connecting ions and water molecule within the same 2D H-bonded sheet.

The 2D H-bonded sheets are connected to adjacent sheets *via* extensive H-bonding interactions as illustrated in Figure 5.16(a) and listed in Table 5.3. The $[Cu(C_7H_3NO_4)_2(H_2O)]^{2-}$ ion forms two H-bonds to two other $[Cu(C_7H_3NO_4)_2(H_2O)]^{2-}$ ions of the next 2D H-bonded sheet *via* the coordinated water molecule (Figure 5.16(b)). O5-H5A···O1^{f} and O5-H5B···O8^{g} are very similar: in each, the acceptor is an oxygen atom of

the peripheral carboxylate group. O5-H5A···O1[f] has the shorter D···A distance of 2.739(3) Å compared to 2.790(3) Å for O5-H5B···O8[g], but both have angles of approx. 163° (163(4)° for O5-H5A···O1[f] and 163(3)° for O5-H5B···O8[g]).

Figure 5.16(c) shows the H-bonds between sheets formed from the *m*-xylylenediammonium ion and the water molecule. O10-H1A···O2[h] is formed between the water molecule and an oxygen atom of a peripheral carboxylate group, and is moderately strong with a D···A distance of 2.739(4) Å and a large angle of 171(4)°.

There are five charge-assisted H-bonds from the ammonium groups of the *m*-xylylenediammonium ion to the carboxylate oxygen atoms of the $[Cu(C_7H_3NO_4)_2(H_2O)]^{2-}$ ions. This includes a bifurcated H-bond formed by H3C to an oxygen atom of a peripheral carboxylate group (N3-H3C···O2[j]) and to a non metal-coordinating oxygen atom of a metal-coordinating carboxylate group of another $[Cu(C_7H_3NO_4)_2(H_2O)]^{2-}$ ion (N3-H3C···O3[a]). The latter is the stronger of the interactions with a D···A distance of 2.865(3) Å and an angle of 136(2)°, while N3-H3C···O2[j] has a longer D···A distance of 3.280(4) Å and an even lower angle of 128(2)°. H3B forms an H-bond to an oxygen atom of a peripheral carboxylate group of another $[Cu(C_7H_3NO_4)_2(H_2O)]^{2-}$ ion. N3-H3B···O9[j] is among the strongest of the H-bonds in this complex, with a D···A distance of 2.726(4) Å and a large angle of 171(3)°. N4-H4A···O9[d] is formed from the other ammonium group to an oxygen atom of a peripheral carboxylate group of a $[Cu(C_7H_3NO_4)_2(H_2O)]^{2-}$ ion. It is a moderately strong interaction with a D···A distance of 2.821(3) Å and an angle of 154(3)°. N4-H4B···O3[g] is formed to a non metal-coordinating oxygen atom of a metal-coordinating carboxylate group of another $[Cu(C_7H_3NO_4)_2(H_2O)]^{2-}$ ion. It has a similar D···A distance to the comparable interaction N3-H3C···O3[a], of 2.875(4) Å, but unlike N3-H3C···O3[a], it has a very low angle of 104(2)°. This may be due to the fact that N4-H4B is also involved in an H-bond to a water molecule of the same 2D H-bonded sheet, N4-H4B···O10[c].

There is a bifurcated H-bond from a hydrogen atom of a CH_2 group of the *m*-xylylenediammonium ion to carboxylate oxygen atoms of two $[Cu(C_7H_3NO_4)_2(H_2O)]^{2-}$ ions: one is a peripheral carboxylate oxygen atom, C15-H15B···O2[a], and the other is a non metal-coordinating oxygen atom of a metal-coordinating carboxylate group of another $[Cu(C_7H_3NO_4)_2(H_2O)]^{2-}$ ion, C15-H15B···O3[j]. The former has a long D···A distance of 3.666(3) Å and an angle of 141(2)°, while the latter has a shorter D···A distance of 3.088(3) Å but a lower angle of 128(2)°. C21-H21A···O4[a] is formed from a hydrogen atom of a CH_2 group of the other alkyl chain to a metal-coordinating oxygen atom of a $[Cu(C_7H_3NO_4)_2(H_2O)]^{2-}$ ion. It has a D···A distance of 3.278(4) Å and an angle of 132(2)°. C17-H17···O5[g] is formed between a C-H group of the benzyl ring to the coordinating oxygen

atom of a $[Cu(C_7H_3NO_4)_2(H_2O)]^{2-}$ ion, with a D···A distance of 3.456(3) Å and an angle of 147°.

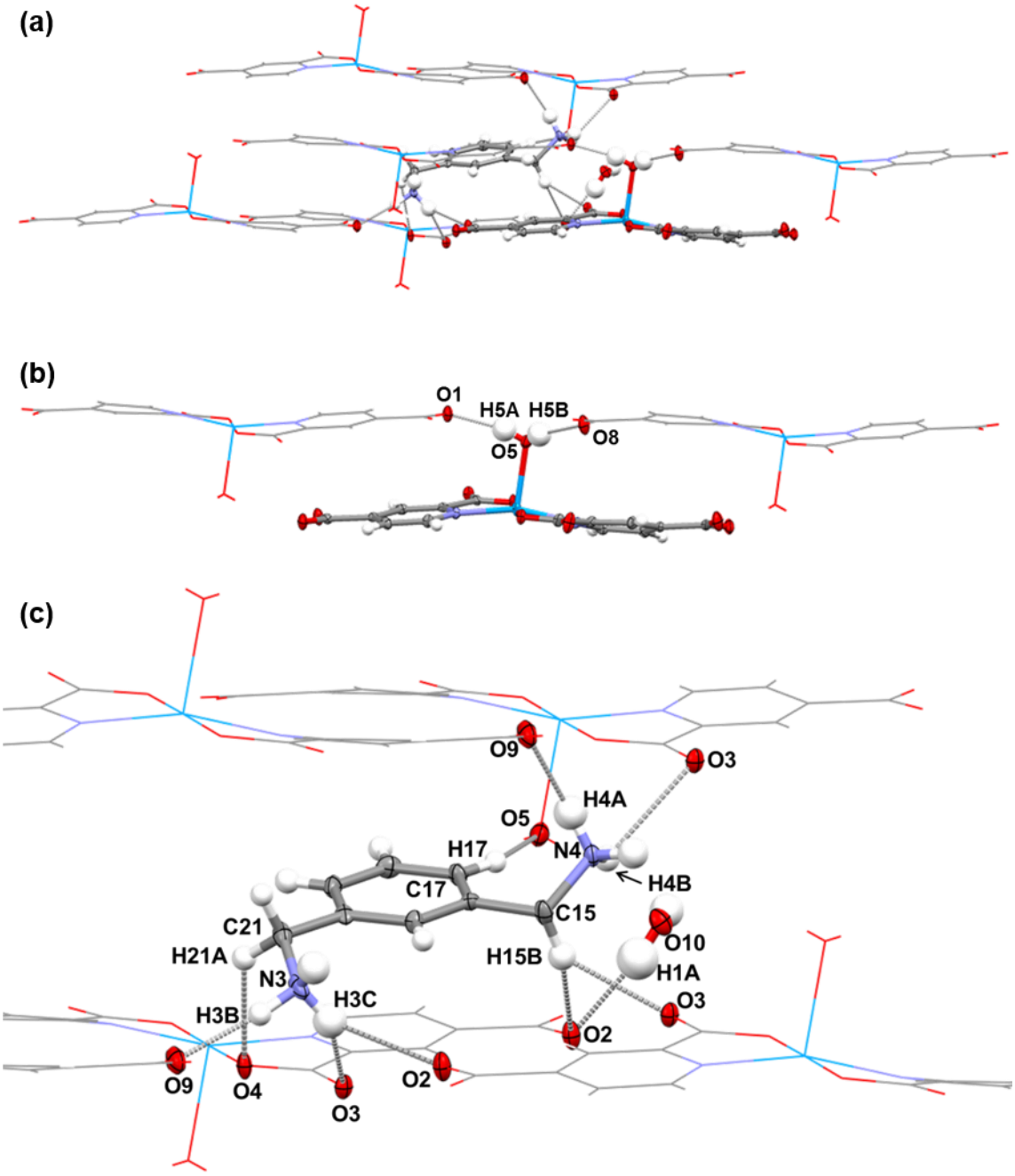

Figure 5.16. Crystal structure of **(16)**. (a) Three adjacent 2D H-bonded sheets. (b) H-bonds originating from the $[Cu(C_7H_3NO_4)_2(H_2O)]^{2-}$ ion shown in ellipsoid setting in (a) connecting between sheets. (c) H-bonds originating from the *m*-xylylenediammonium ion and water molecule shown in ellipsoid setting in (a) connecting between sheets (H15A has been removed for clarity).

Table 5.3. Geometries of H-bonds in **(16)**.

D-H···A Interaction	D-H (Å)	H···A (Å)	D···A (Å)	D-H···A (°)
(Figure 5.15(b)) H-bonds within plane				
O10-H1B···O1[a]	0.78(4)	2.00(4)	2.782(3)	175(5)
N3-H3A···O6[b]	0.91(2)	2.07(2)	2.897(3)	153(2)
N4-H4B···O10[c]	0.91(2)	2.13(2)	2.924(3)	145(2)
N4-H4C···O10[d]	0.92(3)	1.89(3)	2.795(4)	167(3)
*C10-H10···O9[e]	0.93	2.88	3.771(4)	161
*C19-H19···O7	0.93	2.31	3.198(4)	159
C21-H21B···O7[b]	0.98(3)	2.34(3)	3.066(3)	131(3)
(Figure 5.16(b) and (c)) H-bonds between layers				
O5-H5A···O1[f]	0.83(3)	1.94(3)	2.739(3)	163(4)
O5-H5B···O8[g]	0.82(4)	2.00(4)	2.790(3)	163(3)
O10-H1A···O2[h]	0.82(5)	1.93(5)	2.739(4)	171(4)
N3-H3B···O9[i]	0.91(2)	1.82(2)	2.726(4)	171(3)
N3-H3C···O2[j]	0.91(2)	2.64(2)	3.280(4)	128(2)
N3-H3C···O3[a]	0.91(2)	2.14(3)	2.865(3)	136(2)
N4-H4A···O9[d]	0.91(2)	1.98(2)	2.821(3)	154(3)
N4-H4B···O3[g]	0.91(2)	2.51(3)	2.875(4)	104(2)
C15-H15B···O2[a]	0.96(3)	2.86(3)	3.666(3)	141(2)
C15-H15B···O3[j]	0.96(3)	2.40(3)	3.088(3)	128(2)
*C17-H17···O5[g]	0.93	2.64	3.456(3)	147
C21-H21A···O4[a]	1.01(3)	2.52(3)	3.278(4)	132(2)

Symmetry codes: [a](2-x, 1-y, 1-z) [b](2-x, -y, 1-z) [c](1-x, 1-y, -z) [d](x, -1+y, z) [e](1-x, 2-y, 1-z) [f](2-x, 1-y, 2-z) [g](1-x, 1-y, 1-z) [h](-1+x, y, -1+z) [i](1+x, -1+y, z) [j](x, -1+y, -1+z) *H-bond features aromatic hydrogen atom fixed in idealised position.

HSM and DSC analysis were used to characterise the thermal behaviour of **(16)**. During HSM, the crystal underwent a phase transformation very abruptly between 148 °C and 149 °C, blackening as it lost crystallinity. The material then started to bubble but did not melt on heating to 350 °C. Afterwards, the material was still blue, but had become extremely brittle and had lost crystallinity. The DSC trace (Appendix B, Figure A21) shows two endothermic events: one broad and relatively weak peak at 128.3 °C, and a strong, intense peak at 270.7 °C. A similar pattern of events was observed in the DSC trace of the starting material **(I3)**, however the peaks are at higher temperatures, (173.7 °C and 317.1 °C).

5.4. Combining 2,4-Pyridine Dicarboxylic Acid and Magnesium Salts

In order to obtain a crystal structure of the intermediate complex **(I1)** to confirm its identity as that of the magnesium analogue of the TM (Figure 5.1) or not, **(I1)** was dissolved in a range of solvent systems in an attempt to recrystallise the complex to grow crystals suitable for scXRD. Evaporative crystallisation experiments were set up but these did not yield any crystals suitable for diffraction.

Further crystallisation experiments were prepared combining magnesium and calcium salts with both 2,4-pdcam and 3,5-pdca. These experiments included both evaporative and vapour diffusion techniques, and were carried out under a range of temperatures.

One new material synthesised form these experiments was **(A3)**: a complex of pure 2,4-pyridine dicarboxylic acid monohydrate. A crystal structure of this hydrate has previously been reported by Sander *et al*,[140] but in the reported structure [**SUTVEJ**; CSD V5.35 October 2014], 2,4-pdca is in its zwitterionic form, with the *ortho*- carboxyl group deprotonated and the pyridyl nitrogen protonated, whereas in **(A3)** the complex is neutral. **(A3)** is reported in full in Appendix D.

5.4.1. *Reaction of magnesium(II) nitrate hexahydrate and 2,4-pyridine dicarboxylic acid monohydrate to give product* **(I4)**

(I4) was prepared by solvent evaporation of a 1:1 stoichiometric mixture of 2,4-pdcam and magnesium(II) nitrate hexahydrate dissolved in methanol at 30 °C. The visually homogeneous, clear, colourless crystalline shards that were produced were found to be too low in quality to allow scXRD data to be obtained. The crystallisation experiment was also carried out using different solvents (water, ethanol, isopropanol, ACN, THF, acetone and ethyl acetate), using a 2:1 stoichiometric mixture of 2,4-pdcam and magnesium(II) nitrate hexahydrate, and by crystallising at lab temperature or 40 °C. Of these various

experiments, four resulted in clear, colourless crystals of the starting material magnesium(II) nitrate hexahydrate. The PXRD pattern of **(I4)** is shown in Figure 5.17. It matches neither of the patterns of the staring materials, with unique peaks at about 7° and 16.5°.The PXRD pattern is also compared to those of the complexes **(17)**, **(18)** and **(19)** (Appendix B, Figure A23), to the previously reported complexes *bis-[(μ$_2$-pyridine-2,4-dicarboxylato)-triaqua-magnesium(II)]* [**SUYLEE01**; CSD V5.35 October 2014][97] and *bis-(pyridinium-2,4-dicarboxylato)-diaqua-magnesium(II)*[171] [**ZIMJIQ**; CSD V5.35 October 2014] (Appendix B, Figure A24) and to **(I1)**, **(A3)** and **SUTVEJ** (Appendix B, Figure A25), to check whether it was a previously prepared material, a known complex consisting of 2,4-pyridine dicarboxylate and magnesium or if it was 2,4-pdca monohydrate in the form of **(A3)**, or in the same zwitterionic form as in **SUTVEJ**. The PXRD pattern of **(I4)** does not however, show a striking similarity to any of these other potentially formed complexes, except the strong peak at about 24.5° does match with a peak in the PXRD pattern of **(I1)**, however this is the only instance where these two patterns agree.

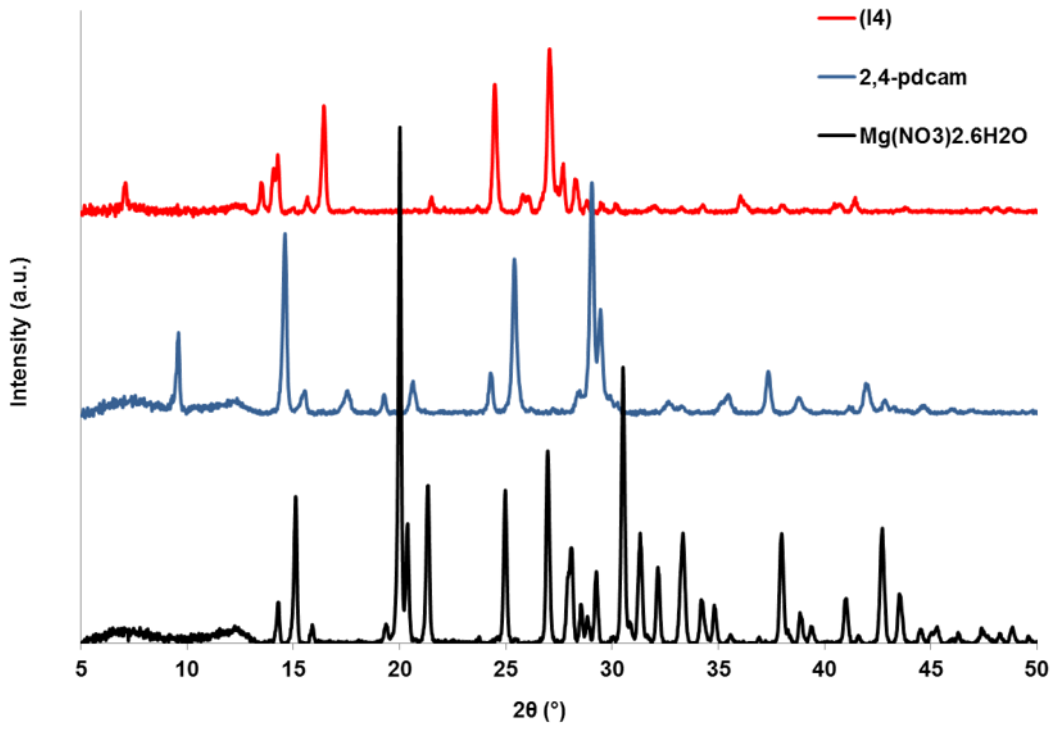

Figure 5.17. PXRD pattern of **(I4)** compared to the patterns of the starting materials.

The DSC trace of **(I4)** is shown in Figure 5.18. There is a strong endotherm at 124.5 °C with a shoulder at 160.9 °C, followed by another endotherm at 260.1 °C. None of these peaks match the melting points of either of the starting materials: $(Mg(NO_3)_2.6H_2O$ m.p. 89 °C; 2,4-

pdcam m.p 246 – 248 °C). These endothermic events provide more evidence that **(I4)** is a new complex, as opposed to a physical mixture of the starting components.

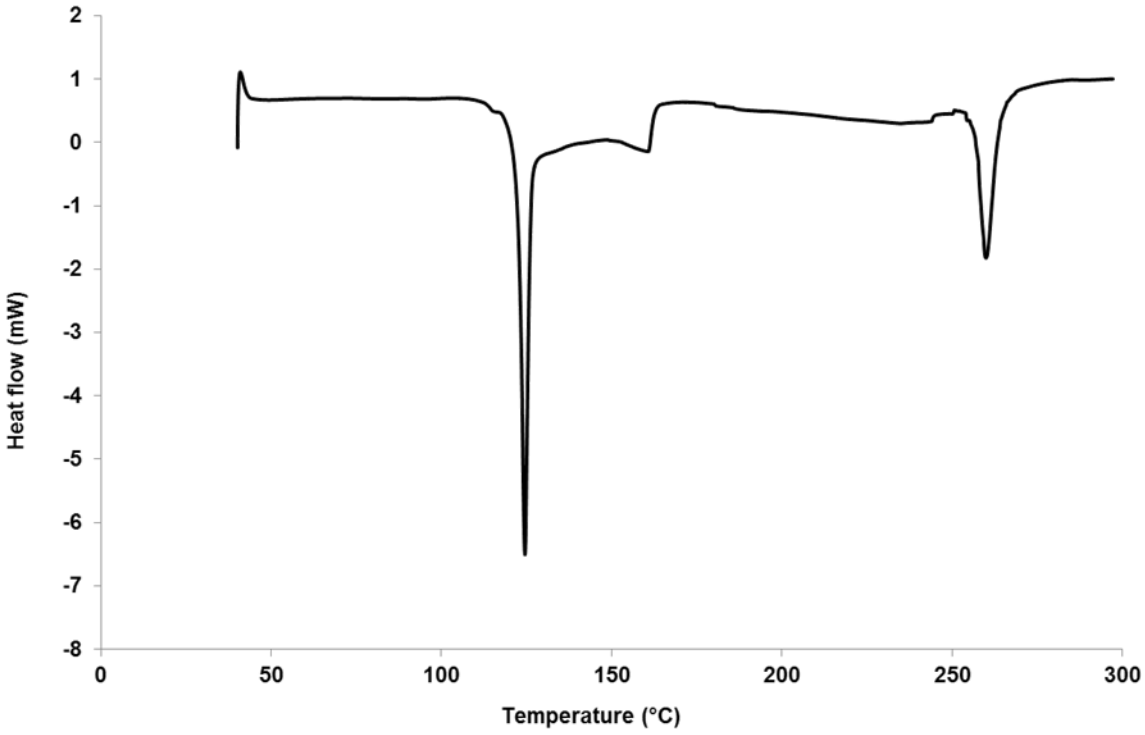

Figure 5.18. DSC trace of **(I4)** on a 1.5 mg sample with a temperature ramp of 10 °C min^{-1}.

The IR spectra of **(I4)** and 2,4-pdcam are compared in Figure 5.19. The broad absorption band at 3511 cm^{-1} in the spectrum of 2,4-pdcam corresponds to O-H stretching which may originate from the carboxyl group or water. This band is absent in the spectrum of **(I4)**, therefore the carboxyl group may have become deprotonated and the material may not feature water. The C=O absorption band at 1759 cm^{-1} in the spectrum of 2,4-pdcam has become much sharper and has shifted to the lower frequency of 1685 cm^{-1} in the spectrum of **(I4)**, indicating that the C=O bond has become more polarised, i.e. the oxygen atom may be coordinated to a metal centre.

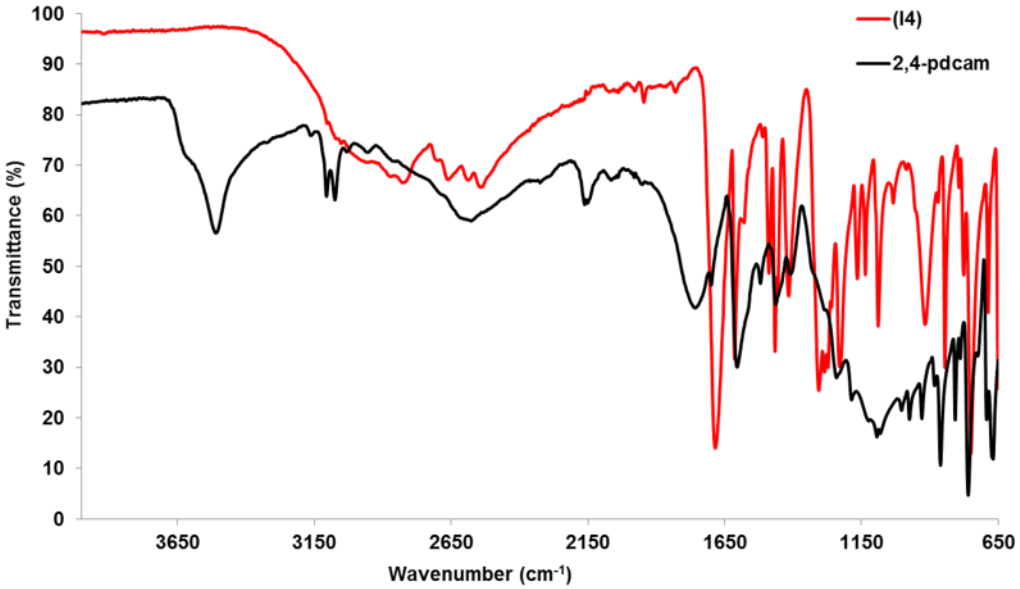

Figure 5.19. IR spectrum of **(I4)** compared to that of 2,4-pdcam.

5.4.2. *Pyridine-2,4-dicarboxylato-tetraaqua-magnesium(II) hemihydrate* **(17)**

$[Mg(C_7H_3NO_4)(H_2O)_4].0.5H_2O$

The PXRD pattern, thermal behaviour (as monitored by DSC) and the IR spectra of **(I4)** suggest that this material is a new complex. Therefore, **(I4)** was used as an 'intermediate' starting material to be combined with a diamine to produce a new magnesium-organic-organic complex. **(I4)** was re-dissolved in methanol in the vial in which it was originally produced, and to this an aqueous solution of *m*-xylylenediamine was added (see Experimental) and the mixture left to crystallise by solvent evaporation at 50 °C. Small, rounded, clear, colourless platelet crystals of **(17)** formed within one week (Figure 5.21(a)). Crystals of this complex were also obtained from further experiments under a range of conditions when combining a diamine with a previously prepared magnesium intermediate complex (see Experimental).

Once the solvent had evaporated (from the original evaporative crystallisation experiment that produced crystals of **(17)**), the PXRD pattern was obtained for the bulk material, shown in Figure 5.20. The PXRD pattern of **(17)** matches the calculated pattern very well, suggesting that the single crystal is a good representation of the bulk sample. The pattern does not match the PXRD patterns of either the intermediate or the original starting materials.[#]

[#] *m*-xylylenediamine is a liquid at room temperature and so the PXRD pattern of this starting material is not included in any Figure.

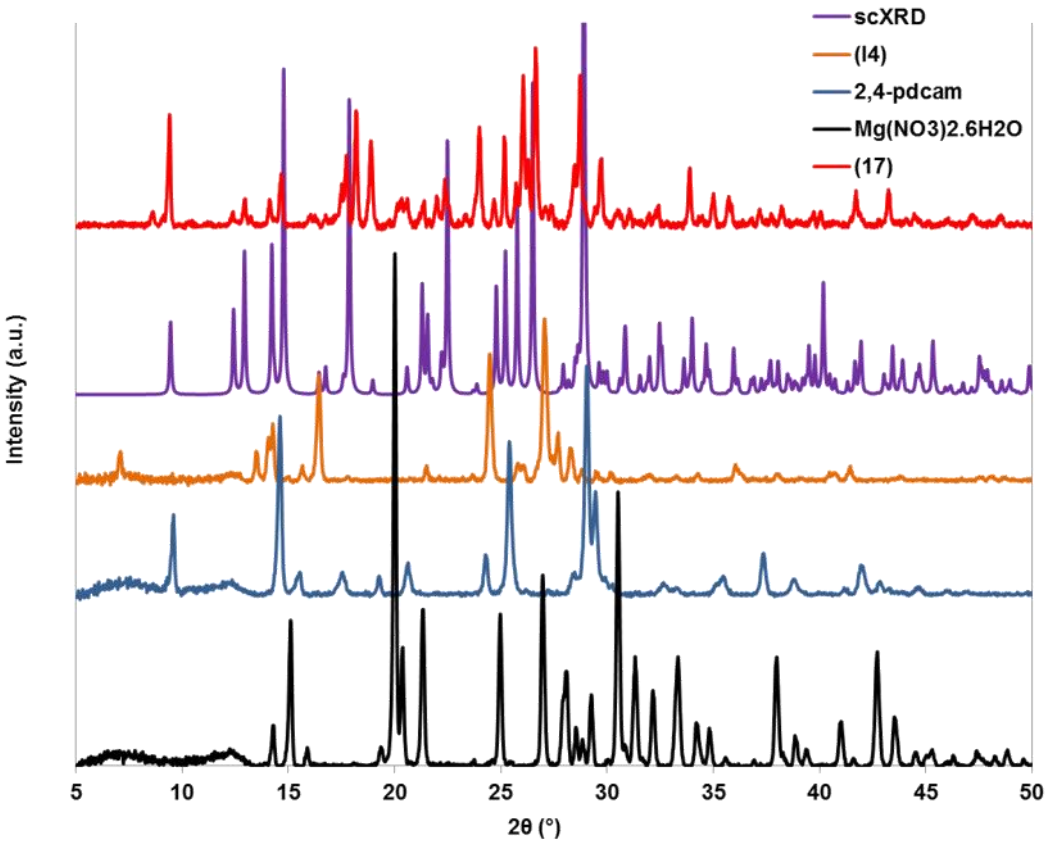

Figure 5.20. PXRD pattern of **(17)** compared to the calculated pattern and patterns of the starting materials including **(I4)**.

The structure of **(17)** is 0D in that it is composed of discrete units of the asymmetric unit (Figure 5.21(b)). The asymmetric unit consists of a magnesium centre, N,O-chelated by one 2,4-pyridine dicarboxylate ligand by coordination *via* both the pyridyl nitrogen atom (N1) and one carboxylate oxygen atom (O1). There are four coordinated water molecules and half a non-coordinated water molecule, 50:50 disordered over an inversion centre. The magnesium centre is in a distorted octahedral environment (Table 5.4) with O-Mg-O/N angles ranging from 76.1(1)° for O1-Mg1-N1, formed between the two coordinating atoms of the chelating 2,4-pyridine dicarboxylate ligand, to 97.6(2)° and 97.5(1)° for O3-Mg1-O5 and O4-Mg1-N1, respectively, the former being the angle formed between two coordinating water atoms *trans* to the smallest angle formed by the chelating ligand. The longest coordination distance is that from the pyridyl nitrogen atom at 2.203(4) Å. The coordination distance from the carboxylate oxygen atom, Mg1-O1, is shorter at 2.066(3) Å, which is comparable to the coordination distance of Mg1-O4, where O4 is the oxygen of a

coordinating water molecule, at 2.067(3) Å. The other coordination distances from water oxygen atoms are 2.092(3) Å for Mg1-O2, 2.050(4) Å for Mg1-O5 and 2.024(4) Å for Mg1-O3.

The metal-organic unit of **(17)** is similar to that of **UFAPEX** (Figure 1.9(a)), except in the latter, the magnesium centre is N,O-chelated by two picoliniate ligands rather than one 2,4-pyridine dicarboxylate ligand. The Mg-O and Mg-N distances follow a similar pattern however, in that the Mg-N distances are the longest at 2.222(1) Å and 2.205(1) Å, and the Mg-O distances to the carboxylate and water oxygen atoms are shorter.

The geometries of the carboxylate groups of the 2,4-pyridine dicarboxylate ligand in **(17)** vary slightly. There is a greater difference between the C-O bond distances for the metal-coordinated carboxylate group: C6-O1 is 1.284(5) Å, and C6-O6 is 1.236(5) Å. The other carboxylate group has distances of 1.259(5) Å and 1.272(5) Å for C7-O7 and C7-O8, respectively. In both cases, the C-O bond distances in each carboxylate group are longer, and shorter, than the C=O and C-OH bond distances, respectively, as was observed for 2,4-pdca in **(A3)**, indicating the delocalisation of the negative charge. Both carboxylate groups have similar O-C-O angles of 125.0(4)° for O1-C6-O6 and 124.8(4)° for O7-C7-O8, both of which are comparable to the O=C-O angles of 2,4-pdca in **(A3)** (at 125.0(2)° and 125.4(2)°). However, both of these angles are smaller than the O-C-O angle of the carboxylate group of the zwitterionic 2,4-pdca molecule in **SUTVEJ** at 128.5(3)°.

The carboxylate groups are both twisted from coplanarity with the pyridyl ring – to a lesser extent for the metal-coordinated carboxylate group. The torsion angle of O1-C6-C5-N1 is -6.7(6)°, and that of O8-C7-C3-C4 is -12.2(6)°.

The structure of **(17)** can be described as layered, with the $Mg(C_7H_3NO)_2(H_2O)_4$ units aligning parallel to the {-204} plane (Figure 5.21(c)). The $Mg(C_7H_3NO)_2(H_2O)_4$ units form 2D H-bonded layers along the {002} plane, through which run the 2_1 screw axes with the non-coordinated, disordered water molecules residing between these layers.

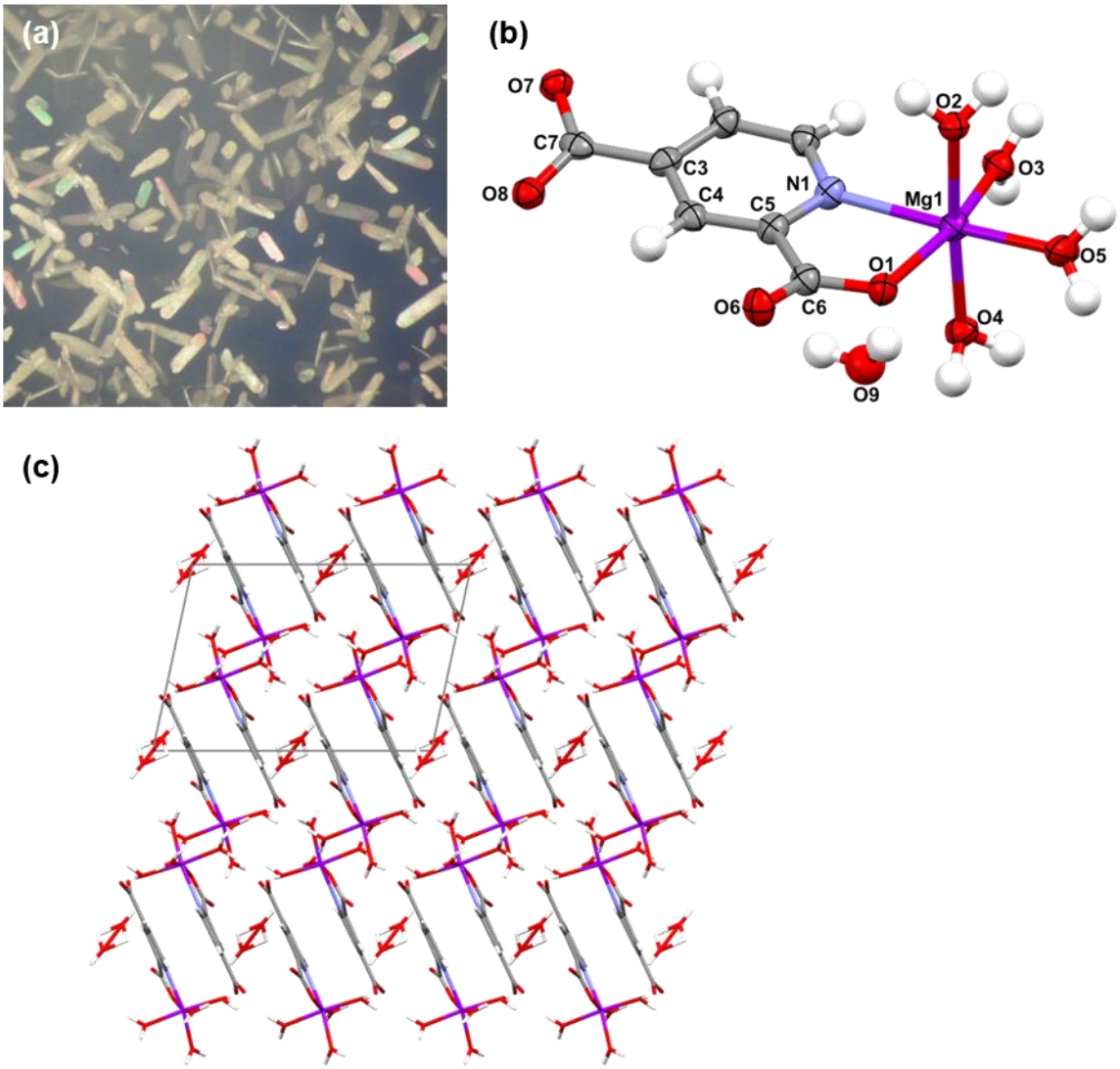

Figure 5.21. Crystal structure of **(17)**. (a) Crystals of **(17)** in solution. (b) Asymmetric unit showing the Mg centre with four coordinating water molecules and one N,O-chelating 2,4-pyridine dicarboxylate ligand, and non-coordinated 50:50 disordered water molecule. (c) View down the *b* axis showing the global packing of **(17)**.

Table 5.4. O-Mg-O/N angles and Mg-N/O distances in **(17)**.

Coordination	O-Mg-O/N angle (°)	Interaction	Distance (Å)
O3-Mg1-O5	97.6(2)	Mg1-O3	2.024(4)
O5-Mg1-O1	96.3(2)	Mg1-O5	2.050(4)
O3-Mg1-O4	88.5(1)	Mg1-O1	2.066(3)
O5-Mg1-O4	91.2(2)	Mg1-O4	2.067(3)
O1-Mg1-O4	88.0(1)	Mg1-O2	2.092(3)
O3-Mg1-O2	94.5(1)	Mg1-N1	2.203(4)
O5-Mg1-O2	83.4(1)		
O1-Mg1-O2	90.3(1)		
O3-Mg1-N1	90.7(2)		
O1-Mg1-N1	76.1(1)		
O4-Mg1-N1	97.5(1)		
O2-Mg1-N1	87.5(1)		

Each $Mg(C_7H_3NO)_2(H_2O)_4$ unit forms H-bonds to six neighbouring $Mg(C_7H_3NO)_2(H_2O)_4$ units *via* the coordinated water ligands, and in one case also *via* an H-bond form a C-H group of the pyridyl ring. It also forms two H-bonds to two non-coordinated, disordered water molecules *via* C-H groups of the pyridyl ring.

Figure 5.22(a) shows five $Mg(C_7H_3NO)_2(H_2O)_4$ units of the same 2D H-bonded layer motif along the {002} plane and the H-bonds connecting between them (listed in Table 5.5). All four of the coordinated water molecules form H-bonds, and in four of these interactions, carboxylate oxygen atoms are the acceptors. O5-H5A forms a bifurcated H-bond to two carboxylate oxygen atoms: one metal-coordinated oxygen atom in O5-H5A···O1^a, and its carboxylate group pair in O5-H5A···O6^a. The latter is the stronger interaction due to its shorter D···A distance of 2.742(5) Å and large angle of 178(8)°, compared to the former's longer D···A distance of 3.470(5) Å and smaller angle of 129(6)°. The oxygen atom O1^a is the acceptor in two other H-bonds: O2-H2B···O1^a of 2.708(4) Å and 152(7)°, and the second weakest of the three H-bonds formed by O3-H3A: O3-H3A···O1^a has a D···A distance of 3.291(5) Å and an angle of 126(5)°. O3-H3A also interacts with the oxygen atoms of two water molecules coordinated to the same Mg centre as O1^a. These

interactions are different in their strengths although both are formed between water molecules. O3-H3A···O2[a] is stronger with a D···A distance of 2.817(4) Å and angle of 158(7)° compared to O3-H3A···O5[a] with a D···A distance of 3.503(5) Å and angle of 124(5)°.

O3-H3B···O8[b] and O4-H4B···O7[c] both form moderately strong interactions to the different carboxylate oxygen atoms of the non metal-coordinating carboxylate group of two $Mg(C_7H_3NO)_2(H_2O)_4$ units. O3-H3B···O8[b] has the shorter D···A distance of 2.687(4) Å and an angle of 169(8)°, while O4-H4B···O7[c] has the longer distance of 2.776(4) Å and an angle of 177(7)°. A weak H-bond is formed from a C-H group of the pyridyl ring to the oxygen atom of a coordinated water molecule of the same $Mg(C_7H_3NO)_2(H_2O)_4$ unit as that which accepts the H-bond O3-H3B···O8[b]. Although C2-H2···O4[b] has a long D···A distance of 3.699(6) Å, it has an angle of 150(3)° which is comparable to the angles of the stronger interactions O2-H2B···O1[a] and O3-H3A···O2[a].

The H-bonds connecting between the $Mg(C_7H_3NO_4)(H_2O)_4$ units along the *c* direction are illustrated in Figure 5.22(b) (and listed in Table 5.5). O2-H2A forms a bifurcated H-bond to both of the carboxylate oxygen atoms of the non metal-coordinating carboxylate group of another $Mg(C_7H_3NO_4)(H_2O)_4$ unit. O2-H2A···O7[d] is the stronger component of this interaction with a D···A distance of 2.696(4) Å and an angle of 162(8)°. O2-H2A···O8[d] on the other hand has a longer D···A distance of 3.395(4) Å and a smaller angle of 136(5)°. O4-H4A···O5[e] is formed between two coordinated water molecules of neighbouring $Mg(C_7H_3NO_4)(H_2O)_4$ units along the *c* direction and O5-H5B···O8[f] is formed between a coordinated water molecule and a carboxylate oxygen atom of the non metal-coordinating carboxylate group of another $Mg(C_7H_3NO_4)(H_2O)_4$ unit along the *c* direction. O5-H5B···O8[f] has a shorter D···A distance of 2.629(5) Å and an almost linear angle of 176(7)°, whereas O4-H4A···O5[e] has a longer D···A distance of 3.196(5) Å and a smaller angle of 142(7)°. The difference in their strengths is likely due to the fact that O5-H5B···O8[f] involves an acceptor atom on which there is a delocalised negative charge, whereas in O4-H4A···O5[e] the acceptor is a neutral atom.

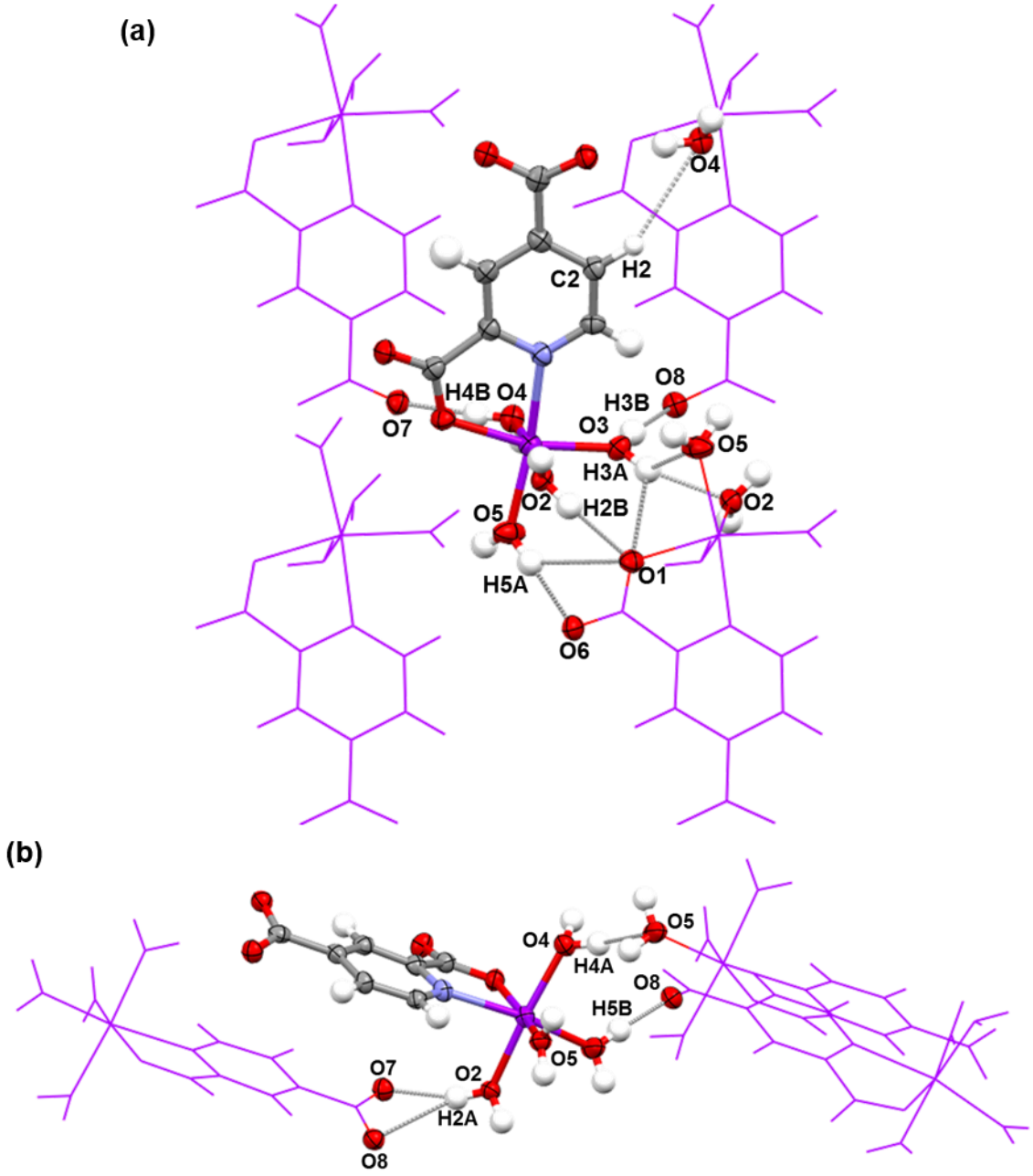

Figure 5.22. Crystal structure of **(17)**. H-bonds connecting directly between $Mg(C_7H_3NO_4)(H_2O)_4$ units (a) within the 2D H-bonded layers along the {002} plane, as viewed down the *c* axis, and (b) along the *c* direction. Only H-bonds originating from the central molecule (ellipsoids, coloured by element) are shown.

The non-coordinated, disordered water molecule connects the $Mg(C_7H_3NO_4)(H_2O)_4$ units along the *c* and *b* directions as shown in Figure 5.23(a) and (b), respectively, (listed in Table 5.5). The water molecule forms H-bonds from each H atom to a coordinated water molecule, O9-H9A···O4, and to a non-coordinated carboxylate oxygen atom of the

coordinating carboxylate group, O9-H9B···O6[b]. These are moderately strong interactions with D···A distances and angles of 2.701(9) Å and 154(14)° for O9-H9A···O4, and 2.806(9) Å and 153(13)° for O9-H9B···O6[b]. The $Mg(C_7H_3NO_4)(H_2O)_4$ units form two H-bonds to adjacent water molecules *via* two C-H groups of the pyridyl ring. These are weak interactions with D···A distances of 3.326(9) Å and 3.228(9) Å and angles of 147(3)° and 155(5)°, for C2-H2···O9[b] and C4-H4···O9[c], respectively.

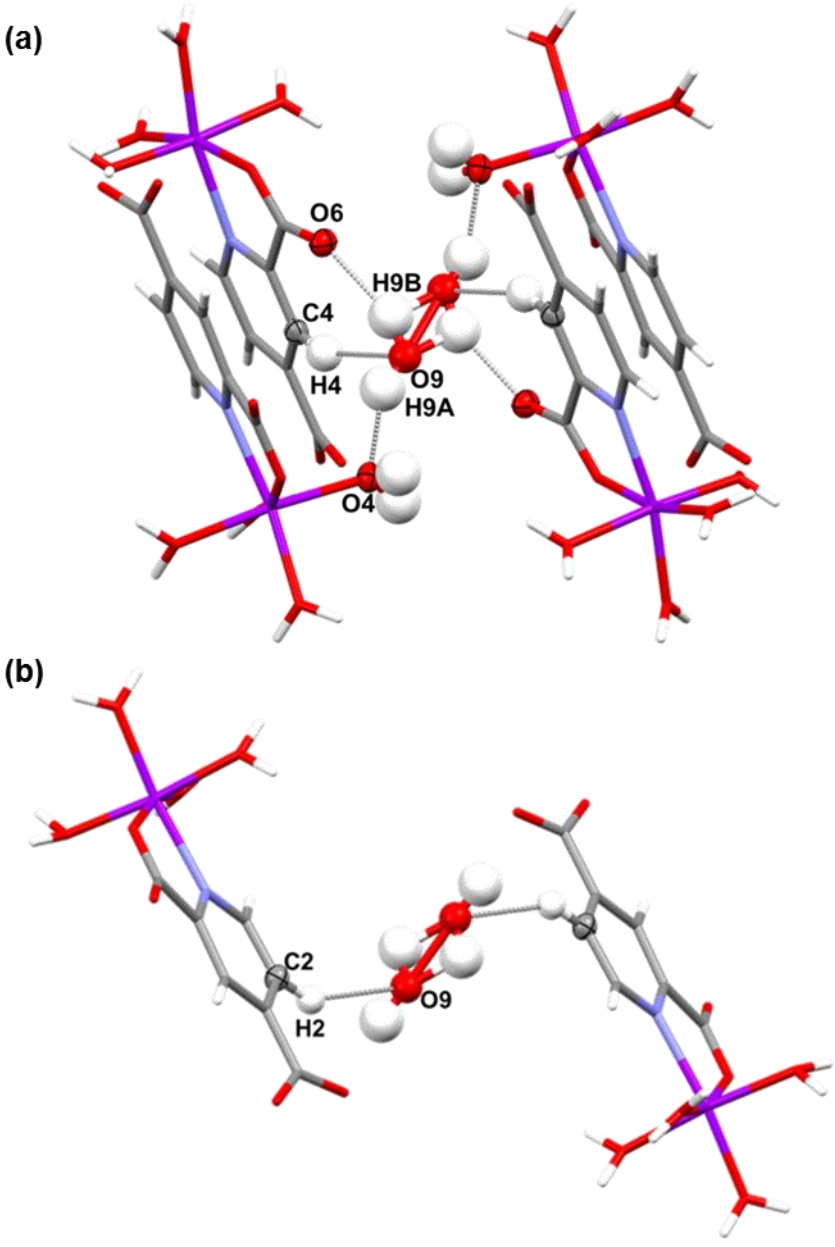

Figure 5.23. Crystal Structure of **(17)**. H-bonds connecting between $Mg(C_7H_3NO_4)(H_2O)_4$ units *via* the non-coordinated water molecule (a) along the *c* direction, and (b) along the *b* direction.

Table 5.5. Geometries of H-bonds in **(17)**.

D-H···A Interaction	D-H (Å)	H···A (Å)	D···A (Å)	D-H···A (°)
(Figure 5.22(a)) H-bonds connecting $Mg(C_7H_3NO_4)(H_2O)_4$ units in {002} plane				
O2-H2B···O1[a]	0.87(1)	1.91(4)	2.708(4)	152(7)
O3-H3A···O1[a]	0.87(1)	2.70(7)	3.291(5)	126(5)
O3-H3A···O2[a]	0.87(1)	1.99(3)	2.817(4)	158(7)
O3-H3A···O5[a]	0.87(1)	2.94(7)	3.503(5)	124(5)
O3-H3B···O8[b]	0.87(1)	1.82(2)	2.687(4)	169(8)
O4-H4B···O7[c]	0.87(1)	1.90(1)	2.776(4)	177(7)
O5-H5A···O1[a]	0.87(1)	2.86(7)	3.470(5)	129(6)
O5-H5A···O6[a]	0.87(1)	1.87(1)	2.742(5)	178(8)
C2-H2···O4[b]	1.04(4)	2.76(5)	3.699(6)	150(3)
(Figure 5.22(b)) H-bonds connecting $Mg(C_7H_3NO_4)(H_2O)_4$ units along c direction				
O2-H2A···O7[d]	0.87(1)	1.85(3)	2.696(4)	162(8)
O2-H2A···O8[d]	0.87(1)	2.71(6)	3.395(4)	136(5)
O4-H4A···O5[e]	0.87(1)	2.46(5)	3.196(5)	142(7)
O5-H5B···O8[f]	0.87(1)	1.76(1)	2.629(5)	176(7)
(Figure 5.23(a) and (b)) H-bonds between $Mg(C_7H_3NO_4)(H_2O)_4$ units and non-coordinated disordered water molecule				
O9-H9A···O4	0.87(1)	1.89(7)	2.701(9)	154(14)
O9-H9B···O6[b]	0.87(1)	2.00(7)	2.806(9)	153(13)
C2-H2···O9[b]	1.04(4)	2.40(5)	3.326(9)	147(3)
C4-H4···O9[c]	1.03(6)	2.27(6)	3.228(9)	155(5)

Symmetry codes: [a](1-x, -½+y, ½-z) [b](2-x, -½+y, ½-z) [c](2-x, ½+y, ½-z) [d](2-x, -y, 1-z) [e](1-x, -y, -z) [f](-1+x, ½-y, -½+z)

HSM was carried out on a single crystal of **(17)**. At about 150 °C the crystal started to look stressed and developed a chequered appearance, and at about 160 °C the crystal started

releasing bubbles. At about 173 °C the crystal 'blackened' and the bubbling continued. Between 220 °C and 240 °C a crack formed in the side of the crystal. The bubbling ceased at about 260 °C. The crystal did not melt on heating to 300 °C: all that was left of it was a skeletal residue. The DSC trace (Figure 5.24) shows two small endothermic events at 155.2 °C and 173.0 °C. The former is sharper and coincides with the first appearances of stress observed in the crystal during HSM. The second event is slightly broader and corresponds to the 'blackening' and bubbling of the crystal, and possibly represents the loss of water, although this would be expected at a lower temperature.

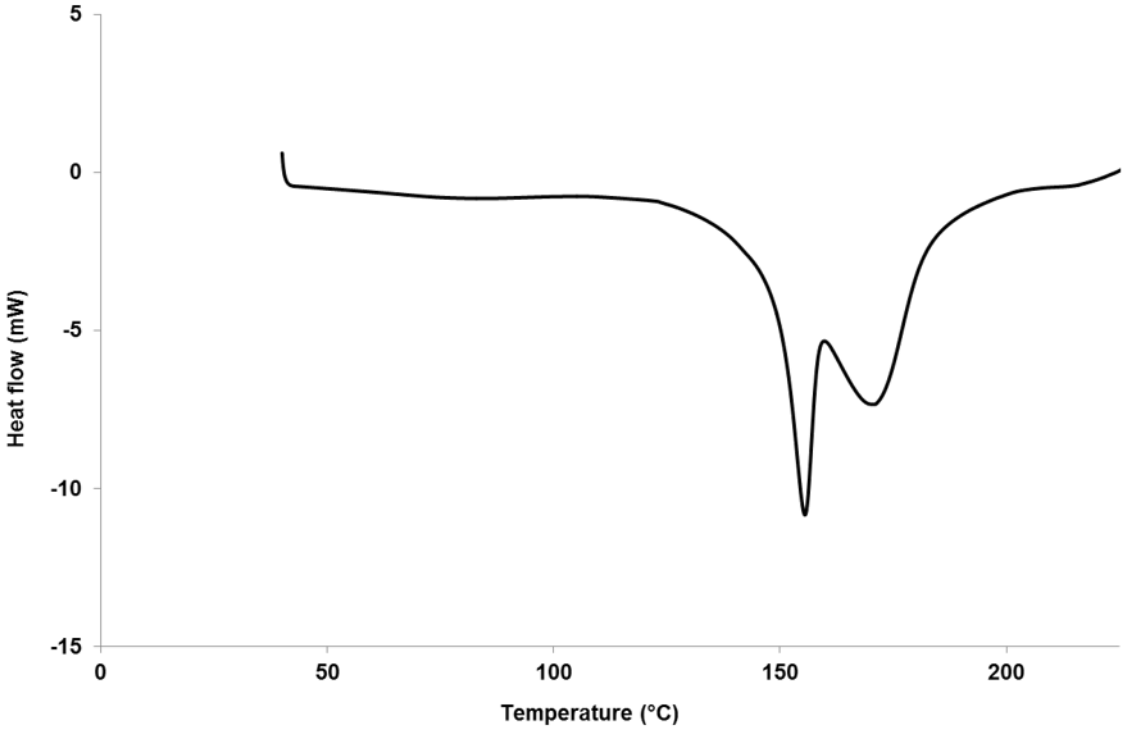

Figure 5.24. DSC trace of **(17)** on a 4.1 mg sample with a temperature ramp of 10 °C min^{-1}.

5.5. Hydrothermal Method to Produce *$[Mg(C_7H_3NO_4)(H_2O)_3]_2$* (SUYLEE01)

Single crystals of a group 2 analogue of the TM were not produced using evaporative or vapour diffusion techniques. Therefore, hydrothermal techniques were considered. The preparation procedure of *bis-[(μ_2-pyridine-2,4-dicarboxylato)-triaqua-magnesium(II)]* [**SUYLEE01**; CSD V5.35 Oct 2014][97] was followed with the intention of then combining the resulting magnesium-organic complex with a diamine to attempt to develop a new magnesium-organic-organic complex. This involved reacting a 1:1 stoichiometric mixture of 2,4-pdcam with magnesium(II) acetate tetrahydrate dissolved in water at 150 °C for 72 hours. However, the complex reported by Mallick *et al.* was never obtained. The experiment was repeated and again the product was **(18)**, a 2D metal-organic complex. The product

material (shown in Figure 5.25(a)) consisted of clear, colourless large petal-shaped angular crystalline chunks. The crystals were left in their mother liquor in the sealed vial on the crystallisation shelf. After ten weeks the crystals had changed from **(18)** to **(19)**, a 0D metal-organic complex. It was not established whether this transformation involved the dissolution of **(18)** followed by the recrystallisation of **(19)**. The resulting crystals (shown in Figure 5.25(b)) were a large homogeneous mass of very flat, clear, colourless platelet shards, many of which were twinned. If crystals of **(18)** were left in fomblin on a glass slide, they did not convert to **(19)** over time; only if left in the mother liquor did **(18)** transform into **(19)**.

The hydrothermal reaction was repeated using a 2:1 stoichiometric mixture of 2,4-pdcam and magnesium(II) acetate tetrahydrate. On opening the autoclave, the vial contained a clear colourless solution, however, after leaving the vial sealed on the crystallisation shelf for one month, crystals of **(19)** had grown in solution. A control experiment was carried out in which the starting materials were combined and left in a sealed vial on the crystallisation shelf, however the reactants never dissolved in the first place and no crystals were produced.

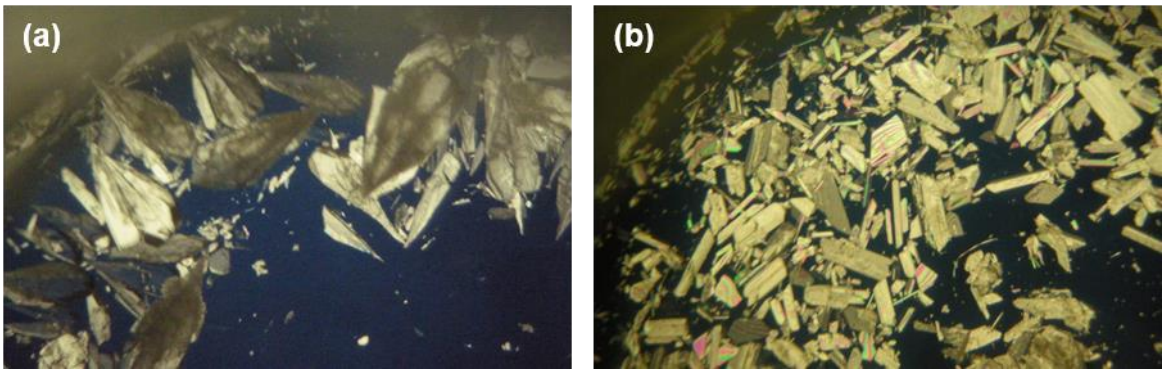

Figure 5.25. Crystals of (a) **(18)**, and (b) **(19)** in their mother liquor.

5.5.1. *Catena-[(μ$_3$-pyridine-2,4-dicarboxylato)-diaqua-magnesium(II)]* **(18)**

[Mg(C$_7$H$_3$NO$_4$)(H$_2$O)$_2$]

The PXRD pattern of **(18)** (shown in Figure 5.26) was obtained from a sample prepared by removing some of the crystals from solution and drying them in paper towel before grinding into a powder. This was carried out nine days after opening the autoclave in which **(18)** was synthesised. The experimentally obtained and calculated patterns are in good agreement with a significant number of coinciding peaks, taking into account the expected shifting of this pattern to slightly higher 2θ values. This confirms that the single crystal used to determine the crystal structure is representative of the bulk material removed from the mother liquor.

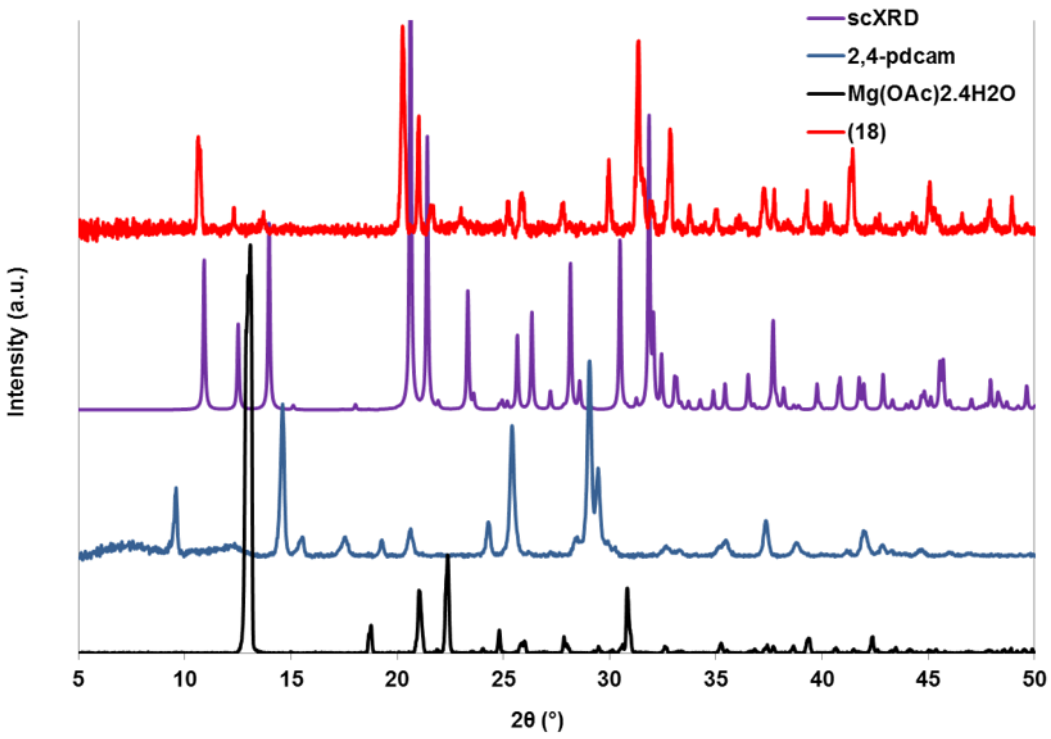

Figure 5.26. PXRD pattern of **(18)** compared to the calculated pattern and patterns of the starting materials.

The crystal structure of **(18)** is composed of 2D coordination polymeric sheets formed by the coordination of magnesium centres by 2,4-pyridine dicarboxylate ligands and water molecules. The magnesium centre in **(18)** is coordinated by two water molecules and three 2,4-pyridine dicarboxylate ligands: two *via* one carboxylate oxygen atom, and one *via* N,O-chelation (Figure 5.27(a)). The magnesium centre is in a distorted octahedral environment (geometries listed in Table 5.6) with angles ranging from 75.70(5)° for N1-Mg1-O1, the angle formed between the coordinating atoms of the chelating ligand, to 100.70(6)° for $O6^{a}$-Mg1-O3, the angle *trans* to this, formed between a coordinating water molecule and a carboxylate oxygen atom. The angles between the coordinating carboxylate oxygen atoms are: 98.11(5)° for $O5^{b}$-Mg1-$O6^{a}$, the angle between oxygen atoms of the ligands not chelating the magnesium centre of interest; 88.75(5)° for $O5^{b}$-Mg1-O1 and 93.04(5)° for O1-Mg1-$O6^{a}$, the angles between the oxygen atom of the chelating ligand and another carboxylate oxygen atom of another ligand.

The longest coordination distance is that from the nitogen atom at 2.217(2) Å, whereas the distance from the oxygen atom of the same chelating ligand, Mg1-O1, is 2.048(1) Å. This is longer than the coordination distances from the other carboxylate oxygen atoms that are both 2.011(1) Å. The coordination distances from the water ligands are both longer than the

distances for any of the carboxylate oxygen atoms at 2.141(1) Å for Mg1-O2 and 2.060(1) Å for Mg1-O3.

Figure 5.27(b) shows the bridging of the μ_3 2,4-pyridine dicarboxylate ligand. The Mg-O-C angles within the eight-membered ring formed by the bridging of two magnesium centres by a carboxylate group are quite similar at 143.4(1)° for $Mg1^{c}$-O5-C8 and 148.1(1)° for $Mg1^{d}$-O6-C8. The O-C-O angle of the bridging carboxylate group (O5-C8-O6) is 126.6(2)°, while that of the carboxylate group involved in chelation (O1-C2-O4) is 125.7(2)°. The C-O bond distances of the bridging carboxylate group are more similar than those of the other carboxylate group. C8-O5 is 1.244(2) Å and C8-O6 is 1.250(2) Å, while C2-O1 is a longer bond at 1.270(2) Å and C2-O4 is 1.242(2) Å.

The bridging carboxylate group is essentially coplanar with the pyridyl ring with a O5-C8-C6-C7 torsion angle of 0.4(2)°, while the carboxylate group involved in chelation is slightly twisted with a O1-C2-C1-N1 torsion angle of 4.1(2)°.

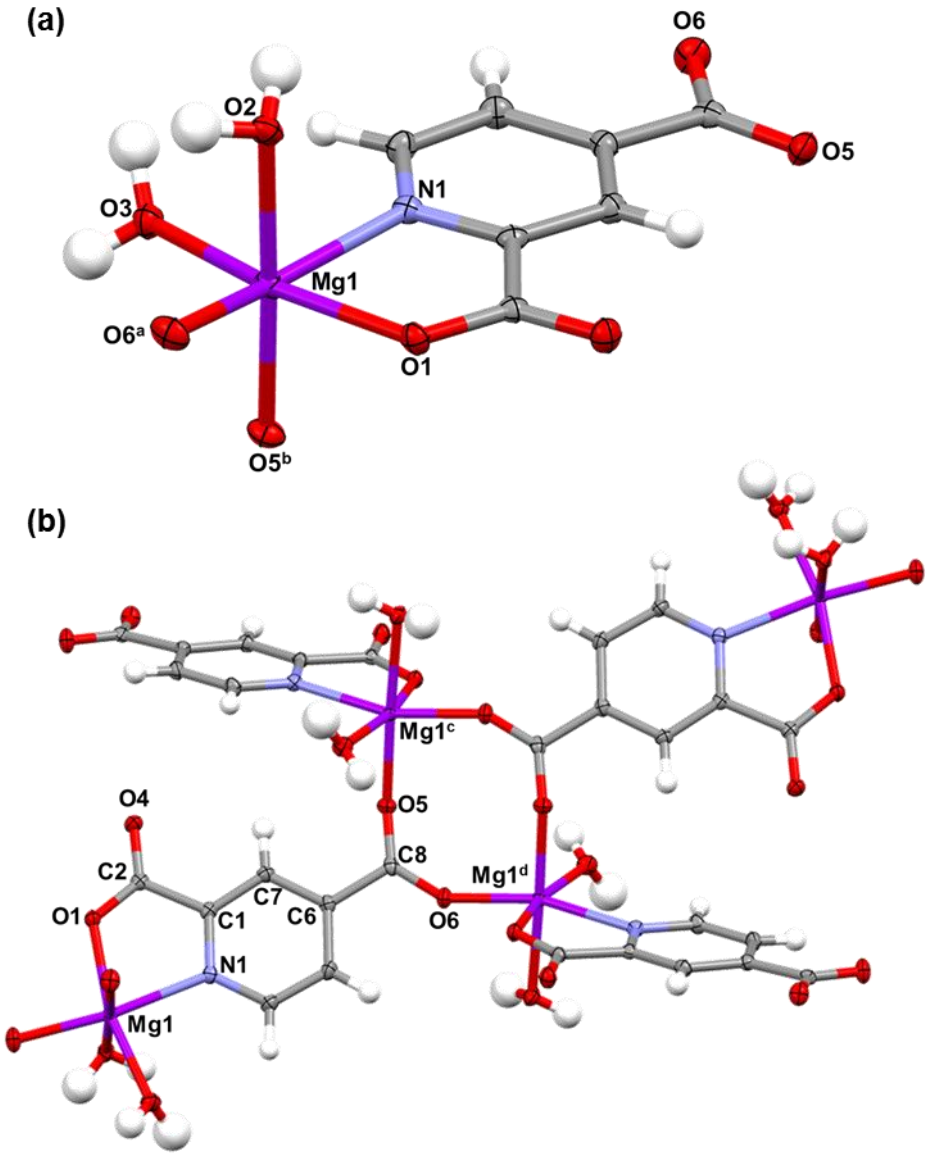

Figure 5.27. Crystal structure of **(18)**. (a) Formula unit showing magnesium centre with one N,O-chelating 2,4-pyridine dicarboxylate ligand, two coordinating carboxylate oxygen atoms and two coordinating water molecules. (b) μ_3-2,4-pyridine dicarboxylate ligands bridging magnesium centres. Symmetry codes: [a](-1+x, ½-y, -½+z) [b](2-x, ½+y, ½-z) [c](2-x, -½+y, ½-z) [d](1+x, ½-y, ½+z)

Table 5.6. O-Mg-O/N angles and Mg-N/O distances in **(18)**.

Coordination	O-Mg-O/N angle (°)	Interaction	Distance (Å)
O2-Mg1-N1	88.02(5)	Mg1-N1	2.217(2)
O2-Mg1-O1	91.82(5)	Mg1-O1	2.048(1)
O2-Mg1-O6[a]	79.55(5)	Mg1-O2	2.141(1)
O2-Mg1-O3	90.90(5)	Mg1-O3	2.060(1)
O5[b]-Mg1-N1	94.37(5)	Mg1-O5[b]	2.011(1)
O5[b]-Mg1-O1	88.75(5)	Mg1-O6[a]	2.011(1)
O5[b]-Mg1-O6[a]	98.11(5)		
O5[b]-Mg1-O3	89.08(6)		
N1-Mg1-O1	75.70(5)		
O1-Mg1-O6[a]	93.04(5)		
O6[a]-Mg1-O3	100.70(6)		
O3-Mg1-N1	90.94(6)		

Symmetry codes: [a](-1+x, ½-y, -½+z) [b](2-x, ½+y, ½-z)

The structure of **(18)** is composed of zigzag 2D coordination polymeric sheets that lie along the {-102} plane as illustrated in Figure 5.28(a). The sheets are made of coordinating rings of four magnesium centres and four bridging 2,4-pyridine dicaboxylate ligands which are linked by the eight-membered ring formed by the bridging carboxylate group of the organic ligand and two magnesium centres (Figure 5.28(b)).

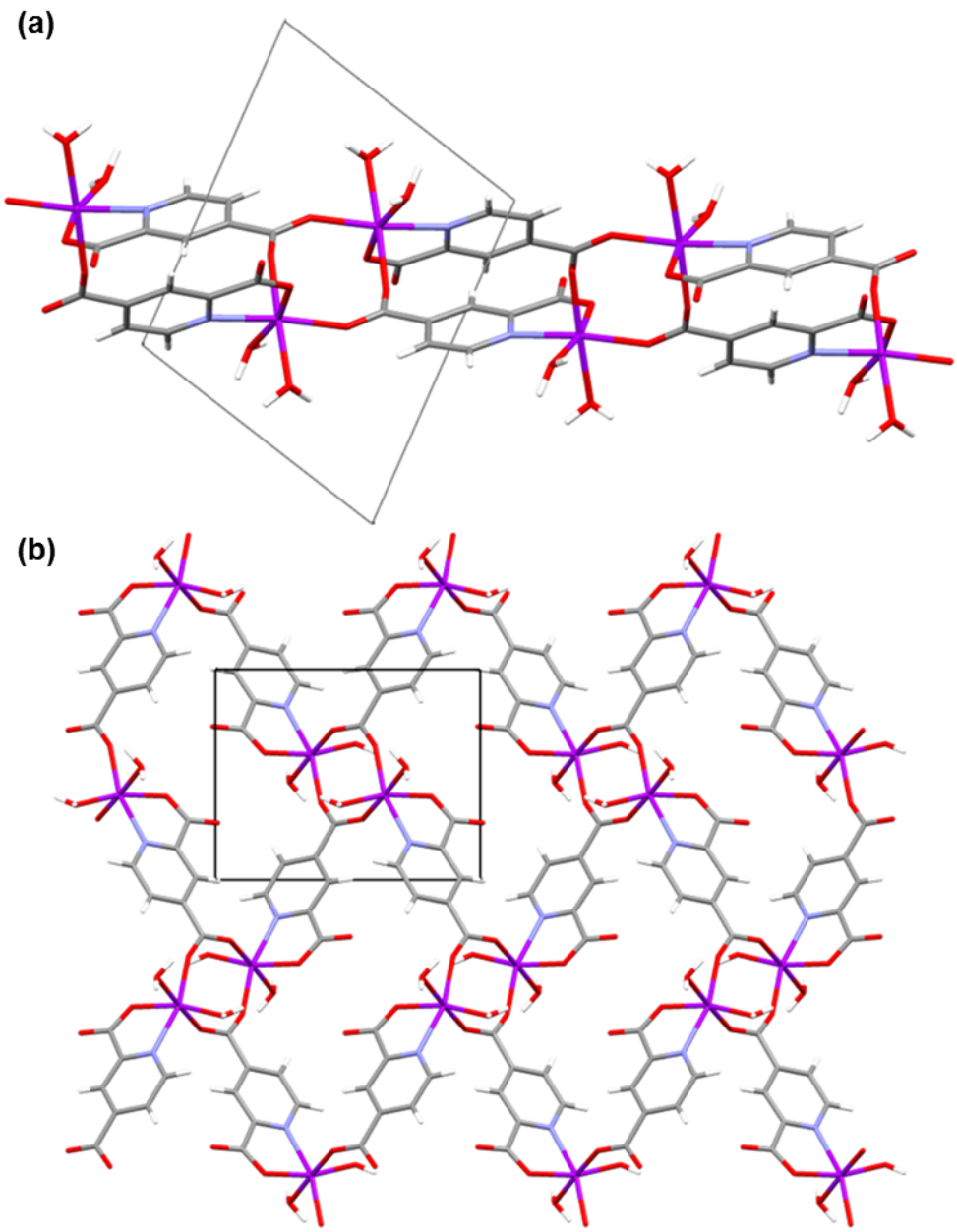

Figure 5.28. Crystal structure of **(18)**. View down (a) *b* axis and (b) *c* axis, showing 2D sheet on {-103} plane.

The zigzag 2D coordination polymeric sheets are connected by H-bonding interactions as depicted in Figure 5.29(a) and listed in Table 5.7. There are six H-bonds formed by the coordinating water molecules, two of which are bifurcated (Figure 5.29(b)). O3-H3A···O1^{e}O2^{e} is formed to a metal-coordinating carboxylate oxygen atom and an oxygen atom of a water molecule coordinating to the same magnesium centre as the carboxylate oxygen atom, respectively. O3-H3B···O1^{e}O4^{f} is formed to the same metal-coordinating carboxylate oxygen atom as before, and a non metal-coordinating oxygen

atom of a metal-coordinating carboxylate group associated with a different metal centre, respectively. These bifurcated H-bonds have moderate length D···A distances but very variable angles indicating that they each have one stronger component. O3-H3A···O2^{e} has a D···A distance of 2.961(2) Å and an almost linear angle of 173(3)° while O3-H3A···O1^{e} has a shorter D···A distance of 2.912(2) Å but a very low angle of 109(2)°. O3-H3B···O4^{f} has a D···A distance of 2.814(2) Å and an angle of 156(3)° while O3-H3B···O1^{e} has a D···A distance of 2.912(2) Å and a very low angle of 103(2)°.

The other coordinated water molecule forms two moderately strong H-bonds. O2-H2B···O1^{f} is formed to a metal-coordinated carboxylate oxygen atom and has the shortest D···A distance of the H-bonds within this structure at 2.724(2) Å and an angle of 165(2)°. O2-H2A···O4^{e} is formed to a non metal-coordinating oxygen atom of a metal-coordinating carboxylate group and has a D···A distance of 2.883(2) Å and an angle of 153(3)°.

There are two weaker H-bonds formed from C-H groups of the pyridyl ring which connect between the 2D sheets (Figure 5.29(c)). C4-H4···O4^{f} is formed to a non metal-coordinating oxygen atom of a metal-coordinating carboxylate group and has a D···A distance of 3.389(2) Å and an angle of 141(1)°. C5-H5···O3^{g} is formed to the oxygen atom of a coordinating water molecule and has a D···A distance of 3.547(2) Å and an angle of 150(2)°.

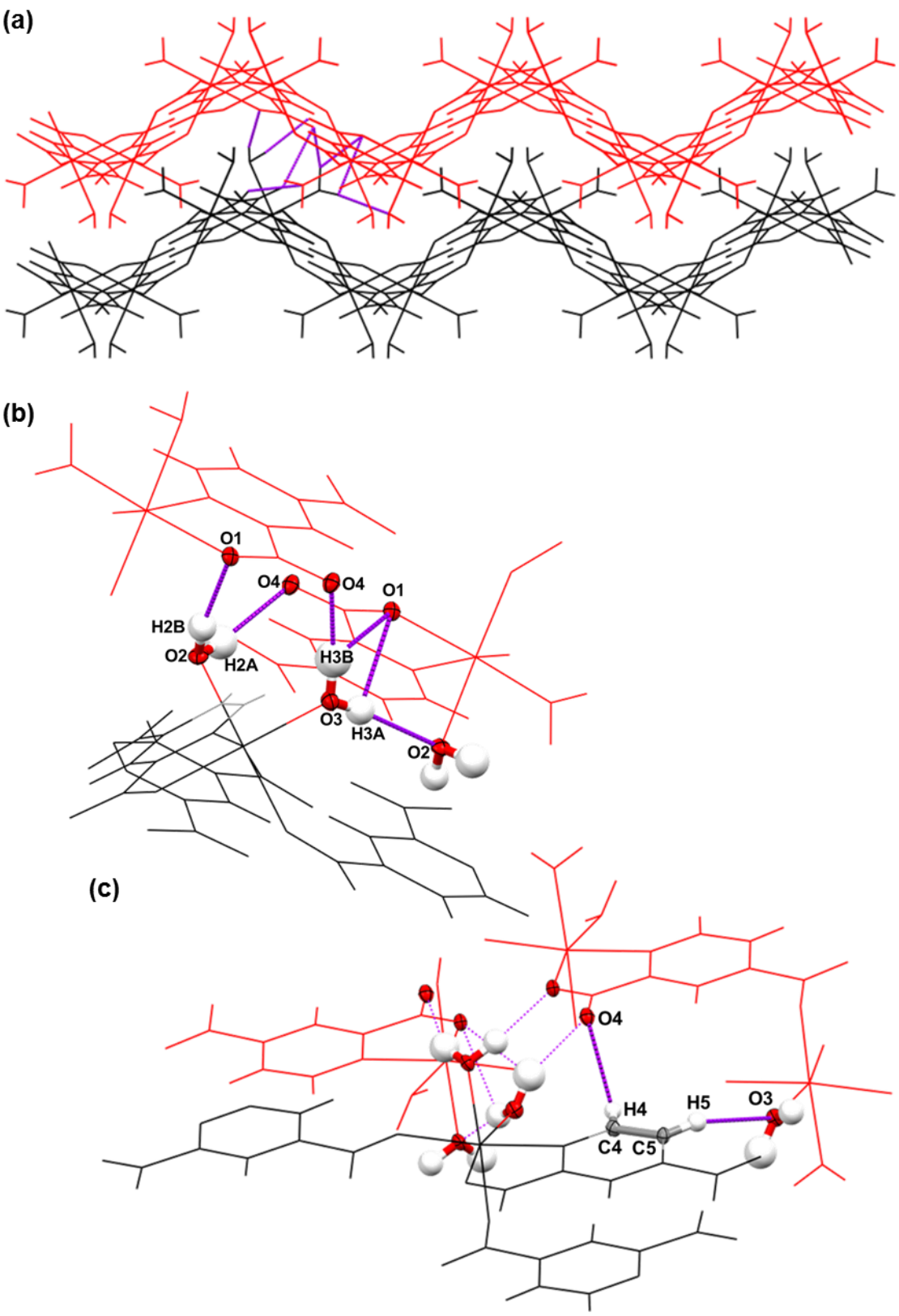

Figure 5.29. Crystal structure of **(18)**. (a) H-bonds connecting between adjacent 2D sheets. H-bonds originating from (b) coordinated water molecules, and (c) C-H groups connecting between layers (only H-bonds from black layer are shown, reciprocal H-bonds are omitted for clarity).

Table 5.7. Geometries of H-bonds in **(18)**.

D-H···A Interaction	D-H (Å)	H···A (Å)	D···A (Å)	D-H···A (°)
(Figure 5.29(b) and (c)) H-bonds between polymeric sheets				
O2-H2A···O4[e]	0.87(3)	2.08(3)	2.883(2)	153(3)
O2-H2B···O1[f]	0.84(3)	1.90(3)	2.724(2)	165(2)
O3-H3A···O1[e]	0.81(3)	2.55(3)	2.912(2)	109(2)
O3-H3A···O2[e]	0.81(3)	2.16(3)	2.961(2)	173(3)
O3-H3B···O1[e]	0.90(3)	2.57(3)	2.912(2)	103(2)
O3-H3B···O4[f]	0.90(3)	1.97(3)	2.814(2)	156(3)
C4-H4···O4[f]	0.99(2)	2.57(2)	3.389(2)	141(1)
C5-H5···O3[g]	0.92(2)	2.72(2)	3.547(2)	150(2)

Symmetry codes: [e](-x, ½+y, ½-z) [f](x, ½-y, ½+z) [g](2-x, 1-y, 1-z)

The thermal behaviour of **(18)** was investigated by HSM and DSC analysis. The DSC trace (Appendix B, Figure A27) shows a broad endotherm at 247.6 °C and no further events until 500 °C when the experiment was stopped. The endotherm occurs within the melting range of 2,4-pdcam (m.p. 246 – 248 °C), however it is unlikely that this indicates that the bulk sample is composed purely of the starting material. DSC analysis was carried out on a sample prepared in the same way as was the sample for PXRD analysis, three days prior to PXRD analysis. The PXRD pattern does not suggest that the bulk sample is composed of the starting material 2,4-pdcam but rather that it is primarily composed of the magnesium-organic complex **(18)**. Therefore it can be concluded that the endotherm at 247.6 °C is related to an event experienced by **(18)**. HSM showed that the crystal began bubbling at about 200 °C and this was accompanied by fracturing and 'blackening' and decomposition around 250 °C. Therefore the peak in the DSC trace may be associated with the decomposition of **(18)**.

5.5.2. *Hexaaqua-magnesium(II) bis-(pyridine-2,4-dicarboxylato)-diaqua-magnesium(II) trihydrate* **(19)** *$[Mg(H_2O)_6][Mg(C_7H_4NO_4)_2(H_2O)_2].3H_2O$*

The PXRD pattern of **(19)** is shown in Figure 5.30. The material was obtained 79 days after opening the autoclave in which **(18)** was synthesised, and the sample for PXRD was

prepared in the same way as that by which the sample for PXRD of **(18)** was acquired. The experimentally obtained PXRD pattern matches the calculated pattern very well. That both the PXRD pattern of the bulk samples of **(18)** and **(19)** match their calculated patterns well suggests that the transformation of **(18)** to **(19)** is homogeneous.

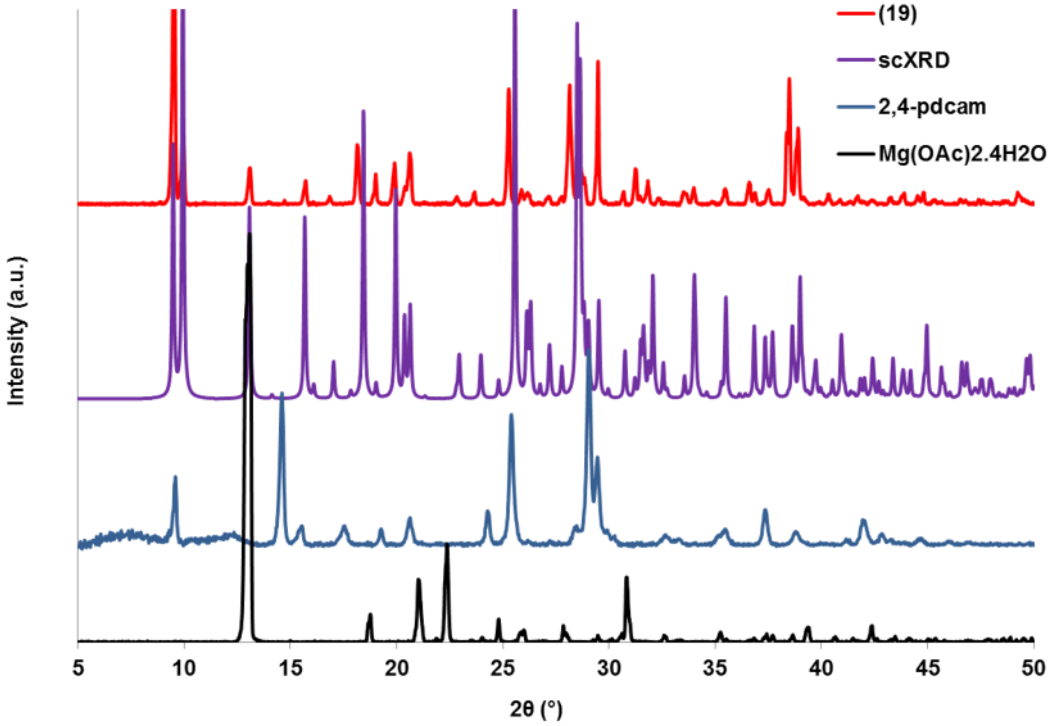

Figure 5.30. PXRD pattern of **(19)** compared to the calculated pattern and patterns of the starting materials.

(19) is a 0D metal-organic hydrate featuring two different magnesium centres. Mg1 is N,O-chelated by two bidentate 2,4-pyridine dicarboxylate ligands and two water molecules, within the $[Mg(C_7H_3NO_4)_2(H_2O)_2]^{2-}$ ion. The 2,4-pyridine dicarboxylate ligands are doubly deprotonated and feature peripheral non-coordinated carboxylate groups. This ion, shown in Figure 5.31(a), corresponds to the doubly deprotonated TM, and is the magnesium analogue of the ion that features extensively in metal-organic complexes developed by Beatty *et al*. Therefore, this ionic metalloligand constitutes an ideal and versatile building block as a possible precursor for lightweight, further functionalised group 2 metal-organic complexes. The -2 charge of this dianion is counterbalanced by the presence of a $[Mg(H_2O)_6]^{2+}$ ion, shown in Figure 5.31(b). The magnesium centres are both located on crystallographic centres of inversion and have distorted octahedral geometries (listed in Table 5.12 and Table 5.13 for Mg1 and Mg2, respectively). Mg2 has a near perfect octahedral geometry with O-Mg-O angles ranging from 89.3(1)° for O6/O6^b-Mg2-O7/O7^b to

90.7(1)° for O6/O6^{b}-Mg2-O7^{b}/O7. The coordination distances are more uniform in Mg2, with Mg2-O6/O6^{b} and Mg2-O8/O8^{b} distances of 2.068(3) Å and 2.065(2) Å respectively, while Mg2-O7/O7^{b} is shorter at 2.044(3) Å.

Mg1 has a more distorted octahedral geometry due to the chelation of the two κ^2 ligands reducing the O2/O2^{a}-Mg1-N1/N1^{a} angle, formed by the coordinating atoms of the same ligand, to 77.8(1)°. This angle is wider than the O-Mg-N angles of both **(17)** (76.1(1)°) and **(18)** (75.70(5)°). It is also slightly larger than the comparable O-Mg-N angle in **SUYLEE01** of 75.82(5)°. The angle O2/O2^{a}-Mg1-N1^{a}/N1, formed between the coordinating atoms of different organic ligands in Mg1 is 102.2(1)°.

The $[Mg(C_7H_3NO_4)_2(H_2O)_2]^{2-}$ ion can be compared to analogous ions within a number of structures reported in the CSD (for which coordinates are available), [refcodes: **PIDYOR**[173] (Mn); **VIZXAF**[174] (Co); **TUTHUL**[175] (Ni); **DORBIW**, **DORBOC**, **DORBUI**, **DORCAP**,[94] **DUKMEC**,[176] **DUMFOH**[177] (Cu); **UNOFAF**,[178] **UZOYAK**, **UZOYEO**, **UZOYIS**, **UZOYOY**[95] (Zn), V5.35 October 2014].

When contrasted to the transition metal-containing analogous ions (in all of which the metal is located on either a crystallographic centre of inversion or in the case of **VIZXAF**, a 2-fold rotation axis, therefore the 2,4-pyridine dicarboxylate ligands are crystallographically equivalent), it is apparent that the angles equivalent to O2/O2^{a}-Mg1-N1/N1^{a} and O2/O2^{a}-Mg1-N1^{a}/N1 of Mg1 are closest to those observed in the Co analogue (Table 5.8).

Table 5.8. Comparison of the O2-Mg1-N1 and O2-Mg1-N1^{a} angles in **(19)** with the equivalent angles in transition metal-containing analogous ions.

Angle	(19)	Mn (1)	Co (1)	Ni (1)	Cu (6)	Zn (5)
O2-Mg1-N1	77.8(1)°	75.74°	78.80°	80.22°	83.35°	79.66°
O2-Mg1-N1^{a}	102.2(1)°	104.27°	101.20°	99.78°	96.65°	100.34°

(Bracket next to transition metal indicates number of structures from which data is obtained, if >1 the average angle is given).

In Mg1, the angles formed between the organic ligands and the coordinated water molecules are closer to 90°, but the angles involving the nitrogen atom show the largest deviation. O3/O3^{a}-Mg1-N1/N1^{a} has an angle of 87.9(1)° and O3/O3^{a}-Mg1-N1^{a}/N1 an angle of 92.1(1)°.

The coordination distance Mg1-N1/N1[a] is 2.190(3) Å, which is closer to the equivalent distance in **(17)** of 2.203(4) Å than that in **SUYLEE01** of 2.220(1) Å, which is more similar to the Mg-N distance in **(18)** of 2.217(2) Å. The distance from the coordinating carboxylate oxygen atom, Mg1-O2/O2[a], is 2.064(2) Å, equivalent to that in **(17)** of 2.066(3) Å, and more similar to the magnesium – carboxylate oxygen atom distances in **SUYLEE01** of 2.100(1) Å and 2.061(1) Å, than the distance from the coordinating oxygen atom of the chelating carboxylate group in **(18)** of 2.048(1) Å.

The distance from the coordinating water molecule, Mg1-O3/O3[a], is 2.036(2) Å. For **(17)**, **(18)** and **SUYLEE01**, which have more than one coordinating water molecule, these coordination distances vary: from 2.024(4) Å to 2.092(3) Å in **(17)**; from 2.060(1) Å to 2.141(1) Å in **(18)**; from 2.014(2) Å to 2.092(1) Å in **SUYLEE01**.

The coordination environment of Mg1 in **(19)** and the transition metal-containing analogous ions differ in the coordination distance from the water molecule. This is the shortest coordination distance in **(19)**, whereas, excluding cobalt, it is the longest in the transition metal containing analogous ions, with the copper analogues having an average metal – water oxygen atom distance of 2.506 Å (Table 5.9). In all of the N,O-chelated magnesium complexes, **(17)**, **(18)**, **(19)** and **SUYLEE01**, the Mg-N coordination has the longest distance, while this is not true of the transition metal-containing analogous ions. This is also the case in **(16)**, in which the Cu-N coordination distances are shorter than the metal-water oxygen atom distance. These observations indicate the relatively weak interaction between the magnesium centre and the nitrogen atom that is expected due to the hard acid character of the Mg^{2+} ion and the soft base nature of the nitrogen donor atom of pyridine, relative to the oxygen donor atoms of the carboxylate groups and water ligands.

Table 5.9. Comparison of the Mg1-O3, Mg1-O2 and Mg1-N1 distances in **(19)** with the equivalent distances in transition metal-containing analogous ions.

Distance	(19)	Mn (1)	Co (1)	Ni (1)	Cu (6)	Zn (5)
Mg1-O3	2.036(2) Å	2.243 Å	2.082 Å	2.113 Å	2.506 Å	2.155 Å
Mg1-O2	2.064(2) Å	2.153 Å	2.091 Å	2.054 Å	1.959 Å	2.085 Å
Mg1-N1	2.190(3) Å	2.235 Å	2.083 Å	2.043 Å	1.990 Å	2.103 Å

(Bracket next to transition metal indicates number of structures from which data is obtained, if >1 the average distance is given).

In common with **(17)**, the metal-coordinated carboxylate group displays a greater difference between the C-O bond distances than for the non metal-coordinated carboxylate group. C6-O1 is 1.228(4) Å while C6-O2, where O2 is coordinating to the metal centre, is longer at 1.275(5) Å. The non metal-coordinated carboxylate group has similar C-O distances of 124.7(4) Å and 1.239(4) Å for C7-O4 and C7-O5, respectively. A similar situation was observed in **(18)** whereby the C-O distances of the metal-coordinating non-bridging carboxylate group were more different than the bridging carboxylate group, with C2-O1, involving the metal-coordinating oxygen atom of the non-bridging carboxylate group having a distance of 1.270(2) Å, similar to 1.275(5) Å of C6-O2 of **(19)**. O1-C6-O2 has a larger angle of 125.7(3)°, compared to the peripheral carboxylate group with angle O4-C7-O5 of 124.4(4)°.

The carboxylate groups are not coplanar with the pyridine ring. The chelating carboxylate group is twisted slightly more from coplanarity with a O2-C6-C5-N1 torsion angle of -11.6(5)° compared to the torsion angle of 1.3(5)° for O4-C7-C3-C4. This is in contrast to **(17)** in which the uncoordinating carboxylate group is twisted more than the chelating group (O8-C7-C3-C4 is -12.2(6)° and O1-C6-C5-N1 is -6.7(6)°). The carboxylate groups of **(18)** are both more coplanar with the pyridyl ring (O5-C8-C6-C7 is 0.4(2)° and O1-C2-C1-N1 is 4.1(2)°).

When comparing these torsion angles of **(19)** to the equivalent torsion angles of the transition metal-containing analogous ions, it seems that unlike **(19)**, in general the uncoordinating carboxylate group is less coplanar than the chelating group (Table 5.10). The torsion angles of the Cu analogues are especially variable, however, with the magnitudes of the torsion angles equivalent to O4-C7-C3-C4 as follows: **DORBIW** 4.04°; **DORBOC** 3.01°; **DORBUI** 2.59°; **DORCAP** 0.66°; **DUKMEC** 23.33°; **DUMFOH** 9.41°.

Table 5.10. Comparison of the O2-C6-C5-N1 and O4-C7-C3-C4 torsion angles in **(19)** with the magnitudes of the equivalent torsion angles in transition metal-containing analogous ions.

Torsion angle	(19)	Mn (1)	Co (1)	Ni (1)	Cu (6)	Zn (5)
O2-C6-C5-N1	-11.6(5)°	2.45°	3.03°	2.79°	7.53°	2.59°
O4-C7-C3-C4	1.3(5)°	0.04°	22.71°	15.25°	7.17°	5.14°

(Bracket next to transition metal indicates number of structures from which data is obtained, if >1 the average torsion angle is given).

In **(19)**, the planes of the pyridyl rings of the two parallel 2,4-pyridine dicarboxylate ligands lie at a distance of approx. 0.803 Å apart. This is greater than the equivalent distances in all of the transition metal-containing analogous ions, for which the zinc analogues have the shortest distance between the planes with an average distance of 0.078 Å (Table 5.11).

Table 5.11. Comparison of the distances between the planes of parallel pyridyl rings of 2,4-pyridine dicarboxyate ligands chelating a central metal in **(19)** with the equivalent distances in transition metal-containing analogous ions.

	(19)	**Mn (1)**	**Co (1)**	**Ni (1)**	**Cu (6)**	**Zn (5)**
Distance	0.803 Å	0.227 Å	-	0.372 Å	0.588 Å	0.078 Å

(Bracket next to transition metal indicates number of structures from which data is obtained, if >1 the average torsion angle is given. The pyridyl rings in the Co analogue **VIZXAF**, are not parallel).

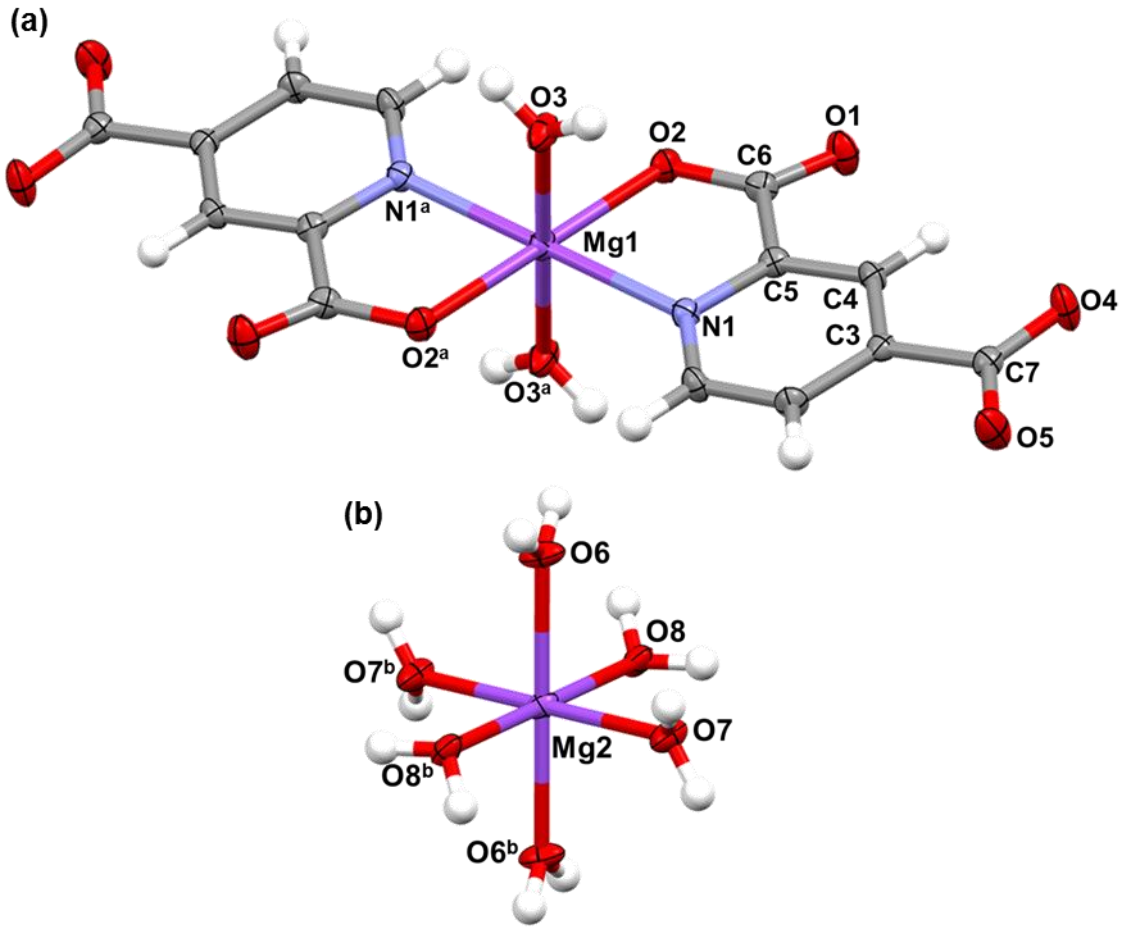

Figure 5.31. Crystal structure of **(19)**. (a) Mg1 centre with two N,O-chelating 2,4-pyridine dicarboxylate ligands and two coordinating water molecules. (b) Mg2 centre with six coordinating water molecules. Symmetry codes: [a](1-x, 1-y, -z) [b](-x, -y, -z)

Table 5.12. O-Mg-O/N angles and Mg-N/O distances involving Mg1 in **(19)**.

Coordination	O-Mg-O/N angle (°)	Interaction	Distance (Å)
O3/O3[a]-Mg1-O2/O2[a]	90.4(1)	Mg1-N1/N1[a]	2.190(3)
O3/O3[a]-Mg1-O2[a]/O2	89.6(1)	Mg1-O2/O2[a]	2.064(2)
O3/O3[a]-Mg1-N1/N1[a]	87.9(1)	Mg1-O3/O3[a]	2.036(2)
O3/O3[a]-Mg1-N1[a]/N1	92.1(1)		
O2/O2[a]-Mg1-N1/N1[a]	77.8(1)		
O2/O2[a]-Mg1-N1[a]/N1	102.2(1)		

Symmetry code: [a](1-x, 1-y, -z)

Table 5.13. O-Mg-O angles and Mg-O distances involving Mg2 in **(19)**.

Coordination	O-Mg-O angle (°)	Interaction	Distance (Å)
O6/O6^{b}-Mg2-O7/O7^{b}	89.3(1)	Mg2-O6/O6^{b}	2.068(3)
O6/O6^{b}-Mg2-O7^{b}/O7	90.7(1)	Mg2-O7/O7^{b}	2.044(3)
O6/O6^{b}-Mg2-O8/O8^{b}	89.6(1)	Mg2-O8/O8^{b}	2.065(2)
O6/O6^{b}-Mg2-O8^{b}/O8	90.4(1)		
O7/O7^{b}-Mg2-O8/O8^{b}	90.5(1)		
O7/O7^{b}-Mg2-O8^{b}/O8	89.5(1)		

Symmetry code: ^{b}(-x, -y, -z)

In addition to the $[Mg(C_7H_3NO_4)_2(H_2O)_2]^{2-}$ and the $[Mg(H_2O)_6]^{2+}$ ions, the structure of **(19)** also features three non-coordinated water molecules; two are crystallographically equivalent and related through a centre of inversion and the other is located on a crystallographic centre of inversion and is disordered over two positions.

In the structure of **(19)** the components are arranged in columns running down the *a* direction (Figure 5.32(a)). The $[Mg(C_7H_3NO_4)_2(H_2O)_2]^{2-}$ ions are linked by H-bonds and π-π interactions creating 2D tapes parallel to the *ac* plane (Figure 5.32(b) and Table 5.14). The H-bonds are formed between the coordinated water molecules of one ion to the carboxylate oxygen atoms of the peripheral carboxylate groups of ions located along the *a* direction.

O3-H3A···O5^{c} is the strongest of these interactions with the shortest D···A distance of 2.721(4) Å and the largest angle of 173(4)°. O3-H3B forms a bifurcated H-bond to two oxygen atoms of the same carboxylate group. The stronger component of this interaction is O3-H3B···O4^{e} with a D···A distance of 2.989(4) Å and an angle of 167(3)°, while O3-H3B···O5^{e} has a longer D···A distance of 3.136(4) Å and a smaller angle of 134(4)°.

The pyridyl groups exhibit interplanar π-π stacking contacts. The centroid – centroid distance of (N1,C1,C2,C3,C4,C5) - (N1,C1,C2,C3,C4,C5)^{c} is 4.601(2) Å which is too long to constitute a π-π stacking interaction, however the centroid – centroid distance of the π-bond (C2,C3) - (C2,C3)^{c} is approx. 3.509 Å. There is better overlap of the pyridyl rings (N1,C1,C2,C3,C4,C5) - (N1,C1,C2,C3,C4,C5)^{d} for which the centroid – centroid distance is 3.830(2) Å.

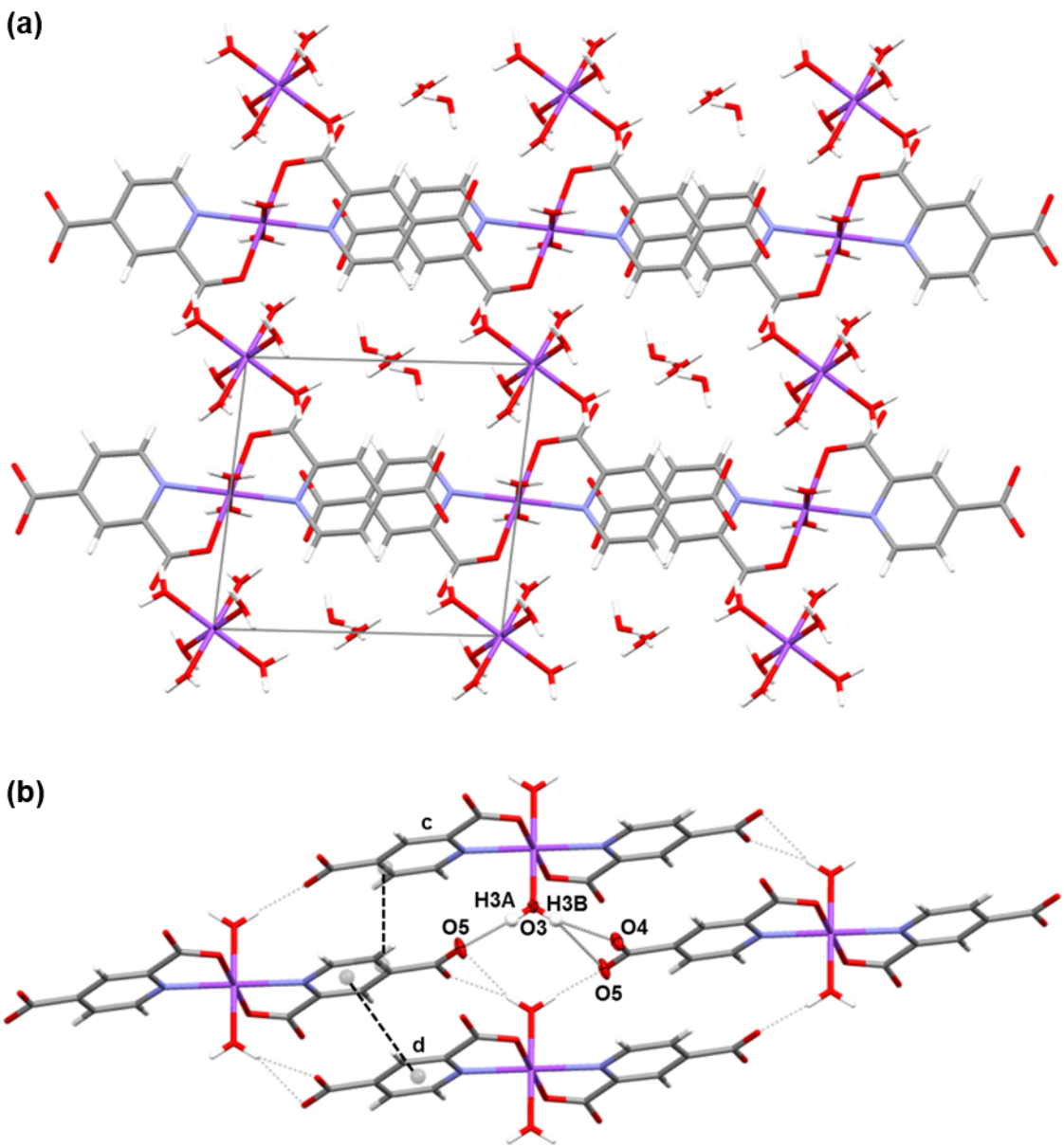

Figure 5.32. Crystal structure of **(19)**. (a) View down *a* axis showing global packing: $[Mg(C_7H_3NO_4)_2(H_2O)_2]^{2-}$ ions with overlap of their pyridyl rings forming 2D H-bonded motifs parallel to the *ac* plane. (b) H-bonds and π-π interactions connecting between $[Mg(C_7H_3NO_4)_2(H_2O)_2]^{2-}$ ions. Symmetry codes of pyridyl rings: [c](-x, 1-y, 1-z) [d](1-x, 1-y, 1-z)

The structure is connected along the *b* direction by H-bonds between the $[Mg(C_7H_3NO_4)_2(H_2O)_2]^{2-}$ ions and the $[Mg(H_2O)_6]^{2+}$ ions and non-coordinated water molecules (Figure 5.33(a) and (b) and Table 5.14). The $[Mg(H_2O)_6]^{2+}$ ion forms five H-bonds to adjacent $[Mg(C_7H_3NO_4)_2(H_2O)_2]^{2-}$ ions and one H-bond to a non-coordinated water molecule, O7-H7A···O9 (D···A distance 2.692(4) Å and angle 168(4)°). The five H-bonds to the $[Mg(C_7H_3NO_4)_2(H_2O)_2]^{2-}$ ions are all formed to carboxylate oxygen atoms. O6-

H6A···O4[c] and O7-H7B···O5[f] are formed to an oxygen atoms of the non-coordinated carboxylate group. They are moderately strong interactions with D···A distances of 2.749(4) Å and 2.712(4) Å and large, linear angles of 173(4)° and 174(3)°, respectively. The acceptor atom of O8-H8B···O1[a] is an uncoordinating carboxylate oxygen atom of the coordinating carboxylate group. This H-bond has a shorter D···A distance of 2.689(4) Å and an angle of 173(3)°. The coordinated carboxylate oxygen atom is the acceptor of the H-bonds O6-H6B···O2[a] and O8-H8A···O2[g]. These are also moderately strong interactions, with slightly longer D···A distances than the previous H-bonds at 2.811(4) Å and 2.878(4) Å and large angles of 177(3)° and 169(3)° for O6-H6B···O2[a] and O8-H8A···O2[g], respectively. The $[Mg(C_7H_3NO_4)_2(H_2O)_2]^{2-}$ ion forms an H-bond from a C-H group of the pyridine ring to the non-coordinated water molecule. C4-H4···O9[c] has a long D···A distance of 3.506(5) Å and an angle of 154°.

The two types of crystallographically inequivalent non-coordinated water molecules each form two H-bonds: one to carboxylate oxygen atoms, O9-H9A···O4[c] and O10-H10A···O1[c], and one to each other, O9-H9B···O9[f] and O10-H10B···O9.

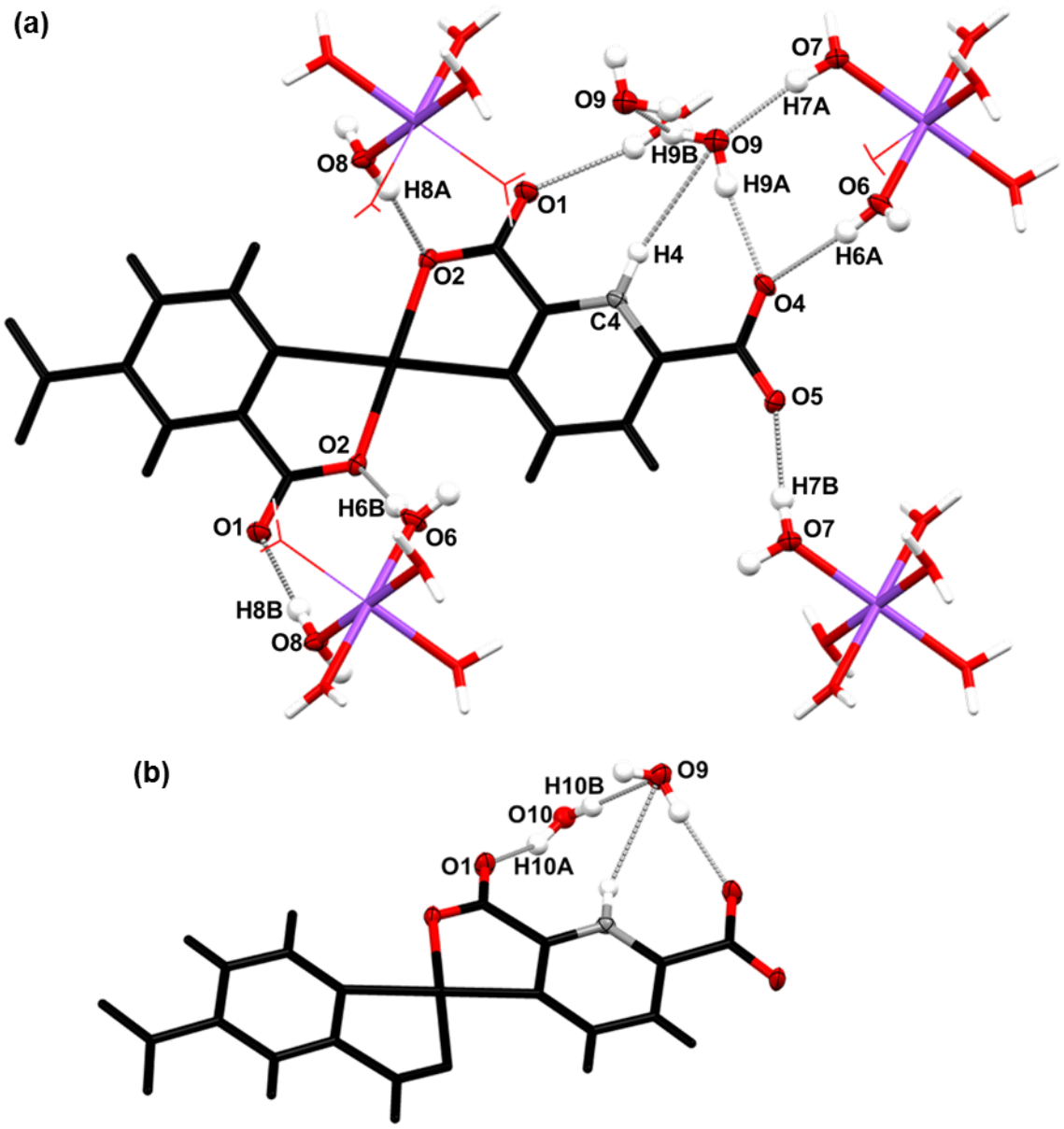

Figure 5.33. Crystal structure of **(19)**. (a) H-bonds between the $[Mg(C_7H_3NO_4)_2(H_2O)_2]^{2-}$ and $[Mg(H_2O)_6]^{2+}$ ions and water molecules connecting the structure along the *b* direction, with (b) detailing H-bonds formed by the disordered water molecule (coordinated water molecules omitted, for clarity).

Table 5.14. Geometries of H-bonds in **(19)**.

D-H···A Interaction	D-H (Å)	H···A (Å)	D···A (Å)	D-H···A (°)
(Figure 5.32(b)) H-bonds betwen $[Mg(C_7H_3NO_4)_2(H_2O)_2]^{2-}$ ions				
O3-H3A···O5[c]	0.84(2)	1.89(2)	2.721(4)	173(4)
O3-H3B···O4[e]	0.84(3)	2.16(2)	2.989(4)	167(3)
O3-H3B···O5[e]	0.84(3)	2.49(4)	3.136(4)	134(4)
(Figure 5.33(a) and (b)) H-bonds connecting structure along b direction				
O6-H6A···O4[c]	0.84(4)	1.91(4)	2.749(4)	173(4)
O6-H6B···O2[a]	0.84(3)	1.98(3)	2.811(4)	177(3)
O7-H7A···O9	0.85(3)	1.85(3)	2.692(4)	168(4)
O7-H7B···O5[f]	0.84(2)	1.88(2)	2.712(4)	174(3)
O8-H8A···O2[g]	0.85(3)	2.04(3)	2.878(4)	169(3)
O8-H8B···O1[a]	0.84(3)	1.85(3)	2.689(4)	173(3)
O9-H9A···O4[c]	0.85(2)	1.96(2)	2.799(4)	170(4)
O9-H9B···O9[f]	0.82(2)	2.25(3)	2.716(5)	116(2)
O10-H10A···O1[c]	0.85(8)	2.35(8)	3.065(3)	141(7)
O10-H10B···O9	0.86(4)	1.83(5)	2.685(4)	170(7)
*C4-H4···O9[c]	0.95	2.627	3.506(5)	154

Symmetry codes: [a](1-x, 1-y, -z) [c](-x, 1-y, 1-z) [e](x, y, -1+z) [f](-x, -y, 1-z) [g](x, -1+y, z) *H-bond features aromatic hydrogen atom fixed in idealised position.

Single crystals of **(19)** were analysed by HSM. This showed small cracks beginning to appear in the crystals at about 49 °C, followed by a blackening of the crystals until about 90 °C. Between around 140 °C and 150 °C major cracks appeared almost splitting the crystal, but no melt was recorded and the heating ramp was stopped at 350 °C. The DSC trace of the bulk sample (Appendix B, Figure A29) shows two endothermic events: the first is at 107.6 °C and the second at 190.6 °C. Neither of these events were apparent during HSM.

The $[Mg(C_7H_3NO_4)_2(H_2O)_2]^{2-}$ ion of **(19)** is the doubly deprotonated magnesium analogue of the TM. It was attempted to combine this complex with the diamines to produce new alkaline earth metal-organic-organic complexes; a method that was tried extensively with the intermediate complexes **(I1)** and **(I2)**, and that was successful in producing **(16)** from **(I3)** and *m*-xylylenediamine. These experiments yielded crystals of **(17)** and **(18)**, and experiments in which *o*-tolidine was used as the diamine sometimes resulted in crystals of *o*-tolidine; no new complexes were produced. In order to promote the formation of charge-assisted H-bonds, the diamine solutions were acidified to about pH 4 in order to shift the equilibrium to favour the formation of the ammonium group. Crystals formed in these experiments were either of **(17)** or **(18)**. The presence of the $[Mg(H_2O)_6]^{2+}$ ions posed a problem in using **(19)** as a starting material for further metal-organic-organic complexes due to it being necessary to balance the charge of the $[Mg(C_7H_3NO_4)_2(H_2O)_2]^{2-}$ ion.

5.6. Conclusions

Three 'intermediate' complexes have been synthesised in powder form. The PXRD patterns and the thermal analyses of **(I1)** and **(I2)** suggest the materials contain the same complex and MS data provides evidence that in each, the magnesium analogue of the TM was formed. **(I3)** is *bis-(pyridine-2-carboxylato-4-carboxyl)-diaqua-copper(II)* and **(I4)**, the product of magnesium(II) nitrate hexahydrate and 2,4-pdcam, is an inconclusively characterised material. These 'intermediates' have been combined with the diamines *o*-tolidine and *m*-xylylenediamine, resulting in the purely organic material **(15)**, the new complex *bis-(pyridine-2,4-dicarboxylato)-aqua-copper(II) 1,3-xylylenediammonium* **(16)** and *pyridine-2,4-dicarboxylato-tetraaqua-magnesium(II) hemihydrate* **(17)**.

Crystallisation experiments combining group 2 metal salts with 2,4- or 3,5-pyridine dicarboxylic acid ligands were not found to produce new crystalline complexes as was readily achieved using pyridine carboxylic acid ligands.

The preparation of *bis-[(μ_2-pyridine-2,4-dicarboxylato)-triaqua-magnesium(II)]* (**SUYLEE01**) through hydrothermal methods was never accomplished: a different product **(18)** resulted, which transformed into **(19)** over a period of several months. This phenomenon was reproducible, but the process by which it occurred was not established. **(19)** was found to contain the magnesium analogue of the doubly deprotonated TM which presents a potentially very useful molecular building block with which to incorporate a magnesium centre into a framework structure. This ionic metalloligand may not be as robust as the transition metal analogues however, albeit that the coordination distances are generally shorter than the equivalent distances in the transition metal analogues. Comparison of the

coordination geometries highlighted that for **(19)** (and indeed, also for **(17)**, **SUYLEE01** and **(18)**), the Mg-N bond has the longest coordination distance, while for the transition metal analogues this distance is more comparable to the M-O coordination distances and in the case of the Ni complex, it is the shortest. This observation indicates the relative weakness of the Mg-N interaction due to the hard acid character of the Mg^{2+} ion. This is in full agreement with what has been reported in the literature regarding the apparent weaker relative binding energy of the Mg–N bond compared to that of the Mg–O bond.[111, 112] Furthermore, the structure of the ionic metalloligand was not always retained on combining with the diamines and single crystals of **(17)** and **(18)** often resulted from these experiments.

Although the doubly deprotonated magnesium analogue of the TM was synthesised reproducibly, an alkaline earth metal-organic-organic complex, comprising a magnesium centre coordinated by a pyridine dicarboxylic acid ligand derivative and H-bonded to a diamine derivative to form an H-bonded coordination network was not achieved. The objective was complicated by the ionic nature of the TM and that it was accompanied by the $[Mg(H_2O)_6]^{2+}$ ion, so that in order to combine the dianion with a diamine through charge-assisted H-bonds, it was necessary to protonate the diamine. This was attempted by acidifing the diamine solutions to about pH 4 in order to shift the equilibrium to favour the formation of the ammonium group, however, either crystals of **(17)** or **(18)** resulted from these experiments.

Chapter 6. Supramolecular Ligand Approach to Metal-Organic Complexes using Chloranilic Acid

6.1. Introduction

In Chapter 5, new H-bonded metal-organic-organic complexes were targeted by first preparing a metalloligand and then combining this with a second organic component. A different approach to designing new complexes involved first preparing a 'supramolecular ligand' and combining this with a metal salt. This study was built upon work carried out by Adam *et al*.[136] who successfully produced salts featuring predictable bifurcated H-bonded synthons from methylpyridine isomers and chloranilic acid (Figure 6.1(a)). In order to develop more functionalised group 2 metal-organic-organic complexes, it was intended to utilise a supramolecular approach based on these synthons. First, a supramolecular ligand would be prepared using chloranilic acid and pyridine carboxylic acids, rather than methylpyridines. If a bifurcated H-bonded synthon formed between the protonated pyridyl nitrogen atom and the deprotonated hydroxyl and carbonyl oxygen atoms of the chloranilate dianion, as for the methylpyridines (Figure 6.1(b)), or if another robust supramolecular synthon could be established, this may allow the carboxyl group of the pyridine carboxylic acids to be available for metal coordination in subsequent synthetic steps, and give rise to a new group 2 metal-organic-organic complex.

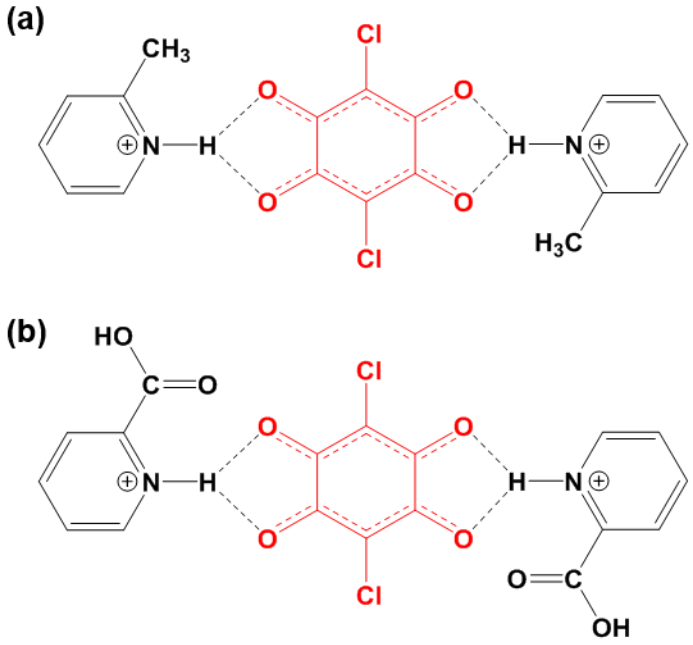

Figure 6.1. (a) H-bonded supramolecular unit of $(C_6H_8N)_2(C_6Cl_2O_4)$.[136] (b) Targeted H-bonded supramolecular unit using 2-pyridine carboxylic acid.

This chapter first describes the structure and thermal properties of salts and co-crystals of picolinic acid, nicotinic acid and isonicotinic acid with the co-former chloranilic acid. These complexes have previously been isolated by the Wilson group (Wittering, M.Chem Project, 2011). **(20)** is a salt hydrate consisting of two partially protonated picolinic acid ions and one hydrogen chloranilate ion. It displays proton disorder between the picolinic acid dimers and also between the hydrogen chloranilate ion and the disordered water molecules. **(21)** is a co-crystal featuring two zwitterionic picolinic acid molecules and one chloranilic acid molecule. **(22)** is a salt comprising two protonated nicotinic acid ions and a chloranilate dianion. A minor side product of one experiment in which isonicotinic acid was combined with chloranilic acid was **(A4)**, a salt hydrate of two protonated isonicotinic acid molecules, and two hydrogen chloranilate ions. **(A4)** is discussed fully in Appendix D.

The next section concerns the products from combination of the 'supramolecular ligands' with both alkaline earth and transition metal salts. **(A5)** is a salt of protonated isonicotinic acid nitrate which is discussed fully in Appendix D. **(23)** is a 0D complex featuring two copper centres bridged by a chloranilate dianion and terminated by chelating picolinate ions.

The third section briefly describes attempts to produce a magnesium/chloranilic acid complex and instead the identification of a new sodium/chloranilate complex **(A6)**, which was a minor product of two of these experiments. **(A6)** is discussed fully in Appendix D.

The final two crystal structures discussed all resulted from experiments in which samples of **(13)**, from Chapter 4, were combined with chloranilic acid. **(24)** has a 3D calcium-chloranilate framework containing dimethylammonium ions and **(25)** is a calcium-chloranilate 1D coordination polymer with six coordinated DMF ligands. Another product from these experiments is **(A7)**, an organic salt of chloranilate and dimethylammonium ions which is discussed fully in Appendix D.

The coordination behaviour of chloranilic acid, as well as the pyridine carboxylic acid ligands, was of interest and so the C-O, C=O and C-Cl bond distances as well as the C-C and C=C bond distances of the conjugated six-membered ring were noted in each complex and compared to the equivalent bond distances of chloranilic acid in its pure form as shown in Figure 6.2. This allowed the effect of metal coordination from the oxygen and chlorine atoms, and in turn its effect on the bonds within the ring, to be observed.

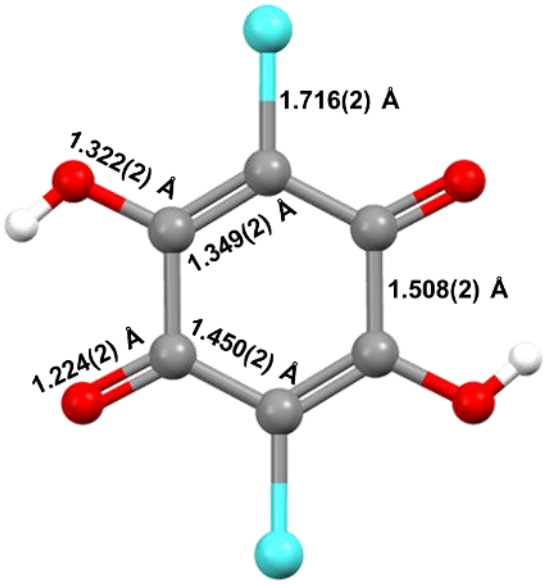

Figure 6.2. Chloranilic acid [**CLANAC11**; CSD V5.35 Feb 2015][142] labelling, C-O, C=O, C-C, C=C and C-Cl bond distances.

6.1.1. Known complexes of chloranilic acid and pyridine carboxylic acid

Experiments in which pyridine carboxylic acids and chloranilic acid were combined to produce 'supramolecular ligands' resulted in two materials that have been reported in the literature. *Pyridinium-3-carboxylic acid hydrogen chloranilate* [**PAZHOO**; CSD V5.35 Feb 2015][169] and *pyridinium-4-carboxylic acid hydrogen chloranilate hydrate* [**YERXUP**; CSD V5.35 Feb 2015][179] were reliably produced and were combined with metal salts in the next step in efforts to produce new metal-organic-organic complexes. *Pyridinium-2-carboxylic acid hydrogen chloranilate* [**HOLPEE**; CSD V5.35 Feb 2015][180] is also reported in the literature, however this material was never encountered during the screening of crystals from these experiments and was therefore not combined with metal salts in the next step.

Pyridinium-3-carboxylic acid hydrogen chloranilate **(PAZHOO)** *($C_6H_6NO_2$)($C_6HCl_2O_4$)*

The asymmetric unit of **PAZHOO** features one protonated nicotinic acid ion and one hydrogen chloranilate ion. The ions form columns along the *b* direction, and alternating 2D H-bonded motifs parallel to the *bc* plane. Figure 6.3(a) shows the strongest H-bonds in black. These feature the bifurcated H-bond from the protonated pyridyl nitrogen atom to the deprotonated hydroxyl and carbonyl oxygen atoms of the hydrogen chloranilate ion, as was consistently observed in the H-bonded synthons reported by Adam *et al*. except these featured the chloranilate dianion as opposed to the non-symmetrical hydrogen chloranilate

ion observed in **PAZHOO**. The shortest H-bond is formed from the hydroxyl oxygen atom of the carboxyl group of the protonated nicotinic acid to the deprotonated hydroxyl oxygen atom of the hydrogen chloranilate ion; this interaction has a D···A distance of 2.576(3) Å. The hydroxyl group of the hydrogen chloranilate ion H-bonds to the carbonyl oxygen atom of the carboxyl group of the protonated nicotinic acid ion. The hydrogen chloranilate ions form type-II halogen bonds along the *c* direction (Figure 6.3(b)); these have distances of 3.447(1) Å for Cl2···Cl1^{a}, and 3.511(1) Å for Cl2···Cl1^{b}, and angles C-Cl2···Cl1^{a}, 173.0(1)°; C-Cl1^{a}···Cl2, 81.6(1)°; C-Cl2···Cl1^{b}, 81.0(1)°; C-Cl1^{b}···Cl2, 172.0(1)°.

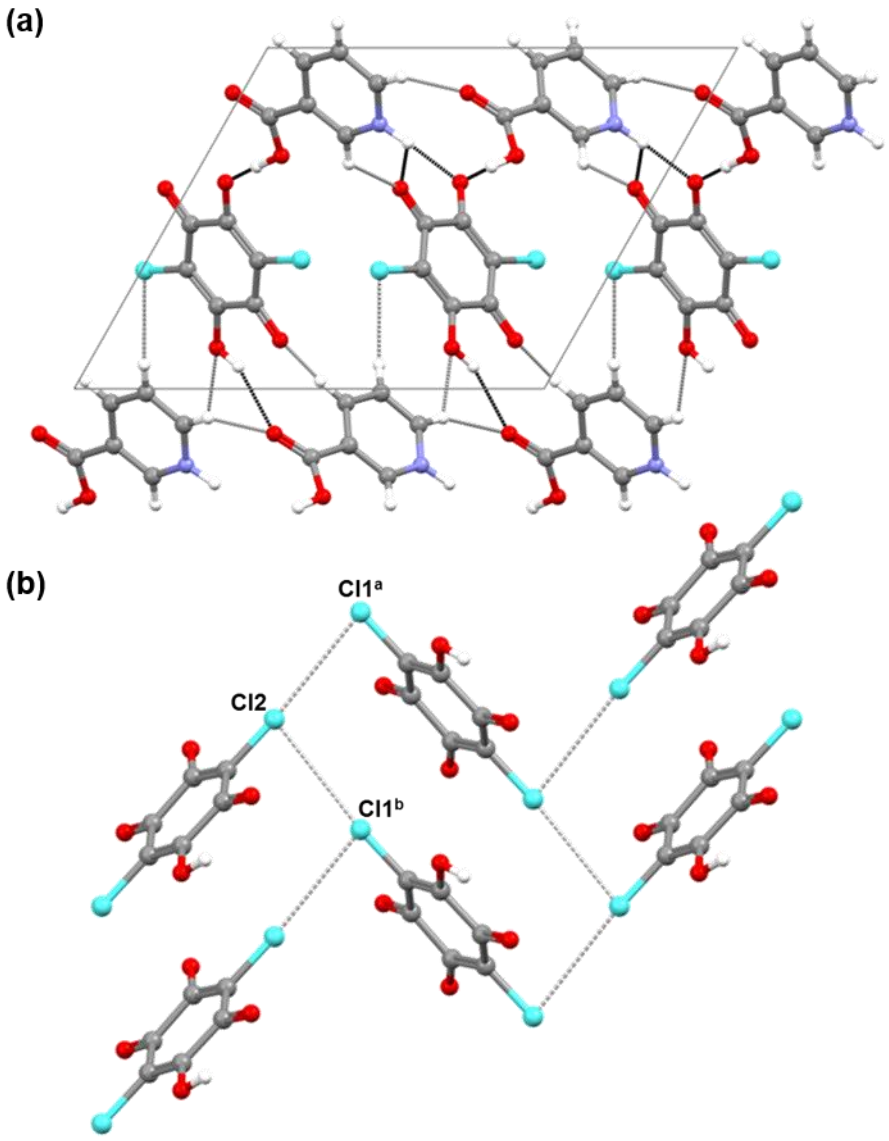

Figure 6.3. Crystal structure of **PAZHOO**. (a) View down the *b* axis showing 2D motifs parallel with the *bc* plane, and O/N-H···O H-bonds (black) and C-H···O/Cl H-bonds (grey). (b) Cl···Cl halogen bonds between hydrogen chloranilate ions. Symmetry codes: ^{a}(x, -y, ½+z) ^{b}(x, -1-y, ½+z)

Pyridinium-4-carboxylic acid hydrogen chloranilate hydrate **(YERXUP)** *($C_6H_6NO_2$)($C_6HCl_2O_4$).H_2O*

The asymmetric unit of **YERXUP** featues one protonated isonicotinic acid ion and one hydrogen chloranilate ion and one water molecule. The ions from columns along the *b* direction, and 2D motifs parallel to the {202} plane (Figure 6.4(a)). In each column, the ions are related to their immediate neighbours through a centre of inversion. The ions are connected primarily through H-bonds *via* the water molecule (Figure 6.4(b)). A bifurcated H-bond is formed from the water molecule to the deprotonated hydroxyl and carbonyl oxygen atoms of the hydrogen chloranilate ion. H-bonds are also formed from the water molecule to the carbonyl oxygen atom of the carboxyl group of the protonated isonicotinic acid ion; from the N-H group of the pyridyl ring to the water molecule, from the hydroxyl group of the hydrogen chloranilate ion to the water molecule, and the strongest H-bond is from the hydroxyl oxygen atom of the carboxyl group to a carbonyl oxygen atom of the hydrogen chloranilate ion (D⋯A distance 2.563(2) Å; angle 175(3)°). The hydrogen chloranilate ions are connected *via* type-I halogen bonds of Cl⋯Cl distance 3.507(1) Å and angles C-Cl1⋯Cl2, 163.95(6)° and C-Cl2⋯Cl1, 168.19(5)° (Figure 6.4(c)). **YERXUP** does not display the bifurcated H-bonded synthons reported by Adam *et al*., however the water is situated in a position which may be possible to occupy with a metal centre, allowing coordination by the organic ligands.

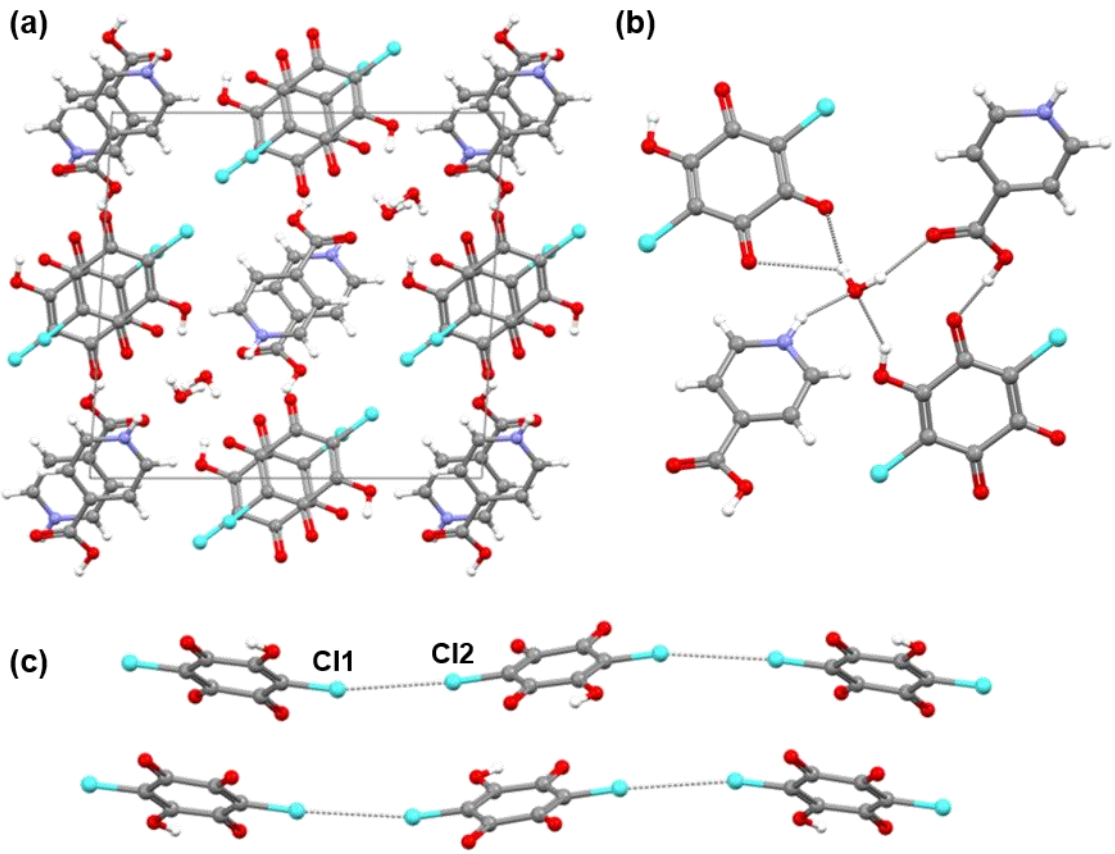

Figure 6.4. Crystal structure of **YERXUP**. (a) View down *b* axis showing 2D H-bonded motifs parallel to the {202} plane. (b) H-bonds connecting between ions. (c) Cl···Cl halogen bonds between hydrogen chloranilate ions.

6.2. New Chloranilic Acid and Pyridine Carboxylic Acid Complexes

6.2.1. *Hydrogen bis-(pyridinium-2-carboxylato) hydrogen chloranilate dihydrate* **(20)**
$(C_6H_{5.5}NO_2)_2(C_6HCl_2O_4).2H_2O$

The complex **(20)** was obtained under a range of conditions. It was prepared by solvent evaporation of a mixture of picolinic acid and chloranilic acid under slightly varying preparation permutations using the various stoichiometric ratios of 1:1, 1:2 or 2:1, dissolved in the solvent systems: acetone at lab temperature; ethanol at lab temperature or water and ACN at 30 °C (see Experimental). The crystals varied in their morphologies with some in the form of large, dark, almost black, crystalline blocks, and others being very dark red, flat needle crystals arranged in clusters. The preparations in which acetone or ethanol were used as the solvent were liable also to produce crystals of **(21)**, while preparations in which water and ACN were used as the solvent more favourably produced **(20)**. Figure 6.5 shows the PXRD pattern of the material produced using a 1:2 stoichiometric ratio and ethanol as the solvent (in red) compared to that of the material produced using a 2:1 stoichiometric

ratio and water and ACN as the solvent (in pink). As might be expected, the pattern of the 2:1 sample is of far better quality to that of the 1:2 sample as the starting materials were used in the same ratio in which they appear in the crystal structure, and it was prepared using water and ACN. Both patterns however display some common peaks with the calculated pattern at about 6°, 12°, 13° and 14°.

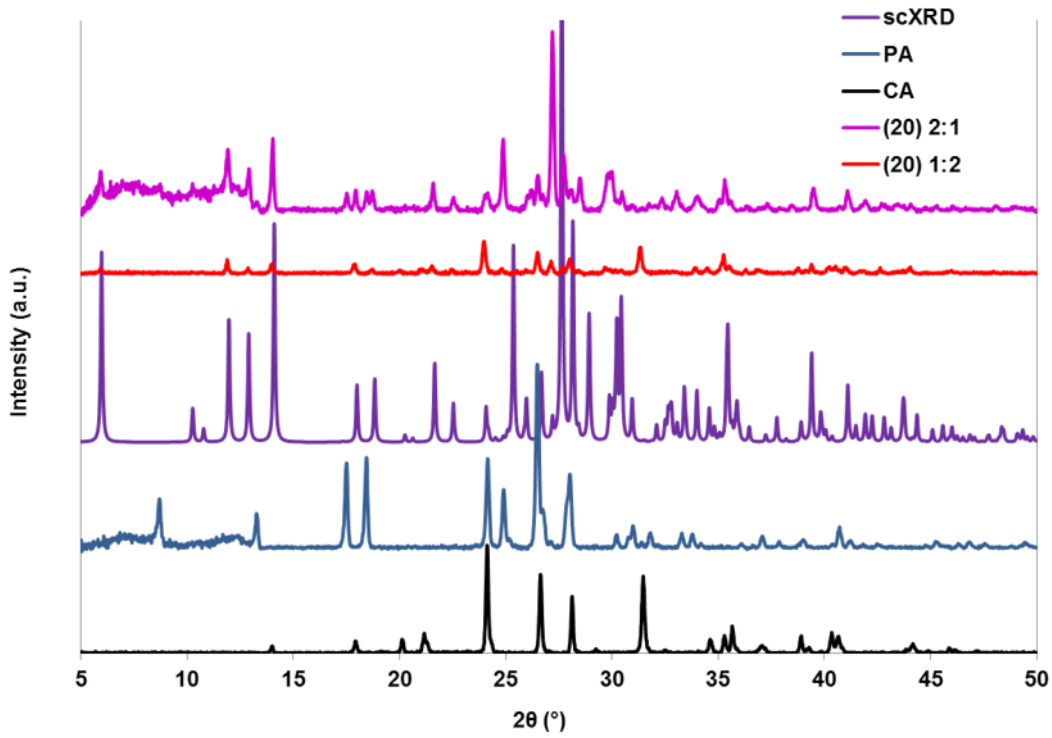

Figure 6.5. PXRD pattern of **(20)** compared to the calculated pattern and patterns of starting materials.

The formula unit of **(20)**, shown in Figure 6.6(a), features two crystallographically equivalent picolinic acid ions, one hydrogen chloranilate ion and two crystallographically equivalent water molecules. The picolinic acid ions, related through an inversion centre, have a protonated pyridyl nitrogen atom and are H-bonded to one another by the hydrogen atom shared between their carboxyl groups (H8). The Fourier difference map shown in Figure 6.6(b) illustrates the spread of the electron density associated with H8. The hydrogen chloranilate ion is located on a centre of inversion and the hydroxyl groups are half occupied by the hydrogen atom H1C. One hydrogen atom of the water molecules is also disordered about two positions (H1W and H2W). Thus, the disordered hydrogen atom (H1) is shared between the water molecule as H1W, and the hydrogen chloranilate ion as H1C. This sharing is illustrated in Figure 6.6(c). The oxygen atom of the water molecule is also disordered about two positions (O5A and O5B). Therefore the water molecule exists either

as H2-O5B-H1W, with an H-O-H angle of 107(3)°, or as H2-O5A-H2W, with a wider angle of 114(3)°. These angles are comparable to the average H-O-H angle of approx. 106.8°, for a water molecule in an organic crystal, calculated from structures reported in the CSD from data collected at temperatures between 100 and 153 K.

The C-O distances of the carboxyl group of the picolinic acid ion are 1.229(2) Å for C1-O3 and 1.282(2) Å for C1-O4. The C=O and C-O bonds are slightly longer than the equivalent distances in the pure ligand (1.213(2) Å and 1.279(2) Å, respectively). The O=C-O angle O3-C1-O4 is 128.8(2)°, about 2° wider than in the pure ligand (126.8(1)°). The O4-C1-C2-N1 torsion angle is -24.1(2)°, indicating the non-coplanarity of the pyridinium ring and the carboxyl group, in contrast to pure picolinic acid where the equivalent torsion angle is -4.0(1)°. In their solid state structures, the picolinic acid ion in **(20)** and the molecule in the pure form are similar in that they form H-bonded dimers that connect *via* a shared hydrogen atom. In pure picolinic acid, the hydrogen atom is disordered between the pyridyl nitrogen atom and the carboxyl group, but in **(20)** the pyridyl nitrogen atom is fully protonated forming the pyridinium ring, and the ion has an overall +½ charge, compensated by the overall -1 charge of the hydrogen chloranilate ion. The presence of water in **(20)** affects the picolinic acid ion by the formation of the H-bond N1-H7···O5^{f}, possibly causing the twisting of the molecule about the C1-C2 bond.

The hydrogen chloranilate ion has a C=O distance, C7-O2, of 1.236(2) Å, slightly longer than the C=O distance of pure chloranilic acid (1.224(2) Å), while the C-O distance, C8-O1, of 1.290(2) Å, is shorter than the C-O distance of the pure ligand (1.322(2) Å). Accordingly, the C=C bond distance (C8-C9) is 1.374(2) Å, and the C-C bond distance (C7-C9^{a}) is 1.431(2) Å; these distances are longer and shorter, respectively, when compared to the corresponding distances of chloranilic acid (C=C 1.349(2) Å; C-C 1.450(2) Å) indicating the delocalisation of the partial negative charge over either O2-C7-C9^{a}-C8^{a}-O1^{a} or O1-C8-C9-C7^{a}-O2^{a}. The C-C distance (C7-C8) of 1.533(2) Å, and the C-Cl distance (C9-Cl1) of 1.738(2) Å are longer than the corresponding distances observed in pure chloranilic acid (1.508(2) Å; C-Cl 1.716(2) Å).

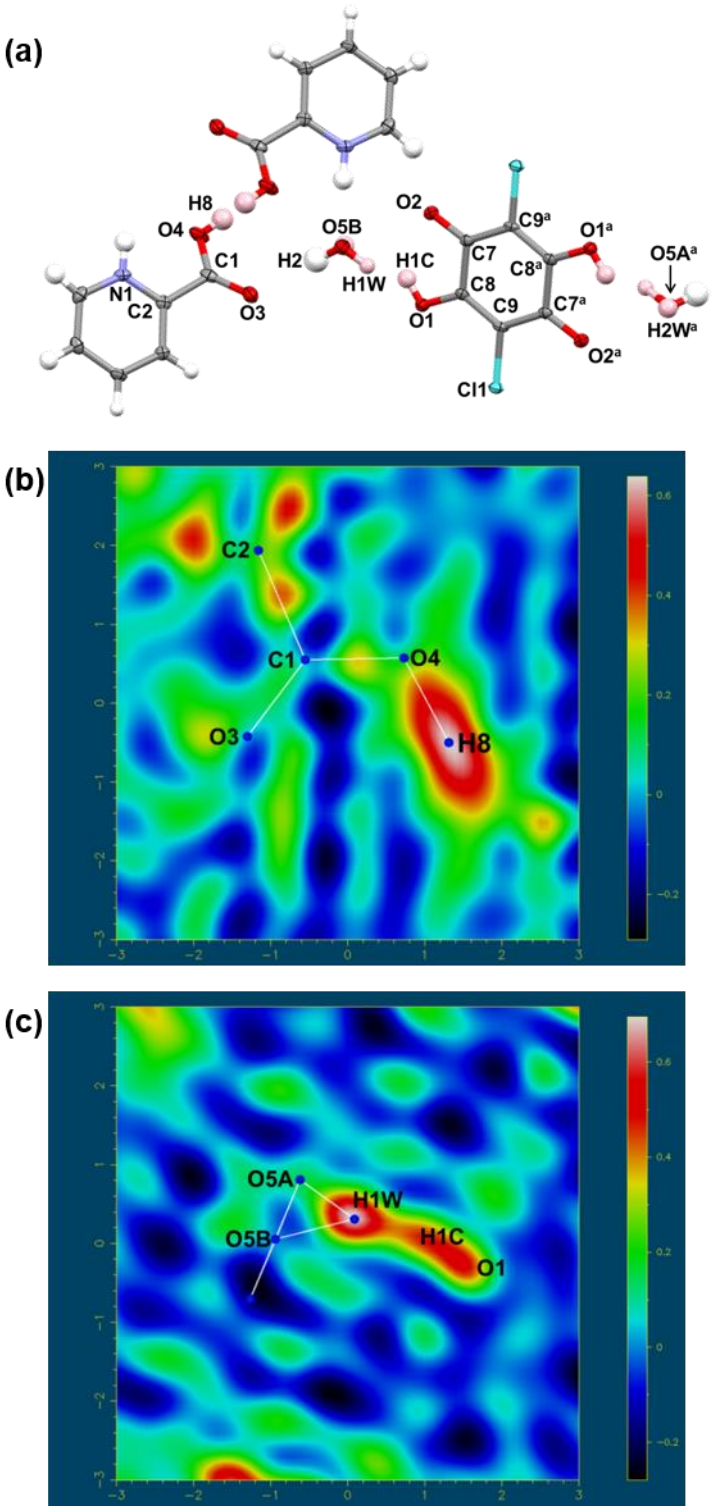

Figure 6.6. Crystal structure of **(20)**. (a) Formula unit of two half-protonated picolinic acid ions, one hydrogen chloranilate ion and two water molecules. Hydrogen atoms of half occupancy are coloured in pink (O5A is obstructed by H2W). (b) Fourier difference map showing the electron density assigned as H8. (c) Fourier difference map showing the electron density assigned as half occupied hydrogen atoms H1W and H1C. Symmetry codes: [a](2-x, 1-y, 1-z)

(20) is composed of 2D motifs of hydrogen chloranilate ions that lie parallel to the *bc* plane, separated by layers of picolinic acid dimers and water ligands (Figure 6.7(a) and Figure 6.8(a)). The hydrogen chloranilate ions interact *via* type-II halogen bonds, Cl1···Cl1^{d}/Cl1^{c}···Cl1^{d} of distance 3.359(1) Å, and angles C-Cl1···Cl1^{d}/C-Cl1^{d}···Cl1^{c} of approx. 127.48° and C-Cl1^{d}···Cl1/ C-Cl1^{c}···Cl1^{d} of approx. 163.30°. They also interact *via* π-π stacking interactions between their C=C bonds, with a centroid-centroid separation of 3.655(1) Å (Figure 6.7(b)).

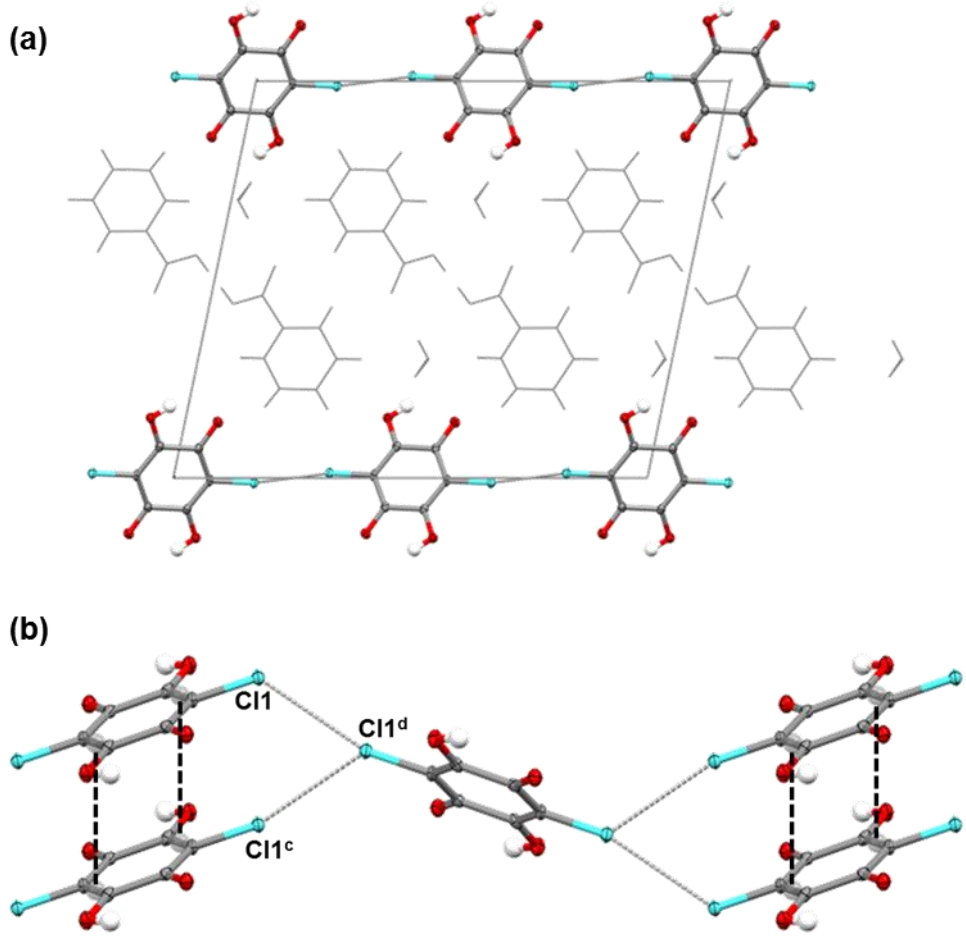

Figure 6.7. Crystal structure of **(20)**. (a) View down the *b* axis showing hydrogen chloranilate ions forming a 2D sheet parallel to the *bc* plane. (b) Interactions between the hydrogen chloranilate ions. Symmetry codes: ^{c}(x, -1+y, z) ^{d}(2-x, -½+y, ½-z)

The picolinic acid dimers are paired *via* the H-bond O4-H8···O4^{e}, (Figure 6.8(b) and Table 6.1). This is a short and strong H-bond with a D···A distance of 2.443(2) Å. The angle, when measured using the location of the half occupied H8 atom is 169(5)°, but if the centroid between the two half occupied H8 atoms, H8 and H8^{e}, is used, the angle is approx. 180°.

If the average position of H8 is taken, this equates to a centred short, strong H-bond with equal D-H and H···A distances of approx. 1.222 Å.

The picolinic acid dimers are linked to neighbouring dimers directly through the weak H-bonds, C3-H3···O3^{g} and C4-H4···O3^{g} from C-H groups of the pyridinium ring to the carboxyl oxygen atom O3 (Figure 6.8(b) and Table 6.1). They are also linked *via* the water molecule. The N-H group of the pyridinium ring forms moderately strong H-bonds to the disordered water molecule oxygen atoms: N1-H7···O5A^{f} and N1-H7···O5B^{f} have D···A distances of 2.734(3) Å and 2.739(1) Å, and angles of 160(2)° and 174(2)°, respectively. C4-H4 also forms the H-bond C4-H4···O5A^{g} to one water molecule while the oxygen atom is in one of its two positions.

The disordered water molecule forms a moderately strong H-bond to the carboxyl oxygen atom O3, while O5 is in either of its positions. O5A-H2···O3 has a D···A distance of 2.820(3) Å and an angle of 146(2)°, while O5B-H2···O3 has a D···A distance of 2.926(1) Å and an angle of 159(2)°.

The water molecule also forms an H-bond to the hydrogen chloranilate ion, as illustrated in Figure 6.8(c) and listed in Table 6.1. O5A-H1W···O1 and O5B-H1W···O1 are moderately strong interactions with D···A distances of 2.804(3) Å and 2.676(3) Å and angles of 149(3)° and 161(4)°, respectively. This H-bond is reciprocated, in the appropriate disordered H configurations, by the hydrogen chloranilate ion in O1-H1C···O5A and O1-H1C···O5B, which have equivalent D···A distances to the interactions involving H1W, and angles of 141(4)° and 147(4)°, respectively. The N-H group of the pyridinium ring H-bonds to the carbonyl oxygen atom of the hydrogen chloranilate ion; N1-H7···O2^{f} has a very low angle of 107(2)° and a D···A distance of 3.236(1) Å.

C4-H4, C5-H5 and C6-H6 also form H-bonds to the hydrogen chloranilate ion: C4-H4 to the hydroxyl oxygen atom, C4-H4···O1^{g}; C5-H5 also to this oxygen atom C5-H5···O1^{g}, and also to two chlorine atoms located above and below the pyridinium ring relative to the *b* direction, C5-H5···Cl1^{g} and C5-H5···Cl1^{h}; C6-H6 also forms an H-bond to a chlorine atom C6-H6···Cl1^{j}, and to two carbonyl oxygen atoms located above and below the pyridinium ring relative to the *b* direction, C6-H6···O2^{i} and C6-H6···O2^{f}. These H-bonds are moderately weak to weak interactions with D···A distances ranging from 3.181(2) Å for C6-H6···O2^{f} to 3.734(2) Å for C5-H5···Cl1^{g}, and angles from 114(2)° for C5-H5···Cl1^{h} to 151(2)° for C5-H5···Cl1^{g}.

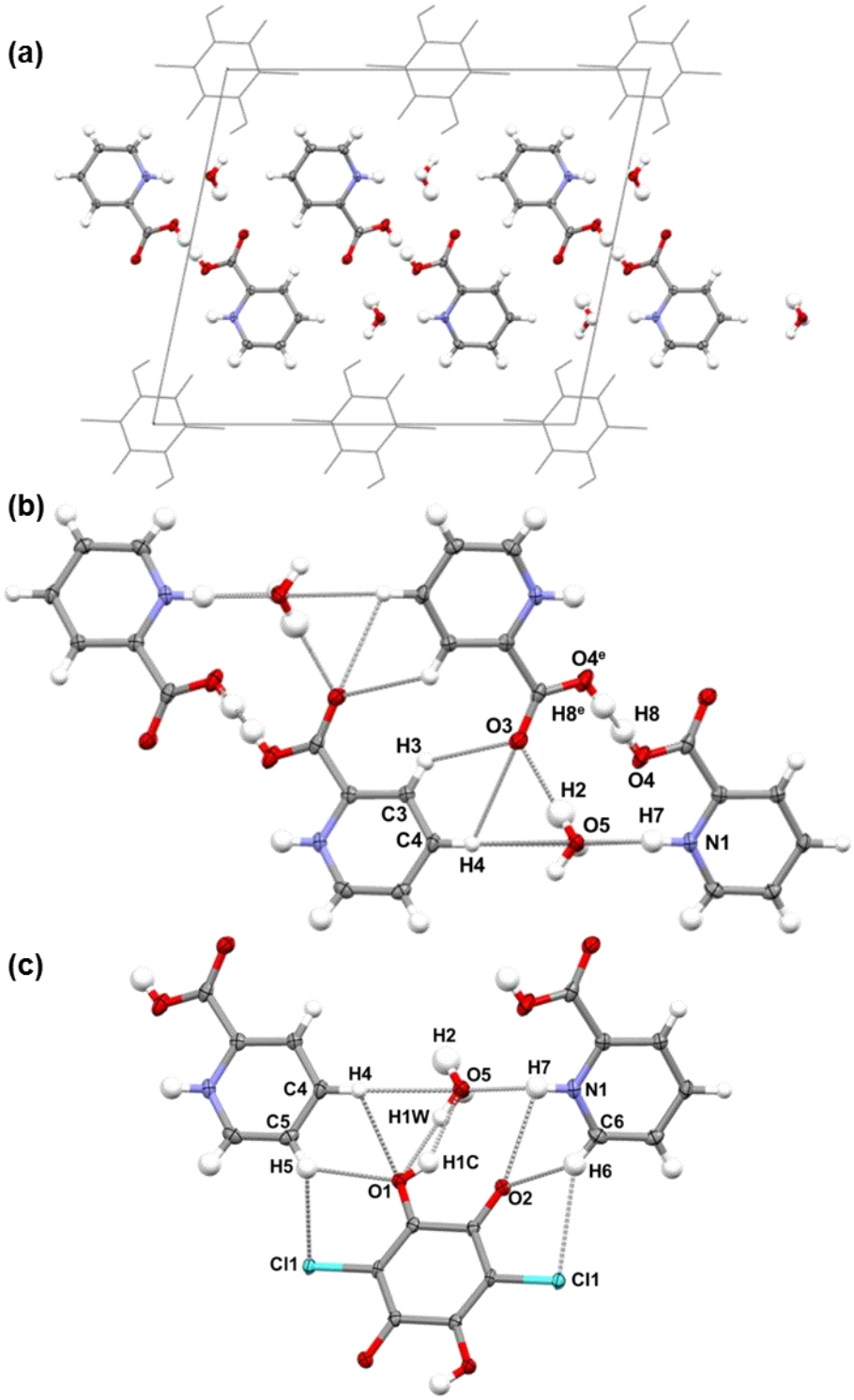

Figure 6.8. Crystal structure of **(20)**. (a) View down the *b* axis showing the layer of picolinic acid dimers and water molecules between the 2D motifs formed by the hydrogen chloranilate ions. (b) H-bonds connecting picolinic acid ions and water molecules. (c) H-bonds connecting picolinic acid ions and water molecules to hydrogen chloranilate ions.

The water molecule also forms an H-bond to another water molecule located along the *b* direction, O5A-H2W···O5B^{k}, Figure 6.9(a) and Table 6.1. This is a moderately strong interaction with a D···A distance of 2.838(4) Å and a near linear angle of 174(5)°. The picolinic acid dimers also stack along the *b* direction *via* π-π stacking interactions in which the centroid-centroid distance, as it was for the hydrogen chloranilate π-π stacking interaction distance, is 3.655(1) Å (Figure 6.9(b)). The packing of **(20)** as viewed down the *c* axis is shown in Figure 6.9(c), illustrating the 2D motifs of hydrogen chloranilate ions parallel to the *bc* plane, the columns of water molecules parallel to the *b* direction, and the criss-crossing of picolinic acid dimers.

The water ligand plays a central role in the connectivity of **(20)** and the short, strong H-bond connecting the picolinic acid dimers is also fundamental to the structure. This H-bond makes the carboxyl group of picolinic acid effectively unavailable to interact with hydrogen chloranilate ion, such that the interactions associating the two organic substituents are weaker C-H···O, C-H···Cl H-bonds and a weak N-H···O interaction. Although the structure is influenced by π-π stacking interactions, these are 'homogeneous' in that when they are observed, they involve only one type of ion. This complex may offer some potential to incorporate as a 'supramolecular ligand' if a metal ion could occupy the location in which the water molecule resides. This would make the oxygen atoms of the hydrogen chloranilate ion, a carboxyl oxygen atom and the nitrogen atom of one picolinic acid ion and a carboxyl oxygen atom of another picolinic acid molecule available for metal coordination. However in order to satisfy the preferred octahedral geometry of a magnesium ion, for example, significant rearrangement of the organic components would be necessary, which would negate this possibility.

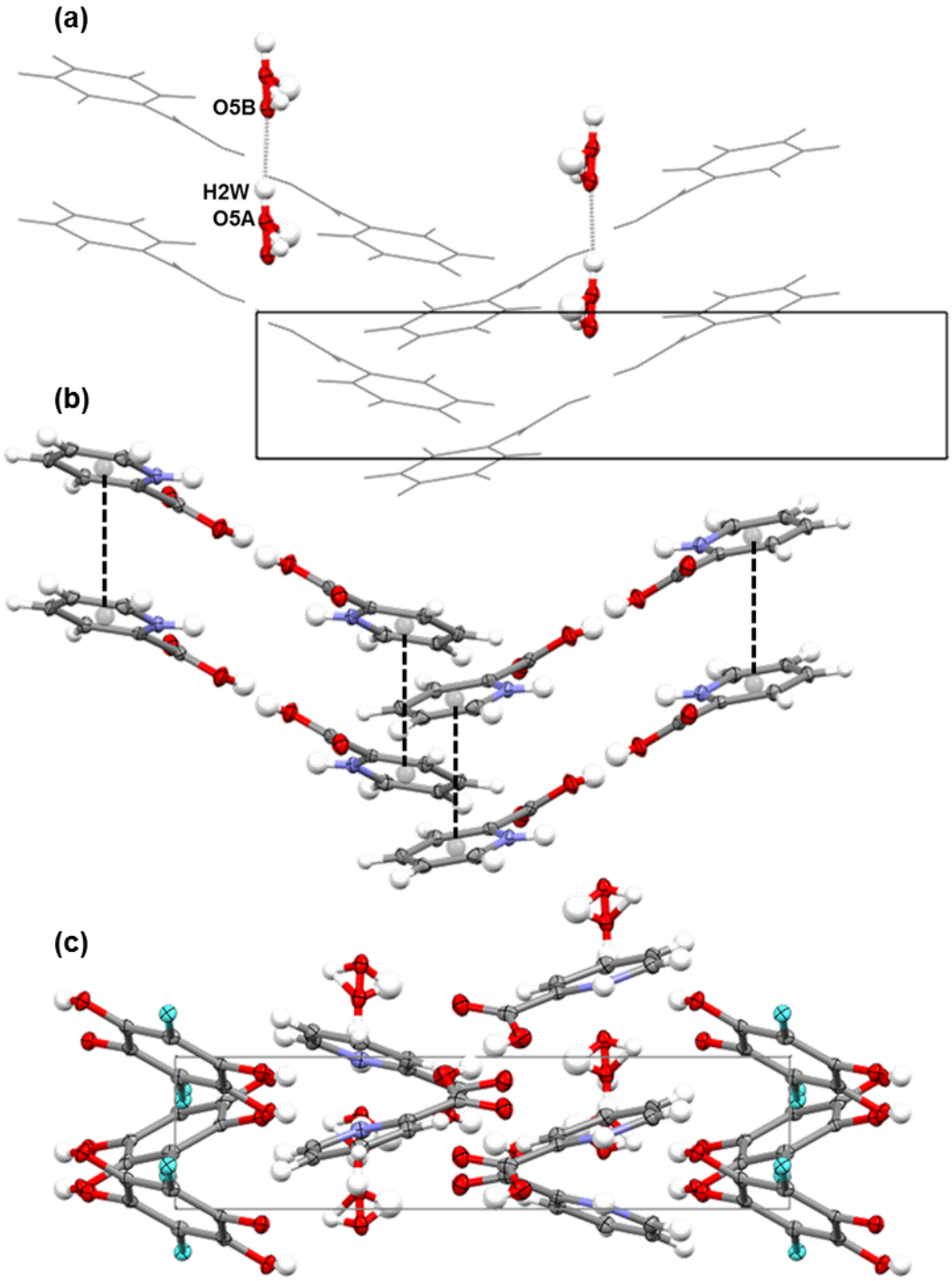

Figure 6.9. Crystal structure of **(20)**. View down the *a* axis showing (a) H-bonds between water molecules, and (b) π-π stacking interactions between picolinic acid ions, connecting the structure along the *b* direction. (c) View down the *c* axis showing zigzag packing of **(20)**.

Table 6.1. Geometries of H-bonds in **(20)**.

D-H···A Interaction	D-H (Å)	H···A (Å)	D···A (Å)	D-H···A (°)
(Figure 6.8(b)) H-bonds between picolinic acid ions and water molecules				
N1-H7···O5A[f]	0.89(2)	1.88(2)	2.734(3)	160(2)
N1-H7···O5B[f]	0.89(2)	1.85(1)	2.739(1)	174(2)
*N1-H7···O5[f]	0.89(2)	1.820	2.706	171.9
O4-H8···O4[e]	0.78(5)	1.67(5)	2.443(2)	169(5)
*O4-H8···O4[e]	1.222	1.222	2.443(2)	180.0
O5A-H2···O3	0.87(3)	2.06(3)	2.820(3)	146(2)
O5B-H2···O3	0.90(3)	2.06(3)	2.926(1)	159(2)
*O5-H2···O3	0.784	2.06(3)	2.844	173.5
C3-H3···O3[g]	0.93(2)	2.72(1)	3.227(1)	115(1)
C4-H4···O3[g]	0.93(2)	2.80(1)	3.290(1)	114(1)
C4-H4···O5A[g]	0.93(2)	2.65(2)	3.564(3)	167(2)
*C4-H4···O5[g]	0.93(2)	2.805	3.689	158.7
(Figure 6.8(c)) H-bonds between hydrogen chloranilate ions, picolinic acid ions and water molecules				
N1-H7···O2[f]	0.89(2)	2.87(4)	3.236(1)	107(2)
O1-H1C···O5A	0.82(5)	2.12(5)	2.804(3)	141(4)
O1-H1C···O5B	0.82(5)	1.96(5)	2.676(3)	147(4)
O5A-H1W···O1	1.06(4)	1.84(5)	2.804(3)	149(3)
O5B-H1W···O1	0.87(4)	1.84(5)	2.676(3)	161(4)
*O1-H1···O5	1.299	1.402	2.676(3)	164.7
C4-H4···O1[g]	0.93(2)	3.01(2)	3.372(2)	114(1)
C5-H5···O1[g]	0.92(2)	2.65(2)	3.329(2)	132(2)
C5-H5···Cl1[g]	0.92(2)	2.91(2)	3.734(2)	151(2)
C5-H5···Cl1[h]	0.92(2)	3.07(2)	3.546(2)	114(2)
C6-H6···O2[i]	0.90(2)	2.49(2)	3.186(2)	135(2)
C6-H6···O2[f]	0.90(2)	2.68(2)	3.181(2)	117(2)
C6-H6···Cl1[j]	0.90(2)	2.85(2)	3.650(2)	149(2)
(Figure 6.9(a)) H-bond between water molecules				
O5A-H2W···O5B[k]	0.83(4)	2.02(4)	2.838(4)	174(5)

Symmetry codes: [e](1-x, 3-y, 1-z) [f](1-x, 3-y, 1-z) [g](1-x, -½+y, ½-z) [h](1-x, ½+y, 1-z) [i](1-x, 1-y, 1-z) [j](-1+x, y, z) [k](x, 1+y z) *H-bond distances and angles measured using centroids between disordered atoms.

The thermal behaviour of **(20)** was investigated by HSM and DSC. During HSM, there was bubbling from the crystal at around 80 °C, with no other event observed until the crystal fractured and decomposed from about 154 – 170 °C; by 200 °C only a dark skeletal trace of the crystal remained. The events observed during HSM do not correspond with the melting of the starting materials (picolinic acid m.p. 139 – 142 °C; chloranilic acid m.p. >300 °C). DSC analysis (Figure 6.10) shows a very broad endotherm at 94.8 °C, likely to be the loss of water from the structure, followed by a second event which may indicate recrystallisation at about 210 °C, before final decomposition.

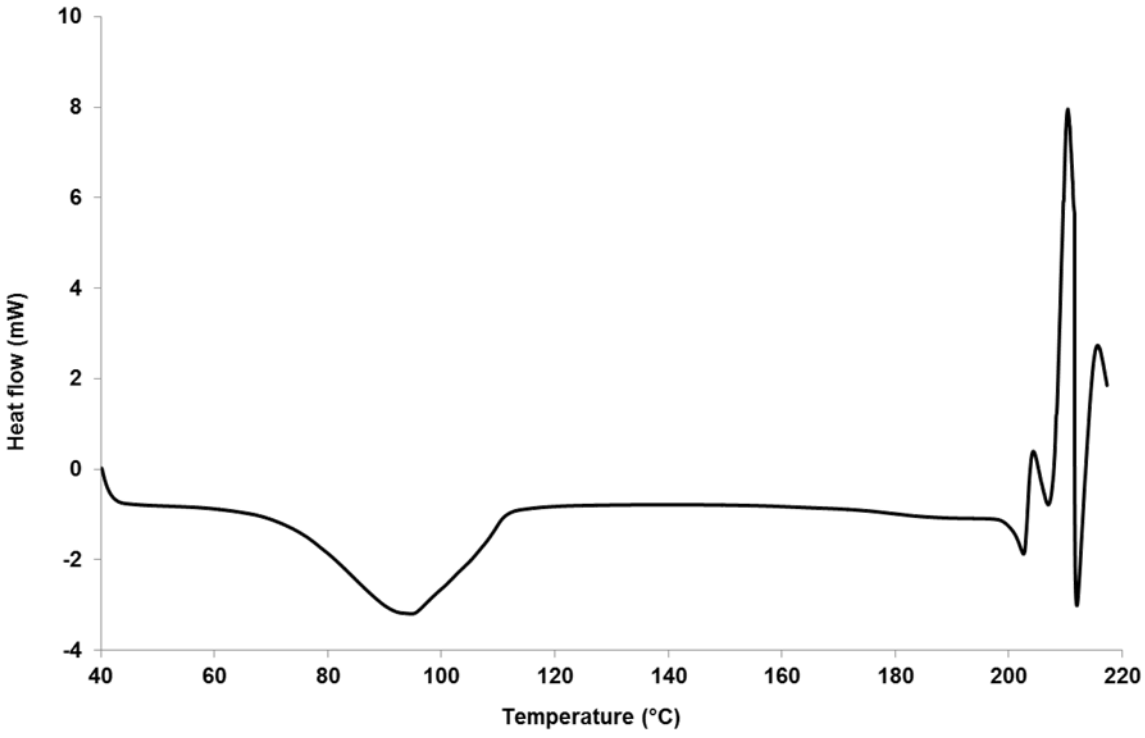

Figure 6.10. DSC trace of **(20)** on a 3.2 mg sample with a temperature ramp of 10 °C min^{-1}.

6.2.2. *Bis-(pyridinium-2-carboxylato) chloranilic acid* **(21)** *($C_6H_5NO_2)_2(C_6H_2Cl_2O_4$)*

(21) was prepared by solvent evaporation of a 2:1 stoichiometric mixture of picolinic acid and chloranilic acid dissolved in either acetone or ethanol at lab temperature. However, some repeat preparations of **(21)** resulted in exclusively **(21)** while others resulted in a visible mixture of both **(21)** and **(20)** (see Experimental). The crystals could be distinguished by appearance as unlike the darker **(20)**, **(21)** is in the form of clear orange/red crystals.

The PXRD pattern of the bulk sample from four crystallisation experiments which produced crystals of **(21)** is shown in Figure 6.11, indicating very little agreement between the experimentally obtained and calculated patterns, or the starting materials. Comparing the

PXRD pattern of **(21)** to the calculated patterns of both **(21)** and **(20)**, (Figure 6.12), it is apparent from the strong correlation between the two patterns that the bulk sample mostly contains **(20)**.

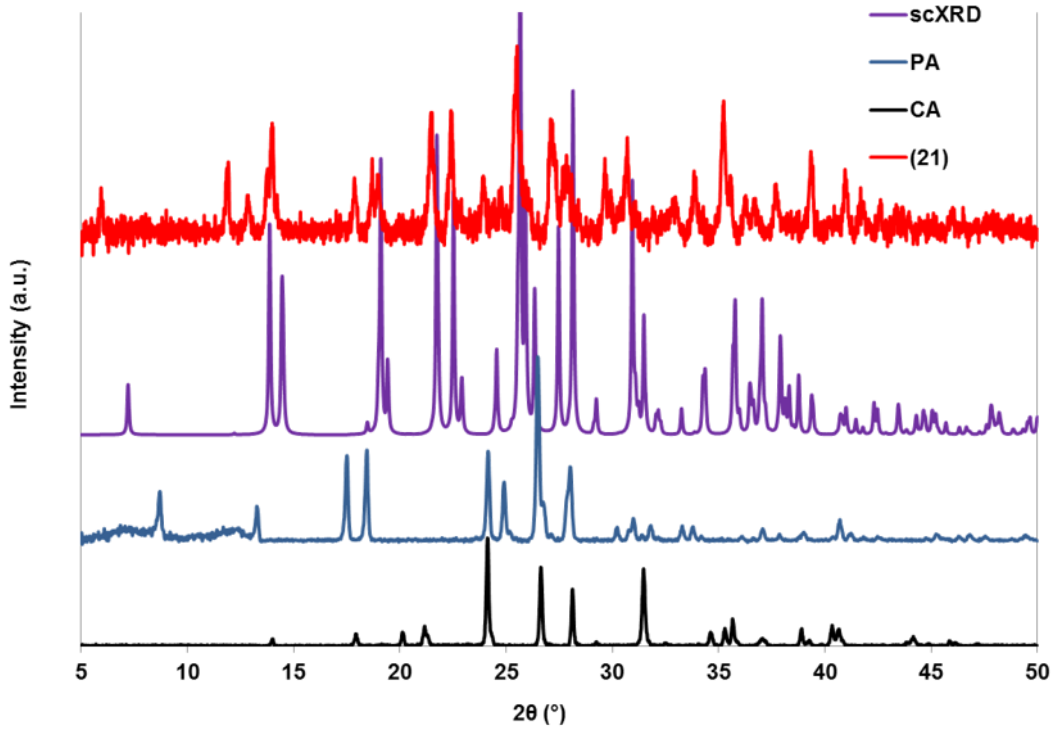

Figure 6.11. PXRD pattern of **(21)** compared to the calculated pattern and patterns of starting materials.

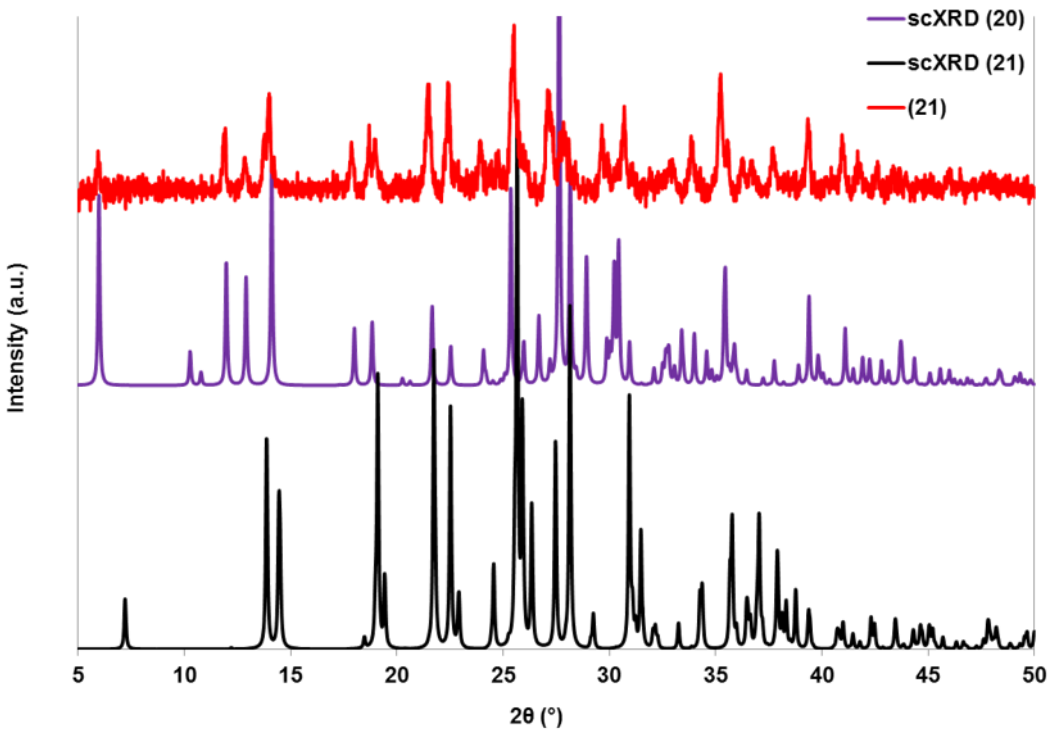

Figure 6.12. PXRD pattern of **(21)** compared to the calculated pattern of **(21)** and **(20)**.

The formula unit of **(21)** (Figure 6.13(a)), consists of two molecules of zwitterionic picolinic acid, and one molecule of chloranilic acid. The crystal structure of **(21)** is similar to that of **(20)** in that the chloranilic acid molecules form 2D motifs parallel to the *bc* plane, between which are layers of picolinic acid molecules. The packing is shown in Figure 6.13(b), which reveals that the structure has a similar zigzag pattern to that of **(20)**. The structures differ in that **(21)** does not feature water, and the picolinic acid molecules are fully deprotonated at the carboxyl group, meaning that they interact with one another to form dimers in a different manner.

The picolinic acid molecule has C-O distances of 1.256(2) Å and 1.241(2) Å for C1-O3 and C1-O4, respectively. The difference between the C-O lengths is less than observed for the C-O and C=O distances of the picolinic acid ion in **(20)**, due to the full delocalisation of the negative charge. The O-C-O angle is 128.0(2)°, close to the equivalent angle in **(20)** of 128.8(2)°. The torsion angle O4-C1-C2-N1 is 3.4(3)°; slightly less than that for pure picolinic acid (-4.0(1)°). Therefore, the pyridinium ring and the carboxylate group of picolinic acid in **(21)** are more planar than in the picolinic acid ion in **(20)**, which has a O4-C1-C2-N1 torsion angle of -24.1(2)°.

As expected, the chloranilic acid molecule has C-O, C=O, C-C, C=C and C-Cl distances more similar to those in pure chloranilic acid than the hydrogen chloranilate ion of **(20)**. The

C-O distance (C9-O2) is 1.318(2) Å and the C=O distance (C7-O1) is 1.220(2) Å; both of these distances are close to the equivalent distances of pure chloranilic acid (C-O 1.322(2) Å; C=O 1.224(2) Å). The C-C bond distances C7-C8 and C7-C9^{a} are 1.456(5) Å and 1.512(3) Å, respectively, and the C=C bond distance C8-C9 is 1.354(3) Å, and the C-Cl bond distance C8-Cl1 is 1.722(2) Å: all of these distances are close to those of pure chloranilic acid.

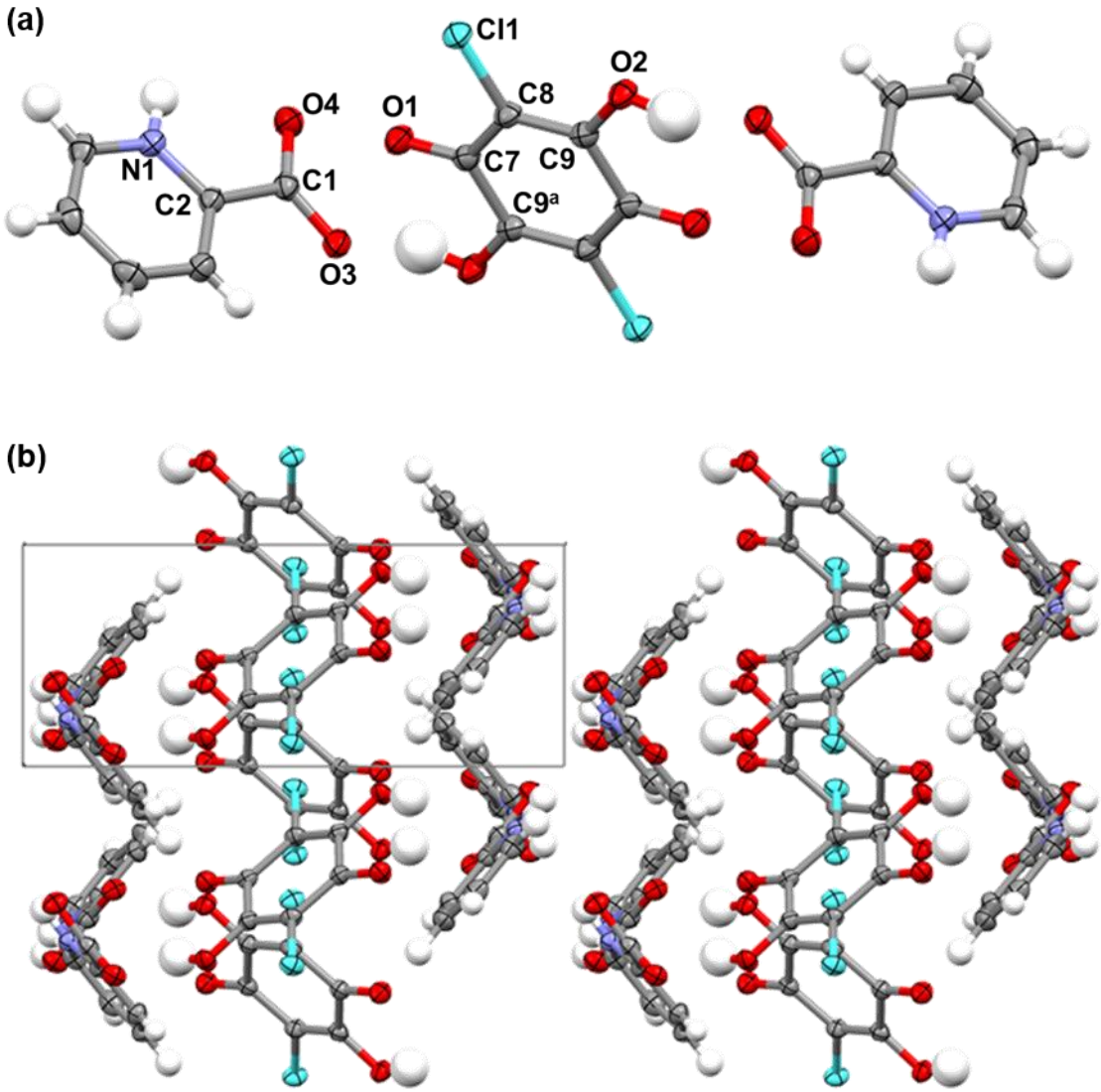

Figure 6.13. Crystal structure of **(21)**. (a) Formula unit of two zwitterionic picolinic acid molecules and one chloranilic acid molecule. (b) View down the *c* axis showing zigzag packing. Symmetry codes: ^{a}(2-x, 1-y, 1-z)

Figure 6.14(a) and Figure 6.15(a) show the packing of **(21)** with the 2D motifs of chloranilic acid molecules parallel to the *bc* plane, and the layers of picolinic acid dimers between them. The chloranilic acid molecules interact *via* type-II halogen bonds,

Cl1···Cl1^{b}/Cl1···Cl1^{c} of distance 3.446(1) Å, slightly shorter than the Cl···Cl halogen bond in **(20)**. The angles of these interactions are; C-Cl1···Cl1^{b}/C-Cl1^{c}···Cl1, 172.15(7)°; C-Cl1^{b}···Cl1/ C-Cl1···Cl1^{c}, 94.33(7)°. Unlike **(20)**, there are no π-π stacking interactions, with a long centroid-centroid distance of 5.019(1) Å. Therefore the zigzag packing of **(21)** is more open than that of **(20)**, as can be seen when comparing Figure 6.9(c) and Figure 6.13(b).

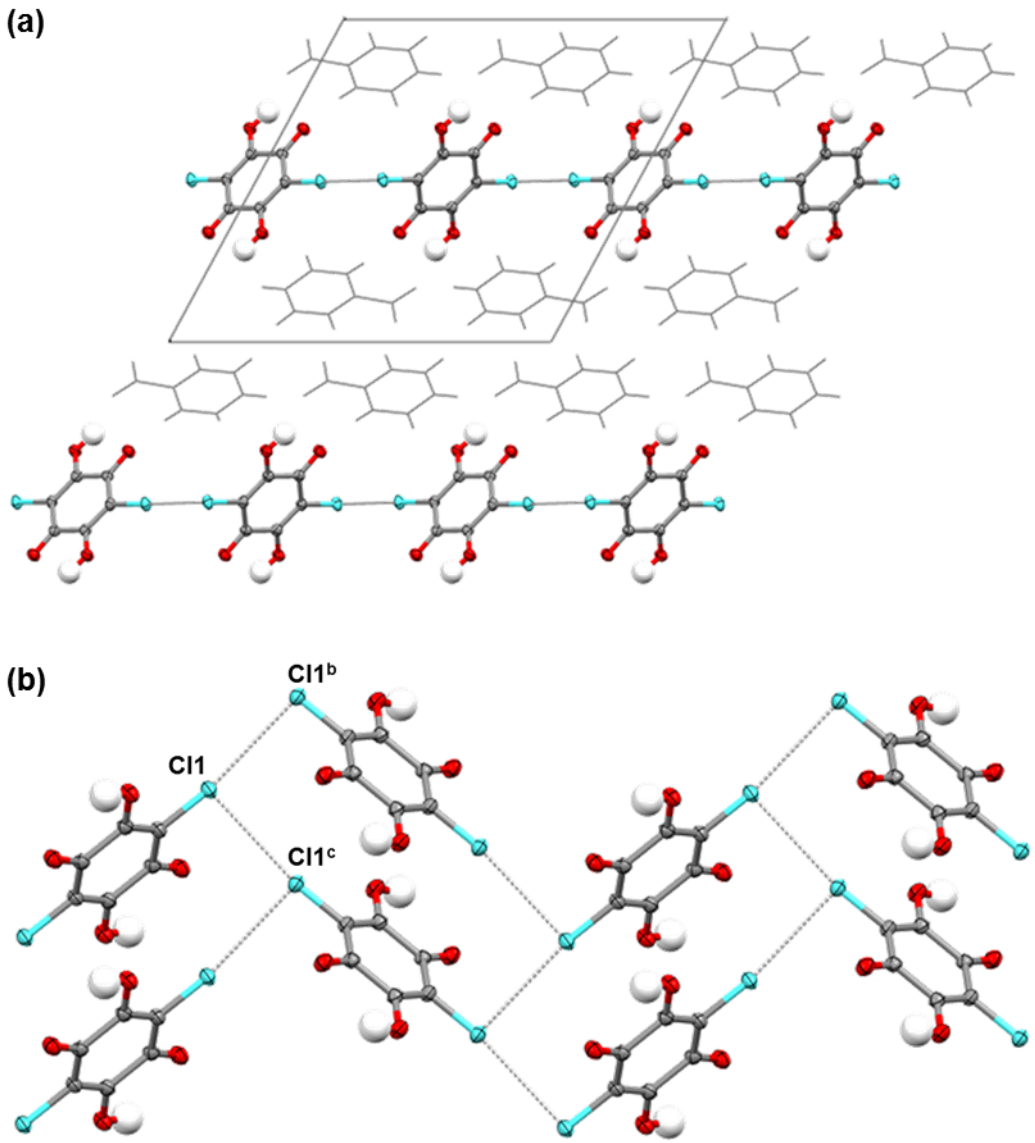

Figure 6.14. Crystal structure of **(21)**. (a) View down the *b* axis showing chloranilic acid molecules forming 2D sheets parallel to the *bc* plane. (b) Cl···Cl halogen bonds between chloranilic acid molecules. Symmetry codes: ^{b}(1-x, ½+y, 1½-z) ^{c}(1-x, -½+y, 1½-z)

The picolinic acid dimers form layers between the 2D motifs formed by the chloranilic acid molecules (Figure 6.15(a)). The dimers are formed by the moderately strong H-bond N1-H1···O4^{d} (Figure 6.15(b) and Table 6.2). This interaction has a D···A distance of 2.715(2) Å

and an angle of 154(3)°. The picolinic acid dimers are positioned at an angle of approx. 80° from the next picolinic acid pair along the *c* direction. They are connected to the neighbouring molecules through four H-bonds from the C-H groups of the pyridinium ring to the carboxylate oxygen atoms of the next picolinic acid dimers. These H-bonds are moderately weak to weak interactions with D···A distances of 3.181(3) Å for C6-H6···O3^{f} to 3.453(3) Å for C5-H5···O4^{f}, and angles from 115(2)° for C6-H6···O3^{f} to 138(2)° for C5-H5···O3^{e}.

The picolinic and chloranilic acid molecules are connected by four H-bonds (Figure 6.15(c) and Table 6.2). O2-H2···O3^{d} is formed between the hydroxyl group of chloranilic acid to a carboxylate oxygen atom of picolinic acid. This H-bond has a short-medium length of 2.538(2) Å and a medium angle of 153(4)°. The picolinic acid molecule forms an H-bond to the carbonyl group of chloranilic acid, C3-H3···O1, with a D···A distance of 3.258(3) Å and an angle of 163(2)°. C5-H5 also forms an H-bond to this oxygen atom, C5-H5···O1^{e}, with a longer D···A distance of 3.658(2) Å and an angle of 130(2)°. The picolinic acid molecule forms an H-bond to the hydroxyl oxygen atom of the chloranilic acid molecule, C4-H4···O2^{c}, the shortest of these carbon donor H-bonds with a D···A distance of 3.190(3) Å and an angle of 147(2)°.

In common with **(20)**, the components of **(21)** are quite distinct from one another with the picolinic acid molecules, again, seeming preferentially to form dimers between themselves, this time through the H-bond N1-H1···O4^{d}. The only strong interaction between picolinic acid and chloranilic acid is the H-bond O2-H2···O3^{d}, however a robust ‘supramolecular motif’ is not observed.

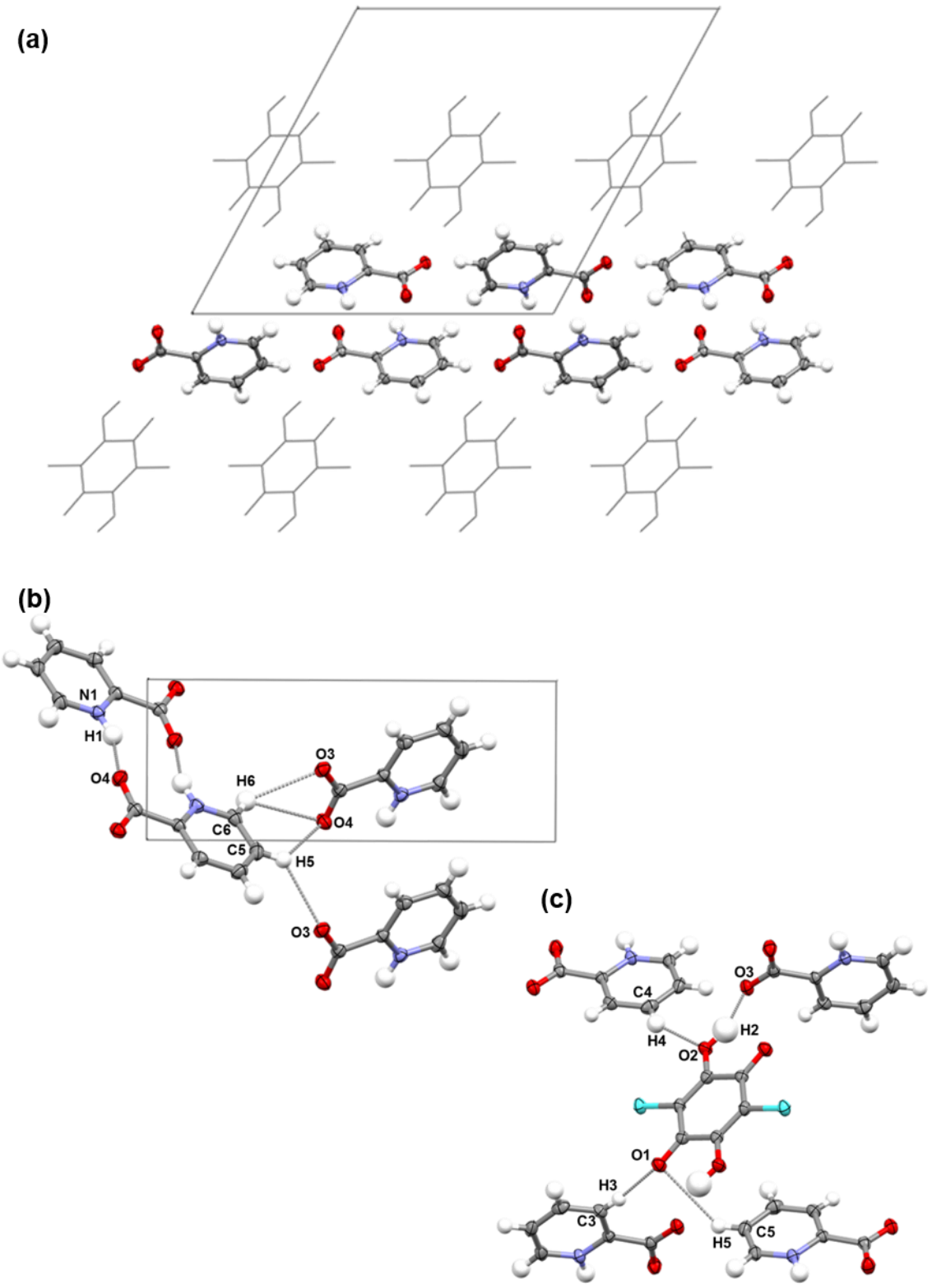

Figure 6.15. Crystal structure of **(21)**. (a) View down the *b* axis showing picolinic acid molecules between the 2D motifs formed by the chloranilic acid molecules. (b) View down the *a* axis showing H-bonds between picolinic acid molecules. (c) H-bonds between picolinic and chloranilic acid molecules.

Table 6.2. Geometries of H-bonds in **(21)**.

D-H···A Interaction	D-H (Å)	H···A (Å)	D···A (Å)	D-H···A (°)
(Figure 6.15(b)) H-bonds between picolinic molecules				
N1-H1···O4[d]	0.94(3)	1.84(3)	2.715(2)	154(3)
C5-H5···O3[e]	0.93(2)	2.60(3)	3.358(3)	138(2)
C5-H5···O4[f]	0.93(2)	2.83(3)	3.453(3)	125(2)
C6-H6···O3[f]	1.02(3)	2.62(2)	3.181(3)	115(2)
C6-H6···O4[f]	1.02(3)	2.80(3)	3.441(3)	121(2)
(Figure 6.15(c)) H-bonds between picolinic and chloranilic acid molecules				
O2-H2···O3[g]	0.94(5)	1.67(5)	2.538(2)	153(4)
C3-H3···O1	0.86(3)	2.43(3)	3.258(3)	163(2)
C4-H4···O2[c]	0.94(3)	2.36(3)	3.190(3)	147(2)
C5-H5···O1[e]	0.93(2)	2.89(2)	3.658(2)	130(2)

Symmetry codes: [c](1-x, -½+y, 1½-z) [d](1-x, 2-y, 2-z) [e](x, 1½-y, -½-+z) [f](2-x, 3-y, 2-z) [g](x, 2½-y, -½+z)

Single crystals of **(21)** were analysed by HSM. The crystals appeared to bubble from about 170 °C and there was a well defined melt from 200 – 203 °C. The DSC trace from thermal analysis of the bulk sample (Figure 6.16) does show this melt, but it is immediately followed by an equally strong exothermic event at approx. 209 °C, possibly indicating a recrystallisation event, which was not observed during HSM, but which is familiar from the DSC trace of **(20)**. There is also a broad endotherm at 89.4 °C, which is also observed in the DSC trace of **(20)**, albeit at the higher temperature of 94.8 °C. As the PXRD of the bulk samples from crystallisation experiments resulting in **(21)** revealed that the sample mostly contained **(20)**, it is likely that this event originates from the loss of water from the crystalline structure of **(20)**.

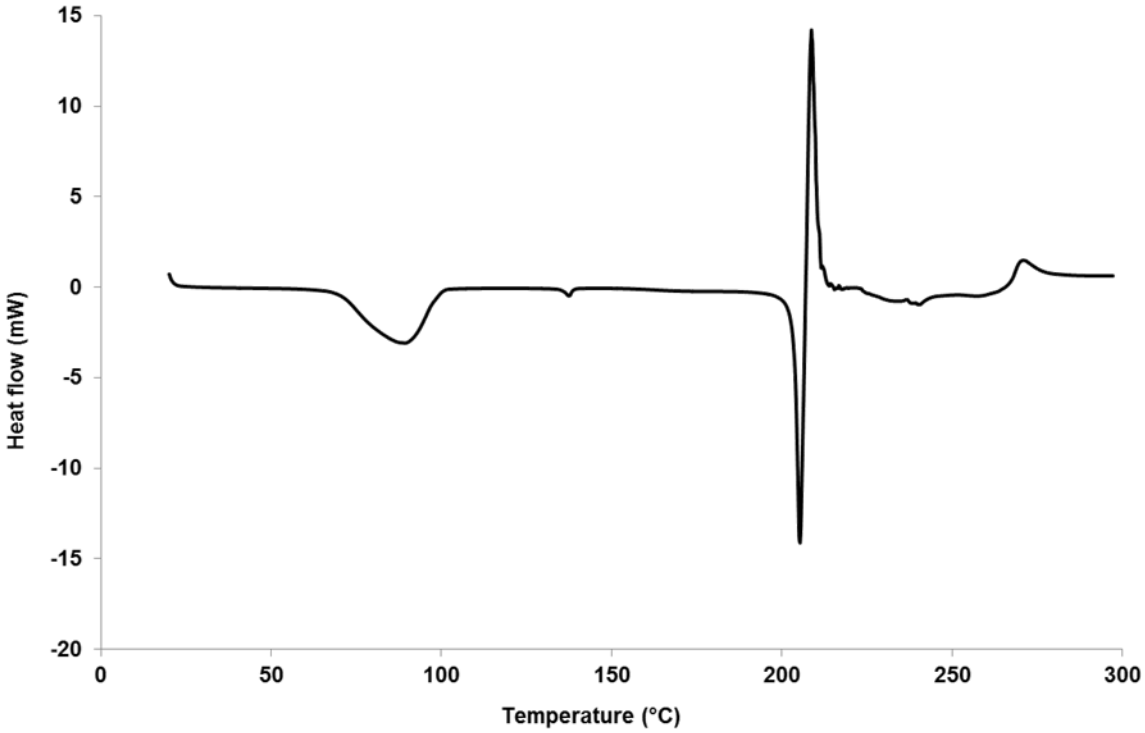

Figure 6.16. DSC trace of **(21)** on a 3.2 mg sample with a temperature ramp of 10 °C min^{-1}.

6.2.3. *Bis-(pyridinium-3-carboxylic acid) chloranilate* **(22)** *($C_6H_6NO_2)_2(C_6Cl_2O_4$)*

(22) was prepared by solvent evaporation of a 2:1 stoichiometric mixture of nicotinic acid and chloranilic acid dissolved in water and ACN at 30 °C. The product was consistently homogeneous and in the form of dark orange/red needle crystals which varied in size from very fine and hair-like, to larger thick needles. When the starting materials were used in a 1:1 stoichiometric ratio, the resulting crystals were of **PAZHOO**. The PXRD pattern from the bulk product of a preparation of **(22)** in which the starting materials were used in a 2:1 stoichiometric ratio (Appendix C, Figure A31) is not of very good quality, but it is evident that there are peaks that coincide with the calculated pattern, indicating that the single crystal is representative of the bulk sample, confirming what could be deduced visually.

The formula unit of **(22)** (Figure 6.17), features two protonated nicotinic ions and one chloranilate dianion, situated on a centre of inversion. A bifurcated H-bond is formed between the N-H group of the pyridinium ring and the deprotonated hydroxyl and carbonyl oxygen atoms of the chloranilate dianion, forming the targeted H-bonded synthon similiar to that reported by Adam *et al*. **(22)** differs from **PAZHOO**, in which the substituents are present in a 1:1 ratio and the chloranilic acid was singly deprotonated. Due to the protonation of nicotinic acid and double deprotonation of chloranilic acid in **(22)**, the nicotinic acid ion does not form dimers with itself and instead there are more extensive interactions

between the pyridine carboxylic acid and chloranilic acid derivatives than was observed in either **(20)** or **(21)**.

The C-O distances of the carboxyl group of the protonated nicotinic acid ion are very close to those of pure nicotinic acid (C=O 1.211(4) Å; C-O 1.308(4) Å). In **(22)**, C1-O1 is 1.212(2) Å and C1-O2 is 1.312(2) Å. The O1-C1-O2 angle is 125.6(1)°, which is wider than the equivalent angle in nicotinic acid (123.2(3)°). The carboxyl group and pyridinium ring are more coplanar in **(22)** than the carboxyl group and the pyridine ring in the pure material. The O1-C1-C2-C3 torsion angle is 0.7(2)°, whereas the equivalent torsion angle of nicotinic acid is approx. 4.7°.

Looking at the chloranilate dianion, the C-O bond distances C9-O4 and C8-O3 are 1.236(2) Å and 1.280(2) Å, respectively, which are shorter and longer, respectively, than the C-O and C=O distances of pure chloranilic acid (C-O 1.322(2) Å; C=O 1.224(2) Å), indicative of the delocalisation of the negative charges across O3-C8-C7-C9^{a}-O4^{a} and O4-C9-C7^{a}-C8^{a}-O3^{a}. Accordingly, C7^{a}-C9 and C7-C8 are shorter, and longer, respectively, than what can be considered as their equivalent bonds in chloranilic acid at 1.428(2) Å and 1.376(2) Å (compared to 1.450(2) Å and 1.349(2) Å, respectively). The C-C bond between the carbon atoms bonded to the oxygen atoms (C8-C9) is 1.534(2) Å, longer than the equivalent bond in chloranilic acid (1.508(2) Å), and C7-Cl1 is also longer than in chloranilic acid at 1.731(1) Å, (compared to 1.716(2) Å).

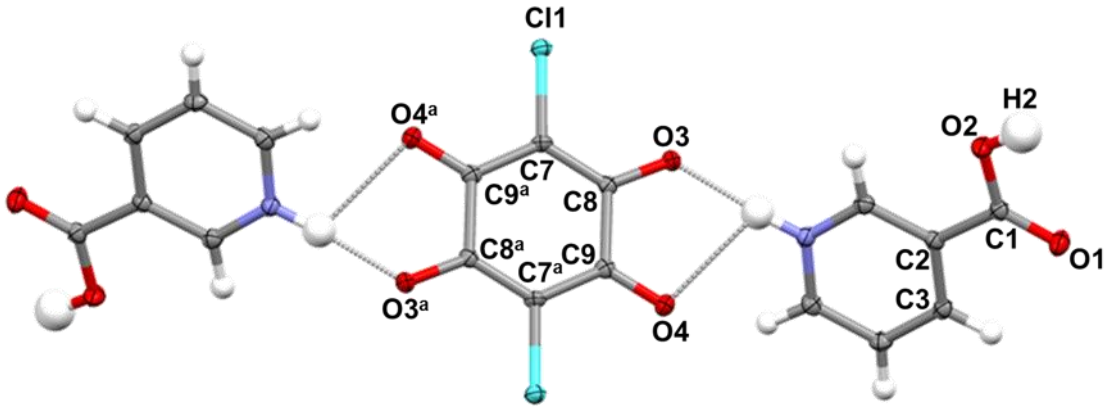

Figure 6.17. Formula unit of **(22)**: two protonated nicotinic acid ions and one chloranilate dianion connected by N-H···O/O bifurcated H-bonds. Symmetry code: ^{a}(-x, -y, 1-z)

The structure of **(22)** is composed of columns of protonated nicotinic acid ions and chloranilate dianions parallel to the *a* direction. Moderately strong H-bonds, including the bifurcated H-bond and one between the hydroxyl group of the carboxyl group of the protonated nicotinic acid to an oxygen atom of the chloranilate dianion, connect these ions

into 2D zigzag layers that lie along the {101} plane, (Figure 6.18(a)). H-bonds originating from C-H groups of the pyridinium ring, and π-π stacking interactions connect ions within the 2D zigzag layers and connect between layers.

The H-bonds connecting ions within the same 2D zigzag layer are illustrated in Figure 6.18(b). N1-H1···O3^{b} and O2-H2···O3^{c} are the strongest H-bonds in this crystal structure with D···A distances of 2.728(1) Å and 2.596(1) Å and near linear angles of 174(2)° and 177(2)°, respectively. N1-H1···O4^{b}, completing the bifurcated H-bond, has a distance of 2.855(1) Å and a very low angle of 108(1)°. It was intended to maintain the bifurcated H-bonded motif and coordinate this to a metal centre *via* the carboxyl group of the protonated nicotinic acid. Therefore, the strengths of the interactions in the bifurcated H-bond relative to the strength of O2-H2···O3^{c} would determine whether this motif would persist when **(22)** was employed as a 'supramolecular ligand'.

C-H groups of the pyridinium ring connect the nicotinic acid ion to two chloranilate dianions and to another nicotinic acid ion *via* the relatively weak interactions C3-H3···Cl1, C5-H5···O4^{d}, and C6-H6···O1^{c}. C3-H3 is also attracted to another chlorine acceptor atom, connecting between 2D zigzag layers; C3-H3···Cl1 is the shorter interaction at 3.217(1) Å, and has the slightly lower angle of 110(1)°. C5-H5···O4^{d} is a slightly stronger H-bond with a D···A distance of 3.068(2) Å and an angle of 132(1)°. C6-H6···O1^{c} is the only H-bond directly between nicotinic acid ions and is of comparable length to C5-H5···O4^{d}, with a D···A distance of 3.092(2) Å, but a larger angle of 146(1)°.

The nicotinic acid and chloranilate dianions interact with like-ions through π-π stacking to form columns parallel to the *a* direction, in each case with a centroid-centroid distance of 3.868(1) Å (Figure 6.18(c)).

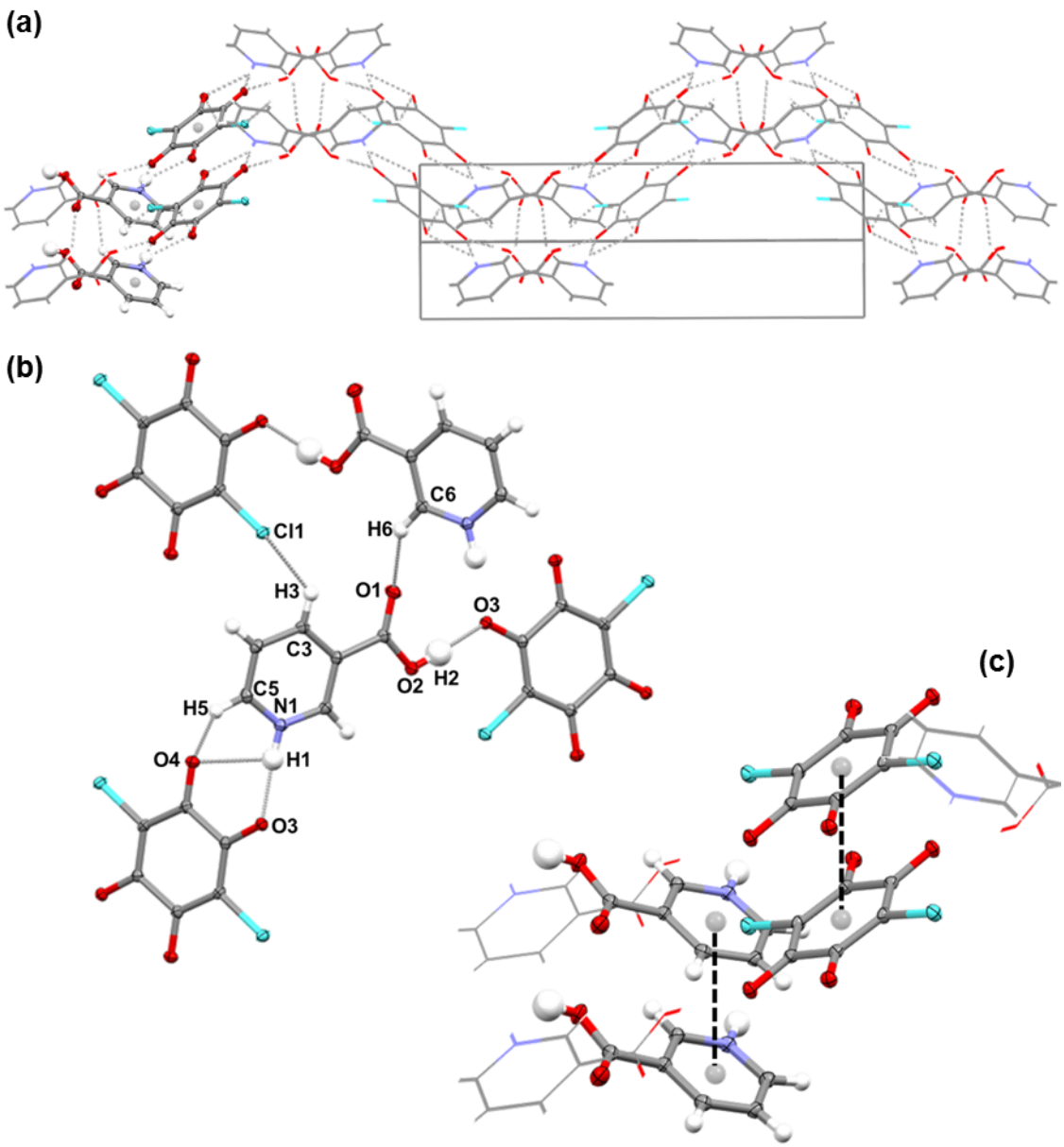

Figure 6.18. Crystal structure of **(22)**. (a) Packing of one 2D zigzag layer along the {101} plane, with nicotinic acid and chloranilate dianions that eclipse when viewed down the *a* axis and display π-π stacking interactions (shown in ellipsoid setting). (b) H-bonds connecting ions in the 2D zigzag layer. (c) Zoomed view of (a) showing the π-π stacking interactions.

Figure 6.19(a) shows the stacking of two 2D zigzag layers. Three H-bonds from C-H groups of the pyridinium ring of the nicotinic acid ion to an oxygen and chlorine atom of the chloranilate dianion, connect solely between these adjacent 2D zigzag layers (Figure 6.19(b)). C4-H4 forms an H-bond to each acceptor; C4-H4⋯ Cl1^{e} has the longer D⋯A distance of 3.558(1) Å, and the lower angle of 119(1)°, compared to C4-H4⋯O4^{f} which has

a shorter D···A distance of 3.408(2) Å and a larger angle of 154(1)°. C3-H3···Cl1^{e} has a D···A distance of 3.529(1) Å and an angle of 123(1)°.

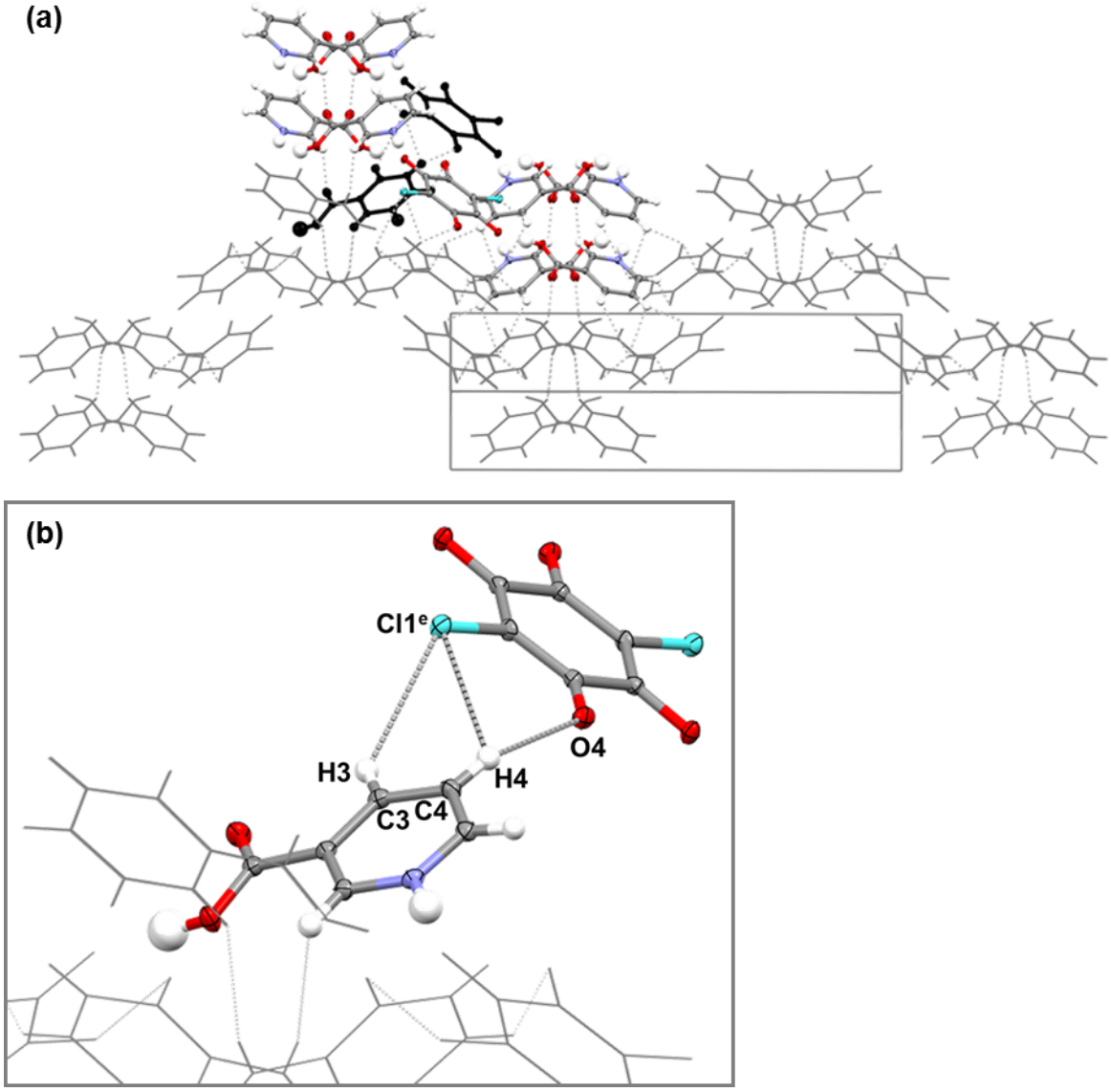

Figure 6.19. Crystal structure of **(22)**. (a) As Figure 6.18(a), also showing part of a second 2D zigzag layer (shown in ellipsoid setting). (b) Zoomed view of the ions coloured black in (a), illustrating the H-bonds connecting solely between the 2D zigzag layers.

Table 6.3. Geometries of H-bonds in **(22)**.

D-H···A Interaction	D-H (Å)	H···A (Å)	D···A (Å)	D-H···A (°)
(Figure 6.18(b)) H-bonds connecting ions in 2D zigzag layer				
N1-H1···O3[b]	0.96(2)	1.78(2)	2.728(1)	174(2)
N1-H1···O4[b]	0.96(2)	2.42(2)	2.855(1)	108(1)
O2-H2···O3[c]	0.92(2)	1.68(2)	2.596(1)	177(2)
C3-H3···Cl1	0.95(2)	2.76(2)	3.217(1)	110(1)
C5-H5···O4[d]	0.94(2)	2.36(2)	3.068(2)	132(1)
C6-H6···O1[c]	0.96(2)	2.25(2)	3.092(2)	146(1)
(Figure 6.19(b)) H-bonds solely connecting between 2D zigzag layers				
C3-H3···Cl1[e]	0.95(2)	2.91(2)	3.529(1)	123(1)
C4-H4···Cl1[e]	0.92(2)	3.02(2)	3.558(1)	119(1)
C4-H4···O4[f]	0.92(2)	2.56(2)	3.408(2)	154(1)

Symmetry codes: [b](x, y, -1+z) [c](-½+x, ½-y, -½+z) [d](1+x, y, -1+z) [e](1+x, y, z) [f](1-x, -y,1-z)

The melting range of **(22)** was found to be 190 – 203 °C by HSM, comparable to that of **(21)** (200 – 203 °C). The crystal seemed to undergo decomposition from about 170 °C, fragmenting in a way reminiscent of **(20)**, before the material smoothened and appeared to melt. The DSC trace of the bulk sample (Appendix C, Figure A32) does not show an endotherm at this temperature range, but rather there is a very weak endotherm at 223.2 °C, too low to be the melt of nicotinic acid (m.p. 236 – 239 °C), followed by a strong exothermic event at about 242 °C, higher than the recrystallisation events observed in the DSC traces of **(20)** and **(21)** which happened at around 210 °C, before likely decomposition.

6.3. Combining Chloranilic Acid and Pyridine Carboxylic Acid 'Supramolecular Ligands' with Metals

Once the optimum conditions for the preparation of **(20)**, **(21)**, **(22)**, **PAZHOO** and **YERXUP** were established (listed in Table 6.4), they were combined in crystallisation experiments with magnesium salts. The sample vials in which the 'supramolecular ligands' were synthesised were inspected for the characteristic crystals and these were removed carefully

using a spatula and weighed into a clean vial. These were combined with magnesium(II) nitrate hexahydrate or magnesium(II) chloride in a roughly 1:1 molar ratio and left to crystallise under a range of conditions using vapour diffusion, solvent layering and evaporative crystallisation techniques. One new crystalline material produced from these experiments was a simple organic salt. **(A5)** comprises 2D H-bonded layers of protonated isonicotinic acid and nitrate ions, and is discussed fully in Appendix D.

After many crystallisation experiments, combination of the 'supramolecular ligands' with magnesium salts did not result in any new metal-organic-organic complexes. Among the resulting materials from these crystallisation preparations were amorphous powders, crystals of the starting materials **(20)**, **(21)**, **(22)**, **PAZHOO** and **YERXUP**, crystals of chloranilic acid [**CLANAC11**; CSD V5.35 Feb 2015][142], crystals of chloranilic acid hydrate [**CLANDH**; CSD V5.35 Feb 2015][141] and crystals of various morphologies that were too low in quality to be identified.

Table 6.4. Optimum preparation conditions of **(20)**, **(21)**, **(22)**, **PAZHOO** and **YERXUP** by solvent evaporation.

Complex	Reagents	Solvent(s)	Temperature
(20)	PA and CA (2:1)	Water and ACN	30 °C
(21)	PA and CA (2:1)	Acetone	Lab temp.
(22)	NA and CA (2:1)	Water and ACN	30 °C
PAZHOO	NA and CA (1:1)	Water and ACN	40 °C
YERXUP	IA and CA (1:1)	Water and ACN	50 °C

6.3.1. *(μ$_2$-chloranilato)-bis-[(pyridine-2-carboxylato)-aqua-copper(II)]* **(23)**

[$Cu_2(C_6H_4NO_2)_2(H_2O)_2(C_6Cl_2O_4)$]

In order to investigate the viability of achieving a new metal-organic-organic complex from combining a 'supramolecular ligand' with a transition metal, a small side study was set up in which **(20)** was combined with iron(III) acetylacetonate, copper(II) sulfate pentahydrate and zinc(II) acetate dihydrate, while **YERXUP**, **PAZHOO** and **(22)** were combined with copper(II) sulfate pentahydrate.

A preparation involving solvent evaporation of a 2:1 stoichiometric mixture of **YERXUP** and copper(II) sulfate pentahydrate dissolved in water and ACN at 30 °C resulted in clear, gold

coloured homogeneous clusters of small triangular crystals. Analysis by scXRD revealed these to be crystals of a coordination polymer consisting of copper centres bridged by chloranilate dianions, *catena-[(μ_2-chloranilato)-diaqua-copper(II)] hydrate* [**VOMNAM**; CSD V5.35 September 2014].[181]

Fine, dark green needle crystals of **(23)** were obtained by solvent evaporation of a 1:1 stoichiometric mixture of **(20)** and copper(II) sulfate pentahydrate dissolved in ACN and water at 30 °C, 40 °C or 50 °C. The same preparation using a 2:1 stoichiometric ratio but **YERXUP** as the organic starting material resulted in crystals of **VOMNAM**, and all other variations of this experiment using **YERXUP**, **PAZHOO** or **(22)** as the organic starting material did not result in crystals of sufficient size or quality for diffraction.

The PXRD pattern of the bulk sample of a preparation that produced **(23)** (Figure 6.20) displays some common peaks with the calculated pattern at about 9°, 11°, 12°, 17°, 18° and 23° although the last may originate from traces of **(20)** in the samples.

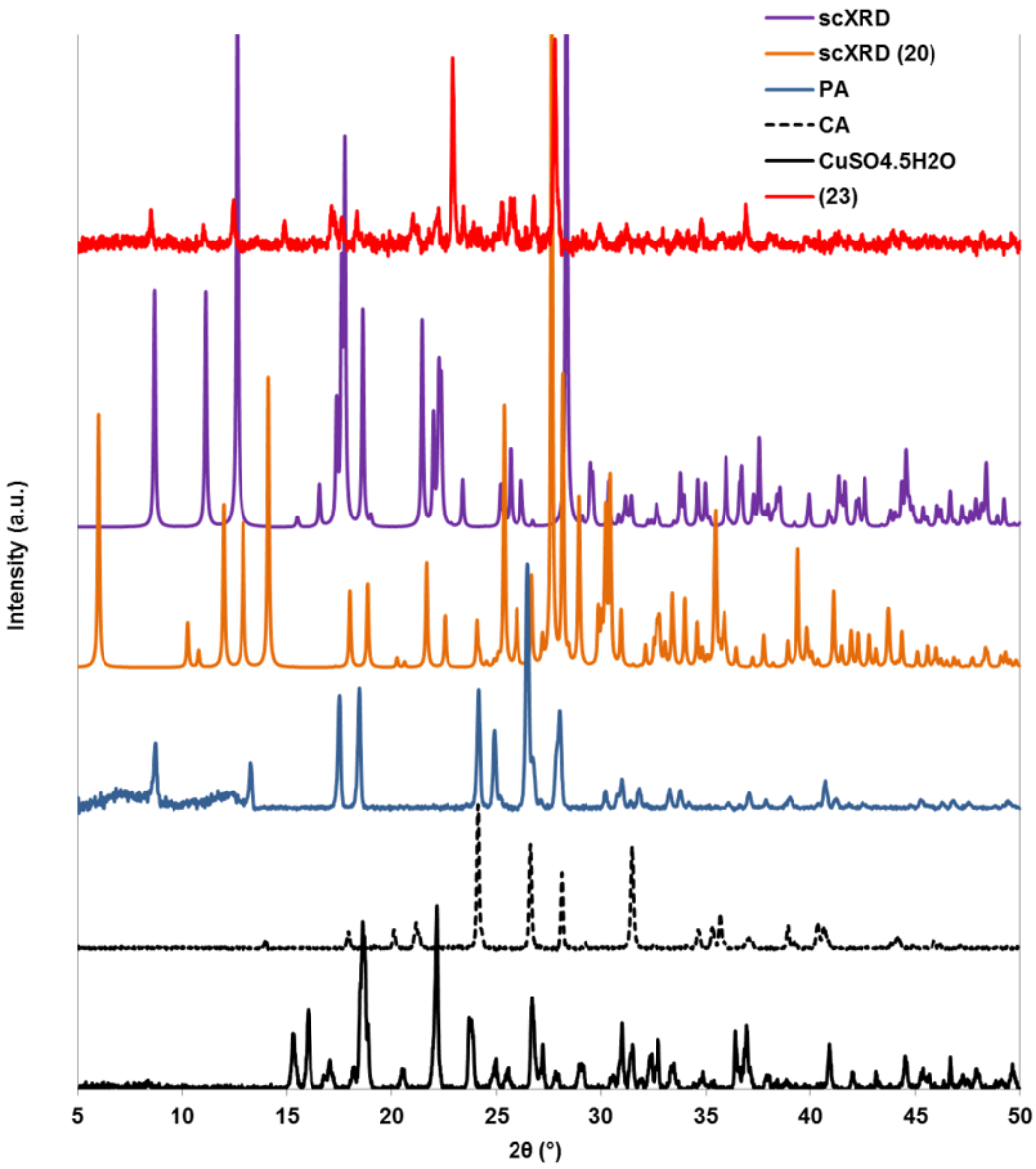

Figure 6.20. PXRD pattern of **(23)** compared to the calculated pattern and patterns of starting materials, (including CA, PA and **(20)**).

The structure of **(23)** is composed of discrete units of the formula unit (Figure 6.22(a)), arranged into layers along the {10-3} plane (Figure 6.22(b)). The formula unit consists of two copper centres in a square pyramidal geometry, bridged by one chloranilate dianion (located on an inversion centre) through chelation by both pairs of oxygen atoms. Each Cu centre is coordinated by one water molecule and chelated by one picolinate ligand *via* the pyridyl nitrogen atom and one carboxylate oxygen atom. A similar arrangement is observed in the formula unit, or as part of the formula unit, in previously reported Cu complexes in which the terminal ligand chelates the Cu centres by two nitrogen atoms; **EFETUF**,[182] **GURCOM**,[183] **WIDBAM**,[184] or three nitrogen atoms; **ERAQIX**,[185] **FUWWUP** and

FUWXAW[186] [CSD V5.35 September 2014]. All of these complexes feature a central chloranilate dianion bridging between the two Cu centres, as depicted in Figure 6.21. **(23)** is different from these structures in that the terminal ligands chelate to the Cu centre *via* an oxygen and a nitrogen atom. In the structures in which terpyridine chelates the Cu centre, the metal adopts a distorted octahedral (**ERAQIX**) or severely distorted trigonal bipyramidal geometry (**FUWWUP** and **FUWXAW**, which have no coordinated solvent 'X'). In the structures in which two nitrogen atoms chelate the Cu centre, the metal adopts a square pyramidal geometry. Not taking into account the axially coordinated water molecule, the structure of the formula unit of **(23)** is planar. **WIDBAM** is the most planar of the analogous structures, whereas **GURCOM** and **EFETUF** are non-planar, and the structures featuring terpyridine are non-planar due to the perpendicular arrangement of the heterocyclic ligand relative to the chloranilate dianion.

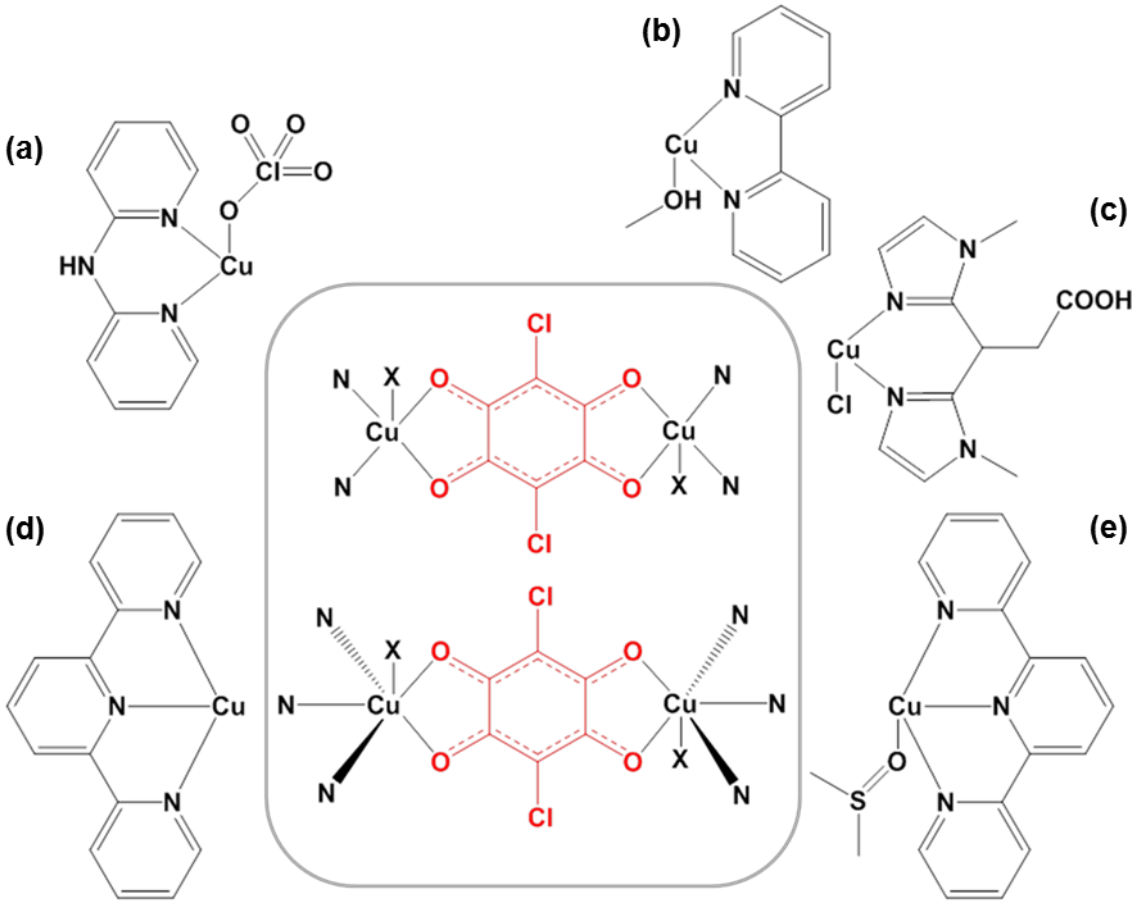

Figure 6.21. Analogous structures to **(23)** reported in the literature. (Centre) chloranilate dianion bridging between Cu centres each coordinated by two (top) or three (bottom) nitrogen atoms of two terminal ligands: (a) **GURCOM**; (b) **WIDBAM**; (c) **EFETUF**; (d) **FUWWUP** and **FUWXAW** and (e) **ERAQIX**. (Full coordination spheres for (a) – (e) are not shown).

The Cu centre of **(23)** has a square pyramidal geometry (Figure 6.22(a) and Table 6.5) with Cu-O distances to the equatorial substituents varying slightly between 1.944(2) Å (Cu1-O3) to 1.984(3) Å (Cu1-O5) with a Cu1-N1 distance of 1.967(3) Å, while the Cu-O1 distance to the axially coordinated water molecule is longer at 2.239(3) Å. The angles formed between the coordinating water oxygen atom and the equatorial atoms are all slightly obtuse with the angles O1-Cu1-O3 and O1-Cu1-O5 being 91.8(1)° and 91.9(1)°, respectively, and O1-Cu1-N1 and O1-Cu1-O4 being larger at 99.7(1)° and 96.6(1)°, respectively. Looking at the angles formed between the equatorial atoms, those formed by atoms of the same ligand are constrained to be significantly smaller at 82.5(1)° for O5-Cu1-O4 and 83.7(1)° for N1-Cu1-O3, compared to 93.8(1)° for O4-Cu1-N1 and 98.4(1)° for O3-Cu1-O5.

The picolinate ligand (Figure 6.22(a)) has C-O distances of 1.234(4) Å and 1.271(5) Å for C1-O2 and C1-O3, respectively. The former is longer than the C=O distance of pure picolinic acid (1.213(2) Å), while the latter is similar to the C-O distance of the pure ligand (1.279(2) Å). This trend in the difference in the C-O distances of the chelating picolinate ligand was also observed, although to a lesser extent, in **(12)** and also in the 2,4-pyridine dicarboxylate ligand of **(16)**: in all cases the metal-coordinating oxygen atom of the carboxylate group has the longer C-O distance. The O-C-O angle is 125.8(4)°, slightly smaller than the pure ligand (126.8(1)°, and the torsion angle O3-C1-C2-N1 is 1.6(5)°; less so than for the corresponding measurement in the pure ligand (-4.0(1)°).

The chloranilate dianion (Figure 6.22(a)) has equal C-O distances of 1.260(5) Å and 1.253(4) Å for C7-O4 and C8-O5, respectively, and equal C-C distances of 1.388(5) Å and 1.387(5) Å for C8-C9 and C7-C9^{a}, respectively, indicating the delocalisation of the negative charges, characteristic of the chloranilate dianion. The C-C bond C7-C8 is 1.533(3), and the C-Cl distance C9-Cl1 is 1.725(4) Å; in both cases these bonds are longer than the equivalent distances in pure chloranilic acid (C-C 1.508(1) Å; C-Cl 1.716(2) Å.)

(23) does not retain any features of the supramolecular ligand **(20)** from which it was synthesised. The picolinic acid ions of **(20)** have become deprotonated, and so the dimers formed by the strong H-bond between the carboxyl groups have separated. The hydrogen chloranilate ion of **(20)** is fully deprotonated in **(23)** and coordinates to the Cu centres by all four oxygen atoms. It accepts only a weak C-H···O H-bond from the picolinate ion.

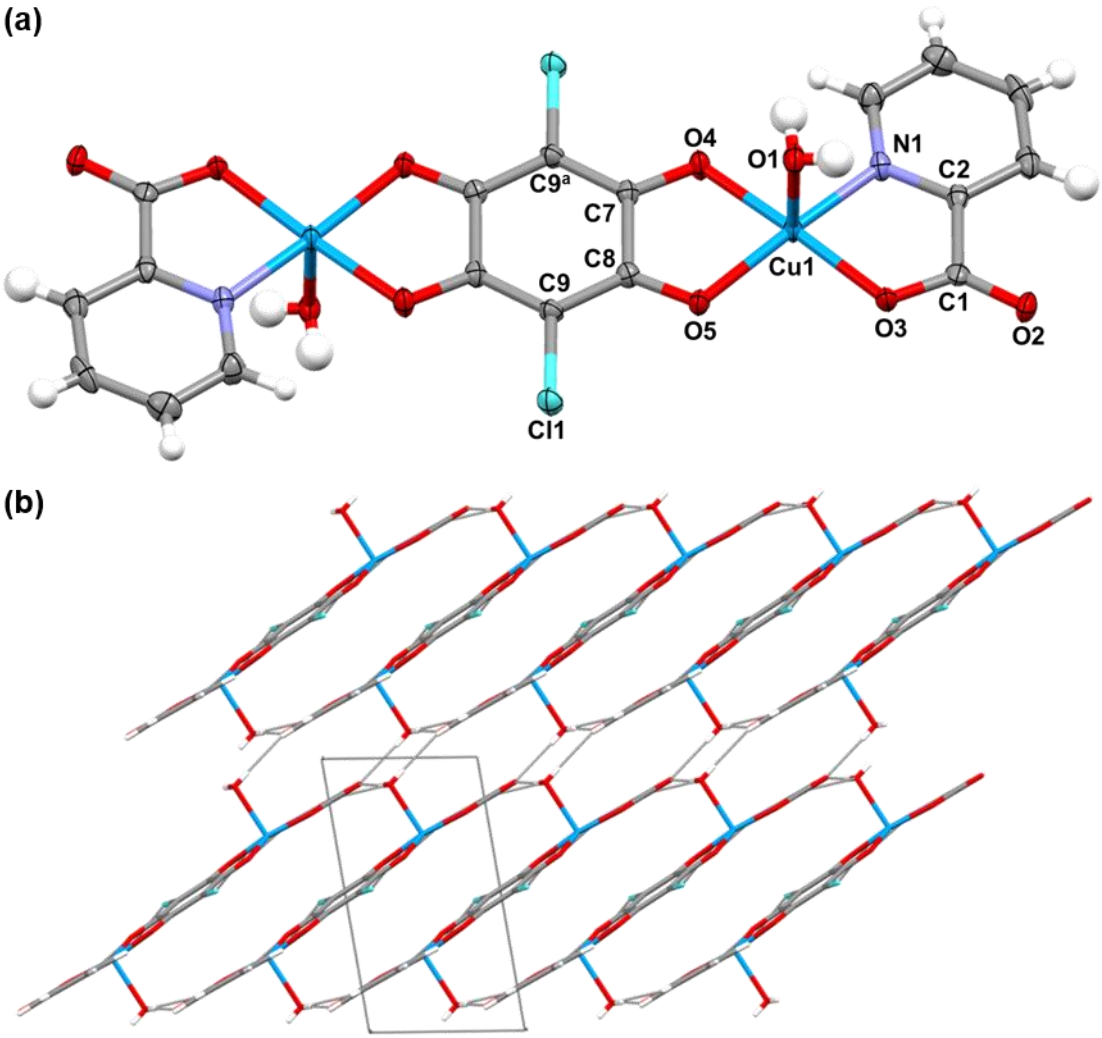

Figure 6.22. Crystal structure of **(23)**. (a) Formula unit of two square pyramidal Cu centres, bridged by the chloranilate dianion, coordinated by water, and chelated by the picolinate ion. (b) View down the *b* axis showing layers of formula units along the {10-3} plane, connected by H-bonds. Symmetry code: [a](-x, 1-y, 1-z)

Table 6.5. N/O-Cu-O angles and Cu-N/O distances in **(23)**.

Coordination	N/O-Cu-O angle (°)	Interaction	Distance (Å)
O1-Cu1-N1	99.7(1)	Cu1-N1	1.967(3)
O1-Cu1-O3	91.8(1)	Cu1-O1	2.239(3)
O1-Cu1-O4	96.6(1)	Cu1-O3	1.944(2)
O1-Cu1-O5	91.9(1)	Cu1-O4	1.972(2)
N1-Cu1-O3	83.7(1)	Cu1-O5	1.984(3)
O3-Cu1-O5	98.4(1)		
O5-Cu1-O4	82.5(1)		
O4-Cu1-N1	93.8(1)		

The formula units aligned on the {10-3} planes are connected along the *b* direction through two weak H-bonds and Cl···Cl halogen bonds (Figure 6.23 and Table 6.6). C5-H5···O5^{b} and C6-H6···Cl1^{b} are long H-bonds with D···A distances of 3.632(6) Å and 3.525(5) Å, and angles of 165(4)° and 143(3)°, respectively. The interactions between the formula units in this direction are reinforced by type-I halogen bonds located on a centre of inversion, of distance Cl1···Cl1, 3.306(1) Å, and C-Cl1···Cl1 angle, 125.6(1)°.

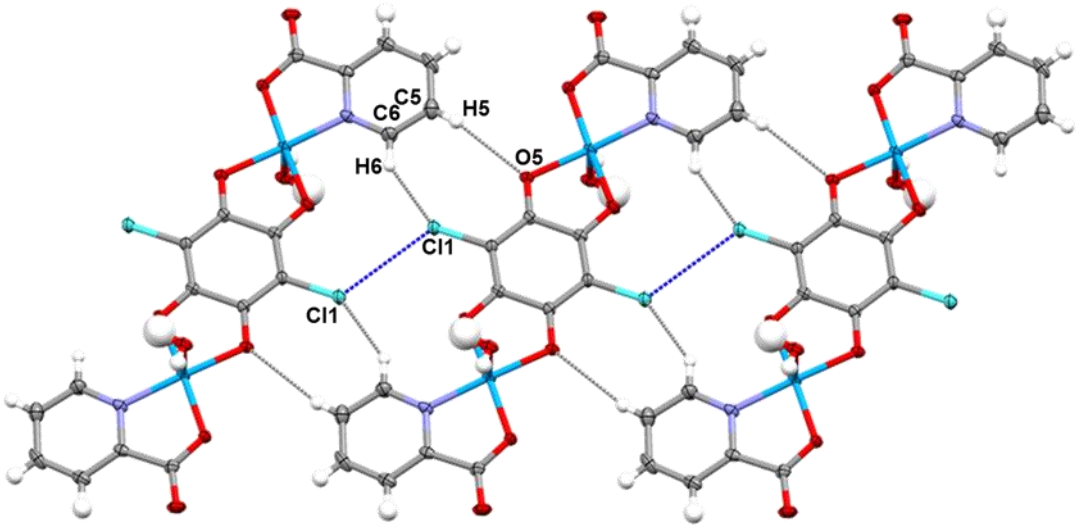

Figure 6.23. Crystal structure of **(23)**, showing H-bonds (grey) and Cl···Cl halogen bonds (blue) connecting the formula units on the {10-3} plane along the *b* direction.

The formula units are connected between layers through three H-bonds all involving the axially coordinated water molecule (Figure 6.24(a) and (b) and Table 6.6). O1-H1A···O2^{c} and O1-H1B···O2^{d} are formed from the water molecule to two non-chelating carboxylate oxygen atoms of neighbouring formula units. These are the strongest H-bonds in this structure with O1-H1A···O2^{c} having a D···A distance of 2.804(5) Å and an angle of 169(5)°, and O1-H1B···O2^{d} having a shorter D···A distance of 2.700(5) Å and an angle of 175(10)°. The oxygen atom of the water molecule is the acceptor of the H-bond C4-H4···O1^{e}, originating from a C-H group of the pyridyl ring. This is the shortest of the C-H H-bonds reported in this structure with a D···A distance of 3.307(6) Å and an angle of 164(4)°. Also connecting between layers are Cl···π interactions from the chlorine atom of the chloranilate dianion to the aromatic ring of the picolinate ion, and to the π-systems of the five-membered Cu–chelate rings, Figure 6.24(c). The distances of these interactions, as measured from the Cl atom to the centroid of the rings are 3.689(2) Å to (N1,C2,C3,C4,C5,C6)^{f}, 3.370(2) Å to (Cu1,N1,C2,C1,O3)^{g} and 3.485(2) Å to (Cu1,O4,C7,C8,O5)^{g}.

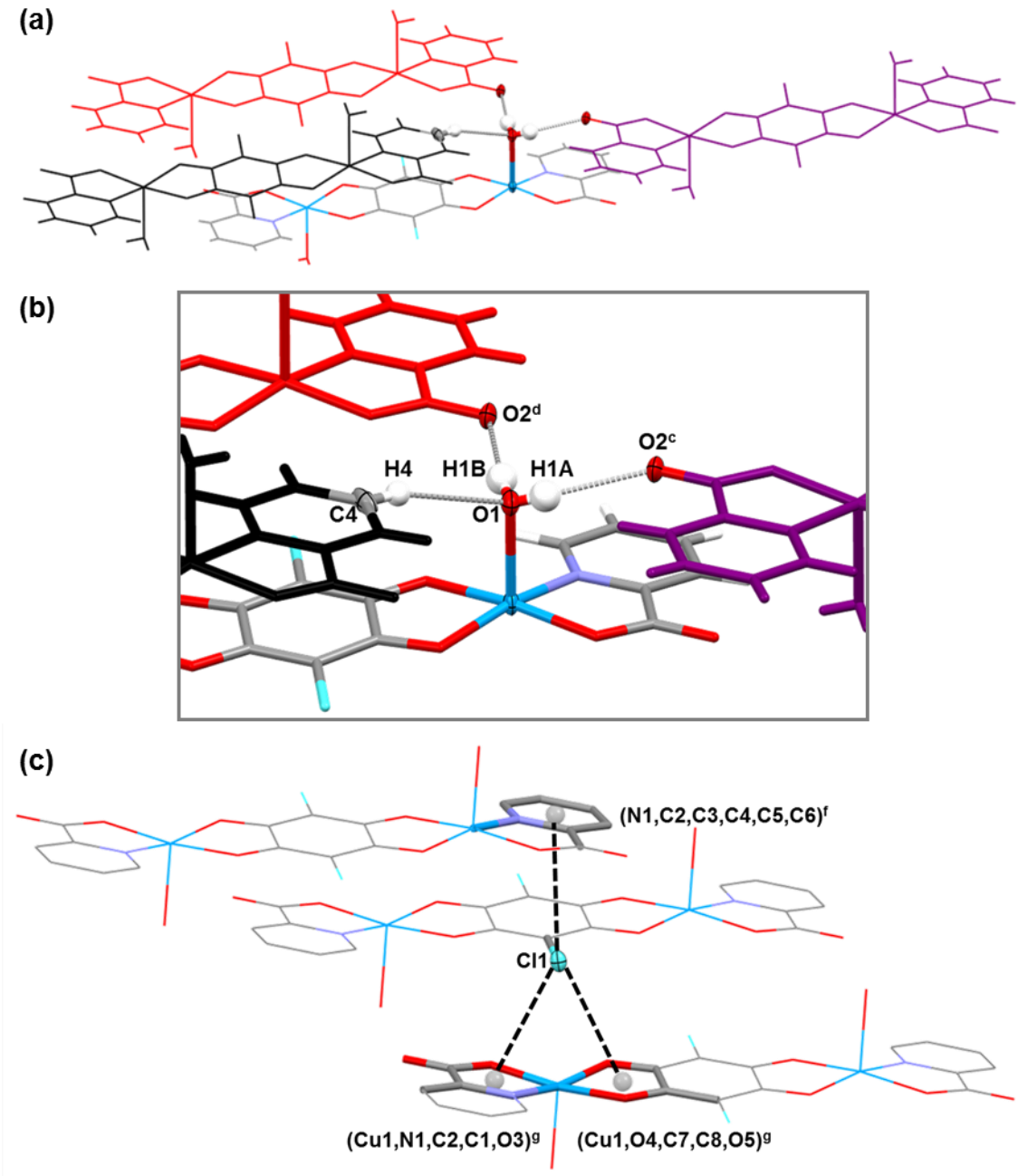

Figure 6.24. Crystal structure of **(23)**. (a) H-bonds connecting the formula units between planes, with (b) showing a zoomed view of (a). (c) Cl···π interactions between the formula units of different layers. Symmetry codes for O atoms: [c](2-x, 2-y, 2-z) [d](-1+x, y, z), for rings: [f](-1+x, -1+y, z) [g](1-x, 1-y, 1-z)

Table 6.6. Geometries of H-bonds in **(23)**.

D-H···A Interaction	D-H (Å)	H···A (Å)	D···A (Å)	D-H···A (°)
(Figure 6.23) H-bonds connecting formula units along b direction				
C5-H5···O5[b]	0.81(4)	2.85(5)	3.632(6)	165(4)
C6-H6···Cl1[b]	0.91(5)	2.76(4)	3.525(5)	143(3)
(Figure 6.24(b)) H-bonds connecting between layers of formula units				
O1-H1A···O2[c]	0.67(5)	2.14(5)	2.804(5)	169(5)
O1-H1B···O2[d]	0.78(8)	1.93(8)	2.700(5)	175(10)
C4-H4···O1[e]	0.80(5)	2.53(5)	3.307(6)	164(4)

Symmetry codes: [b](x, 1+y, z) [c](2-x, 2-y, 2-z) [d](-1+x, y, z) [e](1+x, 1+y, z)

HSM of a single crystal of **(23)** showed bubbling from about 142 °C but no melt was observed before 350 °C. The DSC trace of what small amount of adequately pure bulk sample could be gathered is very complicated (Appendix C, Figure A33), possibly due to instrument problems on the DSC, such that a meaningful trace was not obtained for this material. The TGA trace (also Appendix C, Figure A33) shows evidence of a gradual 10 % mass loss which may involve the loss of coordinated water molecules (however these only constitute a mass of 5.9%), until between about 240 – 250 °C when there is a greater mass loss with a shoulder at about 320 °C, coinciding with what may be an exothermic event indicated in the poor quality DSC trace.

6.4. Sodium and Chloranilic Acid

As it became evident that combining the supramolecular ligands with magnesium salts would be very challenging, it was decided to concentrate on producing magnesium/chloranilic acid complexes, not least since to date there are no structures in the CSD featuring a chloranilic acid derivative coordinated to magnesium and only four in which it is coordinated to calcium.[134] Two-component evaporation crystallisation experiments were prepared in which magnesium(II) nitrate hexahydrate, magnesium(II) chloride, magnesium(II) hydroxide or calcium(II) nitrate tetrahydrate were combined with chloranilic acid, however these preparations did not result in crystals of sufficient size or quality for analysis by XRD. Nevertheless, a new sodium/chloranilate complex, *catena-[(μ_3-chloranilato)-tris-(μ_2-aqua)-aqua-disodium]* **(A6)**, was produced by a solvent evaporation

experiment of a 1:4:1 stoichiometric mixture of chloranilic acid, sodium hydroxide and magnesium(II) chloride dissolved in water, and the material was encountered on a second occasion, resulting from a gel preparation. The synthesis and structure of **(A6)** are discussed fully in Appendix D.

6.5. Calcium and Chloranilic Acid

Due to the apparent propensity for chloranilic acid to form Cl···Cl halogen bonds, it was attempted to introduce this feature into the established crystal structure of **(13)**, a material composed of 2D coordination polymeric sheets, formed by the coordination of calcium centres by two chloride ions and four zwitterionic nicotinic acid ligands, as discussed in Chapter 4. This approach targeted the formation of a 2D layered metal-organic complex, connected by chloranilic acid molecules *via* the often predictable Cl···Cl halogen bonds with the axially coordinated chloride ions. The related bromanilic acid ligand was also of interest, given its similar potential to form halogen bonds.

To this end, a set of experiments were prepared employing evaporation crystallisation and vapour diffusion crystallisation techniques. First, samples of **(13)** were prepared under the most optimum synthesis condition: solvent evaporation of a 2:1 stoichiometric mixture of nicotinic acid and calcium(II) chloride dissolved in isopropanol at 30 °C. Once the solvent had evaporated, the resulting material was combined with chloranilic acid or bromanilic acid in a 1:1 stoichiometric ratio, dissolved in a range of solvent systems and allowed to crystallise under a range of temperatures. Three of these experiments resulted in crystals, all of which included a chloranilate danion: **(24)** was prepared by growth from a solution of **(13)** and chloranilic acid dissolved in isopropanol and DMF at 40 °C; **(A7)** was prepared by vapour diffusion (at lab temperature) in which **(13)** was dissolved in DMF and chloranilic acid was dissolved in THF; and **(25)** was prepared by growth from a solution of **(13)** and chloranilic acid dissolved in THF and DMF at 50 °C.

(24) and **(25)** are both coordination polymers composed of chloranilate dianions bridging two calcium centres. **(24)** features non-coordinated dimethylammonium ions from the hydrolysis of DMF, while **(25)** features calcium-coordinated DMF solvent molecules. **(A7)** does not feature calcium and is composed solely of chloranilate dianions and dimethylammonium ions. It is discussed fully in Appendix D.

The new calcium coordination polymers were of most interest. In order to test the necessity of including nicotinic acid, and the best method by which to do this in their preparation, the initial preparations were repeated exactly as before, and also with two variations. In one of these variations, **(13)** was not synthesised prior to combination with chloranilic acid and

instead, nicotinic acid, calcium(II) chloride and chloranilic acid were used in a roughly 2:1:2 stoichiometric ratio in a three-component crystallisation experiment. In the second variation, nicotinic acid was omitted from the preparation and calcium(II) chloride and chloranilic acid were used in either a 1:2 or 1:1 stoichiometric ratio.

Nicotinic acid was not found to be a necessary component in the synthesis of these crystals, since all of the preparation variations resulted in a mixture of crystals of both **(24)** and **(25)** and possibly also crystals of **(A7)**, according to visual inspection (see Experimental, and Figure 6.25). The solvent of the sample photographed in Figure 6.25(b), (c) and (d) (produced by a repeat preparation of **(24)** without nicotinic acid) was allowed to evaporate and after removing the sample and drying in an oven at about 75 °C, a sticky, wet, purple solid was obtained. This material gave the PXRD pattern shown in Figure 6.26. When compared to the calculated patterns of **(24)**, **(25)** and **(A7)** it is clear that the bulk sample consists primarily of **(24)** while there are a few peaks at about 15° and 22° which coincide with peaks relating to **(A7)** and possibly also **(25)**.

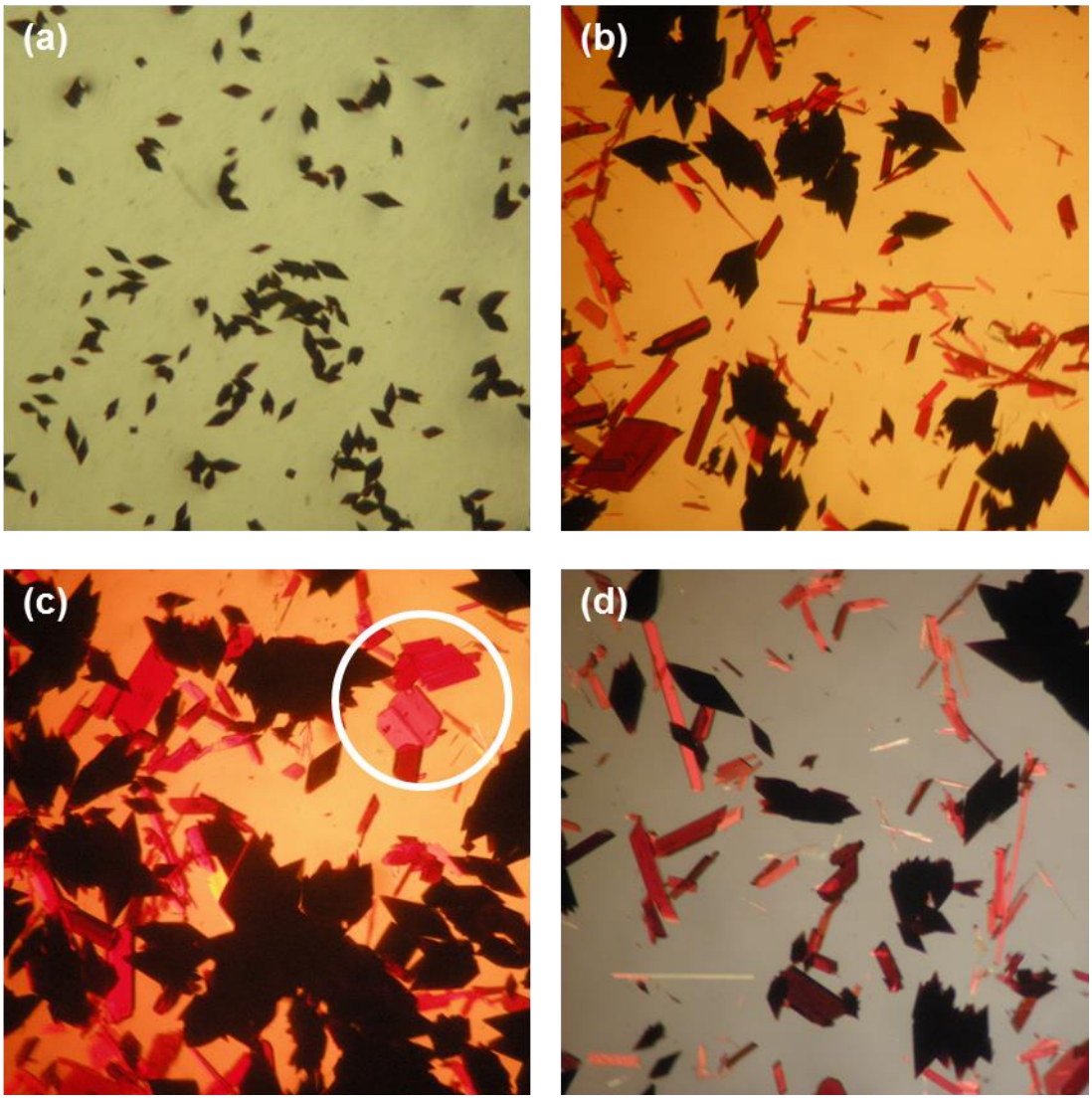

Figure 6.25. Crystals of **(24)**, **(25)** and **(A7)**. (a) Dark red octahedral shaped crystals of **(24)** from original preparation (approx. size of crystals: 2 x 1 x 1 mm). (b), (c) and (d) Crystals of **(24)** and pink rectangular needle crystals of **(25)** grown by a repeat preparation of **(24)**, without nicotinic acid. The larger, flat pink platelet crystals circled in (c) are visually characteristic of **(A7)** (although not confirmed by scXRD in this instance).

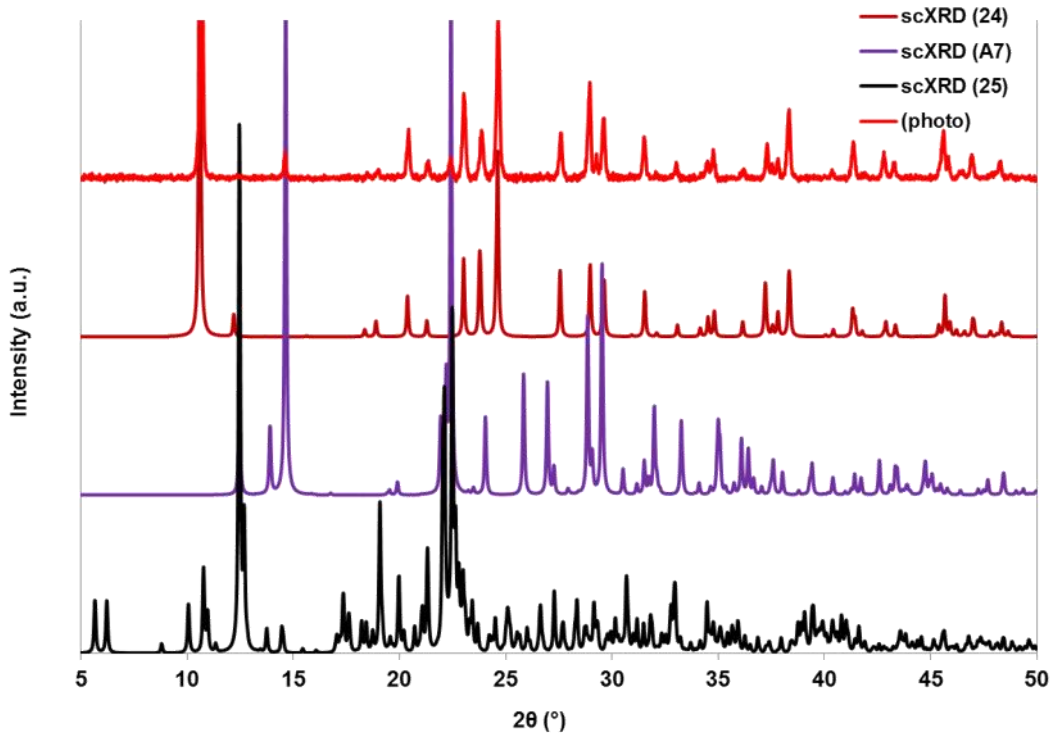

Figure 6.26. PXRD pattern obtained from the dry material photographed in Figure 6.25(b), (c) and (d) (top), compared to the calculated patterns of **(24)**, **(A7)** and **(25)**.

6.5.1. *Catena-[bis-(μ_2-chloranilato)-calcium(II)] bis-dimethylammonium* **(24)**

$[Ca(C_6Cl_2O_4)_2].2C_2H_8N$

The PXRD pattern of **(24)** (Figure 6.27) was obtained from a sample from a repeat preparation of **(24)** in which nicotinic acid was not included (a repeat preparation of the sample whose PXRD pattern is shown in Figure 6.26). This resulted in a large number of dark red octahedral crystals characteristic of **(24)** and a very small number of pink needle crystals characteristic of **(25)** in a bright fuchsia solution. The PXRD sample was prepared by removing the red octahedra from solution and drying them in paper towel before grinding into a powder. As expected, the experimentally obtained PXRD pattern matches the calculated pattern very well, indicating that the mass of red octahedra are indeed crystals of **(24)**.

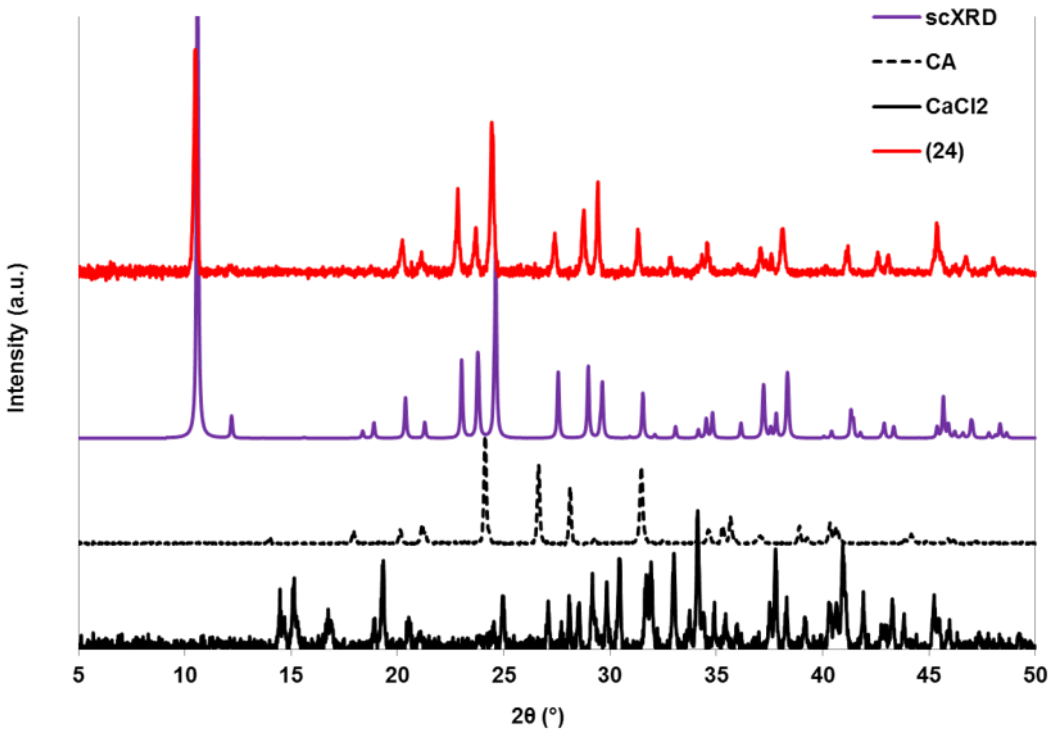

Figure 6.27. PXRD pattern of **(24)** compared to the calculated pattern and patterns of starting materials.

The formula unit of **(24)** features one calcium ion, two chloranilate dianions and two dimethylammonium ions. Each calcium centre is located on a four-fold rotoinversion axis and is eight-coordinate, coordinated by four crystallographically equivalent chelating chloranilate dianions *via* two oxygen atoms. The calcium centre and chloranilate dianions form sheets along the {101} and {10-1} planes, and the {011} and {01-1} planes, with the plane pairs intersecting at an angle of about 33.4°. This forms an anionic 3D coordination polymer framework of diamond-like connectivity with 'channels' in the *a* and *b* directions (Figure 6.28(a)). The charged framework is balanced by the presence of dimethylammonium ions within these 'channels' which form H-bonds to the framework. The necessary presence of these ions precludes porosity by preventing isolated cavities from connecting to form channels: therefore this material can be described as having 'virtual porosity' i.e. it is non-porous.[187] The total potential solvent accessible void volume, calculated from PLATON[166] and using a probe radius of 1.2 Å, is 2.3 % of the unit cell volume. If the dimethylammonium ions are not modelled during structure solution and not included in the void volume calculation, the void space in the structure displays 3D connectivity and the total potential solvent accessible void volume is 37.7 % of the unit cell

volume. However, even without the dimethylammonium ions present, the chlorine atoms penetrate into the channels forming off-set pillars, further reducing porosity.

(24) has a similar structural geometry to *catena-[oxonium bis-(μ_2-chloranilato)-yttrium(iii)] methanol solvate* [**MOBBIO**; CSD V5.35 September 2014][188], illustrated in Figure 6.28(b), with the two structures' crystallographic data listed in Table 6.7. The crystal structures differ in their metal cation, but in both, the cationic cores are identically bridged by a chelating chloranilate dianion. **MOBBIO** is charge-balanced by the presence of a hydronium ion, and also features methanol solvent molecules.

The unit cell of **MOBBIO** has a larger volume than that of **(24)** but **(24)** has a longer *c* axis. The structure of **(24)** is more compressed than that of **MOBBIO** due to the positioning of the coordinating oxygen atoms (Figure 6.28(c) and (d)).

Table 6.7. Crystal data of **(24)** and **MOBBIO**.

	(24)	**MOBBIO**
Formula	*$[Ca(C_6Cl_2O_4)_2].2C_2H_8N$*	*$[Y(C_6Cl_2O_4)_2]H_3O.8CH_3OH$*
M/g mol^{-1}	546.19	778.20
Crystal system	Tetragonal	Tetragonal
Space group	I $4_1/a$	I $4_1/a$
a (Å)	8.7092(3)	11.578(1)
b (Å)	8.7092(3)	11.578(1)
c (Å)	28.9919(11)	25.391(4)
α (°)	90	90
β (°)	90	90
γ (°)	90	90
V (Å^3)	2199.04(17)	3403.7(7)

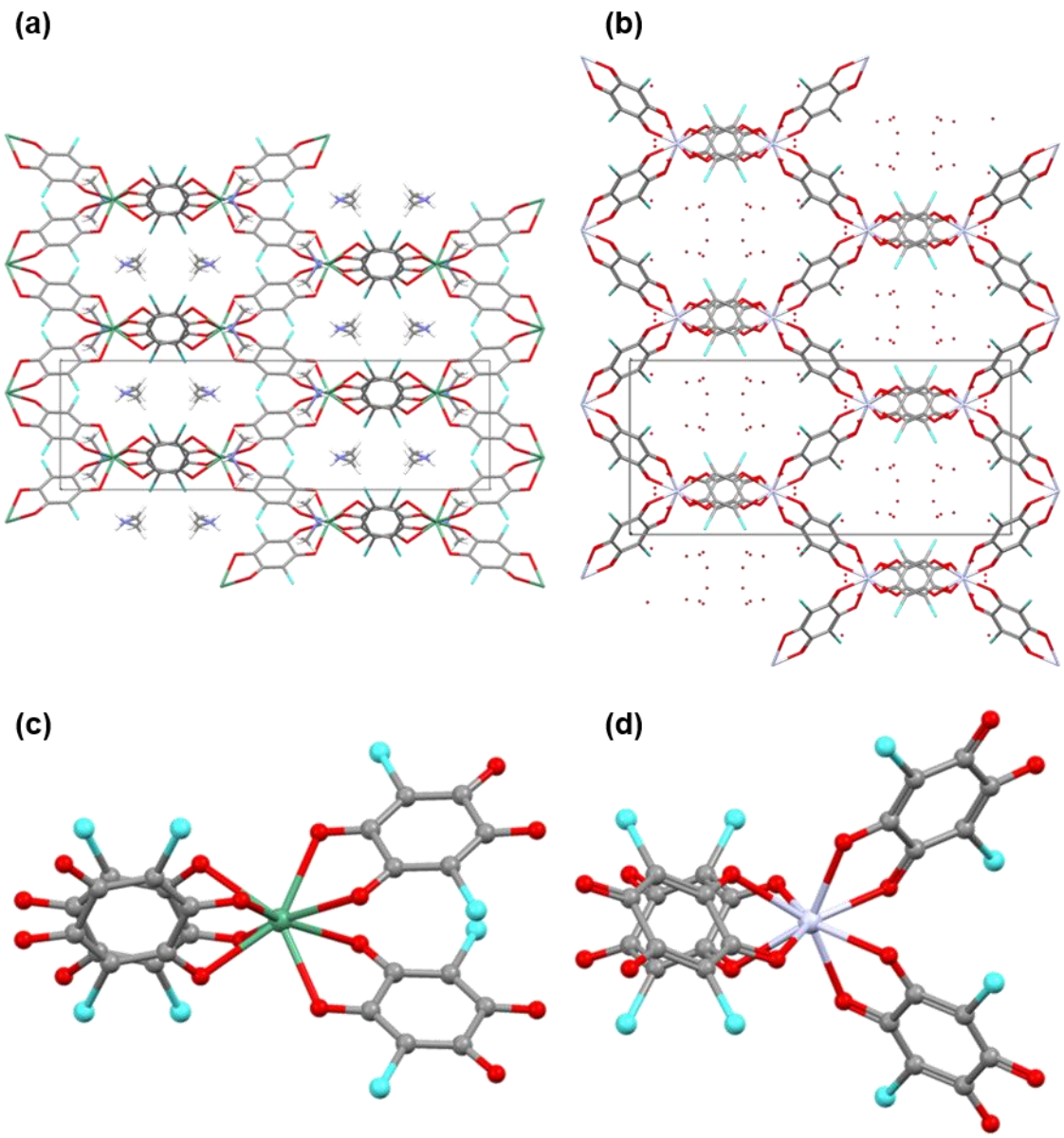

Figure 6.28. Crystal structures as viewed down the *a* axis of (a) **(24)** and (b) **MOBBIO**. (c) Coordination environment of the Ca centre in **(24)** and (d) of the Y centre in **MOBBIO**.

The Ca centre and one coordinating chloranilate dianion of **(24)** are shown in Figure 6.29(a) with the coordination geometries listed in Table 6.8. The Y-O coordination distances in **MOBBIO** are 2.396(6) Å and 2.306(7) Å, shorter than the Ca-O distances of **(24)**, which are 2.458(6) Å and 2.406(6) Å for Ca1-O1 and Ca1-O2, respectively. The angle formed between the Ca centre and the two coordinating oxygen atoms of the same chloranilate dianion is 65.4(2)°. The equivalent angle observed in **MOBBIO** is slightly larger at 67.2(2)°.

The chloranilate dianion has C-O bond distances C1-O1 of 1.247(10) Å, and C2-O2 of 1.267(9) Å, while the C2-C3 and C1-C3^{a} distances are essentially equal at 1.39(1) Å and

1.40(1) Å, consistent with the delocalisation of the negative charges within the chloranilate dianion. C1-C2 is 1.56(1) Å, much longer than the corresponding distance of the pure ligand (1.508(2) Å). This is similar in **MOBBIO**, in which the corresponding C-C distance is 1.55(1) Å. The C3-Cl1 bond distance is also longer in **(24)** at 1.740(8) Å, compared to the pure ligand (1.716(2) Å).

Although the crystal structure of **(24)** is constructed by metal-coordination, intramolecular interactions are also present (Figure 6.29(b)). The dimethylammonium ions present in the metal-organic framework form H-bonds to the oxygen atoms of the chloranilate dianion (Table 6.9). N1-H1 forms a moderately strong interaction, N1-H1···O2, with a D···A distance of 2.808(9) Å and an angle of 163(10)°. The methyl groups form weaker H-bonds; C4-H4B···O1^{c} and C4-H4C···O1^{e} have D···A distances of 3.35(1) Å and 3.27(1) Å and angles of 131° and 133°, respectively. There are also interactions between the chlorine atom of the chloranilate dianion and the conjugated π-electron system of the next chloranilate dianion located along the *b* direction. Measured from the chlorine atom to the centroid of C1^{a}, C3 and C2, this distance is about 3.717 Å.

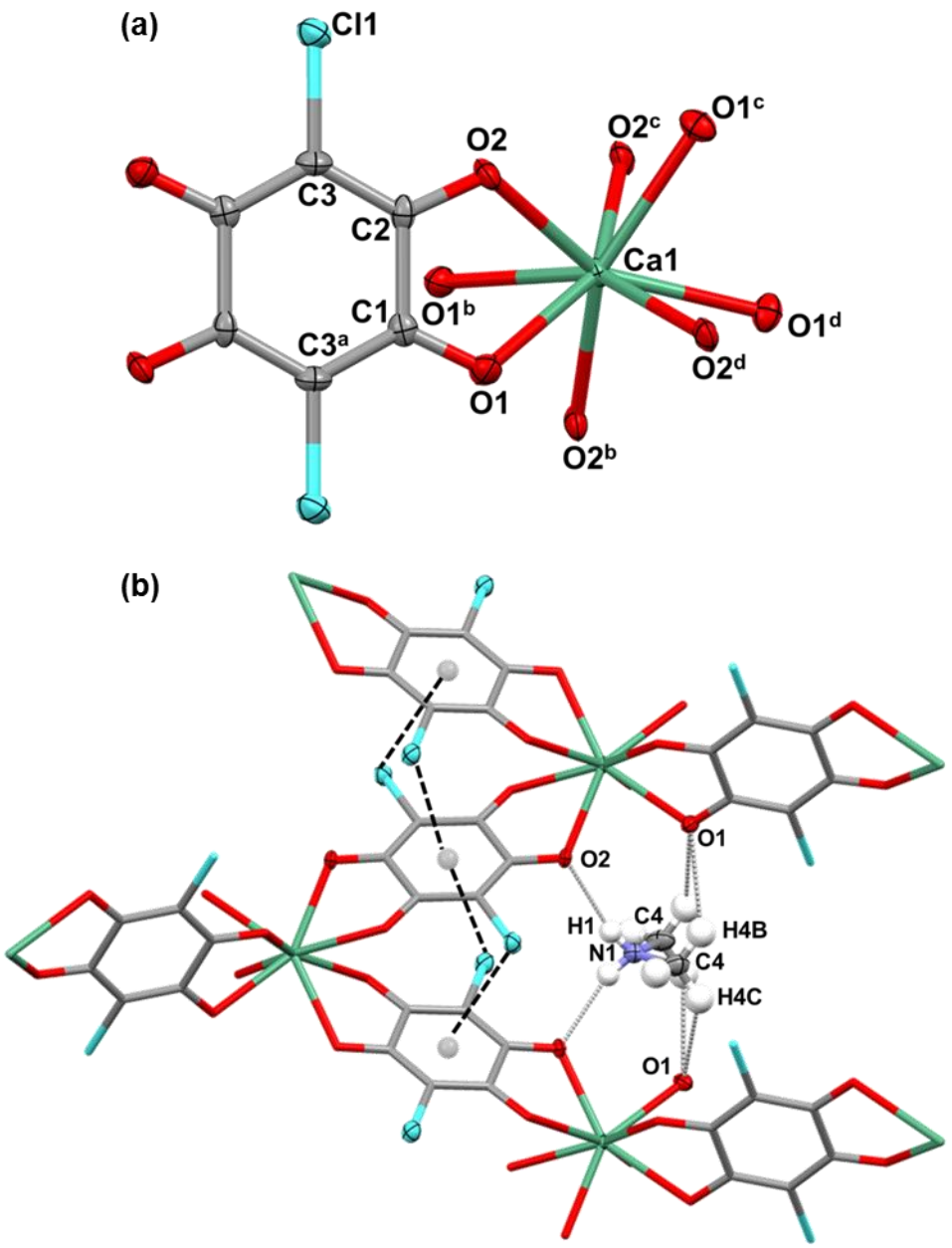

Figure 6.29. Crystal structure of **(24)**. (a) Eight coordinate Ca centre showing one of four chelating chloranilate dianions. (b) Section of the framework showing H-bonding of the dimethylammonium ion to the oxygen atoms of the chloranilate dianions and interactions between the chlorine atoms and the delocalised π-electron system of neighbouring chloranilate dianions (centroid of ring indicated for clarity). Symmetry codes: [a](-x, 1-y, -z) [b](-x, ½-y, z) [c](-¼+y, ¼-x, ¼-z)[d](¼-y, ¼+x, ¼-z)

Table 6.8. O-Ca-O angles and Ca-O distances in **(24)**.

Coordination	O-Ca-O angle (°)	Interaction	Distance (Å)
O1-Ca1-O1^{b} O1^{c}-Ca1-O1^{d}	74.9(3)	Ca1-O1/O1^{b}/O1^{c}/O1^{d}	2.458(6)
O1-Ca1-O1^{c}/O1^{d} O1^{b}-Ca1-O1^{c}/O1^{d}	129.1(2)	Ca1-O2/O2^{b}/O2^{c}/O2^{d}	2.406(6)
O1-Ca1-O2 O1^{b}-Ca1-O2^{b} O1^{c}-Ca1-O2^{c} O1^{d}-Ca1-O2^{d}	65.4(2)		
O1-Ca1-O2^{d} O1^{d}-Ca1-O2^{b} O1^{b}-Ca1-O2^{c} O1^{c}-Ca1-O2	76.6(2)		
O1-Ca1-O2^{b} O1^{b}-Ca1-O2 O1^{c}-Ca1-O2^{d} O1^{d}-Ca1-O2^{c}	77.5(2)		
O1-Ca1-O2^{c} O1^{c}-Ca1-O2^{b} O1^{b}-Ca1-O2^{d} O1^{d}-Ca1-O2	149.9(2)		
O2-Ca1-O2^{c}/O2^{d} O2^{b}-Ca1-O2^{c}/O2^{d}	99.1(1)		
O2-Ca1-O2^{b} O2^{c}-Ca1-O2^{d}	133.1(3)		

Symmetry codes: ^{b}(-x, ½-y, z) ^{c}(-¼+y, ¼-x, ¼-z) ^{d}(¼-y, ¼+x, ¼-z)

Table 6.9. Geometries of H-bonds in **(24)**.

D-H···A Interaction	D-H (Å)	H···A (Å)	D···A (Å)	D-H···A (°)
N1-H1···O2	0.8(1)	2.1(1)	2.808(9)	163(10)
*C4-H4B···O1[c]	0.96	2.64	3.35(1)	131
*C4-H4C···O1[e]	0.96	2.53	3.27(1)	133

Symmetry codes: [c](-¼+y, ¼-x, ¼-z) [e](¼-y, 1¼+x, ¼-z) *H-bond features methyl group hydrogen atom fixed in idealised position.

The crystal structure of **(24)** has a particularly interesting framework architecture due to the channels that would otherwise be present if not for the dimethylammonium ion, albeit that these are interrupted by the protruding chlorine atoms (Figure 6.30). In order for the counter ion to be redundant, and hence potentially realise a more porous structure, it would be necessary to use a +4 metal ion to act as an eight-coordinate 4-connecting node, therefore this is not possible to achieve using group 2 metals.

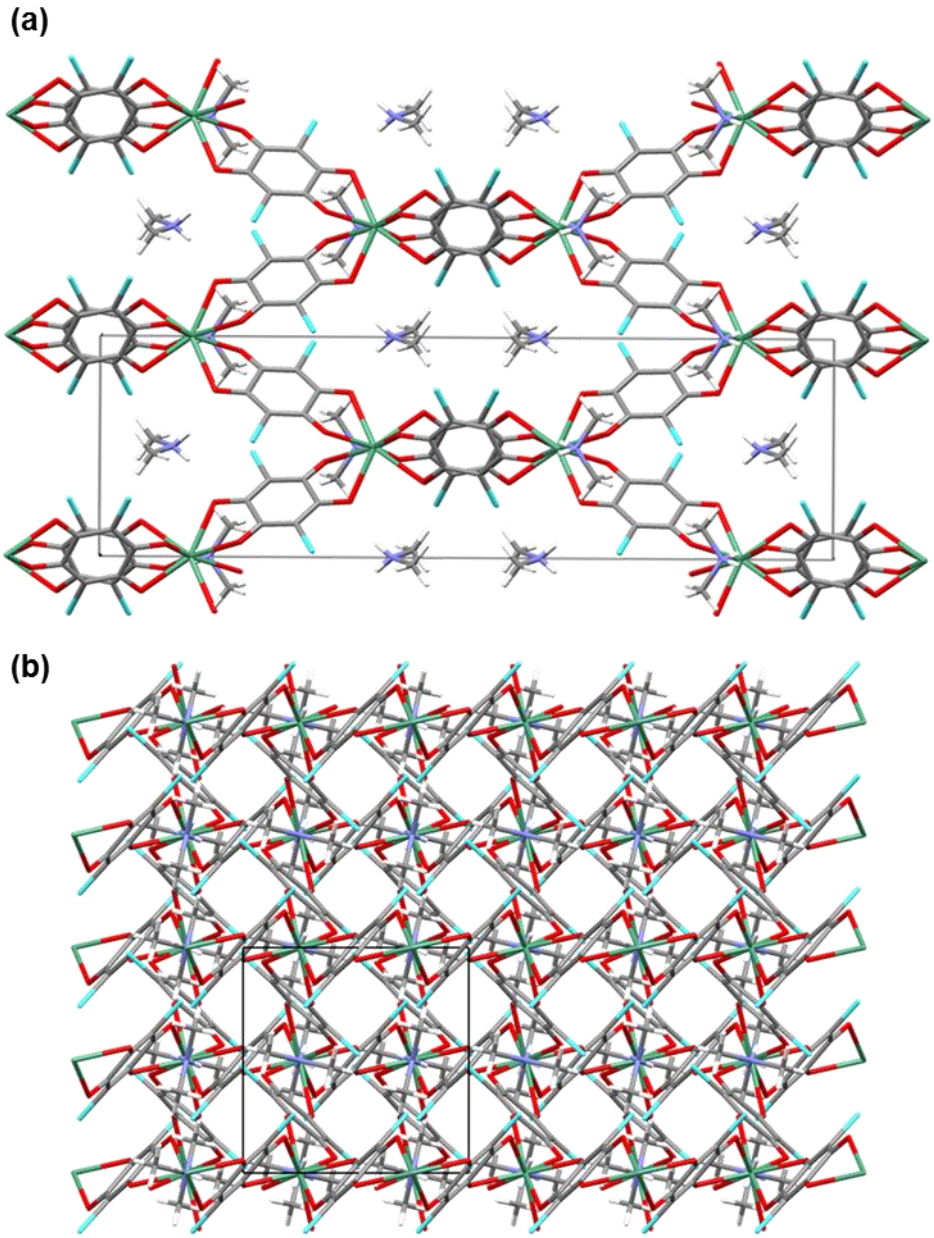

Figure 6.30. Crystal packing of **(24)**. View down (a) the *b* axis, and (b) the *c* axis.

A single crystal of **(24)** was analysed by HSM. At around 100 °C, bubbles began to emerge from the crystal, and between 200 °C and 375 °C the crystal bubbled furiously. After the heat ramp, the crystals remained octahedral in shape and were still red, but had lost all crystallinity. DSC analysis of a sample of **(24)** (Appendix C, Figure A34) did not reproduce what was observed by HSM. Rather, there are no significant events until about 180 °C when a very slight endotherm occurs, while at 294.8 °C there is a very strong exothermic event, possibly indicating recrystallisation. This event coincides with the abrupt weight loss of approximately 30 %, evident in the TGA trace (also Appendix C, Figure A34).

6.5.2. *Catena-[bis-((μ$_2$-chloranilato)-tris-dimethylformamide-calcium(II))]* **(25)**

[$Ca_2(C_6Cl_2O_4)_2(C_3H_7NO)_6$]

The preparation by which crystals of **(25)** alone were most favourably produced (by visual inspection) was the original evaporation crystallisation preparation which included nicotinic acid in the form of **(13)**. However, once the solvent had evaporated from this sample vial, the remaining bulk material of pink needles in a light brown crust was found to be too oily to prepare a sample for PXRD. Due to this unfavourable consistency, a PXRD pattern was obtained from another preparation that produced crystals of **(25)**. The pattern shown in Figure 6.31 was obtained from a sample from a repeat preparation of **(25)** in which nicotinic acid was used in a three-component crystallisation experiment. As was obvious from visual inspection of the vial before the clear orange solvent had evaporated, there were small dark red octahedra, likely to be crystals of **(24)** as well as large pink rectangular needle crystals of **(25)** in the vial. Therefore it is expected that the PXRD pattern of the bulk sample does not match the calculated pattern of **(25)**. When comparing this experimentally obtained PXRD pattern to the calculated patterns of both **(24)** and **(25)** (Figure 6.32), it is clear that it coincides much better with the calculated pattern of **(24)**. Although crystals of **(25)** were observed in solution, they do not seem to grind into a fine crystalline powder very well and so diffraction from the crystallites of **(24)** dominate the scattering. Furthermore, due to the shape of the crystals of **(25)**, they do not agglomerate as well as crystals of **(24)** and are more likely to be left behind in the vial after a sample for PXRD is taken, therefore being under-represented in the PXRD pattern.

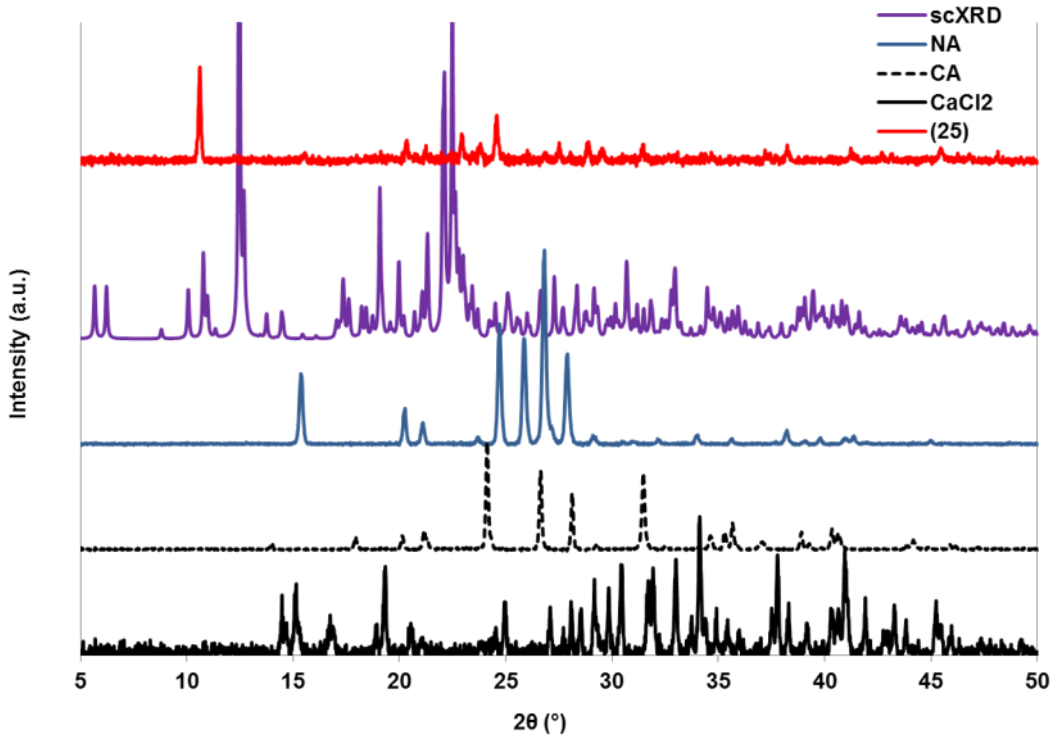

Figure 6.31. PXRD pattern of **(25)** compared to the calculated pattern and patterns of starting materials.

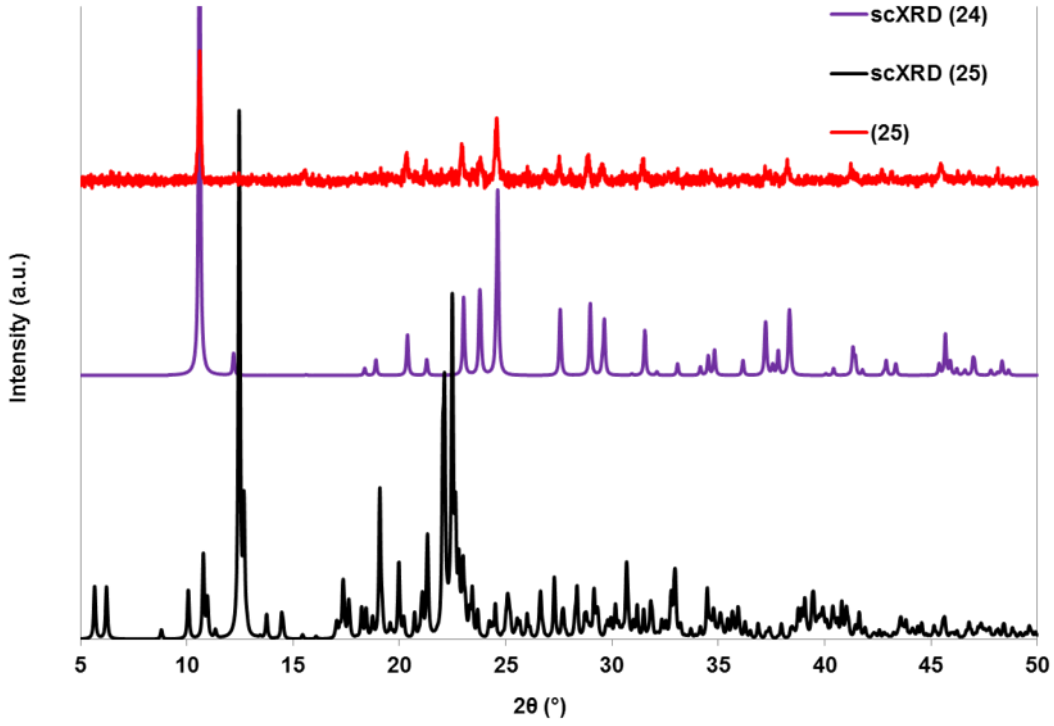

Figure 6.32. PXRD pattern of **(25)** compared to the calculated patterns of **(25)** and **(24)**.

(25) is composed of 1D coordination polymeric chains consisting of two crystallographically inequivalent calcium centres bridged alternately by two crystallographically inequivalent chloranilate dianions, each coordinating *via* two oxygen atoms per metal centre. The calcium centres are also coordinated by three dimethylformamide solvent molecules *via* the oxygen atom. The chain, shown in Figure 6.33(a), extends along the *c* direction.

The calcium centres of **(25)** are seven-coordinate and have distorted pentagonal bipyramidal geometries (Figure 6.33(b), (c) and Table 6.10 and Table 6.11). Generally the Ca-O distances to the oxygen atoms of the coordinating DMF solvent molecules are shorter than those to the coordinating oxygen atoms of the chloranilate ligands, however these distances are slightly longer concerning Ca2 than Ca1. The distances Ca1-O1, Ca1-O2 and Ca1-O6 are 2.344(4) Å, 2.336(4) Å and 2.332(4) Å, respectively, while the distances Ca2-O3, Ca2-O4 and Ca2-O5 are 2.362(4) Å, 2.388(4) Å and 2.372(4) Å, respectively. The O-Ca-O angles formed between the coordinating oxygen atoms of the DMF molecules tend to be closer to 90° than those formed between the oxygen atoms of the DMF molecules and the oxygen atoms of the chloranilate dianions. O6-Ca1-O2 is 92.4(2)°, O1-Ca1-O2 is 85.6(1)° while O5-Ca2-O4 is 89.7(1)° and O3-Ca2-O4 is 93.1(2)°. The exceptions are O1-Ca1-O10 with an angle of 89.5(1)° and O3-Ca2-O14 with an angle of 92.1(1)°. The angles formed between the coordinating oxygen atoms of the same chloranilate ligands are in a very narrow range from 65.8(1)° for $O9^{a}$-Ca1-$O12^{a}$, to 66.5(1)° for O8-Ca2-O13. The equivalent angle observed in **(24)** was very slightly smaller at 65.4(2)°.

The chloranilate dianions can be assigned as CA1 and CA2, as indicated in Figure 6.33(d) with their bond distances listed in Table 6.12. The C-O bond distances are essentially equal, with distances in the narrow range from 1.243(6) Å for C12-O12, to 1.252(6) Å for C5-O13. As was observed in both **(24)** and **(A7)**, the C-C bond lengths are consistent with the delocalisation of the negative charge; in this case across O11-C1-C6-C5-O13 and O10-C2-C3-C4-O8 in CA1, and across O7-C8-C9-C12-O12 and O14-C7-C10-C11-O9 in CA2. In Ca1, the C-C bond distances C2-C3, C5-C6, C1-C6 and C3-C4 range from 1.390(7) Å to 1.396(7) Å, and in CA2, the C-C bond distances C7-C10, C12-C9, C9-C8 and C10-C11 range from 1.390(6) Å to 1.402(7) Å. There is an elongation of the C-C bond distance which is 1.508(2) Å in pure chloranilic acid. In CA1 these distances are 1.537(7) Å and 1.539(7) Å, for C1-C2 and C4-C5, respectively, and in CA2, 1.535(7) Å and 1.541(7) for C7-C8 and C11-C12, respectively. Similarly, the C-Cl bond distances are longer in **(25)** than in the pure ligand (1.716(2) Å): in CA1 C6-Cl5 and C3-Cl6 are 1.739(5) Å, and 1.744(5) Å, respectively, and in CA2, 1.745(5) Å and 1.737(5) Å for C9-Cl3 and C10-Cl4, respectively.

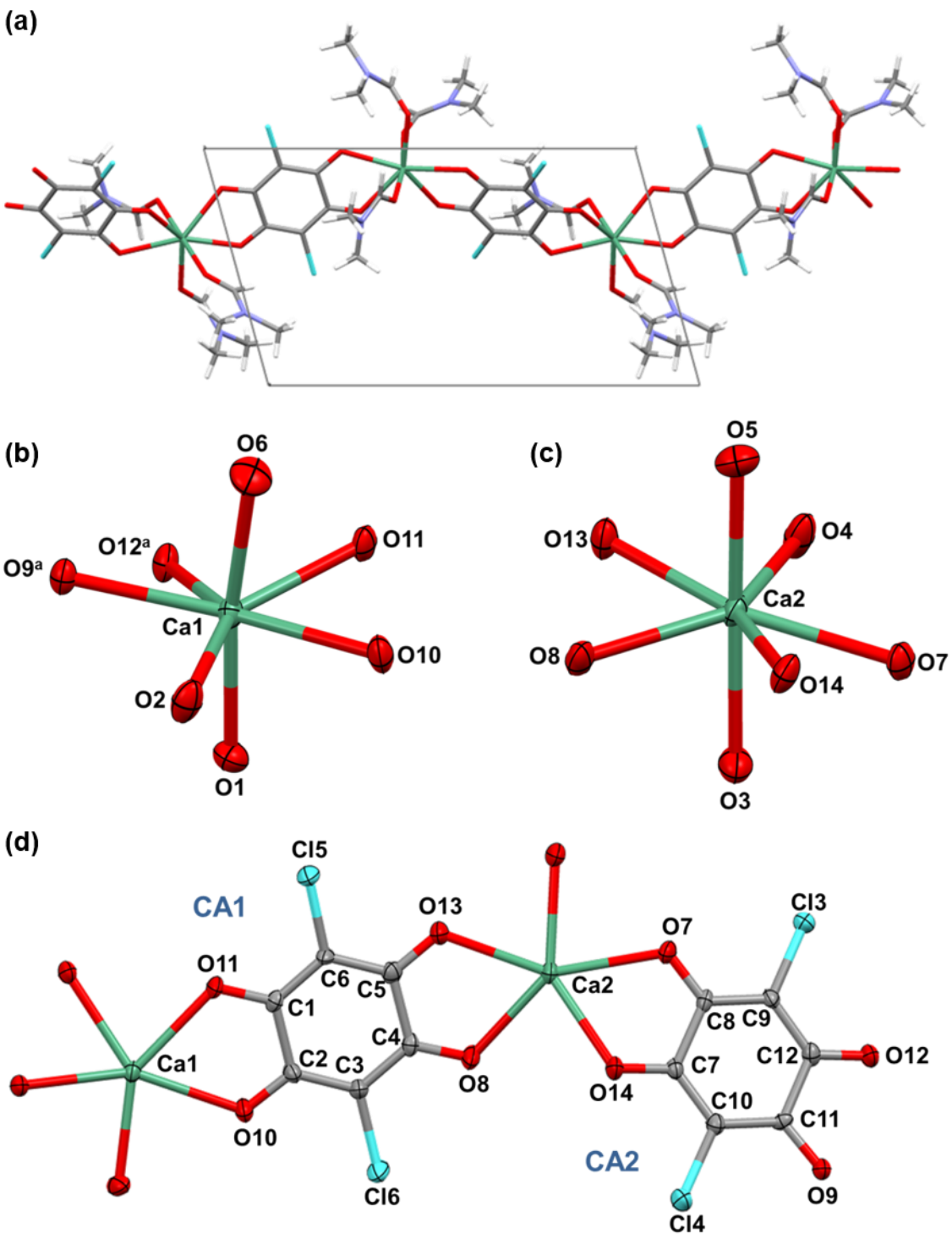

Figure 6.33. Crystal structure of **(25)**. (a) View down the *b* axis showing the 1D coordination polymeric chain extending along the *c* direction. (b) Seven coordinate Ca1 centre, and (c) Ca2 centre, each with four coordinating oxygen atoms of two chloranilate ligands, and three coordinating oxygen atoms of the DMF solvent molecules. (d) Bridging chloranilate ligands, CA1 and CA2, (two coordinating oxygen atoms per Ca centre removed for clarity).

Table 6.10. O-Ca-O angles and Ca-O distances involving Ca1 in **(25)**.

Coordination	O-Ca-O angle (°)	Interaction	Distance (Å)
O6-Ca1-O11	79.2(1)	Ca1-O1	2.344(4)
O6-Ca1-O10	82.3(1)	Ca1-O2	2.336(4)
O6-Ca1-O2	92.4(2)	Ca1-O6	2.332(4)
O6-Ca1-O9[a]	85.8(1)	Ca1-O9[a]	2.434(3)
O6-Ca1-O12[a]	106.3(1)	Ca1-O10	2.425(3)
O1-Ca1-O11	97.6(1)	Ca1-O11	2.398(4)
O1-Ca1-O10	89.5(1)	Ca1-O12[a]	2.401(3)
O1-Ca1-O2	85.6(1)		
O1-Ca1-O9[a]	101.6(1)		
O1-Ca1-O12[a]	80.1(1)		
O11-Ca1-O10	66.3(1)		
O10-Ca1-O2	76.7(1)		
O2-Ca1-O9[a]	80.0(1)		
O9[a]-Ca1-O12[a]	65.8(1)		
O12[a]-Ca1-O11	77.6(1)		

Symmetry code: [a](x, y, 1+z)

Table 6.11. O-Ca-O angles and Ca-O distances involving Ca2 in **(25)**.

Coordination	O-Ca-O angle (°)	Interaction	Distance (Å)
O5-Ca2-O4	89.7(1)	Ca2-O3	2.362(4)
O5-Ca2-O7	103.7(1)	Ca2-O4	2.388(4)
O5-Ca2-O14	84.4(1)	Ca2-O5	2.372(4)
O5-Ca2-O8	94.8(1)	Ca2-O7	2.416(3)
O5-Ca2-O13	82.0(1)	Ca2-O8	2.423(4)
O3-Ca2-O4	93.1(2)	Ca2-O13	2.373(3)
O3-Ca2-O7	75.0(1)	Ca2-O14	2.388(3)
O3-Ca2-O14	92.1(1)		
O3-Ca2-O8	84.4(1)		
O3-Ca2-O13	100.7(1)		
O4-Ca2-O7	77.4(1)		
O7-Ca2-O14	66.4(1)		
O14-Ca2-O8	81.0(1)		
O8-Ca2-O13	66.5(1)		
O13-Ca2-O4	73.2(1)		

Table 6.12. Geometries of selected bond distances of chloranilate ligands in **(25)**.

CA1		**CA2**	
C6-Cl5	1.739(5) Å	C9-Cl3	1.745(5) Å
C3-Cl6	1.744(5) Å	C10-Cl4	1.737(5) Å
C1-O11	1.245(5) Å	C8-O7	1.247(5) Å
C4-O8	1.248(5) Å	C11-O9	1.246(5) Å
C2-O10	1.246(6) Å	C7-O14	1.246(6) Å
C5-O13	1.252(6) Å	C12-O12	1.243(6) Å
C2-C3	1.396(7) Å	C7-C10	1.390(6) Å
C5-C6	1.394(7) Å	C12-C9	1.392(6) Å
C6-C1	1.390(7) Å	C9-C8	1.399(7) Å
C3-C4	1.396(7) Å	C10-C11	1.402(7) Å
C1-C2	1.537(7) Å	C8-C7	1.535(7) Å
C4-C5	1.539(7) Å	C11-C12	1.541(7) Å

The structure of **(25)** consists of 1D coordination polymeric chains that extend along the *c* direction. Within these chains is a bifurcated intracomplex H-bond C29-H29A···O2/O9[a] (Figure 6.34 and Table 6.13) formed from a methyl group of one DMF molecule to the oxygen atom of another DMF molecule, and to the oxygen atom of a chloranilate ligand. C29-H29A···O2 has the longer D···A distance of 3.823(8) Å which, for a C-H···O H-bond, would suggest that the interaction is more van der Waals in nature, but this interaction has the larger angle of 163°, compared to 130° for C29-H29A···O9[a]. In each case both oxygen atoms are coordinated to the same Ca centre as the DMF molecule of the methyl group forming the H-bond.

Figure 6.34 shows two parallel 1D chains and the interactions connecting them along the *a* direction. The chlorine atoms of two crystallographically equivalent chloranilate dianions of different chains form type-I halogen bonds, Cl5···Cl6[b]/Cl6···Cl5[d], of 3.644(2) Å, and angles C-Cl5···Cl6, 138.9(2)° and C-Cl6···Cl5, 135.1(2)°. Eight weak H-bonds, all but one originating from methyl groups, also connect the structure along the *a* direction (Figure 6.34 and Table 6.13). C26-H26···Cl3[c] is formed between a C-H group of the DMF molecule, to a chlorine atom of a chloranilate ligand. This is the most linear of these interactions, with

an angle of 177(8)°, and it is also one of the longest with a D···A distance of 3.773(6) Å. Another H-bond in which a chlorine atom is the acceptor is C21-H21C···Cl4^{b}, but in this case the donor is a carbon atom of a methyl group. This H-bond has a similarly long distance as that previous, of 3.771(7) Å, and a lower angle of 150°. C29 is the donor atom of another bifurcated, and this time intermolecular, H-bond, C29-H29B···O4^{c}/O7^{c}, where the acceptors are again an oxygen atom of a DMF molecule and an oxygen atom of a chloranilate ligand.

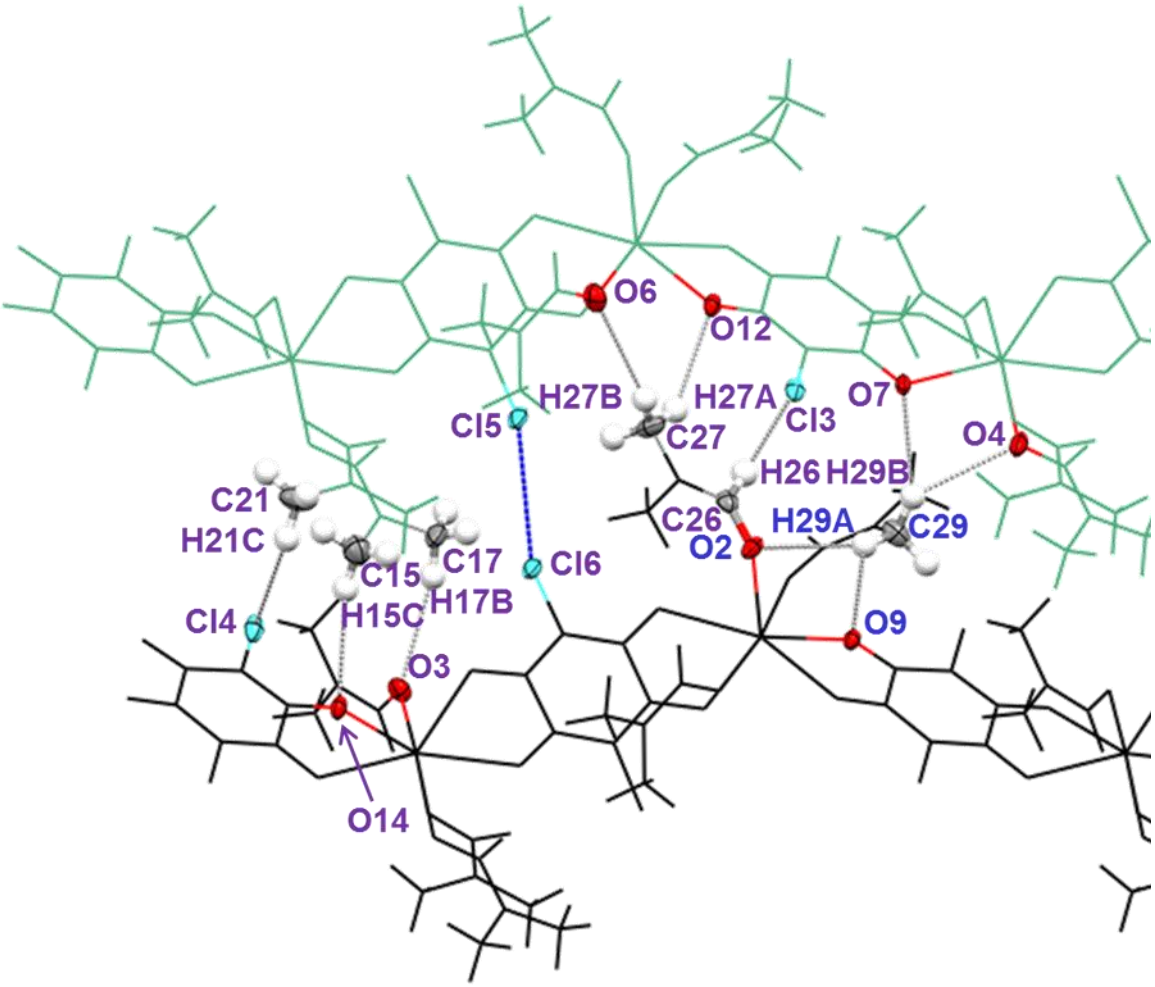

Figure 6.34. Two 1D chains, showing the intracomplex H-bonds C29-H29A···O2 and C29-H29A···O9^{a}, the halogen bond Cl5···Cl6^{b}/Cl6···Cl5^{d}, and H-bonds connecting the 1D chains along the *a* direction.

The 1D chains pack along the *b* direction in a staggered manner as depicted in Figure 6.35. Here, as well as the halogen bond, Cl5···Cl6^{b}/Cl6···Cl5^{d}, connecting 1D chains along the *a* direction, another halogen bond, Cl3···Cl3^{i}, connecting chains along the *b* direction is also

observed. This type-I halogen bond, between crystallographically equivalent chlorine atoms of two chloranilate ligands, is shorter than Cl5···Cl6^{b}/Cl6···Cl5^{d} with a distance of 3.416(2) Å, and has angles C-Cl3···Cl3^{i}/C-Cl3^{i}···Cl3, 161.1(2)°.

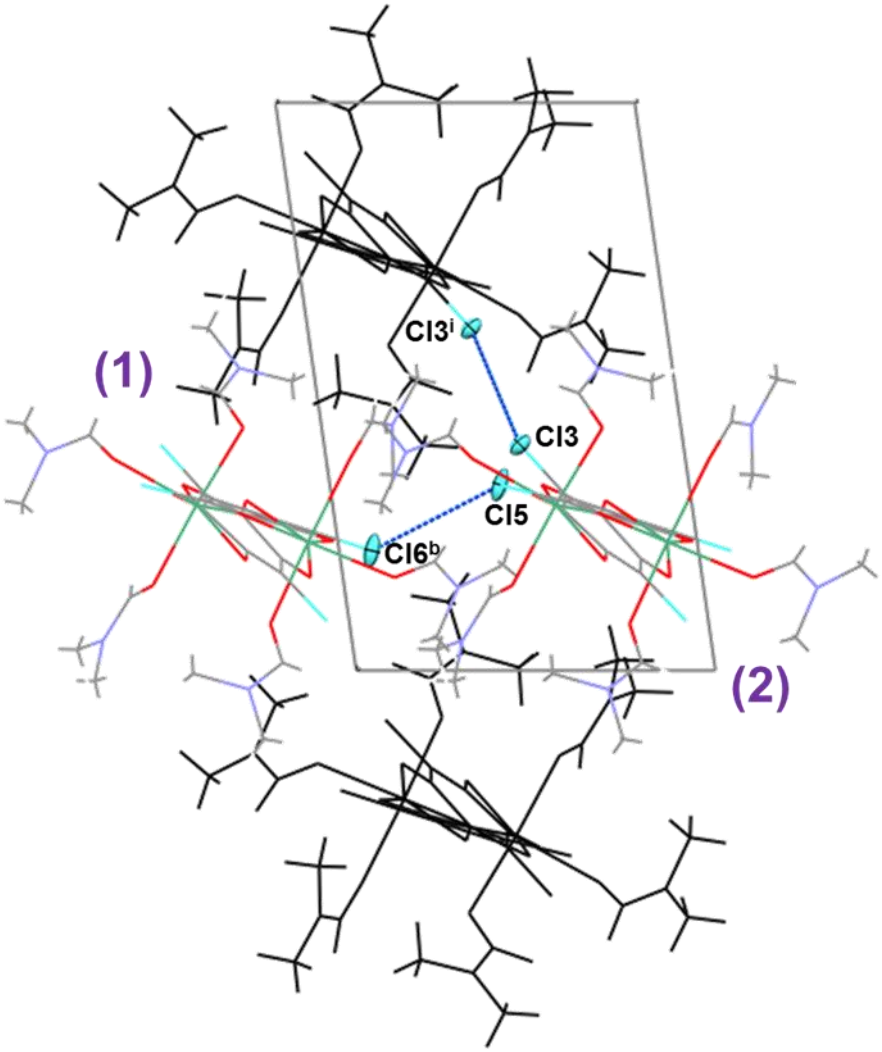

Figure 6.35. View down the *c* axis showing four 1D chains connected by Cl5···Cl6^{b} / Cl6···Cl5^{d}, and Cl3···Cl3^{i} halogen bonds. The two 1D chains coloured by element are labelled (1) and (2) for the purpose of more clearly illustrating the H-bonds connecting chains along the *b* direction in Figure 6.36 and Figure 6.37. Symmetry codes: ^{b}(1+x, y, z) ^{d}(-1+x, y, z) ^{i}(1-x, 1-y, -1-z)

Accompanying the Cl3···Cl3^{i} halogen bonds, there are seventeen weak H-bonds or short contacts that connect the 1D chains along the *b* direction, sixteen of which originate from methyl groups of the DMF molecules. These are illustrated in Figure 6.36 and Figure 6.37 with respect to the 1D chains as labelled in Figure 6.35, and listed in Table 6.13. These include two bifurcated H-bonds: C17-H17A···O3^{e}/O13^{e} and C21-H21B···O5^{g}/O8^{g} both of

which are formed between a methyl group and the oxygen atoms of another DMF molecule and a chloranilate ligand. C17-H17A···O13^{e} has the longest D···A distance of these H-bonds at 3.757(8) Å, which, for a C-H···O H-bond, this length suggests the interaction is more van der Waals in nature. However the directionality of the bond with its angle of 170° suggests it may indeed be an H-bond, especially given that it is a component part of a bifurcated H-bond, and the corresponding part, C17-H17A···O3^{e}, has a much lower angle of 111°.

Three H-bonds are formed to accepting chlorine atoms of the chloranilate ligands. C25-H25A···Cl4^{h} has a D···A distance of 3.601(8) Å, and an angle of 125°. C13-H13···Cl5^{e} and C14-H14C···Cl5^{e} share a common acceptor, and are very similar in their geometries with slightly longer D···A distances than C25-H25A···Cl4^{h}. The former has a D···A distance of 3.636(7) Å, and an angle of 139(3)°, and the latter has a D···A distance of 3.695(7) Å and an angle of 134°. C13-H13···Cl5^{e} is the only H-bond connecting the 1D chains along the *b* direction which is formed from a C-H group of the DMF molecule.

Of the H-bonds formed between methyl groups and oxygen atoms, those with the shortest D···A distances are C25-H25B···O9^{h} and C25-H25C···O9^{h} at 3.263(7) Å. It is likely these H-bonds have the shortest D···A distances due to the combined attractive force of two hydrogen atoms of the same methyl group. The positioning of the participating atoms, however, constrains these interactions to have the smallest angles of 105° and 101°, respectively. The H-bond of the largest angle is C20-H20C···O14^{g} where the acceptor is an oxygen atom of a chloranilate ligand, which has an angle of 175°.

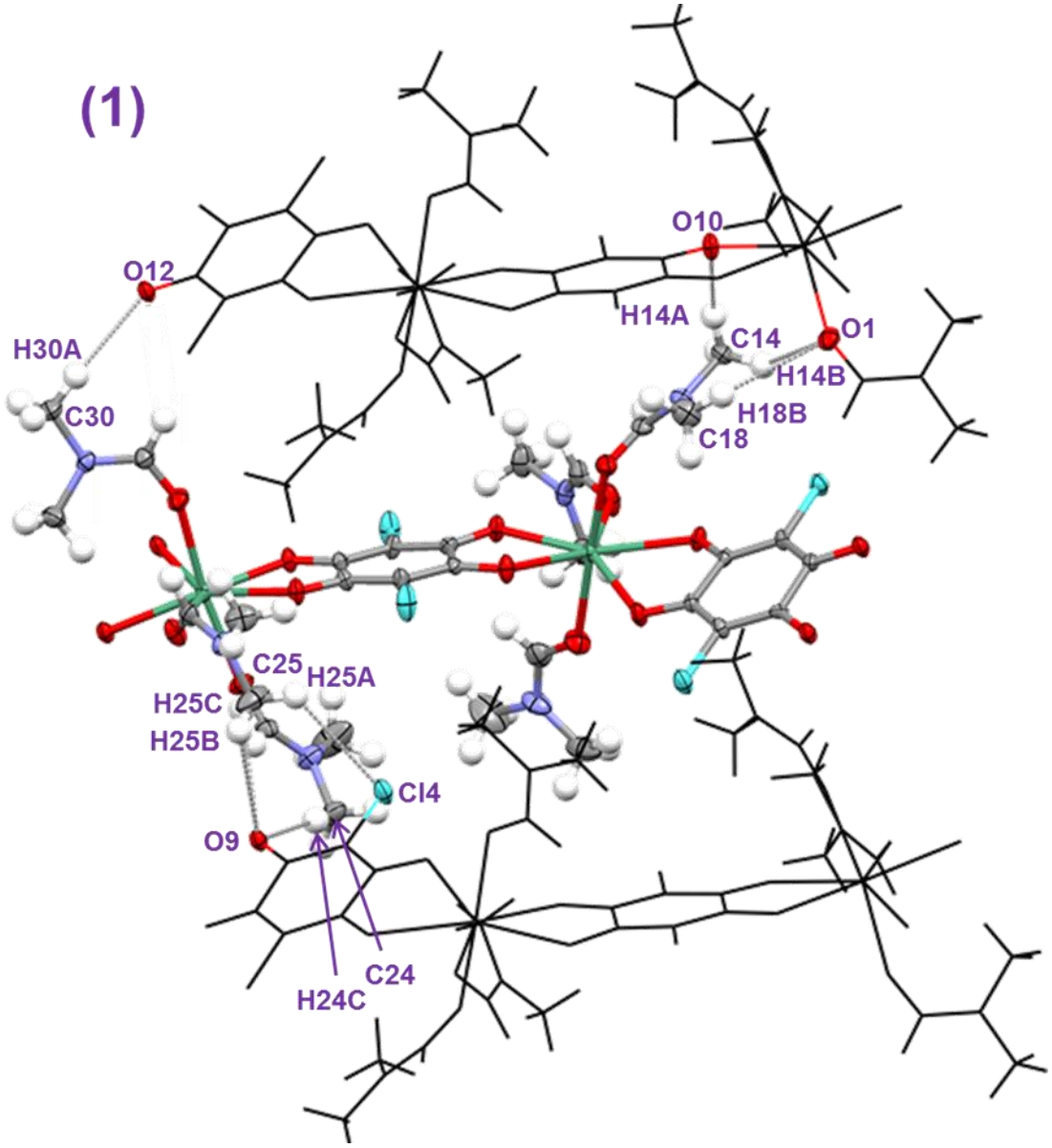

Figure 6.36. The same two 1D chains coloured in black, and the 1D chain coloured by element, that was labelled (1) in Figure 6.35, illustrating the relevant H-bonds connecting the 1D chains along the *b* direction. Only H-bonds originating from the central 1D chain (coloured by element) are shown for clarity.

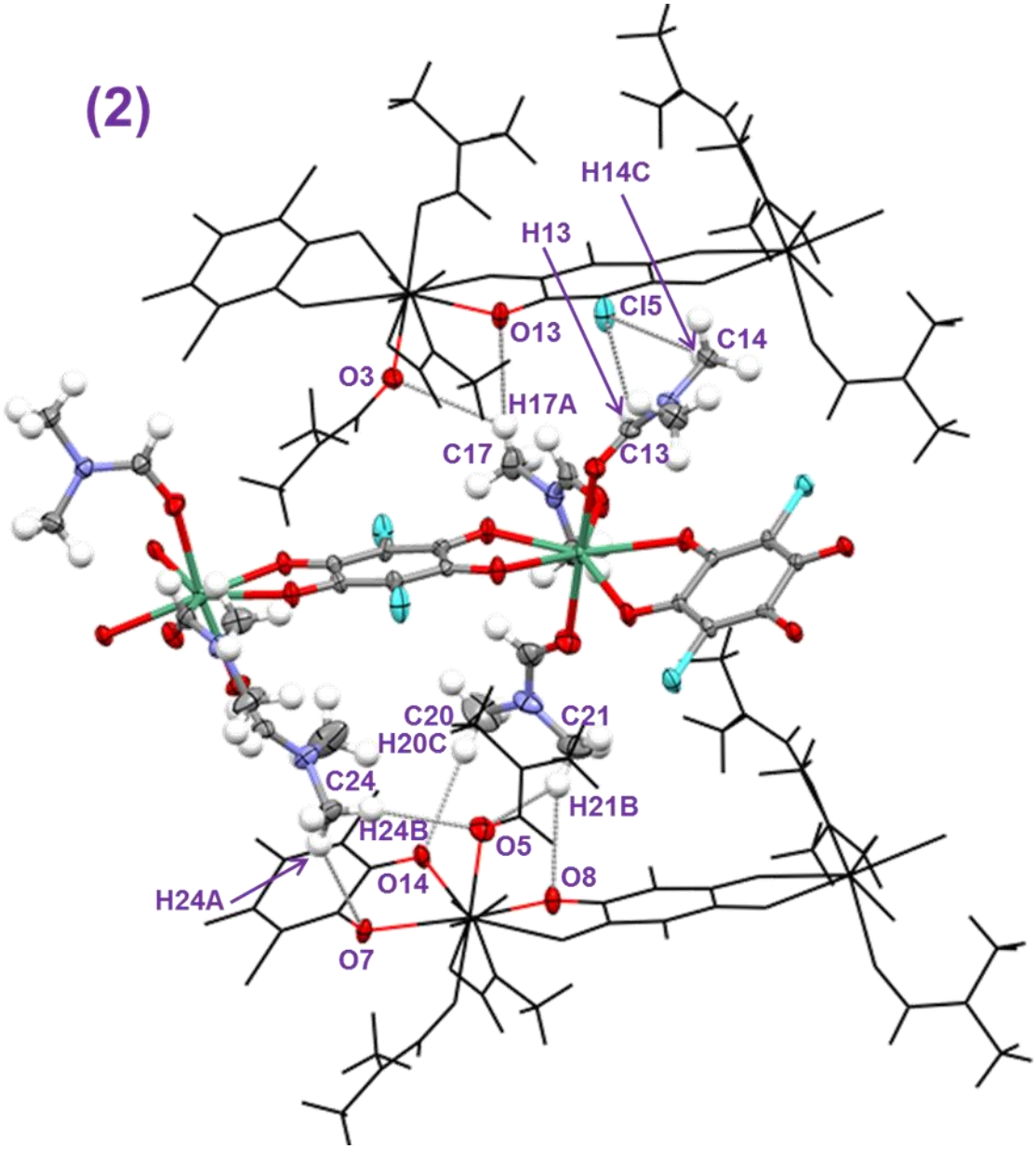

Figure 6.37. The same two 1D chains coloured in black, and the 1D chain coloured by element, that was labelled (2) in Figure 6.35, illustrating the relevant H-bonds connecting the 1D chains along the *b* direction. Only H-bonds originating from the central 1D chain (coloured by element) are shown for clarity.

Table 6.13. Geometries of H-bonds in **(25)**.

D-H···A Interaction	D-H (Å)	H···A (Å)	D···A (Å)	D-H···A (°)
(Figure 6.34) Intracomplex H-bonds				
*C29-H29A···O2	0.96	2.90	3.823(8)	163
*C29-H29A···O9[a]	0.96	2.65	3.353(6)	130
(Figure 6.34) H-bonds connecting chains along a direction				
*C15-H15C···O14[b]	0.96	2.95	3.684(8)	135
*C17-H17B···O3[b]	0.96	2.69	3.626(7)	165
*C21-H21C···Cl4[b]	0.96	2.91	3.771(7)	150
C26-H26···Cl3[c]	1.00(6)	2.77(6)	3.773(6)	177(8)
*C27-H27A···O12[c]	0.96	2.53	3.245(7)	131
*C27-H27B···O6[d]	0.96	2.73	3.605(8)	151
*C29-H29B···O4[c]	0.96	2.68	3.449(6)	138
*C29-H29B···O7[c]	0.96	2.63	3.509(7)	153
(Figure 6.36 and Figure 6.37) H-bonds connecting chains along b direction				
C13-H13···Cl5[e]	1.08(6)	2.75(5)	3.636(7)	139(3)
*C14-H14A···O10[f]	0.96	2.42	3.301(7)	153
*C14-H14B···O1[f]	0.96	2.88	3.543(7)	127
*C14-H14C···Cl5[e]	0.96	2.97	3.695(7)	134
*C17-H17A···O3[e]	0.96	2.96	3.422(8)	111
*C17-H17A···O13[e]	0.96	2.81	3.757(8)	170
*C18-H18B···O1[f]	0.96	2.71	3.640(7)	164
*C20-H20C···O14[g]	0.96	2.60	3.556(9)	175
*C21-H21B···O5[g]	0.96	2.84	3.528(8)	130
*C21-H21B···O8[g]	0.96	2.71	3.574(8)	150
*C24-H24A···O7[g]	0.96	2.60	3.421(7)	143
*C24-H24B···O5[g]	0.96	2.67	3.557(7)	155
*C24-H24C···O9[h]	0.96	2.61	3.570(7)	175
*C25-H25A···Cl4[h]	0.96	2.96	3.601(8)	125
*C25-H25B···O9[h]	0.96	2.88	3.263(7)	105
*C25-H25C···O9[h]	0.96	3.26	3.263(7)	101
*C30-H30A···O12[f]	0.96	2.47	3.415(7)	168

Symmetry code: [a](x, y, 1+z) [b](1+x, y, z) [c](-1+x, y, 1+z) [d](-1+x, y, z) [e](1-x, 1-y, -z) [f](-x, 1-y, -z) [g](1-x, -y, -z) [h](-x, -y, -z) *H-bond features methyl group hydrogen atom fixed in idealised position.

HSM was carried out on single crystals of **(25)**. The crystals started to release bubbles from about 150 °C and this continued until the temperature ramp was stopped at 375 °C. Afterwards, the crystals were still pink but had turned opaque, having lost all crystallinity. A small sample of crystals of **(25)** were analysed by DSC (Appendix C, Figure A35). The trace is complicated and shows no agreement with the observations from HSM. The crystals were selected from the solution of a repeat preparation in which nicotinic acid was used in a three-component crystallisation experiment, and the sample was placed in a mortar to dry. After the solvent had evaporated, a white material was also present which was difficult to separate cleanly from the pink crystals of **(25)**. It is possible that this was nicotinic acid precipitate, which then contaminated the sample used for DSC. This is somewhat evident in the DSC trace which shows a broad endotherm at 238.8 °C – within the melting range of nicotinic acid (m.p 236 – 239 °C).

6.6. Conclusions

The three 'supramolecular ligands' **(20)**, **(21)** and **(22)** have been identified and characterised and can be reproducibly synthesised. **(22)** displays the characteristic bifurcated H-bond that was identified by Adam *et al*.[136] The combination of these materials, as well as the complexes **PAZHOO** and **YERXUP** with magnesium salts did not result in a new magnesium-organic-organic complex: only a simple isonicotinic acid nitrate salt was identified from these experiments **(A5)**. Combination of **(20)** with copper(II) sulfate pentahydrate fomed the new complex **(23)**, however the framework of the 'supramolecular ligand' is not carried through into the metal complex, suggesting that the 'supramolecular ligand' dissociated completely on dissolution prior to combination with the transition metal. In **(23)**, the picolinate ion N,O-chelates to the copper centre; therefore it is not possible for the other isomers of the pyridine carboxylic acid to interact with the copper centre in the same way. A crystallisation experiment combining the 'supramolecular ligand' **YERXUP** with copper(II) sulfate pentahydrate resulted in the previously reported complex, **VOMNAM**, which does not contain the pyridine carboxylic acid ligand. It is likely that due to the greater H-bonding potential of the pyridine carboxylic acid molecules over the methylpyridines, robust and discrete supramolecular synthons do not form, and rather, moderate H-bonds connect the 3D structure.

Incorporating chloranilic acid into the structure of **(13)** was not achieved. Again the pre-prepared complex dissociated into its constituent parts and the pyridine carboxylic acid ligand was not incorporated into the new calcium-chloranilate complexes **(24)** and **(25)**. The inclusion of nicotinic acid either in the form of **(13)**, or as a pure starting material along with

$CaCl_2$ and chloranilic acid was not found to be a necessary factor in the preparation of these complexes. The syntheses often resulted in a mix of phases including crystals of **(24)**, **(25)** and possibly also crystals of **(A7)**, a salt composed of chloranilate and dimethylammonium ions. **(24)** was normally the most dominant product from these experiments. The use of DMF was obligatory in the preparation of these materials; it is a neutral coordinating ligand in **(25)**, and the hydrolysed product, dimethylammonium, is a counterion in **(24)**. This material is isostructural to a known yttrium complex, **MOBBIO**, and is potentially very attractive in that it features what would be channels inter-connected in two directions, if it were not for the presence of the counterions. The challenge remains to design this complex without the need for the counterions. As this would involve the use of a +4 metal ion, naturally, it cannot be realised using group 2 metals.

Chapter 7. Conclusions and Further Work

7.1. Conclusions

This work presents a series of new, crystalline, metal-organic and organic complexes, synthesised from pyridine carboxylic, dicarboxylic and chloranilic acid ligands. The materials are prepared primarily by evaporative crystallisation and characterised primarily by scXRD. The magnesium- and calcium-organic complexes reported contribute to the growing knowledge of alkaline earth metal-organic complexes and support the general growing belief that these metals do have the potential to be employed in the development of functional crystalline materials. In attempting to prepare these group 2 complexes, this work has highlighted the greater ease with which equivalent transition metal complexes can be synthesised, compared to the targeted alkaline earth metal-organic complex analogues.

The metal-organic complexes display varying levels of coordination dimensionality (Table 7.1). Of the 19 alkaline earth metal-organic complexes, the magnesium complexes exhibit the highest number of complexes of 0D coordination dimensionality, showing only two 1D complexes and one 2D complex. In contrast, the calcium complexes generally have a higher degree of coordination connectivity, with the greatest number of 1D complexes, one 2D complex and two 3D complexes. The magnesium complex of the highest coordination dimensionality, **(18)**, was the only complex reported which was synthesised by hydrothermal methods. Both of the copper complexes reported are 0D.

Table 7.1. Coordination dimensionality of all reported Mg and Ca complexes.

Coordination dimensionality	Mg complexes	Ca Complexes
0D	**(1)**, **(2)**, **(5)**, **(6)**, **(17)**, **(19)**	**(3)**, **(4)**
1D	**(7)**, **(8)**	**(9)**, **(10)**, **(11)**, **(12)**, **(25)**
2D	**(18)**	**(13)**
3D	_	**(14)**, **(24)**

A recurring coordination mode whereby two metal centres are doubly bridged by coordinating oxygen atoms of the carboxylate groups of two organic ligands to form an eight-membered-ring was observed in three magnesium- and four calcium-organic complexes, reported in Chapter 4. This coordination mode was also observed within the 2D

coordination polymeric sheet of **(18)** featuring a pyridine dicarboxylate ligand, as reported in Chapter 5.

It was noted that some complexes are related as constitutional isomers (**(3)** and **(10)**, **(5)** and **(6)**, and **(5)** and **(7)**), or as 'molecular building block structural isomers' (**(6)** and **(7)**). Transformation from one crytal structure to another was observed on two occasions: from **(8)** to **(7)** and from **(18)** to **(19)**. In both of these cases the nature of the transformation was not established, but it was possibly due to a dissolution/recrystallisation process.

As is often observed in the literature, magnesium was always six coordinate with an octahedral, or distorted octahedral, geometry. The magnesium centres were never seven coordinate with a pentagonal bipyramidal geometry, as reported in the literature for some complexes in which magnesium is coordinated by 2,4,6-pyridine tricarboxylate,[114] and 3,5-pyridine dicarboxylate.[113] Again, as observed regularly in the literature, the calcium centres have a variable coordination number which are generaly higher than that of the magnesium centres due to the larger size of the ion. Three complexes display a calcium centre of octahedral geometry (**(11)**, **(13)**, **(14)**), two complexes display one of pentagonal bipyramidal geometry (**(4)**, **(25)**), while five complexes are eight coordinate (**(3)**, **(9)**, **(10)**, **(12)**, **(24)**). Two complexes exhibit a calcium centre O,O'-chelated by bidentate nitrate counterions (**(3)** and **(10)**), while that in **(12)** is coordinated by bridging water molecules: neither of these features are displayed by the reported magnesium complexes, however one magnesium complex (**(8)**) is (singly) coordinated by a nitrate ion.

It can be inferred that the coordination geometries of the alkaline earth metal-organic complexes are generally governed by the ligand steric effects and are therefore less predicatable than those of the transition metal-organic complexes. The hard acid character of the Mg^{2+} and Ca^{2+} ions leads to metal-ligand coordination that is more ionic in nature, compared with late transition metal-ligand coordination which is more covalent and directional due to the d electron orbitals of these metals.

It was found that water readily coordinates to both magnesium and calcium centres, which is in accordance with what is reported in the literature. Other than one example in which a nitrate ion coordinates to the magnesium centre, no other counterions or solvent molecules are observed to coordinate to magnesium. Calcium is coordinated by chlorine atoms in two examples (**(11)** and **(13)**), both complexes featuring calcium in an octahedral geometry, and by a DMF molecule in one structure (**(24)**).

The pyridine carboxylic acid ligands were found to coordinate readily with magnesium and calcium to produce new coordination complexes, as discussed in Chapter 4. On the other hand, the evaporation crystallisation experiments in which pyridine dicarboxylic acids were

combined with these metal salts did not yield coordination complexes, new or otherwise, as discussed in Chapter 5. Only the hydrothermal reaction of 2,4-pyridine dicarboxylic acid and magnesium(II) acetate tetrahydrate, which was intended to produce *bis-[(μ_2-pyridine-2,4-dicarboxylato)-triaqua-magnesium(II)]* (**SUYLEE01**),[97] instead resulted in a 2D coordination complex (**(18)**). This complex transformed into **(19)**, which features the first example of a 0D metalloligand composed of magnesium N,O-chelated by two 2,4-pyridine dicarboxylate ligands and two water molecules; this is a potential building block for incorporating a magnesium centre into more functionalised H-bonded frameworks.

The 'supramolecular ligands' synthesised from pyridine carboxylic acid ligands and chloranilic acid were not successfully combined with an alkaline earth metal. Combination with copper was achieved, but with the loss of the original supramolecular ligand motif, as described in Chapter 6. Experiments combining chloranilic acid with alkaline earth metal salts were generally unsuccessful in producing coordination complexes, however two new complexes composed of chloranilate dianions and calcium centres are reported in Chapter 6.

H-bonds are present in all of the structures reported in this work, and make a significant contribution to the overall crystal structures of the 0D, 1D and 2D complexes. Counterions and water molecules, as well as organic ligands, play a major role in the H-bonding of these complexes. As reported in the literature, H-bonds are often formed from coordinated and non-coordinated water molecules, to carboxylate oxygen atoms or other water molecules. The H-bonding present is very unpredictable, generally because the stoichiometry of the complex itself, and therefore the presence of counterions, cannot be known with certainty until the crystal structure is solved. The products of the crystallisation experiments are often very sensitive to the complex solution chemistry and are easily influenced by factors such as the temperature, concentration and pH of the system. Therefore, the H-bonding motifs are very difficult to 'engineer', but there are some general consistencies. Since coordination to an alkaline earth metal is favoured from the carboxylate group over the pyridyl nitrogen atom, the nitrogen atom is often protonated and the pyridine carboxylic acid ligands are often in their zwitterionic form. Therefore it can be expected that the nitrogen atom of the pyridinium ring will form an H-bond. Also, when combining metal complexes synthesised from the pyridine dicarboxylic acid ligands with diamines, as could be predicted, proton transfer occurred from the carboxyl group to the amine group forming charge-assisted H-bonds between the ammonium group and the carboxylate group as observed in **(15)** and **(16)**, and as reported in the literature.[92, 94, 95] Due to the deprotonation of the carboxyl group and the clear preference of pyridine carboxylic acid ligands to coordinate alkaline earth metals *via* the carboxylate oxygen atom(s), as reported in this work and by others',[115]

carboxyl groups were not available as H-bond donors to form supramolecular synthons, such as the carboxyl dimer, in these metal-organic complexes.

The intermolecular interactions π-π stacking and halogen bonds are also observed in the complexes reported. The π-π stacking interactions are commonly observed between the aromatic rings of the pyridine carboxylic acid ligands but are not believed to play a major role in directing the crystal structure as they tend to be longer than the π-π stacking interactions of the pure ligands. Halogen bonds are observed in most complexes synthesised from chloranilic acid, as is reported the literature.[169, 179]

7.2. Further Work

This study focused on using the three isomers of pyridine carboxylic acid and only two isomers of pyridine dicarboxylic acid, so naturally, further work could expand the range of pyridine-based ligands under study, or indeed use other ligands possessing carboxyl groups. Similarly, other alkaline earth metals such as strontium and barium could be experimented with to investigate their behaviours on ligand coordination and to compare them to the behaviours of magnesium and calcium.

It would be desirable to gain better control over the complexes synthesised from magnesium and picolinic acid (**(6)**, **(7)** and **(8)**). This would require further crystallisation experiments to be carried out to establish the precise conditions under which each complex is formed homogeneously. This would involve further experimentation with solvent, temperature, stoichiometries, and crystallisation techniques. Optimising the synthesis of these materials would allow more reliable analysis to be carried out by DSC, and the characterisation could be extended to include TGA.

Since *bis-[(μ_2-pyridine-2,4-dicarboxylato)-triaqua-magnesium(II)]* (**SUYLEE01**) proved elusive, further experimentation with the hydrothermal synthesis may yield this complex, or hopefully, the magnesium analogue of the target metalloligand, so nearly achieved in the structure of **(19)**. Factors that may be altered are the stoichiometries of the reactants, the solvent in which they are dissolved, the temperature of the oven and the length of time in which the autoclave is left in the oven.

Further work could also focus on investigating the nature of the transformations of **(8)** to **(7)** and of **(18)** to **(19)**, to establish whether these involve a dissolution/recrystallisation process or a single-crystal-to-single-crystal transformation.

The combination of the ‘intermediate’ complexes with diamines could also be optimised by extending the range of solvents used and the crystallisation techniques employed. Greater

use of vapour diffusion, solvent layering, and crystallisation from gels may yield new crystal structures with the targeted H-bonding between the metalloligand and the diamine. Furthermore, crystallisation using monoamines, or a greater range of diamines, may be usefully investigated.

Regarding the incorporation of the organic 'supramolecular ligands' with metal salts to yield a metal-organic-organic complex, it is worth experimenting with the order in which the components are combined. Addition of chloranilic acid to a coordination complex synthesised from magnesium or calcium and a pyridine carboxylic acid such that metal-ligand coordination is achieved first, followed by the addition of the second organic component, expected to H-bond with the coordinating ligand, was not attempted. This would follow a similar methodology to that employed in combining the 'metalloligand' synthesised using 2,4-pyridine dicarboxylic acid with a diamine, which has been found to be a successful approach in producing more functionalised H-bonded metal-organic-organic complexes, at least with copper and zinc, the former as reported in this work, and by Beatty and co-workers.[95]

This work has reported an interesting 3D calcium-chloranilate coordination polymer **(24)**, containing dimethylammonium counterions. Due to the anionic framework, these ions cannot be evacuated to reveal channels, however it would be worth carrying out cation exchange experiments, as have been demonstrated by An and Rosi for the exchange of dimethylammonium in the channels of a porous zinc MOF.[76]

Appendices

The Appendices can be found on the disk attached.

Appendix A includes PXRD patterns and DSC traces of materials reported in Chapter 4, and a table listing the C-O / M-O distances and O-C-O / M-O-C angles of carboxylate groups and O-C-C-C / O-C-C-N torsion angles observed in ligands derived from pyridine carboxylic acids in complexes **(1)** – **(14)**.

Appendix B includes PXRD patterns, DSC traces and IR spectra of materials reported in Chapter 5.

Appendix C includes PXRD patterns, DSC and TGA traces of materials reported in Chapter 6.

Appendix D includes the experimental details and full structural analysis of complexes **(A1)** – **(A7)**.

Appendix E includes the experimental details and discussion of the 'unsuccessful attempts' to produce the 'intermediate' complexes **(I5)** – **(I7)**.

Appendix F includes tables summarising the syntheses of all reported materials.

References

1. J. Hulliger, *Angew. Chem. Int. Ed.,* **1994**, *33*, 143-162

2. G. R. Desiraju, *Angew. Chem. Int. Ed.,* **2007**, *46*, 8342-8356

3. J. C. Tan, A. K. Cheetham, *Chem. Soc. Rev.,* **2011**, *40*, 1059-1080

4. L. Brammer, *Chem. Soc. Rev.,* **2004**, *33*, 476-489

5. A. M. Beatty, *Coord. Chem. Rev.,* **2003**, *246*, 131-143

6. M. Dincă, J. R. Long, *J. Am. Chem. Soc.,* **2005**, *127*, 9376-9377

7. J. M. Thomas, *Nature,* **1981**, *289*, 633-634

8. G. Schmidt, *Pure Appl. Chem.,* **1971**, *27*, 126

9. G. R. Desiraju, *Crystal Engineering: The Design of Organic Solids*, Elsevier, Amsterdam, **1989**, Vol. 54

10. N. Schultheiss, A. Newman, *Cryst. Growth Des.,* **2009**, *9*, 2950-2967

11. G. R. Desiraju, *Chem. Comm.,* **2005**, 2995-3001

12. M. D. Hollingsworth, *Science,* **2002**, *295*, 2410-2413

13. J. D. Dunitz, *Pure Appl. Chem.,* **1991**, *63*, 177-185

14. J. D. Wright, *Molecular crystals,* Cambridge University Press, **1995**

15. G. R. Desiraju, *Angew. Chem. Int. Ed. Eng.,* **1995**, *34*, 2311-2327

16. M. C. T. Fyfe, J. F. Stoddart, *Acc. Chem. Res.,* **1997**, *30*, 393-401

17. G. M. Whitesides, E. E. Simanek, J. P. Mathias, C. T. Seto, D. Chin, M. Mammen, D. M. Gordon, *Acc. Chem. Res.,* **1995**, *28*, 37-44

18. G. M. Whitesides, B. Grzybowski, *Science,* **2002**, *295*, 2418

19. J. D. Dunitz, A. Gavezzotti, *Cryst. Growth Des.,* **2005**, *5*, 2180-2189

20. J. D. Dunitz, W. B. Schweizer, *CrystEngComm.,* **2007**, *9*, 266-269

21. M. C. Etter, *Acc. Chem. Res.,* **1990**, *23*, 120-126

22. P. Bombicz, T. Gruber, C. Fischer, E. Weber, A. Kalman, *CrystEngComm.,* **2014**, *16*, 3646-3654

23. D. Braga, F. Grepioni, *Making Crystals by Design: Methods, Techniques and Applications*, Wiley-VCH, **2007**

24. L. Pauling, *The Nature of the Chemical Bond*, Cornell University Press, **1939**

25. E. Arunan, G. R. Desiraju, R. A. Klein, J. Sadlej, S. Scheiner, I. Alkorta, D. C. Clary, R. H. Crabtree, J. J. Dannenberg, P. Hobza, *Pure Appl. Chem.,* **2011**, *83*, 1637-1641

26. G. R. Desiraju, T. Steiner, *The Weak Hydrogen Bond: In Structural Chemistry and Biology*, Oxford University Press, **1999**

27. G. A. Jeffrey, *An Introduction to Hydrogen Bonding*, Oxford University Press, **1997**

28. A. Bondi, *J. Phys. Chem.,* **1964**, *68*, 441-451

29. P. Metrangolo, F. Meyer, T. Pilati, G. Resnati, G. Terraneo, *Angew. Chem. Int. Ed.,* **2008**, *47*, 6114-6127

30. P. Metrangolo, H. Neukirch, T. Pilati, G. Resnati, *Acc. Chem. Res.,* **2005**, *38*, 386-395

31. G. Mínguez Espallargas, F. Zordan, L. Arroyo Marín, H. Adams, K. Shankland, J. van de Streek, L. Brammer, *Chem. Eur. J.,* **2009**, *15*, 7554-7568

32. T. T. T. Bui, S. Dahaoui, C. Lecomte, G. R. Desiraju, E. Espinosa, *Angew. Chem. Int. Ed.,* **2009**, *48*, 3838-3841

33. C. B. Aakeröy, M. Fasulo, N. Schultheiss, J. Desper, C. Moore, *J. Am. Chem. Soc.,* **2007**, *129*, 13772-13773

34. P. Smart, Á. Bejarano-Villafuerte, L. Brammer, *CrystEngComm.,* **2013**, *15*, 3151-3159

35. P. Metrangolo, G. Resnati, *Science,* **2008**, *321*, 918-919

36. C. A. Hunter, J. K. M. Sanders, *J. Am. Chem. Soc.,* **1990**, *112*, 5525-5534

37. C. A. Hunter, K. R. Lawson, J. Perkins, C. J. Urch, *J. Chem. Soc., Perkin Trans. 2* **2001**, 651-669

38. C. R. Martinez, B. L. Iverson, *Chem. Sci.,* **2012**, *3*, 2191-2201

39. J. D. Dunitz, J. Bernstein, *Acc. Chem. Res.,* **1995**, *28*, 193-200

40. W. McCrone, *Interscience, New York* **1965**, *2*, 726-767

41. J. Bernstein, *Polymorphism in Molecular Crystals*, Oxford University Press, **2008**

42. S. A. Kulkarni, E. S. McGarrity, H. Meekes, J. H. ter Horst, *Chem. Comm.,* **2012**, *48*, 4983-4985

43. G. R. Desiraju, *Science,* **1997**, *278*, 404-405

44. B. Spingler, S. Schnidrig, T. Todorova, F. Wild, *CrystEngComm.,* **2012**, *14*, 751-757

45. S. R. Miller, D. Heurtaux, T. Baati, P. Horcajada, J.-M. Grenèche, C. Serre, *Chem. Comm.,* **2010**, *46*, 4526

46. H. Wu, H. Yu, Z. Yang, X. Hou, X. Su, S. Pan, K. R. Poeppelmeier, J. M. Rondinelli, *J. Am. Chem. Soc.,* **2013**, *135*, 4215-4218

47. B. V. Harbuzaru, A. Corma, F. Rey, P. Atienzar, J. L. Jordá, H. García, D. Ananias, L. D. Carlos, J. Rocha, *Angew. Chem. Int. Ed.,* **2008**, *47*, 1080-1083

48. S. Kitagawa, R. Kitaura, S.-i. Noro, *Angew. Chem. Int. Ed.,* **2004**, *43*, 2334-2375

49. J.-R. Li, R. J. Kuppler, H.-C. Zhou, *Chem. Soc. Rev.,* **2009**, *38*, 1477-1504

50. Z. Chang, D.-S. Zhang, Q. Chen, X.-H. Bu, *Phys. Chem. Chem. Phys.,* **2013**, *15*, 5430-5442

51. A. R. Millward, O. M. Yaghi, *J. Am. Chem. Soc.,* **2005**, *127*, 17998-17999

52. M. Maes, M. Trekels, M. Boulhout, S. Schouteden, F. Vermoortele, L. Alaerts, D. Heurtaux, Y. K. Seo, Y. K. Hwang, J. S. Chang, *Angew. Chem.,* **2011**, *123*, 4296-4300

53. T. Grant Glover, G. W. Peterson, B. J. Schindler, D. Britt, O. Yaghi, *Chem. Eng. Sci.,* **2011**, *66*, 163-170

54. A. Phan, A. U. Czaja, F. Gándara, C. B. Knobler, O. M. Yaghi, *Inorg. Chem.,* **2011**, *50*, 7388-7390

55. J. L. Harding, M. M. Reynolds, *J. Am. Chem. Soc.,* **2012**, *134(7),* 3330-3333

56. Y. Liu, C. Hu, A. Comotti, M. D. Ward, *Science,* **2011**, *333*, 436

57. D. Dutta, S. Vasudevan, *Inorg. Chem.,* **2012**, *51*, 8064-8072

58. M. Yoshizawa, J. K. Klosterman, M. Fujita, *Angew. Chem. Int. Ed.,* **2009**, *48*, 3418-3438

59. A. P. Côté, A. I. Benin, N. W. Ockwig, M. O'Keeffe, A. J. Matzger, O. M. Yaghi, *Science,* **2005**, *310*, 1166

60. X. Feng, X. Ding, D. Jiang, *Chem. Soc. Rev.,* **2012**, *41*, 6010-6022

61. T. Tozawa, J. T. A. Jones, S. I. Swamy, S. Jiang, D. J. Adams, S. Shakespeare, R. Clowes, D. Bradshaw, T. Hasell, S. Y. Chong, *Nature Mater.,* **2009**, *8*, 973-978

62. J. R. Holst, A. Trewin, A. I. Cooper, *Nature Chem.,* **2010**, *2*, 915-920

63. A. I. Cooper, *Angew. Chem. Int. Ed.,* **2012**, *51*, 7892-7894

64. M. Mastalerz, I. M. Oppel, *Angew. Chem. Int. Ed.,* **2012**, *51*, 5252-5255

65. P. S. Wheatley, P. Chlubná-Eliášová, H. Greer, W. Zhou, V. R. Seymour, D. M. Dawson, S. E. Ashbrook, A. B. Pinar, L. B. McCusker, M. Opanasenko, J. Čejka, R. E. Morris, *Angew. Chem. Int. Ed.,* **2014**, *53*, 13210-13214

66. T. R. Cook, Y.-R. Zheng, P. J. Stang, *Chem. Rev.,* **2013**, *113*, 734-777

67. J. L. C. Rowsell, O. M. Yaghi, *Microporous Mesoporous Mater.,* **2004**, *73*, 3-14

68. S. Fordham, X. Wang, M. Bosch, H.-C. Zhou, *Lanthanide Metal-Organic Frameworks*, ed. by P. Cheng, Springer Berlin Heidelberg, **2015**, Vol. 163

69. J.-P. Zhang, Y.-B. Zhang, J.-B. Lin, X.-M. Chen, *Chem. Rev.,* **2011**, *112*, 1001-1033

70. C. Baerlocher, L. B. McCusker, D. Olson, I. Z. A. S. Commission, *Atlas of zeolite framework types*, Elsevier, **2007**

71. M. Eddaoudi, D. B. Moler, H. Li, B. Chen, T. M. Reineke, M. O'Keeffe, O. M. Yaghi, *Acc. Chem. Res.,* **2001**, *34*, 319-330

72. O. M. Yaghi, M. O'Keeffe, N. W. Ockwig, H. K. Chae, M. Eddaoudi, J. Kim, *Nature,* **2003,** 423, 705-714

73. M. D. Allendorf, V. Stavila, *CrystEngComm.,* **2015**, *17*, 229-246

74. R. Robson, *J. Chem. Soc., Dalton Trans.* **2000**, 3735-3744

75. M. Eddaoudi, J. Kim, N. Rosi, D. Vodak, J. Wachter, M. O'Keeffe, O. M. Yaghi, *Science,* **2002**, *295*, 469-472

76. J. An, N. L. Rosi, *J. Am. Chem. Soc.,* **2010**, *132*, 5578-5579

77. E. D. Bloch, D. Britt, C. Lee, C. J. Doonan, F. J. Uribe-Romo, H. Furukawa, J. R. Long, O. M. Yaghi, *J. Am. Chem. Soc.,* **2010**, *132*, 14382-14384

78. H. Furukawa, N. Ko, Y. B. Go, N. Aratani, S. B. Choi, E. Choi, A. Ö. Yazaydin, R. Q. Snurr, M. O'Keeffe, J. Kim, O. M. Yaghi, *Science,* **2010**, *329*, 424-428

79. T. Ben, H. Ren, S. Ma, D. Cao, J. Lan, X. Jing, W. Wang, J. Xu, F. Deng, J. M. Simmons, *Angew. Chem.,* **2009**, *121*, 9621-9624

80. J. K. Schnobrich, K. Koh, K. N. Sura, A. J. Matzger, *Langmuir.,* **2010**, *26*, 5808-5814

81. H. K. Chae, D. Y. Siberio-Pérez, J. Kim, Y. B. Go, M. Eddaoudi, A. J. Matzger, M. O'Keeffe, O. M. Yaghi, *Nature,* **2004**, *427*, 523-527

82. T. A. Makal, J.-R. Li, W. Lu, H.-C. Zhou, *Chem. Soc. Rev.,* **2012**, *41*, 7761-7779

83. X. Lin, J. Jia, P. Hubberstey, M. Schröder, N. R. Champness, *CrystEngComm.,* **2007**, *9*, 438-448

84. Q. Wang, J. Luo, Z. Zhong, A. Borgna, *Energy Environ. Sci.,* **2011**, *4*, 42

85. R. Vaidhyanathan, S. S. Iremonger, G. K. H. Shimizu, P. G. Boyd, S. Alavi, T. K. Woo, *Science,* **2010**, *330*, 650-653

86. D. Britt, H. Furukawa, B. Wang, T. G. Glover, O. M. Yaghi, *Proc. Natl, Acad. Sci.,* **2009**, *106*, 20637-20640

87. R. A. Smaldone, R. S. Forgan, H. Furukawa, J. J. Gassensmith, A. M. Z. Slawin, O. M. Yaghi, J. F. Stoddart, *Angew. Chem. Int. Ed.,* **2010**, *49*, 8630-8634

88. J. J. Gassensmith, H. Furukawa, R. A. Smaldone, R. S. Forgan, Y. Y. Botros, O. M. Yaghi, J. F. Stoddart, *J. Am. Chem. Soc.,* **2011**, *133*, 15312-15315

89. A. D. Burrows, C. W. Chan, M. M. Chowdhry, J. E. McGrady, D. M. P. Mingos, *Chem. Soc. Rev.,* **1995**, *24*, 329-339

90. C. B. Aakeröy, A. M. Beatty, D. S. Leinen, *J. Am. Chem. Soc.,* **1998**, *120*, 7383-7384

91. S.-i. Noro, H. Miyasaka, S. Kitagawa, T. Wada, T. Okubo, M. Yamashita, T. Mitani, *Inorg. Chem.,* **2005**, *44*, 133-146

92. A. M. Beatty, B. A. Helfrich, G. A. Hogan, B. A. Reed, *Cryst. Growth Des.,* **2006**, *6*, 122-126.

93. A. M. Beatty, K. E. Granger, A. E. Simpson, *Chem. Eur. J.,* **2002**, *8*, 3254-3259

94. C. L. Chen, A. M. Beatty, *J. Am. Chem. Soc.,* **2008**, *130*, 17222-17223

95. G. A. Hogan, N. P. Rath, A. Beatty, *Cryst. Growth. Des.,* **2011**, *11*, 3740-3743

96. G. Yang, H. G. Zhu, B. H. Liang, X. M. Chen, *J. Chem. Soc., Dalton Trans.* **2001**, 580-585

97. A. Mallick, S. Saha, P. Pachfule, S. Roy, R. Banerjee, *J. Mater. Chem.,* **2010**, *20*, 9073-9080

98. Z. Hulvey, A. K. Cheetham, *Solid State Sci.,* **2007**, *9*, 137-143

99. S. Ma, J. A. Fillinger, M. W. Ambrogio, J.-L. Zuo, H.-C. Zhou, *Inorg. Chem. Comm.,* **2007**, *10*, 220-222

100. Q. Zhai, Q. Lin, T. Wu, S.-T. Zheng, X. Bu, P. Feng, *Dalton Trans.,* **2012**, *41*, 2866-2868

101. Y.-L. Huang, Y.-N. Gong, L. Jiang, T.-B. Lu, *Chem. Comm.,* **2013**, *49*, 1753-1755

102. S. J. Geier, J. A. Mason, E. D. Bloch, W. L. Queen, M. R. Hudson, C. M. Brown, J. R. Long, *Chem. Sci.,* **2013**, *4*, 2054-2061

103. Z.-F. Wu, B. Tan, M.-L. Feng, A.-J. Lan, X.-Y. Huang, *J. Mater. Chem. A.,* **2014**, *2*, 6426-6431

104. N. L. Rosi, J. Kim, M. Eddaoudi, B. Chen, M. O'Keeffe, O. M. Yaghi, *J. Am. Chem. Soc.,* **2005**, *127*, 1504-1518

105. P. D. C. Dietzel, V. Besikiotis, R. Blom, *J. Mater. Chem.,* **2009**, *19*, 7362

106. P. D. C. Dietzel, Y. Morita, R. Blom, H. Fjellvåg, *Angew. Chem.,* **2005**, *117*, 6512-6516

107. A. C. McKinlay, B. Xiao, D. S. Wragg, P. S. Wheatley, I. L. Megson, R. E. Morris, *J. Am. Chem. Soc.,* **2008**, *130*, 10440-10444

108. M. A. Sharif, H. Aghabozorg, E. Motyeian, M. Ghadermazi, J. Attar Gharamaleki, *Acta Crystallogr., Sect E: Struct. Rep.Online,* **2007**, *63*, m2235-m2236

109. Z. Karimov, G. M. Ismailova, *Uzb.Khim.Zh.,* **1997**, (CSD refcode **NISJEE**)

110. T. Liu, D. Luo, D. Xu, H. Zeng, Z. Lin, *Dalton Trans.,* **2013**, *42*, 368-371

111. Y.-C. He, J. Guo, H.-M. Zhang, J. Yang, Y.-Y. Liu, J.-F. Ma, *CrystEngComm.,* **2014**, *16*, 4210-4214

112. R. Oliva, L. Cavallo, *J. Phys. Chem. B.,* **2009**, *113*, 15670-15678

113. D. Banerjee, J. Finkelstein, A. Smirnov, P. M. Forster, L. A. Borkowski, S. J. Teat, J. B. Parise, *Cryst. Growth Des.,* **2011**, *11*, 2572-2579

114. M. C. Das, S. K. Ghosh, E. C. Sanudo, P. K. Bharadwaj, *Dalton Trans.,* **2009**, 1644-1658

115. F. Gschwind, O. Sereda, K. M. Fromm, *Inorg. Chem.,* **2009**, *48*, 10535-10547

116. A. Lazarescu, S. Shova, J. Bartolome, P. Alonso, A. Arauzo, A. M. Balu, Y. A. Simonov, M. Gdaniec, C. Turta, G. Filoti, R. Luque, *Dalton Trans.,* **2011**, *40*, 463-471

117. B. Barszcz, M. Hodorowicz, A. Jabłońska-Wawrzycka, J. Masternak, W. Nitek, K. Stadnicka, *Polyhedron,* **2010**, *29*, 1191-1200

118. W. Starosta, J. Leciejewicz, *J. Coord. Chem.,* **2009**, *62*, 1240-1248

119. W. Starosta, H. Ptasiewicz-Bąk, J. Leciejewicz, *J. Coord. Chem.,* **2003**, *56*, 33-39.

120. W. Starosta, H. Ptasiewicz-Bąk, J. Leciejewicz, *J. Coord. Chem.,* **2002**, *55*, 985-990

121. M. K. Kim, K.-L. Bae, K. M. Ok, *Cryst. Growth Des.,* **2011**, *11*, 930-932

122. G. Strahs, R. E. Dickerson, *Acta Crystallogr., Section B: Struct. Sci.* **1968**, *24*, 571-578

123. W. Starosta, H. Ptasiewicz-BĄk, J. Leciejewicz, *J. Coord. Chem.,* **2002**, *55*, 873-881

124. W. Starosta, H. Ptasiewicz-Bąk, J. Leciejewicz, *J. Coord. Chem.,* **2002**, *55*, 1147-1153

125. W. Starosta, H. Ptasiewicz-Bąk, J. Leciejewicz, *J. Coord. Chem.,* **2002**, *55*, 469-478

126. H. Aghabozorg, S. Daneshvar, A. Nemati, *Acta Crystallogr., Section E: Struct. Rep. Online,* **2008**, *64*, m1063-m1064

127. S. Kawata, H. Kumagai, K. Adachi, S. Kitagawa, *J. Chem. Soc., Dalton Trans.* **2000**, 2409-2417

128. K. Molčanov, M. Jurić, B. Kojić-Prodić, *Dalton Trans.,* **2014**, *43*, 7208-7218

129. K. Molčanov, B. Kojić-Prodić, A. Meden, *Croat. Chem. Acta.,* **2009**, *82*, 387-396

130. K. Molčanov, B. Kojić-Prodić, *CrystEngComm.,* **2010**, *12*, 925-939

131. K. Molčanov, B. Kojić-Prodić, A. Meden, *CrystEngComm.,* **2009**, *11*, 1407-1415

132. F. H. Allen, *Acta Crystallogr., Section B: Struct. Sci.* **2002**, *58*, 380-388

133. H. Burzlaff, J. Lange, R. Spengler, M. I. Karayannis, P. G. Veltsistas, *Acta Crystallogr., Section C:* **1995**, *51*, 190-193

134. B. F. Abrahams, M. J. Grannas, T. A. Hudson, S. A. Hughes, N. H. Pranoto, R. Robson, *Dalton Trans.,* **2011**, *40*, 12242-12247

135. S. Kashino, H. Ishida, T. Fukunaga, S. Oishi, *Acta Crystallogr., Section C: Cryst. Struct. Commun.* **2001**, *57*, 18-19

136. M. S. Adam, A. Parkin, L. H. Thomas, C. C. Wilson, *CrystEngComm.,* **2010**, *12*, 917-924

137. H. Hamazaki, H. Hosomi, S. Takeda, H. Kataoka, S. Ohba, *Acta Crystallgr., Section C: Cryst. Struct. Commun.* **1998**, *54*

138. A. Kutoglu, C. Scheringer, *Acta Crystallgr., Section C: Cryst. Struct. Commun.* **1983**, *39*, 232-234

139. F. Takusagawa, A. Shimada, *Acta Crystallogr., Section B: Struct. Sci.* **1976**, *32*, 1925-1927

140. J. R. Sander, D. K. Bučar, R. F. Henry, J. Baltrusaitis, G. G. Zhang, L. R. MacGillivray, *J. Pharm. Sci.,* **2010**, *99*, 3676-3683

141. E. Andersen, *Acta Crystallogr.,* **1967**, *22*, 188-191

142. G. Dutkiewicz, H. S. Yathirajan, Q. N. M. H. Al-arique, B. Narayana, M. Kubicki, *Acta Crystallogr., Section E: Struct. Rep. Online,* **2010**, *66*, o497-o498

143. G. H. Stout, L. H. Jensen, *X-Ray Structure Determination: A Practical Guide*, Wiley, **1989**

144. W. Massa, *Crystal Structure Determination*, Springer, **2004**

145. A. J. Blake, W. Clegg, J. M. Cole, *Crystal Structure Analysis: Principles and Practice*. Editor, Oxford University Press, **2009**

146. W. Clegg, *Crystal Structure Determination*, Oxford University Press, **1998**

147. D. Sherwood, J. Cooper, *Crystals, X-rays and Proteins: Comprehensive Protein Crystallography*, OUP Oxford, **2011**

148. J. D. Dunitz, *X-Ray Analysis and the Structure of Organic Molecules*, Cornell University Press, **1979**

149. T. Hahn, *International Tables for Crystallography, Space-Group Symmetry*, Wiley, **2005**

150. W. C. Rontgen, *Science, (New York, N.Y.)* **1896**, *3*, 227-31

151. P. K. W. Friedrich, M. Laue, *Sitzungsberichte der mathematisch-physikalischen Klasse der K B Akademie Weissenschaften zu München* **1912**, pp 302 - 322

152. W. Bragg, W. Bragg, *Proceedings of the Royal Society of London. Series A* **1913**, *88*, 428-438

153. W. L. Bragg, *Proceedings of the Royal Society of London. Series A, Containing Papers of a Mathematical and Physical Character,* **1913**, *89*, 248-277

154. W. H. Bragg, *Philosophical Transactions of the Royal Society of London. Series A, Containing Papers of a Mathematical or Physical Character,* **1915**, *215*, 253-274

155. J. M. Mermet, M. Otto, R. Kellner, M. V. Cases, *Analytical Chemistry: a Modern Approach to Analytical Science*, Wiley-VCH, **2004**

156. I. M. Vitez, A. W. Newman, M. Davidovich, C. Kiesnowski, *Thermochimica Acta.,* **1998**, *324*, 187-196

157. D. A. Skoog, D. M. West, F. J. Holler, *Fundamentals of Analytical Chemistry*, Saunders College Pub., **1996**

158. www.thermoscientific.com/content/dam/tfs/ATG/CMD/CMD%20Documents/BR-11007-FLASH-2000-Series-Organic-Elemental-Analyzers.pdf visited 8/4/15

159. D. S. Hage, J. R. Carr, J. D. Carr, *Analytical Chemistry and Quantitative Analysis*, Prentice Hall, **2011**

160. CRYSTALCLEAR_v1.4.0, Rigaku Americas Corporation, 9009 New Trails Drive, The Woodlands, Texas, USA, **2009**

161. CrysAlisPRO, Oxford Diffraction / Agilent Technologies, UK Ltd, Yarnton, England, **2009**

162. T. Higashi, *ABSCOR Rigaku Corporation*, Tokyo, Japan. **1995**

163. G. M. Sheldrick, SADABS Programme for Empirical Absorption Correction of Area Detector Data, University of Gottingen, Germany, **1996**

164. G. M. Sheldrick, *Acta Crystallogr., Section A: Found. Crystallogr,* **2008**, *64*, 112-122

165. L. Farrugia, *J. App. Crystallogr.,* **2012**, *45*, 849-854

166. A. L. Spek, *Acta Crystallogr., Section D: Biol. Crystallogr.* **2009**, *65*, 148-155

167. C. F. Macrae, P. R. Edgington, P. McCabe, E. Pidcock, G. P. Shields, R. Taylor, M. Towler, J. van de Streek, *J. App. Crystallogr.,* **2006**, *39*, 453-457

168. S.-i. Noro, H. Miyasaka, S. Kitagawa, T. Wada, T. Okubo, M. Yamashita, T. Mitani, *Inorg. Chem.,* **2004**, *44*, 133-146

169. Y. Tabuchi, A. Takahashi, K. Gotoh, H. Akashi, H. Ishida, *Acta Crystallogr., Section E: Struct. Rep. Online,* **2005**, *61*, o4215-o4217

170. G. Mehlana, S. A. Bourne, G. Ramon, L. Öhrström, *Cryst. Growth Des.,* **2013**, *13*, 633-644

171. Y. Chang, Q. Shuai, Z. Pei, *J. Coord. Chem.,* **2013**, *66*, 3137-3148

172. S. A. Chawdhury, A. Hargreaves, R. A. L. Sullivan, *Acta Crystallogr., Section B: Struct. Sci.* **1968**, *24*, 1222-1228

173. C.-X. Zhang, C.-B. Ma, M.-Q. Hu, C.-N. Chen, Q.-T. Liu, *Acta Crystallogr., Section E: Struct. Rep. Online,* **2007**, *63*, m1424-m1426

174. T.-W. Tseng, T.-T. Luo, C.-C. Su, H.-H. Hsu, C.-I. Yang, K.-L. Lu, *CrystEngComm.,* **2014**, *16*, 2626-2633

175. E. E. Sileo, A. S. de Araujo, G. Rigotti, O. E. Piro, E. E. Castellano, *J. Mol. Struct.,* **2003**, *644*, 67-76

176. G.-H. Wang, Z.-G. Li, H.-Q. Jia, N.-H. Hu, J.-W. Xu, *Acta Crystallogr., Section E: Struct. Rep. Online,* **2009**, *65*, m1568-m1569

177. J.-D. Wang, S.-M. Han, *Acta Crystallogr., Section E: Struct. Rep. Online,* **2010**, *66*, m206-m207

178. H. Aghabozorg, F. Jafarbak, M. Mirzaei, B. Notash, *Acta Crystallogr., Section E: Struct. Rep. Online,* **2011**, *67*, m435-m436

179. K. Gotoh, Y. Tabuchi, H. Akashi, H. Ishida, *Acta Crystallogr., Section E: Struct. Rep. Online,* **2006**, *62*, o4420-o4421

180. K. Gotoh, H. Nagoshi, H. Ishida, *Acta Crystallogr., Section E: Struct. Rep. Online,* **2009**, *65*, o614

181. S. Kawata, S. Kitagawa, M. Kondo, M. Katada, *Synth. Met.,* **1995**, *71*, 1917-1918

182. P. C. A. Bruijnincx, M. Viciano-Chumillas, M. Lutz, A. L. Spek, J. Reedijk, G. van Koten, R. J. M. Klein Gebbink, *Chem. Eur. J.,* **2008**, *14*, 5567-5576

183. Y.-H. Chung, S.-I. Fang, S.-H. Fang, H.-H. Lin, S.-Y. Liou, *J. Chin. Chem. Soc.,* **2009**, *56*, 1099-1107

184. C. Fujii, M. Mitsumi, M. Kodera, K.-I. Motoda, M. Ohba, N. Matsumoto, H. Okawa, *Polyhedron,* **1994**, *13*, 933-938

185. M. Kawahara, M. K. Kabir, K. Yamada, K. Adachi, H. Kumagai, Y. Narumi, K. Kindo, S. Kitagawa, S. Kawata, *Inorg. Chem.,* **2003**, *43*, 92-100

186. J. V. Folgado, R. Ibanez, E. Coronado, D. Beltran, J. M. Savariault, J. Galy, *Inorg. Chem.,* **1988**, *27*, 19-26

187. L. J. Barbour, *Chem. Comm.,* **2006**, 1163-1168

188. B. F. Abrahams, J. Coleiro, K. Ha, B. F. Hoskins, S. D. Orchard, R. Robson, *J. Chem. Soc., Dalton Trans.,* **2002**, 1586-1594